WL-TR-95-2089

COMBUSTOR LBO DESIGN MODEL EVALUATION

G. STURGESS

UNITED TECHNOLOGIES CORPORATION
PRATT & WHITNEY, GOV'T ENGINES & SPACE
P.O. BOX 109600
WEST PALM BEACH FL 33410-9600

MAY 1995

FINAL REPORT FOR 09/11/87-05/31/94

APPROVED FOR PUBLIC RELEASE; DISTRIBUTION IS UNLIMITED.

19960524 068

AERO PROPULSION & POWER DIRECTORATE
WRIGHT LABORATORY
AIR FORCE MATERIEL COMMAND
WRIGHT PATTERSON AFB OH 45433-7251

DTIC QUALITY INSPECTED 1

DISCLAIMER NOTICE

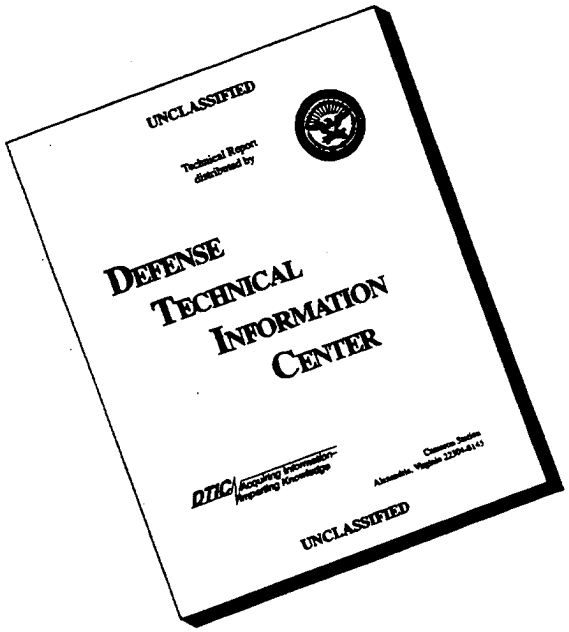

THIS DOCUMENT IS BEST QUALITY AVAILABLE. THE COPY FURNISHED TO DTIC CONTAINED A SIGNIFICANT NUMBER OF PAGES WHICH DO NOT REPRODUCE LEGIBLY.

NOTICE

WHEN GOVERNMENT DRAWINGS, SPECIFICATIONS, OR OTHER DATA ARE USED FOR ANY PURPOSE OTHER THAN IN CONNECTION WITH A DEFINITE GOVERNMENT-RELATED PROCUREMENT, THE UNITED STATES GOVERNMENT INCURS NO RESPONSIBILITY OR ANY OBLIGATION WHATSOEVER. THE FACT THAT THE GOVERNMENT MAY HAVE FORMULATED OR IN ANY WAY SUPPLIED THE SAID DRAWINGS, SPECIFICATIONS, OR OTHER DATA, IS NOT TO BE REGARDED BY IMPLICATION, OR OTHERWISE IN ANY MANNER CONSTRUED, AS LICENSING THE HOLDER, OR ANY OTHER PERSON OR CORPORATION; OR AS CONVEYING ANY RIGHTS OR PERMISSION TO MANUFACTURE, USE, OR SELL ANY PATENTED INVENTION THAT MAY IN ANY WAY BE RELATED THERETO.

THIS REPORT IS RELEASABLE TO THE NATIONAL TECHNICAL INFORMATION SERVICE (NTIS). AT NTIS, IT WILL BE AVAILABLE TO THE GENERAL PUBLIC, INCLUDING FOREIGN NATIONS.

THIS TECHNICAL REPORT HAS BEEN REVIEWED AND IS APPROVED FOR PUBLICATION.

Dale T. Shouse

DALE T. SHOUSE
Project Engineer
Combustion Branch
Fuels & Lubrication Division
Aero Propulsion & Power Directorate

Royce P. Bradley

ROYCE P. BRADLEY, Chief
Combustion Branch
Fuel & Lubrication Division
Aero Propulsion & Power Directorate

Walter J. Lauderdale

WALTER J. LAUDERDALE, Capt, USAF
Deputy, Fuels & Lubrication Division

IF YOUR ADDRESS HAS CHANGED, IF YOU WISH TO BE REMOVED FROM OUR MAILING LIST, OR IF THE ADDRESSEE IS NO LONGER EMPLOYED BY YOUR ORGANIZATION PLEASE NOTIFY WL/POSC WRIGHT-PATTERSON AFB OH 45433-7103 TO HELP MAINTAIN A CURRENT MAILING LIST.

Copies of this report should not be returned unless return is required by security considerations, contractual obligations, or notice on a specific document.

DISCLAIMER NOTICE

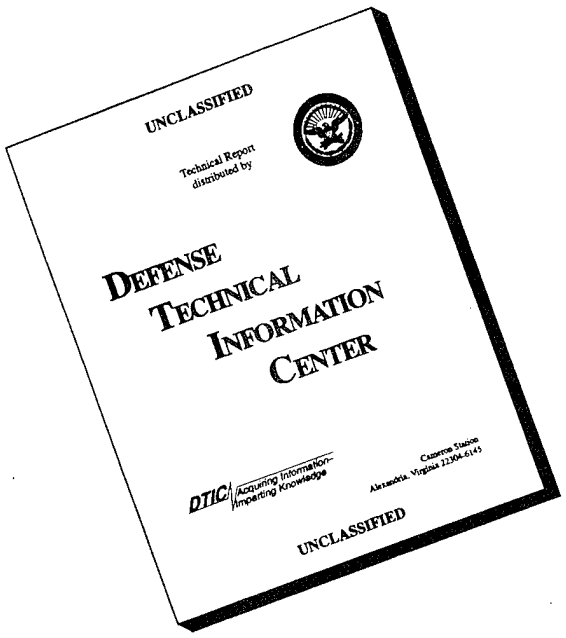

THIS DOCUMENT IS BEST QUALITY AVAILABLE. THE COPY FURNISHED TO DTIC CONTAINED A SIGNIFICANT NUMBER OF PAGES WHICH DO NOT REPRODUCE LEGIBLY.

REPORT DOCUMENTATION PAGE

Form Approved
OMB No. 0704-0188

Public reporting burden for this collection of information is estimated to average 1 hour per response, including the time for reviewing instructions, searching existing data sources, gathering and maintaining the data needed, and completing and reviewing the collection of information. Send comments regarding this burden estimate or any other aspect of this collection of information, including suggestions for reducing this burden to Washington Headquarters Services, Directorate for Information Operations and Reports, 1215 Jefferson Davis Highway, Suite 1204, Arlington VA 22202-4302, and to the Office of Management and Budget, Paperwork Reduction Project (0704-0188), Washington, DC 20503.

1. AGENCY USE ONLY *(Leave blank)*	2. REPORT DATE	3. REPORT TYPE AND DATES COVERED
	1 MAY 1995	FINAL SEP 87 to MAY 94

4. TITLE AND SUBTITLE

Combustor LBO Design Model Evaluation

5. FUNDING NUMBERS

C-F33615-87-C-2822
PE 62203F
PR 3048
TA 05
WU 72

6. AUTHOR(S)

G. J. Sturgess

7. PERFORMING ORGANIZATION NAME(S) AND ADDRESS(ES)

United Technologies Corp. Pratt & Whitney
Government Engines & Space Propulsion
P. O. Box 109600
West Palm Beach, Florida 33410-9600

8. PERFORMING ORGANIZATION REPORT NUMBER

9. SPONSORING / MONITORING AGENCY NAME(S) AND ADDRESS(ES)

Aero Propulsion & Power Directorate
Wright Laboratory (WL/POSC)
Air Force Materiel Command
Wright-Patterson AFB OH 45433-7103
Dale T. Shouse (513) 255-8623

10. SPONSORING/MONITORING AGENCY REPORT NUMBER

WL-TR-95-2089

11. SUPPEMENTARY NOTES

12A. DISTRIBUTION / AVAILABILITY STATEMENT

APPROVED FOR PUBLIC RELEASE: DISTRIBUTION IS UNLIMITED.

12B. DISTRIBUTION CODE

123. ABSTRACT (Maximum 200 words)

Long-term goals of the Air Force are to develop high-performance gas turbine combustors, and the design systems that can produce them. One aspect of an advanced combustor design system is the ability to calculate flame stability under fuel-lean conditions. Towards satisfying this latter desire the program had three principal objectives: 1) design, conduct and analyze experiments that establish a fundamental understanding of lean blowout, 2.) provide a data-base for evaluating and refining computer models of gas turbine combustion, and, 3.) devise a calculation procedure for lean blowout. Two laboratory and one rig-standard combustors were successfully designed, fabricated and operated. A novel procedure using excess nitrogen as a diluent for simulating sub-atmospheric pressures was calibrated and verified. The sequence of events leading to lean blowout was identified, and observed to be common in all the combustors. Advanced diagnostic techniques were applied to enhance understanding of blowout. Some advanced mathematical modeling was shown to be inadequate for calculating blowout. A hybrid calculation procedure was devised that successfully modeled the influences on blowout of many important operating conditions and design variables. In this manner the program objectives were met.

14. SUBJECT TERMS

Lean blowout, Flame stabilization, Combustor design modeling, Turbulent combustion, Laser diagnostics

15. NUMBER OF PAGES

354

16. PRICE CODE

17. SECURITY CLASSIFICATION OF REPORT	18. SECURITY CLASSIFICATION OF THIS PAGE	19. SECURITY CLASSIFICATION OF ABSTRACT	20. LIMITATION OF ABSTRACT
UNCLASSIFIED	UNCLASSIFIED	UNCLASSIFIED	SAR

NSN 7540-01-280-500

Standard Form 298 (Rev. 2-89)
Prescribed by ANSI Std. 239-18
298-102

PREFACE

This final report was submitted by Pratt & Whitney (P&W) under Contract No. F33615-87-C-2822 sponsored by the U.S. Air Force Wright Laboratory, Aero Propulsion and Power Directorate, Wright-Patterson Air Force Base, Ohio. Dr. W.M. Roquemore of WL/POSC was the Air Force Technical Director, and the Air Force Program Monitors were Lt. A. Lesmerises and Mr. D. Shouse, Dr. G.J. Sturgess of Pratt & Whitney was the Program Manager, and the P&W Principal Investigator was Dr. D.G. Sloan. This report covers work performed during the period September 11, 1987 through May 31, 1994.

The Program Manager wishes to express his gratitude and appreciation to Dr. W.M. Roquemore for his encouragement and support, and to all the many contributors to this work from Wright Laboratory, on-site contractors, and the visiting university faculty.

TABLE OF CONTENTS

Section			Page
	SUMMARY		1
1.0	**INTRODUCTION**		3
	1.1	Background	3
	1.2	Specific Problem	5
	1.3	Blowout Design Requirements	6
2.0	**PROGRAM APPROACH**		9
3.0	**BASIC STUDIES: TASK 100 COMBUSTOR**		11
	3.1	Intent	11
	3.2	P&W Task 100 combustor Design	11
	3.3	Flow Field in Research Combustor	14
	3.4	Simulation of Low Pressures	15
	3.5	Flame Structures and LBO Sequence	17
	3.6	Effects of Back–Pressure	22
	3.7	Stability Characteristics	24
	3.8	Summary	26
4.0	**APPLIED STUDIES: TASK 150 COMBUSTOR**		27
	4.1	Intent	27
	4.2	PW Task 150 Combustor Design	27
	4.3	Fuel Injectors and Dome Interface	28
	4.4	Isothermal Flow Field	28
	4.5	Characteristic Flame Shapes	30
	4.6	OH – Imaging for Instantaneous Flame Structures	33
	4.7	Velocity Fields in Reacting and Nonreacting Flows	35
	4.8	Temperature Fields	37
	4.9	Energy Release Rates	40
	4.10	Gas Sampling	42
	4.11	Blowout Characteristics	43
	4.12	Summary	44
5.0	**GENERIC GAS TURBINE COMBUSTOR STUDIES: TASK 200 COMBUSTOR**		45
	5.1	Intent	45
	5.2	PW Task 200 Combustor Design	45
	5.3	Rig and Facility	47
	5.4	Temperature Fields	47
	5.5	Flame and Blowout Characteristics	53
	5.6	Summary	58
6.0	**MODELLING CONSIDERATIONS**		59
	6.1	Intent	59
	6.2	Modeling for Data Correlation	59
	6.3	Phenomenological Modeling	60

TABLE OF CONTENTS (CONT'D)

Section			Page
6.4	Representation of PW100 Research Combustor as a Stirred Reactor		70
6.5	Kinetic Mechanism Evaluation		81
6.6	Eddy Dissipation Concept in CFD Modeling		90
	6.6.1	Introduction	90
	6.6.2	Fluid Dynamics	91
	6.6.3	Reaction Rates	103
	6.6.4	Fast Chemistry Limit	106
	6.6.5	Adjustment Factors	107
	6.6.6	Extinction Criteria for Fast Chemistry Limit	108
	6.6.7	Application of the Extinction Residence Time	110
	6.6.8	Chemical Kinetics for EDC	111
	6.6.9	EDC Model Implementation	113
	6.6.10	Preliminary Test of EDC Model in 2D–PREACH	117
6.7	Hybrid Modeling		118
	6.7.1	Introduction	118
	6.7.2	Hybrid CFD/Stirred Reactor Modeling Concept	118
	6.7.3	Reactor Network Determination	119
	6.7.4	CFD for a Generic Combustor	120
	6.7.5	Reactor Network for the Generic Combustor	128
	6.7.6	Chemical Reaction Mechanism	130
	6.7.7	Heat Losses	132
	6.7.8	Definition of Blowout	132
	6.7.9	Reactor Network Code	132
	6.7.10	Preliminary Test of Hybrid CFD/Stirred Reactor Modeling	133
6.8	Modeling Summary		134
7.0	MODEL EVALUATION		137
7.1	Intent		137
7.2	Evaluation of EDC Combustion Model in the PW100 Combustor		137
	7.2.1	Basic Flowfield (Case N23)	137
	7.2.2	Reacting Flow with EBU Combustion Model (Cases F23 and F63)	139
	7.2.3	Reacting Flow with EDC Combustion Model (Case F23)	140
	7.2.4	Case F41: Reacting Flow with EDC Model	143
	7.2.5	Case F63: Reacting Flow with EDC Model	144
	7.2.6	Case F80: Reacting Flow with EDC Model and Revised Calculation Procedure	145
	7.2.7	Summary of EDC Model Evaluation	148
7.3	Evaluation of Hybrid CFD/Stirred Reactor Modeling in PW200 Combustor		149
	7.3.1	Effects of Primary Zone Airflow	149
	7.3.2	Influence of Operating Pressure	150
	7.3.3	Effects of Dome Airflow	151
	7.3.4	Summary of Hybrid CFD/Stirred Reactor Model Evaluation	159
8.0	DISCUSSION		161
9.0	CONCLUSIONS		167
10.0	RECOMMENDATIONS		169
11.0	REFERENCES		171

TABLE OF CONTENTS (CONT'D)

Section		*Page*
Appendix A	Design And Development Of A Research Combustor For Lean Blow–out Studies	177
Appendix B	Acoustic Characteristics Of A Research Step Combustor	185
Appendix C	Isothermal Flow Fields In A Research Combustor For Lean Blowout Studies	195
Appendix D	Effects Of Back–pressure In A Lean Blowout Research Combustor	207
Appendix E	Lean Blowout In A Research Combustor At Simulated Low Pressures	221
Appendix F	Experimental And Theoretical Studies In A Gas–fueled Research Combustor	233
Appendix G	Aspects Of Flame Stability In A Research Dump Combustor	251
Appendix H	Studies Of Lean Blowout In A Research Combustor	267
Appendix I	Observations Of Flame Behavior From A Practical Fuel Injector Using Gaseous Fuel In A Technology Combustor	277
Appendix J	Lean Blowout Research In A Generic Gas Turbine Combustor With High Optical Access	293
Appendix K	Relation Of Cars Temperature Fields To Lean Blowout Performance In An Aircraft Gas Turbine Generic Combustor	307

LIST OF FIGURES

		Page
Figure 1–1.	Combustor Cross–Section	1
Figure 1–1.	Combustor Cross–Section	3
Figure 1–2.	Design System Based on Models and Design Practices	4
Figure 1–3.	Typical Engine Operating Envelope	6
Figure 1–4.	LBO Characteristics for Two Combustors, Showing Design–Specific Nature	7
Figure 1–5.	LBO Characteristic with Engine Operating Lines, Showing Under– and Over–Shoots	8
Figure 3–1.	Flow Patterns in a Modern Annular combustor Showing "Inside Out" Recirculation (Water–Tunnel Results)	11
Figure 3–2.	Cross–Section of Task 100 Research Combustor Rig	13
Figure 3–3.	Major Flow Features in Task 100 Research Combustor Near–Field (Isothermal Flow)	14
Figure 3–4.	Calibration Curve for Simulation of Low Pressures Using Excess Nitrogen Technique (Air–Propane–Nitrogen Systems)	17
Figure 3–5.	Blowout Characteristic for Task 100 Research Combustor Using Excess Nitrogen	17
Figure 3–6.	Time–Mean, Available Light Photographs of Attached and Lifted Flames in the Task 100 Research Combustor	18
Figure 3–7.	Time History and Frequency Spectra of Relative Temperature from a Thin Filament Pyrometer in the Attached Flame Region at Fuel–Rich and Fuel–Lean Equivalence Ratios	19
Figure 3–8.	Spatial Composite of Instantaneous PLIF OH–Images at an Equivalence Ratio of 1.56 with a Higher–Value combustor Loading (Attached Flame)	20
Figure 3–9.	Spatial Composite of Instantaneous PLIF OH–Images at an Equivalence Ratio of 0.78 with a Lower Vale Combustor Loading (Lifted Flame)	21
Figure 3–10.	Flame Behavior as Lean Blowout is Approached at Low Combustor Loadings with 45% Exit Blockage	21
Figure 3–11.	Influence on LBO of Exit Blockage at High Combustor Loading	22
Figure 3–12.	Dependency of Position of Maximum MTF On Exit Blockage for Lifted and Attached Flames in the 4.9 L/D Combustor	23
Figure 3–13.	Influence of Exit Blockage and combustor Loading (low values) on Equivalence Ratio for Onset of Axial Movements of the Lifted Flame	23
Figure 3–14.	Measured Lean–Portion of Experimental Stability Loop Compared to Well–Stirred Reactor Calculations; via the Loading Parameter	25

LIST OF FIGURES (CONT'D)

		Page
Figure 4–1.	Overall View of the PW Task 150 Technology Combustor	27
Figure 4–2.	Cross–Section of Dome Region, Showing Dome Interfacing and Fuel Injector in the Technology Combustor	28
Figure 4–3.	Isothermal flowfield in the Task 150 Combustor for the HS Injector at a Simulated Equivalence Ratio of 0.72	29
Figure 4–4.	Characteristic Flame Shapes for the HS Injector in the 4.9 L/D Task 150 Combustor with 45% Exit Blockage and Constant Dome Airflow of 310 SLPM	31
Figure 4–5.	Characteristic Flame Shapes for the LS Injector in the 4.9 L/D Task 150 Combustor with 45% Exit Blockage and Constant Dome Airflow of 310 SLPM	32
Figure 4–6.	Spatial Composites of OH–Images of Heat Release from the HS Injector at a Range of Dome Equivalence Ratios	34
Figure 4–7.	Time–Sequence of Instantaneous OH–Images from the HS Injector at a Dome Equivalence Ratio of 1.29	35
Figure 4–8.	LDV Mean Velocity Component Distributions for the HS Injector at 0.72 Equivalence Ratio (Airflow of 500 slpm)	36
Figure 4–9.	LDV Mean Velocity Component Distributions for the HS Injector at 1.49 Equivalence Ratio (Airflow of 500 slpm)	36
Figure 4–10.	Distributions of Mean Temperature Over a Range of Equivalence Ratios for the LS Injector	38
Figure 4–11.	Distributions of Mean Temperature Over a Range of Equivalence Ratios for the HS Injector	39
Figure 4–12.	Comparison of Digitized Characteristic Flame Images with Derived Distributions for Time–Mean Volumetric Energy Release Rates for the HS Injector at Lean and Rich Conditions	41
Figure 4–13.	Stability Characteristics of HS and LS Fuel Injectors in the PW150 Combustor	44
Figure 5–1.	Diagrammatic Cross–Section of PW200 Combustor Rig Test Section	46
Figure 5–2.	Flow Distributions in the PW200 Combustor	46
Figure 5–3.	Schematic Flow Path of Rig and Facility	47
Figure 5–4.	Measurement Planes for CARS Data, Showing Regions of Valid Data Free From Spurious Side–Wall Effects	48
Figure 5–5.	Isotherms of Measured Mean Temperatures for a Lifted Flame at Near–Blowout in the PW200 Combustor	50
Figure 5–6.	Isotherms of Measured Fluctuating Temperatures for a Lifted Flame at Near–Blowout in the PW200 Combustor	52

LIST OF FIGURES (CONT'D)

		Page
Figure 5–7.	Isotherms of Measured mean Temperatures for an Attached Flame at Near Blowout in the PW200 Combustor	53
Figure 5–8.	Influence of Primary Zone Airflow on Flame Type and Blowout at Atmospheric Pressure for 15 Percent Dome Flow	54
Figure 5–9.	Photographs of Lifted and Attached Flame Conditions	55
Figure 5–10.	Influence of Primary Zone Airflow on Blowout at 0.4 Atmospheres Equivalent Pressure for 15 Percent Dome Flow	55
Figure 5–11.	Influences of Dome Flow on PW200 COmbustor Stability, Showing the Effects of Flame Type for Primary Zone Burning	56
Figure 5–12.	Effect of Equivalent Pressure on Blowout at Fixed Airflow for 10 and 20 Percent Dome Flows, Showing Primary Zone Burning and Jet–Stabilized Burning	57
Figure 5–13.	Stability Characteristic for the 10 Percent Dome Flow Combustor, Showing Extended Flame Holding on Transverse Air Jets	58
Figure 6–1.	Diagrammatic Representation of simple Bunsen Flame for Model Development	61
Figure 6–2.	Experimental Dependency of Relative flame speed on Mole Fraction of Oxygen for Propane/Oxygen/Nitrogen Systems	69
Figure 6–3.	Comparison of Calculated and Measured laminar Flame Speeds with Variation in Oxygen Mole Fraction	69
Figure 6–4.	Limited Validation of Temperature Correction to Flame Speed	70
Figure 6–5.	PW100 Combustor Losses in Total Pressure with Isothermal Flow	75
Figure 6–6.	PW100 Combustor Losses in Total Pressure with Reacting Flow	75
Figure 6–7.	Representation of the PW100 COmbustor Co–Axial Jets/Set System as a Turbulence Generation Device to Define the Undistorted Mean Velocity	76
Figure 6–8.	Calculated Streamlines in PW100 COmbustor Near Blowout, Used for Mixing Assessment	77
Figure 6–9.	Calculated Curves of Total Dissipation Gradient Along Y–Grid Lines	78
Figure 6–10.	Enlargement of the Initial Region of Y–Grid Gradients	78
Figure 6–11.	Calculated Curves of Total Dissipation Gradient Along X–Grid Lines	79
Figure 6–12.	Spatial Contours of Total Dissipation Gradient in PW100 Study Case	80
Figure 6–13.	Calculated Field of Turbulence Kinetic Energy in PW100 Study Case	80
Figure 6–14.	High–Range Values in the Calculated Rate of Turbulence Dissipation Field	81
Figure 6–15.	Low–Range Values in the Calculated Rate of Turbulence Dissipation Field	81

LIST OF FIGURES (CONT'D)

Page

Figure 6–16. Characteristic S–Shaped Curve Showing all Possible Modes of Premixed Reaction Behavior 83

Figure 6–17. Representation of Solution Arc–Length 84

Figure 6–18. Calculated Solution Points Using the Colket Reaction Mechanism in PSR/CHEMKIN–II with Arc–Length Continuation Strategies, for the Hottel, et al. WSR Experiment 85

Figure 6–19. Comparison of Calculated Stability for the Colket Reaction Mechanism with the Measured Stability for the Hottel et al. WSR Experiments 85

Figure 6–20. Comparison of Stability Loops Calculated with Colket "Full" and Paczko et al. "Partial" Mechanisms, Against the WSR Experiments of Clarke et al. (Injector A) 87

Figure 6–21. Comparison of Experimental Data of Clarke et al. (Injector A) Against Calculated Stability Using Reaction Mechanisms of Table 6–1 88

Figure 6–22. Comparison of Measured and Calculated Stability Loops for Clarke et al. (Injector A) WSR Experiments, Using Kretschmeer & Odgers Calibrated Mechanism 90

Figure 6–23. Comparison of Measured and Calculated Stability Loops for Clarke et al. (Injector D) WSR Experiments, using Kretschmer & Odgers Calibrated Mechanism 90

Figure 6–24. Schematic Illustration of a Fine Structure Vortex Tube BeingStrained by Larger Eddies . 98

Figure 6–25. Cross–Section of a Fine–Scale Eddy Rotating About Its Center 100

Figure 6–26. Schematic Representation of a Reacting Fine Structure as a Well–Stirred Reactor 104

Figure 6–27. diagrammatic Representation of Solution for Fine–Structure Extinction Time Scale 109

Figure 6–28. Extinction Residence Times as Functions of Inlet Temperature and Equivalence Ratio as Calculated from the Kretschmer & Odgers ALP Expression . 110

Figure 6–29. Logic Flowchart for Extinction Calculations using the Fast Chemistry/Characteristic Time Version of the EDC Model 114

Figure 6–30. Representation of the EDC Model Extincition Criterion at the Flame Anchor Point . 116

Figure 6–31. Comparison of measured and Calculated Flame Lift Heights for a Simple Jet Diffusion Flame 117

Figure 6–32. Plane Orientation and Grid Assessment for CFD Calculations of the PW200 Combustor 121

Figure 6–33. Isothermal CFD Calculation of Iso–Surfaces of Mean Axial Velocity (at Magnitude 1) Showing Swirlig Jet From Fuel Injector Exhibiting Lobate Formation at First Row Combustion Air Jets 122

LIST OF FIGURES (CONT'D)

Page

Figure 6–34. Vertical View of Isothermal CFD Calculation with Iso–Surfaces of Mean Axial Velocity (At Magnitude 2), Showing Lateral Spreading of Colliding Transverse Combustion Air Jets 123

Figure 6–35. Section Through Fuel Injector with Calculated Iso–Vels of Mean Axial Velocities, Showing Reverse Flow Regions 124

Figure 6–36. Section Out of Fuel Injector Plane with Iso–Vels of Calculated Mean Axial Velocities, Showing Reverse Flow Regions 124

Figure 6–37. Tracer particle Trajectories for the Inner Regions of the Fuel Injector Jet (Reacting Flow): Along and Across (Upstream of Combustion Air Jets) the Combustor, (Note the Absence of Swirl) 125

Figure 6–38. Tracer Particle Trajectories for the Outer Regions of the Fuel Injector Jet (Reacting Flow): Along the Combustor 126

Figure 6–39. Tracer Particle Trajectories for the 1st Row Combustion Air Jets (Reacting Flow): Along the Combustor 126

Figure 6–40. Tracer Particle Trajectories for the 1st Row Combustion Air Jets (Reacting Flow): Across the Combustor 127

Figure 6–41. Left and Right Hand Views of a Limiting Surface Contour Representing a Dissipation Gradient Value of 10.0 to Define a Perfectly Stirred Reactor Region for the PW200 Combustor 128

Figure 6–42. Network of Reactors Representing the PW200 Combustor at Near–Lean Blowout Conditions 129

Figure 6–43. Comparison of Network Reactor Outlet Temperatures Against CARS Temperature Measurements Inline with a Fuel Injector on the PW200 Combustor Horizontal Mid–Plane 133

Figure 6–44. Comparison of Network Recirculation Reactor OutletTemperature Against CARS Temperature Measurements Between Fuel Injectors on the PW200 Combstor Horizontal Mid–Plane .. 134

Figure 7–1. Comparison of Calculated and measured Centerline Mean Axial Velocities for Case N23 138

Figure 7–2. Comparison of Calculated and Measured Radial Profiles of Mean Axial Velocity for Case N23 139

Figure 7–3. Calculated Temperature Field for Case F23 (Reacting, j = 0.59) Using the EBU Combustion Model 140

Figure 7–4. Calculated Temperature Field for Case F63 (Reacting, j = 1.62) Using the EBU Combustion Model 140

Figure 7–5. Case F23 Showing Calculated Regions of Reaction Exclusion and Reaction Rates Using the EDC Combustion Model 141

Figure 7–6. Calculated Temperature Field for Case F23 With the EDC Combustion Model 142

LIST OF FIGURES (CONT'D)

		Page
Figure 7–7.	Comparison of the Variation with Equivalence Ratio of CARS Mean Temperatures and EDC Model Calculated Temperatures at a Coordinate Position (5, 25 mm) in the Step Region	142
Figure 7–8.	Calculated Regions of Exclusion for Case F41 using the EDC Model	143
Figure 7–9.	Calculated Temperature Field for Case F41 with the EDC Model	143
Figure 7–10.	Calculated Regions of Exclusion and Reaction Rate field for Case F63 with the EDC Model	145
Figure 7–11.	Calculated Regions of Reaction Exclusion for the Very Rich F80 Case with Deadspace Model and Specified Wall Temperatures	147
Figure 7–12.	Calculated Isotherms for the F80 Case Showing Evidence of Wall and Step Thermal boundary Layers	147
Figure 7–13.	Effect of Primary Zone Airflow on Stability for 15% Dome Flow: Comparison of Calculations with Experimental Data	150
Figure 7–14.	Effect of Pressure on Stability for 15% Dome Flow at Several Primary Zone Airflows: Comparison of Calculations with Experimental Data	151
Figure 7–15.	Calculated Relationship Between Overall Blowout Equivalence Ratio and combustion Efficiency for Network Controlling Reactor (No. 3) for 10% Dome Flow at Several Airflows and Pressures	153
Figure 7–16.	Calculated Relationship Between Overall Blowout Equivalence Ratio and Outlet Temperature of No. 1 Reactor in Network for 10% Dome Flow at Several Airflows and Pressures	153
Figure 7–17.	Calculated relationship Between Overall Blowout Equivalence Ratio and Residence tie in Network Controlling Reactor (No. 3) for 10% Dome Flow at Several Airflows and Pressures	154
Figure 7–18.	Stability Characteristic of Network Controlling Reactor (No. 3) for 10% Dome Flow	154
Figure 7–19.	Comparison of Calculated and Measured Stability for Primary Zone Burning with a 10% Dome Flow Combustor	155
Figure 7–20.	Calculation of Stability for Primary Zone Burning with a 10% Dome Flow Combustor, Showing Change of Flame Holding	156
Figure 7–21.	Calculated Stability for Primary Zone Burning with a 20% Dome Flow Combustor, Showing Change of Flame Holding	157
Figure 7–22.	Comparison of Calculated Stabilities for Primary Zone Burning with 10% and 20% Dome Flows	158
Figure 7–23.	Comparison of Calculated and measured Stabilities for Primary Zone Burning with a 20% Dome Flow Combustor	158

LIST OF TABLES (CONT'D)

		Page
Table 1–1.	Combustion Chamber Design Requirements	4
Table 1–2.	Data–Base Design Methods	5
Table 4–1.	LS Fuel Injector Component Equivalence Ratios	32
Table 4–2.	Energy Comparisons for HS Injector	42
Table 4–3.	Gas Sampling of Major Species for PW100 and PW150 Combustors	43
Table 6–1.	Comparison of Various Kinetic Mechanisms for Propane	83
Table 6–2.	Kollrack's Reaction mechanism and Rate constants for JP5/Jet A Fuel	131
Table 7–1.	Case Descriptions for PW100 Combustor CFD Calculations	138

SUMMARY

A long-term goal of the Air Force is to Develop high-performance gas turbine engines with combustors that operate at near-stoichiometric conditions, burn broad-specification fuels, have low maintenance and high durability, and result in a low-observable engine exhaust plume. It was recognized that to achieve these goals the capabilities of current combustor design systems would be severely strained in many respects. To address the concerns associated with this, in 1987 the U.S. Air Force established the ***Combustor Design Model Evaluation (CDME)*** program, with the intent of improving physical modeling to facilitate design work. Under the CDME effort a joint industry/Government laboratory/university research program was initiated to address combustion stability associated with lean blowout (LBO).

To perform this task, a program was formulated that divided the LBO problem into two distinct parts by separating the effects of liquid fuel atomization and spray evaporation from the aerothermochemical effects, and addressing the aerothermochemical effects on LBO first. This was achieved by operating initially with gaseous propane as the primary fuel; gaseous methane was a secondary fuel.

The aerothermochemical aspects of LBO were investigated by a joint mathematical modeling portion and a simultaneous and complimentary experimental portion. The modeling portion involved conventional phenomenological, computational fluid dynamics, and well-stirred reactor network approaches. The experimental portion utilized three combustors; these combustors began with a very simple configuration and progressively increased in complexity and realism to a gas turbine generic combustor.

Flame stability in the primary zone of gas turbine combustors is achieved by means of recirculation. In an annular combustor configuration, recirculation between adjacent fuel injector modules plays an important role in LBO. The program therefore involves detailed studies of the major primary zone flow features, and especially concentrated on the recirculating flow. It was shown that flame-lift and subsequent flame blowout were controlled in this context by the recirculating flow and the local stoichiometry set up by the fuel injector.

The physical modeling used for simulating the combustion process in the CFD studies was found to be inadequate to calculate the blowout sequence, although flame-lift was calculated. The experimental evidence suggested that nonstationary behavior of the mean flow field influenced the fuel/air mixing in a way unaccounted for in the stationary-state CFE. This was true for both the simplest of the combustors and the generic combustor. Phenomenological modeling proved useful for data correlation purposes, but could not represent the flame-lift satisfactorily.

A hybrid modeling approach was devised that is suitable for engineering-quality calculations of LBO in real combustors. In this hybrid procedure, the LBO process was modeled in the generic combustor by representing it, from a process point of view, as a simple, 8-element network of plug-flow and well-stirred reactors. The network connectivity, reactor type and reactor size were determined from isothermal CFD calculations, using techniques established during the component studies. The detailed chemistry was then solved on the network, uncoupled from the fluid dynamics. This hybrid procedure provided successful calculations of the pressure and primary zone total airflow effects on LBO, the effects of variation in the combustor dome airflow, the influence of combustor loading on the lean stability characteristics, and the effects of fuel type.

These studies have provided a valuable contribution to the understanding of lean stability in gas turbine combustors, and have also sounded a timely warning on the application of stationary–state mathematical modeling to combustion in turbulent, recirculating flows. Phenomenological modeling was produced for the correlation of LBO experimental data. In addition, a simple, inexpensive and convenient experimental technique for simulating subatmospheric pressures by introduction of excess nitrogen, has been verified. A calculation procedure was devised that successfully calculates the influence of many of the relevant parameters on lean blowout. The research described above has led to presentation of 12 technical society papers, of which 7 were subsequently archival journal publications; 3 additional papers were incorporated in symposia proceedings. In addition, two master's theses (Brigham Young University) resulted from this work.

The final report describes the experimental and model results,and gives conclusions for all of the work performed on this contract.

SECTION 1.0
INTRODUCTION

1.1 Background

The U.S. Government's ***Integrated High Performance Turbine Engine Technology (IHPTET)*** Initiative is aimed at taking engine technology well beyond that seen in the Advanced Tactical Fighter (ATF) with its P&W F119 engine. For fighter/attack applications the goals, relative to current engines, are to double thrust/weight ratio together with a halving of specific fuel consumption; for subsonic transport applications the goal is a 30 percent decrease in specific fuel consumption. The payoffs resulting from satisfaction of these goals are seen as:

- Sustained Mach 3+ cruise capability in an F–15 size aircraft
- 100 percent range/loiter/payload increase in an F–14 size aircraft

These are ambitious goals. Attaining them will stretch all of the engine component technologies, and especially the design systems. In the combustor area this latter observation is especially true.

The combustor, Figure 1–1, is a small but important component of the engine, and it is one of deceptive simplicity. The design requirements that this component has to satisfy are listed in Table 1–1.

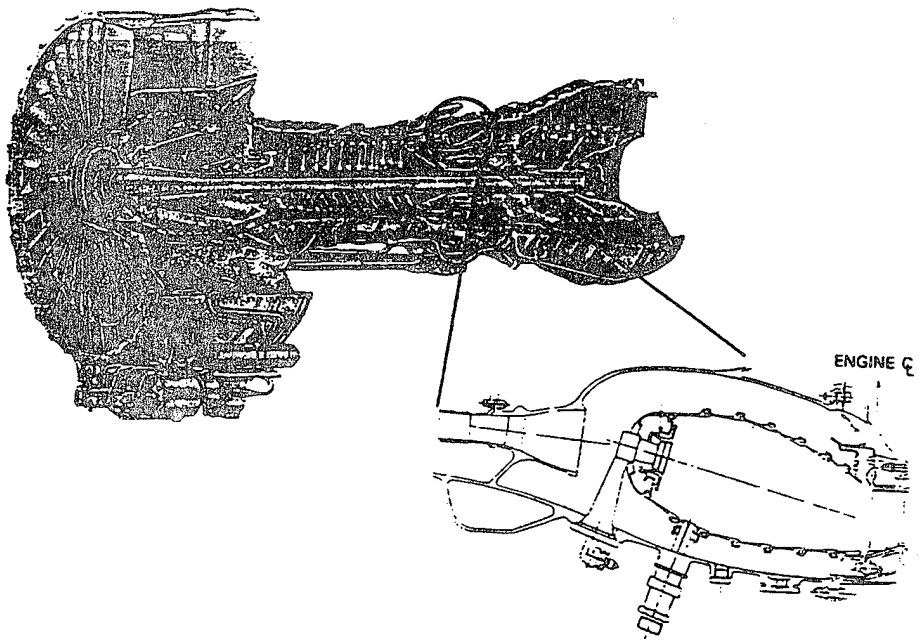

Figure 1–1. Combustor Cross–Section

Table 1–1. Combustion Chamber Design Requirements

All combustors should satisfy the following:

- minimum pressure loss
- high combustion efficiency
- wide stability limits
- suitable outlet temperature distributions
- adequate durability
- freedom from interior coke formation/carbon deposits
- low exhaust emissions of smoke, unburned hydrocarbons and oxides of nitrogen
- low weight
- low initial cost
- ease of maintenance

Special requirements as needed:

- ultra low oxides of nitrogen
- multifuel capability, etc.

The combustor has to meet these design requirements at the engine aero–design point and the design point for the combustor, which are not usually the same. These might actually be several combustor design points, depending on the intended application, e.g., take–off (military power), plus a supersonic, medium altitude flight condition (either maximum afterburner or supercruise), or, emissions points. The combustion system has to achieve this performance while fitting in a spatial envelope that itself imposes certain design layout constraints, e.g., accommodation of aircraft bleeds, intrusion of bearing compartments, structural load–carrying paths, etc. Further, in keeping with historical trends, the system also has to be designed to accommodate at least a 10 to 15 percent engine growth potential (by throttle–bend) without major changes.

Many of the combustor design requirements described above are conflicting, and the developed design will entail a series of optimized compromises in order to meet them. The design system that is used to produce the initial design is historically founded on two important components – models and design practices, (Figure 1–2), which are used together. The models are used to size the critical dimensions in the combustion chamber in order to satisfy a design requirement. The design practices are a series of rules for all parts of the system, that are based on hard, practical experience, and which govern acceptable choices to be made for the majority of the critical dimensions.

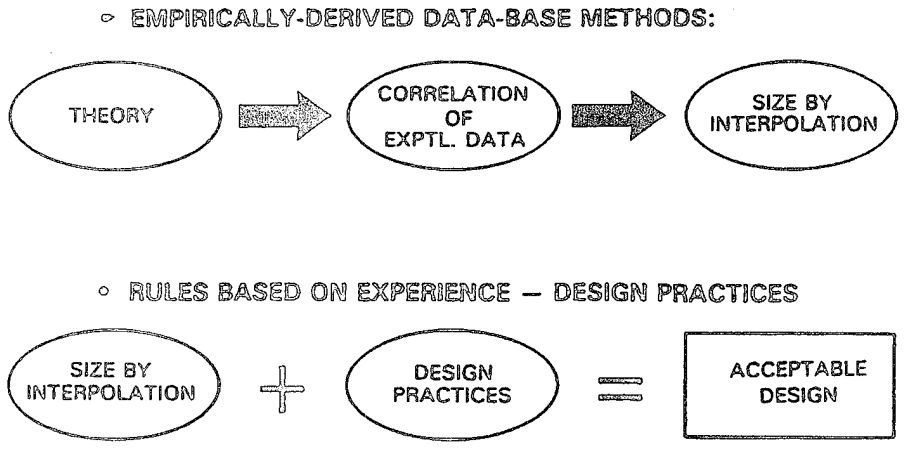

Figure 1–2. Design System Based on Models and Design Practices

The design system described results in a **preliminary design**, which then requires development testing in order to simultaneously meet all the goals. The **development testing** these days will include some analysis/simulation by computational fluid dynamic (CFD) methods, but will involve extensive rig and experimental engine testing that is both expensive and time consuming. Any simulation that is carried out involves the preliminary design produced by the design system, i.e., the CFD itself does not contribute directly to establishing the preliminary design.

The strengths and weaknesses of data–base methods are given in Table 1–2. The most serious deficiencies are that they are nonpredictive, and handle novel solutions very poorly. If, when experimentally tested, the combustor does not satisfy any of the design requirements, nonpredictive data–base methods do not provide the reasons for the failure. The potentials offered by CFD (but not currently delivered) are those of prediction and extrapolation.

Table 1–2. Data–Base Design Methods

Strengths	Weaknesses
• simple to understand • Easy to use • Good record of success	• basic theory gets forgotten • "Blind" use is dangerous • Interpolation rapidly becomes extrapolation • Data–base expensive to update • Handles novel situations poorly • Nonpredictive

Use of data–base design systems for combustion components in engines intended to satisfy ***IHPTET*** goals really exposes the weaknesses inherent in the system. Recognizing these difficulties the U.S. Air Force in 1987 established the ***Combustion Design Model Evaluation (CDME)*** program, with the goal of improving physical modeling to facilitate design work. The intent of the ***CDME*** program was originally to develop advanced diagnostic techniques and to establish a technology base for the evaluation of combustion models. Later, these intents were extended to include improvement of the available physical modeling such that engineering–tool CFD computer codes could be upgraded to advance the design methodology of advanced combustors in a comprehensive fashion.

1.2 Specific Problem

There are many areas of physical modeling related to gas turbine combustion that require improvement. Prioritization is therefore needed. Fortunately, there are some models that naturally stand out in importance. Stability modeling is one of these. Of all the combustor design requirements that must be satisfied combustor stability is considered to be one of the most important since it directly concerns aircraft safety.

The stability of a combustor has great relevance with respect to the operating envelope required of an engine. Figure 1–3 shows an example of an operating envelope *a, b, c, d* and *e*, in terms of aircraft flight Mach Number and flight altitude. Displayed over the envelope are a number of conditions which, taken together, define in this instance, relighting capability. Some limits are set by the engine and its subsystems, and not directly by the combustor stability characteristics. For example, such limits include the minimum engine speed (based on the windmilling drag of the engine) at which the fuel pumps will supply the minimum fuel flow rate. Also shown are enrichment needs due to excess airflow relative to the normal minimum fuel flow rates, and to provide adequate engine acceleration. In addition, for this particular engine there is a fuel atomization limit (due to use of an airblast–atomization fuel injector). Heat loss limits for a cold–soak combustor are indicated. Finally, there is a true combustor stability limit, indicated by the line *c* – *c*. Note that this latter limit has the text–book form of a stability loop, but is oriented according to the

windmilling characteristics of the engine in flight at altitude. The various limitations can take considerable "bites" out of the required operating envelope, which must be restored by design improvements.

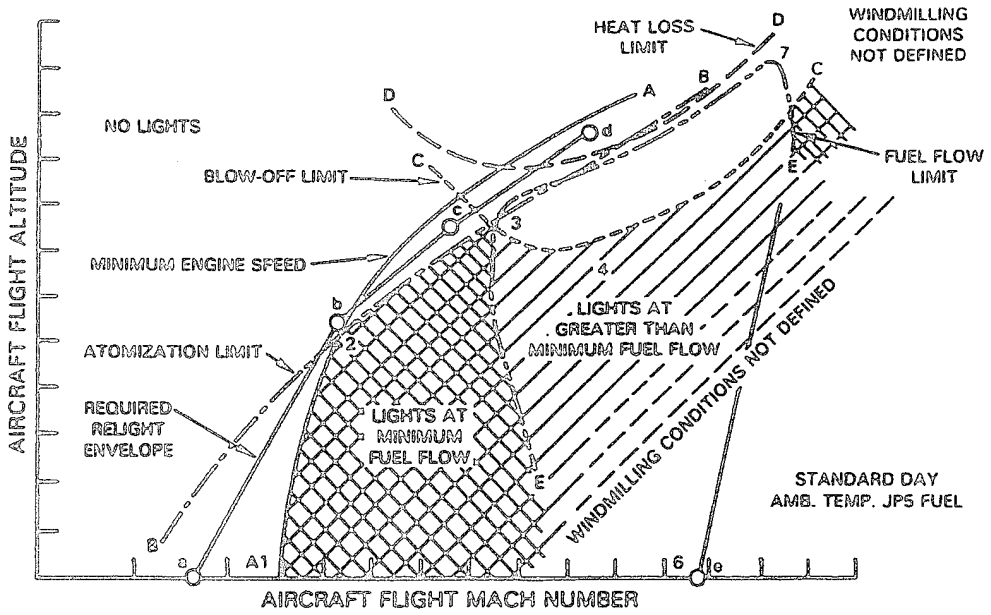

Figure 1–3. Typical Engine Operating Envelope

1.3 Blowout Design Requirements

The flame holding characteristics of the combustor are sometimes referred to as the blow–off limits. Stability in this context is defined as the range of operating fuel/air ratios within which a time–mean stationary flame can be maintained inside the combustor. Implied is the existence at any operating point (combustor loading) of two limiting fuel/air ratios, one involving excess fuel (rich) and the other involving excess air (lean) over the values to completely burn all the reactants. Blow–off at fuel–rich conditions is difficult to achieve under normal circumstances, except near the peak heat release rate condition for a particular combustor. Of more practical interest is blow–off at fuel–lean conditions. This is normally referred to as lean blowout (LBO).

Current modeling practice for combustor blowout is phenomenological, and the data–correlations obtained are design specific, as Figure 1–4 shows.

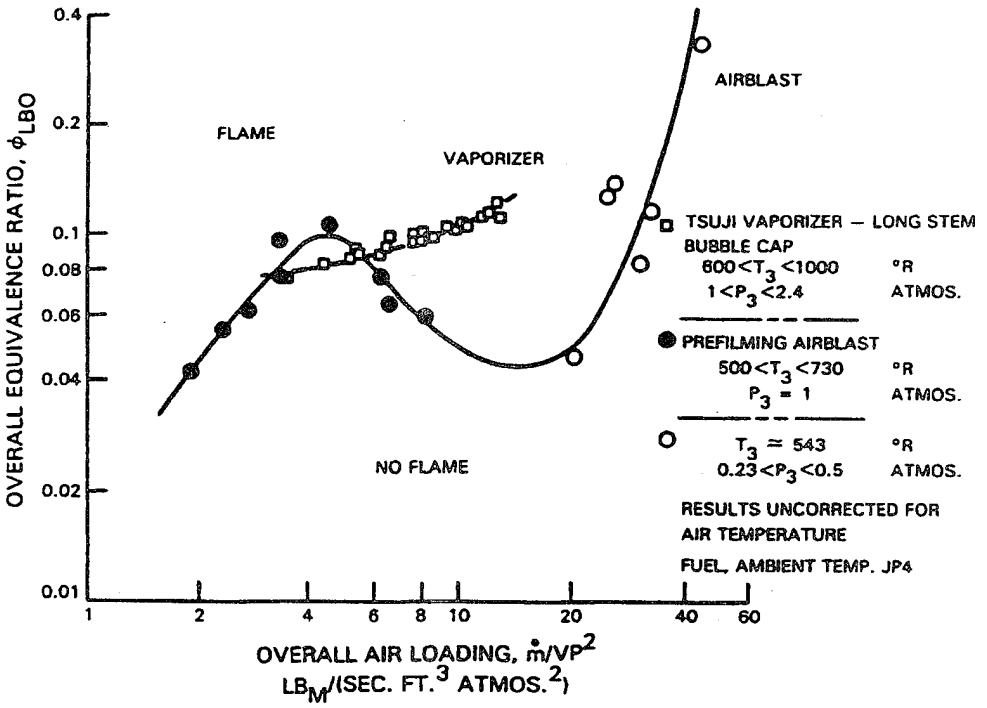

Figure 1–4. LBO Characteristics for Two Combustors, Showing Design–Specific Nature

It is the task of the combustion engineer to design a combustor that will be stable for all required flight operating conditions. With that, all engine steady–state operating points should lie inside an envelope defined by the combustor loading and the rich/lean fuel/air ranges within which combustion can be sustained. This envelope should be extensive enough to encompass the under– and over–shoots associated with the different response rates to throttle movements, of the fuel system and the rotating machinery; adequate allowance for safety margins should also be included. Figure 1–5 illustrates this behavior.

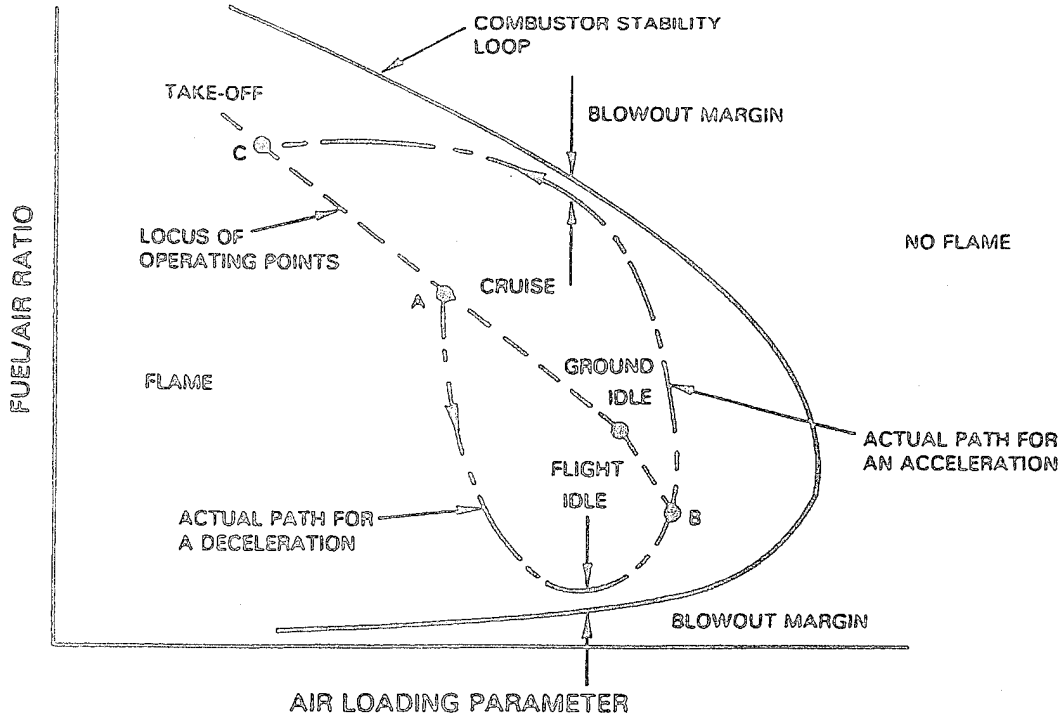

Figure 1–5. LBO Characteristic with Engine Operating Lines, Showing Under– and Over–Shoots

The difficult and important design task described is being made more difficult by the engine design trends under *IHPTET*. For a single example, in a simple system high temperature rise combustors are incompatible with the military need for smokeless engine exhausts (low observables), and compromises to alleviate this adversely impact stability margins for fixed system combustors [1.].

Published material on stability that is available to assist the designer is very limited. The majority of the relevant published material on flame stability is for bluff–body flameholders of various types, or is for well–stirred reactors, as reviewed by Lefebvre [2.]. The quality of experimental data published in the open literature for practical gas turbine combustors is much less extensive, and systematic investigations are largely lacking, although some such work of limited scope for can–type combustors is reported by Jeffs [3.] and Stewart [4.]. Almost all of the information on the annular–type of combustor currently used for aircraft applications is confined to relatively inaccessible private company reports. The information that is available for practical combustors is expressed in global terms, and there are no detailed interior flowfield descriptions at near–blowout conditions. The large number of geometric and flow variables encountered makes rational comparison of data difficult.

It was for these reasons that the Air Force established under the *CDME* effort, a research program to address lean blowout.

SECTION 2.0
PROGRAM APPROACH

In establishing the ***CDME*** /LBO study the Air Force elected to make it a joint effort involving industry, Wright Laboratory and its on–site contractors, and universities through the Laboratory Summer Professor program. Experimental work was to be conducted on–site at Wright Laboratory, but program direction was to reside with industry. The reasoning behind this structure was that the likelihood of success would be maximized by utilizing these wide–ranging talents in combination, to produce an in–depth study while ensuring that the effort remained firmly grounded in the practical needs behind the study.

The overall strategy adopted to address the ***CDME***/LBO program objective, involved three broad but distinct steps:

1. Provide by experimental means, an improved understanding of the physics involved in lean blowout.
2. Model the lean blowout process, and integrate the modeling with CFD codes.
3. Provide experimental data–bases against which the modeling is tested and calibrated.

The following procedure for implementing the strategy was devised: The total problem was divided into two separate phases that separated out liquid fuel preparation and evaporation from the basic aerodynamics and combustion chemistry. If the initial phase, in which gaseous fuels were to be used, was unsuccessful then the second phase for liquid fuels (ethanol, JP8/Jet A) would not proceed. Propane was selected for the Phase I gaseous fuel due to its similar chemistry to jet–fuels; methane was the secondary fuel.

A step–by–step procedure was applied to the Phase I study. This procedure moves from gaining an understanding of the combustor basic primary zone behavior in, initially, a simplified environment, and then, through progressively more realistic situations leading to a simplified version of a real gas turbine combustor. Understanding of LBO in a gas turbine combustor therefore relies on a superpositions method.

As a consequence of the step–by–step procedure, the experimental portion of the program utilizes three combustors as test vehicles to achieve the desired progression in flow complexity. These respective combustors consist of:

a) a research combustor for basic studies and understanding (Task 100 Combustor)

b) a technology–development combustor with characteristics between a) above and b) below (Task 150 Combustor)

c) a gas turbine generic combustor of simplified configuration (Task 200 Combustor).

The modeling component of the program followed the same progression as the experimental portion, and the two components were mutually supporting.

- 100 percent range/payload increase in a CH–47 size helicopter

SECTION 3.0
BASIC STUDIES: TASK 100 COMBUSTOR

3.1 Intent

The intent of Task 100, which resulted in the PW Task 100 Combustor, was to address the fundamentals of the blowout process with the aim of providing a clearer understanding of the physics involved. It was concluded that this would be best done experimentally. Task 100 was also intended to serve to develop the novel instrumentation and experimental techniques necessary to probe the nonstationary processes inherently associated with blowout. The pilot program element was to be conducted in a simplified combustor having reasonable optical access to permit these techniques to be used.

3.2 P&W Task 100 combustor Design

In a modern annular gas turbine combustor, flame is stabilized by producing a local recirculation zone in the general flow field. This zone is generated by a combination of three mechanisms, namely: an axial swirling air jet associated with each fuel introduction, sudden expansion of the axial swirling jets as they enter the primary zone, and back–pressure provided by an array of transverse air jets at the end of the primary zone. The recirculation zone itself serves a triple purpose of (i) producing a region of low velocity where flame can be held, (ii) providing high local residence time for flame to propagate into the incoming fresh mixture, and (iii) acting as a source of continuous ignition by supplying hot gas and active radicals for the incoming combustible fuel/air mixture, [2.].

To obtain low exhaust emissions of unburned hydrocarbons (UHC) at low engine powers, P&W since the late 1970's has tailored the combustor flow control mechanisms to produce an "inside–out" recirculation pattern, which is different to the classical recirculation described in Reference 2, and is illustrated in Figure 3–1. This flow pattern keeps incompletely–reacted fuel out of the relatively cool liner film cooling air, where it could become chemically frozen [5.]. Note the central, coherent, swirling axially–directed jet that is initially near–cylindrical in shape, and the back–pressure effect of the opposed transverse air jets that, in conjunction with its swirl, cause the axial jet to abruptly spread radially and be recirculated upstream to the forward bulkhead of the combustor.

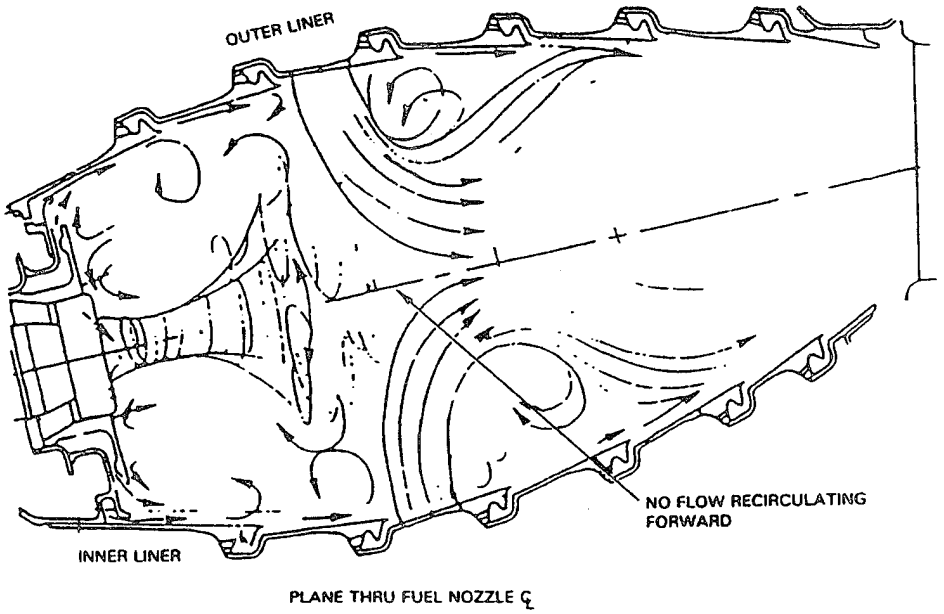

Figure 3–1. Flow Patterns In a Modern Annular combustor Showing "Inside Out" Recirculation (Water–Tunnel Results)

The flow field described above and in Figure 3–1, is the primary zone that the research combustor needed to emulate. The dominant feature is the toroidal recirculation zone surrounding the central fuel and combustion–air jet, that is confined at its forward end by the combustor bulkhead and at its aft end by the transverse air jets.

The flow emulating the combustor primary zone was to be contained in as simple a combustor as possible to facilitate CFD modeling and to provide good optical access. An axisymmetric combustor is the simplest configuration possible in which the desired flowfield could be established. However, there were concerns with suitable optical access for diagnostic measurements in an axisymmetric combustor. Although these difficulties have been overcome in other circumstances by use of correcting optics, it was not felt to be a desirable approach for the present program. A compromise cross–section was determined as one with flat side–windows for optical access, but having substantial circular–arc corner pieces to minimize secondary–flow vorticity generation by wall boundary layer interactions.

It was believed that the inside–out recirculation zone could be generated by means of a combination of jet sudden expansion and back–pressure, but without the need for introduction of swirl. The transverse air jet back–pressure effect was to be represented by restriction of the combustor outlet, and orifice plates were selected for this purpose. The fuel injector flow and associated airflow were to be respectively represented by a central, circular, low–momentum jet of propane with a concentric, high–momentum jet of air, both being introduced with a purely axial velocity. The forward end of the combustor was to be closed with a simple step–bulkhead.

Details of the design process for the simple research combustor with these features are presented in Reference 6, which is contained in Appendix A, and some of its development as a clean experimental vehicle is described in Reference 7 which is given as Appendix B.

In final form the research combustor, Figure 3–2, consists of a central jet of gaseous fuel surrounded by an unheated co–axial air jet, with the confluence of the jets centrally–located in a nominally circular cross–section duct. The duct has a hydraulic diameter of 150 mm, and is closed at its forward end to give a backwards–facing step of 55 mm height. The discharges from the fuel and air supply tubes are flush with each other and with the step. The constant outer diameter fuel tube has an inner diameter at exit of 29.97 mm with a 2–degree half–angle taper over 120 mm of its interior length to give a thin lip at its exit. The outer wall of the air passage converges sharply to its discharge, where the exit diameter is 40 mm. To ensure that spurious acoustic effects were minimized a baffle is installed in the fuel tube to acoustically isolate the fuel supply system from the combustor. The baffle is far enough upstream in the fuel tube that the turbulence generated by it, while not entirely dissipated, is at least uniformly distributed across the tube diameter by the discharge plane.

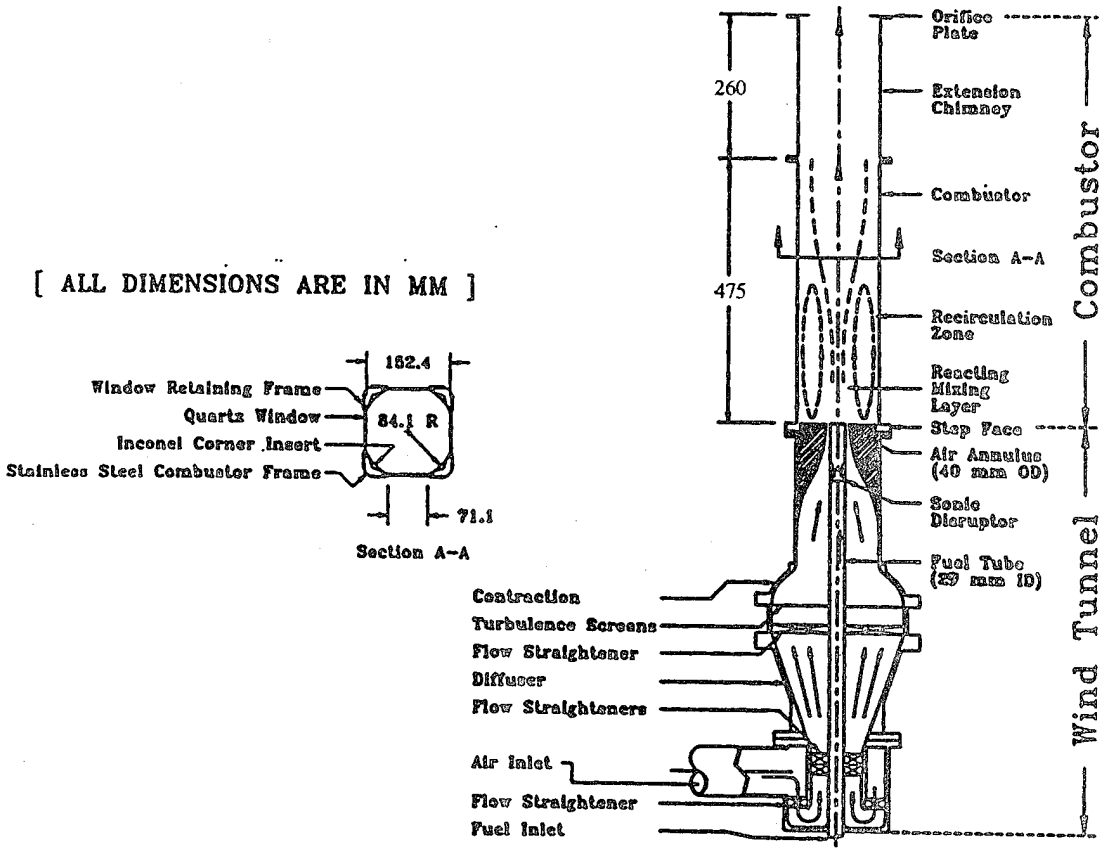

Figure 3–2. Cross–Section of Task 100 Research Combustor Rig

The combustor is designed and constructed in two main sections – a fixed upstream window section of 475 mm length providing optical access as needed, and, a replaceable downstream chimney. The chimney is available in two lengths, and the combustor can be run with either of these, or both, or with no chimney at all. The combustor has never actually been run with both chimneys mounted simultaneously. The other arrangements give length to diameter ratios (L/D) of 4.9, 6.513 and 3.167 respectively. Provision is made for exit blockage, with geometric values of 21.0, 45.1 and 62.0 percent tunnel blockage. These blockages are achieved by thin orifice plates. For the 45.1 percent geometric blockage, "top–hat" exits with tailpipe L/D's of 1.0 and 2.1 respectively, are also available. The "preferred configuration" for which most experimental testing was conducted was an L/D of 4.9 with a 45.1 percent geometric exit blockage by orifice plate.

The combustion tunnel cross–section was achieved by means of optical windows of thin, flat, fuzed–quartz, which form the four sides of the fixed upstream window section. The windows were retained in the corner frames by thin, sheet–metal, circular arc corner fillets. A later redesign replaced these with machined corner pieces that are integral with the frames. The resulting effective optical window, within which laser diagnostics data can be obtained, is defined by $-68.7 < x < +68.7$ mm and $-22 < y < +33$ mm, where axes x and y are defined in relation to an entering laser beam in Figure 3–2. In the downstream direction the window is $+2 < z < +358$ mm, where the z–origin is in the plane of the step.

The optical windows can be replaced as desired by metal plates containing either arrays of thermocouples for wall temperature measurements, or interior–flush tappings for static pressure measurements. The combustor may be run with any combination of windows and plates. Ignition is accomplished by means of a removeable propane torch ignitor that is inserted via an access boss mounted

interior–flush on a single, permanently–installed metal side–plate. When the ignitor is removed a flush plug is inserted into the boss. The combustor is uncooled.

The combustor was mounted vertically on the air–conditioning (wind tunnel) unit, that delivers a smooth flow of reactants to the combustor. The combustor and air–conditioning unit together translated vertically and horizontally through a square cut–out in a fixed optical bench, so that traversing with laser diagnostics could be easily made. A water–cooled exhaust extractor was positioned vertically above the combustor exit.

Both the fuel and air flows were continuously monitored and controlled by separate electronic flow control units to within 2 percent of set values. It was therefore relatively easy to set and hold a given operating condition within these constraints for long periods of time. Blowouts were found to be reasonably consistent, with a typical repeatability on equivalence ratio at fixed operating conditions being within 0.06.

3.3 Flow Field in Research Combustor

Under isothermal conditions the flowfield in the PW Task 100 research combustor was established by means of laser Doppler velocimeter (LDV) measurements. The basic information is presented in Reference 8, which is contained in Appendix C. Figure 3–3 shows the major features in the combustor.

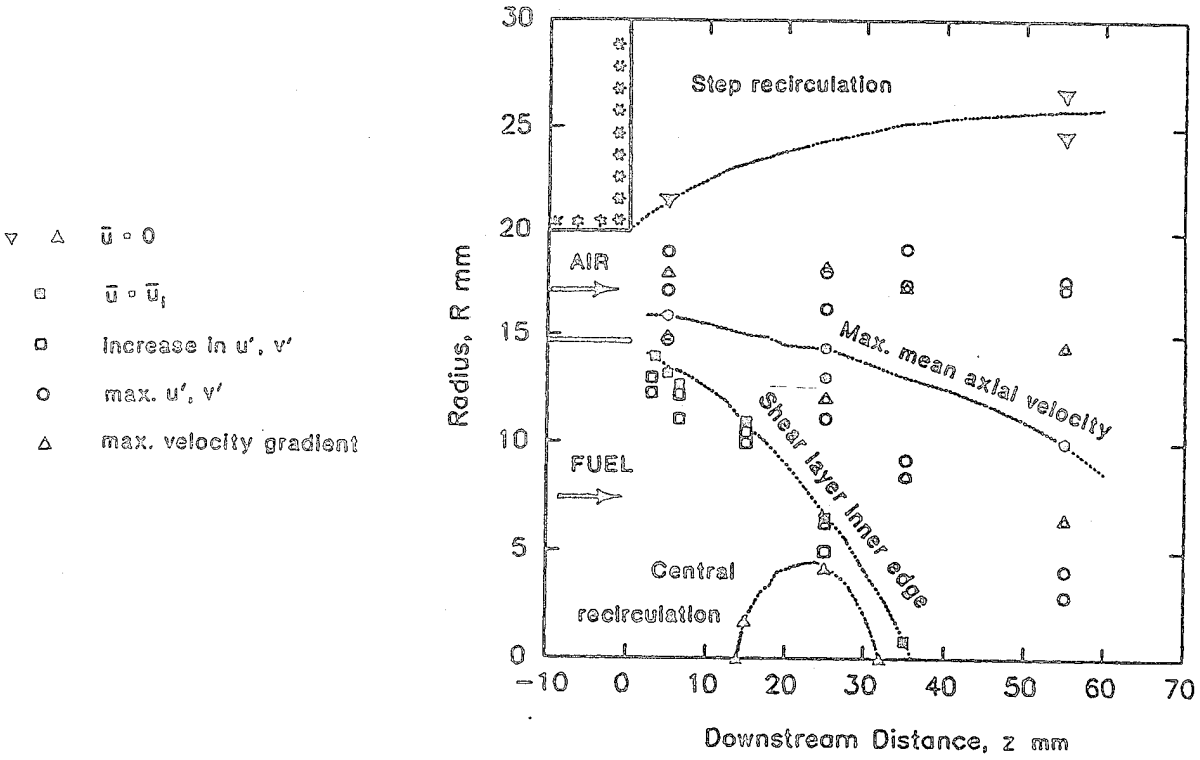

Figure 3–3. Major Flow Features in Task 100 Research Combustor Near–Field (Isothermal Flow)

The momentum ratio of the air to fuel jets ranged from about 6 to 22 over the conditions of interest. These ranges caused the fuel jet to be strongly entrained by the air jet. This entrainment, together with the sudden expansion that the jets undergo upon entering the combustor, generated a small, central recirculation bubble of length about 19 mm and width about 9 mm, with its leading edge about 13 mm downstream from the step–plane. The strength of this bubble, as defined by the magnitude of the combustor centerline axial velocity depression, was entirely consistent on a jet momentum ratio basis with measurements in a similar geometry by Owen (1965), Habib & Whitelaw (1979) and Johnson & Bennett

(1981). (In combusting flow, visualization using Mie–scattering from titanium dioxide particles, revealed that the location of this recirculation bubble was not stationary. It became off–set, and precessed about the combustor centerline within the jet shear layers; it also moved axially and its forward stagnation point could even momentarily enter the discharge plane of the fuel jet.)

The step generated a toroidal vortex which was centered radially at 60 percent of the combustor radius and axially about 3.1 step heights downstream from the step plane. The re–attachment plane was 7.7 step heights (about 3 combustor diameters downstream), and was consistent at the test Reynolds number with the collected data of Morrison et al. (1987). The step recirculation was very symmetrical about the combustor centerline.

The addition of orifice plate blockage at the combustor exit, Reference 9 which is presented as Appendix D, generated a toroidal vortex formed on the forward face of the orifice plate. The effect on the flow in the combustor was to cause a velocity acceleration along the centerline as the *vena contracta* in the orifice was approached. The magnitude of the effect depends on the diameter of the orifice plate, and the extent to which it was felt in the front of the combustor depended on the combustor L/D. For the 4.9 L/D combustor with 45 percent exit blockage the general flow characteristics were unaffected, except for centerline mean axial velocity accelerations of the order of about 6 percent at 300 mm downstream from the step, to about 9.8 percent at 125 mm downstream.

The static pressure in the step recirculation zone for isothermal flow was a function of jet velocity ratio with a free exit from the combustor. The addition of exit blockage eliminated the jet velocity ratio dependency.

The jet shear layers in the near–field region of the combustor appeared to behave as conventional shear layers, and quickly reached self–similar conditions. The velocity profiles in these layers were in reasonable agreement with Schlichting's classical profile for plane shear layers. The Reynolds stresses were in good agreement with those calculated from the mean profiles using Prandtl's mixing length theory. The inner–edge of the jet shear layer reached the combustor centerline about 36 mm downstream from the step plane, just downstream of the central recirculation bubble.

In the far–field region of the combustor the individual jets interacted vigorously with each other, and were merged by 138 mm from their confluence. Having lost their individuality subsequent development took place as though the two jets were a single round jet. For measurement stations from 138 to 358 mm downstream, the mean axial velocity profiles were self–similar, and agreed well with those of Forstall & Shapiro's submerged round jets.

The fluctuating velocity profiles in the far–field were not self–similar, and did not agree with those for Wyganski & Fiedler's, or Corrsin's, free round jets. It was concluded that the fluctuating velocities in the far–field were not directly associated with or derived from, the mean velocity profiles at the same axial stations, i.e., convection of turbulence was a dominant feature in the research combustor. Comparison of the local turbulence intensities with those of Habib & Whitelaw (1979) measured in a similar configuration showed good agreement.

It was concluded that there was no abnormal flow behavior in the research combustor. The configuration selected for the research combustor satisfied its design intent by generating a flow field that successfully reproduced the desired features of a combustor primary zone. The optical access provided reasonable probing capability to assess behavior in the combustor.

3.4 Simulation of Low Pressures

The stability of a combustor is most difficult to attain under operating conditions of low inlet temperatures, low combustion pressures and high mass flow rates. Together, they determine the combustor loading. Therefore these conditions are the ones of direct interest in any LBO study.

Operation at low combustor inlet temperatures is expensive, and is made moreso because the combustion air must be dried to avoid internal icing problems; in addition, heavy insulation of supply

ducting is required to minimize external icing difficulties. For reasons of cost and convenience t[illegible]fore, it was decided to operate the research combustor at ambient temperatures.

Conducting low combustion efficiency and blowout testing at subatmospheric pressures is an expensive and inherently dangerous operation. This is because potentially explosive fuel/air mixtures from the combustor exist in the exhaust system, and can be ingested by the exhaust blowers pumping the rig down to subatmospheric pressures. For reasons of safety therefore, it was decided to operate the research combustor at atmospheric pressure.

Achievement of sufficiently high loadings in the research combustor to be able to construct a significant portion of its lean stability characteristic by means of airflow alone was not feasible. The most readily-available air supplies in the vicinity of the lasers required for diagnostic purposes did not have sufficient capacity. Therefore, some form of simulation was needed for blowout testing.

The quantities involved in combustor loading -- airflow, air temperature and operating pressure -- are those which influence the speed at which chemical activity converts reactants to products. When the combustor inlet conditions cannot be directly manipulated to achieve a desired loading, as was so for the research combustor, the chemical reaction can be influenced by some other means to yield a similar rate of reactants conversion. If pressure is made the variable of influence, then a suitably altered chemical reaction would reflect the effects of the "simulated low pressure."

Low pressures can be simulated by the introduction of an inert diluent that slows down the chemical reaction in approximately the same way that true low pressures do. The addition of the diluent has two effects -- first, it lowers the reaction temperature by virtue of its heat capacity, and second, it lowers the reaction temperature by reducing the concentration of reactants. Thus, tests may be made at atmospheric pressure, and a high combustor loading still achieved.

It was decided to use simulation of low pressures as the means of achieving high loadings in the research combustor. Gaseous nitrogen was selected as the diluent, and it was considered as an inert under the conditions of LBO testing. Nitrogen is convenient to use, and is relatively inexpensive.

Based on an appropriate global reaction, it was demonstrated that reaction rate expressions in terms of combustion pressure and fractional of fuel burned, and, the ratio of excess nitrogen to fuel masses and fraction of fuel burned, have the same shape. Since the reaction rate shapes are the same, this forms the basis of the simulation. This information is contained in Reference 10, which is attached as Appendix E. Since a given global rate expression cannot be expected to adequately represent all the actual reaction taking place over wide ranges of operating conditions, the simulation does require some form of calibration.

An ideal calibration would be based on a comparison of the simulated pressure technique using excess nitrogen against true low pressure tests in the same reactor. Unfortunately, such a direct approach was not immediately available for the research combustor. Therefore, an indirect approach was used.

The empirical calibration of the Arrhenius rate expression for the propane/air/excess nitrogen system by Kretschmer & Odgers (1972) served as the basis of the calibration procedure for the low pressure simulation technique based on the introduction of excess nitrogen as a diluent to the research combustor air supply. Figure 3-4 shows the resulting calibration curve. A blowout characteristic for the research combustor is given in Figure 3-5. It is noted that the technique tends towards saturation at high values of nitrogen to fuel mass ratios.

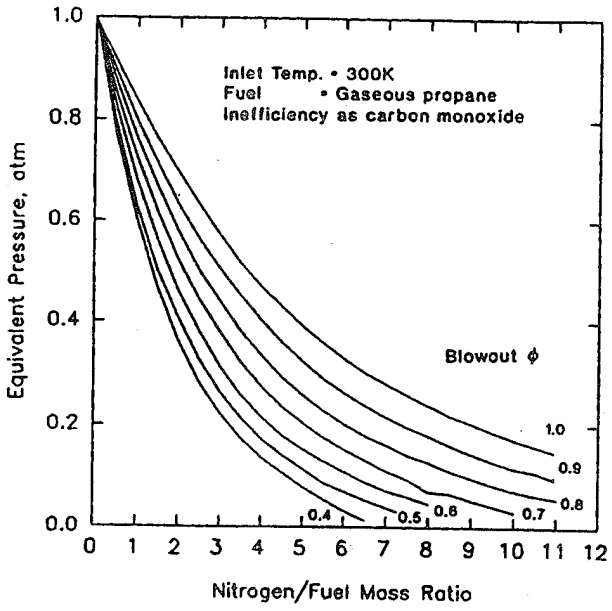

Figure 3–4. Calibration Curve for Simulation of Low Pressures Using Excess Nitrogen Technique (Air–Propane–Nitrogen Systems)

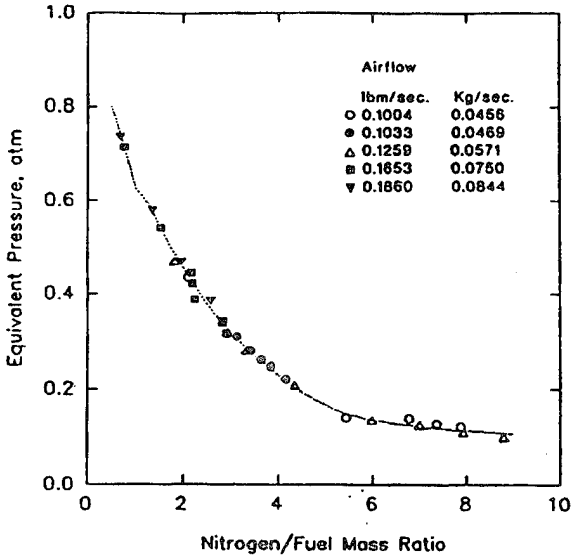

Figure 3–5. Blowout Characteristic for Task 100 Research Combustor Using Excess Nitrogen

The excess nitrogen was introduced into the research combustor air supply, upstream in the air–conditioning unit, so that it was well–mixed with the air at entry to the combustor.

3.5 Flame Structures and LBO Sequence

Three flame configurations existed in the combustor, depending on the equivalence ratio. For operation at about stoichiometric conditions over a wide range of jet Reynolds Numbers, a steady sheath–flame originated on the combustor step at the outer–edge of the air jet. Visually, this attached flame appeared quite thin at its origin, and maintained a roughly constant overall diameter and thickness for about 20 mm downstream. Beyond this 20 mm station the thickness of the flame increased by growing significantly towards the combustor centerline, and also radially outwards; strong radial expansion of the

reacting jet shear layers began thereafter. It appeared that the initial thickening at 20 mm was due to the ignition of the inner shear layer (see Figure 3–3), where the thickened flame had a "turbulent flame brush" appearance, i.e., "fuzzy–blue."

When the bulk equivalence ratio reached 1.5 to 2.0 (depending on combustor loading), and before a rich blowout, a separated flame condition was established, where the lower part of the attached flame originating from the outer–edge of the air jet was not visible to the eye; for low combustor loadings this took place at an equivalence ratio of 1.8 (see Appendix D). The detached flame then originated about 30–40 mm downstream from the step plane. A rich blowout occurred suddenly at this condition, and did not involve further flame–lift.

As fuel was reduced from the near–stoichiometric condition, (or airflow increased at constant fuel flow) the attached flame remained fixed in position but became visibly intermittent in both circumferential and axial extent, i.e., it evidenced "holes," and at an equivalence ratio of 1.05 (for propane/air) was no longer apparent to the eye. The character of the intermittency of the inner shear layer burning was much more severe than that in the outer shear layer. Eventually, shear layer burning was no longer present, and the flame lifted to move far downstream (160–300 mm), and existed in distributed fashion across most of the combustor diameter. Figure 3–6 compares the attached and lifted flame conditions.

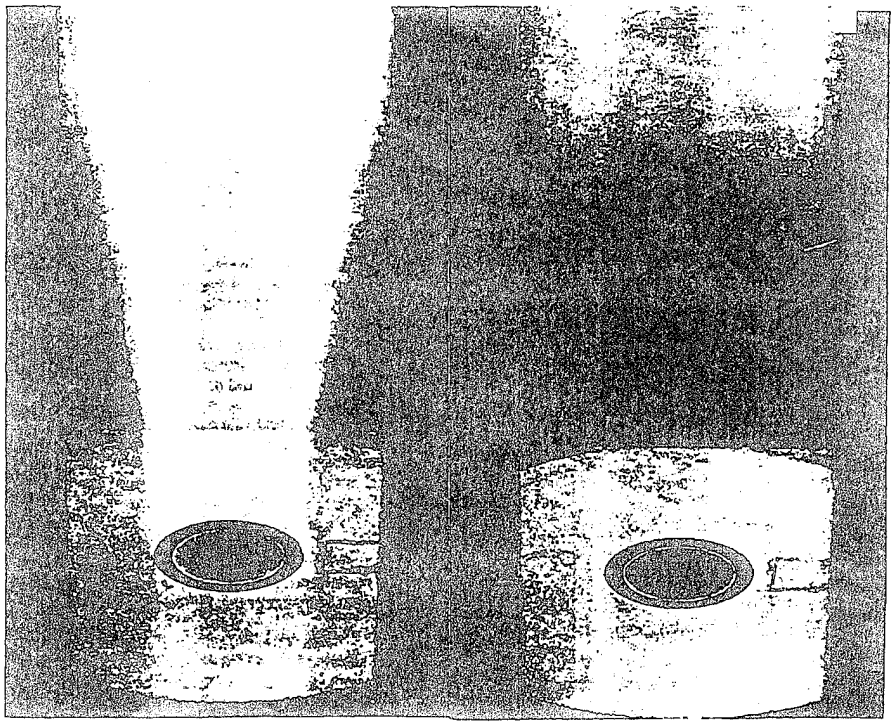

Figure 3–6. Time–Mean, Available Light Photographs of Attached and Lifted Flames In the Task 100 Research Combustor

The characteristics of the attached flame near its initiation position were studied using spontaneous OH–imaging, thin–filament pyrometry (TFP), coherent anti–Stokes Raman spectroscopy (CARS), planar laser–induced OH–imaging (PLIF), and reactive Mie–scattering from

TiO_2 particles. These studies are described in References 11 and 12, which are submitted as Appendices F and G respectively.

The spontaneous OH–imaging of the attached flame at about 15 mm above the step, revealed that the visually–observed flame–lift equivalence ratio of 1.05 represented a break in the gradient of u.v. emission

intensity with equivalence ratio. For equivalence ratios less than 1.05 the attached flame was still present but with very high intermittency. In intermittent form it was present at equivalence ratios right down to blowout. It clearly did not release sufficient heat to stably pilot the shear layer flame, and this was what caused lift of the main flame; also, the luminosity was not sufficient for normal visibility at equivalence ratios below 1.05.

The TFP measurements found that at 10 mm above the step, the attached flame was about 5 mm thick, and, that the peak temperatures oscillated about a mean radius of 24 mm with a displacement of about 4 mm and a frequency less than 10 hertz. The intermittency at equivalence ratios less than 1.05 was confirmed, Figure 3–7.

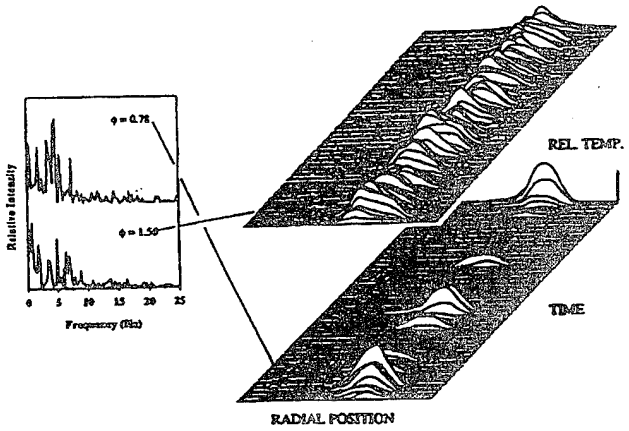

Figure 3–7. Time History and Frequency Spectra of Relative Temperature from a Thin Filament Pyrometer in the Attached Flame Region at Fuel–Rich and Fuel–Lean Equivalence Ratios

The CARS measurements of radial mean temperature profile at 5 mm downstream from the step established that for visually–lifted flames, low (inlet) temperatures existed out to a radius of 19 mm; for visually–attached flames there was a sharp temperature rise from a radius of 17 mm. The CARS p.d.f.'s were strongly bi–modal for radii between 14 and 19 mm for the visually–attached flame, and absolute mean temperature levels were in excess of 1300°K at 25 mm radius.

The PLIF OH–images of the attached flame in the near–field strongly suggested that the radial oscillations of the flame sheath observed by the TFP and supported by the CARS p.d.f.'s, could be associated with eddy formation in the jet shear layers. Reactive Mie–scattering by TiO_2 particles formed from $TiCl_4$ vapor seeding of the jet streams, confirmed that the size of the eddies in the jet shear layers had a characteristic dimension that was consistent with the amplitude of the oscillations indicated by the TFP measurements, and supported this observation. The estimated frequency of the shear layer eddies was also consistent with that observed by the TFP for oscillation of the attached flame.

The PLIF OH–images also indicated that the necessary fuel for the attached flame was recirculated to the step by the step vortices. However, it appeared that a significant mode for fuel entering the step vortices was not straight–forward recirculation of unburned fuel from the jet shear layer that was delivered to the reattachment plane of the step–vortex. Rather, it was direct radial injection of fuel into the step recirculation, by nonstationary eruptions through the jet shear layers, as Figure 3–8 illustrates. This behavior was also observed in a movie of nonreacting flow visualizations (fluoroscene dye in water) made at UTRC in a similar geometry, by Johnson [13]. The CARS measurements for this equivalence ratio at a radius of 24–26 mm and 5 mm downstream from the step indicated mean temperatures around 1500K. Such temperatures in this region of the combustor are indicative of the attached flame.

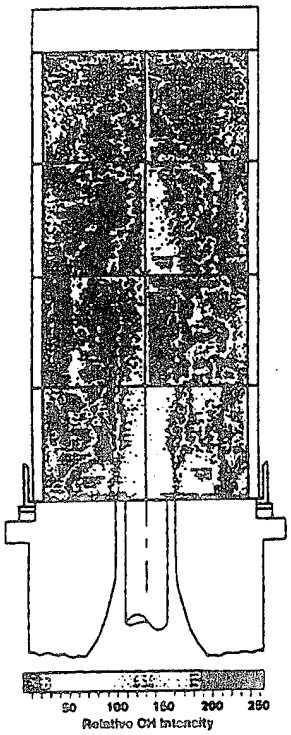

Figure 3–8. Spatial Composite of Instantaneous PLIF OH–Images at an Equivalence Ratio of 1.56 with a Higher–Value combustor Loading (Attached Flame)

For the lifted flame, the PLIF OH–images did not show shear layer burning in the near–field, but a lifted shear layer burning at heights greater than 150 mm above the step–plane, Figure 3–9. The reattachment plane for the lifted shear layer burning was in the range 230–310 mm above the step. Considerable OH was shown in the step recirculation back at the step. The was due to straight–forward recirculation. The CARS measurements indicated a mean temperature of about 1250–1300°K at a radius of 24–26 mm and 5 mm downstream from the step. These temperatures are less than the generally–accepted value of about 1480°K required to result in a visual flame.

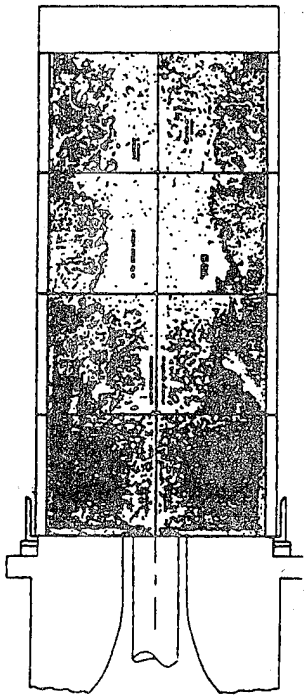

Figure 3–9. Spatial Composite of Instantaneous PLIF OH–Images at an Equivalence Ratio of 0.78 with a Lower Vale Combustor Loading (Lifted Flame)

Figure 3–10 describes the LBO sequence for the 4.9 L/D combustor with 45% outlet blockage over a range of combustor (low–end) loadings. The Reynolds Number of the annular air jet was between 24,800 and 46,000 in this map. The map indicates that when equivalence ratio was further reduced following loss of the attached flame and lift of the main flame, intermittency progressively grew in the main flame. This intermittency increased with combustor loading. As blowout was approached, large–scale axial movements of the lifted flame region occurred.

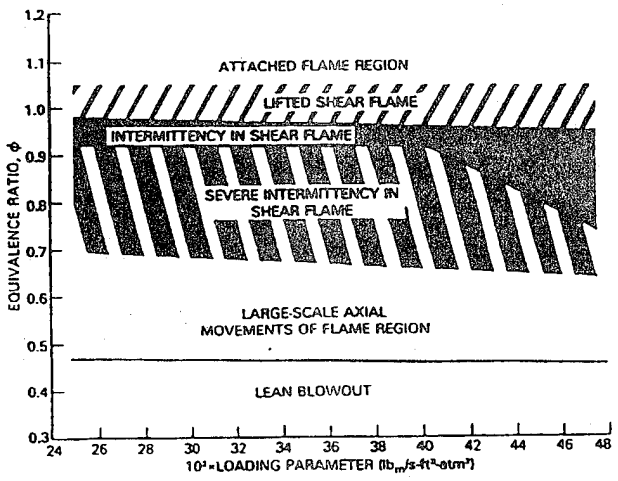

Figure 3–10. Flame Behavior as Lean Blowout is Approached at Low Combustor Loadings with 45% Exit Blockage

3.6 Effects of Back–Pressure

Orifice plates on the combustor outlet were provided to simulate the back–pressure that exists in real gas turbine combustors due to the presence of the combustion and dilution air jets, and the turbine inlet guide vanes. Back–pressure was found to exert a number of effects on combustion in the Task 100 Research Combustor. These are described in Reference 9, which is included as Appendix D.

Back–pressure by means of exit blockage did exert an effect on the LBO characteristics of the combustor. The effect was weakest at low combustor loadings near the flammability limits, and strongest at high combustor loadings near the peak heat release rate, Figure 3–11. The magnitude of the effect was changed with combustor L/D.

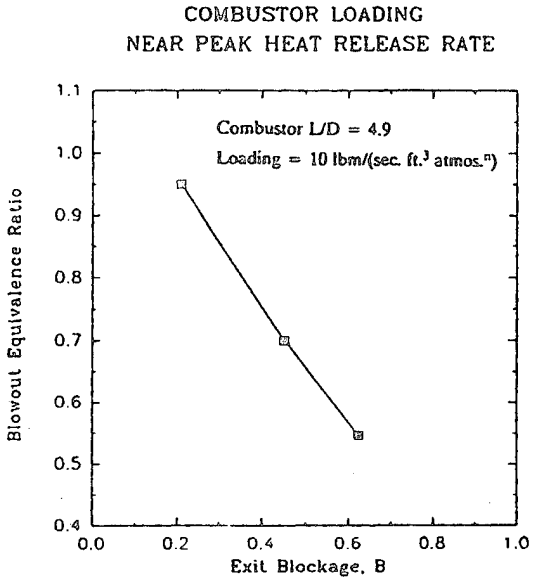

Figure 3–11. Influence on LBO of Exit Blockage at High Combustor Loading

The effects of back–pressure were two–fold: 1.) changes to the mean flowfield, and, 2.) changes to the nonstationary characteristics of a blowout sequence.

Changes to the mean fields were evidenced as changes in the position at which the combustor walls reached a maximum temperature, as expressed through *metal temperature factor,* MTF, where,

$$MTF = \frac{T_s - T_{in}}{T_{ad.\,fl.} - T_{in}}$$

The maximum temperature experienced by the combustor walls was associated with the re–attachment plane for the step recirculation.

As expressed by MTF, the maximum wall temperature was only a function of equivalence ratio, and was not influenced by exit blockage. For attached flames the position of maximum MTF was reached at about 450 mm downstream from the step (4.9 L/D combustor), with a value of about 0.42. For lifted flames the position of maximum MTF was a complex function of exit blockage and equivalence ratio, as Figure 3–12 shows, and the value of max. MTF increased with decreasing overall equivalence ratio to about 0.47.

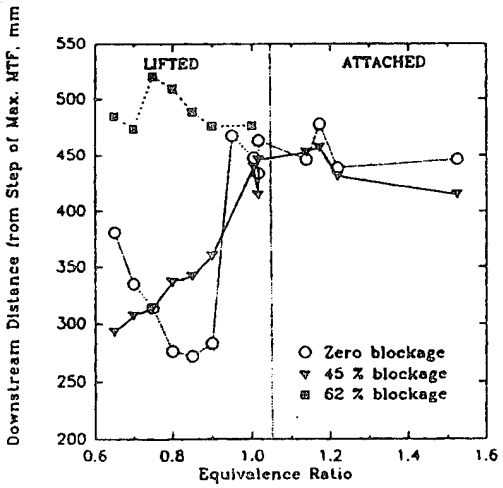

Figure 3–12. Dependency of Position of Maximum MTF On Exit Blockage for Lifted and Attached Flames in the 4.9 L/D Combustor

The effect is induced by influence of the stagnation recirculation region set up on the forward face of the orifice plate, with that of the step recirculation zone. In Figure 3–12 the behavior for zero exit blockage was consistent with the findings of Morrison et al. [14.], Pitz & Daily [15.] and Stevenson et al. [16.], for premixed flames, that a step recirculation zone at fixed (turbulent) Reynolds number decreases in size with increasing equivalence ratio. The minimum distance at this zero blockage, occurring at an equivalence ratio of 0.9 in the Task 100 combustor, suggested that the pilot flame attachment was becoming evident before the directly–observed equivalence ratio of 1.05. This was confirmed by Roquemore et al. [11.] and Chen [17.] with the pilot–flame intermittency measurements.

As exit blockage was increased at low loadings in the 4.9 L/D combustor the equivalence ratio for the onset of the large–scale axial movements of the lifted flame immediately preceding an LBO, was increased. Figure 3–13 illustrates this destabilizing action. The blowouts at these combustor loadings were only weakly improved by increased exit blockage. This suggests that the destabilizing effect of the increased large–scale axial movements at these loadings, off–set the strong stabilizing effect of exit blockage.

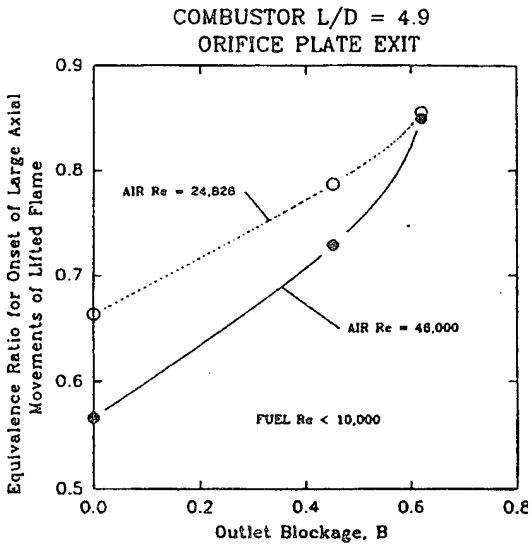

Figure 3–13. Influence of Exit Blockage and combustor Loading (low values) on Equivalence Ratio for Onset of Axial Movements of the Lifted Flame

3.7 Stability Characteristics

One of the classical ways of presenting LBO data is to plot the blowout equivalence ratio against the combustor loading parameter, which derives from well–stirred reactor approaches. This method follows that of Bragg [18.], who proposed that a gas turbine combustor could be modeled as a well–stirred reactor representing the primary zone, followed by a plug–flow reactor representing the intermediate zone; the dilution zone was considered as redundant, i.e., nonreacting. While this is now recognized as being too simple a representation, ideas arising from it proved to be very useful. For this reason the combustor loading parameter continues as a correlating group of merit, if used with care.

The form of the loading parameter used presently follows that of Kretschmer & Odgers [19.], where the order of the global reaction representing the real reaction kinetics is made a function of equivalence ratio. This results in fractional reaction orders, which is not physically real, but comes from the sweeping simplifications arising from use of a single global reaction to represent the real chemistry. Additional modifications are introduced into this loading parameter to account for the presence of the excess nitrogen used to simulate low combustion pressures. The excess nitrogen affects residence time in addition to acting as a heat sink and reactant–diluent. Thus, the loading parameter LP, is defined,

$$LP = \frac{\dot{m}_{Tot}}{V P^n F}$$

where,

$\dot{m}_{Tot} = \dot{m}_f + \dot{m}_a + \dot{m}_{N2}$ lbm/sec.

V = effective reactor volume, ft^3

P = combustion pressure, atmos.

n = apparent global reaction order = $2\phi_{LBO}\ (1 + \dot{m}_{N2} / \dot{m}_a)_{tt}$

$$F = \frac{10^{0.00143\,T}}{3.72}$$

T = fuel/air inlet temperature, K

ϕ_{LBO} = equivalence ratio at LBO

The exponential temperature correction factor F is to correct the data to a constant 400K inlet temperature, and represents a tribute to the pioneering well–stirred reactor work of Longwell et al. [20.], where an actual inlet temperature of 400K was used.

The difficulty in applying the loading parameter to the Task 100 combustor is associated with making a choice for the effective reactor volume V. This is, by definition, the volume within which the fuel–air mixture is well–stirred, and the equivalence ratio is within the rich and lean flammability limits for the reactants.

To establish the reactor volume, recourse was made to the CFD tool, and calculations were made of the flowfields in the research combustor using the 2D–PREACH code. The calculated flowfields were interrogated using the total dissipation gradient methodology of Swithenbank [21.] to establish the well–stirred regions of the combustor, according to a standardized definition of "well–stirred." These estimates [12.] suggest that the combustor was effectively well–stirred across its entire radius by a distance of 650 mm (4.3 L/D) downstream from the step. Within this distance, there were local regions, such as in the step recirculation zone, around the step–recirculation reattachment plane, and in the downstream parts of the shear layers, where the flow was also effectively well–stirred. Account was taken of the flame–lift through the experimental observations of that height. Since the flame–lift allowed time for some degree of fuel distribution and premixing of reactants to take place within the well–stirred regions prior to reaction, it was assumed that all well–stirred regions, except for the step recirculation, constituted reacting volumes.

The LBO data were correlated on the basis of loading parameter, and a good correlation was obtained over a wide range of total mass flow rates and equivalent pressures. At low values of loading parameter the correlated LBO equivalence ratio asymptotically approached the limiting condition represented by the lean flammability limit for propane/air mixtures [22.].

Implicit in the data–correlation is the assumption that in the lifted–flame condition from which a lean blowout occurs, the research combustor behaves like a simple, single, well–stirred reactor. Two steps were taken to check the validity of this: 1.) A comparison was made with actual well–stirred reactor experimental data from the literature, and, 2.) the correlated research combustor data were compared to a calculated stability line obtained using a well–stirred reactor computer code.

A comparison of correlated research combustor LBO data with well–stirred reactor data from the literature is contained in References [6.] and [23.], with the latter reference being attached as Appendix H. The data from the research combustor at low loadings are consistent with a large amount of the literature data.

The well–stirred reactor code used was a version of the MARK2I stirred reactor network code by David Pratt and Brian Pratt. MARK2I uses the CREK chemical kinetics code of Pratt & Wormeck [24.]; the hydrocarbon reaction mechanism used was a simulation of Jet A fuel by Roberts et al. [25.]. This was considered appropriate for propane (see Section 6.0).

The research combustor near to blowout was modeled in MARK2I as a single, perfectly–stirred reactor with separate air and fuel inlets, and a single discharge of products; there was no external recirculation of products. Heat losses were not accounted for. The reactor volume was made the same as the active volume of the research combustor. No cases with excess nitrogen were run, but true combustion pressure variation was made. Thus, comparison with the experimental data also serves as a check on the calibration of the excess nitrogen low–pressure simulation technique.

Figure 3–14 shows the comparison. The good agreement of the calculated stability with the well–correlated experimental data is apparent in the figure. The agreement confirms that the research combustor at LBO behaves like a well–stirred reactor due to the premixing of reactants allowed by the lifted flame condition.

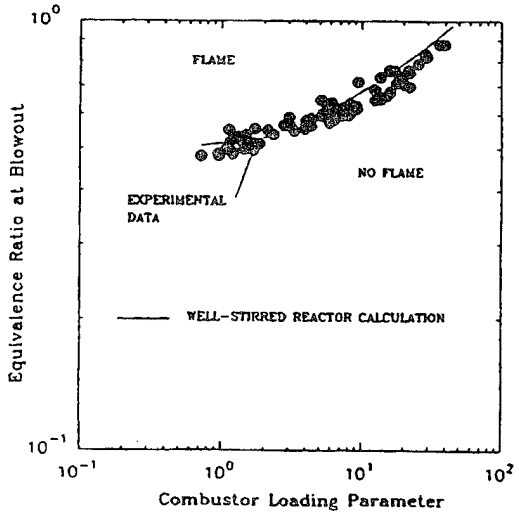

Figure 3–14. Measured Lean–Portion of Experimental Stability Loop Compared to Well–Stirred Reactor Calculations; via the Loading Parameter

3.8 Summary

The research combustor was intended to represent a simplified version of a primary zone. Experimentally, it revealed some important features concerning blowouts.

The role of recirculation in maintaining stability was clearly brought out. Recirculation provided a piloting action of an attached flame that kept the main flame anchored in the jet shear layers close to the fuel injection plane. Fuel distributions, especially in the step recirculation zone, were strongly, and favorably, influenced by nonstationary behavior of the mean flow field. The nonstationary behavior directly introduced more fuel radially into the step recirculation zone than was provided via conventional jet shear layer re-attachment and recirculation from downstream. The piloting action of the attached flame was enhanced by this additional fuel source for the step recirculation. The nonstationary behavior appeared to arise from interactions of a precessing, small, central, recirculation bubble, situated in the near-field of the fuel stream, with the individual eddies of the jet shear layers. With reduction of the total fuel flowrate, insufficient fuel was introduced into the step recirculation to provide adequate energy to the attached flame for piloting the main, jet shear layer, flame. The fuel reduction was from both the conventional path and from the nonstationary flow path. When the pilot flame was lost, the main flame lifted in the jet shear layers, and was more distributed across the combustor. The flame-lift allowed significant premixing of fuel and air to take place prior to the downstream reaction. Final blowout was of the character of a premixed flame. Back-pressure on the system exerted some significant influences on the flowfield, flame behavior, and blowout. These influences depended on the combustor loading and the operating equivalence ratio.

SECTION 4.0
APPLIED STUDIES: TASK 150 COMBUSTOR

4.1 Intent

The intent of the PW Task 150 Combustor was to continue the Task 100 effort of addressing the fundamentals of the blowout process, by studying practical fuel injector combustion characteristics in isolation from the other complications of gas turbine combustors. While many detailed studies exist in the literature concerning jet flames, both free and enclosed, almost nothing is directly available on the flame characteristics produced by practical devices for introducing reactants into a combustor. The PW Task 150 "technology combustor" goes some way towards remedying this situation.

4.2 PW Task 150 Combustor Design

The PW Task 150 Technology Combustor design was modified from that of the PW Task 100 Research Combustor, Figure 3–2. The combustion tunnel section, consisting of the 475 mm length window piece, 260 mm length extension chimney (4.9 L/D total), and the outlet orifice plate (45% geometric blockage), were retained from the research combustor. A new bulkhead replaced the jet system and step, however. The new bulkhead accommodated a practical fuel injector, taken from an engine, together with the engine combustor dome interfacing, which consisted of injector guide containing an "insert swirler," and a dome cooling air deflector. To accommodate the fuel injector the central, propane fuel tube was removed from the wind tunnel (air conditioning section), see Figure 3–2, together with the contraction–piece. A 240 mm length plenum chamber spool–piece was provided in place of the contraction–piece. The spool–piece also accommodated a mounting pad for the fuel injector support stem and flange. Figure 4–1 shows an overall view of the Technology Combustor.

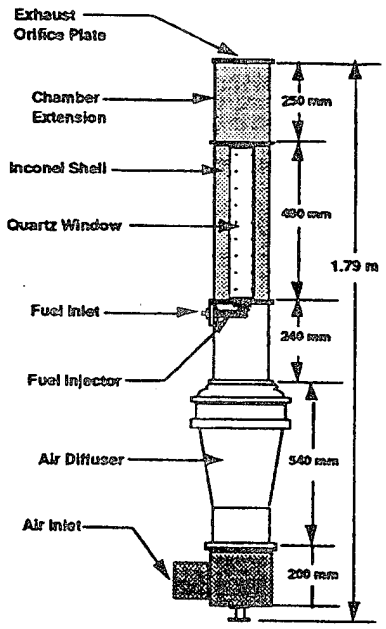

Figure 4–1. Overall View of the PW Task 150 Technology Combustor

The fuel injectors used were of the prefilming airblast atomizing type, and contained swirlers in the air passages to provide good circumferential fuel distribution, and to assist in establishing the "inside–out recirculation" flowfield shown in Figure 3–1 and simulated in the PW Task 100 Research Combustor. The only modification made to the fuel injectors from the engine configuration was the removal of a fuel–line trim orifice contained in the injector support. The purpose of the trim orifice was for final adjustment of the flow

number so as to increase the production yield of injectors. Its removal was necessary to pass the required mass flow rate of gaseous propane in this combustor, but did not affect the injector performance.

Figure 4–2 shows the installation of the fuel injector package in the combustor dome. The only air addition to the technology combustor was that introduced through the dome via the fuel injector, insert swirler and dome cooling. The correct dome interfacing was provided to ensure that the fuel source should have boundary conditions virtually identical to those in an engine.

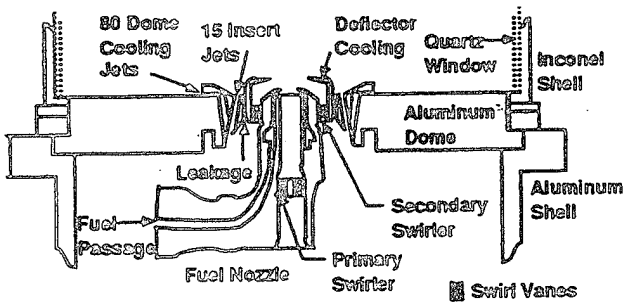

Figure 4–2. Cross–Section of Dome Region, Showing Dome Interfacing and Fuel Injector In the Technology Combustor

4.3 Fuel Injectors and Dome Interface

The airblast fuel injectors used coswirling airstreams on either side of a coswirling annular fuel sheet, with the outer air passage and fuel passage both converging on the central air passage. Thermal protection for the outer air passage deflector cap was provided by tapping off a small amount of film cooling air from the outer airflow. The cooling film was discharged to flow radially inwards on the flame–side of the deflector cap. The spent cooling air was subsequently entrained into the injector main passage discharges.

Two injectors of this configuration were used. A high–swirl (HS) injector had a nominal swirl number (based on vane angles and mass–weighted for the swirler flow splits) of 1.41, and, a low–swirl (LS) injector had a nominal swirl number of 1.05; both in the fully turbulent flow regime. The total air passage effective areas were 0.176 in^2 for the HS injector, and 0.266 in^2 for the LS injector, with outer to inner passage flow splits of 2.8 and 2.2 respectively. The outer swirler vane angle was 55 degrees for both injectors, while the inner swirler vane angle was 70 degrees for the HS injector and 45 degrees for the LS injector. The inner passage swirl numbers were 1.91 and 0.69 for the HS and LS injectors respectively, and the outer passage respective swirl numbers were 1.24 and 1.21, respectively.

The dome interfacing was the same for both fuel injectors. The insert swirlers were angled 12.5 degrees into the injector centerlines; the swirl angle was zero in this instance. The purpose of the insert swirlers is described in Reference [5.]. Dome cooling air was introduced with, but separated from, the insert swirler air, and was then turned to flow radially outwards along the dome surface, by a circular deflector plate. The total effective air flow area of the dome excluding the fuel injector, was 0.160 in^2.

4.4 Isothermal Flow Field

Two copies of the Task 150 combustor were manufactured by the Air Force. One was run at Wright Laboratory, and the other was run by the Advanced Combustion Engineering Research Center in the Chemical Engineering Department of Brigham Young University at Provo, Utah. Experimental data to be reported were taken at both of these sites, and is contained in References [26–29]; Reference [29] is presently attached as Appendix I.

LDV measurements were made in the Task 150 combustor with the HS injector flowing air at 288K and simulation of the propane fuel by flowing gaseous nitrogen at 273K. The airflow was 500 slpm, and the

nitrogen flow was 14 slpm; these flowrates corresponded to a fuel–lean equivalence ratio (mass basis) of 0.72. Data were generally taken at 11 transverse planes axially disposed downstream from the dome, although additional planes were added as necessary. On each plane the radial increments from the centerline were 0.5 or 1.0 mm where large velocity gradients existed, and up to 10.0 mm increments where the velocity profiles were relatively flat. Measurements were only made on one half of the combustor; measured and calculated fields were duplicated and reversed to provide complete images.

From the velocity data fields the zero axial velocity contours were obtained by interpolation. From these zero velocity contours, together with the other velocity components, the associated recirculation zones were estimated. This information is presented in Figure 4–3.

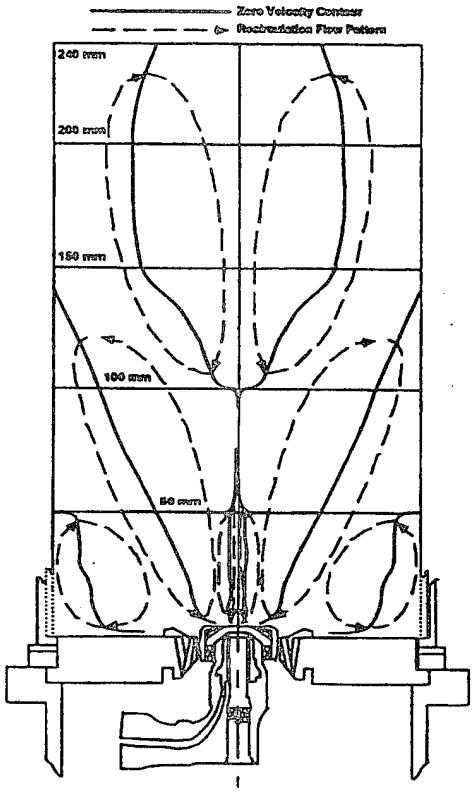

Figure 4–3. Isothermal flowfield in the Task 150 Combustor for the HS Injector at a Simulated Equivalence Ratio of 0.72

It can be seen from Figure 4–3 that the flow field in the Task 150 combustor contains several recirculation zones. In the far–field (distances greater than 100 mm from the dome), a large but very weak recirculation zone existed on the combustor centerline. This was somewhat different from what would exist in an engine combustor, due to the absence in the Task 150 combustor, of transverse combustion air jets, (the exit orifice plate simulates their back–pressure however, as described in Section 3.0). This zone was generated by the strong, toroidal–shaped, rotating main recirculation zone that establishes the "spray angle" which exists when a liquid fuel is used. It extended from the injector to about 120 mm downstream. This zone is analogous to the step recirculation zone in the Task 100 research combustor. Fuel following this trajectory reached the combustor wall at about 150 mm downstream. This is much closer to the dome (by a factor greater than 2.0) than the step–vortex reattachment plane in the research combustor, and illustrates the benefit of swirl in shortening flame length.

Contained within the main toroidal recirculation was a small, narrow, recirculation on the injector centerline. It extended from the injector to about 60 mm downstream, and is analogous to the small, central

recirculation bubble seen in the research combustor. A large toroidal recirculation region existed at large radius in the corners formed between the dome and the combustor walls. It was generated by a combination of the radially–outwards flow of the dome film cooling air with the injector main toroidal recirculation, and extended about 50 mm downstream. Because it was generated by a combination of flows, it was much larger than its (negligibly) small equivalent in the research combustor. The trajectory of the annular fuel stream in the near–field was between the small, central recirculation bubble and the larger, toroidal main recirculation, as it was in the research combustor.

It can be appreciated from Figure 4–3, that the HS injector in the Task 150 combustor generated an isothermal flowfield that had many similarities with that of the research combustor, (Figure 3–3). However, the presence of swirl did introduce some significant differences that must be examined. The velocity field generated by the LS injector was even closer in appearance to that of the research combustor.

4.5 Characteristic Flame Shapes

The flame structures in the Task 150 combustor were studied by direct visual observation and by recorded–image video. Still images from the video were digitized and filtered using computer techniques to produce isochromatic contour plots from the grey–scale images, that provided a photographic flame characterization. The shape of the flame yields qualitative insights to the mixing processes and location of flame fronts. Variation in location of these fronts relative to the injector with operating conditions is of obvious interest. It must be remembered that these images represent the exterior of the flame or, a spatial integration through its thickness.

Figure 4–4 shows characteristic flame shapes for the HS injector at a constant airflow of 310 slpm as the fuel flow (gaseous propane) was varied to give overall equivalence ratios from 2.38 to 0.46. The range of Reynolds Numbers at this overall airflow for the various passages was determined by the flow splits and passage dimensions. On this basis flow from the insert swirler jets was completely turbulent, flow from the outer swirler was in the transitional region, and flow from the inner swirler was in the transitional region also, but only barely so. These observations hold for the LS injector. However, Reynolds Number effects are very small relative to other effects. Figure 4–5 shows the characteristic flame shapes for the LS injector at 310 slpm airflow for equivalence ratios from 1.42 to 0.71. The linear cut–offs to some of the contour plots in both figures represent window–edges in the combustor.

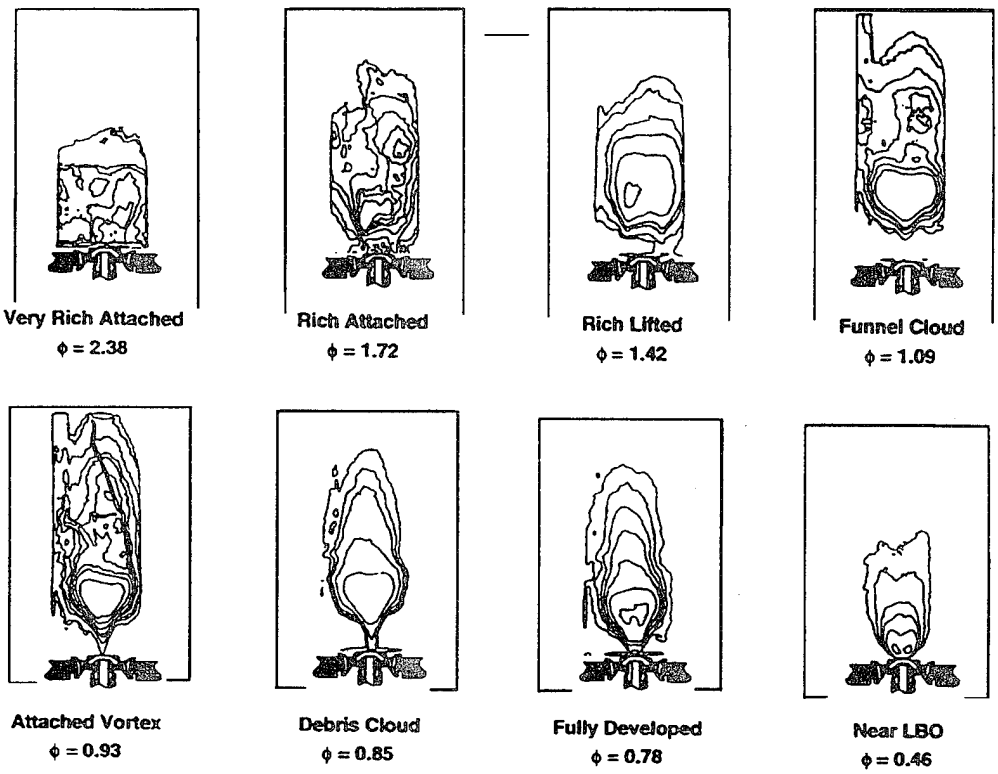

Figure 4–4. Characteristic Flame Shapes for the HS Injector in the 4.9 L/D Task 150 Combustor with 45% Exit Blockage and Constant Dome Airflow of 310 SLPM

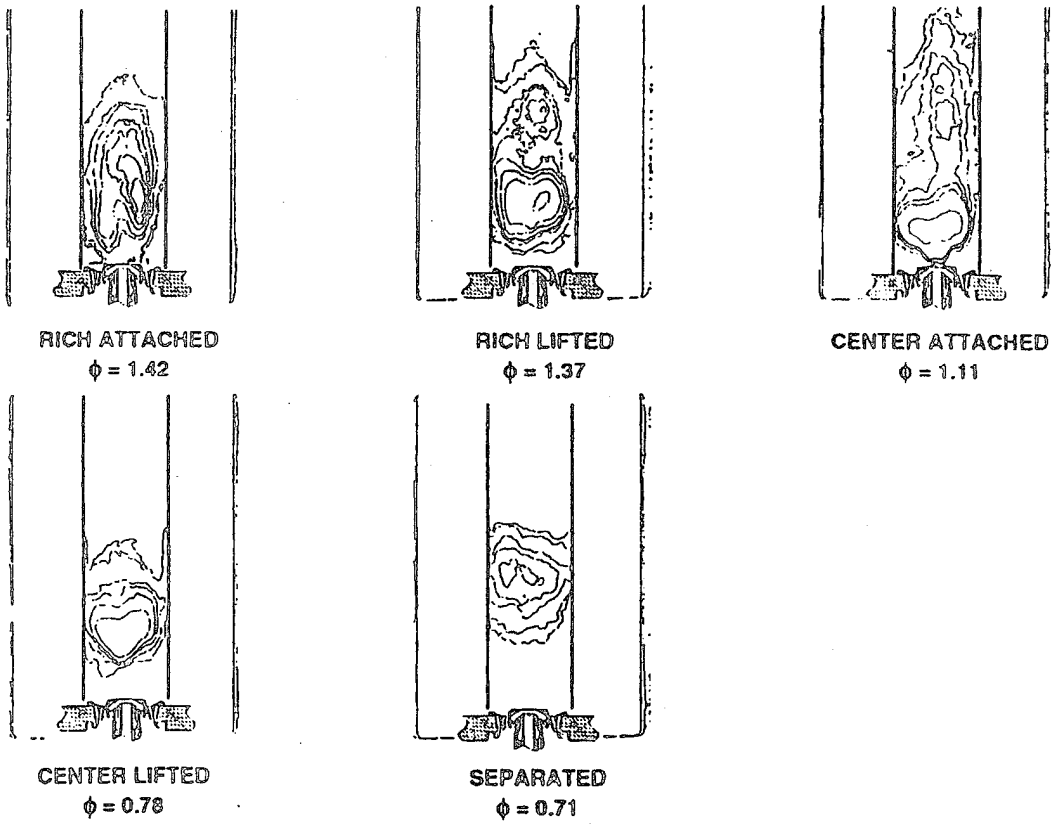

Figure 4–5. Characteristic Flame Shapes for the LS Injector in the 4.9 L/D Task 150 Combustor with 45% Exit Blockage and Constant Dome Airflow of 310 SLPM

To assist in interpretation of the flame shapes, recourse is made to Figure 4–3, and to the stoichiometry of the fuel injector components. These are shown in Table 4–1 [28.] for the LS injector; the distributions for the HS injector are similar.

The flame shapes for the two injectors were governed by the injector stoichiometry and the swirl characteristics. The HS injector at this airflow had about the same lean stability as the LS injector, which was rather surprizing. For an overall equivalence ratio of 0.78 the HS injector had an attached flame which could be attributed to the strong central swirl, while the LS injector had a lifted flame that was similar in many respects to the lifted flame of the research combustor. LBO for the LS injector was from the lifted–flame condition, and occurred at an overall equivalence ratio about 0.46, which was a little better than for the research combustor (Figure 3–14); LBO for the HS injector at this airflow was about 0.49 equivalence ratio from an attached flame condition.

Table 4–1. LS Fuel Injector Component Equivalence Ratios

Overall Phi	Inner Swirler	Injector	Inj. + Insert
0.62	4.17	1.11	0.80
0.72	4.84	1.29	0.93
1.08	7.26	1.94	1.39
1.29	8.67	2.32	1.66
1.49	10.02	2.67	1.92

Table 4–1 for the LS injector, indicates that for overall (dome) equivalence ratios at and above 0.72, there was insufficient injector air to burn all of the introduced fuel. The insert swirler air therefore played an important role in the combustion process. For overall (dome) equivalence ratios of unity and above, dome cooling air also had to play a role in combustion. Thus, at very rich overall equivalence ratios, above 1.5 for both injectors, it would be expected that flame would be distributed across the combustor and attached in the dome region. The characteristic flame shapes did show this. This condition was analogous to the attached flame condition in the research combustor.

Comparison of the flame shapes in Figure 4–4 and Figure 4–5 is complicated by the airflow difference between the two injectors, (see Section 4–3). For a constant dome airflow, (as in the figures) the LS injector flows 1.1921 times the air of the HS injector, i.e., the equivalence ratio of the LS injector is 0.8389 times that of the HS injector. Thus, for comparative purposes with equal injector equivalence ratios at a fixed dome airflow, the dome equivalence ratio with the LS injector should be 1.1921 times the dome equivalence ratio with the HS injector.

Therefore, by applying this correction, the flame structure for a dome equivalence ratio of 0.93 with the HS injector is directly comparable to that for a dome equivalence ratio of 1.11 with the LS injector. Such a comparison from Figure 4–4 and Figure 4–5 shows both flames are attached to the injector via a flame core generated by the inner swirler. The flame core is more compact for the HS injector due to the higher inner swirl number of this injector. Similarly, a comparison for the HS injector at a dome equivalence ratio of 1.09 is comparable with a LS injector at a dome equivalence ratio of 1.3. Comparison from Figure 4–4 at 1.09 equivalence ratio with Figure 4–5 at the nearest equivalence ratio of 1.37 shows a rich, lifted flame in both instances. Comparison of the LS injector at a dome equivalence ratio of 0.71 with a lifted flame from Figure 4–5, with Figure 4–4 for the HS injector would require an equivalence ratio of 0.6; the nearest two equivalence ratios in Figure 4–4 are 0.78 and 0.46, and these both show an attached flame core for the higher swirl case.

The flame structures of Figure 4–4 and Figure 4–5 can be explained with reference to the recirculation zone structure shown in Figure 4–3, and the component equivalence ratios for the dome, given in Table 4–1.

With reference to Figure 4–4, for dome equivalence ratios 0.93 to 0.46, the central attached flame was stabilized inside and between the structure of the main toroidal recirculation and that of the small central recirculation bubble. The central swirler alone does not provide sufficient air for combustion so mixing with additional air due to recirculation must have taken place. The influence of the insert swirler jets on the base of the main flame can be detected (inwards dimples). As fuel flow rate was increased the combined injector and insert swirler airflows again were insufficient to react all of the fuel supplied. Due to the air deficiency along the combustor centerline, the flame lifted (rich lifted flame) until it found sufficient air (provided by the dome cooling convected downstream) to stabilize within the flammability limits. The large but weak, centrally–located recirculation shown in Figure 4–3 was not present in reacting flow. With further increases in total fuel flow rate, large quantities of unburned fuel were recirculated to the dome by the main toroidal recirculation and the large–diameter toroidal recirculation in the combustor corners formed by the dome and walls. This recirculated unburned fuel was then able to react directly with the dome cooling air to give the rich attached flame (dome equivalence ratios of 1.72 and 2.38).

The functioning of the so–called "rich–dome" approach to combustor design is well–described by the Task 150 combustor, the flame behavior seen relates well to that seen in the Task 100 research combustor.

4.6 OH – Imaging for Instantaneous Flame Structures

The OH radical is an important marker for hydrocarbon flames since it is produced in large quantities during the combustion process. This radical therefore gives a good indication of flame–fronts and regions of significant heat release. Care has to be taken in interpreting OH images since there is a concentration

level below which the radical cannot be detected, and in some circumstances, it can persist for long times and is therefore subject to convection from its sites of origin.

A series of OH–images was made in the Task 150 combustor using PLIF (planar laser–induced fluorescence) imaging by means of a dye laser tuned in the ultra–violet to about 283 nm wavelength, pumped at 10 ns by a Nd:YAG laser. The near–instantaneous images were captured at 308 nm wavelength by an intensified CCD camera. Unlike the digitized flame photographs, these images represent vertical sections through the center of the combustor.

Images were taken for the HS injector at a fixed dome airflow rate of 500 slpm and equivalence ratios from 0.62 to 1.75. Figure 4–6 shows spatial composites of these instantaneous images at 0.62, 1.08 and 1.49 dome equivalence ratios. The highest regions of OH concentration indicate the main heat release regions, and can be well–related to the digitized flame structure images in Figure 4–4, and to the explanation given above of the roles of recirculation and local equivalence ratio.

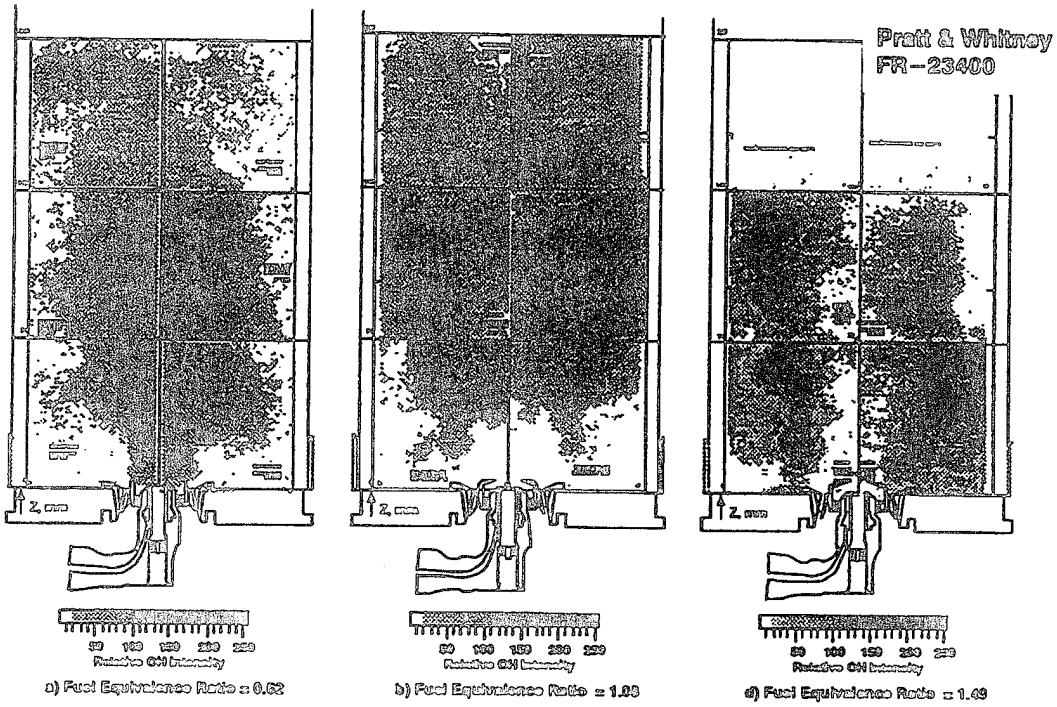

Figure 4–6. Spatial Composites of OH–Images of Heat Release from the HS Injector at a Range of Dome Equivalence Ratios

Figure 4–6 a) at 0.62 dome equivalence ratio represented the attached central core flame with central burning; Figure 4–6 b) at 1.08 dome equivalence ratio ratio represented the rich–lifted flame and showed the penetrations of the insert swirler jets into the extensive and distributed flame; and, Figure 4–6 c) at 1.49 dome equivalence ratio represented the rich–attached flame and showed the burning of recirculated and partially–reacted fuel at the dome cooling air film, together with most of the reaction being associated with the main toroidal recirculation zone (Figure 4–3). For this latter condition note the absence of reaction along the combustor centerline due to the air–deficiency of the injector.

Figure 4–7 provides a time–sequence of OH images for the HS injector at a dome equivalence ratio of 1.29. It can be seen that the heat release process "puffs," and that the flame puffing has a significant effect on the main toroidal recirculation, together with the quantity of unburned or partially–burned fuel recirculated back to the dome. At no time is reaction detected on the combustor centerline at this equivalence ratio. Figure 4–7 supports the observation made for the Task 100 research combustor, that

mass transport in axisymmetric, turbulent, recirculating, nonpremixed flames is dominated by nonstationary flow phenomena.

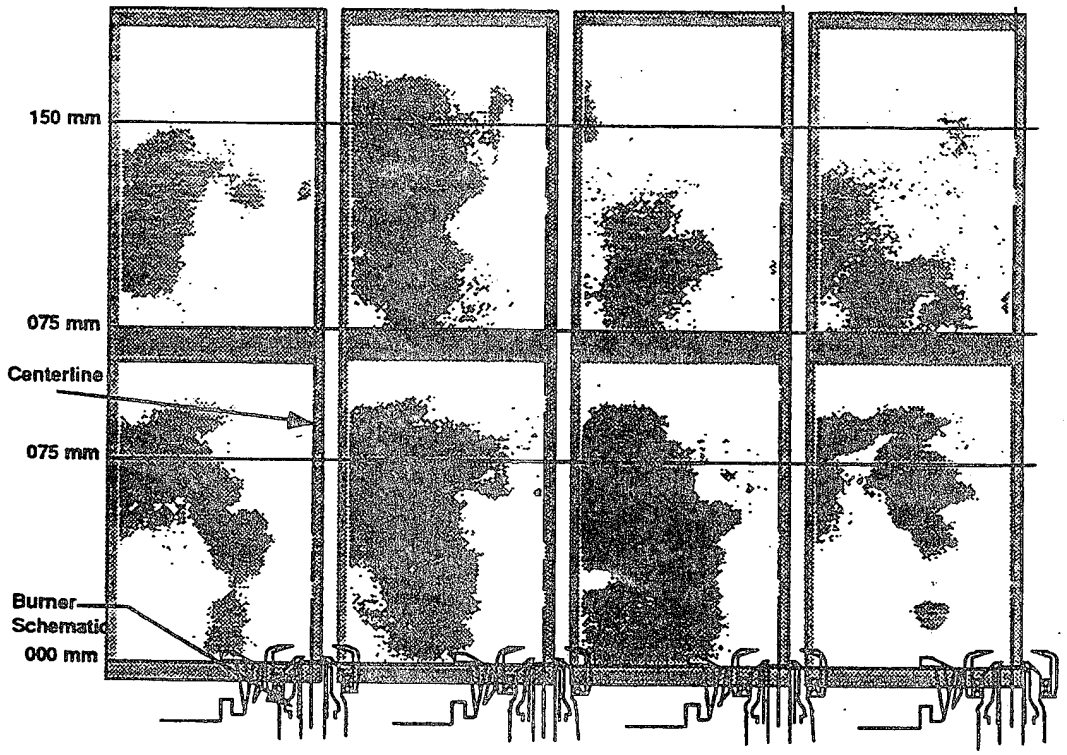

Figure 4–7. Time–Sequence of Instantaneous OH–Images from the HS Injector at a Dome Equivalence Ratio of 1.29

Averaged OH images from 6 to 10 separate instantaneous laser shots at 0.72 and 1.49 equivalence ratios [26.] represent the mean flame structure, and resemble the instantaneous images (Figure 4–6). The averaged images at these two equivalence ratios bring out the control exerted by the injector/dome component local equivalence ratios on where the flame is held.

4.7 Velocity Fields In Reacting and Nonreacting Flows

LDV was used to make measurements of the gas velocity fields in both reacting and nonreacting flows. The matrix of measurement stations was as described in Section 4.4. For the HS injector the operating conditions at which measurements were taken was a constant airflow of 500 slpm, and dome equivalence ratios of 0.72 and 1.49; for the nonreacting cases gaseous nitrogen was substituted for the propane fuel.

Isovels of mean axial, tangential and radial velocity components for the HS injector at equivalence ratios of 0.72 and 1.49 are given in Figure 4–8 and Figure 4–9, respectively [29.]. The flame at 0.72 equivalence ratio was attached to the center of the injector, and at 1.49 equivalence ratio it was attached to the insert jets and dome film cooling (Figure 4–4 and Figure 4–6).

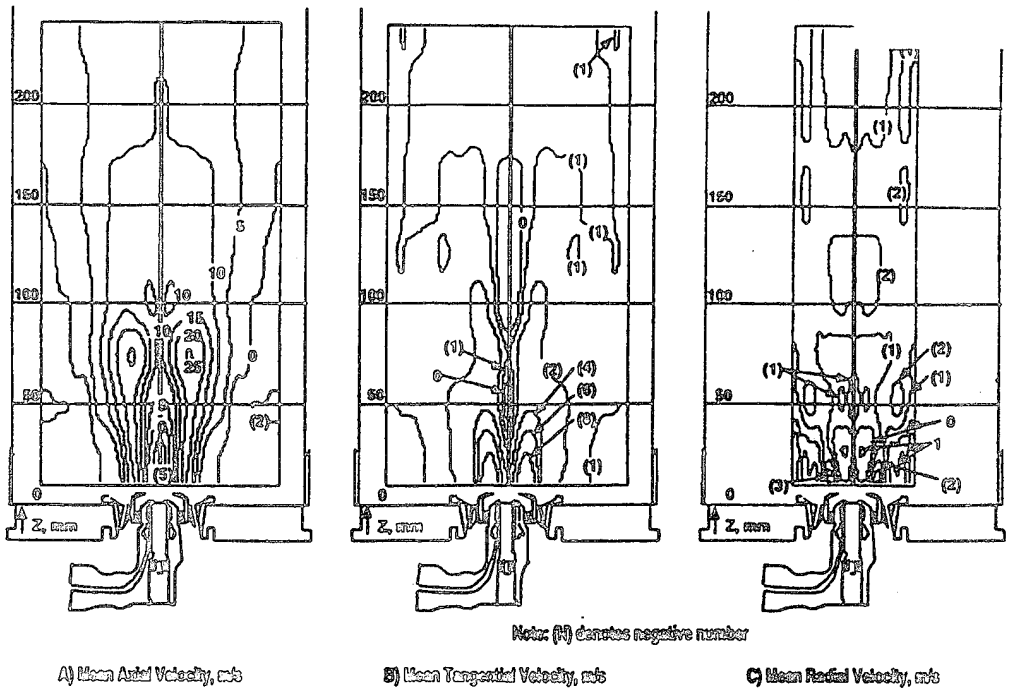

Figure 4–8. LDV Mean Velocity Component Distributions for the HS Injector at 0.72 Equivalence Ratio (Airflow of 500 slpm)

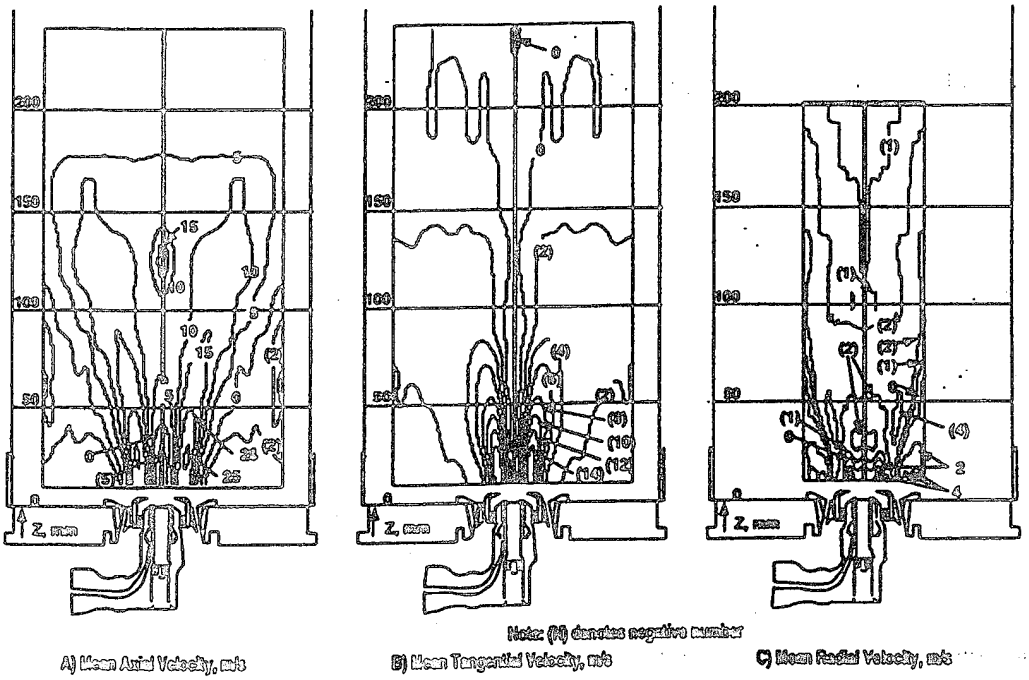

Figure 4–9. LDV Mean Velocity Component Distributions for the HS Injector at 1.49 Equivalence Ratio (Airflow of 500 slpm)

A sharp annular peak in axial velocity (Figure 4–8A) was evident close to the injector, together with a small, central reverse velocity. This peak was driven by main injector flow (air + propane) and the insert swirler jet airflows, moving between the central recirculation bubble and the main toroidal recirculation (see Figure 4–3). On the injector centerline close to the discharge there was a reverse velocity of 5 m/s, whereas the nominal one–dimensional mean velocity leaving the primary swirler was a positive 23 m/s. Momentum transfer across the large velocity gradient quickly overcomes the reverse flow however. Note that the large, downstream and central recirculation bubble seen in nonreacting flow (Figure 4–3) was not evident when combustion was present. The confining influence of the nonswirling insert jets was noticeable. Little of the strongly–swirling flow from the injector discharge was transmitted to the outer recirculation regions. The toroidal recirculation situated in the combustor corners was not much changed in size by the heat release at this equivalence ratio, but was of quite low velocity. This toroidal vortex also rotated rather slowly around the combustor circumference. Tangential velocities were nearly zero by 100 mm downstream. The magnitudes of the radial velocity components were all rather small compared to the axial components and even to the tangential components. This might be a contributing factor for the strong resemblance to the Task 100 research combustor characteristics. Absolute axial and tangential RMS values of velocity were similar in both value and distribution, and had peaks associated with the shear layers of the annular axial velocity peak.

At 1.49 equivalence ratio (Figure 4–9) the general flowfield in terms of recirculation regions and general characteristics, was similar to that for 0.72 equivalence ratio. The sharp annular peak in axial velocity can be seen to decay much more rapidly than for the lower equivalence ratio, and "lobing" was evident and extensive. As a result, the main toroidal vortex was widened. The radial velocity components were low for both equivalence ratios, but had different patterns. Again, the absolute axial and tangential RMS values of velocities were similar in magnitude and distribution. The velocity field differences can be associated with the influences of heat release on the flow velocities, and the changes in flame structure, Figure 4–4 and Figure 4–6, that take place with increasing equivalence ratio.

4.8 Temperature Fields

Coherent anti–Stokes Raman spectroscopy (CARS) in a folded BOXCARS phase matching arrangement, was used to obtain gas temperature measurements at equivalence ratios of 0.75, 1.00, 1.25 and 1.50 for the HS injector [28.],[29.], with a constant airflow of 500 slpm; similarly for the LS injector [27.]. The CARS lasers and spectrometer were remote from the combustor, and fiber optics were used as beam and signal carriers. Where the large temperature gradients existed, closely–spaced radial traverses were used, similarly to the LDV measurements. Temperature data were taken to a radius of 30 mm and an axial distance of about 300 mm. Again, image rotation was used to obtain symmetrical displays of data.

Figure 4–10 shows the isotherms of mean temperatures for the LS injector, and Figure 4–11 shows them for the HS injector. In both cases the isotherms can be related to the characteristic flame shapes in Figure 4–5 and Figure 4–4, respectively.

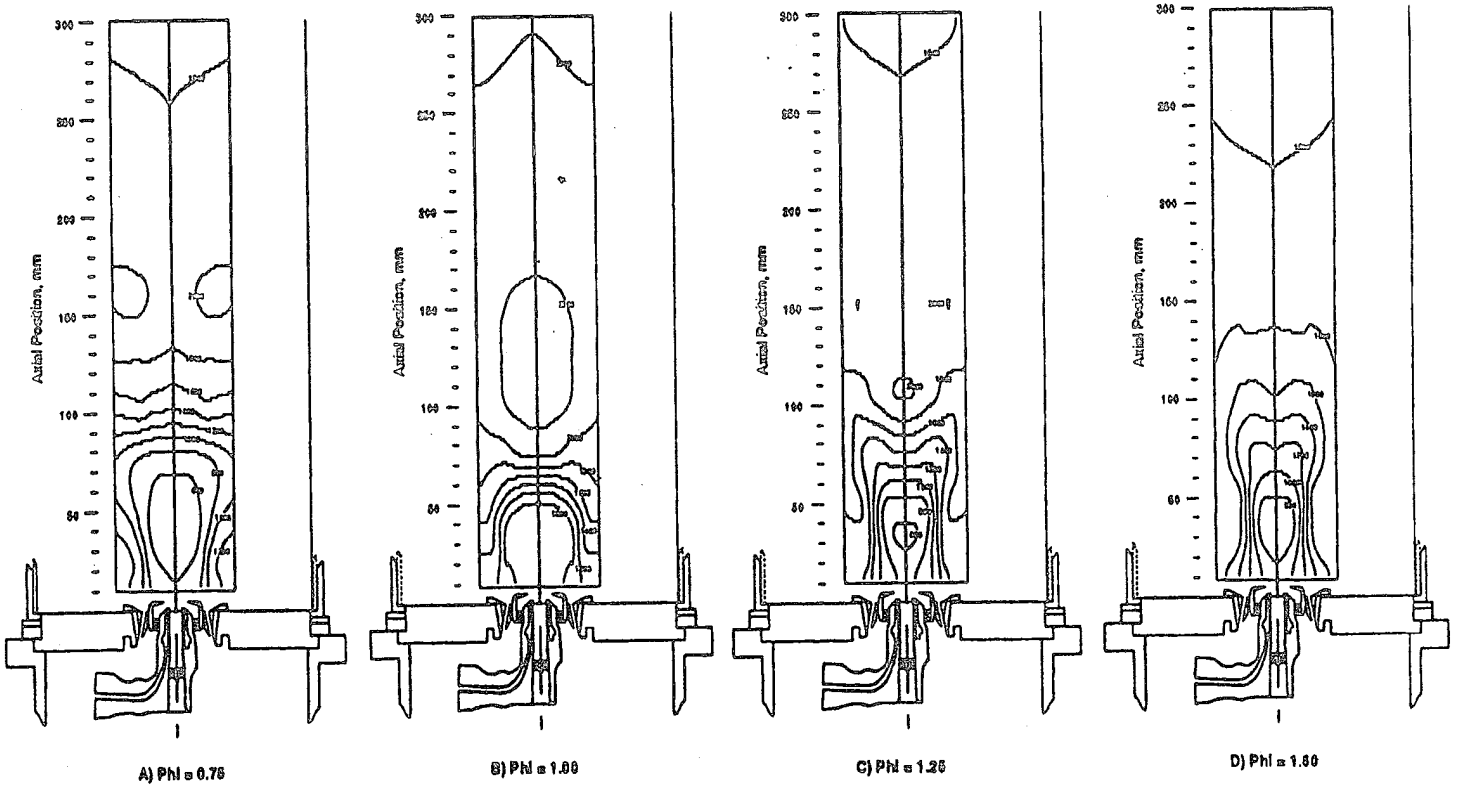

Figure 4–10. Distributions of Mean Temperature Over a Range of Equivalence Ratios for the LS Injector

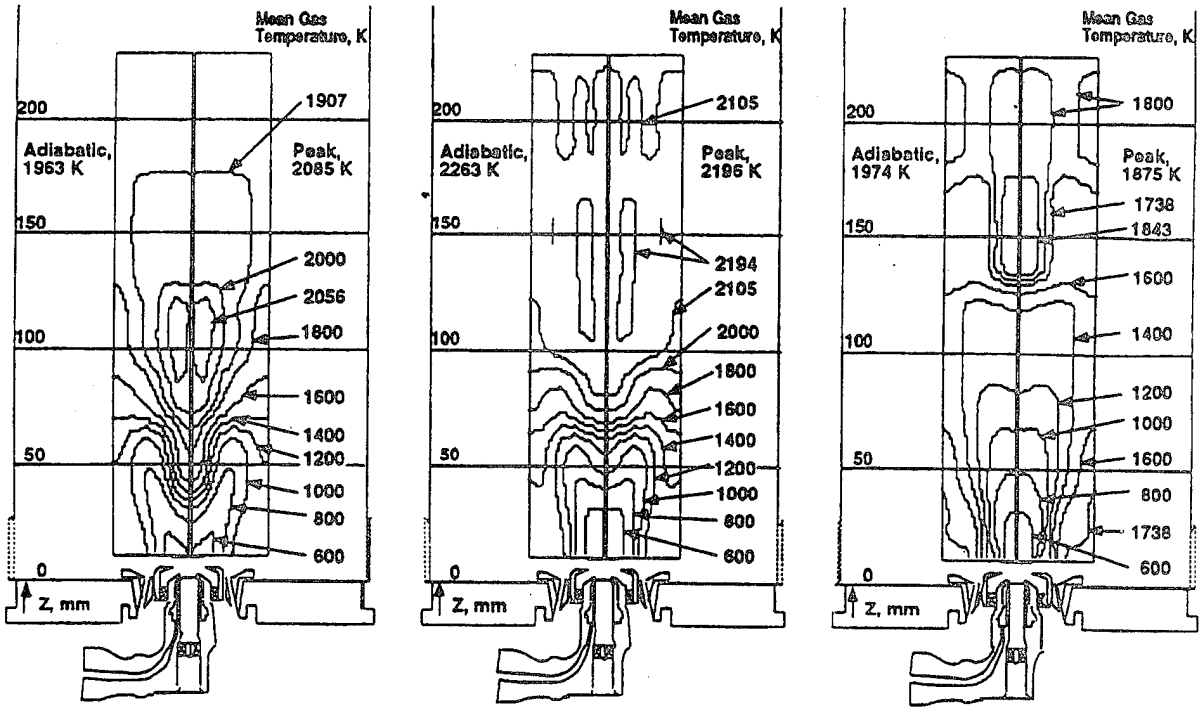

Figure 4–11. Distributions of Mean Temperature Over a Range of Equivalence Ratios for the HS Injector

For the LS injector at the lowest equivalence ratio it can be seen that the lifted flame condition (Figure 4–5, ϕ 's of 0.78 and 0.71) represented mean temperatures of 1,000–1,800°K (Figure 4–10) in a parallel band across the combustor from about 85–130 mm downstream from the dome. There was a toroidal flame at over 2,000°K about 165 mm downstream. This toroidal flame may be associated with the remnants of the downstream central recirculation seen in Figure 4–3. Temperatures in the dome recirculation were about 1,200°K.

At an equivalence ratio of unity the center–attached flame had the parallel band of isotherms across the combustor moved closer to the injector, and closer together, from 45–70 mm. The higher–temperature toriodal flame at 2,000°K was now a much larger flame that extended from 75–270 mm from the dome, and filled most of the combustor; it had a cooler central core extending 90–165 mm.

For an equivalence ratio of 1.50 the rich–attached flame had strong radial temperature gradients in the first 50 mm downstream, with a cool central region (less than 800°K) and temperatures in the dome recirculation of 1,600–1,800°K. These may be associated with the OH–distributions seen in Figure 4–6 showing reaction confined to the outer regions of the flow.

For the HS injector at 0.75 equivalence ratio, the fully developed, attached characteristic flame (Figure 4–4) had a somewhat different temperature distribution than that for the LS injector This was a consequence of the higher swirl of the HS injector. The central isotherms for distances closer than 75 mm were drawn down towards the injector. This was due to the influence of the central recirculation shown in Figure 4–3 and evidenced in Figure 4–8. Temperature levels were very similar to those for the LS injector. There was a central high temperature region extending from about 75–175 mm where levels were at and above 2,000°K.

At unity equivalence ratio the isotherm distribution was similar to that for the lower equivalence ratio, but everything was moved downstream, with an elevation in temperature level. This opening–up of the flame reduced the temperature gradients. Peak temperatures were attained in a toroidal region close to the centerline at 110–170 mm downstream, and peak temperature levels were close to the adiabatic flame temperature (2,263 K). The isotherms at this equivalence ratio were very similar to those for the LS injector.

For 1.50 equivalence ratio the isotherms for both injectors again looked very similar. The peak temperatures for the HS injector were on the centerline at about 150 mm, and were close to the adiabatic flame temperature. Close to the dome there were strong radial temperature gradients that agreed with the OH–distribution seen in Figure 4–6.

Comparison of Figure 4–10 and Figure 4–11 shows the influence of the stronger swirl of the HS injector in "tightening–up" the flame via velocity field changes. However, the general patterns of the isotherms were determined by the local stoichiometry distributions.

For the LS injector there were major fluctuations in temperature (400–500 deg. K RMS) existing in the regions of maximum temperature gradients, which themselves were associated with the maximum velocity gradients. These temperature fluctuations were concentrated in the initial 100 mm downstream from the dome. The effect of increasing equivalence ratio was to increase the gradients of temperature fluctuations. For the lifted characteristic flame ($\phi = 0.75$) there was also a fairly concentrated band of temperature fluctuations (150–500 deg. K RMS) from 100–150 mm downstream. The influence of increased swirl for the HS injector was to further concentrate the major fluctuations in the first 100 mm length of the combustor.

4.9 Energy Release Rates

Warren [28.] has conducted an elegantly simple analysis to extract from the temperature and velocity field data sets that were obtained at identical flow conditions, distributions of volumetric energy release rates.

To conduct the analysis, steady–state cylindrical finite difference control volumes were used. Each cylindrical control volume had four distinct sides (its cross–section) across which mass and energy transport could occur. The data fields were divided into such control volumes having widths of 1 mm and heights of 2 mm, rotated about the injector/combustor centerline. Interpolation of the data fields allowed the normal velocities at each boundary to be resolved, and the temperature of the volumes to be determined.

To estimate the mass storage term, the control volume densities were evaluated with the interpolated temperatures based on upwind differencing, and the assumptions of atmospheric pressure and the general composition of pure air. With upwinding, the vertical velocity for the considered control volume with node P, carries mass into P from the South control volume, bearing with it South–volume properties. By applying these assumptions to each side of the considered control volume, the mass fluxes were estimated from the continuity equation. A "conservation of mass error" was then defined as,

$$\% \; Error \; = \left[\frac{net \; mass \; in - net \; mass \; out}{net \; mass \; in} \right] x \; 100$$

which serves as a measure of the quality of the data.

This error check for individual control volumes filling the combustor data view volume was made for the HS injector at the equivalence ratios of 0.75 and 1.50. In general, the error in local mass balance was less than 10 percent, which is considered acceptable given the assumptions made.

Conservation of energy requires that the chemical energy supplied by the fuel be converted into thermal energy to balance a negative thermal energy storage. Unfortunately, the amount of energy that was transported through a control volume in the PW150 combustor was much greater than the amount released in that volume. Thus, even small errors in the mass balance caused severe energy "noise." To address this, the energy balance for heat release was written, with neglect of heat losses, in the form,

$$H_r = \dot{m}_{in}(h_{in}-h_{out})$$

where the incoming thermal energy was associated with the incoming mass and its enthalpy, and the outgoing thermal energy was associated with incoming mass and the characteristics of the considered control volume, (i.e., similar to upwinding). This approach conserved mass, but did not allow kinetic energies to be calculated. However, kinetic energy terms in these flows were three orders of magnitude smaller than the thermal energy terms, and so could be conveniently neglected.

The calculated local heat release rate was normalized by the volume of the associated control volumes. Comparison of the fields of volumetric heat release rate with the characteristic flame images, Figure 4–4, shows remarkable similarity. (This approach might represent a feasible alternative method of postprocessing CFD calculations to simulate flames. However, note that the maximum energy release rate sites do not coincide exactly with the visual flame envelope.) Figure 4–12 shows the comparisons; the units are *kJ / (m^3s)*. Note for the rich flame at 1.50 equivalence ratio there is a separated horizontal band of energy release at about 125 mm from the dome. This implies that unreacted and partially–reacted fuel from the initial flame region is finding an additional oxygen source for some further reaction.

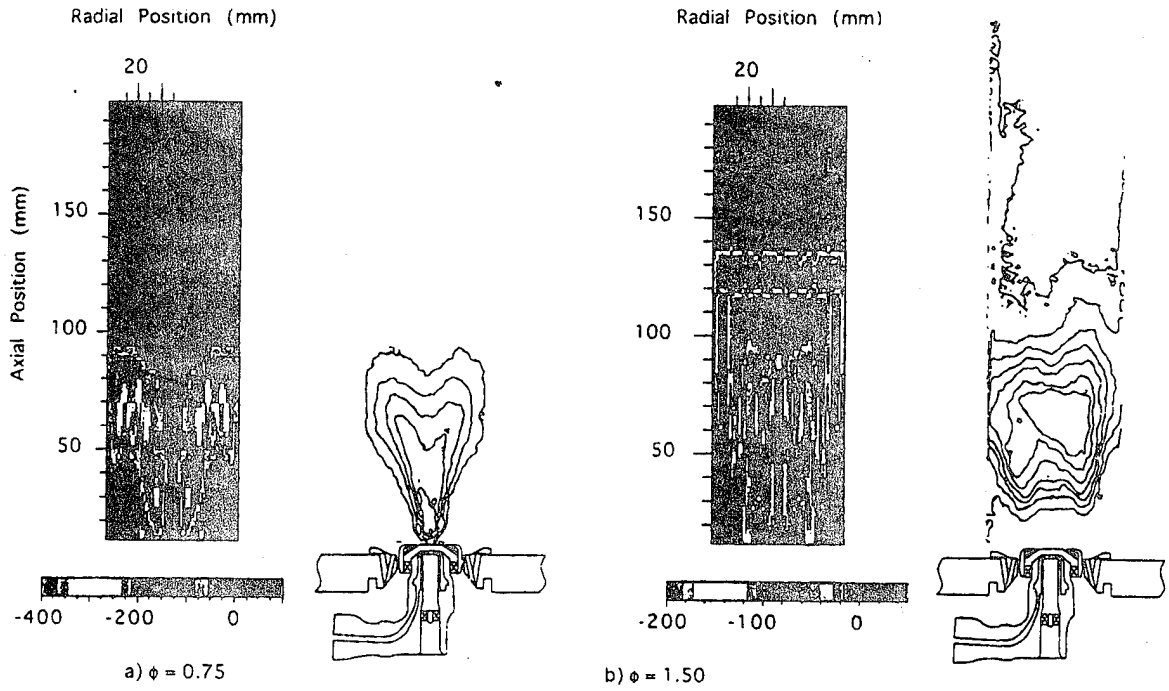

Figure 4–12. Comparison of Digitized Characteristic Flame Images with Derived Distributions for Time–Mean Volumetric Energy Release Rates for the HS Injector at Lean and Rich Conditions

Comparison of these time–mean distributions of energy release rate with the instantaneous OH–images, Figure 4–6, which represent another way of portraying where reaction is taking place, reveals good general agreement for equivalence ratios less than unity; for the rich flame however, there are some major differences. It should be remembered that OH can be persistent, and therefore can be subject to convection effects. For 1.50 equivalence ratio the OH images indicate most of the chemical reaction was taking place at greater radii than do the time–mean energy release rate results.

A comparison of the integrated energy release rate over the entire domain with the rate of energy supply can yield a combustion efficiency value. Such comparisons will not be perfect since the integrations are limited to the fields of view of the original temperature and velocity measurements, and, there was no account of radiation heat losses. The comparisons are given in Table 4–2. The value of 79 % percent for 0.75 equivalence ratio is felt to be in the correct range to be expected.

Table 4–2. Energy Comparisons for HS Injector

Phi	Thermal Energy Released, (kW)	Chemical Energy Introduced (kW)	Approx. Combustion Efficiency, %
0.75	16.3	20.7	78.74
1.50	8.9	41.4	21.50

4.10 Gas Sampling

Some very limited gas sampling was undertaken to ascertain the gas composition in the all–important step–recirculation zone. One wall of the combustor was replaced by a side–plate containing a row of small holes along a vertical centerline. A long hypodermic needle was inserted through these holes, and grab–samples withdrawn. The samples were passed to a gas chromatograph. Sampling was carried out for the HS injector in the PW150 combustor at overall equivalence ratios of 0.75 and 1.50, as well as for the PW100 combustor.

Three common sampling positions were used in each combustor, and these positions were best related to flow features observed in the combustors: Z=0 mm and R=30 mm which was very close to the origin of the attached flame in the PW100 combustor (see Figure 3–6); Z=38 mm and R=40 mm, which was inline with but considerably upstream of the step vortex center in isothermal flow in the PW100 combustor; and, Z=76 mm and R=55 mm, which was close to the step vortex center in reacting flow. In the PW150 combustor these co–ordinates corresponded respectively, to the dome cooling region, upstream in the toroidal vortex, and, downstream in the toroidal vortex (see Figure 4–3).

The major measured species are given in Table 4–3 as (dry) mole percentages. No propane whatsoever was detected in either of the combustors at any location for either of the equivalence ratios. In the PW100 combustor significant quantities of methane and carbon monoxide (partial products) were detected at the rich condition; for the lean condition with a lifted flame, only combustion products of carbon dioxide, nitrogen and depleted amounts of oxygen were measured. For the HS injector in the PW150 combustor at the rich condition, only small amounts of carbon monoxide were found in the toroidal recirculation, increasing with increase in downstream position and radial position. At the lean condition, only combustion products were measured.

Table 4–3. Gas Sampling of Major Species for PW100 and PW150 Combustors

PW100 at 1.50 Equivalence Ratio

Species	Position 1	Position 2	Position 3
CO	9.0	6.3	8.2
CO2	7.7	9.4	8.5
N2	81.1	82.4	80.8
O2	1.2	1.3	1.6
CH4	1.0	0.6	0.8

PW100 at 0.75 Equivalence Ratio

Species	Position 1	Position 2	Position 3
CO	–	–	–
CO2	7.1	6.5	7.9
N2	82.5	80.5	82.5
O2	10.4	13.0	9.6
CH4	–	–	–

PW150 at 1.50 Equivalence Ratio

Species	Position 1	Position 2	Position 3
CO	–	1.1	4.6
CO2	11.6	8.3	10.9
N2	82.5	80.9	79.6
O2	5.9	9.7	4.9
CH4	–	–	–

PW150 at 0.75 Equivalence Ratio

Species	Position 1	Position 2	Position 3
CO	–	–	–
CO2	6.5	4.2	7.1
N2	79.9	80.4	81.5
O2	13.8	15.4	11.4
CH4	–	–	–

Position 1 Z = 0 mm, R = 30 mm; **Position 2** Z = 38 mm, R = 40 mm

Position 3 Z = 76 mm, R = 55 mm.

4.11 Blowout Characteristics

Blowout data for the HS and LS injectors in isolation (no air addition other than through the dome) were collected in the PW150 combustor with an L/D of 4.9 and an outlet blockage plate of 45 %, [27.].

The blowout characteristics for the two injectors are shown in Figure 4–13 as a function of total volumetric airflow rate. The blowouts should be related to the characteristic flame shapes given in Figure 4–4 and Figure 4–5.

For the HS injector at low airflow rates (less than 500 slpm), the flame was attached at blowout; at higher airflows (greater than 500 slpm), the flame was lifted at blowout, even with the high swirl of this injector. For the LS injector the flame was always lifted at blowout for airflows down to 200 slpm. When both flames were lifted, there was essentially no difference in blowout between the HS and LS injectors. For lifted

flames, the stability was improved (at least initially) as airflow was increased. This behavior was probably due to increased turbulence with increased Reynolds number. There are suggestions in the data that for the LS injector, the improved stability was reaching its limit at around 900 slpm airflow, prior to blowout equivalence ratios again increasing with increasing airflow due to decreased residence times, [28.]. For the HS injector, the attached flame at low airflows was initially very stable (by a factor of almost 2.0), but quickly lost that enhanced stability just prior to lift at around 550 slpm airflow.

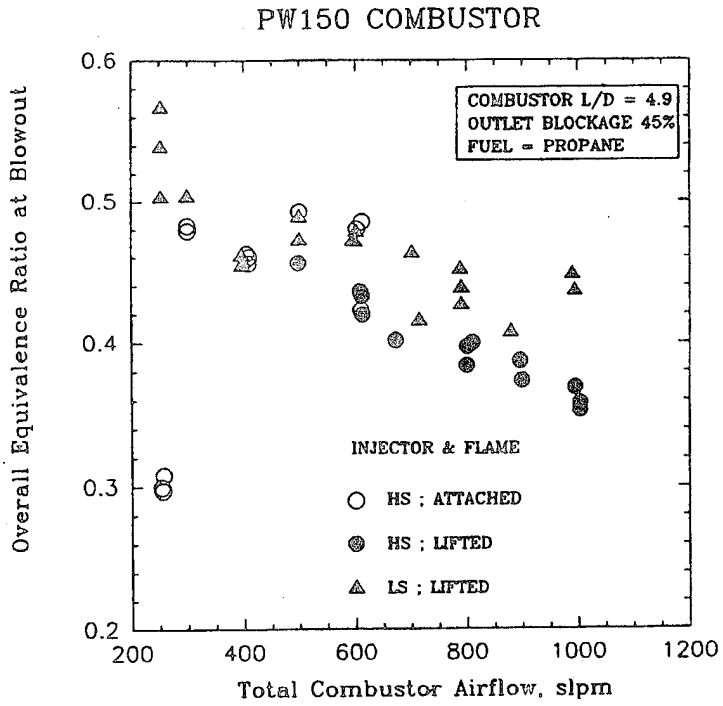

Figure 4–13. Stability Characteristics of HS and LS Fuel Injectors in the PW150 Combustor

4.12 Summary

The purpose of the PW Task 150 Combustor was to study the combustion characteristics of practical fuel injectors, and to relate this behavior to the knowledge of LBO gained in the PW Task 100 Combustor. Experimentally, the PW150 combustor with two versions (HS and LS) of an airblast–atomizing (but operated on gaseous propane) fuel injector, revealed interesting aspects of this combustion behavior, and showed the differences due to the introduction of swirl. Despite these differences, there were many similarities with the behavior observed in the PW 100 combustor.

The major effect of swirl, compared to the PW100 combustor, was a more compact flame; the more swirl, the more compact the flame. When the swirl was strong enough to generate a central separation bubble, the shape of the flame at some operating conditions was more complex than for weaker swirl; however, over a range of operating conditions, there were many similarities in flame shape and behavior. The importance of recirculation again emerged, especially that associated with the combustor step. In the case of the HS injector, the toroidal recirculation generated by the swirl was important. However, when both HS and LS injectors were operated rich, it was the step recirculation that was most important. Like the PW100 combustor, the PW150 combustor with both injectors, operated with significant nonstationary behavior of the mean flowfield that strongly influenced mass transport within the combustion region. The flame types produced and LBO performance, were controlled by the stoichiometry distributions and levels established in the dome. For both injectors, blowout, in the range of Reynolds Numbers of practical interest, was from a lifted flame condition that allowed partial premixing of separately–introduced reactants to take place prior to combustion. Therefore, there was little difference in LBO performance between the two injectors over these conditions.

SECTION 5.0
GENERIC GAS TURBINE COMBUSTOR STUDIES: TASK 200 COMBUSTOR

5.1 Intent

The primary purpose of the PW200 generic gas turbine combustor was to provide an experimental database against which lean blowout modeling of various types might be evaluated and calibrated. A secondary purpose was to develop some additional experimental insight by direct observation into the LBO behavior of the component parts and flow features, studied separately in the PW100 and PW150 combustors, when they are assembled into a practical aircraft gas turbine engine combustion system.

5.2 PW Task 200 Combustor Design

The intent of the PW200 combustor placed four major requirements on its design: First, that it be as close to a real aircraft gas turbine combustor as possible in terms of LBO characteristics and flowfield. Second, that it be flexible enough to allow sufficient variation in relevant geometry and flow distribution to afford some investigation of the important primary zone design parameters, such as equivalence ratio and residence time. Third, that adequate optical access be provided so that direct observation and application of laser diagnostics might yield details of important flow features and their role in providing stability. Fourth, that the layout be simple to avoid geometry complications when attempting to model the combustor. These requirements were rather stringent, and exerted a strong influence on the design approach and configuration selected.

The aerothermodynamic design of the annular combustor that served as the reference for the PW200 combustor, was based on Pratt &Whitney commercial engine design practice circa 1985, which was current practice when this contract was started. For the PW200 combustor the configuration adopted was a four–injector, planar–section, simplified–geometry version of the reference combustor. This configuration represented the best compromise between flow realism, optical access and geometric simplicity, while being commensurate with the air supplies available. The fundamental rig design to accommodate this combustor was carried out by United Technologies Research Center (UTRC), with subsequent on–site modifications made by Wright Laboratory to improve handling, access and window durability. The rig design attempted to incorporate as much flexibility as possible.

Figure 5–1 shows a cross–section of the PW200 combustor rig. The fuel injectors were either the LS or HS injectors described above, incorporating the modifications for gas operation; all of the LBO work to be described was carried out with the LS injector set. The upper shroud, dome, and lower shroud air flows were separately–metered and isolated from one–another by means of sonic venturis. Shroud by–pass valves allowed the levels of liner convective cooling to be set independently of the flows passing through the liners. Upper and lower liners were removeable, permitting the air port arrays to be changed as desired. Two domes were available, one a plain bulkhead and the other a vertically–symmetrical configuration having filleted upper and lower corners, as illustrated in Figure 5–1. Dome cooling was provided by means of impingement jets, with the spent dome cooling air being discharged at the dome/liner interfaces as a liner film. Ignition was by means of a hydrogen–fueled torch–ignitor mounted in the dome.

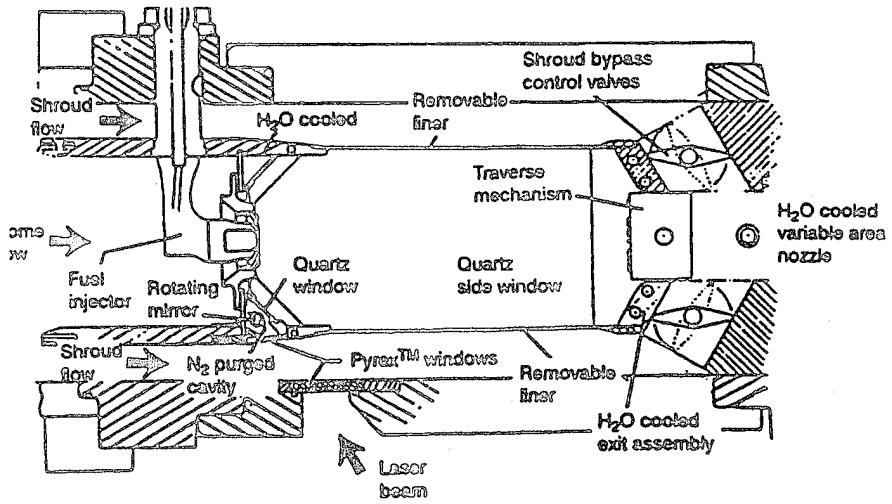

Figure 5–1. Diagrammatic Cross–Section of PW200 Combustor Rig Test Section

The distance between fuel injectors was 7.62 cm and the height between liners was 9.91 cm, while the length of the combustor was 20.83 cm from the fuel injector face to the exit nozzle entrance. The diameters of the liner air ports in the three rows of air addition were 0.635, 1.303 and 0.897 cm respectively, from front to rear, with a lateral spacing between ports in each row of 3.81 cm. Ports in a given row were staggered half a port pitch relative to adjacent rows, while the ports in each row of upper and lower liners were directly opposed. The ports in the first row were positioned with a port directly inline with a fuel injector. The spacings between rows of ports were as follows: first to second, 4.267 cm; and, second to third, 3.962 cm; the centerlines of the first row of ports were positioned 4.902 cm downstream from the injector faces. The port configuration was plain, circular holes.

Figure 5–2 shows the flow distribution in the combustor rig. Careful *in situ* measurements were made of the discharge coefficients for the dome, liner ports and fuel injectors. The measured effective areas for the liner air ports, top and bottom respectively, were as follows: first row – 1.516 and 1.632 cm^2; second row – 4.968 and 5.394 cm^2 and, third row – 2.845 and 2.852 cm^2. The total effective area of the dome was 8.652 cm^2 and that of the fuel injector air passages was 5.929 cm^2 (total of four injectors).

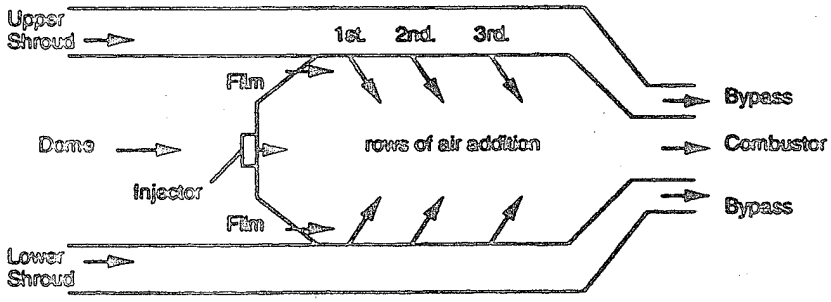

Figure 5–2. Flow Distributions in the PW200 Combustor

Direct optical access to the combustor for visualization and laser diagnostics was provided primarily by the side–walls enclosing the four–injector section. These side–walls were of fused quartz, and were contained in water–cooled housings. Two thicknesses of side–wall were available: 1.905 cm for operation at internal pressures up to 449.2 kN / m^2, and 0.318 cm for operation at atmospheric pressure.

A further optical path was provided by windows in the base of the rig (Figure 5–1), that allowed laser beam access to a high–speed rotating mirror contained by the dome lower fillet–piece, and extending across the width of the dome. Through selectively–opened vertical slits in the dome, the rotating mirror could scan the combustor with vertical, planar sheets of laser light for imaging purposes. For thermal protection, the mirror cavity was purged with a small, pressure–balanced and continuous flow of gaseous nitrogen.

In addition, special upper and lower liners made of fused quartz sheet were available to replace the metal liners and so allow direct vertical access to the reacting flow. These quartz liners contained the hole pattern described above to permit normal combustor operation with them present.

5.3 Rig and Facility

The rig was mounted horizontally in a test cell (Room 20) of Wright Laboratory, Wright–Patterson Air Force Base, Dayton, Ohio, where the LBO tests and laser measurements were conducted by Wright Laboratory personnel. The facility and rig provided flow, metering and control, of air, fuel, nitrogen and cooling water to the PW200 combustor; combustion products were collected and exhausted from the cell by means of existing ducting. A schematic flow path for the rig and facility is given in Figure 5–3.

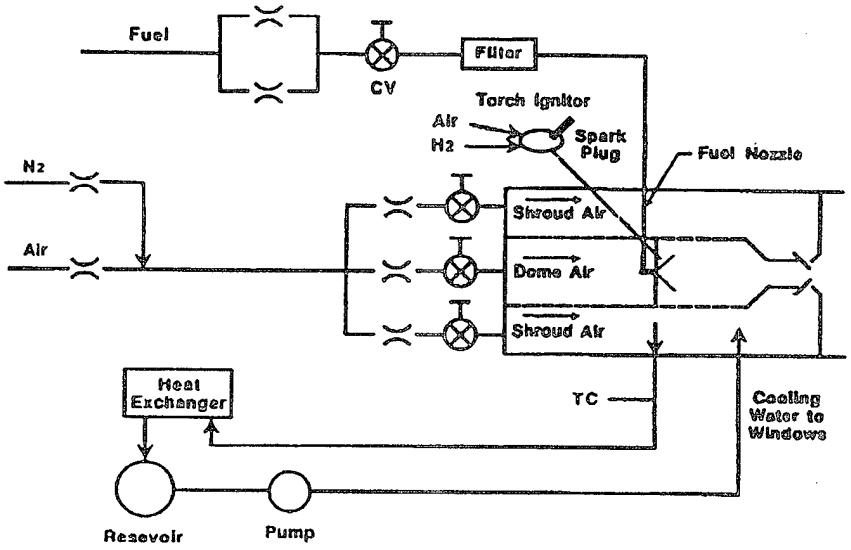

Figure 5–3. Schematic Flow Path of Rig and Facility

The PW200 combustor used the excess nitrogen dilution technique to simulate subatmospheric pressures, as described above (Section 3.4). A high–pressure bottled supply of gaseous nitrogen was used for this purpose.

The PW200 combustor, the rig and facility, are described in Reference 30, which is contained in Appendix J.

5.4 Temperature Fields

Measurements were made of mean and fluctuating temperatures in the PW200 combustor using a hardened LDA/CARS system that was mounted under and on either side of the test section, and used the rig side windows for access, [30.].

The CARS system is described in detail in Reference 31, and briefly as presently used, in folded BOXCARS geometry, in Reference 32, which is itself contained in Appendix K.

The accuracy of the CARS temperature determination was estimated to range between 10 percent at near–room temperatures and 5 percent at near–stoichiometric flame temperatures, with the largest

contribution to uncertainty resulting from shot–to–shot variation in the Stokes–laser spectral distribution. Since it took considerable elapsed time to acquire adequate data for extensive mapping, repeatability was not determined by the CARS system, but by the constancy of the combustor air and fuel flow rates, and the precision with which a selected operating condition could be set and held. During operation both the fuel and air flows were continuously monitored, and were electronically controlled to within 5 percent.

It proved to be difficult to take CARS measurements over extensive regions of the combustor. In probing the central regions of the combustor, i.e., between the central pair of injectors, unreliable results were obtained because of insufficient CARS signal strength. The lack of signal strength was found to be due to turbulent beam–steering as the laser beams passed through the flows associated with the near–pair of fuel injectors. The beam steering was sufficient to prevent the essential overlap of the CARS pump and Stokes beams. Also, holes were burned in the combustor windows by the laser beams when the high intensity laser beam focus volume was approached too close to the side windows. The result of these two difficulties was the placing of rather severe constraints on the allowable extents of the measurement fields.

With the constraints on the possible measurement grid, a horizontal plane through the centerline of all four injectors (y = 0 cm) was selected. This plane extended transversely across the combustor from the axis of symmetry (x = 0 cm) to 11 cm towards the near–side (to the laser beam sources) combustor wall. It extended axially (z–axis) from 1 – 15 cm downstream from the combustor dome. This area was covered with a 1 cm square measurement grid. An additional, smaller, transverse grid was applied normal to the horizontal grid at z = 5 cm, approximating the position of the first row of combustion air jets. The width of this vertical plane extended from x = 0 to x = 7 cm; thus, the second fuel injector centerline was near its center. Again, a 1 cm square grid covered the region of this plane for 3 cm above and below the horizontal plane. Figure 5–4 illustrates these measurement planes.

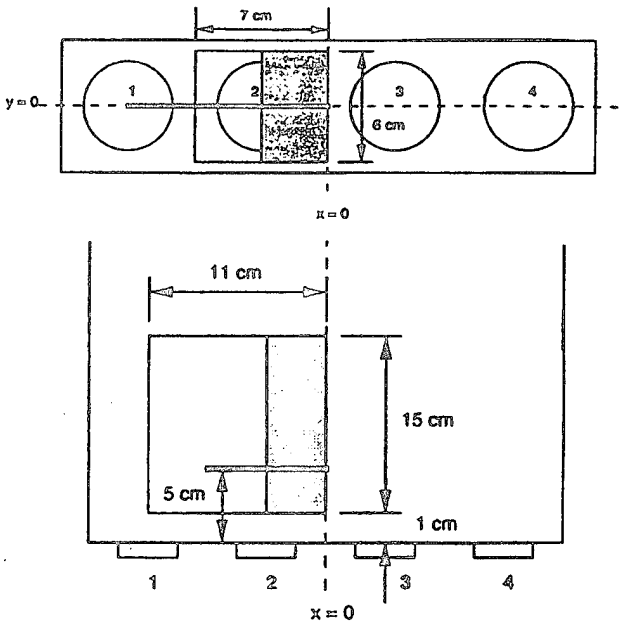

Figure 5–4. Measurement Planes for CARS Data, Showing Regions of Valid Data Free From Spurious Side–Wall Effects

With the measurement grids established, it was necessary to determine where on these grids valid data could be obtained. Valid data in this sense refers to data that was not affected by aerodynamic effects due to the combustor end–walls. End–wall effects were found inside the combustor due to flows interior to the combustor, and inside the combustor due to flows in the shrouds affecting jets penetrations. Details of

this determination are given in Reference 32. When the spurious, side–wall affected, data were removed from consideration, only fields between injectors 2 and 3 could be considered as being reasonably representative of the real combustor. The narrow regions of valid data are represented as the shaded areas in Figure 5–4.

As is to be described below, the normal operating mode of the combustor at lean blowout was a lifted flame. However, an attached flame condition could exist, [30.], and it was interesting because of its quiet operation and improved stability. It was therefore decided to make the temperature measurements to include this attached flame condition.

A typical engine combustor dome flow was 15 % of the combustor air, so this was selected for the temperature measurements, and at this condition a primary zone airflow rate to produce an attached flame was selected from the map below. The total combustor airflow (all four injectors) was 0.7383 lbm/sec. (0.3350 kg/sec.), with a primary zone airflow (see below for definitions) of 0.1422 lbm/sec. (0.0645 kg/sec.); there was no excess nitrogen used, and the fuel was gaseous propane. Observations of the combustor in operation indicated that the normal lifted flame became an attached flame at 0.69 primary zone equivalence ratio, and that the combustor blew out for this airflow at just less than 0.60 equivalence ratio, from an attached flame condition. CARS measurements were taken for a propane flow rate of 0.35 lbm/min. (0.1588 kg/min.).

The combustor loading for these conditions was a low one so that the flame holding was confined to the primary zone. The flame produced was not an attached flame in the region of valid data. It was an attached flame only at injectors number 1 and 4; at injectors number 2 and 3 it was a lifted flame. The effect was traceable to the sidewalls. The attachment was due to the steeper angle of the first row combustion air jets forcing air from the jets upstream into the injector jet, as is to be described below.

Figure 5–5 shows the measured mean isotherms on the horizontal (to the left of the figure) and vertical (to the right of the figure) cross–sectional planes, placed with the horizontal center of the vertical plane at its correct downstream position (just downstream of the first row of air jets) and the vertical center correctly aligned with an injector centerline. The vertical plane is viewed from the rear of the combustor. Super–imposed on the horizontal plane are the temperature pdf's at each measurement point in the plane. Note that the measured data in the horizontal plane for the right–hand–side of injector number 2 have been flipped to the left–hand–side also. The symmetrical image so–formed makes it easier to understand the temperature field for a single representative, (see Figure 5–4), injector. While this is convenient, it should be remembered that the effects of swirl introduce some asymmetries in reality. For the LS injectors the effective swirl strength is low, (see Section 4.3), so that any asymmetries would not be especially large. The data in the vertical plane are not flipped.

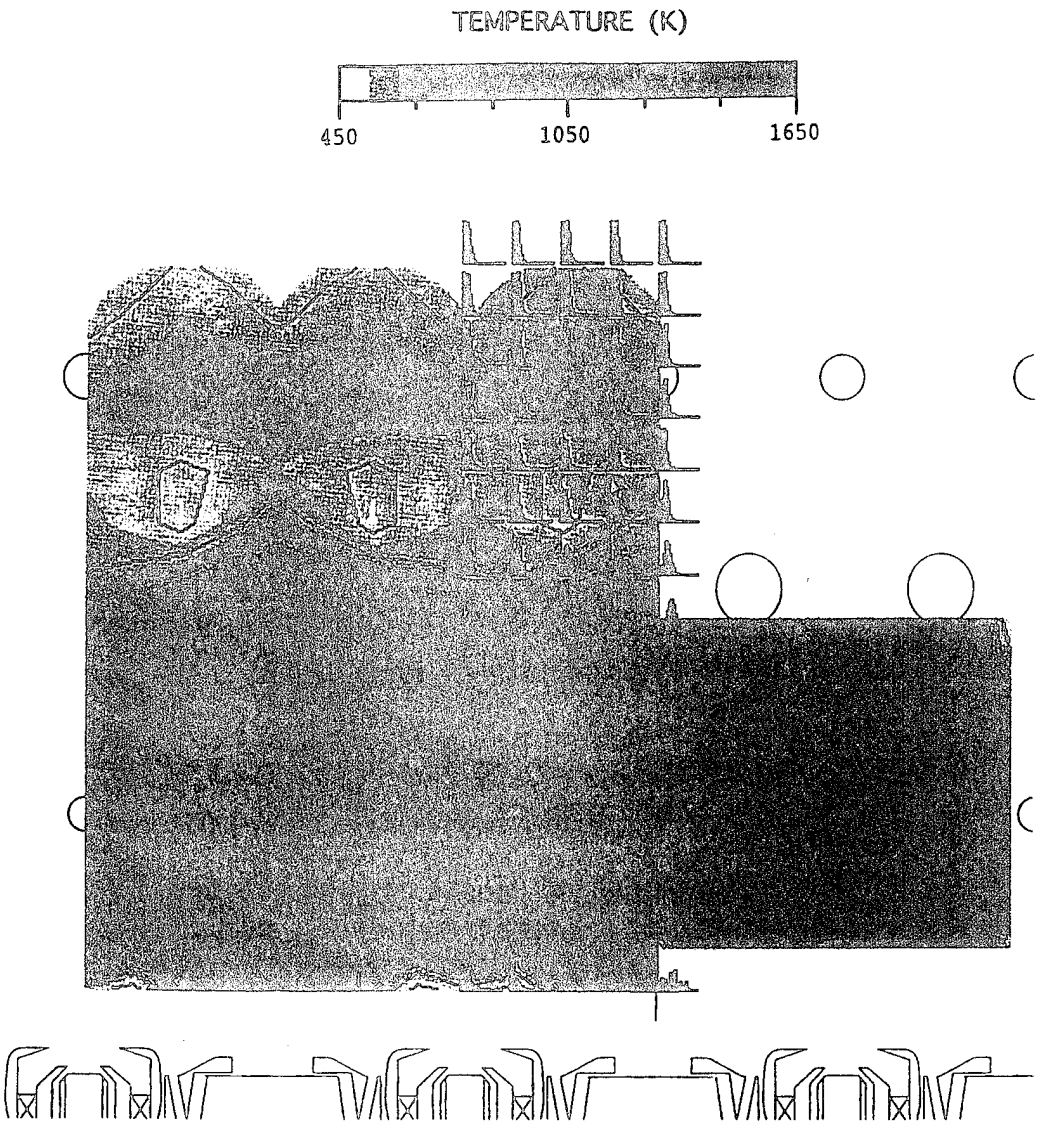

Figure 5–5. Isotherms of Measured Mean Temperatures for a Lifted Flame at Near–Blowout In the PW200 Combustor

The flame shown is a lifted one. On the horizontal plane the peak gas temperatures of around 1500°K were reached inline with the fuel injectors at 5–6 cm downstream, and could be clearly associated with recirculatory action of the axial swirling fuel/air jet from the injector at its confluence with the colliding opposed combustion air jets of the first row, that were inline with the injectors. The equivalence ratio of the swirling axial fuel/air jet is such, (see Table 4–1), that some jet–air is needed for combustion to take place.

In the vertical plane an asymmetric region of high temperatures (about 1350–1400°K) could be identified as flow of the axial injector jet dividing as it moved around the blockage formed by the colliding combustion air jets. Regions of high temperature (about 1300°K) were moved laterally at midcombustor height following the spreading due to combustion air jet impact. It should be noted that, inline with the injectors, the penetration of the lower combustion air jet was not so evident as that for the upper air jet in this ($z = 5$ cm) plane. This might be related to the top to bottom hole effective area differences, (see Section 5.2), and indicated different jet trajectories, top to bottom of the combustor, (bottom jets have greater effective

area.) It can also be observed that between injectors, both combustion air jets can be seen at this plane, but again, the lower jet appeared to have lesser penetration than the upper one.

Note the downstream displacement of temperature events on the central horizontal plane at the position of the first row of air ports due to the initial jet trajectory angles not being normal to the liner surfaces. The hot gases that initially moved laterally from inline with the injectors then entered a reverse flow region between the injectors. They were mixed with jet air and recirculated back upstream to the combustor dome at temperatures about 1150–1200°K.

Temperatures downstream of the first row of combustion air jets were fairly uniform on the central horizontal plane at 1000–1200°K, until the second row of combustion air jets was encountered. Combustion was essentially over on the center plane when the second row of combustion air jets were added, with temperatures falling to less than 800°K downstream of them.

The flow from the injectors was initially cold at inlet temperatures. Temperature increased radially outwards from the injector centerlines as the insert swirler jets entrained the hot gases recirculated to the dome from downstream. For less than 2 cm downstream the local temperatures in the interior of these jets was about 750–800°K. By 2–3 cm downstream temperature rise was evident on the centerline of the injector jets. This appeared to be induced by the interaction with the combustion air jets, and did not propagate from the peripheral shear layers associated with the insert swirler jets.

At the conditions for this test the equivalence ratio of the flow emerging from the fuel injector was 1.488, (using the LS injector effective areas), and with account of all of the insert swirler air it would have fallen to 1.159. All of the insert air would not have been involved however, so the additional air for combustion had to be provided by the reverse flow of combustion jet air from the local recirculation at the jet confluence. (Compare with Figure 4–10D) for the PW150 combustor where the LS injector had no transverse combustion air jets with which to interact.) If this was so, then the reverse flow of combustion air penetrated upstream on the order of 2–3 cm on the centerline of the injector jet. Such a penetration would introduce an increased radial velocity component into the injector jet, causing the jet to open in angle.

The temperature pdf's in the region of the injector were skewed towards the lower inlet temperature, with evidence of strong intermittency towards the jet edges. In the downstream region where the bulk of the heat release took place, the probabilities were more symmetrical about the mean temperatures. For the dome recirculation zones they showed broadened peaks indicating near–equal probabilities of a wide range of temperatures as poorly–mixed combustion products and unreacted or partially–reacted combustion air and fuel were returned together towards the dome region by the reverse flow. The isotherms indicate that some chemical reaction took place in this recirculating flow.

Figure 5–6 shows the fluctuating temperatures expressed as a local intensity. Highest temperature intensities, 40–50 percent, were encountered on the centerline of the injector jet, and in the flow recirculated back to the dome. Intensities in the insert jets were about 30 percent, and rose to 36–38 percent in the periphery of the fuel injector jet as it divided about the combustion air jets. In the reverse flow region immediately upstream of the first row combustion air jets (where the highest temperatures were attained) the intensities were 30 percent or less. Downstream of the second row of combustion air jets the temperature fluctuations increased to give intensities of 32–36 percent.

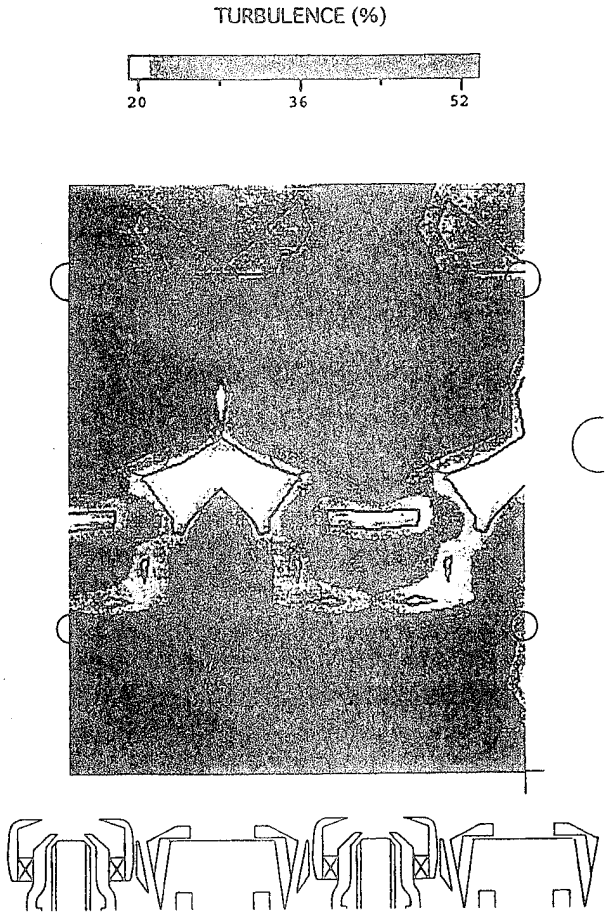

Figure 5–6. Isotherms of Measured Fluctuating Temperatures for a Lifted Flame at Near–Blowout In the PW200 Combustor

The attached flame was produced by air being strongly recirculated upstream in the injector jet from the first row combustion air jets. This was a much more vigorous effect than for the lifted flame. It resulted from a change in combustion air jet trajectory to near–vertical that occurred when the jet dynamic head became high, either by increased airflow or by side–wall interference effects in the shroud at fairly high airflows. The temperature distribution was similar in some respects to that for the lifted flame, but temperature events were markedly shifted upstream.

For the attached flame condition the axially–moving fuel/air jet flow reached 1250°K on the injector centerline within the first centimeter downstream from the injection plane, and the peak 1500°K temperature was attained within 2 cm. There was a widened "spray angle" and increased radial temperature gradient. The first row combustion air jet inline with the injector penetrated to the combustor centerline almost vertically, with only half a hole diameter downstream displacement on the centerplane. This is clearly evident in the isotherms. It was this increased airjet penetration at higher combustor airflow rates that drove the small internal recirculation region formed at the three–jet confluence, further upstream into the swirling fuel/air jet. This provided sufficient air for combustion within the jet itself, and increased the radial velocity component that resulted in a wider angle flame. Figure 5–7 shows mean temperature isotherms for the attached flame; only one–half of the structure is shown in this instance.

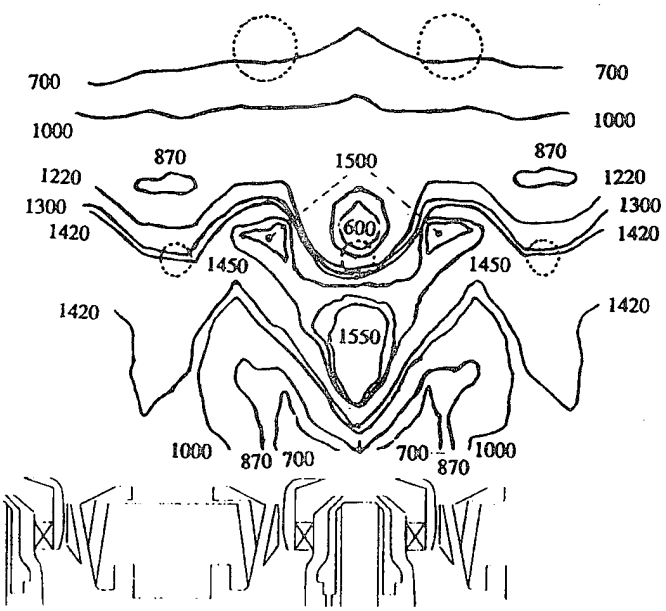

Figure 5–7. Isotherms of Measured mean Temperatures for an Attached Flame at Near Blowout in the PW200 Combustor

5.5 Flame and Blowout Characteristics

Blowout characteristics of the PW200 combustor with the LS injectors and using gaseous propane as fuel, were described in Reference 30, which is attached as Appendix J. The excess nitrogen technique (see Section 3.4) was used to simulate subatmospheric pressures, and together with a range of combustor airflows at ambient inlet temperatures, to vary combustor loading. The flexible capabilities of the rig (see Sections 5.2 and 5.3) were used to vary the dome flow for the filleted dome, from 10 to 20 percent of the combustor total airflow. The shroud by–pass valves were set to an appropriate position for sufficient convective cooling of the liners at low airflow rates, and were then held fixed. The hole pattern in the liners was that described above in Section 5.2.

For zero excess nitrogen and 15 percent dome flow, the blowout equivalence ratio increased with increasing primary zone airflow and eventually showed two different flame characteristics, a normal "lifted flame," and at high airflows, an "attached flame." This behavior was similar in appearance to that seen in the PW100 combustor (Section 3.5) and in the PW150 combustor (Section 4.5). However, its cause in the PW200 combustor was quite different from that in the PW100 combustor. For the LS injector the attached flame condition in the PW200 combustor was related to the characteristic flame shape seen at around 1.11 equivalence ratio for the injector alone in Figure 4–5, but was more robust (present for a wider range of equivalence ratios) than that figure would suggest.

The attached flame in the PW200 combustor was connected with the injector local stoichiometry distribution, just as in the PW150 combustor. However, that distribution was modified by the PW200 combustor aerodynamics, as described above from the temperature measurements, to give the attached flame. The modification was brought about by relatively small changes in the trajectory of the first row of combustion air jets. Increases in total combustor airflow resulted in increases in the pressure drop across the combustor liners because of the fixed position of shroud by–pass valves. The increased liner pressure drop made the first row of combustion air jet enter the combustor at an increasingly steep angle. Since the

first row of air jets were extremely close–coupled with the strongly–coherent fuel/air jets that flowed axially from the injectors, the local stoichiometry was driven into the flammable range by these jet changes.

As the attached flame appeared there was a small improvement in stability, and the combustion noise was noticeably reduced. Figure 5–8 shows this stability behavior at atmospheric pressure for the 15 percent dome flow case. Note that the attached flame appears for a primary zone airflow of 0.0576 kg/sec. (0.127 lbm/sec.). The appearances of the respective flames can be deduced from the isotherms displayed in Figure 5–5 and Figure 5–7. Photographs of the the two flame conditions are displayed in Figure 5–9. For these operating conditions both flames were confined to the primary zone. With reference to Figure 5–2, the airflow distributions were defined as below:

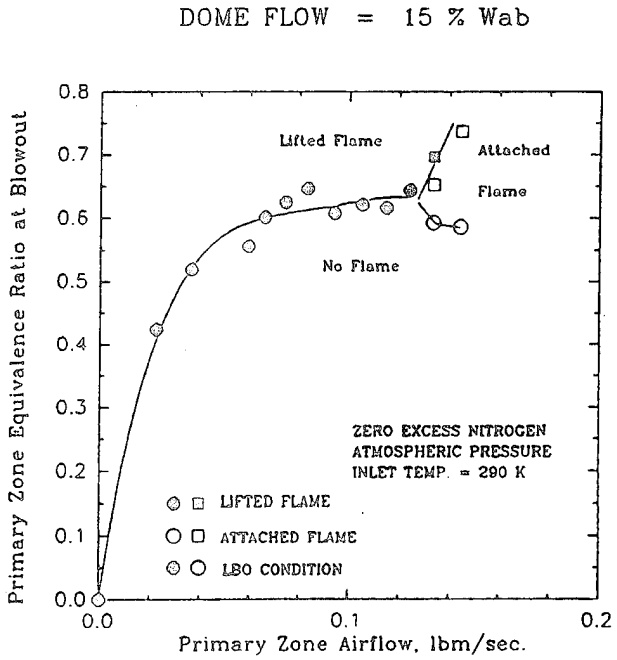

Figure 5–8. Influence of Primary Zone Airflow on Flame Type and Blowout at Atmospheric Pressure for 15 Percent Dome Flow

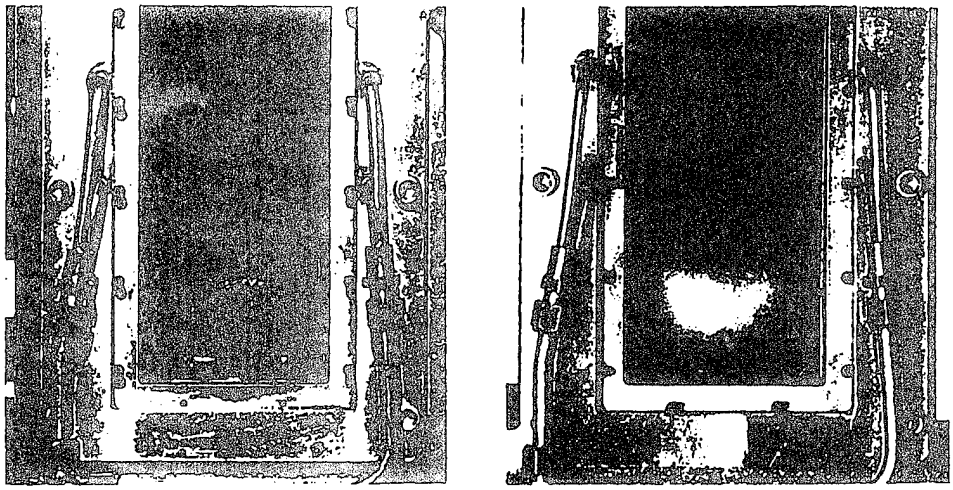

Figure 5–9. Photographs of Lifted and Attached Flame Conditions

The combustor total airflow was defined as the sum of the metered dome flow and the calculated jet flows based on measured pressure drops and the pre–established hole effective areas, i.e.,

$$W_{ab} = W_{dome} + W_{jets}$$

The dome flow was made up of the injector, insert swirler jets and dome cooling flows, i.e.,

$$W_{dome} = W_{injectors} + W_{inserts} + W_{cooling}$$

The primary zone airflow consisted of the dome flow plus 27.9 percent of the first row jet air. This value of primary zone–active jet air was established separately [5.] for the particular primary zone aerodynamic flow pattern used. Thus,

$$W_{P.Z.} = W_{dome} + 0.279 W_{1st.jets}$$

For a particular run, flow split information was established at the set point without combustion, prior to each blowout test point.

When Figure 5–8 was repeated for the 15 percent dome flow at the same residence time, (corrected to zero excess nitrogen conditions), but for 0.4 atmos. equivalent pressure, the attached flame and the accompanying local improvement in stability were not observed in the flow range up to 0.066 kg/sec. (0.145 lbm/sec.) primary zone airflow, as Figure 5–10 shows.

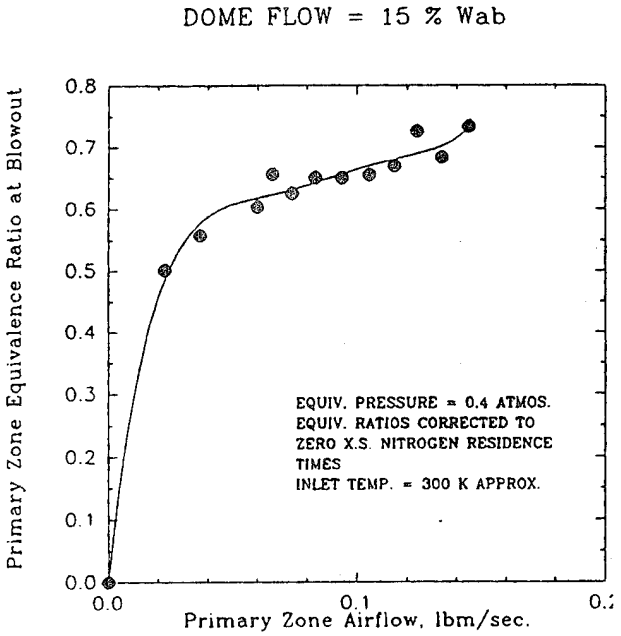

Figure 5–10. Influence of Primary Zone Airflow on Blowout at 0.4 Atmospheres Equivalent Pressure for 15 Percent Dome Flow

The attached flame was most prevalent for the 10 percent dome flow case, and least prevalent for the 20 percent dome flow case. The higher dome flow resulted in an increased mean dynamic head to which the combustion air jets were subject. When the attached flame was established, it would exist as fuel flow rate was reduced, and blowout would take place from the attached condition. The effects on stability and noise

were substantial, as Figure 5–10 illustrates for stability. In the figure the overall (combustor) equivalence ratio was plotted against an overall loading parameter. The loading parameter is defined in general in Section 3.7, and here the volume is the total combustor volume and the mass flow rates are also totals for the combustor.

For the 10 percent dome flow case the two flame types that can exist produced dual LBO limits over a range of combustor overall loading parameter, that depended on flame type, as can be seen in Figure 5–11. Therefore, the stability depended on how the loading was achieved (based on Figure 5–8 and Figure 5–10). Thus, if the loading was achieved at atmospheric pressure by means of high airflow, then attached flames would be produced and stability was enhanced; if the loading was achieved at low airflow with high excess nitrogen, i.e., low equivalent pressures, then lifted flames would be produced and stability was reduced. This behavior arose as a consequence of how the combustor was operated, and the close–coupled primary zone design.

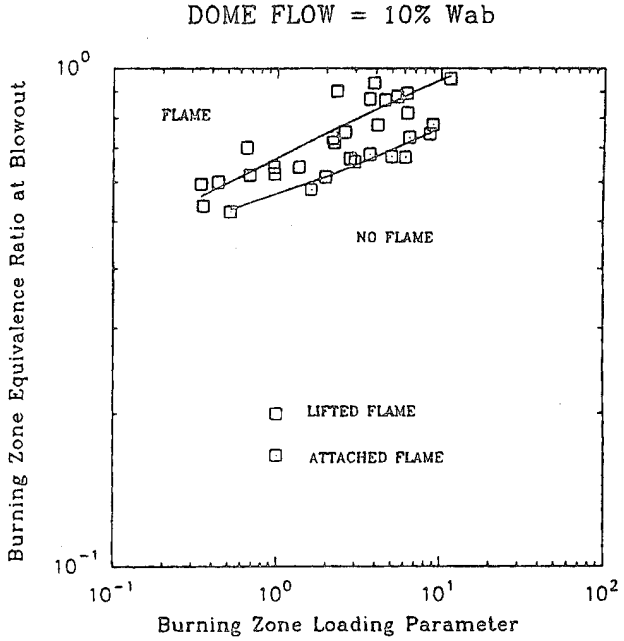

Figure 5–11. Influences of Dome Flow on PW200 COmbustor Stability, Showing the Effects of Flame Type for Primary Zone Burning

The flame structures described have all been confined to the primary zone. However, as combustor loading was increased beyond about 10.0 *lbm/sec. ft^{3}atmos^n* at 400°K for the 10 percent dome flow case, the flame was observed to expand beyond the primary zone as defined above. This was because of reduced residence time or inadequate oxygen, or combinations of these, at the higher loadings. Flame was seen stabilized on the combustion air jets. For jet–stabilized flames, the blowout equivalence ratio became independent of both flame type (attached or lifted) and dome flow. This independence is not surprising.

This characteristic is illustrated in Figure 5–12 for a fixed burning zone airflow of 0.0454 kg/sec. (0.10 lbm/sec.). A "burning zone" was defined as the region in which flame existed. Thus, for primary zone flames it was the primary zone; for extended flames involving the first row of combustion air jets the burning zone included all the first row combustion air and the combustor volume containing them in addition to the primary zone; and so on, as the flame expanded further at still higher loadings.

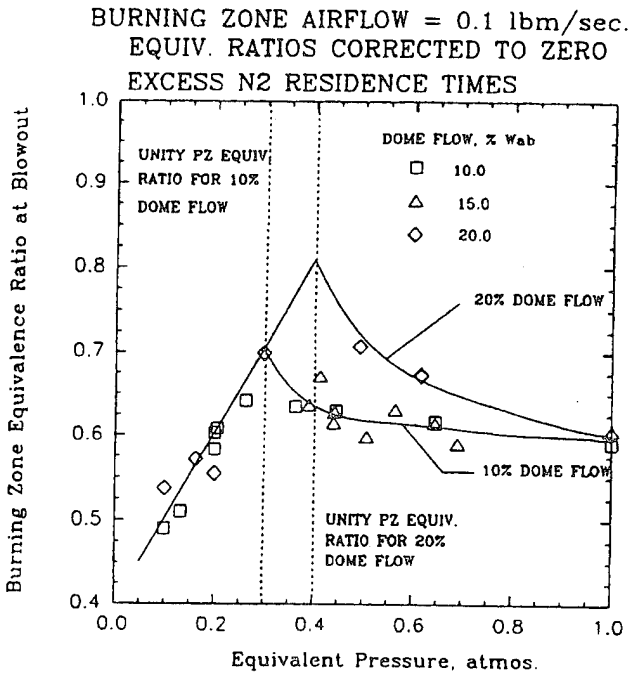

Figure 5–12. Effect of Equivalent Pressure on Blowout at Fixed Airflow for 10 and 20 Percent Dome Flows, Showing Primary Zone Burning and Jet–Stabilized Burning

It can be seen from Figure 5–12 that increased dome flow had an adverse impact on stability for primary zone burning, and, that stability was lost as equivalent pressure was reduced. However, for jet–stabilized flames, blowout was independent of dome flow; for these flames blowout was improved as equivalent pressure was further reduced. The changeover from primary zone burning to jet–stabilized burning occurred when the bulk equivalence ratio in the primary zone reached and exceeded a value of unity.

The expanding flame with increased combustor loading produced a saw–tooth stability curve as flame–holding was progressively transferred down the combustor from jet–row to jet–row. This is illustrated in Figure 5–13 for the 10 percent dome flow combustor. It will be noted from this figure that by this means the maximum value of overall combustor loading attainable (peak heat release rate) was extended to very respectable values, of the order of 60 *lbm/sec. ft*^{3} *atmos.*^{n} at 400°K. This is the same kind of performance that could be expected from a spherical well–stirred reactor, [33.].

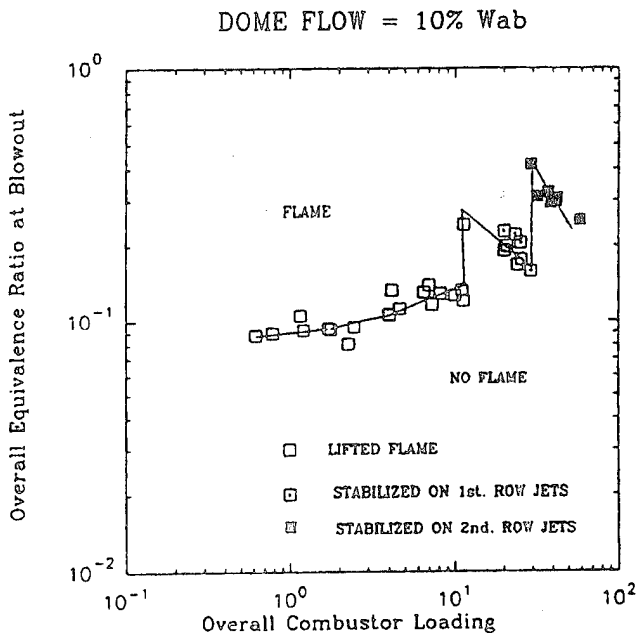

Figure 5–13. Stability Characteristic for the 10 Percent Dome Flow Combustor, Showing Extended Flame Holding on Transverse Air Jets

For increased dome flows, the overall loading at which the flame moved out of the primary zone was increased, but the rate of increase in overall equivalence ratio with loading was greater (Figure 5–11) so that there was a loss in peak heat release rate capability.

5.6 Summary

The stability and flame behavior of the PW200 combustor had many features that were observed in the PW150 combustor. By means of comparison, the PW150 combustor results enabled the interaction effects of the LS injector flow with the PW200 combustor fluid dynamics to be ascertained. The basic understanding of the effects of recirculation on stability obtained from the PW100 combustor contributed greatly to interpreting the behavior in the PW200 combustor. The common feature of all the combustors was the flame–lift that took place at overall equivalence ratios less than unity.

The major aerodynamic feature of the PW200 combustor that emerged was the extremely close coupling that existed between the discharge of fuel and air as a semi–coherent jet from the LS injector, and the first row of transverse jets supplying combustion air. Relatively small changes in the transverse jet trajectories exerted significant impacts on flame type, combustion noise and stability over a range of combustor loadings for which the flame was stabilized in the primary zone.

The amount of air introduced in the dome region exerted a strong influence on the stability, with a loss in stability occurring as dome airflow was increased. For lower values of dome airflow the flame expanded as combustor overall loading was increased, and flame holding was transferred from the primary zone to the transverse airjets. The multiple flame–holding characteristic of rich domes extended the peak heat release capability of the combustor to loadings that were comparable to that of spherical well–stirred reactors.

SECTION 6.0
MODELLING CONSIDERATIONS

6.1 Intent

The modeling effort fell into four parts: First, modeling in support of the experimental portion of the program, to provide suitable correlation groups for comparison purposes. Second, phenomenological modeling of LBO to provide simple analytical expressions to be used in quick assessments of stability for preliminary design purposes. Third, mathematical modeling of LBO to provide *a priori* calculation procedures of LBO for new combustor designs. Finally, a hybrid modeling procedure involving mathematical modeling of fluid dynamics with uncoupled treatment of the chemical kinetics.

6.2 Modeling for Data Correlation

A traditional approach that is commonly used for correlating experimental LBO data is the so–called air loading parameter, defined in original form as,

$$ALP = \frac{\dot{m}_{air}}{VP^2}$$

The form of the ALP comes from a consideration of perfectly–stirred reactors, [34.]

For gas turbine engines use of this expression arises from the assumption that flame is stabilized in the primary zone of the combustor, and that the primary zone may be treated as a single, well–stirred reactor, (WSR). This approach was suggested by Bragg [18.]. Later modifications recognized the influence of reactant inlet temperature, and that imperfect mixing/aerodynamic/heat loss effects could influence the value of the reaction order. ALP became modified to,

$$ALP = \frac{\dot{m}_{air}}{VP^{1.8}F}$$

where,

$$F = \frac{10^{0.00143\ T}}{3.72}$$

The reduced apparent reaction order and the exponential temperature correction to 400°K reflect the experimental WSR work of Longwell and his coworkers, [20.].

Later, Kretschmer & Odgers [19.] realized that the apparent reaction order for a global equation seeking to represent the complex actual reaction mechanism for hydrocarbon/air systems at blowout conditions, would be a variable. For LBO's, they modified the ALP to,

$$ALP = \frac{\dot{m}_{air}}{VP^n F}$$

where,

$$n = 2\phi_{LBO}$$

For correlating LBO data in the PW100 combustor, where the gaseous propane fuel and excess gaseous nitrogen diluent exert a noticeable effect on residence time, the Kretschmer & Odgers form of ALP was modified to a general loading parameter,

$$LP = \frac{\dot{m}_{Tot}}{VP^n F} \qquad (6.1)$$

where,

$$\dot{m}_{Tot} = \dot{m}_f + \dot{m}_a + \dot{m}_{N2} \qquad \text{and,}$$

$$n = 2\,\phi_{LBO} \,/\, (1 + \dot{m}_{N2} \,/\, \dot{m}_a)$$

The use of LP as the basis for correlating experimental data was considered appropriate for the PW100, PW150 and PW200 combustors because of the lifted flames observed as blowout was approached, (see Sections 3.5, 4.5, 4.11, 5.4 and 5.5). The lifted flames in these combustors would have allowed some premixing prior to reaction, even though the fuel and air in each case were introduced into the combustors separately. Therefore, the flames in these combustors could be considered, to first order, as being "well–stirred" to some significant degree.

Equation 6.1 can be applied to combustors in two ways: First, to describe the behavior of a single reaction zone. In this usage the volume V has to be related to the actual volume within which heat release occurs, and this has to be determined in some way. Generally, this form is more conveniently used for geometrically simple combustors, such as the PW100 combustor, (see Appendix G). Second, Equation 6.1 can be used for complex combustors, such as the PW200 combustor, when it is applied in an overall sense so that LP includes the redundancy of the dilution zone. In this usage the volume V is the total volume and the mass flow rates are also totals. Thus, it is easy to calculate the combustor loading. When used in this latter form the comparison of LBO performances for two or more different combustors invokes the implicit assumptions that dilution zones are essentially the same for all combustors, and that the flame–holding in all combustors is concentrated within the primary zone in every operating instance. Section 5.5 illustrates the weakness of this usage.

6.3 Phenomenological Modeling

Many of the modeling concepts for local flame extinction have been derived from studies of lift–off and blowout in simple, turbulent, diffusion jet–flames. The perceived behavior of such flames can be characterized by two generalized views [35.] – premixed flame propagation, and diffusion flamelet theory.

The diffusion flamelet theory involves the subjection of laminar diffusion flamelets to high strain rates; the laminar flames consist of a thin chemical reaction zone between fuel and oxidant. Flow processes lead to stretching of the flame, and through the velocity gradient tend to increase the local, instantaneous strain rate. Strain rate is then proportional to composition and conserved scalar gradients. Local extinction is assumed to occur when the instantaneous strain parameter exceeds a critical value. The instantaneous scalar dissipation rate is a typical measure of the effects of strain. It represents the inverse of a characteristic diffusion time or local residence time. At large rates of scalar dissipation the heat generated due to chemical reaction is exceeded by heat loss. However, if the turbulent mixing or diffusion time scale is comparable to the chemical reaction time scale, local flame quenching occurs.

More traditional theory assumes that a lifted turbulent diffusion flame is stabilized in a region where combustion is controlled by premixing. Even "attached flames" are viewed as having a "dark space" between them and the source of reactants, that is due to heat and active radical losses to the burner surfaces. It is the existence of the dark space that permits premixing prior to combustion.

The flame observations in the PW100, PW150 (LS injector) and PW200 (LS injector/lifted flame) combustors all show an LBO that takes place from lifted flames. The amount of flame lift is sufficient to presume that a significant degree of reactant premixing takes place prior to reaction. Even the LS injector with an attached flame in the PW200 combustor exhibits a dark space at the base of the main flame (see Figure 5–7). Therefore, a phenomenological modeling approach based on premixing would represent a logical choice. It is at least consistent with the modeling used above for data correlation.

If the flame is lifted and stabilized some distance downstream from the burner, a relevant question is, to what degree is the flame premixed? There is some evidence that such lifted flames do incur a degree of premixing, [35] – [41.]. The assumption is therefore adopted that such lifted flames will have a significant degree of reactants premixing on the molecular level, even though large coherent structures that might exist need not themselves be completely premixed.

With premixing therefore, the stability in general will be governed to first order by three conditions:

(i) the flammability limits for the mixture,

(ii) the relationship of the local turbulent burning velocity of the mixture to the mean flow velocity,

(iii) the influence of the local turbulence on mixing rates of premixed reactants with the products of combustion.

Hence, if the premixing assumption is justified, the stability of gaseous, turbulent diffusion flames that are lifted can be characterized by the mixing of small eddies of premixed reactants, which are within mixture flammability limits, with small eddies of hot products of combustion that might serve as ignition sources, [37.].

If a pair of such eddies come into contact and mix very quickly, ignition of the reactants is not likely due to dilution. Also, the resultant temperature of the mixed eddies could be below the ignition temperature of the reactants. For hydrocarbon/air mixtures the (hypothetical) ignition temperature will tend towards the burned temperature of the mixture, [42.]. However, if the rate of mixing is slow enough, then hot products can ignite reactants before dilution and cooling are completed, and a flame front will propagate through the reactants eddy. The consumed reactants eddy, now another hot products eddy, can then serve as a new ignition source for another reactants eddy.

With this conceptual model of ignition, propagation of the flame will not take place in the mixture when the rate of turbulent mixing between the small eddies is greater than the local chemical reaction rate. A stability criterion can be formulated on this basis.

Consider the turbulent Bunsen flame shown in Figure 6–1. For a stable flame, the volumetric flow rate of mixture supplied must equal the volumetric flow rate of mixture burned. Thus, if the value of the turbulent burning velocity S_T, is uniform over the surface of the flame brush,

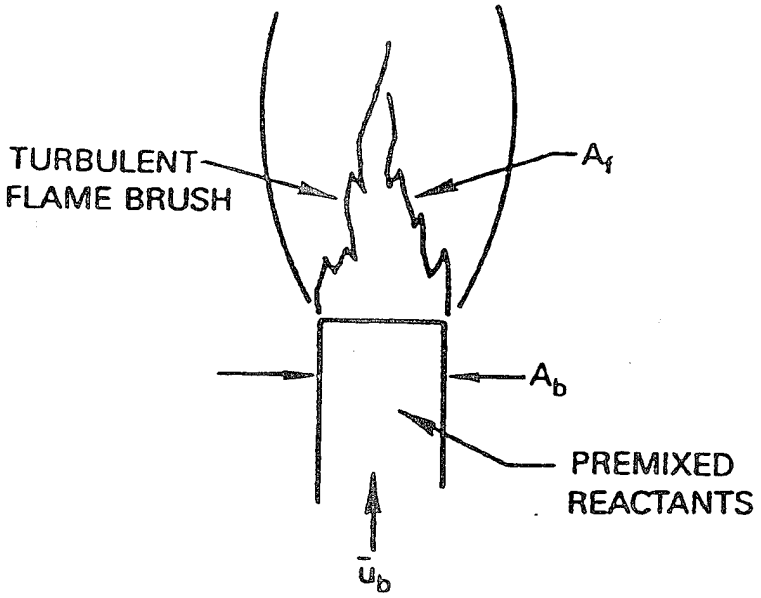

Figure 6–1. Diagrammatic Representation of simple Bunsen Flame for Model Development

$$A_b \bar{u}_b = A_f S_T$$

Now, from conservation of mass,

$$A_b \bar{u}_b = \left(\frac{\dot{m}}{\bar{\rho}}\right)_{REACTANTS}$$

so,

$$S_T A_f = \left(\frac{\dot{m}}{\bar{\rho}}\right)_{REACTANTS}$$

But, for 100 percent combustion efficiency, $\left(\frac{\dot{m}}{\bar{\rho}}\right)_{REACTANTS}$ is equal to the volumetric reaction rate, R_{RR}. Hence,

$$R_{RR} = S_T A_f \tag{6.2}$$

For a lifted flame the arguments resulting in Equation 6.2 will apply to the eddies in the flow at the base of the lifted flame. Thus,

$$R_{RR} = S_T A_e \tag{6.3}$$

where,

A_e = eddy interfacial area

Since chemical reactions take place between molecules, the relevant reactant eddies must be those in which there is significant molecular mixing. In a turbulence energy spectrum, high molecular–level mixing rates are achieved where dissipation of turbulence kinetic energy is a maximum. For fully–developed turbulence a Reynolds Number–independent wave number k_d, can be identified where dissipation reaches a maximum. This wave number is usually theoretically related to the Kolmogorov eddy length scale η, in which viscous effects become very strong indeed and the energy appears as heat in the fluid. However, experimental evidence indicates that most viscous dissipation occurs at $k_d\eta < 0.5$, and for high Reynolds Numbers, $k_d\eta \approx 0.2$. Mixing within an eddy does not have to be perfect for chemical reaction to be initiated. Note also that heat release due to chemical reaction within an eddy can laminarize the fluid within the eddy so that dissipation does to zero, even though the eddy size may be larger than the Kolmogorov length scale.

The Kolmogorov length scale is given by,

$$\eta = \left(\nu^3 / \varepsilon\right)^{1/4} \tag{6.4}$$

where ε is the dissipation rate of turbulence kinetic energy and ν is the kinematic viscosity of the fluid. So, the wave number for maximum viscous dissipation, high–rate, molecular mixing is given by,

$$k_D = 0.2\left(\varepsilon / \nu^3\right)^{1/4} \tag{6.5}$$

Hence, the length scale of the dissipation eddies of interest is given by,

$$k_D = 1 / l_D$$

or,

$$l_D = 5\left(\nu^3 / \varepsilon\right)^{1/4} = 5\eta \tag{6.6}$$

Since such eddies are five times the size of the Kolmogorov eddies, the burning velocity S_T, for these eddies could be affected by the smaller turbulent eddies present, even though laminarization within the eddy itself could take place. If this is so, a burning velocity expression of the Damkohler type, consisting of two components involving a contribution from chemical kinetics and a fluid dynamic contribution, is appropriate, i.e.,

$$S_T = S_L + u_o'$$

where,

S_L = laminar flame speed

u_e' = representative turbulent eddy velocity component for eddies smaller than the dissipation eddies, and moving on a local basis, the flame front formed around the dissipation eddy

With this definition, u_e' would represent the characteristic velocities of all eddies equal to or greater in size than the Kolmogorov eddies, but smaller than the dissipation eddies. Thus, the representative turbulent dissipation eddy velocity is,

$$u'_D > u'_e \geq V$$

where V is the velocity of the Kolmogorov eddies, which is given by,

$$V = (\nu\varepsilon)^{1/4} \tag{6.7}$$

so that with Equation 6.6 and equilibrium turbulence,

$$u_D' = (l_D \varepsilon)^{1/3} = (5\eta\,\varepsilon)^{1/3}$$

giving,

$$u_D' = 5^{1/3}(\nu\varepsilon)^{1/4} \tag{6.8}$$

But, using Equation 6.7,

$$u_D' = 1.71V \tag{6.9}$$

Thus, in the inequality above,

$$V \leq u'_e < 1.71V \tag{6.10}$$

So, if the Damkohler expression for burning is written in the form,

$$S_T = S_L + \alpha V \tag{6.11}$$

to relate to the Kolmogorov eddies, then,

$$\alpha = \frac{u_e'}{V}$$

giving,

$$1.0 \leq \alpha < 1.71 \tag{6.12}$$

At this point the constant α cannot be determined any closer than the inequality 6.12. Hence in Equation 6.3,

$$R_{RR} = \left[S_L + \alpha(\nu\varepsilon)^{1/4}\right]A_c \tag{6.13}$$

which represents the chemical reaction time.

Within the maximum dissipation range of wave numbers, the mass transfer in the dissipation eddies will also depend on the molecular motions and turbulent motions, similar to the burning velocity. Thus, the total flux of chemical species j in the direction x, is given by a Damkohler–like expression,

$$\left[\dot{m}''_{j,x}\right]_{Tot} = \left[\dot{m}''_{j,x}\right]_m + \left[\dot{m}''_{j,x}\right]_t \tag{6.14}$$

where the subscripts m and t denote molecular and turbulent transfer respectively. For both contributions the form of Fick's law of diffusion is taken, i.e., the gradient hypothesis is assumed for the turbulent contribution. Thus,

$$\left[\dot{m}''_{j,x}\right]_m = -D_j \bar{\rho}_j \frac{\partial \bar{m}_j}{\partial x} \qquad \left[\dot{m}''_{j,x}\right]_t = -\Gamma_{t,j} \bar{\rho}_j \frac{\partial \bar{m}_j}{\partial x}$$

where D_j is a diffusion coefficient for j, $\bar{m}_j$ is the mean mass fraction of j, and $\Gamma_{t,j}$ is a turbulent exchange coefficient for j, related to a turbulent Schmidt Number σ_t, through,

$$\sigma_t = \nu_t / \Gamma_t \tag{6.15}$$

and the turbulent viscosity ν_t, is obtained through the eddy viscosity hypothesis as,

$$\nu_t = \frac{C_\mu K^2}{\varepsilon} \tag{6.16}$$

C_μ being a conditional constant of value 0.09, and K is the kinetic energy of turbulence.

Thus, the total mass flux of species j in the direction x, is,

$$\left[\dot{m}''_{j,x}\right]_{Tot} = \dot{\rho}_j \frac{\partial \bar{m}_j}{\partial_x} \left[D_j + \Gamma_{t,j}\right] \tag{6.17}$$

Then, the rate of diffusion per unit length of flame front R_D, is given by

$$R_D = \frac{\left[\dot{m}''_{j,x}\right]_{Tot} A_e}{\bar{\rho}_j \frac{\partial \bar{m}_j}{\partial x}} \cdot \frac{1}{1_D}$$

where l_D is the length over which diffusion takes place, related to the dissipation eddy size. Using Equations 6.6 and 6.17, this expression becomes,

$$R_D = \frac{\left(D_j + \Gamma_{t,j}\right) A_e}{5\eta}$$

or, with Equations 6.15 and 6.16,

$$R_D = \frac{\left[D_j + \frac{C_\mu K^2}{\sigma_t \epsilon}\right] A_e}{5(\nu^3 / \epsilon)^{1/4}} \tag{6.18}$$

which represents the mixing time.

From the original arguments, the flame will be extinguished if the mixing time, represented by Equation 6.18, is very short compared to the chemical reaction time, represented by Equation 6.13. Alternatively, if the mixing time is long in relation to the chemical reaction time, a hot eddy of burned products adjacent to a cold eddy of fresh reactants, can act before it is diluted, as an ignition source for the cold reactants, thereby establishing a flame front around the reactants eddy. Thus, some critical ratio of these two times exists; let it be β. Then,

$$\frac{D + \frac{C_\mu K^2}{\sigma_t \epsilon}}{\left[S_L + a(\epsilon\nu)^{1/4}\right]} \cdot \frac{0.2}{(\nu^3 / \epsilon)^{1/4}} > \beta \tag{6.19}$$

i.e., the ratio of the reaction time to mixing time greater than β denotes the condition for flame extinction. β is related to the number–size densities of the hot products eddies that range in size between the dissipation and Kolmogorov eddies, and which act as ignition sources.

Then,

$$\frac{D + \frac{C_\mu K^2}{\sigma_\epsilon}}{\beta\left[S_L + a(\epsilon\nu)^{1/4}\right]} \cdot \frac{0.2}{(\nu^3 / \epsilon)^{1/4}} > 1.0 \qquad (6.20)$$

A limit analysis can be performed as follows for the fine-grain Kolmogorov eddies, which are encountered near to solid surfaces and in well-mixed regions of a flow. In boundary layers the ratio ε / K ranges from a few hundred to a few thousand $\text{sec.}^{\pm 1}$, and on the solid surfaces $\varepsilon \to \infty$ due to the no-slip condition. Thus, writing Equation 6.20 in the form of a stability parameter, SP,

$$SP = \frac{0.2\left(D + \frac{C_\mu K^2}{\sigma_\epsilon}\right)}{\beta\alpha\nu\left[\frac{S_L}{a(\epsilon\nu)^{1/4}} + 1\right]}$$

and applying the limiting condition,

$$\frac{C_\mu K^2}{\sigma_\epsilon} \qquad \text{and,} \qquad \left[\frac{S_L}{a\ (\epsilon\nu)^{1/4}} + 1\right] \to 0$$

so,

$$SP \to \frac{0.2D}{\beta\alpha\nu} \qquad (6.21)$$

Using the definitions of Schmidt Number and kinematic viscosity, Equation 6.21 becomes,

$$SP = \frac{0.2}{\beta\alpha \cdot S_c} \qquad (6.22)$$

where S_C is the molecular Schmidt Number.

For dilute mixtures of propane in air the molecular Schmidt Number is 1.51. Thus, from Equation 6.22, the limiting value of $\beta\alpha$ is obtained as,

$$\beta\alpha = 0.1325 \qquad (6.23)$$

Therefore, substituting Equation 6.23 into 6.20 gives,

$$SP = \frac{1.5\left(D = \frac{C\mu K^2}{\sigma_\epsilon}\right)}{\nu\left[\frac{S_L}{(\epsilon\nu)^{1/4}} + 1\right]} > 1.0 \qquad (6.24)$$

Equation 6.24 can be applied on a point-by-point basis throughout a calculated flowfield to establish were a flame can exist or is extinguished.

It should be noted that α is not a true constant, but can be shown [43.]to be given by,

$$a = \left(C_1 \frac{\rho_u}{\rho_b}\right)^{1/2}$$

where C_1 is a constant lying between zero and unity, and, ϱ_u and ϱ_b are respectively the unburned and burned densities of the fuel/air mixture.

Since any real turbulent diffusion or partially–premixed flame will always contain a mixture of distributed reaction zones, laminar flamelets and large–scale structures, it is instructive to compare the stability parameter based on chemical and mixing times to the alternative limiting condition of the flame–stretch approach to extinction. This is especially relevant since the Kolmogorov eddies can act on the maximum dissipation eddies, and locally stretch any flame front formed around these larger eddies.

Flame stretch S, is given by,

$$S = \frac{\delta}{S_L} \cdot \frac{d(In\ A)}{dt}$$

where,

δ = flame thickness

A = flame area

If there is a predominant flow direction, as in jet flames for example, i.e., $u = u(x)$, then,

$$S \rightarrow \frac{\delta}{S_L} \cdot \frac{d\bar{u}}{dx} \qquad 6.25$$

This is known as the Karlovitz Number, KN, [35.].

Now, for the Kolmogorov eddies acting on the dissipation eddies,

$$\frac{d\bar{u}}{dx} = \frac{V}{\eta}$$

where η and V are given by Equations 6.4 and 6.7 respectively. Thus,

$$\frac{d\bar{u}}{dx} = \frac{(\nu\epsilon)^{1/4}}{(\nu^3/\epsilon)^{1/4}} = (\epsilon/\nu)^{12}$$

Thus,

$$KN = \frac{\delta}{S_L} \cdot \left(\frac{\epsilon}{\nu}\right)^{1/2}$$

It can be shown [42.] that flame thickness is given by,

$$\delta = \Omega \frac{k}{\rho c_p} \cdot \frac{(T_b - T_i)}{(T_b - T_u)} \cdot \frac{1}{S_L}$$

where subscripts u, b and i respectively signify unburned, burned and ignition conditions, and where,

$$0 < \frac{(T_b - T_i)}{(T_b - T_u)} < 1$$

and,

$$\Omega = 2 \text{ for } \frac{(T_b - T_i)}{(T_b - T_u)} = 0$$

$$\Omega = 1 \text{ for } \frac{(T_b - T_i)}{(T_b - T_u)} = 1$$

For convenience, the $\Omega = 1$ condition is taken, (this implies not being strictly representative for hydrocarbons). Hence,

$$KN = \frac{k}{\rho c_p} \cdot \frac{1}{S_L^2} \left(\frac{\epsilon}{\nu}\right)^{1/2}$$

Introducing Lewis Number, Le, where,

$$Le \equiv \frac{\rho c_p D}{k}$$

and Schmidt Number,

$$KN = \frac{\mu}{Le \cdot Sc} \cdot \frac{1}{S_L^2} \left(\frac{\epsilon}{\nu}\right)^{1/2}$$

or, since $Le \cdot Sc = \Pr$, the Prandtl Number,

$$KN = \frac{(\nu\epsilon)^{1/2}}{Pr \cdot S_L^2}$$

Hence,

$$KN = \frac{V^2}{Pr \cdot S_L^2} \qquad 6.26$$

If the critical Karlovitz Number is around unity, (it is certainly of order unity), then extinction due to flame stretch occurs when the Kolmogorov velocity scale becomes equal to or greater than, the laminar flame speed, i.e.,

$$\frac{V^2}{Pr \cdot S_L^2} \geq 1.0 \qquad 6.27$$

Equation 6.27 may be compared with Equation 6.24 in the case of "weak turbulence." Weak turbulence is typically defined as, eddy fluctuation velocity, u′ << S_L and, u′ → V , so that $\frac{V}{S_L} << 1.0$ and, eddy length scale, $l_e < \delta$ and, $l_e \rightarrow \eta$, so that $\frac{\eta}{\delta} < 1.0$

Therefore, for weak turbulence, from Equation 6.24,

$$\left[\frac{S_L}{(\nu\epsilon)^{1/4}} + 1\right] \rightarrow \frac{S_L}{V} \qquad \text{and} \qquad D + \frac{C_\mu K^2}{\sigma_f \epsilon} \rightarrow D$$

so that,

$$SP \rightarrow \frac{1.5DV}{\nu S_L} \geq 1.0$$

Then, introducing Lewis and Prandtl Numbers,

$$SP \rightarrow 1.5\ Le \cdot \frac{V}{Pr \cdot S_L} \geq 1.0$$

Squaring,

$$2.25 \frac{Le^2}{Pr} \cdot \frac{V^2}{Pr \cdot S_L^2} = 1.0 \qquad 6.28$$

Thus, comparing Equations 6.27 and 6.28, it can be seen that in the limit of weak turbulence the two stability groups, Karlovitz Number the strained–flame criterion for extinction and SP the characteristic time criterion, have the same functional form. Given the common features of the two stability parameters the two should agree on partially–premixed flame extinction in regions of weak turbulence. In regions of high dissipation, SP should result in better predictions than the flame–stretch criterion. Both approaches require further exploration, evaluation and development.

In order to utilize Expression 6.24, a description of laminar flame speed is needed for propane/air combustion, and this description should include account of the excess nitrogen presently used to simulate subatmospheric pressures. Such a description is most conveniently obtained via experimental data, such as that contained in Reference 44.

For propane/oxygen/nitrogen systems, if the mole fraction of oxygen ψ, is,

$$\psi = \frac{O_2}{O_2 + N_2} \qquad 6.29$$

normal air (i.e., zero excess nitrogen) has a value of ψ equal to 0.21, and a relative flame speed $(S_L)_{rel}$, with excess nitrogen can be defined as,

$$(S_L)_{rel} = S_{L,\max} / (S_{L,\max})_{\psi = 0.21} \qquad 6.30$$

where both $S_{L,\max}$'s are the respective maximum flame speed at 300°K. The experimental data [44.] can be represented by the polynomial,

$$(S_L)_{rel} = \pm 0.9825 + 7.1\psi + 11.0\psi^2 \qquad 6.31$$

as Figure 6–2 shows, and which is valid for $0.125 \leq \Psi \leq 0.5$. At 300°K $(S_{L,\max})_{\psi = 0.21} = 0.445$ m/s.

The effect of equivalence ratio for lean mixtures is accounted for by the correlation,

$$S_L / (S_{L,\max}) = 1.1309 \ln \phi + 0.9119 \qquad 6.32$$

which gives the dependencies shown in Figure 6–3 at 300°K. Equation 6.32 represents a correlation of experimental data obtained by the Shadow–method [45.] of measuring flame speed, while the data in Figure 6–3 were measured by the Schlieren–method [45.], (there is not a 1:1 agreement between the two methods). For this reason the agreement in Figure 6–3 is considered satisfactory.

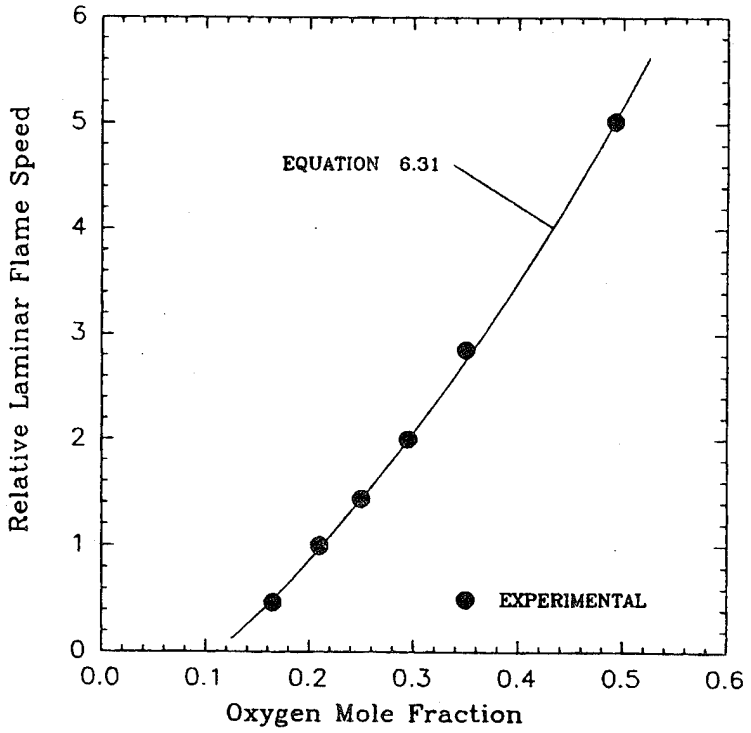

Figure 6–2. Experimental Dependency of Relative flame speed on Mole Fraction of Oxygen for Propane/Oxygen/Nitrogen Systems

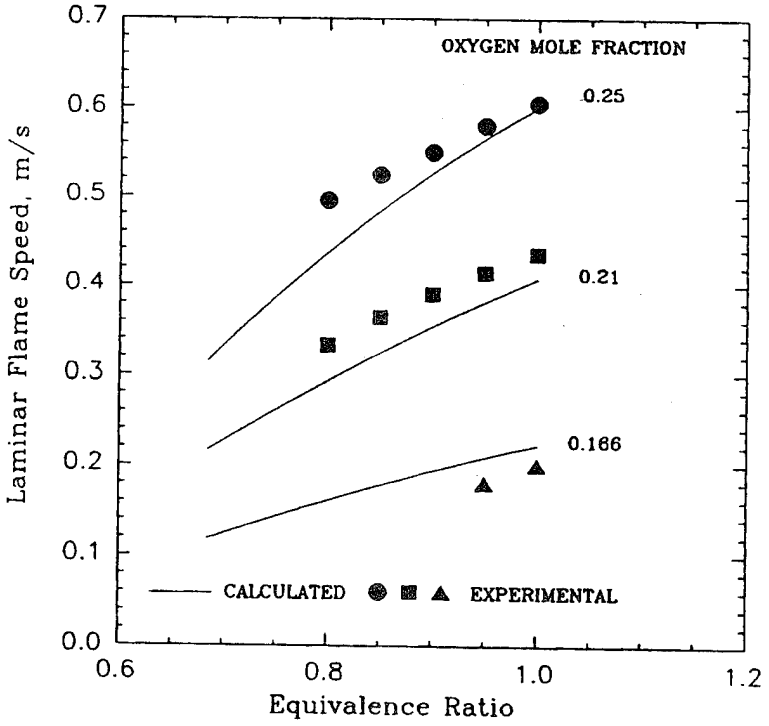

Figure 6–3. Comparison of Calculated and Measured laminar Flame Speeds with Variation In Oxygen Mole Fraction

Unfortunately, it was difficult to find sufficient experimental data to conduct a good and complete assessment of mixture initial temperature effects when there is excess nitrogen present. However, correction of $(S_{L,\max})_{\psi=0.21}$ for temperature using the relation,

$$(S_L)_{ref} = 25 + 0.00085T^2 \qquad 6.33$$

where $(S_L)_{ref}$ is a percentage of the value at an initial temperature of 25C, results in values for the variation of flame speed at unity equivalence ratio with ψ at 422K that are in acceptable agreement with the limited data available [44.], as Figure 6–4 shows.

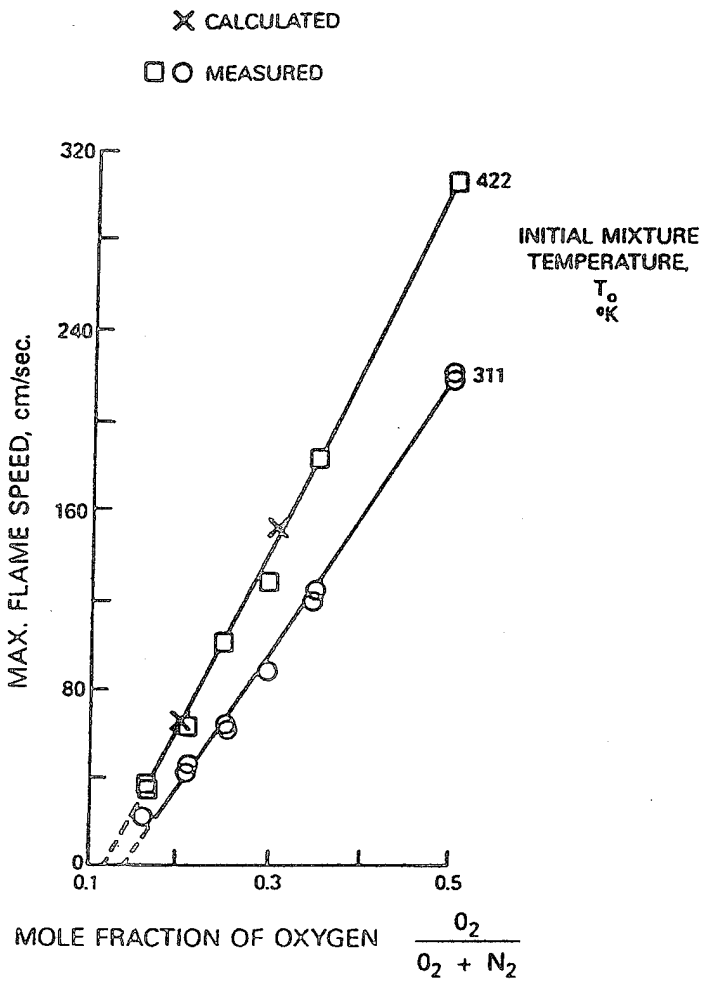

Figure 6–4. Limited Validation of Temperature Correction to Flame Speed

For dilute mixtures of gases in air the Schmidt Number of propane [46.] may be found with sufficient accuracy from,

$$Sc_j = 0.145 M_j^{0.556} \pm 30\% \qquad 6.34$$

where M_j is the molecular weight of chemical species j , i.e., propane in this instance.

6.4 Representation of PW100 Research Combustor as a Stirred Reactor

In Section 6.2 a combustor general loading parameter LP, and defined by Equation 6.1, was presented for the purposes of data correlation. Application of LP to the PW100 combustor is simple, with the exception

of a choice for the reactor volume, V. This choice is complicated by the separate introduction of the fuel and air, and by the lifted–flame condition of this combustor as LBO was approached.

There are three criteria to be satisfied in a choice of the effective reactor volume: First, the region should be "well–stirred," second, the fuel/air mixture in the well–stirred region must be inside its flammability limits, and third, the local flow velocity should not exceed the burning velocity of the mixture.

A perfectly–stirred reactor is defined classically as a steady flow of perfectly–premixed reactants in a reactor within which there exists everywhere uniform chemical composition and temperature distributions that are identical with those of the outgoing stream. It has been observed that the decay of a mixture concentration perturbation in a perfectly–stirred reactor follows an exponential law. Turbulence theory leads to the observation that when the turbulent motion is on a small scale and is locally isotropic, the mixing results in an exponential decay of an initial concentration nonuniformity. Thus, provided Reynolds analogy (velocity and concentrations decay simultaneously in a turbulent flow) is adopted, application of turbulent mixing concepts to reactor flows offers a way to define well–stirred regions in these flows.

Therefore, following Swithenbank [21.], it can be shown as follows, that for mechanical generation of turbulence, the minimum condition for a perfectly–stirred reactor is represented by the resulting pressure loss factor.

If, in a turbulent flow, an instantaneous quantity is represented by the sum of its time–mean and randomly fluctuating values,

$$\phi = \bar{\phi} + \phi'$$

then, $\overline{\phi'} = 0$ and $\phi'_{rms} = \left(\overline{\phi'^2}\right)^{1/2}$, and if u represents velocity, the total turbulence energy spectrum over all wave numbers k, enables the kinetic energy of turbulence K, to be found, i.e.,

$$K = \int_0^\infty E(k)dk = 1/2\ (u'^2_{rms} + v'^2_{rms} + \omega'^2_{rms}) \quad \text{per unit mass of fluid}$$

where $E(k)$ is the average amount of energy of the turbulent motion between k and dk. So, for isotropic turbulence,

$$K = 3/2\bar{\rho}u'^2 \qquad \text{per unit volume, where for convenience,}$$

$$u' \equiv u'_{rms}$$

Production of turbulence in a flow by means of some mechanical device involves a loss in total pressure, ΔP. Thus, the efficiency with which turbulence is produced can be defined,

$$\eta_{Tu} = \frac{3/2\bar{\rho}u'^2}{\Delta P}$$

If ξ is a **pressure loss factor**, defined as $\Delta P / q_1$ where $\Delta P = P_1 \pm P_2$ and $q_1 = 1/2\bar{\rho}\bar{u}_1^2$, and,

"section 1" is defined as being upstream of the turbulence–producing device, and "section 2" is sufficiently far downstream from the turbulence generator that the mean velocity profile is again uniform, then,

$$\Delta P = \xi q_1 = \xi \cdot 1/2\bar{\rho}\bar{u}_1^2$$

so that,

$$\eta_{Tu} = \frac{3/2\bar{\rho}u'^2}{\xi \cdot 1/2\bar{\rho}\bar{u}_1^2} = 3\left(\frac{u'}{\bar{u}_1}\right)^2 \cdot \frac{1}{\xi} \qquad 6.35$$

Now, for 100 percent efficiency in turbulence generation, η_{Tu} is unity, and $(u' / \bar{u}_1)$ is unity also. Thus, from Equation 6.35,

$$3\left(\frac{u'}{\bar{u}_1}\right)^2 \cdot \frac{1}{\xi} = \frac{3}{\xi} \qquad \text{and,} \qquad 1.0 = \frac{3}{\xi}$$

so that,

$$\xi = 3.0$$

But $(u' / \bar{u})$ equal to unity represents the condition of a perfectly–stirred reactor. Hence, the condition for a perfectly–stirred reactor is that,

$$\frac{\Delta P}{q_1} \geq 3.0 \qquad 6.36$$

However, with a direct injection of gaseous fuel into a combustor even with the condition represented by Equation 6.36 satisfied, "well–stirred" conditions are not achieved immediately. The pressure loss is introduced into the inlet streams via some geometric means, e.g., blockage, sudden expansion, confluence of two impinging jets of differing initial velocity, etc. As a result of this mechanical device the pressure drop is initially converted to some distortion of the mean velocity profile. The energy contained in this distorted mean velocity profile is converted to turbulence through the shear generated between layers of differing velocity in the profile. The turbulence so–produced transfers energy down the eddy length scale range by the action of smaller eddies on the bigger eddies of the developing turbulence, until this energy of motion is dissipated eventually, to heat by the action of molecular viscosity. When this condition is reached for all of the energy introduced into the flow, the full pressure loss is achieved. Thus, at any streamwise station in the flow, the energy associated with the loss will exist in all three forms, to give the energy balance,

$$\frac{\Delta P}{q_1} = \frac{KE_{mean}}{q_1} + 3\left(\frac{u'}{\bar{u}_1}\right)^2 + \frac{D}{q_1} \qquad 6.37$$

where the first term on the right–hand side is the loss associated with the mean velocity distortion, the second represents the turbulence generated, and the third is the total dissipation of turbulence energy.

Equation 6.37 can be used to establish the extent of the well–stirred reactor existing in the flow. The discussion is limited to two–dimensional flows for the PW100 combustor.

Far downstream where the full loss is achieved, the distorted profile will have mixed out to become uniform, and turbulence will have dissipated; however, the total dissipation will reach a finite number. When this so the asymptotic condition is reached where,

$$\frac{\Delta P}{q_1} = \frac{D}{q_1} \qquad 6.38$$

Consider the distortion of the mean velocity profile,

$$KE_{mean} = \frac{1}{y} \int_0^{y_{max}} 1/2 \cdot \bar{\rho} \Delta \bar{u}^2 dy$$

where,

$$\Delta \bar{u} = (\bar{u}_1 \pm \bar{u}_{local}) \qquad \text{and} \qquad \bar{u}_{local} = \bar{u}_{local}(x, y)$$

y = cross–stream co–ordinate direction over which $\bar{u}$ varies

x = streamwise co–ordinate direction

Hence,

$$\frac{KE_{mean}}{q_1} = \frac{1}{y_{max}} \int_0^{y_{max}} \left| \left(1 - \frac{\bar{u}_{local}}{\bar{u}_1} \right) \right| dy$$

The total dissipation per unit volume is the rate of dissipation per unit volume, $(\bar{\rho}\varepsilon)$, multiplied by a time–scale τ, i.e.,

$$\frac{dD}{d\tau} = \bar{\rho}\varepsilon$$

or,

$$D = \int_0^{\tau} \bar{\rho}\epsilon d\tau = \int_0^{x} \frac{\bar{\rho}\epsilon}{\bar{u}_1} dx \qquad 6.39$$

and $\varepsilon = \varepsilon(x, y)$.

The dissipation rate can, if desired, be expressed in terms of the turbulence intensity. The rate of energy transfer from large eddies to smaller eddies is u_T / l_T, where u_T is the appropriate eddy velocity scale and l_T is an appropriate eddy length scale. In the smaller eddies the energy supply rate equals the energy dissipation rate. This balance implies,

$$l_T = u_T^3 / \varepsilon$$

The eddies of interest are the energy–containing eddies, so that,

$$u_T = u' \quad \text{and} \quad l_T = l_e$$

Thus,

$$\varepsilon = \frac{(u')^3}{l_e}$$

so that in Equation 6.39,

$$D = \bar{\rho} \int_0^{x} \frac{(u')^3}{\bar{u}_1 l_e} dx$$

Generally,

$$l_e = \lambda y_{\max}$$

where λ is a constant less than unity, and is typically taken as 0.03. i.e.,

$$D = \bar{\rho} \int_0^{x} \frac{(u')^3}{\lambda y_{max}\, \bar{u}_1} dx$$

Hence,

$$\frac{D}{q_1} = \frac{2}{\lambda y_{max}} \int_0^{x} \left(\frac{u'}{\bar{u}_1} \right)^3 dx \qquad 6.40$$

remembering that $u' = u'(x, y)$

Now, mixing is proportional to dissipation, so Equation 6.40 is an appropriate basis for determining the well–stirred portion of a flow. However, as Equation 6.38 indicates, the maximum value of D/q_1 is approached asymptotically. Therefore, differentiating Equation 6.40 yields,

$$\frac{d(D/q_1)}{d_x} = \frac{2}{\lambda y_{max}} \left(\frac{u'}{\bar{u}_1}\right)^3 \qquad 6.41$$

which depends only on the integrated value of $(u' / \bar{u}_1)^3$ over y at each x–station. This quantity will be zero initially, rises to a maximum due to shear effects, and then declines to zero downstream at the asymptotic condition. Therefore, due to the cubic effect, Equation 6.41 represents a rather precise way to establish the extent of the well–stirred region in a reactor.

It is not necessary for $d(D/q_1)/dx$ to be zero. Swithenbank recommends,

$$\frac{d(D/q_1)}{d(x/y_{\max})} \leq 0.1 \qquad 6.42$$

for negligible further mixing. Examination of the spatial variation of the quantity $d(D/q_1)/d(x/y_{\max})$ offers an excellent way to assess a combustor flow field for the presence and extent of well–stirred reactors.

The total pressure loss characteristics of the PW100 combustor flowing air are given in Figure 6–5, where,

P_o = outer jet total pressure

P_{Exit} = combustor exit total pressure

P_1 = total pressure in combustor at step plane

T = inlet temperature

W = sum of jets mass flow rates

λ = jet velocity ratio, outer to inner, where $\lambda = \infty$ signifies no central jet

such that ΔP (Equation 6.36) is equivalent to $(P_0 \pm P_{Exit})$. The orifice plate on the combustor exit was of 45 percent geometric blockage, (see Section 3.2). Figure 6–6 contains the pressure loss characteristics for reacting flow.

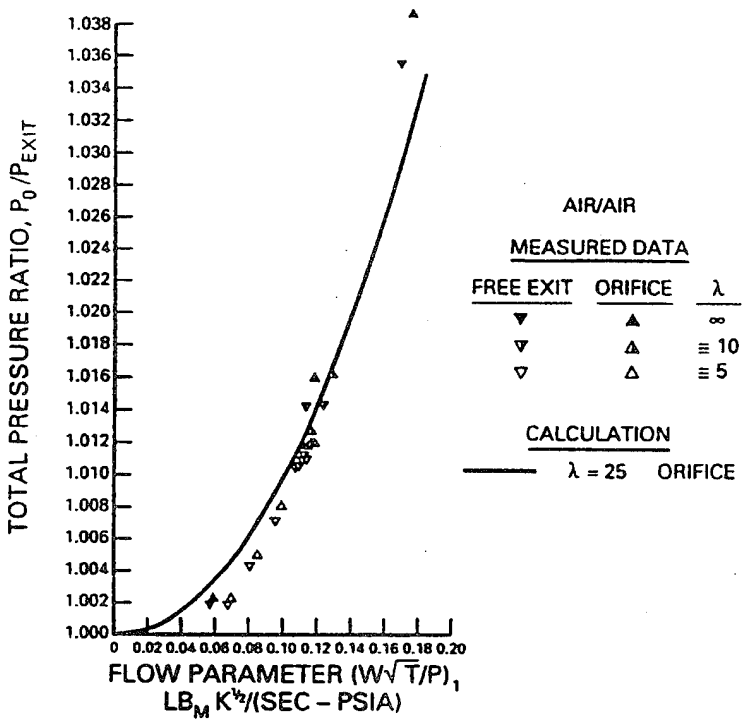

Figure 6–5. PW100 Combustor Losses In Total Pressure with Isothermal Flow

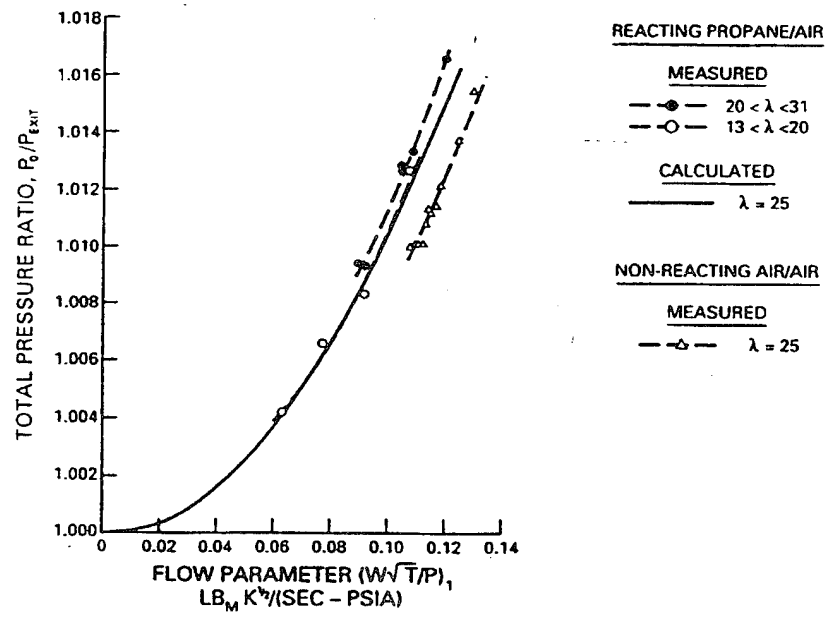

Figure 6–6. PW100 Combustor Losses In Total Pressure with Reacting Flow

The total pressure loss follows a square–law relationship with flow parameter for low values of flow parameter, (incompressible flow). From the two pressure loss figures it can be noted that in isothermal flow the effect on total pressure loss of jet velocity ratio is small, as is combustor exit blockage; heat release increases total pressure losses, and the weak effect of jet velocity ratio is more noticeable.

The PW100 combustor is basically a low–loss device. Its pressure loss characteristics indicate that it should be operated at high values of flow parameter in order to generate sufficient turbulence to contain extensive well–stirred regions.

CFD was used to assess the mixing characteristics within the PW100. The turbulence description was provided by the familiar $K \pm \varepsilon$, or two–equation, model. CFD can be extremely convenient for this purpose since the code output already includes dissipation directly, i.e., it is not absolutely necessary to use Equation 6.41, and this can avoid any length–scale assumptions.

To apply the approach, the dissipation gradient has to be assessed in streamwise and cross–stream directions for the axisymmetric flows in the PW100 combustor. The method adopted was to make a one–dimensional application in each co–ordinate direction along computational grid–lines upon which the flowfield was calculated. From an energy balance point of view this associates the local turbulence with the shear generated by a small portion of the appropriate portion of the distorted mean velocity profile about a given grid–line. It ignores multidimensional effects, together with any effects due to convection of turbulence, and is therefore consistent with Prandtl's mixing hypothesis.

The calculation was axisymmetric. The mean velocity at Station 1, $\bar{u}_1$, was interpreted as illustrated in Figure 6–7, where the co–axial fuel and air jets, and the combustor step, were represented as the mechanical device inserted in a hypothetical undistorted flow existing upstream in an imaginary inlet of cross–section equal to that of the combustor. The fluctuating velocity u', was obtained from the calculated K–field with the assumption of isotropic turbulence. The length scale λ, was taken as 3 percent of the combustor diameter, and consistent with the isotropic turbulence assumption, λ was taken to be constant in both co–ordinate directions. Equation 6.41 was used for dissipation gradient.

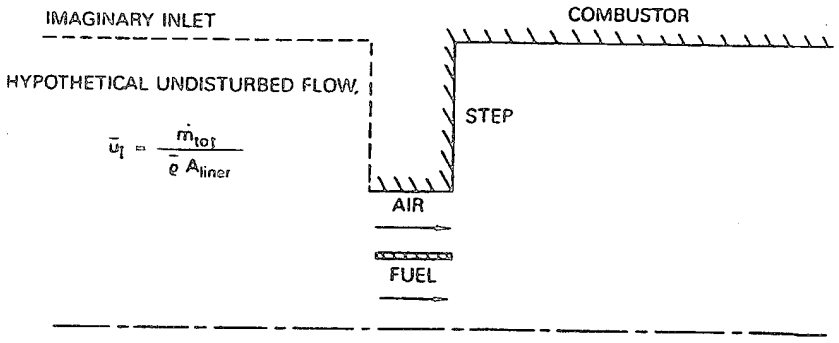

Figure 6–7. Representation of the PW100 COmbustor Co–Axial Jets/Set System as a Turbulence Generation Device to Define the Undistorted Mean Velocity

The study case for the PW100 combustor was as follows: The air jet had an outer diameter of 40 mm and was concentric with a 29 mm inner diameter fuel jet; the combustor diameter was 150 mm and the exit boundary condition (a free outlet) was placed 1.1 m downstream from the step (with reference to Section 3, it can be seen that this represents the 6.5 L/D version). The airflow was 78.26 kg/hr. with a propane flow of 3 kg/hr. for an equivalence ratio of 0.6 representing an LBO condition; both jets had an inlet temperature of 293K. The initial velocity profiles were "top–hat" in shape. The flow was nonreacting (because of the inability of the combustion model then available to calculate a lifted flame). The CFD calculations were made with the P&W 2D–PREACH code.

Figure 6–8 defines the flowfield by means of streamlines; note that in this figure there is a difference in scale of the axes. Features to note include the obvious and dominating step recirculation zone, the extent of which is marked by the stagnation streamline that is shown as a dashed line. This location (about 460 mm) is in fairly good agreement with the measured position (540 mm) at which maximum static pressure is attained, [9.] and Appendix D. The high velocity air jet (30.25 m/s) rapidly expands into the low velocity (0.69

m/s) fuel jet, also seen in the measurements, [8.] and Appendix C, as well as being evident as "waisting" in the attached flame (Section 3).

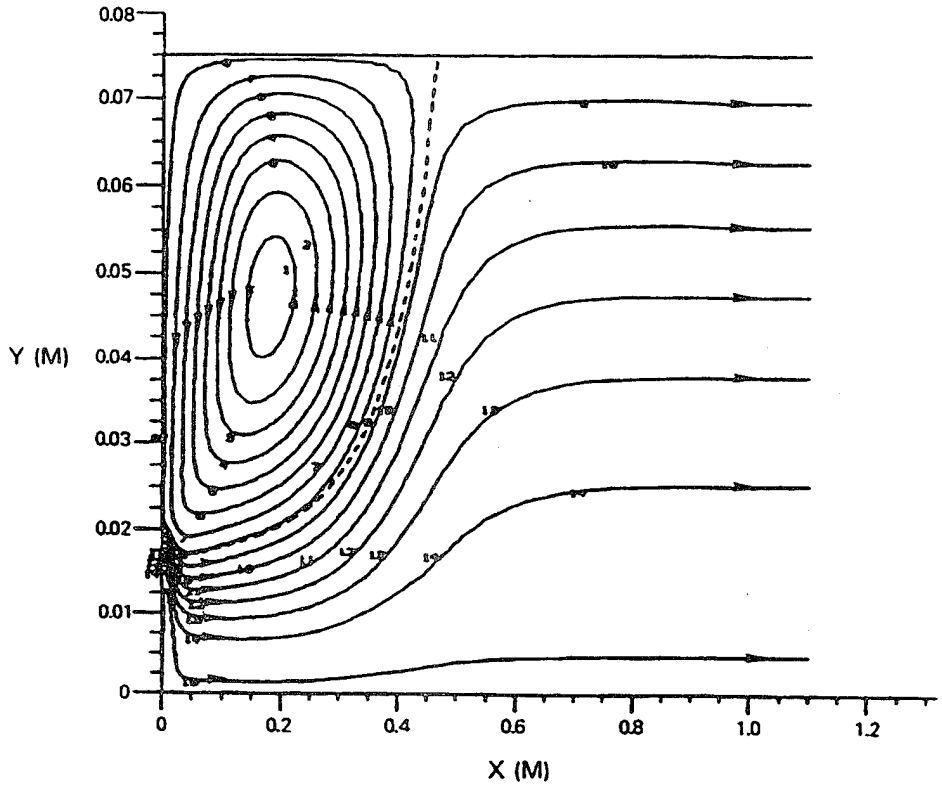

Figure 6–8. Calculated Streamlines In PW100 COmbustor Near Blowout, Used for Mixing Assessment

Shown in Figure 6–9 are curves representing the variation with distance of the total dissipation gradient $d(D/q_t)/d(x/y_{max})$ along $y\pm$gridlines (streamwise direction); the lowest curve shown is closest to the combustor wall. The range of the gradient is from 0.01 to 3,000. Figure 6–10 presents an enlargement of the near–field region. The dissipation gradients in the $y\pm$ co–ordinate direction along $x\pm$gridlines (cross–stream direction) are shown in Figure 6–11.

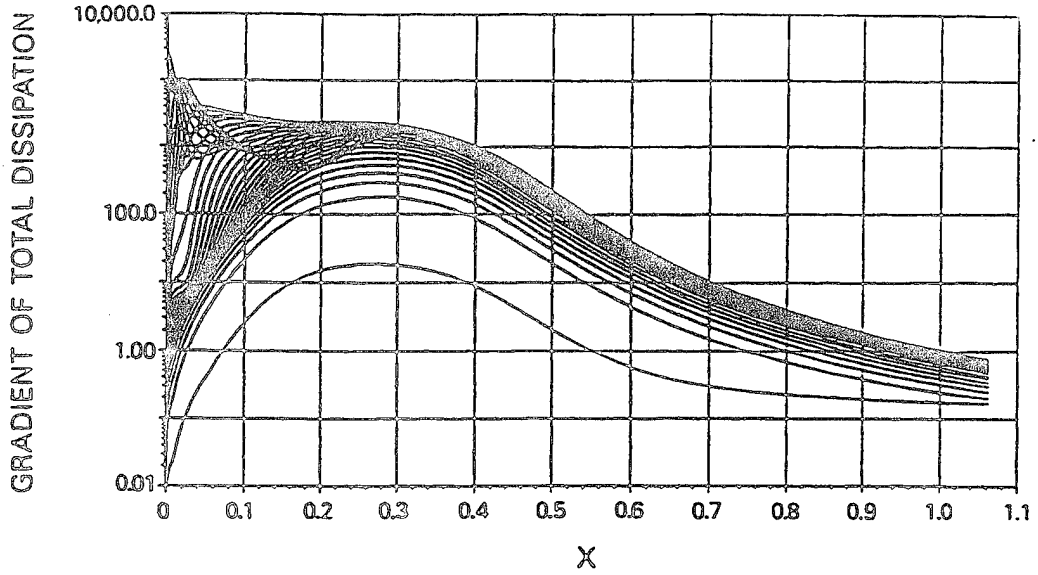

Figure 6–9. Calculated Curves of Total Dissipation Gradient Along Y–Grid Lines

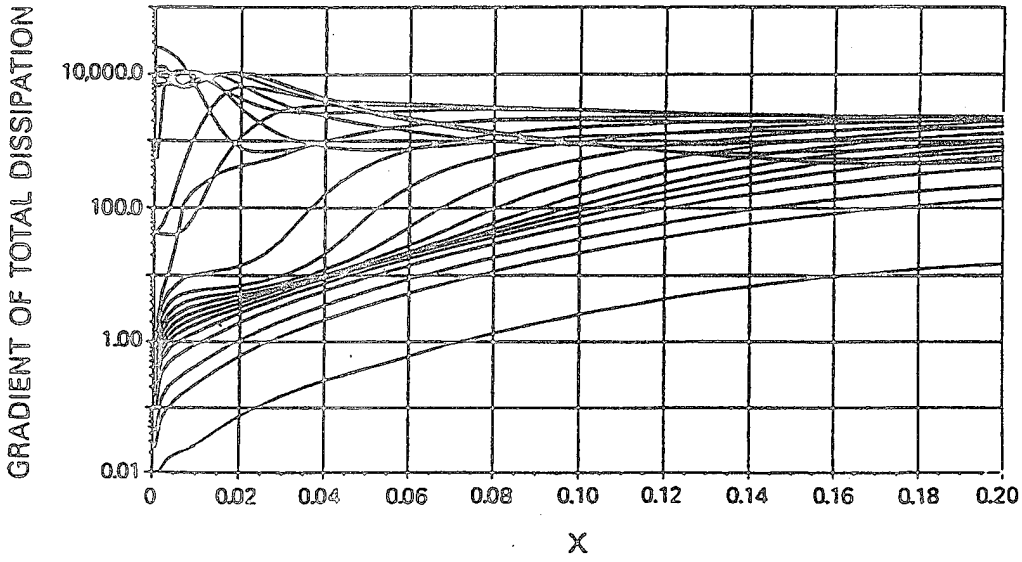

Figure 6–10. Enlargement of the Initial Region of Y–Grid Gradients

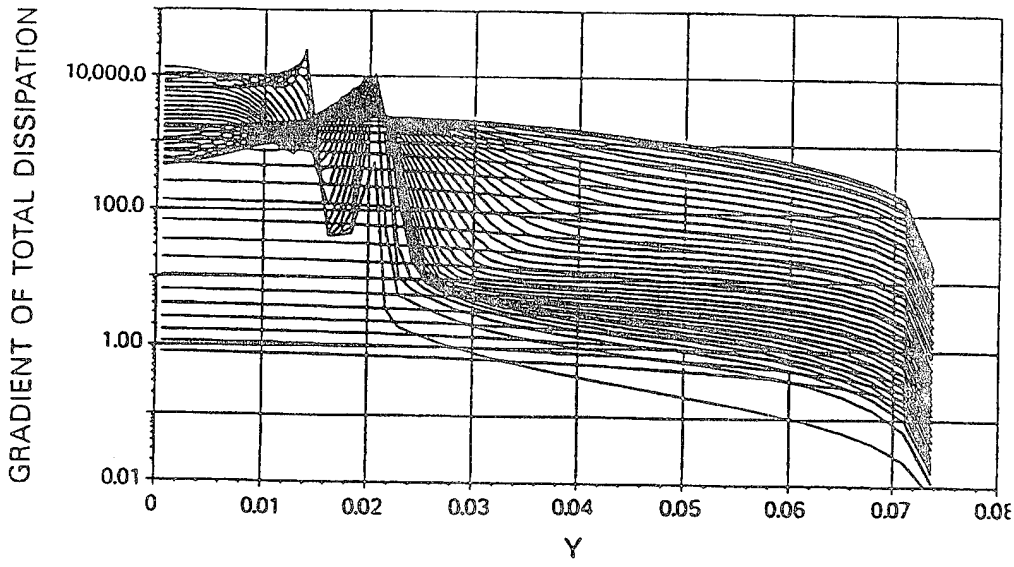

Figure 6–11. Calculated Curves of Total Dissipation Gradient Along X–Grid Lines

The complete calculation domain is shown in Figure 6–12, with contours of dissipation gradient where values of 1.0 and 10.0 respectively are equalled or exceeded. Applying Swithenbank's criterion, Equation 6.42 indicates that most of the combustor is not well–stirred. However, Swithenbank's recommendation was based on grid–turbulence. The turbulence calculated for the PW100 combustor far exceeds the intensities generated by a turbulence grid. Figure 6–13 shows the calculated field of turbulence kinetic energy per unit mass K, and Figure 6–14 and Figure 6–15 display the field of dissipation rate ε. Both K and ε are close to zero at the combustor exit plane, and reach very low values long before the outlet is attained. For example, K reaches 2.0 m^2/s^2, which is 4.2 percent of its maximum well inside the 10.0 contour for dissipation gradient, and ε reaches 100.00 m^2/s^3, which is 1.0 percent of its maximum, well inside the 10.0 contour for dissipation gradient of Figure 6–12. Most of the mixing in the PW100 combustor therefore takes place inside the 10.0 dissipation gradient contour. Therefore, does a limiting spatial contour of total dissipation gradient equal to 10.0 adequately represent a limiting condition for a well–stirred region in the PW100 combustor? It should also be noted (Section 3.5) that near LBO there is a flame–lift of about 160 – 300 mm, (depending on Reynolds Numbers) so that about half of the region inside the 10.0 contour is not a reactor anyway (i.e., high turbulence levels, via Equation 6.24, preclude local combustion).

In view of the calculated turbulence levels and decay characteristics, which were confirmed in level and trend by the PW100 isothermal turbulence measurements [8.] shown in Appendix C, the limiting condition for $d(D/q_t)/d(x/y_{max})$ was taken as 10.0.

With a critical dissipation gradient value of 10.0, and account of flame–lift, the well–stirred reactor volume for the PW100 combustor near blowout was estimated. The resulting well–stirred reactor volume was about 44 percent of the total combustor volume. The estimated well–stirred reactor volume was used in the LBO data correlation, via Equation 6.1. It was also used in a well–stirred reactor code (see below) to calculate the PW100 LBO performance. The comparison of the calculated lean stability against the correlated data is shown in Figure 3–14. Treating the PW100 combustor as a well–stirred reactor, via Equation 6.1 and the WSR volume, resulted in a satisfactory correlation of the experimental data. The calculated stability via the WSR code using the estimated WSR volume, produced a good agreement with the correlated LBO data.

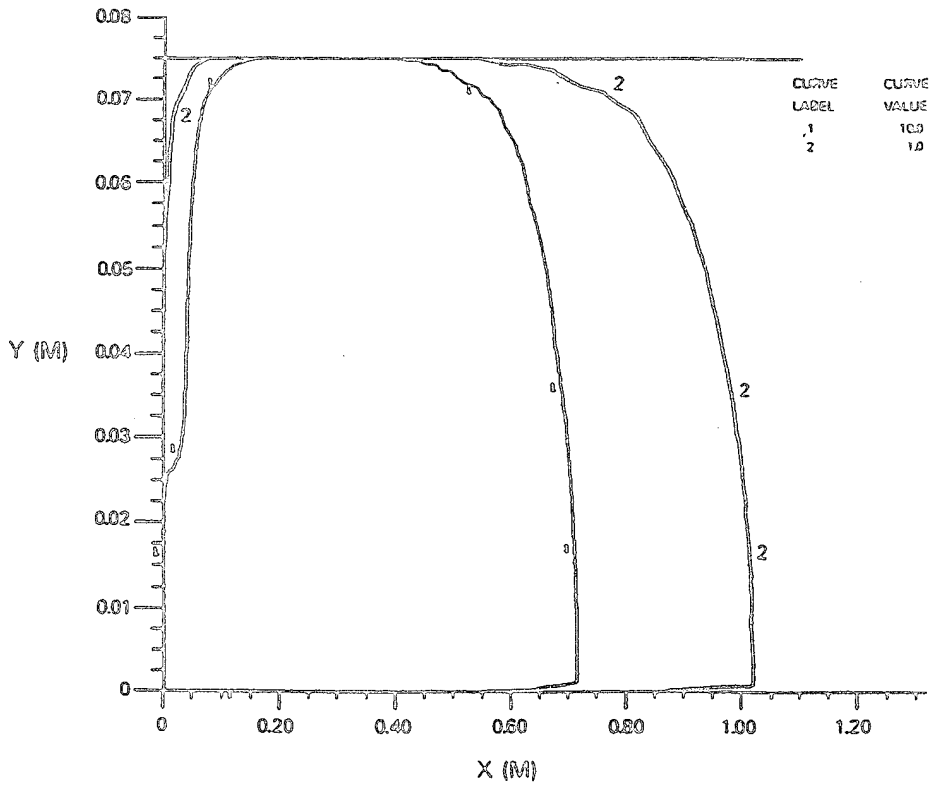

Figure 6–12. Spatial Contours of Total Dissipation Gradient In PW100 Study Case

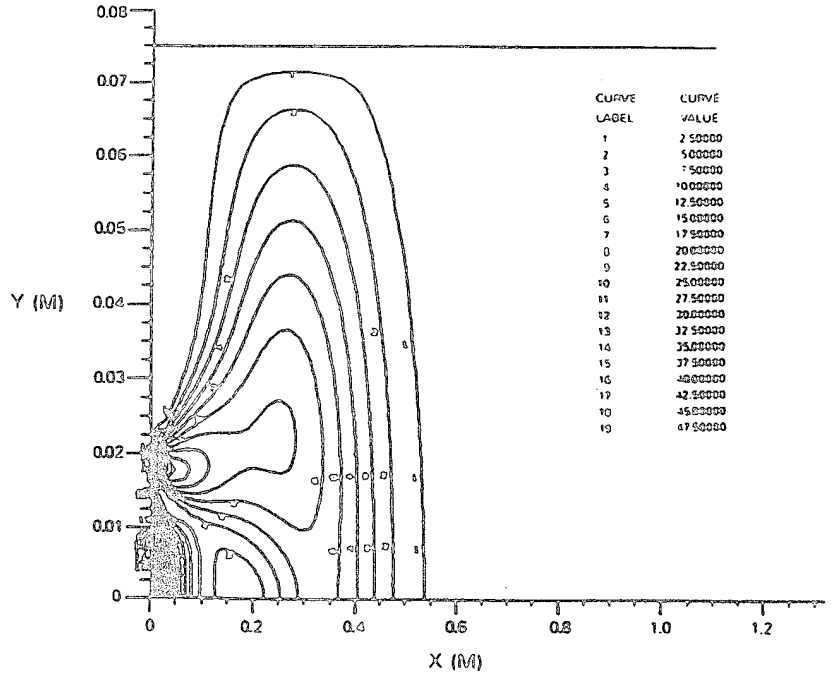

Figure 6–13. Calculated Field of Turbulence Kinetic Energy In PW100 Study Case

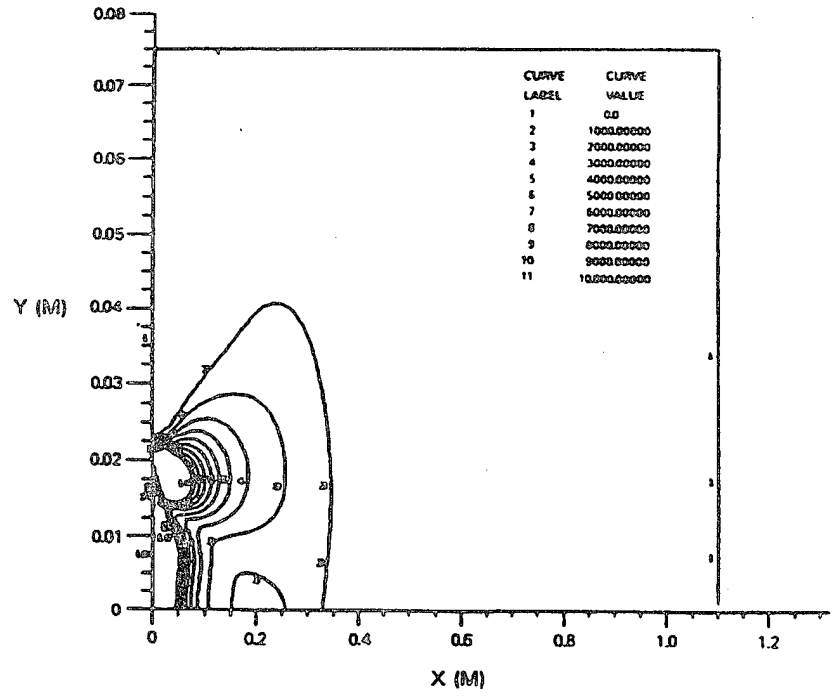

Figure 6–14. High–Range Values in the Calculated Rate of Turbulence Dissipation Field

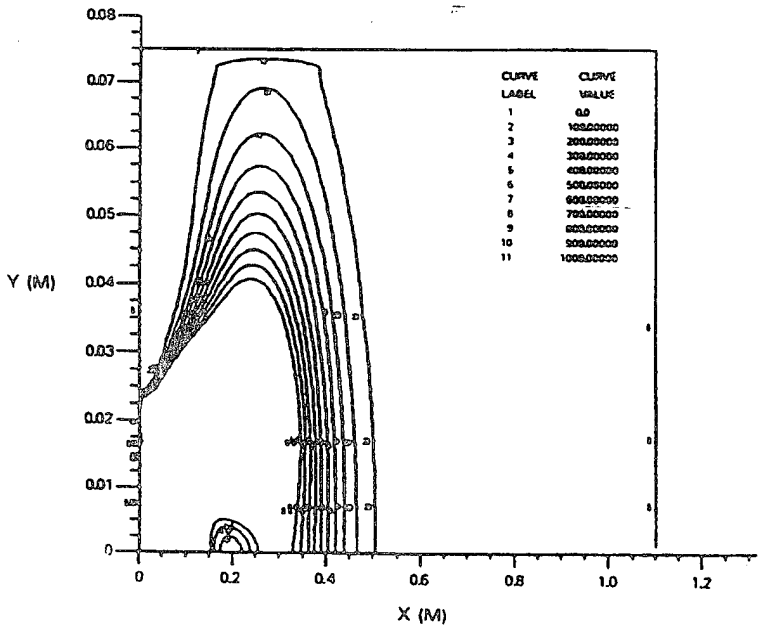

Figure 6–15. Low–Range Values in the Calculated Rate of Turbulence Dissipation Field

6.5 Kinetic Mechanism Evaluation

Problems involving blowout limits constitute particularly difficult computations involving systems of nonlinear differential equations for reaction kinetics. Even with a robust code it is necessary to approach blowout by making a series of steps, beginning with an artificially long residence time or high equivalence ratio with benign inlet conditions (elevated mixture temperature and pressure), such that the initial value for the problem is the equilibrium chemistry condition, and then progressively shortening the residence time or

reducing equivalence ratio and operating conditions, as blowout is approached. This is necessary because the extinction point represents a singularity that causes solution algorithms (Newton's method typically) to become more ill–conditioned as extinction is approached. This, in turn, prevents convergence, and requires the adoption of special procedures (predictor–corrector approaches). The number of solutions to reach the extinction point can represent a severe CPU burden. It is therefore well–worthwhile to consider reducing chemical species by means of a reduced reaction mechanism.

Propane was selected as the gaseous fuel of choice for the present study (see Section 2). It's kinetic mechanism has been fairly well established relative to the higher hydrocarbons, and it's reaction chemistry behavior resembles that of vaporized JP fuels. Some of the propane reduced kinetic mechanisms evaluated here are contained in Table 6–1. Reaction mechanisms are usually tested against their ability to predict flame speed, not their ability to predict extinction. It was therefore necessary to evaluate these mechanisms against extinction directly. An additional mechanism evaluated preliminarily, was the 6–step (global), 7 species mechanism of Jones & Lindstedt [47.]. Although this latter mechanism in an extinction test case gave extinction temperatures in close agreement with those obtained from the Paczko *et al.* mechanisms, there were considerable differences in minimum residence time, and it manifested some unrealistic species concentration behavior near extinction. Further consideration was not given to this mechanism.

With reference to Table 6–1, the Colket mechanism [48.] was a full mechanism, while Pazcko *et al.* had a partial mechanism that contained only those reaction steps that were considered to be important in high–temperature flames. The reduced mechanism also proposed by Pazcko *et al.* , [49.], consisted of relatively complex algebraic expressions formed by the judicious application of partial–equilibrium and steady–state assumptions to the elementary reaction steps. Both the Edelman & Harsha [50.] and Kollrack [51.], [52.] mechanisms were quasi–global in nature; the latter mechanism was for JP5 fuel. It was adapted for propane simulation by both substituting propane thermodynamics for JP5 thermodynamics, and by modifying the global steps for the appropriate C:H ratio. The Kretschmer & Odgers [53.] empirical expression was based on a one–step stoichiometry relationship for propane; it was calibrated to blowout data from stirred reactors.

The reaction mechanisms given in Table 6–1 were incorporated into a well–stirred reactor code in order to examine the accuracy of the various mechanisms in the limit of extinction. The code selected for this purpose was the PSR/CHEMKIN II code [54.]. In the CHEMKIN code the system of nonlinear equations is solved by a modified damped Newton algorithm. If the Newton algorithm fails to converge, the solution estimate is conditioned by a time–integration procedure that provides initial estimates which are more likely to be within the domain of convergence for Newton's method, (continuation method). The continuation method is a "predictor–solver" strategy, where the predictor component is Euler's technique and the solver component is Newton's iterative method. Despite the generally robust convergence conferred by these features, it was necessary to introduce further special modifications to the convergence algorithms when the code was used in the limit of extinction.

The reaction behavior of premixed fuel and oxidant can be conveniently characterized by a plot of reaction temperature versus reactor residence time. The behavior in this form follows an S–shaped curve, as is illustrated in Figure 6–16. From the chemically frozen state an increase in residence time allows weak and slow chemical reactions to occur. Eventually, a point is reached (the ignition state) where the rate of heat release by chemical reaction is greater than heat transport out of the reactor. This allows a rapid increase in temperature, which, via the exponential temperature dependency of Arrhenius kinetics, induces a coupled increase in reaction rate. Eventually, the reaction rate is high enough that significant reaction occurs within the reactor, and the equilibrium state is approached. The extinction state represents a condition where intense burning is not possible, such that the rate of heat release is no longer sufficient for an appreciable amount of reaction to occur in the available residence time. Between the extinction and ignition states is a region of *nonphysical solutions*. The transition between upper and lower branches of the reaction curve occurs precipitously.

Table 6–1. Comparison of Various Kinetic Mechanisms for Propane

Mechanism	Number of Species	Number of Reactions*	CPU Seconds** Per Steady–State Solution	30–Step CPU***	Comments
Colket (1989)	51	249–R	1.376	41.3	Full mechanism
Pazcko, Lefdel, Peters (1988)	29	76–I	0.308	9.24	"Partial" mechanism
Pazcko, Lefdel, Peters (1988)	8	5–G	0.045	1.35	Reduced mechanism
Edelman and Harsha (1978)	10	1–G 12–R	0.044	1.32	Quasi–global mechanism
Kollrack (1976) Roberts, et al (1972)	21	2–G 28–R	0.16	4.8	(a) Quasi–global mechanism (b) Fuel is JP–5
Kretschmer and Odgers (1972) (modified)	7	1	0.015	0.45	Equilibrium product distirubtion

* I = Irreversible elementary step
R = Reversible elementary step
G = Global step

** CPU on IBM 3090 platform

*** 20 to 50 steady state solutions may be required to find the extinction point along the reacting branch of the bifurcastion curve.

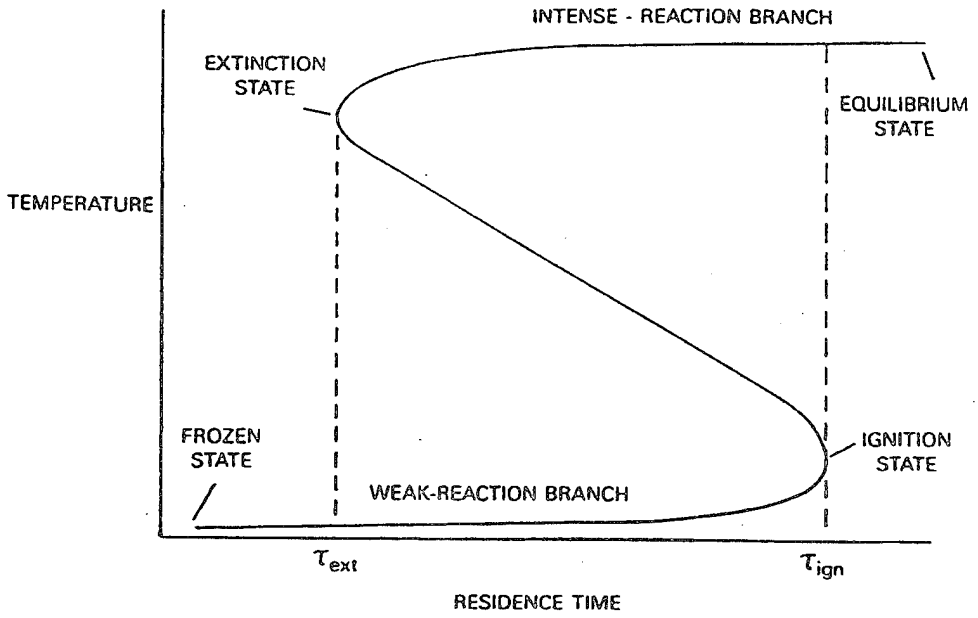

Figure 6–16. Characteristic S–Shaped Curve Showing all Possible Modes of Premixed Reaction Behavior

For various reaction mechanisms the determinant of the Jacobian matrix is positive on the upper branch of the reaction curve, and negative on the intermediate branch. The extinction point is therefore singular, (determinant of Jacobian zero), which causes the Newton algorithm to become more ill–conditioned as extinction is approached. The ill–conditioning precludes successful convergence of the solution algorithm.

Near the extinction point an alternative method, known as arc–length parameterization, must be employed. This method deletes the independent parameterization involving residence time, and absorbs it

as another dependent variable. The augmented vector of dependent variables is now a function of a new and arbitrary independent parameter that is the arc–length of the solution. The arc length is only a function of the temperature within the reactor, and the residence time. This change of variable procedure, in which τ becomes a dependent variable and arc–length becomes an independent parameter, essentially introduces a co–ordinate system transformation such that the turning point singularity disappears. The method was developed by Seydel [55.], and Keller [56.], [57.], and has been applied to extinction by Kee *et al.* [58.] and Giovangigli [59.]. The arc–length is schematically represented in Figure 6–17.

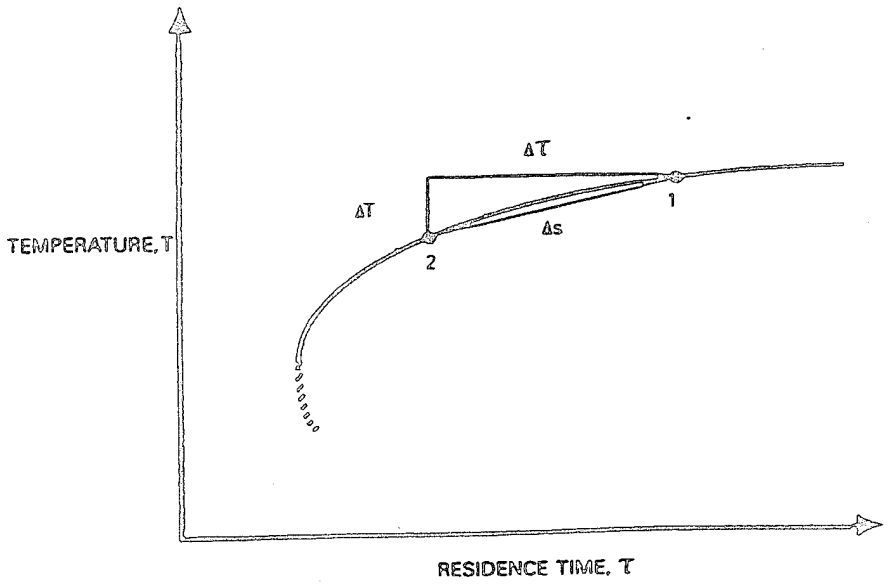

Figure 6–17. Representation of Solution Arc–Length

The robustness and efficiency of the combined arc–length/continuation method are largely a function of step length control. The arc step length (Δs) control should be flexible enough to adapt to the actual convergence behavior in order to achieve a stable solution at minimum CPU–cost. To achieve step–length control the magnitude of the slope near the extinction point was monitored through,

$$Slope = \frac{\left(\frac{\ln t_2 - \ln T_1}{\ln T_1}\right)}{\left(\frac{\ln \tau_2 - \ln \tau_1}{\ln \tau_1}\right)}$$

With reference to Figure 6–17, the magnitude of *slope* is larger near the extinction point than near the flat branch portions corresponding to chemical equilibrium. Hence, slope was used as a switch controlling the degree of severity of a damping factor applied to the updating of a previous solution, such that,

$$\Delta s_{new} = \varsigma(\Delta s_{old})$$

where ς is also a function of the number of Newton iterations for the previous (old) solution. If the Newton iterations completely failed to converge with the adjusted time–step, the calculations were automatically restarted with a severely reduced step–size.

The PSR/CHEMKIN–II code, incorporating the arc–length parameterization and continuation methodologies, was used to investigate the realism and CPU–cost of the various reaction mechanisms. Residence time was decreased in discrete intervals at constant equivalence ratio, reactor pressure and inlet temperature, until extinction occurred. Figure 6–18 presents an example for the Colket mechanism simulating extinction in the Hottel *et al.* [60.], well–stirred reactor experiment. It shows the damped arc

length and continuation effects on step–length as extinction was approached; Figure 6–19 compares the predicted stability loop using the mechanism, against the measured performance, where the locus of calculated extinction points is plotted in terms of equivalence ratio and air loading parameter (see Section 6.2). The extinction points are points of vertical tangency on each of the curves in Figure 6–18.

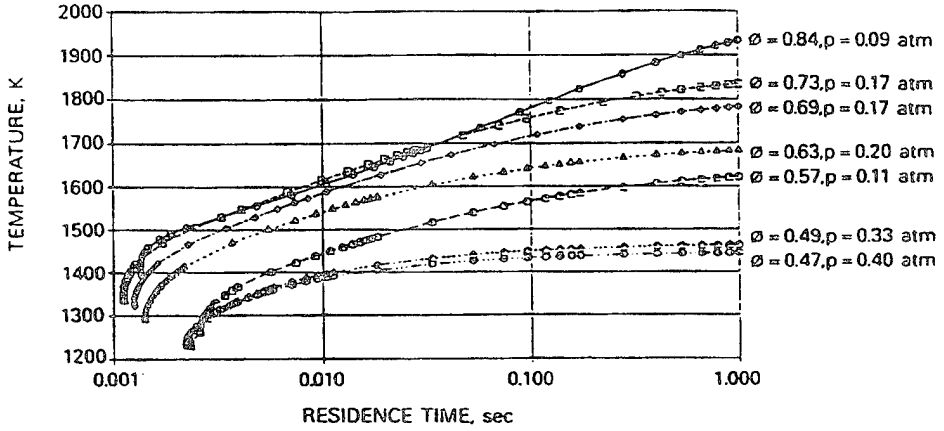

Figure 6–18. Calculated Solution Points Using the Colket Reaction Mechanism In PSR/CHEMKIN–II with Arc–Length Continuation Strategies, for the Hottel, et al. WSR Experiment

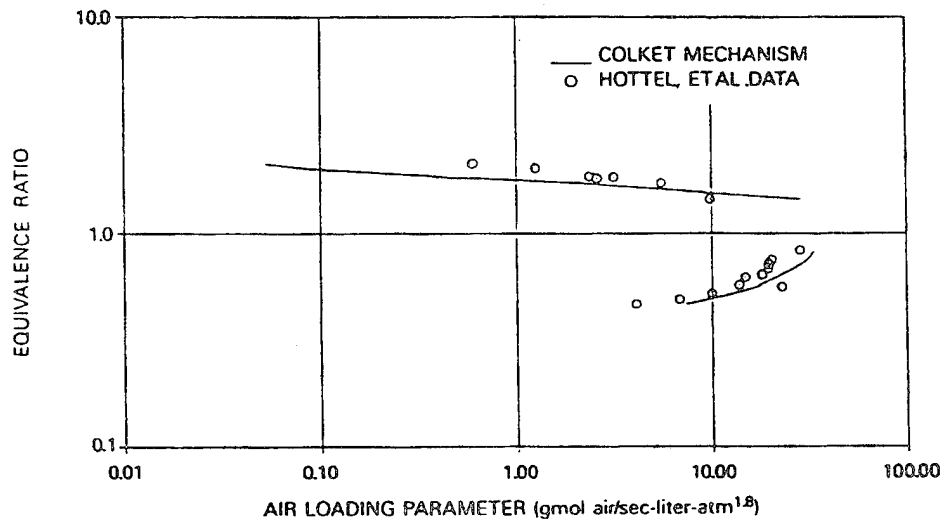

Figure 6–19. Comparison of Calculated Stability for the Colket Reaction Mechanism with the Measured Stability for the Hottel et al. WSR Experiments

Considering the logarithmic scales used in Figure 6–19, the agreement of the calculations with the measurements is not especially good, although it is qualitatively correct. However, given the nature of blowout experiments there will always be some scatter in the experimental data that is being compared against. Furthermore, the "well–stirred reactor" used in the experiments may not have been a "perfectly–stirred reactor." The effects of any unmixedness in the experiment would manifest themselves more near the peak heat release rate conditions, where peak heat release would be reduced. Heat losses from the experimental reactor are also a factor that could influence predictive accuracy. All in all, the full mechanism was considered to have performed well.

Consideration of Table 6–1 reveals that the cost of achieving this degree of predictive accuracy by using a full reaction mechanism was high. The calculations were made on an IBM 3090 mainframe computer at 1.376 sec./point of CPU time for each point shown in Figure 6–18, (there are 305 of them). This is two orders of magnitude computationally more expensive than, for example, the one–step mechanism of Kretschmer & Odgers.

To set the computational cost in better perspective, consider the following CFD example case using 2D–PREACH on a 48 x 45 mesh, with the 3–species eddy break–up combustion model. This model will not predict either flame–lift or blowout as these are beyond its capabilities. The overall time for a single iteration in this calculation was 1.3 CPU seconds on the IBM 3090 platform. This is virtually the same as the CPU time per point for the full reaction mechanism. However, 20 to 50 such points are typically needed to establish the upper branch and give the blowout condition, as Figure 6–18 indicates. This effort would have to be repeated at each node of the computational mesh. Depending on implementation, it might also have to be repeated for the complete mesh at each iteration required for the gas–phase flow–field solution. It would also be necessary as part of this flow–field, to solve additional transport equations for each of the chemical species involved in the kinetic mechanism, i.e., 51 of them for the Colket mechanism. The form of the transport equation is,

$$\frac{\partial}{\partial x_j}\left(\overline{\rho u_j}\,\overline{m}_i - \Gamma_{eff}\frac{\partial \overline{m}_i}{\partial x_j}\right) = S_{\overline{m}_i}$$

where i denotes chemical species, $\overline{m}_i$ is the time–mean mass fraction of i, and $S_{\overline{m}_i}$ is a species source term; Γ_{eff} is a turbulent exchange coefficient. This also results in a significant increase in the computational burden.

It is clear from this example that local application of a full–mechanism PSR calculation within a CFD calculation is not computationally feasible, even for relatively simple geometry combustors..

On the basis of low CPU–usage, Table 6–1 suggests that the reduced mechanism of Pazcko *et al.* and the quasi–global mechanism of Edelman & Harsha appear as candidates for consideration. The best CPU performance is that of the one–step mechanism due to Kretschmer & Odgers. However, the predictive accuracy of the respective mechanisms is the major and over–riding consideration.

In order to assess the relative predictive accuracy of the various mechanisms, the PSR/CHEMKIN–II calculations for each were compared with the experimental data from the well–stirred spherical reactor experiments of Clarke *et al.* [61.]. This experiment was selected because it was for a propane/air/nitrogen system, and provided a comprehensive blowout data set covering wide–ranging conditions. It was also the experiment against which Kretschmer & Odgers calibrated their mechanism. Only one of several data sets was used in the comparisons, that for "Injector A."

Figure 6–20 compares the experimental stability loop with the calculated loops for the Colket full mechanism and the Paczko *et al.* "partial" mechanism (29 species and 76 single–step reactions; rate constants were for 1 atmos.). The calculated stability loops for the Colket and Paczko *et al.* mechanisms are in close agreement. Unfortunately, these mechanisms both over–estimate the measured peak heat release condition by a factor of four in air loading parameter. Closer consideration of Figure 6–19 suggests that the Colket mechanism might also over–estimate the peak heat release rate condition for the Hottel *et al.* reactor, although by not as much as in Figure 6–20. The experimental stability loops of Clarke *et al.* and Hottel *et al.* are in reasonable agreement with each other. Clarke *et al.* did notice a slight effect of pressure loss on their data, indicative of less than perfect mixing. Spherical reactors also have heat losses somewhat greater than about 5 percent. Both these effects would tend to reduce the peak heat release rate achieved. However, it is doubtful that heat losses or reactor mixing limitations in the experiments could account entirely for the significant discrepancy between calculations and measurements. It is possible that a separate physical phenomenon might have controlled global quenching in the Clarke *et al.* and Hottel *et al.*

reactors; for example, acoustic oscillations or combustion–driven instabilities. Such oscillations and instabilities can occur in WSR experiments, although none were reported in the cited experiments.

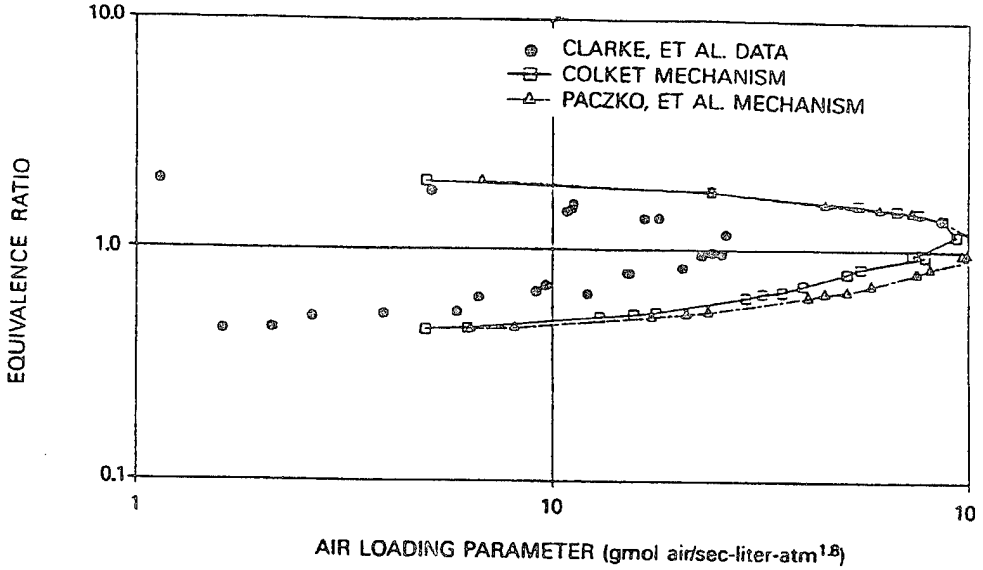

Figure 6–1. Comparison of Stability Loops Calculated with Colket "Full" and Paczko et al. "Partial" Mechanisms, Against the WSR Experiments of Clarke et al. (Injector A)

(It should be noted that more recent WSR experiments [62.] are indicating that higher peak heat release rates can be achieved than those demonstrated by the Hottel *et al.* and Clarke *et al.* experiments; however, the differences between the earlier and more modern reactors would have to be thoroughly researched to definitively resolve this issue.)

A more plausible explanation for the sources of predictive inaccuracy is that the hydrocarbon kinetic mechanisms are inadequate in some way. This inadequacy could be in postulated reaction pathways, or inaccuracies in the experimental rate constants. Rate constants in particular, are normally evaluated at conditions well–removed from blowout, and may not be applicable over wide ranges of conditions.

NO TAG compares the Clarke *et al.* experimental blowout data with calculated blowout for all of the mechanisms given in NO TAG, except for the Kretschmer & Odgers mechanism. The Kollrack mechanism was applied in two ways: as is with propane thermodynamics, and additionally, with reaction steps modified for the propane C:H ratio.

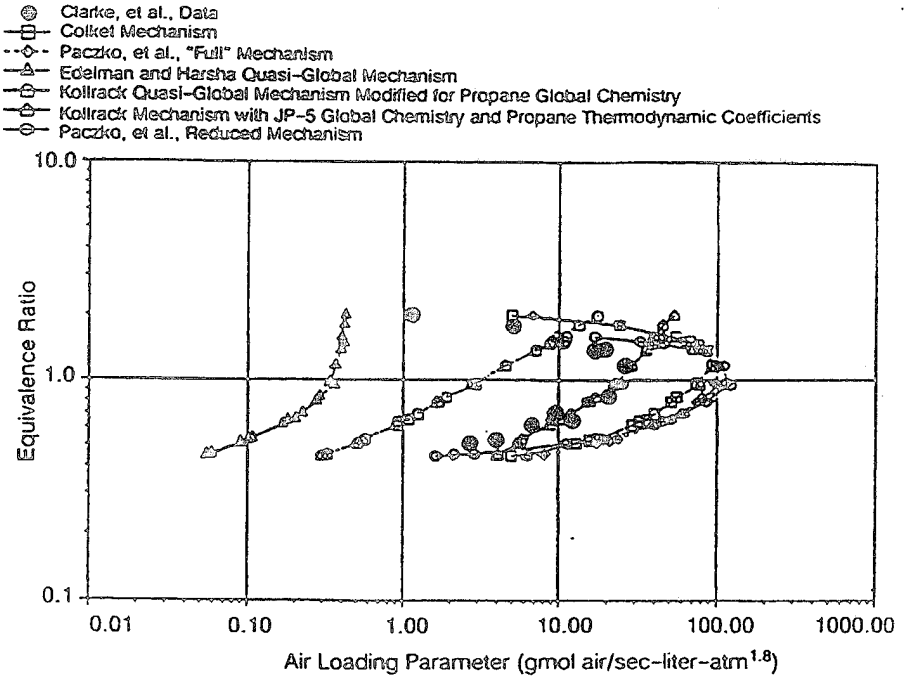

Figure 6–21. Comparison of Experimental Data of Clarke et al. (Injector A) Against Calculated Stability Using Reaction Mechanisms of Table 6–1

For rich blowouts, the Edelman & Harsha quasi–global mechanisms gave trends that were qualitatively incorrect. Only the Colket and Paczko *et al.* "full" and "reduced" mechanisms were qualitatively correct, but were substantially in error quantitatively. For lean blowouts the Kollrack mechanism with propane thermodynamics and modified reaction steps, and the Edelman & Harsha mechanisms were both seriously in error. The Kollrack mechanism with only propane thermodynamics was in good agreement with the experimental data, although there was some fall–off at very low values of air loading parameter.

The Kretschmer & Odgers 7 species, 1 step mechanism was based on the stoichiometry relationship,

$$\phi C_3H_8 + 5(O_2 + aN_2) \rightarrow 3\varepsilon\eta CO_2 + 4\varepsilon\eta H_2O + (\phi \pm \varepsilon\eta)C_3H_8 + 5(1 \pm \eta)O_2 + 5aN_2 \qquad 6.43$$

where,

ϕ = molar equivalence ratio

a = 3.762 moles of N_2/mole O_2 in air

$\eta = \phi$ for $\phi \leq 1$

$= 1$ for $\phi > 1$

ε = fractional (oxidant) consumption efficiency

The reaction rate expression was given in terms of the molar rate of disappearance of oxygen, as,

$$\pm r_O = \pm \frac{dC_O}{dt} = k_O T^m \exp[\pm T_{act} / T] C_F^{\alpha} C_O^{\beta} \qquad 6.44$$

where,

r_O = molar rate of disappearance of oxidant (gmol O_2/liter–sec.)

C_F = molar concentration of fuel (gmol C_3H_8/liter)

C_O = molar concentration of oxidant (gmol O_2/liter)

t = time (sec.)

k_O = preexponential factor based on oxidant

$$= 1.29 \times 10^{10} \frac{(liters)^{\alpha+\beta+1}}{(K)^{m}(gmol)^{\alpha+\beta\pm1}(\text{sec.})}$$

T = temperature (K)

m = exponent on temperature

α, β = exponents on the reactant concentrations

T_{act} = activation temperature (i.e., activation energy divided by the gas constant; in units of K)

For use with blowout curves, the reaction rate equation was couched in terms of an air loading parameter:

$$\frac{N}{VP^{n}} = \frac{k_o}{\Re} \cdot \frac{(a+1)}{\eta\epsilon} (T_{in} + \epsilon\Delta T)^{m-n}\left[exp\ -T_{act}/(T_{in} +)\epsilon\Delta T)\right] x_F^{n/2} x_o^{n/2} \qquad 6.45$$

where,

$$x_F = \text{mole fraction of fuel} = \frac{\phi \pm \varepsilon\eta}{5(a+1) + \phi + \varepsilon\eta} \qquad 6.46$$

$$x_O = \text{mole fraction of oxygen} = \frac{5(1 \pm \varepsilon\eta)}{5(a+1) + \phi + \varepsilon\eta} \qquad 6.47$$

n = overall reaction order = $\alpha + \beta$

$= 2\phi$ for $\phi \preceq 1$

$= 2/\phi$ for $\phi > 1$

$\Re$ = universal gas constant = 0.08205 atm−liter/gmol−K

T_{in} = inlet temperature (K)

ΔT = "undissociated" adiabatic temperature rise (K)

V = reactor volume (liter)

P = static pressure in reactor (atm.)

N = molar flow rate of air into the reactor (gmol air/sec.)

The expression was calibrated by Kretschmer & Odgers to blowout data by tabulating values of the adiabatic temperature rise (ΔT), the activation temperature (T_{act}), and the fractional oxygen consumption efficiency (ε) as a function of inlet temperature (T_{in}) and the inlet equivalence ratio (ϕ). The tabulation was from temperatures of 300 to 900°K and equivalence ratios from 0.4 to 2.0, although reliable confirmation for equivalence ratios greater than unity could not be obtained.

Extinction calculations using Equation 6.45 are compared to the WSR data of Clarke *et al.* for "Injectors A and D," in Figure 6−22 and Figure 6−23, respectively. The calibrated expression attains better predictive accuracy than that exhibited by the multistep mechanisms. It s performance represents the minimum level of accuracy which other mechanisms or techniques should match in order to be considered for extinction calculations.

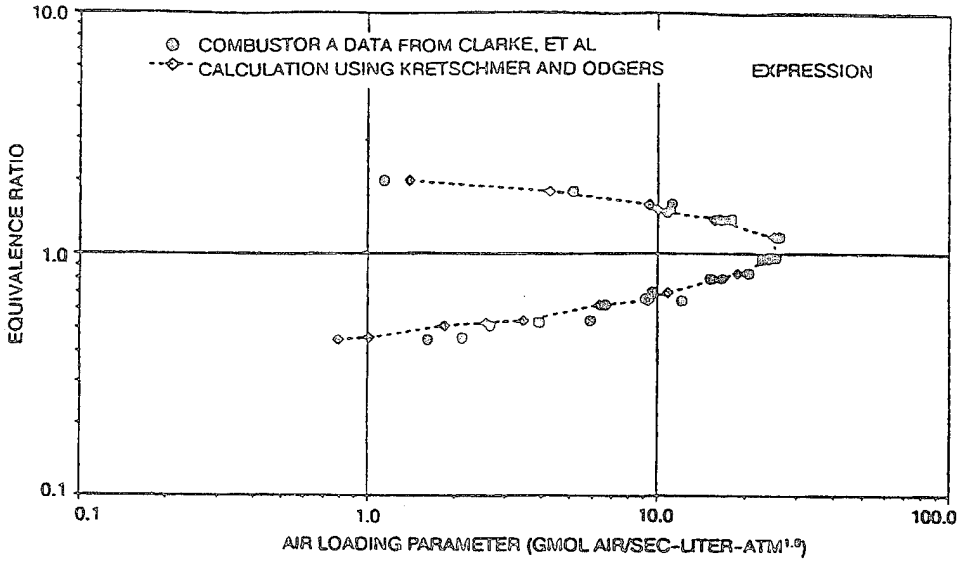

Figure 6–22. Comparison of Measured and Calculated Stability Loops for Clarke et al. (Injector A) WSR Experiments, Using Kretschmeer & Odgers Calibrated Mechanism

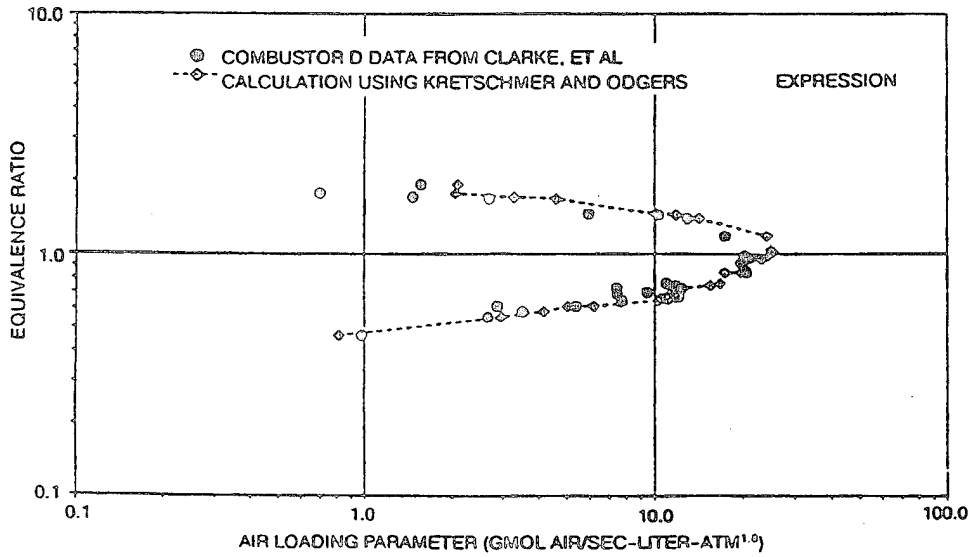

Figure 6–23. Comparison of Measured and Calculated Stability Loops for Clarke et al. (Injector D) WSR Experiments, using Kretschmer & Odgers Calibrated Mechanism

6.6 Eddy Dissipation Concept in CFD Modeling

6.6.1 Introduction

The Eddy Dissipation Concept (EDC) of Magnussen [63.], [41.], [64.–68.], is a general model for chemical reaction in turbulent flow. The approach focuses on the physics of the fine–scale turbulence (much as in Section 6.3).

Microscale processes, such as dissipation of turbulence kinetic energy into heat and molecular–level mixing of reactants, occur within the fine eddy structures of length scale of up to a few times that of the Kolmogorov eddies. The fine structures have dimensions that are small in one or two dimensions, but not in the third. The microscale structures are concentrated within fine–structure regions, that are themselves

severely intermittent spatially, and which have a cumulative volume that is only a small fraction of the total volume of the fluid.

The EDC combustion model is based on the concept that the reactants are homogeneously mixed within the fine eddy structures. Therefore, these fine structures may be regarded as being well-stirred reactors. This approach is entirely consistent with the ideas and concepts followed thus far in Section 6 – Modeling Considerations.

The EDC model partitions the fluid into fine structures that define the well-stirred reactors, and the "surrounding fluid," which includes all of the remaining fluid regardless of turbulence scale. AS befits well-stirred reactors, the fine structures are assumed to have a uniform internal composition and temperature, both of which are determined by the progress of the reactions taking place in these structures. Since the scale of the fine structures would normally be below that which could be resolved by any reasonable CFD computational grid, the fine structure reactors are referred to as subgrid scale reactors. The composition and temperature of the "surrounding fluid" constitute the feed-stream conditions to the subgrid scale reactors.

To be able to model the chemical reactions occurring within the well-stirred reactors, it is necessary to know the fine-scale structure volume, as well as the mass exchange rate between the fine structures and the surrounding fluid. The model supplies a system of equations that describes the chemical reaction process within the fine-structure reactors, and then relates the microscale parameters to the ensemble-averaged mean flowfield. The ensemble-averaged mean scalar quantities are determined by an appropriate linear combination of the fine-structure and surrounding-fluid characteristics. The set of EDC model equations, in conjunction with a stirred reactor calculation methodology and "full" chemical kinetics, may be solved for the fine structure and surrounding-fluid regions of every computational cell of the grid in the flowfield domain. The local hydrodynamic time scales or residence times corresponding to the fine structure eddies, may be calculated from the information supplied through the turbulence model in the CFD code. By calculating the relevant chemical time scale at extinction and comparing it to the hydrodynamic equivalent, computation could be made of local regions of extinction. Hence, a CFD code containing the EDC combustion model potentially might be capable of simulating the phenomena of flame-lift and blowout.

6.6.2 Fluid Dynamics

A turbulent flow consists of eddies of a large number of sizes and velocities. The classical concept is that the largest eddies extract energy from the mean flow, and progressively transfer it down the eddy size range to the smallest eddies where it is eventually dissipated as heat via the action of viscosity. The smallest eddies are known as the Kolmogorov eddies, and the flow inside them is laminar, with zero dissipation of turbulence kinetic energy taking place. The small-scale structures of turbulence within which dissipation is a maximum, are not uniformly distributed in a turbulent motion at high Reynolds Numbers. There are relatively small regions of the flow having intense dissipation, that are scattered through the fluid, leaving large regions with negligible dissipation. The fraction of the fluid volume occupied by fine structures of given size decreases as the turbulence Reynolds Number is decreased. Also, the relative volume occupied by fine structures decreases as the wave number decreases. The average linear dimension of fine structure regions is much larger than the sizes of the fine structures contained within them.

In a turbulent motion an eddy is an envelope of vortex lines, each interacting strongly with one another in the eddy, and comparatively weakly with vortex lines in other eddies. A turbulent flow is therefore an intertwined, three-dimensional, random mass of such vortex-line envelopes. The envelope of vortex lines may take the form of large vortex sheets, ribbons of vorticity, or, vortex tubes. Vortex lines are stretched in preferred directions by the mean shear existing in the flow.

The first task in establishing the EDC model is to define the micro-scales of the fine structures of turbulence. The fine structure is associated with the dissipation of turbulence kinetic energy and

molecular–level mixing of reactants. In Section 6.3, molecular–level mixing was associated with eddies where dissipation of turbulence kinetic energy was a maximum. Assumptions were made that chemical reaction could be initiated with less–than–perfect molecular mixing within an eddy and, that laminarization of eddy internal flow due to heat release could reduce further dissipation to zero. With these assumptions, experimental evidence for high Reynolds Number flows was used to provide a relationship between the length of maximum dissipation eddies and the Kolmogorov eddies, i.e., Equation 6.6,

$$l_D = 5\eta \qquad 6.49$$

The assumption is made that the rate of energy supply to the small eddies of a turbulent motion is equal to the dissipation rate of this energy to heat, via the action of viscosity. Thus, the net rate of change is less than the energy dissipation rate and so, by dimensional reasoning the Kolmogorov scales are established as,

length: $\eta = \left(\nu^3 / \varepsilon\right)^{1/4}$

velocity: $V = (\varepsilon\nu)^{1/4}$

time: $\tau = (\nu / \varepsilon)^{1/2}$

so that the Kolmogorov eddies have a fixed Reynolds Number,

$$\mathrm{Re}_K = \frac{V\eta}{\nu} = 1.0$$

Now, vorticity represents the rotation of an undistorted (solid body) fluid element, and is defined,

$$\zeta = \frac{dC}{dA}$$

where the circulation C, is given by,

$$C = \oint v\cos\alpha \; ds$$

ds being an element of an eddy circumference and $v\cos\alpha$ is the local tangential velocity to the center of eddy rotation. For a circular eddy of radius r, all points on the circumference have the same velocity U, and,

$$C = 2\pi U r$$

In terms of angular velocity ω, $U = \omega r$ and, $C = 2\pi\omega r^2$. Hence,

$$\zeta = 2\omega$$

If u_e is the eddy velocity scale and l_e is it's length scale, then,

$$\xi = 2\frac{u_e}{l_e} \qquad 6.49$$

Hence, ζ represents a vorticity scale for the eddies. Eddies generally exist in a flow as line vortices (small in two directions, but not in the third). As a line vortex is stretched axially due to fluid motion, its radius decreases but angular momentum $\left(r\omega^2\right)$, is conserved. Thus, ω increases, and therefore, ζ increases also. In a general sense, vorticity can be expressed,

$$\xi = \varepsilon_{i,j,k}\frac{\partial u'_k}{\partial x_j}$$

Viscous dissipation by turbulent fluctuations is given, per unit mass, by,

$$\varepsilon = 1/2\nu\left(\frac{\partial u'_i}{\partial x_j} + \frac{\partial u'_j}{\partial x_i}\right)\frac{\partial u'_j}{\partial x_i}$$

which for isotropic turbulence reduces to,

$$\varepsilon = 15\nu\overline{\left(\frac{\partial u'_i}{\partial x_i}\right)^2} \qquad 6.50$$

where the numerical coefficient arises from the summation over the indices i, j, k.

If, as in Section 6.4,

$$u_e = \overline{(u'^2)}^{1/2}$$

then substituting in Equation 6.50,

$$\varepsilon = 15\nu\left(\frac{u_e}{l_e}\right) \qquad 6.51$$

The production of turbulence by the mean shear can be obtained from the K–transport equation, as, per unit mass,

$$P_K = \overline{u'_i u'_j}\frac{\partial u_i}{\partial x_j}$$

where pressure fluctuations are ignored.

Using eddy viscosity modeling,

$$-\overline{u'_i u'_j} = \frac{\mu_t}{\rho}\left(\frac{\partial u_i}{\partial x_j} + \frac{\partial u_j}{\partial x_i}\right) = \nu_t\left(\frac{\partial u_i}{\partial x_j} + \frac{\partial u_j}{\partial x_i}\right)$$

where μ_t is the turbulent viscosity.

Now, an expression for turbulent viscosity can be obtained as follows:

$\nu_t = V_T^m l_T^n$ where V_T and l_T are suitable turbulence scales.

Assume $\nu_t^m = K^{1/2}$ a standard assumption, so that, $\nu_t = K^{1/2} l_T^n$

Now, using dimensional reasoning,

$$\nu_t \supseteq \left[\frac{L^2}{T}\right] \quad ; \quad K^{1/2} \supseteq \left[\frac{L}{T}\right] \text{ so that, } n = 1.0, \text{ and ,}$$

$$\nu_t = K^{1/2} l_T$$

This is a well–established relationship. For isotropic turbulence, $K = 3 / \overline{2u'^2}$ and, if,

$$u_e = \left(\overline{u'^2}\right)^{1/2} \quad \text{then,} \quad K^{1/2} = \sqrt{\frac{3}{2}}u_e \quad \text{so that,} \quad \nu_t = \sqrt{\frac{3}{2}}u_e l_T$$

where l_T now clearly relates to the energy–containing eddies.

Then, in isotropic turbulence, with summation over the indices, per unit mass,

$$P_K = 12\nu_t\left(\frac{\partial u_i}{\partial x_i}\right)^2 \qquad 6.52$$

i.e., substituting for ν_t,

$$P_K = 12\sqrt{\frac{3}{2}}u_e^2\left(\frac{u_e}{l_T}\right) \qquad 6.53$$

At any wave number n, in the energy cascade through the eddy sizes, a balance of energy is,

Energy in given wavenumber (n)	=	energy transferred to next wave number ($n+1$)	+	Energy dissipated as heat in given wavenumber (n)

Using Equations 6.51 and 6.52, the appropriate terms can be substituted into this balance, as follows:

$$\xi\left[12\sqrt{\frac{3}{2}}(u_e^2)_n\left(\frac{u_e}{l_e}\right)_{n-1}\right] = \xi\left[12\sqrt{\frac{3}{2}}(u_e^2)_{n+1}\left(\frac{u_e}{l_e}\right)_n + 15\nu\left(\frac{u_e}{l_e}\right)_n\right]$$

where the coefficient ξ is introduced to account in a crude sense, for "leakage" of energy across wave numbers in the cascade process, and is therefore, less than or equal to unity. Although it is treated here as a constant for all wave numbers, ξ is unlikely to be a constant. Also, at the previous wave number, $(u_e / l_T) \rightarrow (u_e / l_e)$, i.e., the previous wave number always represents eddies larger than the considered wave number.

Denoting the smallest eddies of the eddies in the dissipation range with the subscript *, for equilibrium turbulence,

$$P_* = \varepsilon_*$$

where, using the equations above,

$$P_* = \xi\left[12\sqrt{\frac{3}{2}}(u_e^2)_*\left(\frac{u_e}{l_e}\right)_{*-1}\right]$$

and

$$\varepsilon_* = \xi\left[15\nu\left(\frac{u_e}{l_e}\right)_*^2\right]$$

If the wave number ranges are defined through the vorticity ζ, where each eddy level has a characteristic vorticity scale, each considered wavenumber can be separated from its neighboring wavenumber number ranges by an arbitrary factor of twice the vorticity. This is a plausible approach because the smaller eddies are exposed to the strain–rate field of the larger eddies, this results in the vorticity of the smaller eddies increasing, with a consequent increase in their energy at the expense of the energy of the larger eddies, so that there is a distinct separation in vorticity between the eddy sizes. Therefore, the vorticity for the very small eddies ζ_*, is given by,

$$\xi_* = 2\,\xi_{*-1}$$

Thus, from Equation 6.49,

$$\xi_* = 2\left[2\left(\frac{u_e}{l_e}\right)_{*-1}\right]$$

Then, since $\xi_* = 2(u_e/l_e)$ also, these two expressions may be equated to yield,

$$\left(\frac{u_e}{l_e}\right)_{*-1} = 1/2\left(\frac{u_e}{l_e}\right)_* \qquad 6.54$$

Introducing Equation 6.54 into the expression above for P_*,

$$P_* = \xi\left[12\sqrt{\frac{3}{2}}(u_e^2)_* \frac{1}{2}\left(\frac{u_e}{l_e}\right)_*\right] = \xi\left[12\frac{1}{2}\sqrt{\frac{3}{2}}\left(\frac{u_e^3}{l_e}\right)_*\right]$$

Equating this with the expression for ε_*,

$$\xi\left[12\frac{1}{2}\sqrt{\frac{3}{2}}\left(\frac{u_e^3}{l_e}\right)_*\right] = \xi\left[15\nu\left(\frac{u_e}{l_e}\right)_*^2\right]$$

i.e., there are two simultaneous equations for ε_*,

$$\varepsilon_* = \xi\left[15\nu\left(\frac{u_e}{l_e}\right)_*^2\right]$$

and,

$$\varepsilon_* = \xi\left[12\frac{1}{2}\sqrt{\frac{3}{2}}\left(\frac{u_e^3}{l_e}\right)_*\right]$$

This procedure may be repeated at the next lower wave number, i.e.,

$$\xi_{*-1} = 2\xi_{*-2}$$

Thus,

$$\xi_{*-1} = 2\left[2\left(\frac{u_e}{l_e}\right)_{*-2}\right]$$

or, using Equation 6.49 for vorticity,

$$2\left(\frac{u_e}{l_e}\right)_{*-1} = 2\left[2\left(\frac{u_e}{l_e}\right)_{*-2}\right]$$

i.e., $\left(\frac{u_e}{l_e}\right)_{*-2} = \frac{1}{2}\left(\frac{u_e}{l_e}\right)_{*-1}$ and introducing Equation 6.54,

$$\left(\frac{u_e}{l_e}\right)_{*-2} = \frac{1}{4}\left(\frac{u_e}{l_e}\right)_* \qquad 6.55$$

Hence,

$$P_{*-1} = \xi\left[12\sqrt{\frac{3}{2}}\ (u_e^2)_*\left(\frac{u_e}{l_e}\right)_{*-2}\right] = \xi\left[12\sqrt{\frac{3}{2}}(u_e^2)_*\ \frac{1}{4}\left(\frac{u_e}{l_e}\right)_*\right]$$

Since production is equal to dissipation in this range of wave numbers,

$$\varepsilon_{*-1} = \frac{1}{4}\varepsilon_*$$

or,

$$\varepsilon_* = \xi\left[15\nu\left(\frac{u_e}{l_e}\right)_*^2\right]$$

and, repeating at the higher spectral levels,

$$\varepsilon_{*-1} = \xi\left[15\nu\left(\frac{u_e}{l_e}\right)_{*-1}^2\right] = \xi\left[15\nu\left(\frac{1}{2}\frac{u_e}{l_e}\right)_*^2\right]$$

$$\varepsilon_{*-2} = \xi\left[15\nu\left(\frac{1}{4}\frac{u_e}{l_e}\right)_*^2\right]$$

$$\varepsilon_{*-3} = \xi\left[15\nu\left(\frac{1}{16}\frac{u_e}{l_e}\right)^2\right]$$

etc., etc.

Therefore,

$$\frac{\varepsilon_*}{\varepsilon_{Tot}} = \frac{\varepsilon_*}{\sum_{all\ n}\varepsilon_{*-n}} = \frac{\varepsilon_*}{\varepsilon_*\left(1 + \frac{1}{4} + \frac{1}{16} + \frac{1}{256} + \frac{1}{1024} + \cdots\right)}$$

$$\frac{\varepsilon_*}{\varepsilon_{Tot}} = \frac{\varepsilon_*}{1.333008\varepsilon_*} = 0.7502$$

i.e., three–quarters of the total dissipation takes place in eddies that are part of the fine structure; or alternatively, a negligible dissipation of energy as heat occurs at the highest eddy levels of the cascade representation of turbulence.

Then, if $\varepsilon = \frac{\varepsilon_*}{0.75}$ the two simultaneous equations of ε_* become,

$$\varepsilon = \frac{\xi}{0.75}\left[15\nu\left(\frac{u_e}{l_e}\right)_*^2\right]$$

$$\varepsilon = \frac{\xi}{0.75}\left[12\frac{1}{2}\sqrt{\frac{3}{2}}\left(\frac{u_e^3}{l_e}\right)_*\right]$$

Equating these simultaneous equations,

$$\left[15\nu\left(\frac{u_e}{l_e}\right)^2_*\right] = \left[12\frac{1}{2}\sqrt{\frac{3}{2}}\left(\frac{u_e^3}{l_e}\right)_*\right]$$

$$15\nu\frac{1}{(l_e)_*} = 12\frac{1}{2}\sqrt{\frac{3}{2}}(u_e)_*$$

or,

$$(u_e)_* = \frac{2x15\nu}{12}\sqrt{\frac{2}{3}}\frac{1}{(u_e)_*}$$

and,

$$(l_e)_* = \frac{2x15\nu}{12}\sqrt{\frac{2}{3}}\frac{1}{(u_e)_*}$$

Substituting above for $(l_e)_*$,

$$\varepsilon = \frac{\xi}{0.75}\left[12\frac{1}{2}\sqrt{\frac{3}{2}}(u_e^3)_*\,(u_e)_*\,\frac{12}{2x15\nu}\sqrt{\frac{3}{2}}\right]$$

so,

$$(u_e^4)_* = (\nu\varepsilon)\,\frac{2x15}{12^2}2\frac{2}{3}\,\frac{0.75}{\xi} \qquad \text{so then,} \qquad (u_e)_* = \frac{0.6756}{\xi^{1/4}}\,(\nu\varepsilon)^{1/4}$$

Thus, from the definition of Kolmogorov eddy velocity scale given above,

$$(u_e)_* = \frac{0.6767}{\xi^{1/4}}\,V \qquad 6.56$$

and, hence,

$$(l_e)_* = \frac{2x15\nu}{12}\sqrt{\frac{2}{3}}\cdot\frac{1}{0.6756}\cdot\frac{\xi^{1/4}}{\nu\varepsilon^{1/4}} = 3.0214\xi^{1/4}\left(\frac{\nu^3}{\varepsilon}\right)^{1/4}$$

and again, using the definition of Kolmogorov eddy length scale, also given above,

$$(l_e)_* = 3.0214\xi^{1/4}\,\eta \qquad 6.57$$

The energy leakage coefficient ξ may be estimated from experimental evidence. As in Section 6.3, for low Reynolds, Numbers $(l_e)_* \approx 2\eta$. Hence, in Equation 6.57,

$$\xi = \left(\frac{2}{3.0214}\right)^4 = 0.192$$

Then, with this value,

$$(u_e)_* = 1.0206V$$

For high Reynolds Numbers, $(l_e)_* < 5\eta$, giving $\xi = 1.655$ for an upper limit, which is not physically possible. However, it can be stated that $0.192 \leq \xi \leq 1.0$ is reasonable. If $\xi = 1.0$, then

$$(l_e)_* = 3.0214\eta$$

Magnussen obtained a value of 0.260 for this coefficient. Following Magnussen therefore,

$$(u_e)_* = 1.75V \qquad 6.58$$

$$(l_e)_* = 1.43\ \eta \qquad 6.59$$

Thus, the analysis indicates that the scales of the fine scale structures are of the same order of magnitude as those of the maximum dissipation eddies used in the stability analysis. However, the definition of the fine structures is more restrictive. Not only do the fine structures encompass the maximum rates of dissipation, but they also include most of the total dissipation (three–quarters of it), that is accomplished.

The regions of high dissipation are relatively small regions of the flow that are scattered through the fluid. The vortex lines of the eddies constituting a region of concentrated vorticity and making up the fine structure, are stretched by the action of the larger eddies of the turbulent motion. As a result, there is an intermittency of dissipation at a point in an Eulerian frame of reference. The stretching of vortex lines by shear may be represented as shown in Figure 6–24, where straining of a vortex line is occurring between two bigger eddies.

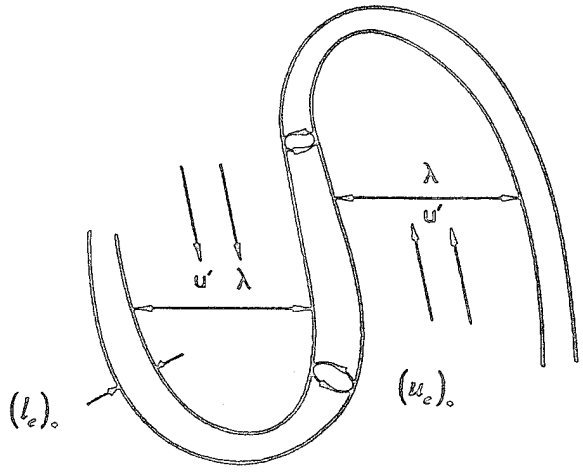

Figure 6–24. Schematic Illustration of a Fine Structure Vortex Tube BeingStrained by Larger Eddies

The average linear dimension λ, of an active fine structure region, will be greater than that of the linear dimension { length scale $(l_e)_*$ } of the small–scale structure contained therein. Therefore, a dissipative intermittency will exist. The volume fraction γ_*, occupied by the dissipative motion, is on the order of,

$$\gamma_* = \frac{vol.\ of\ eddy}{vol.\ of\ region} \cong \frac{(l_e)_*\lambda^2}{\lambda^3} = \frac{(l_e)_*}{\lambda} \qquad 6.60$$

Now, if equilibrium turbulence is taken, i.e., $P_\lambda = P_*$, where, from the discussion above on dissipative eddies,

$$P_* = \xi\left[12\sqrt{\frac{3}{2}}\cdot\frac{1}{2}\cdot\frac{(u_e)_*^3}{(l_e)_*}\right] \quad \text{for the small–scale eddies.}$$

and similarly,

$$P_\gamma = \xi\left[12\sqrt{\frac{3}{2}}\cdot\frac{1}{2}\cdot\frac{(u_e)^3}{l_e}\right]$$ for the larger–scale eddies,

and hence,

$$\xi\left[12\sqrt{\frac{3}{2}}\cdot\frac{1}{2}\cdot\frac{(u_e)_*^3}{(l_e)_*}\right] = \xi\left[12\sqrt{\frac{3}{2}}\cdot\frac{1}{2}\cdot\frac{(u_e)^3}{l_e}\right]$$

or,

$$\frac{(u_e)_*^3}{(l_e)_*} = \frac{(u_e)^3}{l_e}$$

Since for the larger eddies,

$$\frac{u_e^3}{l_e} \equiv \frac{(u')^3}{\lambda} \qquad \text{then} \qquad \frac{(u_e)^3}{(l_e)_*} = \frac{(u')^3}{\lambda}$$

and hence,

$$\gamma_* = \left[\frac{(u_e)_*}{u'}\right]^3 \qquad 6.61$$

Now, it was established above, Equation 6.58, that,

$$(u_e)_* = 1.75(\varepsilon\nu)^{1/4}$$

and for isotropic turbulence,

$$u' = \left(\frac{2}{3}K\right)^{1/2}$$

i.e., implying that the bigger eddies in this case are the energy–bearing eddies, and therefore that λ is really the **Taylor microscale** of turbulence. Hence, inserting these expressions for eddy velocities into Equation 6.61, gives,

$$\gamma_* = 9.7\left(\frac{\varepsilon\nu}{K^2}\right)^{3/4} \qquad 6.62$$

In a region of local isodensity, the volume fraction, Equation 6.62, is also equivalent to a mass fraction.

Magnussen [67.] verified by suitable comparisons with experimental data that Equations 6.58, 6.59 and 6.62 were adequate representations of the significant physics of turbulent flow.

Now that the microscales of the fine structure have been defined, (Equations 6.58 and 6.59), and the fraction of the total fluid that is in the fine structure microscales has been determined, (Equation 6.62), the next step is to obtain the mass exchange between a local fluid volume and the fine structures contained within it.

The approach adopted is based on the model of turbulence proposed by Tennekes [67.], where randomly distributed vortex tubes of diameter $(l_e)_*$, are concentrated in fine–structure regions which have length scales on the order of the Taylor microscale λ, as is illustrated in Figure 6–24. The mass entrainment into the fine structure region occurs through pressure forces induced by rotation of the fine scale eddies.

Following Chomiak [70.], consider a vortex tube in a turbulent motion, and let it rotate about its cross–sectional center with a tangential velocity w_*, at the eddy periphery, (see Figure 6–25). A balance of forces on the rotating eddy yields,

$$\frac{\rho w_e^2}{r} = \frac{dp}{dr}$$

where ρ is the eddy density and r is the effective radius from the center of rotation.

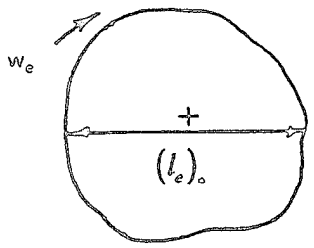

Figure 6–25. Cross–Section of a Fine–Scale Eddy Rotating About Its Center

Vortices, however they originate, tend to free–vortex motion due to the conservation of angular momentum. Viscous friction inside the vortex transfers momentum from the inner streamlines to the outer streamlines. Thus, the centers of vortices tend towards forced–vortex motion; the combined vortex motion is known as a Rankine vortex. The general vortex equation is,

$$wr^n = const.$$

where for free–vortex motion $n = +1$, and for forced–vortex motion, $n = \pm 1$. If subscript 'c' represents the outer limit of the forced vortex core of a Rankine vortex, the general equation can be expressed as,

$$w = w_c(r_c \,/\, r)^n$$

Substituting into the force equation and integrating gives,

$$\int_{p_c}^{p} dp = \rho w_c^2 r_c^{2n} \int_{r_c}^{r} \frac{dr}{r^{2n+1}}$$

yielding,

$$(p - p_c) = -\frac{1}{2}\rho w_c^2 \frac{1}{n}\left[\left(\frac{r_c}{r}\right)^{2n} - 1\right] \qquad 6.63$$

Examination of Equation 6.63 yields the following: For free–vortex outer flow, $n = +1$, r is positive and greater than r_c, giving p_c less than p outside the vortex, i.e., the free–vortex portion of the vortex tends to hold together. For the forced–vortex inner flow, $n = \pm 1$, r is positive but less than r_c, giving p_c greater than p in the core, i.e., the forced vortex portion of the vortex also tends to be held together. Thus, for the very small vortices of interest, which may be considered as being forced in character,

$$(p - p_c) = \frac{1}{2}\rho w_c^2\left[\left(\frac{r}{r_c}\right)^2 - 1\right]$$

Hence, the pressure difference from the edge of such a vortex to its axis of rotation is,

$$\Delta p = \frac{1}{2}\rho w_e^2 \qquad 6.64$$

This pressure gradient results in a positive flow of outside fluid into the eddy.

Applying the Bernoulli equation to the large–scale outside region and the small–scale inside region,

$$P_{outside} - P_{inside} = \frac{1}{2}\rho_{outside} v_1^2 \qquad 6.65$$

where v_1 is the induced inflow velocity. Now, in the limit,

$$P_{outside} - P_{inside} \rightarrow \Delta p$$

Then, equating Equations 6.64 and 6.65, yields the inflow velocity,

$$v_1 = \left(\frac{\rho_{out}}{\rho_{in}}\right)^{1/2} w_e \qquad 6.66$$

Assuming that the density inside the eddy is equal to that at its periphery, Equation 6.66 reduces to,

$$v_1 = w_e \qquad 6.67$$

Consequently, the induced mass flow rate into the fine structure $(\dot{m}_1)_*$, is given by,

$$(\dot{m}_1)_* = (\rho v_1 A_e)_*$$

or, using Equation 6.67,

$$(\dot{m}_1)_* = (\rho A_e w_e)_* \qquad 6.68$$

where $(A_e)_*$ is the external circumferential area of the tube vortex at the outer-edge of its viscous core.

Dividing the mass flow rate into the vortex by the total mass $(m_e)_*$ of the vortex yields the normalized inflow s_*, where,

$$s_* = \frac{(\dot{m}_1)_*}{(m_e)_*} = \frac{(\rho A_e w_e)_*}{(\rho E)_*}$$

and E_* is the volume of the fine-scale eddy. Introducing the values for $(A_e)_*$ and E_* gives,

$$s_* = 4\left(\frac{w_e}{l_e}\right)_* \qquad 6.69$$

Comparison of the right-hand side of Equation 6.69 with Equation 6.49 reveals that when $(l_e)_*$ is taken as an eddy diameter presently, in terms of the original definition where l_* was a radius,

$$s_* = \xi_* = 2\left(\frac{u_e}{l_e}\right)_* \qquad 6.70$$

Applying Equation 6.70 to the cumulative sum of all of the dissipation eddies within a local volume, s_* then represents the mass flow rate transferred through the fine structures, per unit mass of the fine structures.

The parameter 's' has units of reciprocal time, and represents a type of "space-velocity." It denotes the number of reactor volumes of feed at the specified conditions, that can be processed in unit time. In this context the fine-structure eddy represents a steady-state, mixed-flow reactor that processes the mass influx. The "space-time" τ, or mean residence time, is the reciprocal of the space-velocity, i.e.,

$$\tau = \frac{1}{s}$$

It denotes the time required to process one reactor volume of feed measured at the specified conditions.

In terms of the mass fraction of the fine structures in the fluid γ_*, given by Equation 6.62, the space-velocity for the bulk fluid may be expressed as,

$$s = s_* \gamma_* \qquad 6.71$$

The bulk space–velocity denotes the mass flow rate passed through the fine structures per unit mass of the bulk fluid.

If it is further assumed that the fine–scale structures are concentrated into fine–structure regions, the linear dimensions of the fine–structure regions would be much larger than those for the fine structures within them. Such regions appear in highly strained places between the bigger eddies, e.g., in Figure 6–24 the vortex tube shown could also represent a fine–structure region, where the region is itself made up of closely–interacting fine–scale eddies. Such a fine structure region need not be a vortex tube; it could also be in the form of a vortex sheet or vortex ribbon. The mass fraction of the fine–structure region γ_λ, relative to the surrounding fluid, is given by,

$$\gamma_\lambda = \frac{\rho_\lambda A_\lambda (u_e)_*}{\rho_\lambda A_\lambda u'}$$

i.e.,

$$\gamma_\lambda = \frac{(u_e)_*}{u'} \qquad 6.72$$

The mass fraction of the fine structures within a fine–structure region can be defined as,

$$(\gamma_\lambda)_* = \frac{\gamma_*}{\gamma_\lambda} \qquad 6.73$$

Inserting into Equation 6.72 the expression for $(u_e)_*$ from Equation 6.58, and that $u' = \left(\frac{2}{3} K\right)^{1/2}$, gives for γ_λ,

$$\gamma_\lambda = \frac{1.75(\varepsilon\nu)^{1/4}}{\left(\frac{2}{3}K\right)^{1/2}} = 2.143\left(\frac{\varepsilon\nu}{K^2}\right)^{1/4} \qquad 6.74$$

Another equation can be formed by dividing Equation 6.71 by Equation 6.74, such that,

$$s_\lambda = \frac{s}{\gamma_\lambda} \qquad 6.75$$

where s_λ represents the mass transferral rate through the fine structures per unit mass of the fine–structure regions. Then, utilizing Equations 6.58, 6.59, 6.62, and 6.74,

$$s_* = 2\left(\frac{u_e}{l_e}\right)_* = 2.434\left(\frac{\varepsilon}{\nu}\right)^{1/2} \qquad 6.76$$

$$s = s_*\gamma_* = 23.6\left(\frac{\varepsilon\nu}{K^2}\right)^{1/4}\left(\frac{\varepsilon}{K}\right) \qquad 6.77$$

$$s_\lambda = \frac{s}{\gamma_\lambda} = 11.07\left(\frac{\varepsilon}{K}\right) \qquad 6.78$$

The corresponding residence–time scales are reciprocals of the respective space–velocities, and are given by,

$$\tau_* = \frac{1}{s_*} = \frac{\gamma_*}{s} \qquad 6.79$$

$$\tau = \frac{1}{s} \qquad 6.80$$

$$\tau_\lambda = \frac{\gamma_\lambda}{s} \qquad 6.81$$

Such scales may be compared with the chemical kinetic time scales in order to establish whether the reaction is mixing or chemically controlled; they may also be used to establish criteria for flame extinction.

6.6.3 Reaction Rates

The EDC combustion model is based on the concept that the reactants are homogeneously mixed within the fine structures of the turbulence field, and that these fine structures may therefore be treated as well–stirred reactors. The composition and temperature of the surrounding fluid constitutes the feedstream conditions to the individual reactors. The ensemble–averaged mean scalar quantities within a local fluid volume, e.g., a finite–difference cell of a CFD procedure, are determined by an appropriate linear combination of the fine–structure and surrounding fluid characteristics.

A reacting fine structure region may be represented schematically as in Figure 6–26. A species mass balance for such a steady–state, mixed–flow reactor is given by,

$$\left[(m_i)_* \ (\dot{m}_I)_*\right]_{out} - \left[(m_i)_0 \ (\dot{m}_I)_*\right]_{in} = - \ (R_i E)_* \qquad 6.82$$

where the asterisk subscript denotes the fine structure, as above, and the zero subscript denotes the surrounding fluid conditions; $(R_i)_*$ is the mass consumption rate of species i per unit volume, and E_* is the fine structure volume. The parameter $(\dot{m}_I)_*$ is the (induced) mass flow rate into the reactor, and m_i is the species mass fraction, expressed as,

$$m_i = \frac{\rho_i}{\rho} \qquad 6.83$$

The left–hand side of Equation 6.82 represents the net mass transfer rate of species i from the surrounding fluid into the fine structures, while the right–hand side represents the net consumption rate of species i within the fine structures.

Rearranging Equation 6.82 as,

$$\left[(m_i)_0 - (m_i)_*\right] \frac{(\dot{m}_1)_*}{E_*} = (R_i)_* \qquad 6.84$$

Then rearranging the expression for s_* above as,

$$s_* = \frac{(\dot{m}_I))_*}{(m_e)_*} = \frac{(\rho A_e w_e)_*}{(\rho E)_*}$$

into the form,

$$(\dot{m}_I)_* = s_* \ (m_e)_* = s_* \ (\rho E)_*$$

and inserting into Equation 6.84, gives,

$$(R_i)_* = \rho_* s_* \left[(m_i)_0 - (m_i)_*\right] \qquad 6.85$$

Alternatively, introducing Equation 6.71 for s_*, yields,

$$(R_i)_* = \rho_* \frac{s}{\gamma_*} \left[(m_i)_0 - (m_i)_*\right] \qquad 6.86$$

Assuming that reaction occurs only in the fine structures and not in the surrounding fluid, $(R_i)_*$ may be related to the mean reaction rate of species i per unit volume of total fluid $(\overline{R_i})$, through the following expression:

$$\overline{R}_i = (R_i)_* \frac{E_*}{\overline{E}} \qquad 6.87$$

where $\overline{E}$ is the total fluid volume.

Since it may be shown that,

$$\overline{\rho} = \frac{\rho_*}{\gamma_*} \frac{E_*}{\overline{E}} = \frac{\left(\frac{m}{E}\right)_* E_*}{\frac{m_*}{\overline{m}} \overline{E}} = \frac{\overline{m}}{\overline{E}}$$

then the mean species reaction rate becomes,

$$\overline{R}_i = (R_i)_* \left(\frac{\gamma_* \overline{\rho}}{\rho_*}\right)$$

or, with Equation 6.86,

$$\overline{R}_i = \overline{\rho} s \left[(m_i)_0 - (m_I)_*\right] \qquad 6.88$$

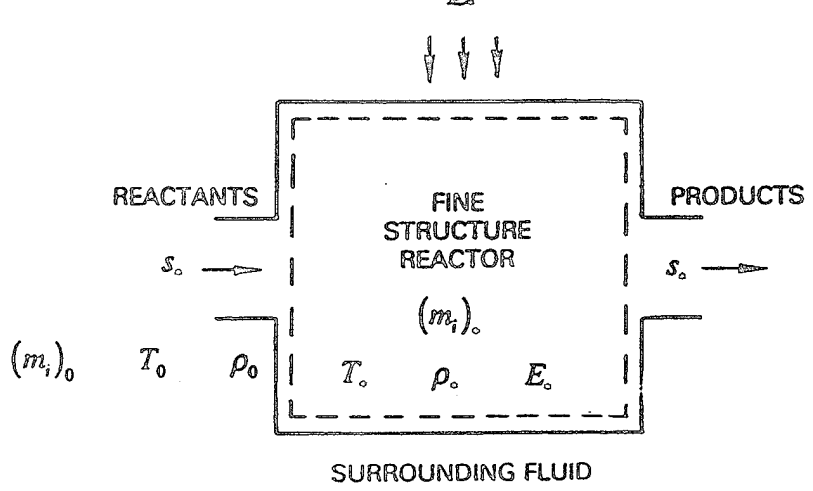

Figure 6–26. Schematic Representation of a Reacting Fine Structure as a Well–Stirred Reactor

When considering reaction, it must be remembered that not all of the fine structures will be sufficiently heated for ignition and subsequent combustion to occur. Both quenching and remoteness from the flame front may severely limit the number of fine structures containing combustible mixtures that actively contribute to the reaction rate expression. Consequently, a heuristic variable χ is introduced into the reaction rate relationships to account for these effects. In addition, Magnussen discovered from a study of flame propagation in premixed gases, that the above combination of governing equations was inadequate to provide sufficiently high reaction rates in the tails of such flames. He therefore found it necessary to introduce a second adjustment factor ^{K}, to align his calculations with the measurements. These factors will be defined in detail below. Therefore, introducing the factors χ and ^{K} into Equations 6.85 and 6.88, yields,

$$(R_i)_* = \rho_* s_* K \left[(m_i)_0 - (m_i)_*\right] \qquad 6.89$$

and,

$$\overline{R}_i = \overline{\rho} s X K \left[(m_i)_0 - (m_i)_*\right] \qquad 6.90$$

Note that χ is not inserted directly into the equation for $(R_i)_*$ since $(R_i)_*$ is understood to be based on only the portion(χ) of the fine structure that is active.

The mass fraction of specie i in the portion χ of the fine structures that participates in the reaction, and the mass fraction in the surrounding fluid, are related to the local, mean mass fraction through the relationship,

$$\overline{m}_i = (m_i)_* \gamma_* X + (m_i)_0 \ (12 - \gamma_* X) \qquad 6.91$$

Solving for $(m_i)_0$ and substituting into Equations 6.89 and 6.90 yields,

$$(R_i)_* = \frac{\rho_* \ s_* \ K}{(l - \gamma_* \ X)} \left[\overline{m}_i - (m_i)_*\right] \qquad 6.92$$

and,

$$\overline{R}_i = \frac{\overline{\rho} s X K}{(l - \gamma_* X)} \left[\overline{m}_i - (m_i)_*\right] \qquad 6.93$$

The relationship between these latter two equations may be found by the substitution of one into the other. The result is a reduced version of the more complete form, given as,

$$\frac{\overline{R}_i}{\overline{\rho}} = \frac{(R_i)_*}{\rho_*} \ (\gamma_* X) + \frac{(R_i)_0}{\rho_0} \ (1 - \gamma_* \ X) \qquad 6.94$$

The last term on the right–hand side accounts for reaction in the surrounding fluid, and may normally be omitted, (except for NO–formation in premixed flames).

The steady–state macroscopic energy balance, neglecting potential energy and work terms, and applied to the fine structure reactor, is given by,

$$H_* - H_0 = Q_* \qquad 6.95$$

where H is the stagnation enthalpy (in joule/kg) and Q is the sum of all thermal energy per unit mass of fine structure reactor crossing the system boundaries by conduction, radiation, etc.

Multiplying both sides of Equation 6.95 by, from above,

$$\left(\frac{\dot{m}}{E}\right)_* = \rho_* \ s_*$$

results in,

$$\rho_* \ s_* \ (H_* - H_0) = \rho_* \ s_* \ Q_* = - q_* \qquad 6.96$$

where, since the temperature of the fine structures will be greater than that of the surrounding fluid due to the heat of reaction, q_* is the net energy transferred to the surrounding fluid by transfer mechanisms such as radiation. Then, following the pattern of Equation 6.91,

$$\overline{H} = H_* \ \gamma_* \ X + H_0 \ (1 - \gamma_* \ X) \qquad 6.97$$

and solving for H_0, inserting this formulation into Equation 6.96, yields an equation that incorporates only the reactor enthalpy and the mean fluid enthalpy,

$$q_* = \frac{\rho_* \ s_* \ K}{(l - \gamma_* x)} \ (\overline{H} - H_*) \qquad 6.98$$

In deriving Equation 6.98 the adjustment factor ^{K} was also introduced as in Equations 6.89 and 6.90.

Equations 6.92, 6.93 and 6.98 constitute a system of equations which can be adapted to the full kinetic treatment of reacting fine structures for both turbulent premixed and diffusion flames.

6.6.4 Fast Chemistry Limit

Since it is computationally–expensive in a CFD code to carry a large number of chemical species i, and because of the disappointing performance in Section 6.5 of full and reduced reaction mechanisms in representing well–stirred reactor stability, it is important to explore the EDC combustion model in the context of the fast chemistry limit.

A simple, irreversible, one–step chemical reaction may be represented by the mass balance,

unit mass of fuel + α mass of oxidant $\rightarrow$ $(1+\alpha)$ mass of products

where α is the stoichiometric mass ratio for the fuel and oxidant. If the chemical reactions proceed extremely fast, then it may be assumed that the rate of combustion will be determined solely by the rate of fuel/oxidant mixing on a molecular level, i.e., in a turbulent flow by the rate of mass transfer between the surrounding, or bulk, fluid and the fine structures contained therein. Under such circumstances the limiting concentration of fuel (in a fuel–lean environment) or oxidant equivalent (in a fuel–rich environment) will go to zero in the fine structures. Consequently, Equations 6.92 and 6.93, with i equal to fuel (subscript fu) reduce to,

$$(R_{fu})_* = \frac{\rho_* s_* K}{(1 - \gamma_* X)} (\overline{m}_{\min}) \qquad 6.99$$

and,

$$\overline{R}_{fu} = \frac{\overline{\rho} s X K}{(1 - \gamma_X)} (\overline{m}_{\min}) \qquad 6.100$$

where,

$$\overline{m}_{\min} = minimum\ of \left\{ \overline{m}_{fu} , \frac{mbar_{ox}}{a} \right\} \qquad 6.101$$

where, $\overline{m}_{ox}$ is the mean mass fraction of oxidant.

Neglecting the kinetic energy contribution to stagnation enthalpy, the energy balance given by Equation 6.96 simplies to,

$$q_* = \rho_* s_* K (h_0 - h_*)$$

where h is the static enthalpy. Inserting the relationship for enthalpy, and assuming a constant specific heat , in the relationship above transforms it to,

$$q_* = \rho_* s_* K \left\{ \sum \left[(m_i)_0 - (m_i)_* \right] (h_{f,i})_0 + c_P (T_0 - T_*) \right\} \qquad 6.102$$

where the subscript on the enthalpy has specific reference to standard–state conditions.

For a one–step reaction, the fast–chemistry approximation is,

$$\sum \left[(m_I)_0 - (m_i)_* \right] (h_{f,i})_0 = (m_{\min})_0 \left[(h_{ffu})_0 + \alpha (h_{f,ox})_0 - (\alpha + 1) \left(h_{f,pr} \right) \right]$$

$$= (m_{\min})_0 (\Delta H_{comb})_0$$

Thus, Equation 6.102 becomes in the fast chemistry limit,

$$q_* = \rho_* s_* K \left[(m_{\min})_0 (\Delta H_{comb})_0 + C_p (T_0 - T_*) \right] \qquad 6.103$$

Applying Equation 6.91,

$$\overline{m}_i = (m_i)_* \gamma_* X + (m_i)_0 (1 - \gamma_* X)$$

by rearranging for $(m_i)_0$, and taking into account that in the fast chemistry limit $(m_i)_*$ goes to zero,

$$(m_i)_0 = \frac{\overline{m}_{\min}}{(1 - \gamma_* X)}$$

Substituting this in Equation 6.103 yields, with rearrangement,

$$T_* = T_0 - \frac{q_*}{c_p \rho_* s_* K} + \frac{\overline{m}_{\min}}{c_p (1 - \gamma_* X)} (\Delta H_{comb})_0 \qquad 6.104$$

Similarly with Equation 6.98,

$$q_* = \frac{\rho_* s_* K}{(1 - \gamma_* X)} (\overline{H} - H_*)$$

eventually yields,

$$T_* = \overline{T} - \frac{(1 - \gamma_* X) q_*}{c_p (\rho_* s_* K)} + \frac{\overline{m}_{\min} (\Delta H_{comb})_0}{c_p} \qquad 6.105$$

Equations 6.104 and 6.105 may be combined to produce:

$$T_* = \overline{T} + \Delta T \qquad 6.106$$

$$T_0 = \overline{T} + \Delta T \frac{\gamma_* X}{(1 - \gamma_* X)} \qquad 6.107$$

$$\overline{T} = T_* (\gamma_* X) + T_0 (1 - \gamma_* X) \qquad 6.108$$

Note that for an exothermic reaction, the temperature of the fine structures T_*, will be significantly higher than both the surrounding fluid temperature T_0, or the local time–mean temperature $\overline{T}$.

6.6.5 Adjustment Factors

Two heuristic adjustment factors, χ and ^{K} were introduced into the equations; χ has some obvious physical basis, and ^{K} is more of a calibration coefficient. These factors are discussed below in the context of the fast chemistry limit.

The factor χ is designed to provide a limit to the extent of reaction in the fine structures during low temperature conditions. It is defined as that portion of the fine structures that is sufficiently heated for ignition and subsequent reaction. The portion of the fine structures which reacts is assumed to be proportional to the ratio of the local concentration of reacted fuel to the sum of the total quantity of fuel that may yet react and, the quantity of fuel that has already reacted. Thus,

$$x = \frac{C}{\gamma_\lambda} \left\{ \frac{\frac{\overline{m}_{pr}}{(1 + a)}}{\left[\frac{\overline{m}_{pr}}{(1 + a)} + \overline{m}_{\min} \right]} \right\} \qquad 6.109$$

where C is a simplified correlation coefficient given by,

$$C = \frac{\left[\frac{\overline{m}_{pr}}{1 + a)} + \overline{m}_{\min} \right]^2}{\left[\frac{\overline{m}_{pr}}{(1 + a)} + \overline{m}_{fu} \right] \left[\frac{\overline{m}_{pr}}{(1 + a)} + \frac{\overline{m}_{ox}}{a} \right]} \qquad 6.110$$

and χ is limited to,

$$X \leq C \qquad 6.111$$

It should be noted that for stoichiometric premixed flames, C is identically equal to unity. The construction of the correlation coefficient implies that $0 < C \leq 1.0$. It should be observed that the presence of reactant mass fractions of unity will cause the expression to become unbounded, and caution should therefore be exercised. The term γ_λ defined through Equations 6.72 and 6.74, has a magnitude less than unity, and will tend to increase the apparent reaction rate, via Equations 6.109 and 6.100. The physical reason for this is that the reaction products formed within the fine structure regions may have a higher concentration within these regions, thus increasing the probability of ignition of structures.

The calibration coefficient κ was found to be necessary when calcuated reaction rates were discovered to be too low in the tails of turbulent premixed flames. This was accounted for by noting that the time–mean, mass–averaged concentrations of reactants will be low in the tail region of a premixed flame; however, the concentrations of the reactants in the unreacted fine structures will still be high. Therefore, the thin reacting interface (the "flame") that separates the reacting fine structures from the nonreacted fine structures will propagate more rapidly than would otherwise be expected on the basis of an unmodified mean reaction rate. This provides some (weak) physical basis for the adjustment factor. It is defined as,

$$\kappa = \frac{1}{\gamma_\lambda} \qquad 6.112$$

with the limitation,

$$\kappa \leq \frac{\left[\frac{\overline{m}_{pr}}{(1+\alpha)} + \overline{m}_{\min}\right]}{\overline{m}_{\min}} \qquad 6.113$$

Analogous equations for χ and κ in the context of full chemical kinetics can be derived, and are similar in form to those above.

6.6.6 Extinction Criteria for Fast Chemistry Limit

The assumption of a one–step, irreversible reaction and fast chemistry requires development of some local extinction or quenching criteria in terms of the local residence–time scale.

For a one–step, irreversible chemical reaction the fractional conversion Y, or reactedness of the fuel mass fraction for the reactor, assuming a fuel–lean state, is given by,

$$Y = \frac{(m_{fu})_0 - (m_{fu})_*}{(m_{fu})_0} \qquad 6.114$$

The mass balance of Equation 6.86 may be applied to the fuel ($i = fu$) and rearranged to give,

$$\left[(m_{fu})_0 - (m_{fu})_*\right] \rho_* \frac{s}{\gamma_*} = (R_{fu})_*$$

Then, Equation 6.79 can be used to give a relationship for s / γ_*, i.e.,

$$\frac{S}{\gamma_*} = \frac{1}{\tau_*}$$

so that the fractional conversion becomes,

$$Y = \frac{(R_{fu})_* \gamma_*}{(m_{fu})_0 \rho_* s} = \frac{(R_{fu})_* \tau_*}{(m_{fu})_0 \rho_*} \qquad 6.115$$

Similarly, for an adiabatic, well–stirred reactor with constant specific heat and with one–step chemistry, using Equation 6.102, with the definition of Equation 6.114,

$$Y = \frac{c^p(T_* - T_0)}{(\Delta H_{comb})_)(m_{fu})_0} \qquad 6.116$$

The fine–structure extinction time scale $(\tau_{ext})_*$, can be found by solving Equations 6.115 (mass balance basis) and 6.116 (energy balance basis) simultaneously, and the solution is illustrated in Figure 6–27, where $(\tau_1)_* > (\tau_{ext})_* > (\tau_2)_*$.

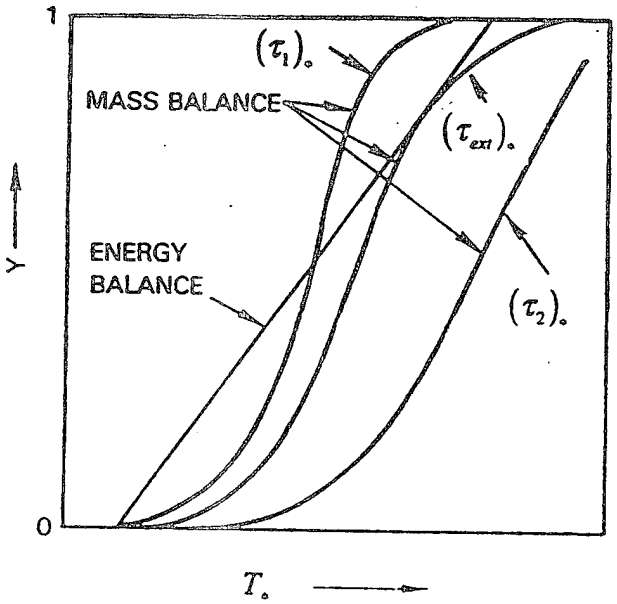

Figure 6–27. Diagrammatic Representation of Solution for Fine–Structure Extinction Time Scale

In Section 6.3 a stability parameter SP, Equation 6.24, was derived by phenomenological modeling, and was a characteristic time approach relating a turbulent mixing time to a turbulent burning time. Flame was assumed to be extinguished if the turbulent mixing time for eddies composed of hot products of combustion with eddies composed of premixed or well–mixed fresh reactants was very short compared to the turbulent burning rate of the mixture. The approach equated mixing to eddy dissipation, and presumed that an adequate degree of molecular–level mixing is achieved in and characterized by, eddies where the dissipation rate of turbulence kinetic energy is at a maximum. Experimental evidence at high Reynolds Numbers was used to relate eddies with maximum dissipation to the Kolmogorov eddy scales. Further, it was assumed that the burning rate can be represented by a Damkohler–type expression, and that the flame front was associated with the dissipation eddies only, which were themselves affected solely by eddies of the Kolmogorov microscale.

Subsequent studies of turbulence/laminar flamelet interactions [71.] showed that on a global basis, the flame front existing in turbulent combustors of the PW100–type would be discontinuous, with eddy–burning as the mode of combustion. The eddies involved in combustion were substantiated as the dissipation eddies, with Kolmogorov eddies acting as large–scale (relative) turbulence to the flame fronts associated with the dissipation eddies.

The fine structure eddies of the EDC model, that contain 75 percent of the dissipation, were shown in Section 6.6.2 to be very similar in size to the maximum dissipation eddies of the SP model. The EDC model takes account of the additional effect of the fine–structure intermittency. This also implies that a globally–continuous flame would not be appropriate.

The characteristic time stability parameter model and the EDC model both assume that separately–introduced reactants are well–stirred on the microscale level prior to combustion in a flow with high Reynolds Number turbulence. Both approaches equate molecular–level mixing to the dissipation of turbulence energy by turbulent eddies. Both also show that the relevant eddies are larger than the Kolmogorov microscale. The fine–structure, energy–containing, eddies of the EDC model are very close in size to the maximum dissipation eddies of the SP model. Both approaches argue by different methods that globally–continuous flame fronts are not possible. Thus, there are no serious conceptual incompatibilities between the EDC model approach and the SP model approach. Therefore, the stabilitiy parameter SP, could also serve as the basis for an extinction criterion that might be used with the fast chemistry assumption, within the EDC local approach, as a low–cost alternative to finite–rate chemistry.

6.6.7 Application of the Extinction Residence Time

The extinction residence time τ_{ext}, is obtained through the simultaneous solution of Equations 6.115 and 6.116. It may be expressed as,

$$\tau_{ext} = \left(\frac{\rho V_R}{\dot{m}}\right)_{ext} \qquad 6.117$$

where V_R is the reactor volume, ρ is the mass density and $\dot{m}$ is the total mass flow rate into the reactor. For a given set of reactants the extinction residence time is independent V_R if $\dot{m}$ is allowed to adjust with it. Consequently, with this provision, extinction residence times may be calculated solely as a function of the inlet temperature and equivalence ratio.

From Section 6.5 the recommended Kretschmer & Odgers air loading parameter expression, Equation 6.45, can be used as a basis for this calculation, as is illustrated in Figure 6–28. As is to be expected, the residence times decrease with increasing temperature, and attain a minimum at unity equivalence ratio. The waviness in the calculated characteristics is due to the tabulated constants in the original expression.

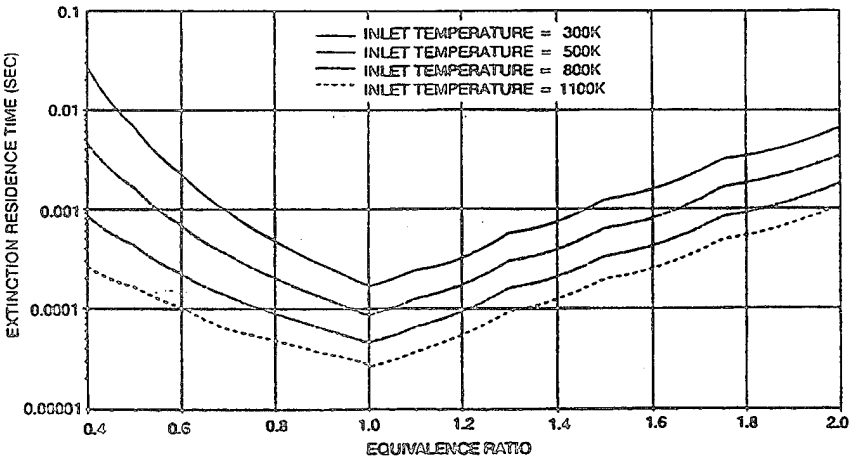

Figure 6–28. Extinction Residence Times as Functions of Inlet Temperature and Equivalence Ratio as Calculated from the Kretschmer & Odgers ALP Expression

The calculated extinction residence times constitute critical chemical time scales. If a local hydrodynamic time scale or residence time is smaller than the prevailing chemical time scale corresponding to extinction, then reaction will not occur and the original reactants entering the reactor volume are recovered.

A set of suitable hydrodynamic time scales is given in Section 6.6.2 as Equations 6.79 – 6.81. Magnussen [72.],[73.], used an alternative, refined, expression that is the characteristic hydrodynamic time for the mass exchange between the reacting fine structures and the bulk fluid, which can be expressed as,

$$\tau_R = \left(\frac{1-\gamma_*X}{K}\right)\tau_* \qquad 6.118$$

where τ_* is given by Equation 6.79. In computational grid cells where zero products exit, the coefficient term in Equation 6.118 is unity and τ_R reduces to τ_*. (Thus, to calculate a flame lift height, for example, only τ_* need be utilized.)

Strictly, since the perfectly–stirred reactors (PSR) are represented by the fine structures, the "inlet" feed quantities to the PSR's are those corresponding to the surrounding fluid. The mean computational grid cell values are a weighted summation of the PSR and surrounding fluid values, e.g.,

$$\bar{\phi} = (\gamma_*\chi)\phi_* + (1 \pm \gamma_*\chi)\phi_0 \qquad 6.119$$

where the subscripts * and 0, respectively, represent the PSR mixture and the fluid in the cell surrounding the fine structures. If τ_* rather than τ_R is used for a hydrodynamic time, it is permissible to take $\bar{\phi} \approx \phi_0$. Therefore, the "inlet" temperature and equivalence ratio used as feed parameters for the Kretschmer & Odgers PSR extinction expression are simply the local mean quantities. The equivalence ratio used can be be based on a composite fuel and air, both of which can themselves be based on appropriate combinations of products and unburned reactants. Therefore, the equivalence ratio parameter is that which would exist in the absence of reaction for the same flow field, i.e., a mixture fraction–type of parameter.

6.6.8 Chemical Kinetics for EDC

For CFD codes the EDC applies the stirred reactor principle on a microscale level in a fully–integrated form, i.e., at every grid–node for each solution iteration. Therefore, it is a computationally–intensive procedure. Complete stirred reactor theory depends on nonequilibrium chemistry. Since chemical reaction kinetics usually involve the solution of sets of ordinary differential equations that become mathematically "stiff," the additional computational cost burden could become completely overpowering when "complete" reaction mechanisms for hydrocarbon combustion are utilized to calculate the singularity represented by blowout. Therefore, devices to reduce this cost burden are sought wherever appropriate.

The EDC defines turbulence microscales within which the reactants are mixed on the molecular level, i.e., perfectly premixed. Therefore, the stirred reactor representation may be limited to the perfectly–stirred case, (as opposed to well– or partially–stirred). By definition, a perfectly–stirred reactor is a finite volume within which the contents are spatially uniform in temperature and composition at the exit (burnt) conditions. Furthermore, the mass flow rate through the reactor is constant. Since the flow is steady–state, the relevant equations for the reactor become algebraic rather than differential. For example, the conservation of chemical species i, is,

$$\dot{m}\left[m_i - (m_i)_{out}\right] = \dot{n}_i M_i V_R \qquad 6.120$$

where,

m_i = mass fraction of i present
$\dot{n}_i$ = molar rate of production of by chemical reaction per unit volume
M_i = molecular weight of species i
V_R =reactor volume

rather than,

$$\frac{dm_i}{dt} = -\frac{1}{\tau}\left[m_i - (m_i)_{out}\right] + \dot{n}_i M_i V_R \qquad 6.121$$

where

τ = the nominal residence time, $\bar{\rho} V_R / \dot{m}$

$\bar{\rho}$ = mean density in reactor

Similarly, the conservation of energy for perfectly–stirred reactors is,

$$\dot{m} \sum_{all\ i} \left[m_i h_i - (m_i)_{out} (h_i)_{out} \right] = \dot{Q} \qquad 6.122$$

where,

$\dot{Q}$ = rate of heat loss from reactor

h = specific enthalpy

The molar rate of production of i is the sum for all reactions in the kinetic reaction mechanism consisting of K reactions, of the concentration progress variable q_k, times the number of moles, such that,

$$\dot{n}_i = \sum_{all\ k} (\phi^r_{i,k} - \phi^f_{i,k}) q_k \qquad 6.123$$

where $\phi^f_{i,k}$ and $\phi^r_{i,k}$ are the stoichiometric coefficients for i of the left–hand side and right–hand side respectively, of the k–th. reaction in the elementary reactions,

$$\sum_{all\ i} \phi^f_{i,k} \psi_i \Leftrightarrow \sum_{all\ i} \phi^r_{i,k}\ \psi_i \qquad (k=1 \ldots K) \qquad 6.124$$

where ψ_i is a symbol representing the i–th. of I chemical species.

The law of mass action is used to define q_k from the difference between the forward f, and reverse r, reaction rates, such that,

$$q_k = c_{f,k} \prod_{i=1}^{I} [\psi_i]^{\phi^f_{i,k}} - c_{r,k} \prod_{i=1}^{I} [\psi_i]^{\phi^r_{i,k}} \qquad 6.125$$

where $[\psi_i]$ is the molar concentration of the i–th. species.

The rate constants c, take the Arrhenius form,

$$c_{f,k} = A_k T^{\beta_k} exp(-E_k / \Re T) \qquad 6.126$$

where, for the k −th. reaction,

A_k = pre−exponential factor

β_k = temperature exponent

E_k = activation energy

Reverse rate constants $c_{r,k}$, are related to the forward rate constants via the equilibrium constant $C_{eq,k}$, as,

$$c_{r,k} = \frac{c_{f,k}}{C_{eq,k}} \qquad 6.127$$

Therefore, the equation set, Equations 6.120 and 6.122, with $I+1$ equations, although algebraic, is highly nonlinear.

Because of the nonlinear character of the equations, variants of Newton's methods can be used to minimize computing costs. However, although correctly posed in stationary terms, the solution can also involve a partial solution of the transient forms of the equations when slow convergence is encountered. Such a dual approach solution algorithm is generally cost−effective and robust, and is therefore convenient for a CFD procedure. The Sandia CHEMKIN PSR code, [54.], uses such a procedure, (see Section 6.5). Furthermore, economy in computational costs can be achieved if both I and K are minimized by means of a reduced chemical reaction mechanism.

6.6.9 EDC Model Implementation

With the failure (Section 6.5) to identify a suitable hydrocarbon chemical reaction mechanism, either full or reduced, that accurately represented blowout, and because of the computational costs associated with such mechanisms (Section 6.6.8.), it was decided to implement the EDC model with the fast chemistry assumption (Section 6.6.4.), and to rely on a characteristic time comparison as the flame extinction criterion (Section 6.6.6.). This characteristic time approach represents a partial implementation of the EDC model, in which a calibrated, single−step rate expression is utilized as a stability criterion in conjunction with a fast chemistry model. With this approach, fast, or equilibrium, chemistry is coupled with the characteristic time criteria extracted from the EDC model to form a relatively simple and CPU−viable prediction package for local extinction in a CFD code. The CFD code, via its turbulence model, provides the necessary turbulence information at each grid node to calculate the hydrodynamic time scales (Section 6.6.2.) for the fine structure eddies. The chemical time scale at extinction for propane fuel is calculated from the Kretschmer & Odgers calibrated expression for blowout.

The fast chemistry EDC combustion model with the described time−scale extinction criterion, was incorporated into the Pratt & Whitney two−dimensional (axi−symmetric) PREACH CFD code [74.]. The logic flowchart for the extinction calculations is shown in Figure 6−29.

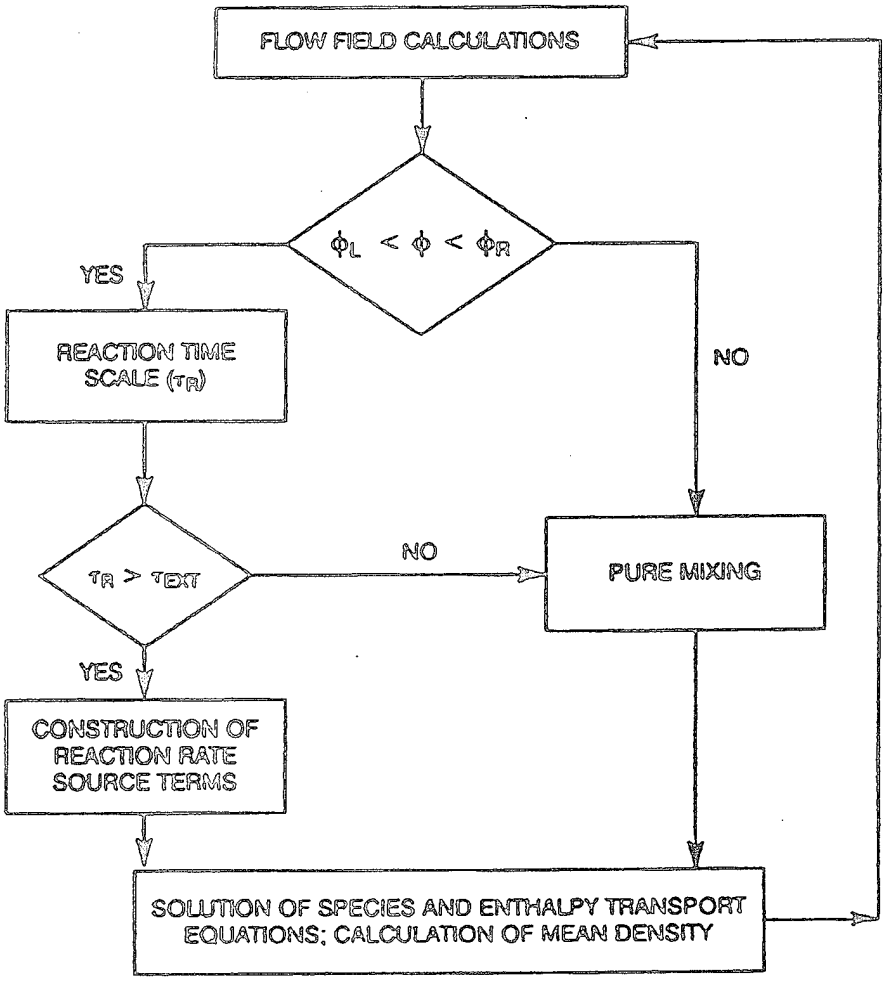

Figure 6–29. Logic Flowchart for Extinction Calculations using the Fast Chemistry/Characteristic Time Version of the EDC Model

With reference to Figure 6–29, following solution of the momentum equations and satisfaction of continuity, the source terms for the species continuity equation are constructed. Two constraints are applied to the construction of the source terms: First, the local equivalence ratio is compared with prespecified "combustion limits." Such limits are conceptually distinct from flammability limits. Plots of extinction residence times as a function of equivalence ratio are parabolic in appearance and concave–upwards, (Figure 6–28). The rich (ϕ_R) and lean (ϕ_L) combustion limits correspond to asymptotes on either side of these curves, or to arbitrarily–selected threshold values of extinction residence time. Such combustion limits are a function of the "inlet" feed temperature to the local PSR's. In the present instance the rich and lean limits were initially selected as constants, 2.0 and 0.4 respectively. These values are similar to traditional flammability limits for propane/air systems, but actually represent the extent to which the curve–fit of the Kretschmer & Odgers ALP expression (Equation 6.45) may be considered valid.

The local equivalence ratio, that is tested against these combustion limits, is based on composite, burned–plus–unburned fuel and air. Use of this type of equivalence ratio produces an expanding flame zone, which is closely aligned with the flame zone resulting from use of the more traditional eddy breakup (EBU) combustion model, [63.]. If the equivalence ratio is based solely on unreacted fuel and air, then a long, thin flame sheet is produced, that is rather poorly resolved with the nonadaptive and relatively coarse

grids commonly used in combustor calculations. As noted above, the composite equivalence ratio is similar to a mixture fraction.

If the combustion limit constraint is satisfied, a second constraint on the flame zone is then applied. The hydrodynamic PSR residence time τ_* (Equation 6.79) or alternatively the "reaction" time scale τ_R (Equation 6.118), is calculated and compared with the extinction time scale $(\tau_{ext})_*$ or τ_{ext}, respectively. If the hydrodynamic time scale is smaller than the extinction time scale, then the combustible material within the reactor is not allowed to react, and simple mixing occurs. In this case, the reaction rate source term is zero. If the opposite is true, then reaction within the fine structures is permitted, and the reaction rate source terms are constructed from the EDC model relationships, Equation 6.100.

The species and enthalpy transport equations are subsequently solved, density is calculated from its equation of state, and the solution algorithm loops back for another gas–phase iteration.

Although in principle the application of this version of EDC modeling is relatively straightforward, in practice implementation of the procedure poses some problems. Some of these difficulties, and their work–arounds, are described below.

As iteration proceeds, certain cells may encounter equivalence ratios and/or residence times that are almost identical in magnitude to the two flame extinction (rich and lean) limits described above. Consequently, any perturbations that might arise in the calculated flow field, due to code–numerics, the solution algorithm, or solution convergence history, may cause the reaction in such a cell to abruptly turn "on" and "off" with iteration. Since behavior in any particular computational cell impacts upon the behavior in adjacent cells, a "flickering flame" can be produced. Such flickering flame behavior may influence enough of the computational domain to induce an adverse and oscillatory effect on the solution convergence characteristics. To help ameliorate this behavior, the reaction rates were modified by a clipped–sinusoid or ramp–like function that allows the blowout (or ignition) process to take place somewhat gradually over a diffused combustion limit. For example, for the rich limit, a ramp function may be applied in smooth fashion between the actual (imposed) rich limit of 2.1 and a value slightly displaced from it, say, 2.0.

In a "stationary" diffusion flame the conceptual existence of a stoichiometric contour in the idealized flame sheet is intuitively obvious. However, in a calculation of such a flame, the computational grid is most unlikely to be able to satisfactorily resolve the location of the stoichiometric contour. Poor resolution of the flame sheet in the calculation may produce nonmonotonic variations in the local equivalence ratio and/or extinction criteria, resulting in an apparent flame "spottiness." While a discontinuous flame sheet can occur in real turbulent diffusion flames, such calculated spottiness is not physically–based. To avoid this difficulty in the extinction residence time, a reactor inlet equivalence ratio of unity is used in every cell where the combustion limits are satisfied in this cell.

The extinction time scale τ_{ext} is a function of the local mean temperature and an equivalence ratio that is set equal to unity to avoid resolution problems (see above). Therefore, in the comparatively isothermal region between the fuel source and the anchor position of a lifted flame, the extinction time scale should remain relatively constant. As is indicated in Figure 6–30 for a simple jet diffusion flame, the hydrodynamic time scale τ_* will be much less than the extinction time scale in the high shear region near the fuel jet exit. It will increase monotonically with downstream distance along the stoichiometric contour. At the lift–off height and in the vicinity of the stoichiometric contour, the hydrodynamic time scale will be equal to the extinction time scale, and reaction will occur with an abrupt temperature rise. Due to the temperature increases the laminar viscosity increases and the density decreases. In the flame region, the entrainment flux increases by a significant amount, and the dissipation rate will increase accordingly. Therefore, the hydrodynamic time scale tends to increase in the flame zone, (see Equations 6.77 and 6.80). Conversely, the extinction time scale decreases with an increase in temperature (see Figure 6–28). Since reaction is permitted wherever $\tau_* > \tau_{ext}$, the fact that τ_* increases and τ_{ext} decreases with increase in temperature, tends to

augment the differences in magnitude between the two time scales. This serves to "lock–in" or stabilize the flame at the calculated initial anchor point. Consequently, during the course of the solution development, if the extinction criteria are based on local cell conditions, the calculated flame may be permanently and spuriously anchored in a high temperature region that would otherwise be only a transient artifice of the solution procedure. The lock–in to the high temperature region may prevent the flame from migrating to its true equilibrium position. A similar situation can be generated when beginning a new calculation from a restart file of a previous combustion situation.

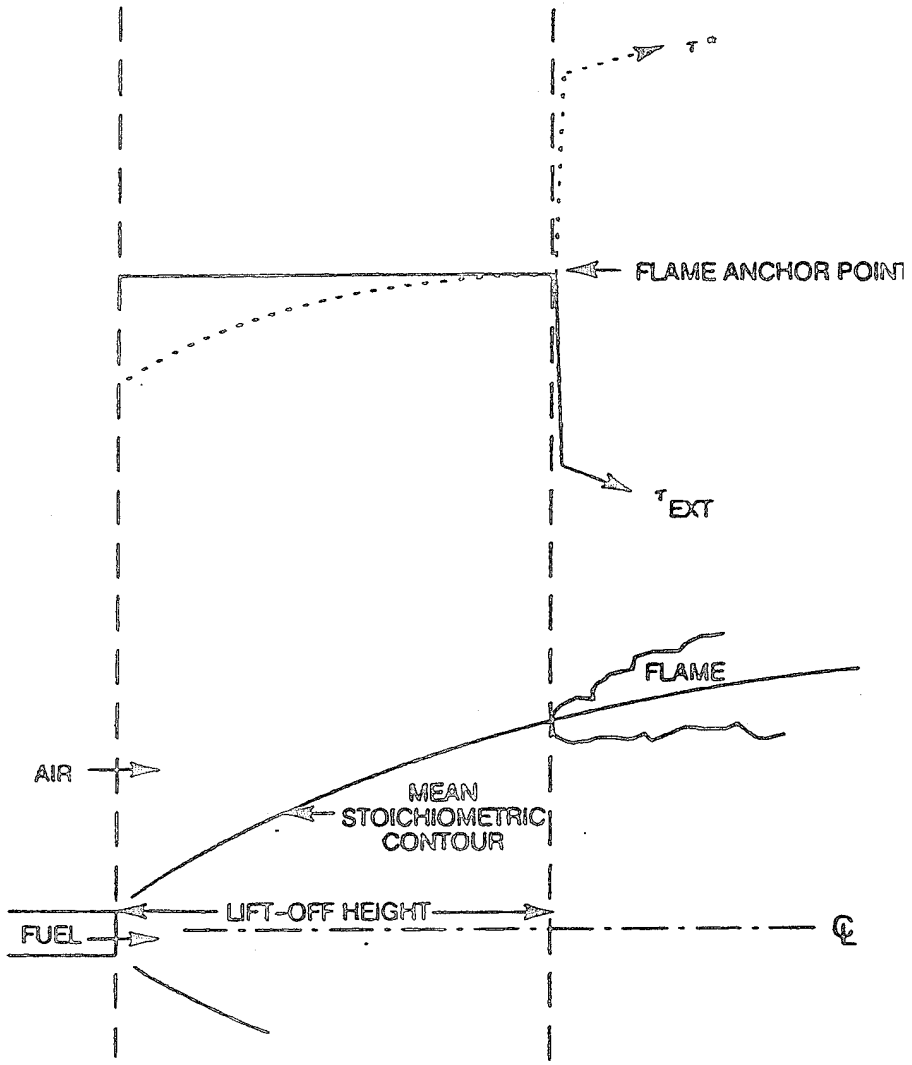

Figure 6–30. Representation of the EDC Model Extinction Criterion at the Flame Anchor Point

To overcome this problem, an upwinding procedure is used in which the extinction criteria τ^{*} and τ_{ext} are functions only of the properties of that neighbor cell that provides both a mass flux into the considered cell, and which has the lowest temperature of any neighbor cell. This approach is based on the premixed flame concept of stabilization whereby the anchor point constitutes a location at which the turbulent flame propagation velocity is equal and opposite to the appropriate flow velocity component. At the flame stabilization surface, the flow feeding the PSR's, representing the fine structures, is to a large degree composed of the unreacted species components coming from the region immediately upstream. Flame stabilization is, in this sense, a planar phenomenon and not a volume (i.e., finite–difference cell)

phenomenon. Only the extinction criteria are upwinded, the reaction rate source terms are a function of the local cell properties.

6.6.10 Preliminary Test of EDC Model in 2D–PREACH

As a preliminary evaluation of the EDC model implemented in the 2D–PREACH CFD code, as described above, calculations were made of flame–lift heights in a turbulent jet flame. The test–case selected was the experiment of Dahm & Dibble, [75.]. In this experiment gaseous propane entered a coflowing airstream in an enclosed square duct of 30 cm side–dimension, by means of a centered round tube of 3.3 mm diameter with a 0.9 mm thick wall. The mean air velocity was 0.58 m/s with a turbulence intensity of 0.4 %; air temperature was 291 °K.

For the calculations the propane was assumed to have a temperature of 260.9°K with a jet initial turbulence intensity of 6.5%. Two fuel–jet velocities were selected as 20 and 40 m/s, and measured flame–lift heights were 0.085 and 0.132 m, respectively. Five finite–difference cells were fitted radially into the fuel tube. The overall length of the calculation domain was 0.8 m, and the grid size was 77 x 53 for one–half of the flowfield. The grid expanded axially and radially, such that around the first lifted–flame position the cell size was approximately 5 mm, and the cell size was about 10 mm at the second lifted–flame position.

A comparison of calculated and measured flame–lift is given in Figure 6–31. It can be seen that at the 40 m/s fuel jet velocity the agreement is very good; however, at the 20 m/s fuel jet velocity the agreement is not so good. Unfortunately, the experimental curve exhibits a sharp change in slope at about 15 m/s fuel jet velocity. With only the two calculated points it is not possible to determine whether the calculation of lift at 20 m/s is inaccurate, or, if the occurrence of the gradient change (a fuel jet Reynolds Number effect?) is not correctly calculated.

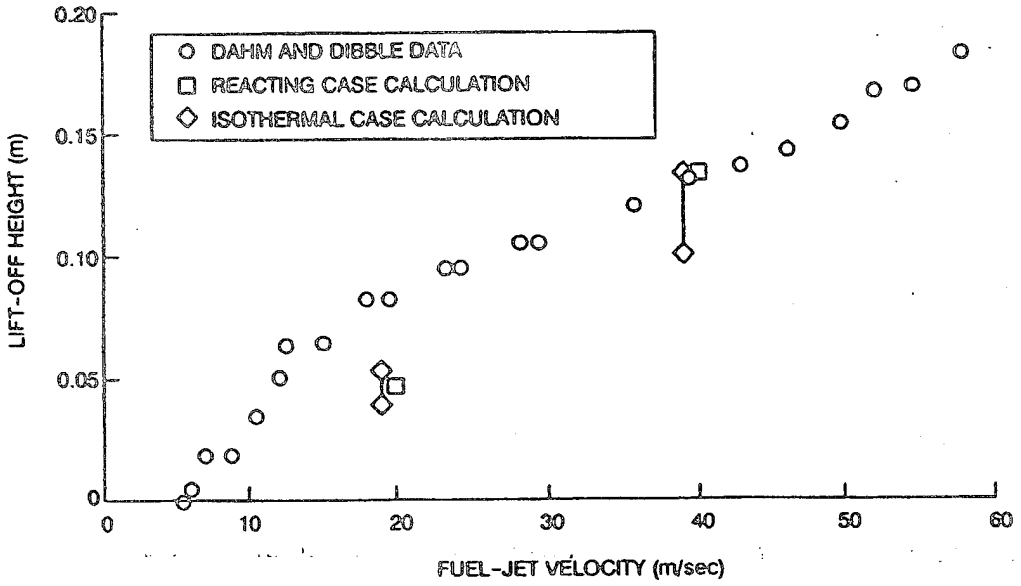

Figure 6–31. Comparison of measured and Calculated Flame Lift Heights for a Simple Jet Diffusion Flame

It was observed during the course of the calculations, that satisfaction of the flame extinction criteria alone was an insufficient condition to produce a high temperature flame. It was necessary that a certain amount of reaction–product was built–up before the reaction rate source term became significant, and a stable flame was established.

Isothermal calculations were also performed to compare with the nonisothermal cases. In this instance, the lift–height was represented by a band in Figure 6–31. The lower limit of the band represents

the axial position at which the extinction criteria were satisfied in a single cell; the upper band limit represents the axial location at which the extinction criteria were satisfied in two or more adjacent cells along a radius. This is a somewhat arbitrary method of accounting for the observed need for a product build–up to establish a stable flame. Although differences in flowfield could be expected between the isothermal and nonisothermal calculations, the agreement of the calculated flame–lifts are in good agreement. The two–cell condition improves the agreement with the measurements.

6.7 Hybrid Modeling

6.7.1 Introduction

Two basic extremes to quantitatively describing LBO behavior have been presented. They are, on one hand, extremely complex and inherently expensive, and on the other hand, extremely simple, initially expensive, and, requiring extrapolation. In Section 6.6 the concept of stirred reactors, developed in Section 6.2 for correlation of LBO data, was further developed at the micro–scale level and applied as a subgrid field calculation integral with a CFD code. Due to cost considerations it was necessary in this procedure to forgo detailed chemistry calculations. The calculations were still computationally expensive, and probably prohibitively so for such purposes as obtaining engine stability characteristics such as illustrated in Figure 1–3. This is the extremely complex and expensive approach. Examination of the LBO data from the PW200 combustor demonstrated [30.],[32.], in Section 5.0, that during the LBO process flame was held in different regions of the combustor, and that universal experimental data correlations for a wide variety of combustors could never be expected. This is the extremely simple approach. Clearly, a middle–ground approach might merit consideration.

Given the difficulties described above, known characteristics of LBO (flame lift and partial premixing – Section 6.3) can be exploited to derive a middle–ground approach that might be suitable for engineering–quality calculations of LBO in real combustors. The approach is a hybrid one, where the chemistry is uncoupled from the aerodynamics, and the chemical calculations are performed as a form of postprocessing activity to the stationary state CFD solution. This separation would imply that mixing and chemical time scales can be treated as being very different. This is not a bad approximation at typical engine LBO conditions. It is however, only true in a global sense (gross fuel/air distributions) and not in an eddy–sense (extremely local fuel/air distributions). Thus, two observed and important aspects of the LBO process are apparently explicitly ignored: the general nonstationary behavior of the mean flow, and, the unity Damkohler Number effects of turbulence/chemistry interactions. (Some aspects of these can be addressed implicitly however, in the detailed development).

6.7.2 Hybrid CFD/Stirred Reactor Modeling Concept

Bragg [18.] proposed that a gas turbine combustor could be modeled as a perfectly–stirred reactor (PSR) or later, as a well–stirred reactor (WSR) representing the primary zone where flame is held, followed by a plug–flow reactor (PFR) representing the intermediate zone where secondary burn–up takes place; the dilution zone was taken not have a combustion function, but served as a mixer. A WSR is a reacting volume within which the time–scales of turbulent mixing are assumed to be finite but are less than the chemical time–scales. For a PSR, the ratio of mixing to chemical times is zero. A PFR is a PSR transversely across the flow direction, but not longitudinally. Thus, a PSR is zero–dimensional, but a PFR is one–dimensional.

Experimental realizations of (near) PSR's, e.g., Longwell et al., [20.] and Longwell & Weiss [76.], when operated at near–blowout conditions have indicated that blowout occurs locally while global stability still exists, [77.]. This implies development of three–dimensionality, and it follows from this that representation of the primary zone by a single reactor is inappropriate.

With this realization, Bragg's idea can be generalized, where the total fluid in the combustor is partitioned into a number of flow structures that define "reactors," and "surrounding fluid," which includes

all of the remaining fluid, regardless of turbulence scale. The composition and temperature of the "surrounding fluid" constitute the feed stream conditions to the reactors. These ideas are common to the Magnussen microscale approach (Section 6.6), but are used here in a supra-grid approach. The "surrounding fluid" providing the feed stream for a given "reactor" could, in fact, be the products streams from other reactors, or fresh reactants, or any combination of these. The resulting network of interconnected reactors of various types and sizes represents the globally active regions of the complete combustor. With such a network, portions of the network can undergo blowout while overall combustion continues via other portions of the network.

To be able to model the chemical reactions occurring within the reactors, it is necessary to know the reactor volumes and types, as well as the mass exchange rates between the reactors and the surrounding fluid, and the connectivity linking the individual reactors into a network. In other words, it is necessary to represent the aerodynamics (hydrodynamics) of the complete combustor. CFD methods can provide all this information.

Such network representations of the combustor have been used previously, e.g., Correa & Overton [78.], with very simple and intuitively-derived networks. In the hybrid approach, the network can be more rigorously derived from a CFD solution using the gradient analysis techniques of Swithenbank (Section 6.4) for reactor definition, together with streakline postprocessing for connectivity; mass exchange and feedstream temperatures can also be obtained from the appropriate CFD fields.

6.7.3 Reactor Network Determination

A CFD solution of the combustor flowfield, for isothermal flow (or with a simple combustion model to establish the effect of heat release on the flowfield) can be postprocessed to establish reactor volumes, types and connectivity.

The "reactor" regions are established through postprocessing the CFD solution to reveal flowfield features such as recirculation zones. For a recirculation zone, for example, the following information is required:

(i) volume

(ii) recirculated mass flow rate

(iii) mean residence time

(iv) temperature or mean equivalence ratio

(v) range of turbulence dissipation gradient values present.

Although great progress is being made, e.g., Globus et al., [79.], direct computation of fluid flow topology in three-dimensional, multispecie, nonisothermal, chemically-reacting flowfields has not yet been derived in sufficient generality for many of the complex flow features present in gas turbine combustors. For this reason an indirect approach was developed for the needed information. The approach involved a Lagrangian technique of particle tracking (using streaklines--the trajectories of zero mass, infinite drag particles) and an algorithm based on the elapsed time interval since a particle at a point of interest was introduced into the computational domain. Neighboring particles residing in other topological features, will have different elapsed times, e.g., a stagnation surface for closed recirculation zones may be defined as the boundary between a region within which particles have infinite residence times and adjacent regions where the residence time is finite. Boundaries of recirculation zones so-defined can be displayed using tangent surfaces and conventional surface contour plotting. The residence times can be computed by tracking a particle backwards, forwards and sideways to the tangent surfaces (zero-velocity boundaries). The recirculated mass flowrate can be computed by summing the mass flowrate of each computational particle along its trajectories, i.e.,

$$\dot{m}_{recirc} = \sum_{i=1}^{N} \left(\frac{\bar{\rho}_i V_i}{t_i} \right) \qquad 6.128$$

where here,

V =cell volume
$\bar{\rho}$ =cell density (to which the particle density is equal)
t =total elapsed time a particle is in the recirculation
N = number of particles in the recirculation

The boundaries of regions for other criteria can be defined by selecting the appropriate elapsed time thresholds. Special procedures are necessary to track streaklines with adequate accuracy in regions of high velocity gradient. Algorithms are also used to perform volume integrations for 3-D surfaces of arbitrary scalars.

To determine whether or not a region of the combustor is designated as a "reactor" or not, the calculated local fuel/air ratios in the region must be within established flammability limits. If a reacting flow CFD solution is used, reaction must be "undone" to estimate the fuel/air ratios. For propane/air systems, the experimental flammability data provided by Barnett & Hibbard [44.], were used. If the calculated local fuel/air ratio was outside of these limits, the region was designated as a nonreacting "mixer."

To ascertain if a designated reactor region is qualified as being perfectly stirred, the dissipation gradient method of Swithenbank [21.], was used. This method was described above in Section 6.4, and this description will not be repeated here. With the dissipation gradients estimated along the major co-ordinate directions from the calculated turbulence fields of the CFD solution, tangent surfaces can be used to establish local volumes that are well-stirred; plane-surfaces normal to flow trajectories can be used to define local volumes that are plugflow, (see definition above). These are both tedious processes, and some "lumping" of regions into larger blocks is generally convenient to keep the task, and the number of reactors resulting, reasonable.

When the established reactor volumes are super-imposed on streakline plots for the flowfield, the connectivity of the reactors in the network can be determined.

6.7.4 CFD for a Generic Combustor

As an example of a reactor network established from CFD to represent a combustor, the simplified PW200 combustor (Section 5.2) was considered to be a suitable vehicle to illustrate this. The combustor rig had high optical access [30.] for flame observations and, an adequate experimental description of its LBO performance (Section 5.5) had been obtained, together with some limited CARS measurements of primary zone temperatures, (Section 5.4).

The CFD calculations of the PW200 combustor were made using the P&W NASTAR stationary-state solution computer code, [80], and preliminary results of these calculations were presented in Reference 32.

The calculation domain represented a (repeating) single fuel injector segment of the combustor, to which periodic boundary conditions were applied on the lateral sides. The calculation domain consisted of the combustor only (no shrouds, etc.) and the domain was filled by a 109 x 53 x 49 (283,073 nodes) body-fitted grid; however, grid-independent solutions are not claimed even with this nodal density. Figure 6-32 gives an orientation and assessment of the grid upon which the calculations were made; treatment of the combustion air ports in the liners is noteworthy.

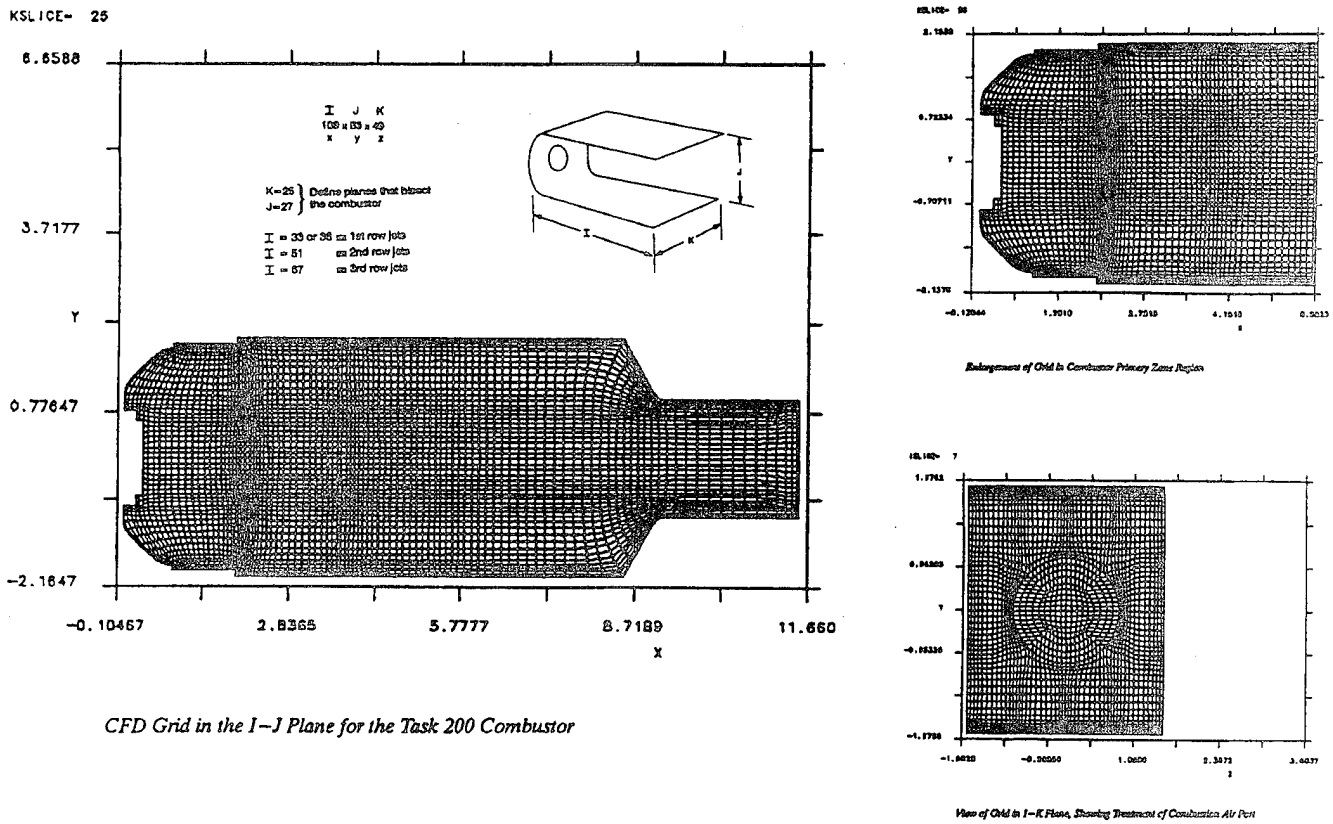

CFD Grid in the I–J Plane for the Task 200 Combustor

Enlargement of Grid in Combustor Primary Zone Region

View of Grid in I–K Plane, Showing Treatment of Combustion Air Port

Figure 6–32. Plane Orientation and Grid Assessment for CFD Calculations of the PW200 Combustor

The calculations were made for both isothermal flow and reacting flow with gaseous propane as fuel. The operating conditions for the isothermal case were an air temperature of 304K and a combustor pressure of 14.31 psia. The total combustor airflow was 0.1716 lbm/sec. (4–injector basis), with flow splits of 15 percent dome, upper liner 42.41 percent and lower liner 42.56 percent. Liner flows were introduced as individual jets, according to the hole patterns and effective areas given in Section 5.2. The two rows of combustion air jets in the liners (Rows 1 and 2, Figure 5–2), were introduced into the combustor with downstream velocity components resulting in jet initial angles of 15 degrees and 8 degrees off the vertical respectively; the dilution air jets had an initial angle of 5 degrees downstream deviation from the vertical to the liners. These jet angles were due to the bypass flows in the shrouds, and the values used were confirmed by measurements in the combustor, made through the windows during hot–flow running. The calculations were started at the discharge from the fuel injector. Fuel injector flow boundary conditions were obtained from LDV measurements of a similar injector, made at United Technologies Research Center. Injector passage effective areas were given in Section 4.3.

The reacting flow case had a total airflow of 1.1632 lbm/sec. (including shroud bypass air) at 297.6K; the bypass air (see Figure 5–1 and Figure 5–2) was 0.422 lbm/sec. Pressure in the combustor was 14.73 p.s.i.a. Flow splits were as for the isothermal case. The combustion model used was the standard EBU–version, which does not provide a good representation for the given operating conditions where chemical kinetics are important.

Only the salient features of the calculated combustor flowfields may be presented here due to the inherent complication involved. Figure 6–33 shows calculated iso–surfaces of mean axial velocity at fixed velocity of, for reference purposes, Magnitude 1, in the isothermal case. This figure conveys a good three–dimensional impression of the major flow features existing in the combustor. The only flow medium used in this calculation was air, although tracer–tagging was used to follow specific flows where desired.

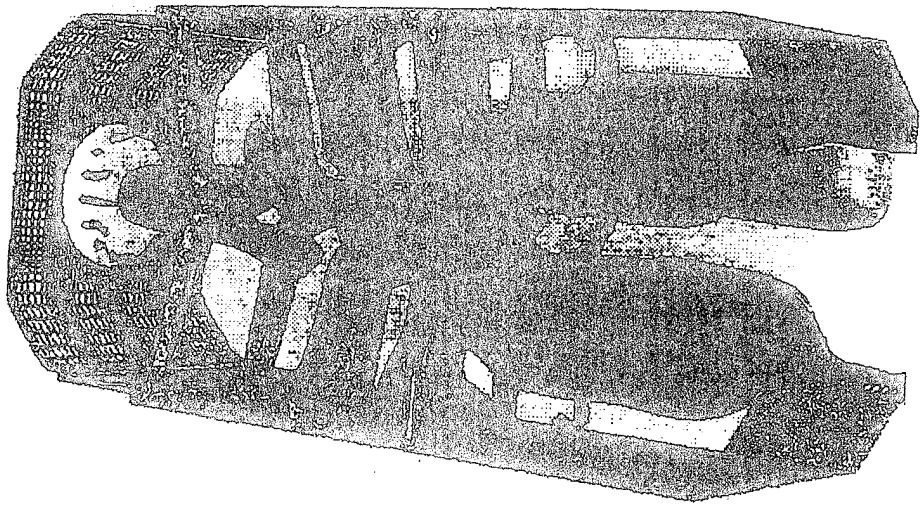

Figure 6–33. Isothermal CFD Calculation of Iso–Surfaces of Mean Axial Velocity (at Magnitude 1) Showing Swirlig Jet From Fuel Injector Exhibiting Lobate Formation at First Row Combustion Air Jets

Immediately identifiable, from the front of the combustor, are the axial swirling jets from the airblast fuel injector, the individual insert swirler jets (for geometric details of the combustor and injector, see Sections 5.2 and 4.3) surrounding the fuel injector, the first row of combustion air jets as opposed pairs on either side of, and inline with, the fuel injector jet, the second row of liner air jets as larger diameter, opposed pairs that are laterally disposed between the first row jets, and so on, along the combustor. Note the account of the effect of shroud bypass flows on the jet initial angles. The spent dome impingement cooling air was discharged axially as a liner cooling film at the upper and lower liner/dome interfaces.

The insert swirler jets (together with the fuel injector internal geometry – see Figure 4–2) act by confinement to prevent the weakly–swirling (LS injectors used) jet leaving the fuel injector from spreading much radially. It can be seen that the first row air jets penetrated to the combustor horizontal centerline before completing their turn to flow axially.

The lateral spreading of the combustion air jets resulting from their high penetration and resulting collision, can be seen in Figure 6–34, where Magnitude 2 velocity is less than Magnitude 1 velocity in Figure 6–33. The view in Figure 6–34 is from the top of the combustor, with the upper liner removed for clarity. As in Figure 6–33, the bounds of the calculation domain that are physical wall are shown by means of the calculation grid projected onto these surfaces.

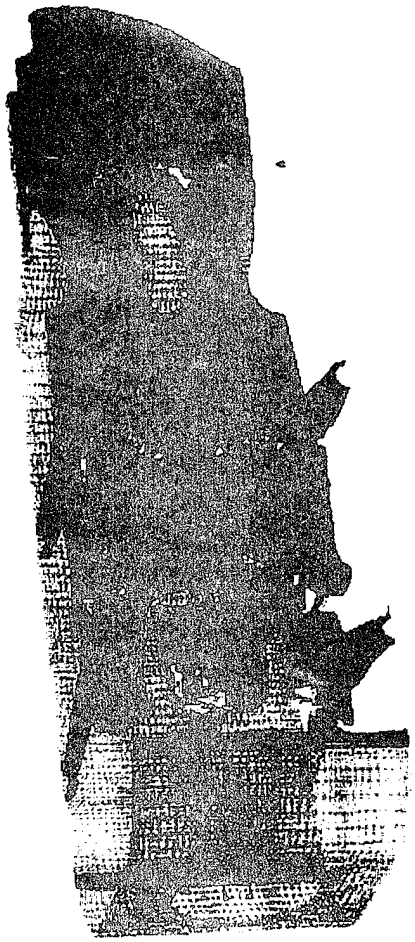

Figure 6–34. Vertical View of Isothermal CFD Calculation with Iso–Surfaces of Mean Axial Velocity (At Magnitude 2), Showing Lateral Spreading of Colliding Transverse Combustion Air Jets

The consequential blockage to exiting primary zone flow represented by the colliding combustion air jets caused the coherent swirling jet from the airblast fuel injector to divide into two diagonally–opposed lobes in order to escape from the combustor primary zone. Asymmetric splitting of the fuel injector jet into two lobes was due to the swirl velocity component that this jet contained.

Figure 6–35 and Figure 6–36, respectively, show contour plots of mean axial velocities on vertical planes inline with, and between, the fuel injectors; the plots reveal the regions of flow reversal (shown as hatched areas).

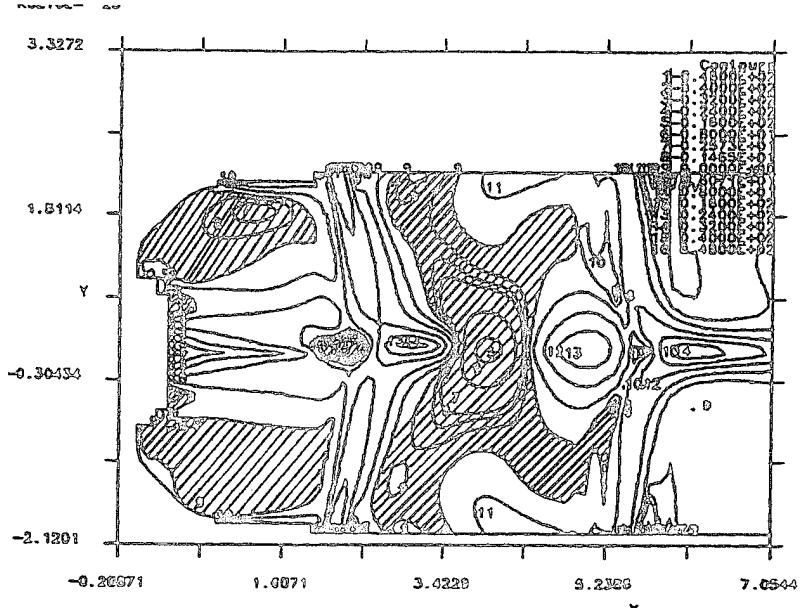

Figure 6–35. Section Through Fuel Injector with Calculated Iso–Vels of Mean Axial Velocities, Showing Reverse Flow Regions

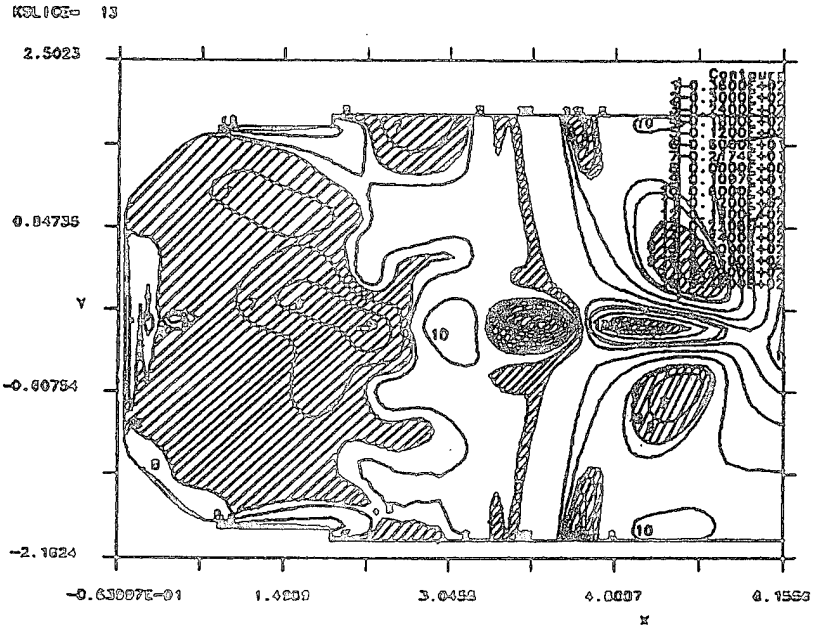

Figure 6–36. Section Out of Fuel Injector Plane with Iso–Vels of Calculated Mean Axial Velocities, Showing Reverse Flow Regions

Note that the blockage of the pairs of combustion air jets inline with the injector produced a small region of reverse flow in the center of the fuel injector jet as it began to split into lobes, and that this caused diagonally–opposed lateral flows of combined combustion jet air and injector fluid into the regions between fuel injectors. Thus, the major recirculation zones were between injectors, with smaller recirculation zones in the injector planes that were placed radially about the injector jets, outboard of the insert swirler jets. Further regions of reverse flow existed in the wake structures downstream of the first row combustion air jets, and, upstream and downstream of the second row of combustion air jets.

With combustion turned on, the primary zone isothermal flowfield features shown in Figure 6–35 and Figure 6–36 were all present, although velocity magnitudes were of course, changed somewhat. Maximum

gas temperatures and the majority of the heat release were contained between the dome and the first row of combustion air jets; some moderately high temperatures were encountered in the immediate wake regions of the first row of combustion air jets. There was no reaction taking place downstream of the second row of combustion air jets. The temperature levels calculated were much above those measured (Section 5.4) due to the limitations of the EBU combustion model. The presence of the small recirculation region on the fuel injector jet centerline due to collision of the first row of air jets, resulted in a "notched flame" appearance; this feature was visually observed in the actual flames during PW200 combustor testing. The "burned equivalence ratio" in the dome recirculations was around 0.6, and in the wakes of the first row combustion air jets it was 0.4 – 0.6; in the small recirculation bubble at the jets confluence it was about 0.5.

Some indication of hot flow tracing can be obtained from Figure 6–37 and Figure 6–38, which show particle trajectories for tracers introduced on the fuel injector centerline and around its periphery, respectively. Figure 6–39 and Figure 6–40 show first row combustion air jet behavior by the same technique.

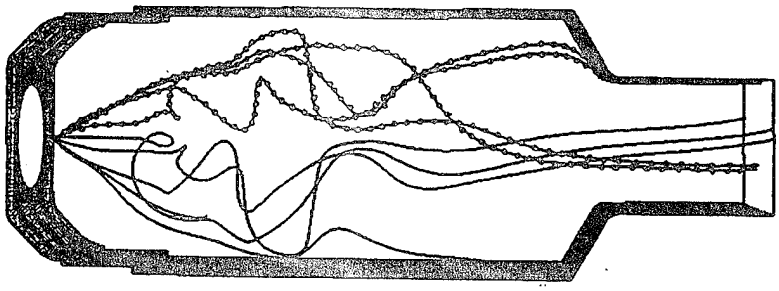

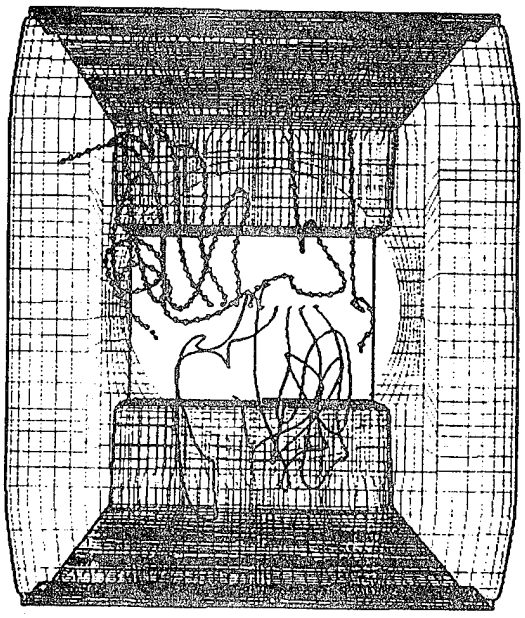

Figure 6–37. Tracer particle Trajectories for the Inner Regions of the Fuel Injector Jet (Reacting Flow): Along and Across (Upstream of Combustion Air Jets) the Combustor, (Note the Absence of Swirl)

Fluid from the center region of the fuel injector jet achieved significant radial displacement as it moved downstream, (Figure 6–37). This resulted from two causes: first, entrainment into the outer regions of the injector jet and insert swirler jets, and second, by encountering the central recirculation at the jets

confluence. It can bean seen that encountering the recirculation bubble caused essentially a 90 degree flow direction change. Fluid on the periphery of the axial injector jet, (Figure 6–38), was distributed across the combustor when it encountered the first row of combustion air jets. Behavior of the combustion air jets was strongly influenced by the interaction with the swirling injector jet, which produced axisymmetric development as shown by Figure 6–40. This behavior could be related to the isothermal flow iso–surface of velocity shown in Figure 6–33.

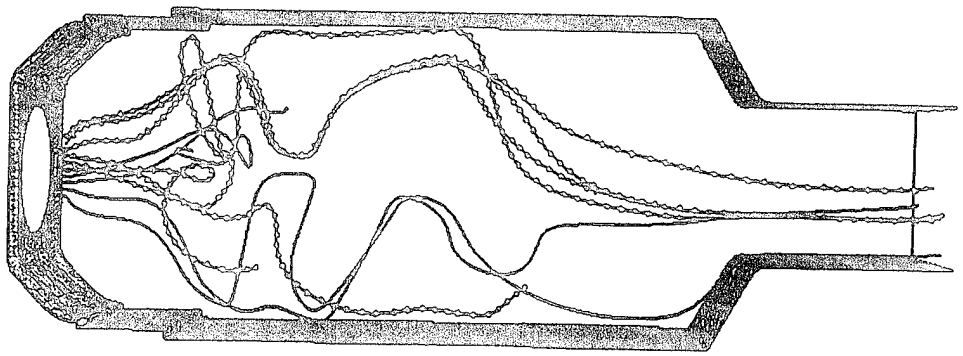

Figure 6–38. Tracer Particle Trajectories for the Outer Regions of the Fuel Injector Jet (Reacting Flow): Along the Combustor

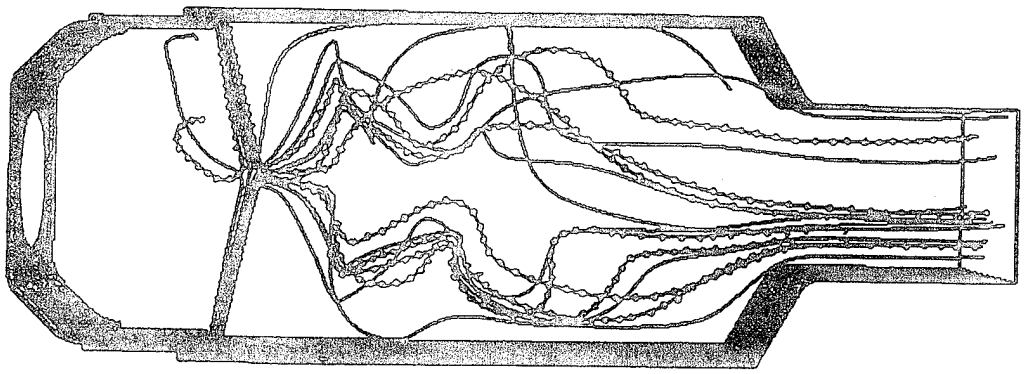

Figure 6–39. Tracer Particle Trajectories for the 1st Row Combustion Air Jets (Reacting Flow): Along the Combustor

Consideration of the traces shown in Figure 6–37 to Figure 6–40 inclusive, reveals that fluid introduced into the combustor via a given source (fuel injector, combustion air jet, etc.) is well–dispersed throughout the combustor volume in a downstream direction. While dispersion is not exactly the same as mixing, the high degrees of dispersion achieved suggests that mixing rates, at least on a global basis, are high in the PW200 combustor.

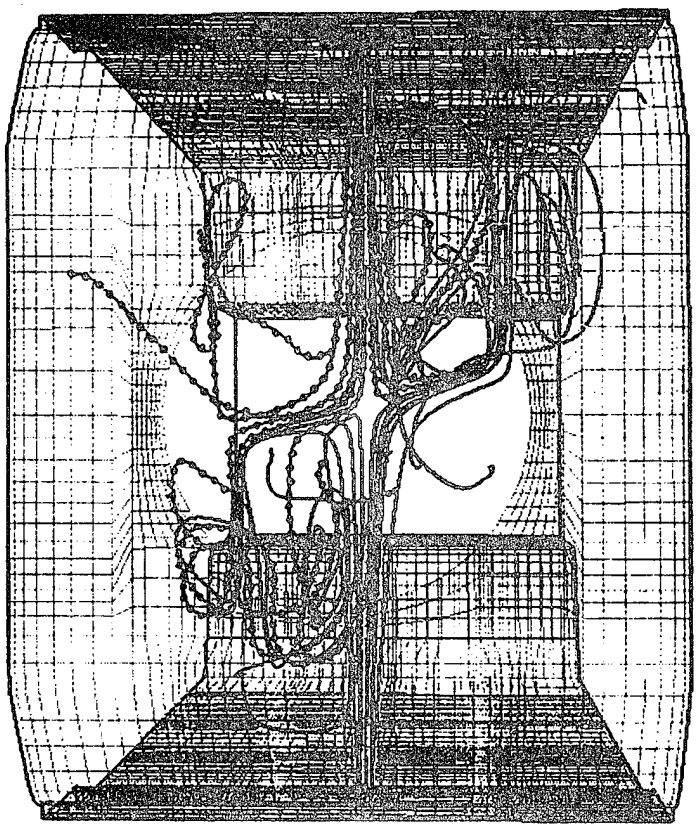

Figure 6–40. Tracer Particle Trajectories for the 1st Row Combustion Air Jets (Reacting Flow): Across the Combustor

The CFD calculations reveal some interesting features concerning the behavior of the PW200 combustor at near–blowout conditions. The swirling jets from the fuel injectors are sufficiently confined by their surrounding insert swirler air jets and the basic internal geometry of the injector itself, that they retain their coherence in the dome region of the combustor. The closeness of the first row of combustion air jets to the dome, their lateral spacing and alignment with the fuel injector centerlines, together with the jet penetration achieved, together result in a close–coupled jet system with the fuel injector in the short primary zone. The consequential aerodynamic blockage to escape of primary zone flow represented by the colliding combustion air jets and their subsequent lateral spreading (Figure 6–34), causes the coherent swirling jet from the airblast fuel injector to divide into two, diagonally–opposed, lobes, in order to exit from the combustor primary zone. The combustion air jet system establishes ample regions of reverse flow to provide jet flame–holding if supplied with suitable fuel/air mixture. The major regions of recirculation providing flame stability are, however, between fuel injectors with recirculation back to the dome. Smaller recirculations to the dome exist above and below the injector centerlines.

The flow features observed in the calculations are established by the combustor geometry, and the strong aerodynamic interaction of the closely–coupled flow features. These structures and their behavior are not significantly changed by the heat release due to combustion at near–blowout operating conditions.

It is interesting to compare the calculated flow fields in the PW200 combustor to the measured behavior in Section 4.0 for a single injector without transverse combustion air jets in the PW150 combustor. The modification of flame behavior due to the closely–coupled first row of combustion air jets is dramatic. The PW150 results do give an added perspective on how the coupling arises, which is not only through the positioning of the first row of transverse air jets but is also a factor of the local stoichiometry.

6.7.5 Reactor Network for the Generic Combustor

From Section 6.4 it was determined that the limiting condition of the dissipation gradient $d(D/q_{\cdot})/d(x/y_{\max})$, to adequately represent a PSR was a value not to exceed 10.0.

Information on the dissipation gradient was obtained from the calculated turbulence field by post–processing. The information is difficult to represent, but Figure 6–41 attempts to do this. In the PW200 generic combustor, the CFD results indicate that the surface contour representing this value of dissipation gradient was confined to the primary zone and the regions around and immediately downstream of, the first row of combustion air jets. Well–stirred reactor (WSR – defined as regions of high turbulence kinetic energy and high turbulence dissipation, but having dissipation gradients greater than 10.0) regions exist downstream of the primary zone in the wake regions downstream and around the other transverse air jets, but being somewhat towards the combustor wall rather than towards the center of the combustor.

Note that the surface contour shown in Figure 6–41 is actually for a value of nondimensionalized turbulence kinetic energy that corresponds to a dissipation gradient value of 10.0, obtained via Equation 6.41.

Global contours of equivalence ratio, together with imposed flammability limits, were used to establish what parts of the identified perfectly–stirred and well–stirred regions of the combustor would sustain chemical reaction. This information, together with the geometric locations of inlet flows, (fuel and air), were used to partition the regions into individual reactors. In making these decisions, some drastic simplifications of the local region geometries were necessary. This was done intuitively, with some trial and error, and involved an inevitable "lumping" of individual regions to fit both the connectivity that was derived from the super–imposed streak–lines, and the one–dimensionality framework of the reactor network.

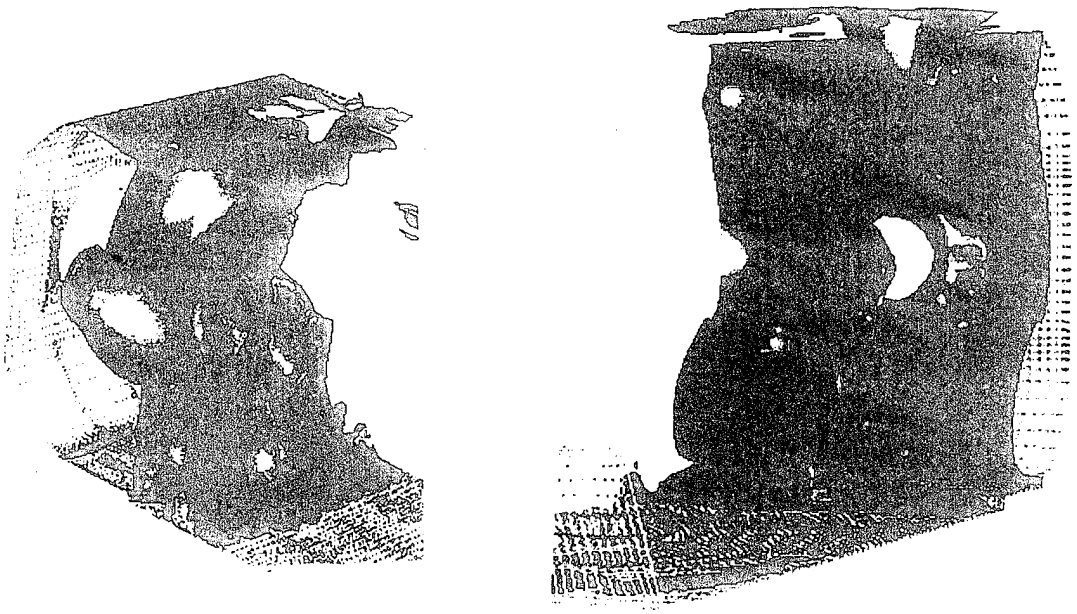

Figure 6–41. Left and Right Hand Views of a Limiting Surface Contour Representing a Dissipation Gradient Value of 10.0 to Define a Perfectly Stirred Reactor Region for the PW200 Combustor

Figure 6–42 illustrates the reactor network established from the CFD results by the procedure described above. The network consists of seven reactors in series, and one reactor in parallel with the first

three series reactors. When Figure 6–42 is compared to the calculated flowfield information in Section 6.74, it is relatively easy to relate the network to the flowfield.

The initial plug–flow reactor (PFR) represents the fuel and air discharges from the fuel injector, together with a portion of the dome flow from the insert swirlers concentric with each injector. The region is a PFR because of the strong unidirectionality of the flow; generally, the stoichiometry exceeds the rich flammability limits (depending on the combustor loading), and conditions are influenced by recirculated flow that is fed back into the inlet by the large parallel reactor. The second region is generally an active reactor because the remainder of the insert swirler air and the dome film cooling air have mixed–in to bring the local equivalence ratio within the flammability limits for lower values of fuel flow. The third reactor in the series represents the recirculations on the injector centerlines that are set up by the impact and interactions of the first row of combustion air jets with the injector jets. The reactor in parallel with the first three reactors provides recirculation, and represents the shaded regions in Figure 6–35 and Figure 6–36 around and between the near–axial jets from the injectors. The dissipation gradients in these regions of the combustor are such that the reactors can be considered as perfectly–stirred (PSR). In the downstream regions of the combustor a general "preferred direction of flow" is again established, and with growing strength with distance from the dome. PSR's would not be totally appropriate under these conditions, so PFR's are used, and individual reactors are associated with the remaining air–addition stages in the combustor.

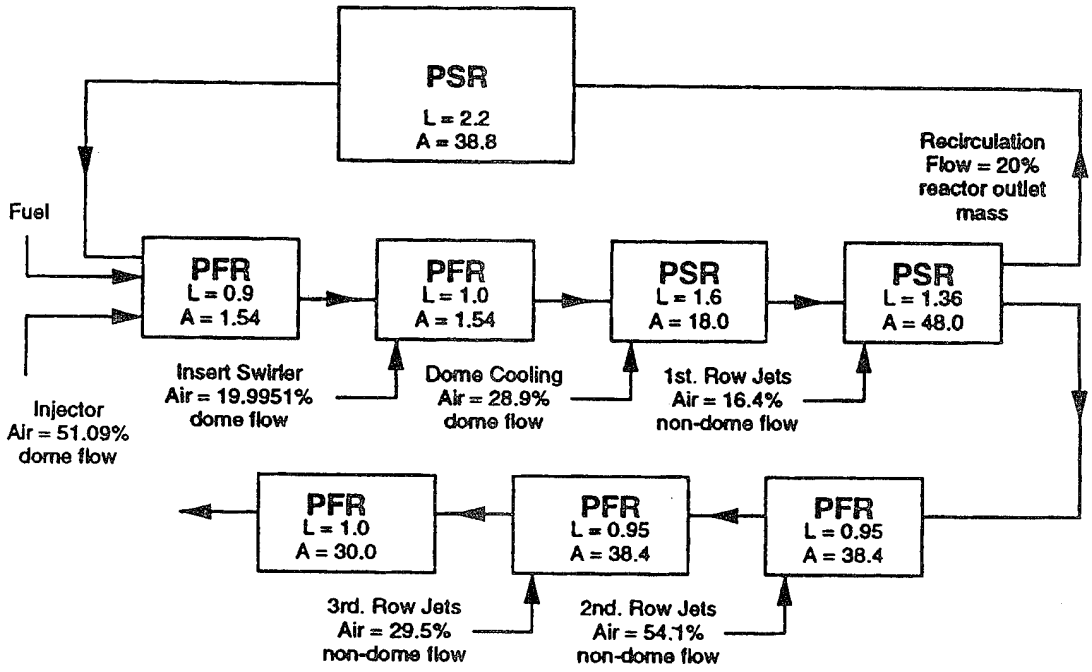

Notes:

1. **Dome and liner mass flowrates separately metered**
2. **L = reactor length, inches**
3. **A = reactor cross-sectional area, sq. inches**

Figure 6–42. Network of Reactors Representing the PW200 Combustor at Near–Lean Blowout Conditions

It should be noted that the sum of the individual reactor volumes does not equate with the total volume of the actual combustor. The analysis of the CFD result used to produce the network suggested that not all of the available combustor volume was effectively utilized for combustion, at least at near–blowout conditions.

The network of Figure 6–42 does not represent the only interpretation of the CFD results that is possible. It is the simplest one, however; complication could be added later as necessary in the event of shortcomings being revealed. Although it is relatively simple, the network of Figure 6–42 represents a considerable improvement over Bragg's original concept of representing the complete combustor as a single PSR for the primary zone, followed by a PFR for the intermediate and dilution zones.

In making lean blowout calculations with the network, it is assumed that the combustor flowfield represented by the reactor network shown in Figure 6–42 is established by the geometric boundary conditions supplying the flows entering the combustor, and by the relationship of these geometric features to each other. The flowfield is assumed not to change substantially with either heat release rate or with combustor operating conditions in the lean blowout range. Changes in operating conditions will only affect individual reactor residence times and equivalence ratios, as will combustor flow–split changes.

Many other well–established practical combustor development tools also rely on this assumption, e.g., rheology or, water–analogy (water–tunnel) rigs [81.]. The heat release part of the assumption is largely verified by comparing the nonreacting and reacting flow CFD calculations given above. Given the closely–coupled flowfield character of the PW200 combustor primary zone and the confining of the flame to the primary zone at LBO conditions, the assumption appears to be reasonable in the present instance at least.

6.7.6 Chemical Reaction Mechanism

LBO of the PW200 generic combustor is to be modeled by representing it, from a process point of view, as a simple, eight–element network of PSR's, PFR's, and recirculating reactors, as constructed from an analysis of CFD calculations for the flowfield. The detailed chemistry is then to be solved on the network, uncoupled from the fluid dynamics.

The chemical reaction mechanism, together with rate constants, used for this detailed chemistry was a reduced, quasi–global one based on that by Kollrack, [51.],[52.], for JP5/Jet A. The reaction chemistry behavior of vaporized JP5/Jet A resembles that of propane, the prime fuel used in the PW200 testing. The reason that this particular mechanism was selected was that, when used with propane thermodynamic properties and modifying the global steps for the appropriate C:H ratio, it gave the best representation of LBO of several competing mechanisms for propane/air combustion, (Section 6.5) when compared to the experimental blowout curve obtained by Clarke et al. [61.], for a well–stirred reactor. The Kollrack mechanism also gave good agreement with the experimental LBO data of the PW100 research combustor (Figure 3–14).

When formulating the mechanism, Kollrack represented the multicomponent real fuel by the generic fuel molecule $C_{12}H_{23}$. The shortened mechanism includes a two–stage fuel molecule breakdown (pyrolysis), and then gives emphasis to the more stable intermediate species via a second stage in which simpler hydrocarbons are reacted, and a third stage that is dominated by recombination reactions and the conversion of CO to CO_2. Included in it is the extended Zeldovich mechanism for thermal NO, but there is no account of "prompt" NO.

There are 30–steps involving 20 species, and the complete mechanism is given in Table 6–2.

Table 6–2. Kollrack's Reaction mechanism and Rate constants for JP5/Jet A Fuel

The forward and backwards rate constants, k_j, are taken as being equal (where appropriate), and are given in Arrhenius form, e.g.,

$$k_j = 10^{B_j} T^{N_j} exp\left(-\frac{T_j}{T}\right)$$

STEP	REACTION	10^{B_j}	N_j	T_j
1.	$C_{12}H_{23} + O_2 \rightarrow 5C_2H_4 + C_2H_3 + 0_2$	4.48	1.5	7900
2.	$C_{12}H_{23} + OH \rightarrow 6C_2H_4 + 0$	7.3	1.0	4500
3.	$C_2H_4 + H \Leftrightarrow C_2H_3 + H_2$	10.48	0.0	9500
4.	$H + H + M \Leftrightarrow H_2 + M$	12.3	−1.0	0.0
5.	$0 + 0 + M \Leftrightarrow 0_2 + M$	11.0	−1.0	0.0
6.	$H + OH + M \Leftrightarrow H_2O + M$	13.85	−1.0	0.0
7.	$H + 0_2 \Leftrightarrow OH + O$	11.35	0.0	8400
8.	$O + H_2 \Leftrightarrow OH + H$	10.24	0.0	4730
9.	$CO + OH \Leftrightarrow CO_2 + H$	−14.75	7.0	−7000
10.	$H + H_2O \Leftrightarrow OH + H_2$	10.92	0.0	10050
11.	$CH_3 + O_2 \Leftrightarrow CH_2O + OH$	9.0	0.0	4000
12.	$HO_2 + M \Leftrightarrow H + O_2 + M$	12.32	0.0	2300
13.	$HO_2 + H \Leftrightarrow 2OH$	9.89	0.0	950
14.	$CH_2O + OH \Leftrightarrow H_2O + HCO$	10.90	0.0	2120
15.	$O + H_2O \Leftrightarrow 2OH$	10.76	0.0	9000
16.	$N_2 + O \Leftrightarrow NO + N$	9.0	0.0	25000
17.	$N + O_2 \Leftrightarrow NO + O$	5.0	1.0	2000
18.	$N + OH \Leftrightarrow NO + H$	9.0	0.0	0.0
19.	$HCO + O_2 \Leftrightarrow HO_2 + CO$	10.48	0.0	7000
20.	$HCO + OH \Leftrightarrow H_2OO + CO$	10.30	0.0	0.0
21.	$C_2H_4 + OH \Leftrightarrow C_2H_3 + H_2O$	9.78	0.0	1750
22.	$CH_2O + HO_2 \Leftrightarrow HCO + 2OH$	9.0	0.0	4500
23.	$C_2H_2 + HO_2 \Leftrightarrow HCO + CH_2O$	9.3	0.0	5500
24.	$C_2H_3 + O_2 \Leftrightarrow C_2H_2 + HO_2$	9.23	0.0	5000
25.	$NO + HO_2 \Leftrightarrow NO_2 + OH$	3.0	1.0	0.0
26.	$C_2H_4 + O \Leftrightarrow CH_3 + HCO$	9.93	0.0	1500
27.	$C_2H_4 + HO_2 \Leftrightarrow CH_3 + HCO + OH$	9.9	0.0	5000
28.	$H_2 + CH_3 \Leftrightarrow CH_4 + H$	7.0	−1.5	7140
29.	$C_2H_2 + OH \Leftrightarrow CH_3 + CO$	8.2	0.0	2500
30.	$CH_3 + O \Leftrightarrow CH_2O + H$	11.11	0.0	1000

6.7.7 Heat Losses

Heat losses from the flame can be important at lean blowout conditions. For the PW200 combustor, where at LBO conditions flame is confined to the primary zone, heat lost from the primary zone through the liner walls to the shroud flow is essentially lost to the combustion process.

Heat losses for the PW200 combustor were estimated as functions of airflow at close to blowout conditions, and were accounted for through a downwards adjustment of the fuel heating value from that for propane.

6.7.8 Definition of Blowout

A careful protocol was established to ensure that the correct LBO solution was achieved, (see Section 6.5). Calculated LBO's of the reactor network were obtained to meet an objective value of combustor loading parameter by first establishing for the appropriate airflow, reaction at or near stoichiometric primary zone fuel/air ratio and atmospheric pressure, then, reducing pressure in several steps to the desired level while maintaining high primary zone temperatures, and finally, progressively reducing the fuel in ever–smaller decrements at the desired and constant pressure level. The fuel decrement step size was decided based on the rate of change of the critical reactor (the one sustaining combustion) outlet temperature.

To avoid confusion between the stable intense–reaction and the unstable weak–reaction branches existing below the equilibrium state, and represented on the characteristic S–shaped curve of temperature versus residence time for a PSR (Figure 6–16), use was made of an extinction/ignition state to establish blowout. At the ignition state the rate of heat release in the reactor is such that it is no longer balanced by the heat transport through the reactor. This leads to an increase in the reaction temperature that induces a coupled increase in the reaction rate, culminating in the runaway event of ignition. For present purposes, no explicit distinction is made between ignition and extinction, which may be viewed as the reverse of ignition. A blowout was thus assumed when the computer code either failed to find a solution (rare), or, when all reactor temperatures had fallen below a conservative 1480°K (2200°F), based on a suggestion of Appleton & Heywood [82.]. Choice of this particular temperature allows for some implicit account of the nonstationary behavior know to preceed a blowout event, (Figure 3–10, for example).

6.7.9 Reactor Network Code

The reaction mechanism given in Table 6–2 was solved on the reactor network illustrated in Figure 6–42 by means of the MARK2I interactive computer code of Pratt & Pratt [83.]. The MARK2I code uses the CREK chemical kinetic package of Pratt & Wormeck [84.], and is conveniently run on a P.C.

6.7.10 Preliminary Test of Hybrid CFD/Stirred Reactor Modeling

The limited fields of mean temperatures measured by CARS in the PW200 combustor (Section 5.0) were used as the basis for a preliminary evaluation of the hybrid CFD/stirred reactor modeling approach.

From the measured distributions of mean temperature, data in an axial band of width 2 cm inline with a fuel injector at the combustor midheight, were extracted. The measured axial distribution was compared against the calculated temperatures at the exit from each of the seven inline reactors of the network, when the network was run with the inlet conditions appropriate to the measurements. Similarly, from the measured data, the maximum and minimum temperatures for a 2 cm wide band midway between fuel injectors was compared with the outlet temperature from the recirculation reactor.

Figure 6–43 shows the comparison of measurements and calculations inline with fuel–injectors. The reactors are marked by number, with Number 1 being the first PFR, and the downstream distance that they each occupy. The measured temperatures are represented by the maximum and minimum values encountered in the 2 cm band width at each measurement distance from the combustor dome. Reactor No. 7 is not shown since it extends beyond the range of the measured data. Figure 6–44 contains similar information for the recirculation region between injectors.

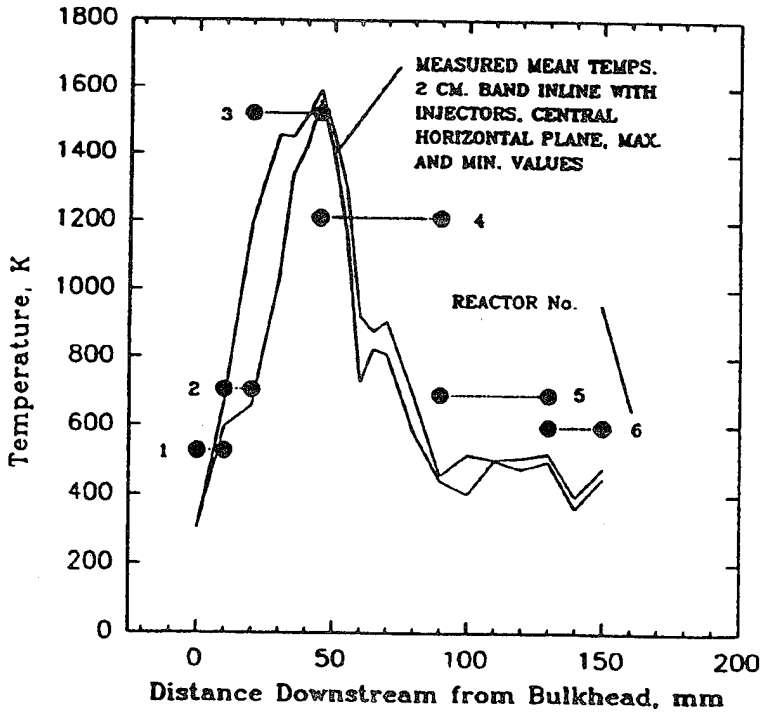

Figure 6–43. Comparison of Network Reactor Outlet Temperatures Against CARS Temperature Measurements Inline with a Fuel Injector on the PW200 Combustor Horizontal Mid–Plane

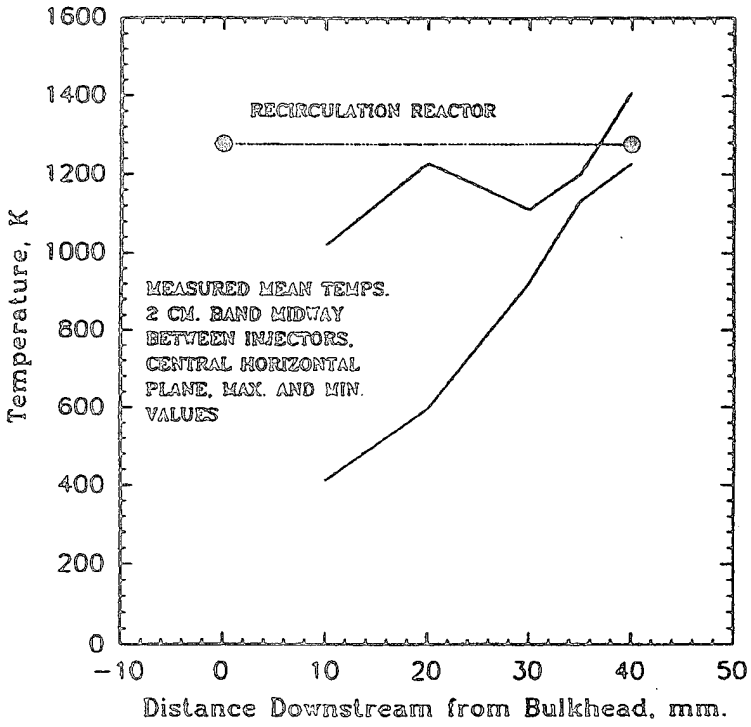

Figure 6−44. Comparison of Network Recirculation Reactor OutletTemperature Against CARS Temperature Measurements Between Fuel Injectors on the PW200 Combstor Horizontal Mid−Plane

In Figure 6−43, the calculated temperatures reproduce well the axial distribution of measured temperatures inline with the fuel injector, and also agree well as to temperature level. The agreements are particularly good for distances 0 − 70 mm, the critical region that determines flame stability. For distances greater than 100 mm from the combustor dome the calculated temperatures are 50 − 100 deg. K higher than the measured values.

In Figure 6−44 the agreement is not so good. However, the recirculation reactor in the calculation represents not only the recirculation region between fuel injectors, but also that portion above and below the injectors (see Figure 6−35 and Figure 6−36 where the recirculation zones are shown as irregularly−shaped toroids about each injector), whereas the mea e.g.,surements are only indicative of the region between injectors; no measurements in the upper and lower portions of the recirculation are available. The implication is that the reactor network might be improved by splitting the recirculation reactor into two separate recirculation reactors with different connectivities.

Although the temperature comparison does not represent a particularly severe test of the CFD/reactor network concept, it suggests that the network does constitute a reasonable representation of the complex reactive flowfield, and that the approach has merit.

6.8 Modelling Summary

Three examples of modeling lean blowout of turbulent diffusion−flame combustion have been developed; these are:

(i) a phenomenological approach of turbulent eddy quenching that is based on a partial premixing assumption that arises through flame−lift,

(ii) a CFD approach utilizing a subgrid scale combustion model applied to the turbulence structure and based on well−stirred reactor methods, that is solved in coupled fashion using a characteristic time blowout criterion,

(iii) a hybrid CFD/stirred reactor network approach wherein the calculated flowfield is used to establish a global network of stirred reactors upon which detailed chemistry is solved uncoupled from the flowfield.

In addition, correlation groups for experimental LBO data were developed in terms of stirred reactor concepts.

There are two commonalities in all of these pieces of work: First, that turbulent diffusion flames near blowout always involve some significant degree of premixing of reactants at some appropriate length scale. Second, that stirred reactor modeling concepts represent a useful method of addressing the partial premixing aspects. These commonalities have been applied in markedly different ways to describe the LBO problem, and the methods of application show different blends of sophistication and pragmatism. The three modeling approaches involve respectively, no chemistry, a single–step reaction, and, multi–step reaction chemistry. The way that chemistry is incorporated reflects concerns of total calculation costs. The preliminary evaluations of the modeling suggest that they all do hold some promise.

THIS PAGE INTENTIONALLY LEFT BLANK

SECTION 7.0
MODEL EVALUATION

7.1 Intent

Preliminary evaluations of the modeling approaches were described in Section 6.0. These evaluations were sufficient to establish the efficacy of each approach, but they were neither extensive nor rigorous enough to establish the validity of an approach for successfully modeling the lean blowout process in a gas turbine engine combustor. For this purpose, the experimental data gathered in the PW100 and PW200 combustors served as an appropriate database. The PW100 combustor was important because it exhibited (Figure 3–6), both attached and lifted flame behavior. The presumption of flame–lift and subsequent partial–premixing of reactants formed a corner–stone idea in all of the modeling approaches. The PW200 combustor was important because it represented a gas turbine generic combustor for which extensive LBO data were available, and which included some flow split variations of significance. The PW150 combustor was viewed only as a diagnostic tool for understanding the behavior of the PW200 combustor, and therefore did not form part of the evaluation database.

7.2 Evaluation of EDC Combustion Model in the PW100 Combustor

The PW100 combustor appeared to be ideal vehicle for a continuation of the evaluation of the EDC model as incorporated into the 2D–PREACH CFD code. The PW100 combustor, being a step–combustor, exhibited in a recirculating (i.e., elliptic as opposed to the parabolic field used in Section 6.10) flowfield, a lifted–flame behavior, (Figure 3–6 and Figure 3–10). The EDC model should be capable of capturing this behavior.

A number of cases of interest were calculated, as described in Table 7–1. Accompanying experimental data (with LDV and CARS measurements) were made for an airflow of 1,000 SLPM. This airflow resulted in Reynolds Numbers that were less than desirable. Since locally–laminarized flame regions have been commonly observed for free propane jets with Reynolds Numbers less than 9,000, these PW100 flow conditions and the resulting Reynolds Numbers may be sufficiently low as to represent transitionally– turbulent conditions. The calculations of course, only address fully–turbulent flow conditions.

The calculations assumed that the mean flows in the combustor were axisymmetric, and that they were stationary. The mesh size used was 77 x 57 for one–half of the combustor from the geometric axis of symmetry, and the grid expanded in both downstream and radial coordinate directions. For the fuel tube, 15 cells were used, and 5 were used in the air annulus. The start of the calculation domain was taken as the physical confluence of the fuel and air jets, and it extended downstream for the combustor length with the 260 mm extension chimney, for a total length of 735 mm. Inlet boundary conditions were estimated from experimental conditions, and from an analysis of the measurements taken at an axial station of 7 mm downstream from the step–plane. The initial value for turbulent Schmidt Number was 0.9. This value is really only appropriate for wall boundary layers; a value of 0.7 has been found appropriate for jet flows, and a value of 0.5 for recirculating flows [85.].

7.2.1 Basic Flowfield (Case N23)

The efficacy of the calculations for flame–lift is not determined solely by the EDC combustion model. It is also governed by the basic abilities of the CFD code to calculate the mean flow field and the turbulent mass transport of fuel, air and products. This latter aspect also involves the presumption that the mean flow is indeed stationary. The nitrogen case N23, (Table 7–1) was used to establish the mean field accuracy.

Table 7–1. Case Descriptions for PW100 Combustor CFD Calculations

Case	Fuel	Fuel Flow Rate (SLPM)	Air Flow Rate (SLPM)	Equivalence Ratio	Fuel Tube* Reynolds Number	Comments
N23	Nitrogen	23	1000	--	1,172	--
F23	Propane	23	1000	0.59	4,003	Lifted 0.15 m)
F41	Propane	41	1000	1.05	7,135	Lifted (0.10 m)
F63	Propane	63	1000	1.62	10,964	Attached

Figure 7–1 shows the comparison of measured and calculated centerline mean axial velocity, and Figure 7–2 gives the radial profiles. The combustor experimental Reynolds Number for this nonreacting case was sufficiently high that the flow was fully turbulent, so that the comparisons are entirely valid.

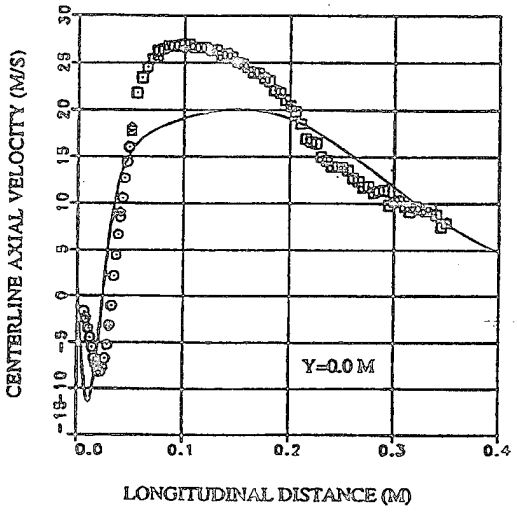

Figure 7–1. Comparison of Calculated and measured Centerline Mean Axial Velocities for Case N23

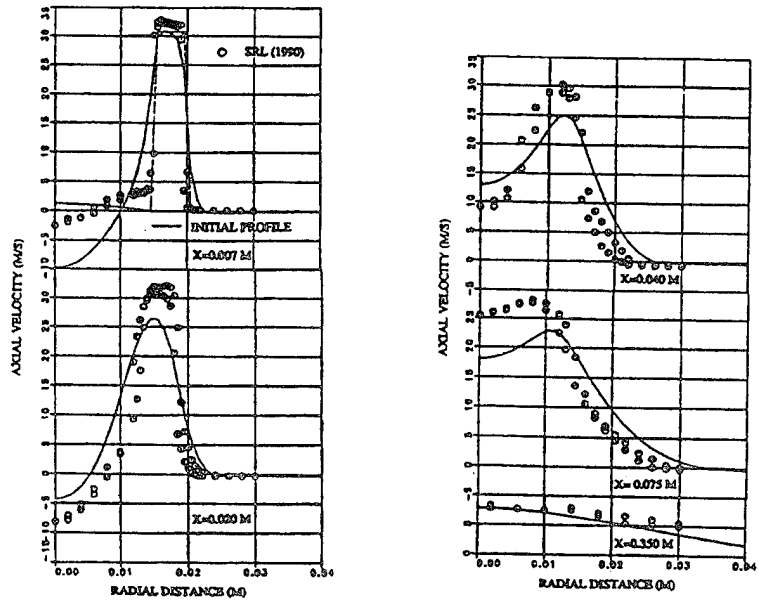

Figure 7–2. Comparison of Calculated and Measured Radial Profiles of Mean Axial Velocity for Case N23

The comparisons reveal that the calculated centerline recirculation bubble (see Figure 3–3 for a different set of measurements at higher Reynolds Number and using pure air) develops more rapidly and its reverse flow velocity is stronger than measured; also, its axial extent is less than that measured. The experimental recovery of centerline mean axial velocity was greater than that calculated. The radial profiles of mean axial velocity suggest that the calculated step recirculation zone length may be longer than that measured. Perturbations of the initial inlet profiles in the calculation did not significantly change this behavior. The behavior is typical of that associated with the turbulence model used in the code [74.]. Clearly, the level of calculation accuracy is determined by the turbulence model, and assessment of the EDC model must be considered in light of this. While the calculative accuracy can only be considered as "fairly good," the quantitative behavior is entirely correct.

7.2.2 Reacting Flow with EBU Combustion Model (Cases F23 and F63)

To provide a combustion model reference base for comparison with the EDC model, calculations were made for the F23 and F63 cases using the standard (mixed–is–burned) Eddy Break–Up, (EBU) model. Adiabatic wall boundary conditions were used for these calculations.

With the EBU model reaction occurs along the stoichiometric contour, and begins as soon as fuel and air mix to form the stoichiometric mixture. Case F23 in Figure 7–3 shows this, and that the flame zone anchors at the end of the fuel tube. In this fuel–lean calculation, ____ , the stoichiometric contour intersects the symmetry axis. Figure 7–4 shows the isotherms for the F63 case ___. Again, the flame is anchored at the end of the fuel–tube, and the high temperature regions follow the jet shear layer developments. Neither the F23 nor the F63 cases exhibited, via the temperatures, the lifted and hour glass–shaped flames (anchored on the outer–edge of the annular air jet) respectively, that are evidenced in Figure 3–6.

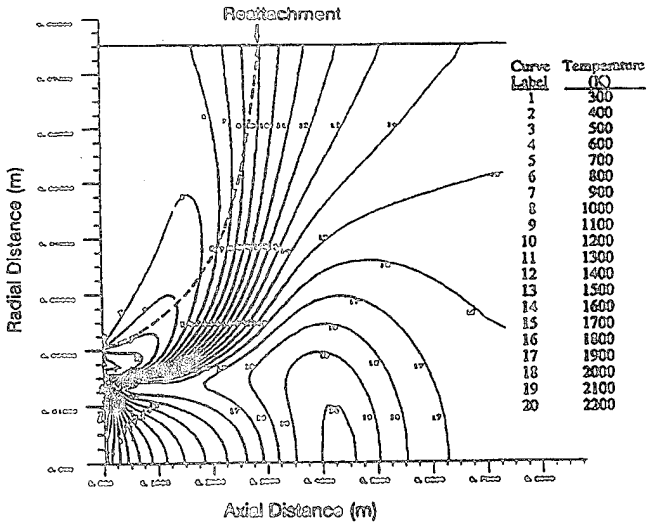

Figure 7–3. Calculated Temperature Field for Case F23 (Reacting, Ø = 0.59) Using the EBU Combustion Model

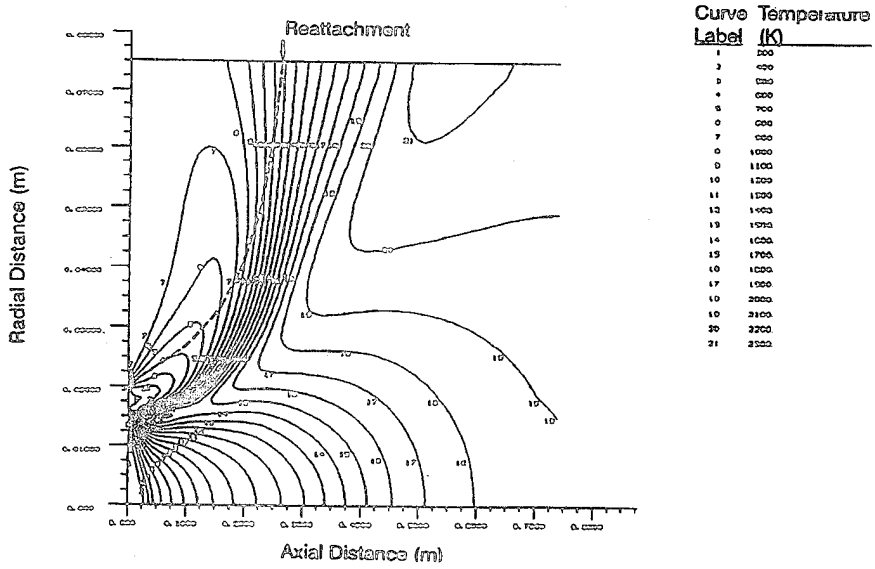

Figure 7–4. Calculated Temperature Field for Case F63 (Reacting, Ø = 1.62) Using the EBU Combustion Model

7.2.3 Reacting Flow with EDC Combustion Model (Case F23)

The calculated combustor characteristics for the 0.59 equivalence ratio case made with the fast–chemistry version of the EDC combustion model would be similar to those made with the EBU model (Section 7.2.2.) in that the high temperature zones would be closely aligned with the stoichiometric contour. However, when the extinction criteria of this version of the model are invoked, then chemical reactions are excluded in certain regions of the combustor flowfield, and this modifies the location of the flame.

Figure 7–5 shows the calculated exclusion regions as shaded areas. For this calculation the equivalence ratio limits were fixed (Section 6.6.9). Also shown on the figure is the stoichiometric contour, which runs to the combustor centerline, and, the zero mean axial velocity line (stagnation streamline) in the step–recirculation zone, which defines the reattachment position.

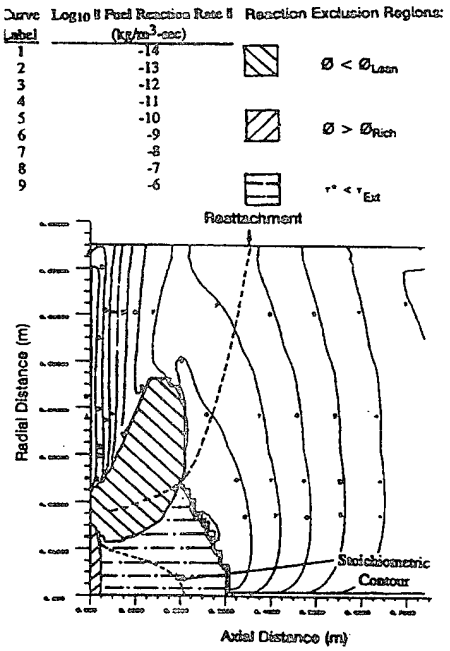

Figure 7–5. Case F23 Showing Calculated Regions of Reaction Exclusion and Reaction Rates Using the EDC Combustion Model

The region adjacent to the annular air jet is too fuel–lean for combustion. Similarly, the region adjacent to the fuel jet is outside the rich combustion limit. Finally, there is a region along the combustor centerline where the cell hydraulic residence times are less than the extinction time scale. (It should be noted that this region actually has overlaps into the other two regions, but the overlap extents are not shown in the figure.) It can be seen that the stoichiometric contour actually passes through the exclusion regions to reach the combustor centerline. Reaction of this mixture is not permitted until the fuel emerges downstream of the exclusion regions. A lifted–flame is therefore calculated. In those regions of the combustor were reaction is permitted, it takes place wholly fuel–lean. This observation suggests that when the reaction exclusion regions due to time–scales become large enough to extend over all regions where flammable mixtures prevail, then blowout occurs. This has been computationally verified.

Also shown on Figure 7–5 are contour lines representing logarithmic values of the absolute reaction rate for the fuel consumption; the contour intervals cover an order of magnitude change in the reaction rate. For the body of the flow, the higher reaction rates occur at the highest (but lean) equivalence ratios immediately downstream of the exclusion regions. Reaction along the step in the step–recirculation takes place, but the rates are very low due to there being very little unreacted fuel that is recirculated from the jet shear layers back to the step.

The consequence of the reaction–exclusion regions is immediately apparent in the calculated isotherms, which are displayed in Figure 7–6. If a limiting flame temperature of 1480°K (Section 6.7.8.) is used to define the beginning of the visible flame region, it can be seen that the lifted–flame on the combustor center–line is evident at 0.33 m downstream from the step–plane, and it is distributed radially across the combustor at about this height, which is closely associated with the calculated reattachment plane for the step recirculation, which itself is in good agreement with the measured position in the reacting flow at high combustor Reynolds Numbers (Section 3.5). The calculated distance is also in good agreement with the measured position of the maximum metal temperature factors (MTF) shown in Figure 3–12, and the direct flame observations reported in Section 3.5. In contrast, Figure 7–3 shows that the EBU model gives a temperature at the step reattachment plane of only 1100°K, and that the reattachment plane is about 0.27 m from the step. At the 0.59 equivalence ratio, CARS measurements (at higher Reynolds Number

values than Table 7–1) compare well to calculated temperatures close to the step wall, as Figure 7–7 shows [12.].

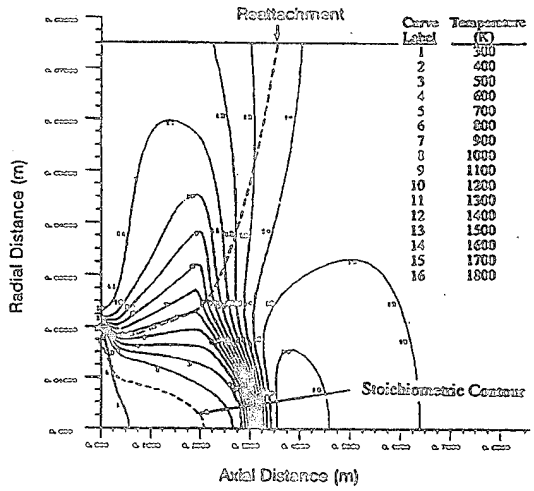

Figure 7–6. Calculated Temperature Field for Case F23 With the EDC Combustion Model

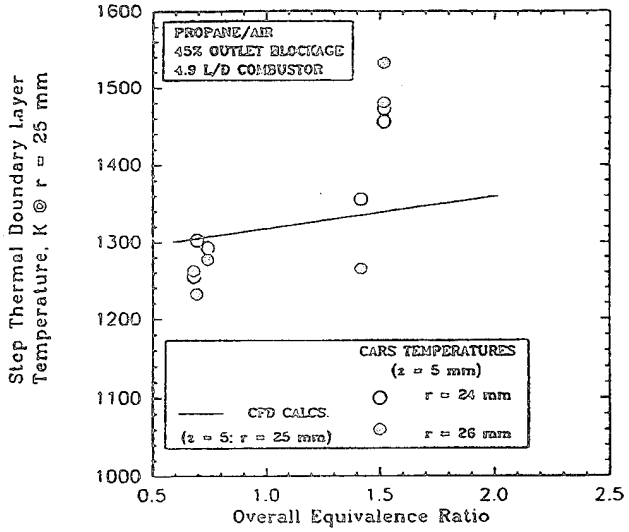

Figure 7–7. Comparison of the Variation with Equivalence Ratio of CARS Mean Temperatures and EDC Model Calculated Temperatures at a Coordinate Position (5, 25 mm) In the Step Region

Note in Figure 7–6, that the stagnation streamline of the step recirculation zone is entrained by the strong annular air jet. The resulting hourglass shape of the streamline, and the arrangement of the temperature contours that are congruent with it, are very reminiscent of the shape of the attached shear layer flame observed in Figure 3–6, although of course, at the equivalence ratio of these calculations an attached flame does not exist. The EBU model calculations do not display this characteristic. All in all, the EDC combustion model with fast chemistry and the characteristic time limitations, does a creditable job of calculating the lifted flame of the PW100 combustor at these conditions.

7.2.4 Case F41: Reacting Flow with EDC Model

Case F41, for which the equivalence ratio is 1.05, represents experimental conditions at which flame–lift occurs, as Figure 3–10 shows. It is therefore, a singularity, and is difficult to calculate. The calculated exclusion regions and reaction rate contours for this case are shown in Figure 7–8, and the isotherms are given in Figure 7–9.

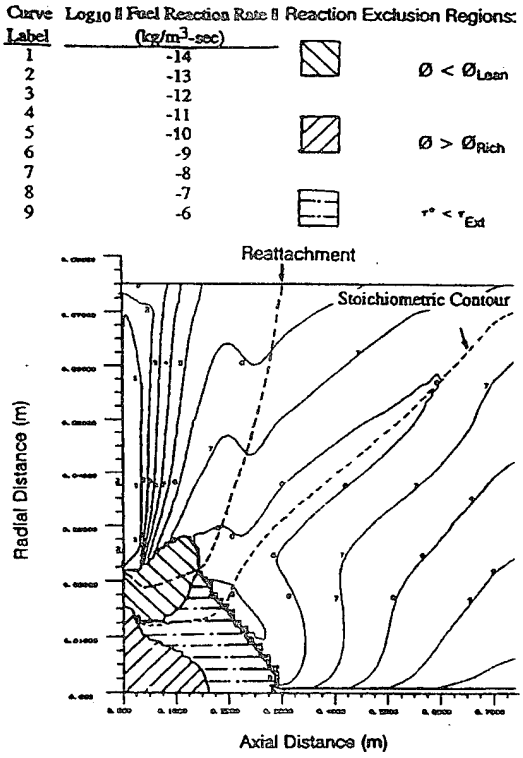

Figure 7–8. Calculated Regions of Exclusion for Case F41 using the EDC Model

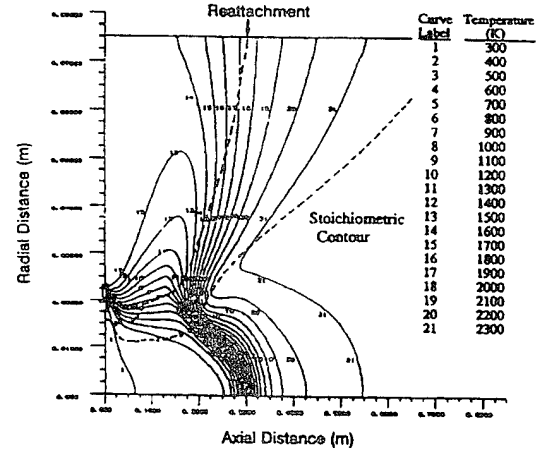

Figure 7–9. Calculated Temperature Field for Case F41 with the EDC Model

The path of the stagnation streamline in Figure 7–8 has the desired hourglass shape, but the exclusion regions indicate a lifted–flame. However, the overall size of the net exclusion region is reduced compared to that for 0.59 equivalence ratio in Figure 7–5. Being an overall fuel–rich case, the fuel–lean constrained region has significantly decreased in size, although the fuel–rich constrained region has naturally expanded; the residence time constrained region is about the same size as for the lower equivalence ratio. The stoichiometric contour now follows the general path of the jet shear layers towards the combustor wall, rather than closing on the combustion centerline as for the overall lean equivalence ratio case. The maximum reaction rate contour is aligned with the stoichiometric contour. Fuel reaction rates in the step recirculation zone are lower than for the lower equivalence ratio, and decrease to become vanishingly small as flow recirculates upstream back towards the step. This indicates that negligible unreacted fuel survives to reach the step.

From the isotherms shown in Figure 7–9, the flame can be seen to be still lifted at this equivalence ratio. "Visible flame" (using the 1480°K definition) on the combustor centerline is at 0.32 m from the step plane. This is almost the same position as shown in Figure 7–6. Compared to the lifted flame at 0.59 equivalence ratio however, the lifted flame at 1.05 equivalence ratio shows more radial distortion. It is 0.19 m downstream from the step at a radius of 0.0175 m. It does not reach the combustor wall, but loops around in the step recirculation zone to intersect the step at a radius of 0.023 m. The CARS measurements in Figure 7–7 at 0.7 and 1.5 equivalence ratios suggest that at 1.05 equivalence ratio mean temperatures between 1300 and 1400 might be expected at a radius of 25 mm and close to the combustor step. The temperature difference between calculated and possible measured values suggests that heat losses from the combustor might be important in the step recirculation zone. The step recirculation zone reattachment plane is at an axial distance of 0.30 m, and the temperature there is about 1950°K.

Although the EDC model has failed to calculate an attached flame at 1.05 equivalence ratio, it does calculate a temperature field which suggests that such a flame is about to be established via the step recirculation zone.

7.2.5 Case F63: Reacting Flow with EDC Model

Case F63, for which the equivalence ratio is 1.62, is well into the experimentally–observed attached–flame region of operation. Given the behavior calculated at 1.05 equivalence ratio, it would reasonable to expect that the EDC model would calculate the observed attached–flame.

Figure 7–10 shows the calculated chemical reaction rate characteristics. Since the overall richness of the case has been further increased, the fuel–rich exclusion region has expanded considerably compared to that in Figure 7–8, while the fuel–lean exclusion region has shrunken further; the residence time constrained region is about the same as previously. The stagnation streamline again has the hourglass shape, and the stoichiometric contour follows it closely to reach the combustor wall just downstream of the step recirculation zone reattachment plane, which is at 0.30 m downstream from the step. As in the 1.05 equivalence ratio case, the peak reaction rates follow the stoichiometric contour. Reaction rates in the recirculation zone are low and decrease to negligible values as the step is approached; again, this indicates little unreacted fuel being recirculated back to the step.

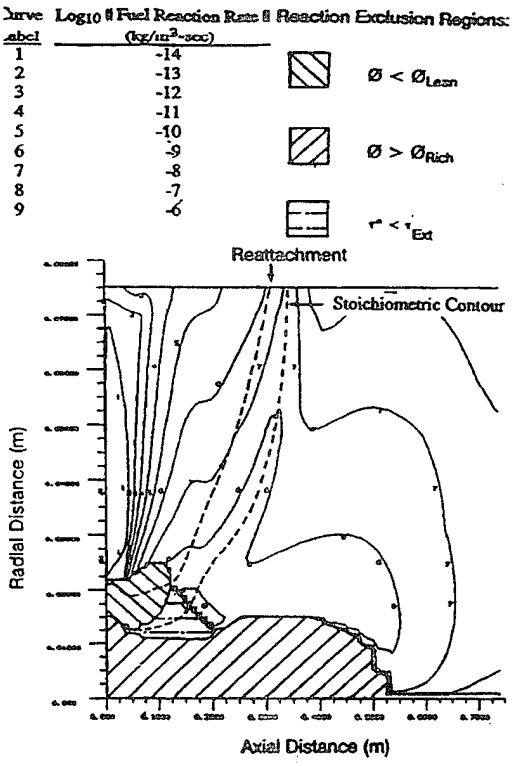

Figure 7–10. Calculated Regions of Exclusion and Reaction Rate field for Case F63 with the EDC Model

The very rich central core calculated precludes reaction on the combustor centerline until distances greater than 0.525 m downstream from the step, as Figure 7–10 shows. However, the spatial composites constructed from instantaneous LIF OH–images at an equivalence ratio of 1.56, indicate centerline reactions by a distance of 0.236 m, due to the radially–inwards growth of the inner–edges of the reacting jet shear layers, [12.].

It is apparent that the attached flame could never be demonstrated by the EDC model with the calculation being done as it was.

7.2.6 Case F80: Reacting Flow with EDC Model and Revised Calculation Procedure

The difficulties described above resulted in calculation of an additional case, F80, for which the bulk equivalence ratio was 2.05. This very fuel–rich case was selected in an attempt to increase the amount of fuel recirculated to the combustor step to see if this would result in an attached–flame.

The results for 1.62 equivalence ratio revealed some clear difficulties with the way that the calculations were made. An obvious one is that the rich and lean combustion–limiting equivalence ratios were held constant. From Section 6.6.9, these combustion limits represent equivalence ratio asymptotes between which the Kretschmer & Odgers ALP expression may be considered as valid. Although these asymptotes are not flammability limits, they can be treated as though they were and made dependent on the local values of temperature. When this is done, for the range of temperatures pertinent to these calculations, the lean limit would vary from 0.5 to 0.2, compared to the original fixed 0.4; the rich limit was maintained constant at 2.0, although if it were a flammability limit some broadening with increased temperature is known to occur.

It was mentioned in Section 7.2 that the 0.9 value for turbulent Schmidt Number was really appropriate to boundary layer flows. The extent of fuel/air mixing was therefore increased by decreasing the turbulent Schmidt Number to 0.5, the value found to be appropriate for recirculating flows. This value was considered to be more realistic for the PW100 combustor flowfield.

It was noted in Section 7.2.4 that heat losses from the combustor appear to be important. Therefore, the combustor boundary condition was changed from an adiabatic wall type to a specified wall temperature type, with the specified temperatures being based on the measured values, (Section 3.0). This change in boundary condition would introduce severe temperature gradients in the gas flow near to the combustor walls and step.

The existence of strong thermal boundary layers on the combustor surfaces introduced the possibility that wall–quenching of chemical reactions might be the source of additional unburned fuel that would be recirculated back to the step. Close to an impervious surface, the luminosity that is associated with visible flame is observed never to extend completely to the surface. The intervening dark region is known as a deadspace. Deadspace is caused by local quenching of chemical reactions due to heat losses through the wall and removal of active radicals by the wall, which acts as a "third body." Fuel entering the deadspace would not be reacted until convected away from the surface at some point.

A deadspace model was developed (Appendix L) and a simplified correlation of wall deadspace was incorporated into the 2D–PREACH code. The deadspace model was applied to the combustor walls and the step, and operated to quench reactions out from the surface to a value of "y^+" equal to 100, where

$$y^+ \equiv \frac{yv^*}{\nu}$$

and v^* is the friction velocity, $\sqrt{\tau_s / \bar{\rho}}$, y is the distance normal to the wall, and τ_s is the wall shear stress, $\mu \left.\frac{\partial \bar{u}}{\partial y}\right|_{y=0}$.

An additional combustion limiting condition was also introduced. This was a premixed burning velocity limit where the local flow velocity was compared to a local turbulent burning velocity; when the local flow velocity was greater than the local turbulent burning velocity, combustion was not allowed. The turbulent burning velocity was of the Damkohler type, i.e.,

$$S_T = S_L + u_e'$$

where u_e' was provided by the $K \pm \varepsilon$ turbulence model, and the laminar flame speed was based on the equations given in Section 6.

The results of the calculations for the F80 case are given in Figure 7–11 and Figure 7–12, showing the reaction–exclusion regions and isotherms respectively.

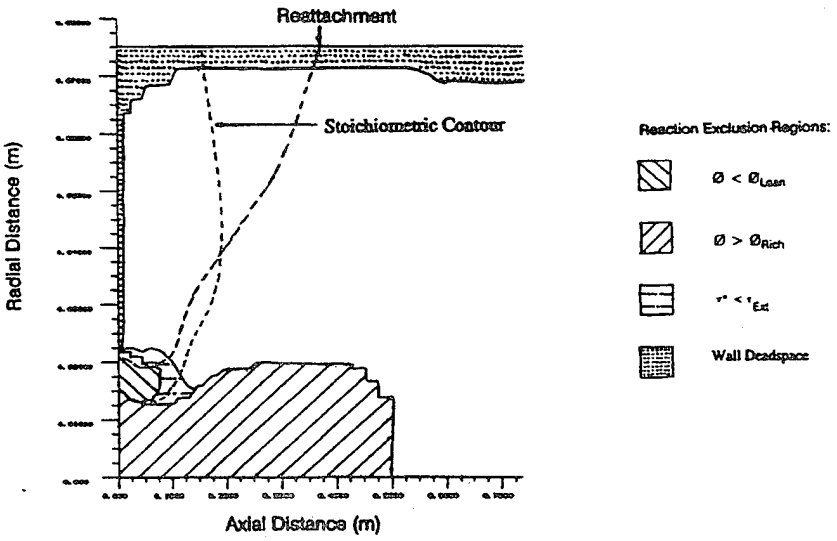

Figure 7–11. Calculated Regions of Reaction Exclusion for the Very Rich F80 Case with Deadspace Model and Specified Wall Temperatures

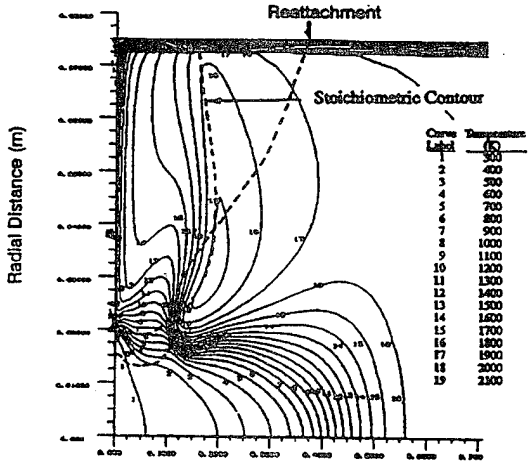

Figure 7–12. Calculated Isotherms for the F80 Case Showing Evidence of Wall and Step Thermal boundary Layers

Figure 7–11 shows that the stoichiometric contour now crosses into the step recirculation zone and reaches the combustor wall about halfway from the step to the reattachment plane. The stagnation streamline indicates that the "coke–bottle waist" is at about 40 mm from the step–plane. The combined combustion criteria now exclude chemical reactions from substantial portions of the combustor, with wall quenching (deadspace) being an obvious new addition. Any unreacted or partially reacted fuel from the jet shear layers that reaches the combustor wall region would be recirculated without further reaction back to the step and thence, to the entering jets. It can be seen that the combination of lean limit and residence time exclusions preclude the existence of an attached flame, even if the deadspace permits additional fuel to be recirculated.

The calculations show that although the level of fuel recirculated is increased, it is still outside the lean–limit. Since the region of exclusion due to time–scales encloses the lean–limit restrained region, it in fact, is the controlling factor limiting combustion in the step/jet interfacial region. The ratio of the

hydrodynamic to the chemical extinction time scales would need to be reduced by a factor of 2–3 to permit the lean combustion limit to become controlling in this region.

The large axial extent of the fuel–rich exclusion region is once again, clearly erroneous, and indicates that broadening of the rich–limit with temperature is in order.

The isotherms in Figure 7–12 reveal the strong thermal boundary layers that exist along the combustor walls and on the step. The recirculation zone is very hot with temperatures exceeding 1500K. However, consideration of Figure 7–7 reveals that the calculations considerably under–estimate the temperatures on the step near to the air jet entrance. The main flame is stabilized in the jet shear layers about 11 cm downstream from the step. It is rather thick with an axis that follows the stoichiometric contour across the step recirculation zone. When compared to the LIF OH images, e.g., Figure 3–8, there is good agreement in position with the concentrated islands of reaction seen in the expanding jet shear layers, that give the sudden thickening visually observed in the flame. Although there is more unreacted fuel on the step at the outer edge of the air jet as consequences of the thermal boundary layers and the deadspace, the mixture strength still is outside the lean flammability limits. Thus, there would be no evidence from the isotherms of an attached flame, such as is seen (Figure 3–6) by direct observation.

7.2.7 Summary of EDC Model Evaluation

The overall accuracy of the CFD calculation with respect to the basic flowfield will determine the absolute accuracy that can be achieved when the EDC combustion model is used. Figure 7–1 and Figure 7–2, for isothermal flow, establish this base–accuracy. The 2D–PREACH code has a predictive accuracy that is characteristic of its generation and the fluid dynamic modeling used in it, e.g., Reference 74. For present purposes, the basic code accuracy should be adequate.

It is obvious by comparing the calculations made with the EBU combustion model (Figure 7–3 and Figure 7–4) with any of the calculations made with the EDC model, that the EDC is the more realistic model of the two for combusting flows. If nothing else, the EDC model does represent an advance on the EBU model.

The EDC model does a creditable job of calculating the lifted flame (Case F23). It qualitatively calculates the "parabolic" flame shape, and its anchor position in the jets shear layers. Quantitative accuracy was limited by the underlying fluid dynamics modeling and the simplicity of the EDC model as implemented in the code. For the attached flame conditions it became readily apparent the the original adiabatic wall boundary conditions were inadequate, and that account of wall thermal boundary layers was necessary. However, even with such an account, the EDC model failed completely to generate an attached pilot flame such as was observed practically.

The inability of the EDC model to calculate the attached flame structure observed in the PW100 research combustor for equivalence ratios greater than unity may be ascribed to at least two contributing factors. The first concerns the influence of chemical kinetics. The modeling implemented in the CFD code involved a fast–chemistry model in conjunction with extinction criteria, some of which appear to be too severe. As an effort was made in the calculations to bring more and more fuel into the recirculation zone by raising the overall equivalence ratio, the stoichiometric contour moved in response, and the model produced correspondingly higher temperatures within the step recirculation zone. The step detachment region of the recirculation must always be fuel–lean, since to be otherwise would cause the stoichiometric contour to circulate back on itself, which is impossible. The high temperatures and flame–sheet type calculation associated with a fast chemistry model essentially preclude any significant amounts of unreacted fuel surviving the jets shear layers and being recirculated back to the step. This is so regardless of the deadspace being accounted for. The jets shear layers consume almost all of the fuel. If it is presumed that in reality it is not pure fuel that is feeding the attached pilot flame on the step but lower hydrocarbons, hydrocarbon fragments and CO left over from the shear layers, then a realistic (i.e., with account of turbulence interaction effects) multi–step kinetic mechanism is required to perform the calculation.

The second factor is concerned with the likelihood that the mean flow field may not be stationary at all, and so, nonstationary flow behavior may dominate the mass transport within the combustor. Immediate evidence of this was recorded in the LIF OH−images, where local, intense "eruptions" of OH (denoting regions of chemical reaction and clearly not subject to secondary convection effects) across the jets shear layers directly into the step recirculation zone can be see, e.g., Figure 3−8. The intermittent nature of the jet shear layers region was also detected by the TFP measurements and the spontaneous OH−imaging [12.]. It has been postulated [11.] that entrainment into the step recirculation is by an intermittent process involving discrete "packets" of "unreacted" fuel. The intermittent nature of the entrainment accounts for the intermittent existence of the attached pilot flame seen in the spontaneous OH−imaging. This entrainment process could occur through the holes in the braid regions of the vortices in the shear layers, where stretching leads to local quenching of the flame. The fuel packets must then be transported around the recirculation in a relatively intact manner until the pilot flame attachment point is reached. The experimental evidence lends creditability to this hypothesis.

7.3 Evaluation of Hybrid CFD/Stirred Reactor Modeling in PW200 Combustor

The PW200 combustor was the ideal vehicle for an evaluation of the hybrid modeling concept because of the large amount and wide variety of LBO data gathered in this generic combustor (Section 5.5), and because of the CFD conducted on it (Section 6.7.4.).

The reactor network of Figure 6−42 was used. This network was established from a CFD calculation (Section 6.7.4.) made for boundary conditions representing a typical LBO point. The presumption is made that this basic flowfield does not change substantially with variations (in the LBO range) of combustor operating conditions, or, with minor changes in the flow splits within the combustor. These are considered to be reasonable assumptions.

The reaction mechanism used was that given in Section 6.7.6., and heat losses were accounted for as previously. The blowout definition and protocol were also as described in Section 6.7.8.

7.3.1 Effects of Primary Zone Airflow

For fixed dome flow equal to 15 percent of the total combustor airflow (see Figure 5−2), it had been observed [30.] that the effect of increased primary zone airflow at atmospheric pressure on LBO equivalence ratio produced a change in flame condition between lifted and attached flames at blowout. As before, primary zone airflow was defined as,

$$W_{PZ} = W_{dome} + 0.279 W_{1st.\,jets}$$

and the increase in W_{PZ} was obtained while increasing the total airflow to the combustor. An important test of the hybrid modeling would be represented by its ability to calculate this behavior.

Figure 7−13 compares the experimental blowout points with the calculated points. The agreement between measurements and calculations is excellent up to a primary zone airflow of about 0.135 lbm/sec. (0.0613 kg.sec.). For primary zone airflows above this value the experimental flame blows out in an attached condition (for photographs of the two flame conditions see Figure 16 of Reference 30, presented as Appendix J), and the measured LBO's show a break in equivalence ratio, with a slight improvement in stability. The calculations reproduce this break in the LBO characteristic, and do so at the correct primary zone airflow.

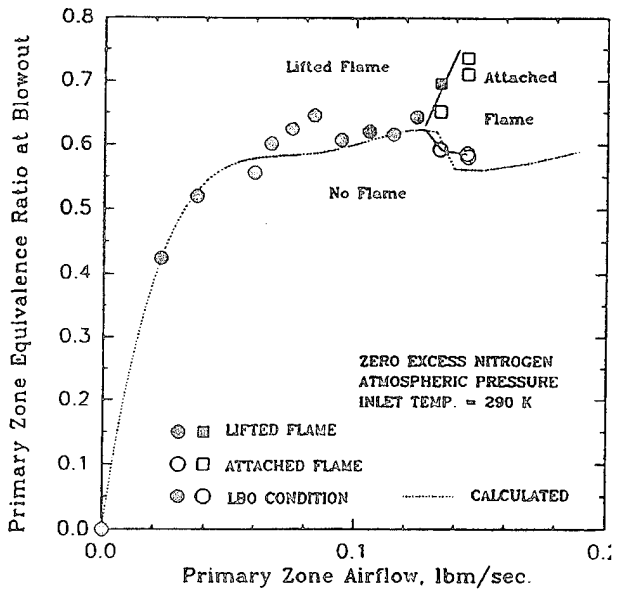

Figure 7–13. Effect of Primary Zone Airflow on Stability for 15% Dome Flow: Comparison of Calculations with Experimental Data

Consideration of the reactor network behavior along the blowout characteristic reveals the following: Blowout is always determined by Reactor No. 3, which represents the condition immediately prior to introduction of the first row combustion air jets. As the primary zone airflow is increased, the outlet temperature of the Recirculation Reactor rises steadily and it eventually exceeds the ignition temperature limit (2,200F, 1480K – see protocol, Section 6.7.8.) at a value around 0.10 lbm/sec. (0.0454 kg/sec.), momentarily taking control of the LBO limit. With further increases in airflow, the Recirculation Reactor temperature falls slightly, and LBO control is returned to Reactor No. 3. At still higher primary zone airflows above 0.17 lbm/sec. (0.077 kg/sec.), the outlet temperature of the Recirculation Reactor begins to increase again, but for the range of the plot does not regain ignition temperature. It is the action of the recirculated flow that serves to boot–strap Reactor No. 3, to give the small improvement in stability observed and calculated.

The Recirculation Reactor, rather obviously, influences the temperatures of Reactors No. 1 and 2, but does not raise them to the arbitrary ignition limit. However, at higher airflows it does increase their temperatures to values where luminosity could be apparent. This could contribute to the observed "attached flame" appearance; however, the network is not sophisticated enough to reproduce true attached flame behavior since this would almost certainly require dynamic changes in reactor size and airflow distribution.

Reactor No. 3 is a critical reactor in the network. Physically, it represents the closely–coupled jet interaction region immediately ahead of the first row of combustion air jets. Observations of the actual flame clearly support the importance of this region in holding flame in the PW200 combustor.

7.3.2 Influence of Operating Pressure

The effects of pressure on LBO were simulated experimentally by means of the separately–calibrated excess nitrogen diluent technique [10.], whereby an equivalent pressure is obtained, (Appendix E). This technique exerts the correct effects on chemical reaction rates, but residence time becomes uncoupled from pressure. The residence time change effect would have to be accounted for through a dynamic change in reactor size in the network, which is not convenient, and is therefore ignored in the network.

Correction is therefore made to the experimental data to account for bulk residence times. A second important test of the hybrid modeling is its ability to calculate the effects of pressure on LBO.

For the 15 percent dome flow case and a number of fixed primary zone airflows, a comparison between calculated and measured LBO's is made in Figure 7−14. Since the presence of the excess nitrogen reduces the combustor residence time, the experimental equivalence ratios at LBO were corrected to a zero excess nitrogen residence time (see Reference 30). For the calculations, true pressures were used, i.e., it was assumed in the comparisons that the excess nitrogen calibration procedure and the residence time corrections were both perfect, and that equivalent pressure was exactly equal to the true pressure used in the calculations.

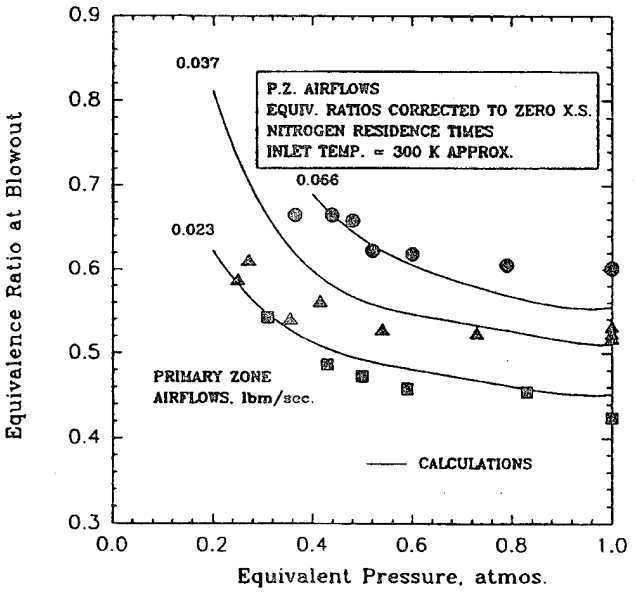

Figure 7−14. Effect of Pressure on Stability for 15% Dome Flow at Several Primary Zone Airflows: Comparison of Calculations with Experimental Data

The agreement of the calculations with the measurements is good for the 0.023 lbm/sec. (0.0104 kg.sec.) primary zone airflow from 1.0 down to about 0.2 atmospheres pressure. The absolute agreements are not so good for the 0.037 and 0.066 lbm/sec. (0.0168 and 0.0299 kg/sec.) airflows; however, the trends with pressure are correct, and the effects of airflow level at low pressures (i.e., the equivalent of Figure 7−13 at say, 0.4 atmospheres), are correct. Generally, given the somewhat imprecise nature of LBO measurements, the agreements can be considered satisfactory overall.

7.3.3 Effects of Dome Airflow

An important combustor design variable is the percent of total combustor airflow that is introduced through the dome. This became particularly significant with the general introduction of airblast atomization of liquid fuels and the need to design for low emissions of pollutants, since both can have important effects on combustor stability due to the trade−offs that exist between emissions and stability, and the general increases in dome airflow that follow.

With separately−controlled and metered airflows in the generic combustor (see Figure 5−3), variation of the dome flow was an easy design variable to investigate. It was shown experimentally [30.] that the percent dome flow exerts a strong influence on stability, with more dome flow reducing stability at all combustor loadings, and it is clearly limiting to the peak heat release rate obtained in a combustor. The combustor loading parameter was defined from well−stirred reactor theory in Section 6.2 by Equation 6.1, where the volume in this instance was taken as the overall value for the complete combustor.

When applied to a complete combustor, this overall definition suffers from the weakness that it treats the flame stability region as though it were a single well–stirred reactor, i.e., as Bragg originally conceived it, [18.]. This weakness was shown in Reference 30, where the LBO data for primary zone flame–holding at 10 percent dome flow in the generic combustor fell into two distinct groups according to flame type. The explanation given was that a given value of loading parameter could be obtained via different combinations of the operating conditions, and so the LBO points could be segregated into either attached or lifted flame types. Based on the experimental measurements of temperature [32.] it would be expected that the segregation into attached or lifted flames would depend on whether the combustor loading was achieved by increased airflow or by reduced equivalent pressure. Another example of failure of the single–reactor representation would be when the flame is stabilized in different parts of the combustor as operating conditions change. This was also observed in Reference 30 for the 10 percent dome flow case where as pressure was reduced the flame expanded beyond the primary zone region.

Use of the present reactor network, Figure 6–42, to represent the generic combustor clearly moves beyond the simple suppositions inherent in the single reactor description of the complete combustor. Since the network also provides a better representation of the critical combustor flows, (via the CFD derivation), the experimental data (deriving from the real airflows) would also be expected to violate the single reactor model. Therefore, breakdown of the loading parameter correlation group might be expected as more complicated (e.g., PW200 combustor versus PW100 combustor) flows arise in geometrically more complex combustors. This was addressed somewhat in Reference 30 by working in terms of "burning zones."

To test the limited applicability and eventual failure of the single reactor correlation group, the stability of the network was calculated with a 10 percent dome flow for the following range of variables: Overall airflow – 0.100 to 0.700 lbm/sec., (0.0454 – 0.3176 kg/sec.); combustion pressure – 1.2 to 0.3 atmos., and, inlet air temperature 87 to 200F (304 to 367K). The resulting range of overall loading parameter defined by Equation 6.1 with appropriate units, was 0.4555 to 4.9643, and the calculated overall equivalence ratios at blowout were 0.05721 and 0.11554 respectively.

These calculations showed that for a range of overall loading parameters representing primary zone flame holding (i.e., flame was always contained within the conventional definition of "primary zone."), LBO in the reactor network was always determined by Reactor No. 3. The combustion efficiency of this individual reactor decreased as overall combustor equivalence ratio at blowout increased with increased overall loading. This behavior is illustrated in Figure 7–15, and suggests that eventually, control of LBO would pass from Reactor No. 3. As a consequence of the characteristic given in Figure 7–15, the outlet temperature of the Recirculation Reactor increased with increased overall loading, which caused the outlet temperature of Reactor No. 1 to also increase, as Figure 7–16 demonstrates. The net effect of the boot–strap temperature increase, together with the increased loading due to increased mass flow rate and reduced pressure, was that the residence time in Reactor No. 3 was decreased. Calculated overall equivalence ratio at blowout therefore correlated with residence time in Reactor No. 3, as is shown in Figure 7–17. Consequently, the relationship between overall loading and residence time in Reactor No. 3 could be expected to be discontinuous over wide ranges. This discontinuous behavior causes the blowout equivalence ratio correlation based on overall loading parameter to breakdown as Reactor No. 3 approaches its peak heat release rate condition, (illustrated in Figure 7–18), if the ranges of operating variables are too large.

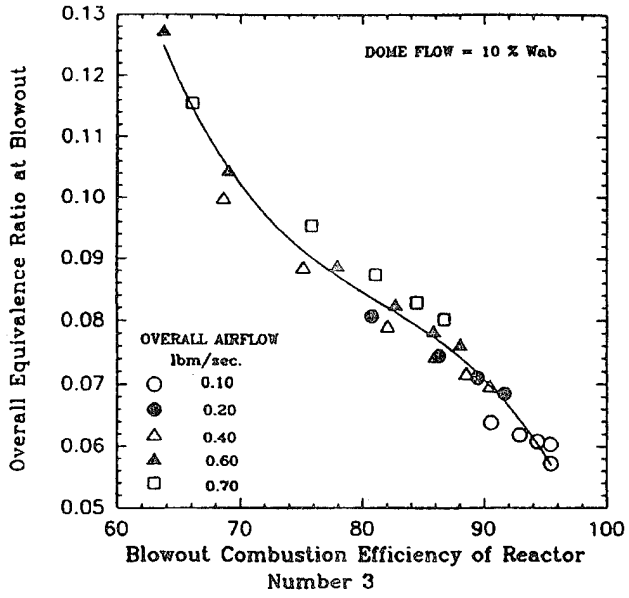

Figure 7–15. Calculated Relationship Between Overall Blowout Equivalence Ratio and combustion Efficiency for Network Controlling Reactor (No. 3) for 10% Dome Flow at Several Airflows and Pressures

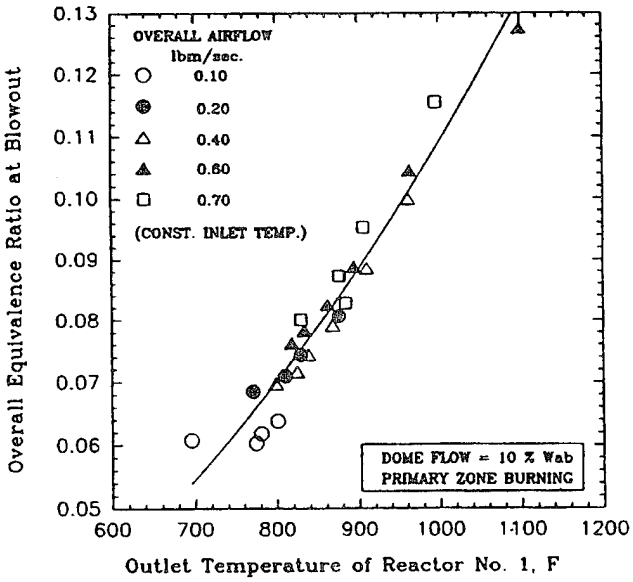

Figure 7–16. Calculated Relationship Between Overall Blowout Equivalence Ratio and Outlet Temperature of No. 1 Reactor in Network for 10% Dome Flow at Several Airflows and Pressures

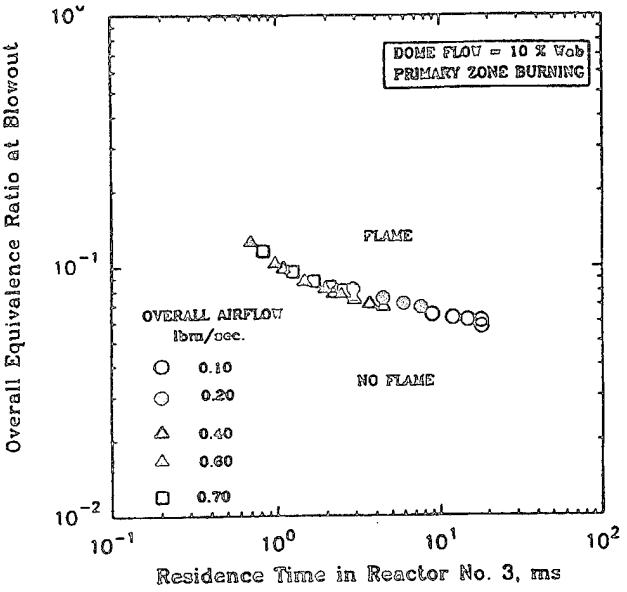

Figure 7–17. Calculated relationship Between Overall Blowout Equivalence Ratio and Residence tie In Network Controlling Reactor (No. 3) for 10% Dome Flow at Several Airflows and Pressures

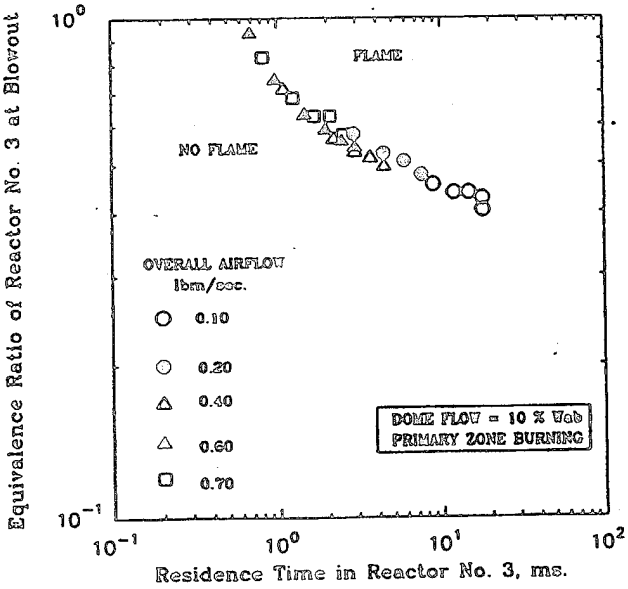

Figure 7–18. Stability Characteristic of Network Controlling Reactor (No. 3) for 10% Dome Flow

Figure 7–19 is a comparison in terms of overall equivalence ratio at blowout against overall loading parameter, of measurements and calculations for the 10% dome flow case. When the LBO is governed by a single region within the total reacting flowfield that is made up of many such regions, the difficulty of adequately defining the pressure dependency through an appropriate equivalence ratio was addressed by making the apparent reaction order 'n' a function of primary zone equivalence ratio, where "primary zone" is defined in Section 5.5, and for,

$$(\phi_{PZ})_{LBO} < 1.0, \qquad n = 2(\phi_{PZ})_{LBO}$$

and,

$$(\phi_{PZ})_{LBO} \geq 1.0, \qquad n = 2.0$$

i.e., in the limit, the reaction becomes a second order one.

In Figure 7–19 it will be noted that the experimental data fall into two distinct groupings, one placed to the left and center of the plot, and the other placed to the right of the plot. Those data points falling in the right–hand grouping represent tests for which the calculated primary zone equivalence ratio was actually greater than unity, but for which the apparent reaction order was taken as 2.0. Data in this grouping was for tests having burning that extended beyond the conventional primary zone. It will be noted that the correlation of the data in the left–hand group, which was for pure primary zone burning cases, are better correlated than the data falling in the right–hand, nonprimary zone burning, grouping.

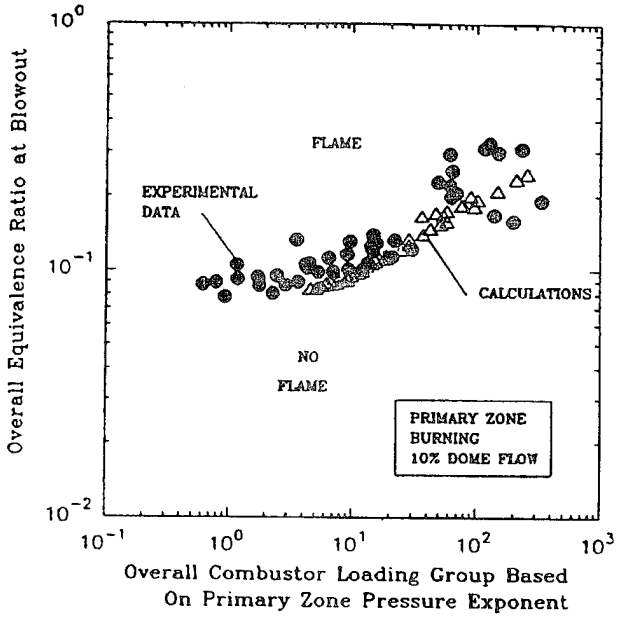

Figure 7–19. Comparison of Calculated and Measured Stability for Primary Zone Burning with a 10% Dome Flow Combustor

The calculated blowouts also exhibit less–than–perfect correlation for loadings greater than about 30.0 (with appropriate units). As reported previously in Section 6.7.8., the reactor network behaves somewhat like a real combustor in that the blowout fuel flow is achieved in a series of decreasing but discrete steps of finite size. For loadings less than about 30.0, the calculated blowouts were controlled by Reactor No. 3; for higher values of loading, control was passed first to the Recirculation Reactor, and subsequently to Reactor No.4. Where control is passing from one reactor to another, the solution procedure slows down and becomes very sensitive to rates of change. It is easy under these circumstances to provoke premature blowout as the real blowout point is approached. This introduces inevitable scatter in the calculated values.

Given the *caveats* on the experimental data, the calculations, the overall loading parameter definition, and the wide variation in loading, (3 – 4 orders of magnitude), the agreement of the calculations with the experimental data can be considered to be remarkably good.

Figure 7–20 repeats the calculation portion of Figure 7–19, but delineates by symbol between reactor control in the reactor network. Points are shown for control (last blowout in stated reactor) by Reactor No. 3 and for control by the Recirculation Reactor.

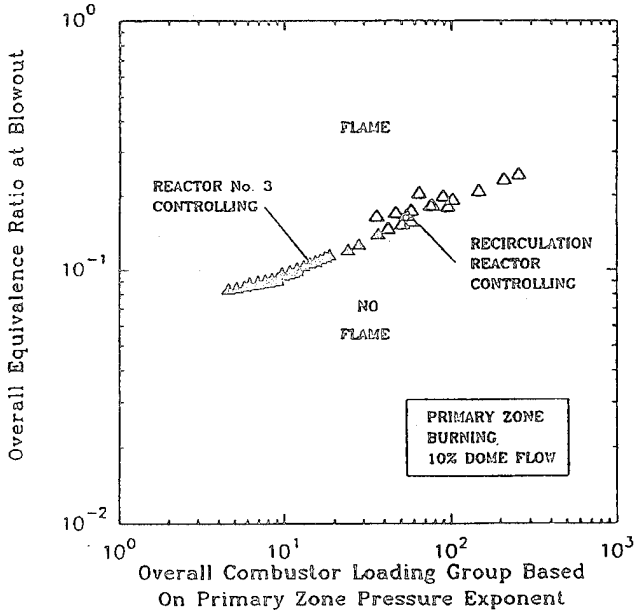

Figure 7–20. Calculation of Stability for Primary Zone Burning with a 10% Dome Flow Combustor, Showing Change of Flame Holding

The modified overall combustor loading group can be seen to successfully correlate the calculated blowouts over a wide range of airflows and pressures, and a more limited range of inlet air temperatures. It provides a clear segregation of where flame holding occurs within the combustor. For overall combustor loadings less than 34.0 (appropriate units), flame holding was provided through Reactor No. 3, which represents the region just immediately ahead of the first row of combustion air jets. This can be related to the small recirculation region on the injector centerlines, visible in Figure 6–35 and Figure 6–36, and provided by the CFD calculations. For overall combustor loading greater than 34.0, flame holding was provided through the Recirculation Reactor, which represents the regions in the combustor dome around the discharges from the fuel injectors. These recirculation regions can be seen in Figure 6–35 and Figure 6–36, to dominate the calculated flowfield in the primary zone, (between the dome and the first row of combustion air jets).

Figure 7–21 shows the calculated stability for the PW200 combustor with 20 percent of the total combustor air introduced through the dome. The overall equivalence ratio at LBO is plotted against the overall combustor loading group with the apparent reaction order (pressure dependency exponent) based on the primary zone equivalence ratio, as before. The solid symbols are for Reactor No. 3 controlling the blowout, and the open symbols are for the Recirculation Reactor controlling the blowout. The calculations cover combustor airflows from 0.100 to 1.300 lbm/sec. (0.0454 to 0.590 kg/sec.) and pressures from 1.2 to 0.3 atmospheres. The resulting combustor loading is varied over three orders of magnitude. The correlation of the calculated blowout points by the overall loading parameter is somewhat improved over that achieved for the 10 percent dome flow combustor.

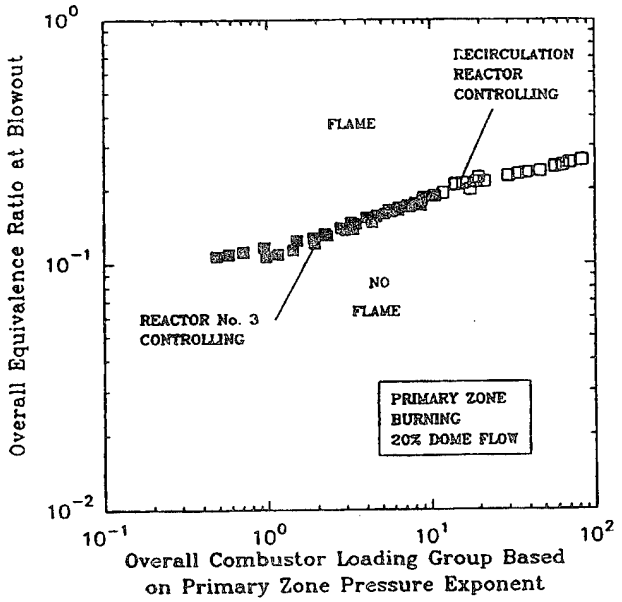

Figure 7–21. Calculated Stability for Primary Zone Burning with a 20% Dome Flow Combustor, Showing Change of Flame Holding

The two PW200 combustor calculated stability curves for 10 and 20 percent dome airflows are compared in Figure 7–22. The doubling of dome airflow has a large and adverse influence on combustor lean stability by increasing the blowout equivalence ratios at all combustor loadings covered by the plots. For both dome flows, control of stability at lower combustor loadings resides with Reactor No. 3 in the network, Figure 6–42. At higher loadings Reactor No. 3 blows out and control is passed to the Recirculation Reactor in both cases. For the 10 percent dome flow combustor this condition takes place at an overall loading of 34 (appropriate units); for the 20 percent dome flow combustor the transfer condition takes place at an overall loading of 10 (appropriate units). Therefore, the 20 percent dome flow combustor not only blows out at consistently higher overall equivalence ratios compared to the 10 percent dome flow combustor, its network stability starts to break down at about one–third of the loading at which breakdown begins for the 10 percent dome flow combustor.

Although not presently shown, the calculated stability curve, and the measured stability points, for the PW200 combustor with a 15 percent dome flow fall between the 10 and 20 percent curves shown in Figure 7–22.

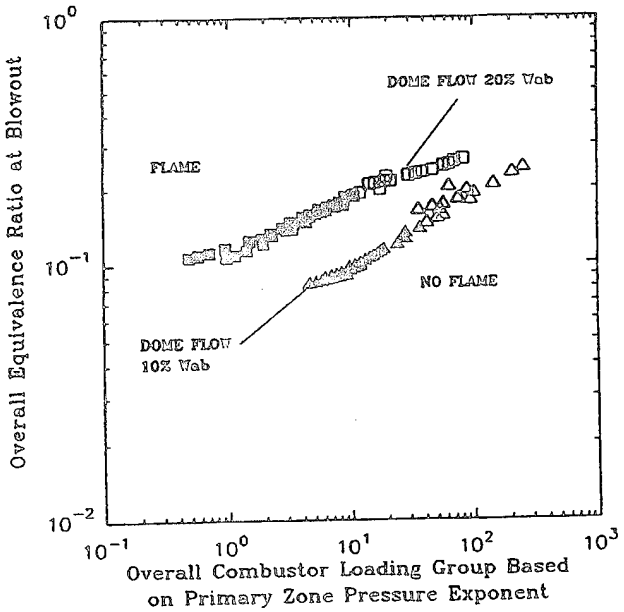

Figure 7–22. Comparison of Calculated Stabilities for Primary Zone Burning with 10% and 20% Dome Flows

A comparison is made in Figure 7–23, of the calculated lean stability for the 20 percent dome flow combustor against the measured data at this condition.

The amount of experimental data for the 20 percent dome flow case is not as extensive as for the 10 percent and 15 percent cases. As for the 10 percent dome flow combustor in Figure 7–19, the experimental data fall into two groups: lower overall loadings where the primary zone equivalence ratio is less than unity, that is well–correlated (left–hand side of plot), and, higher overall loadings where the primary zone equivalence ratio is greater than unity, that exhibits increased scatter (right–hand side of plot). Overall, the calculated stability for this combustor agrees very well with the measured stability.

Figure 7–23. Comparison of Calculated and measured Stabilities for Primary Zone Burning with a 20% Dome Flow Combustor

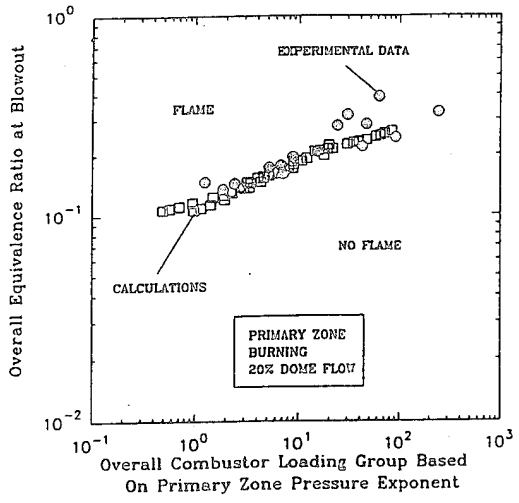

7.3.4 Summary of Hybrid CFD/Stirred Reactor Model Evaluation

The Hybrid CFD/Stirred Reactor Model evaluation was conducted over a wide range of operating conditions in three variations (dome flows) of a generic, simplified gas turbine combustor (PW200 combustor). Although, consistent with the original program decisions (Section 2.0), only a gaseous fuel (propane) was used, the evaluation was still a rather stringent one. Overall, the approach proved to be very successful.

The protocols established to operate the reactor network code and to define a blowout, proved to be successful. The code was easily run in interactive fashion on a 486–based P.C. In finding a solution, the code was found to have progress characteristics that in many ways were similar to those of a real combustor approaching a lean blowout. Handling of the code therefore benefits from experience in operating combustors! Debiting the lower heating value of the fuel to account for combustor heat losses appeared to be a reasonable strategy. Use of the reduced mechanism for JP–5 fuel with propane properties appeared to be acceptable, as was suggested by Section 6.5.

The code successfully calculated the effects of airflow, pressure and airflow distribution on the PW200 combustor stability. Any difficulties encountered appeared to be largely associated with the presentation of the collected data, (both experimental as well as calculated), in correlated form over wide ranges of operating conditions. As a correlating group the loading parameter was not as successful as it was for the simple PW100 and PW150 combustors. This is because it is based on treatment of a complex real combustor as a single stirred reactor, which it clearly is not.

THIS PAGE INTENTIONALLY LEFT BLANK

SECTION 8.0
DISCUSSION

Flame extinction is a singularity. A phenomenological understanding and quantitative description leading to a predictive capability of lean blowout in a real gas turbine combustor therefore represents an extremely complex problem. The initial program decisions (Section 2.0) to break the study down into a series of smaller steps were necessary ones, although they did imply that not all aspects of the complete problem could be addressed with the time, people and fiscal resources available. Valuable progress has been achieved as part of this effort, but much still remains to be uncovered in future work.

The three combustors, PW100, PW150 and PW200 of sequentially increasing geometric complexity, that evolved to address separate aspects of the present study, proved to be extremely useful in building progressive understanding, developing and interpreting various experimental diagnostic techniques, and in testing modeling concepts. It transpired that even "simple" combustors have complex behavior, and that the simplicity is only in the boundary conditions and bounding geometries. This being so, it was found that application of many different diagnostics to a given combustor was essential to develop a comprehensive and necessary understanding of the flow behaviors and combustion characteristics. Each diagnostic had its own story to tell; together, they enhanced one–another! It was especially disconcerting to recognize the extent that nonstationary behavior of the mean flow field plays in "turbulent" mass transport and lean blowout, regardless of the combustor concerned. There are implications of importance here for the mathematical modeling of such flows.

The many similarities in the observed gross behavior of the PW100, PW150 and PW200 combustors were remarkable, and suggested that the PW100 successfully incorporated within its design, the essential features of flame stabilization inherent in the PW200 simplified, generic gas turbine combustor. Specific design details in the more complex combustors were certainly important, but only modified the inherent gross behavior. It was interesting to note that the detailed behavior in the PW100 combustor, the simplest of the three but still representative, contained many features and behaviors that are observed in other, more fundamental, studies of flame holding, flame lift, and blowout. Regardless of the combustor, the basic aerodynamic behavior is associated with shear layer development. The shear layers may be axisymmetric and/or curved, and they may interact with one–another, but they are shear layers nonetheless. It is the detailed, time–resolved, behavior of these shear layers, e.g., the vortical structures in the layer and their manipulation of the local bounding flows, that appears to predominate and control the combustion behavior for diffusion flames. (Since shear layers are inherently unstable, this might account for the general nonstationary behavior observed.) In this respect, the PW100 combustor contains within it the gross flow behavior representative of gas turbine combustors, and the details associated with the fundamentals of flame stability.

The technique of dilution with excess nitrogen to simulate low pressures was successful in all three combustors, and the calibration that was derived from information contained in the literature for propane/excess nitrogen/air systems appears to be valid. The technique does suffer from eventual saturation effects at very high values of nitrogen to fuel mass flow ratios. It also results in decoupling of combustor (cold) residence time from (cold density. This must be allowed for in making comparisons of experimental results obtained using the technique, with other experimental results and calculations made using true pressure variations.

The attention given to providing good optical access in all three combustors was well worth the extra efforts and other compromises it involved. The benefits of the optical access were accrued not only in the ability to apply various laser diagnostic techniques, but also in the direct observation of flame behavior as operating conditions were varied. The "mental models" so–acquired proved to be most valuable in interpreting the LBO characteristics, and in applying aspects of the modeling. The value of the "mental conditioning" was enhanced through the use of super–positioning these mental models from the simpler

PW100 and PW150 combustors, to interpret the impression of the flame structures and behaviors in the more complex PW200 combustor. This was especially so with respect to the expansion of the flame through various burning zones in the PW200 combustor as the effective pressure was reduced and primary zone fuel loading consequently increased.

The PW200 combustor was designed to be a flexible vehicle, and it proved to be so in practice, despite some ergonomic short–comings in its mechanical design. Separating the fuel injectors from the PW200 combustor to stand alone in the PW150 combustor was a wise move, and enabled the relationships between the PW100 and PW200 combustors to be better understood, especially the close–coupling that exists between the injector flows and the first row of combustion air jets. Particularly noteworthy in the PW150 study was how the details of the individual stoichiometries associated with the fuel injector components controlled the flame behavior.

It was observed in the PW100 combustor and for the LS injector in the PW150 combustor, that as lean blowout was approached, flame lift occurred; flame lift also took place under some conditions for the HS injector in the PW150 combustor. This condition was also apparent in the PW200 combustor with LS injectors. Therefore, even though the fuel and oxidant might be introduced separately to give a nominal diffusion flame, flame lift would allow some degree of partial premixing of reactants to take place prior to combustion. This observation is consistent with some arguments made for the stability of classical jet flames, where air entrainment through the darkspace at the burner lip takes place. The observation was the basis for a key postulate for the modeling approaches pursued in this program, i.e., that turbulent diffusion flames near blowout always involve a degree of flame lift with some significant amount of premixing of reactants at some appropriate length scale, as a result.

The modeling effort fell into four parts concerned with 1.) correlation, for experimental data, 2.) phenomenological, for quick status assessments, 3.) mathematical, for *a priori* calculation of detailed flame characteristics, and, 4.) hybrid, as a design analysis tool. In each part, the detailed approach was founded in the key postulate, and relied on partial premixing concepts. In Parts 1, 3 and 4, partial premixing was utilized in the form of well–stirred reactor theory. None of the modeling explicitly addressed the other key observation concerning the presence of flow oscillations.

The experimental data correlation used well–stirred reactor theory directly, by treating the combustor as a single reactor that could be sized by established and methodical procedures (e.g., the dissipation gradient method). The resulting loading parameter approach was very successful for simple combustors that had a single and well–defined reaction zone, and which only operated over a relatively limited range of inlet conditions, e.g., the PW100 combustor. It failed for the more complex PW200 combustor because this vehicle had more than a single potential reaction zone, and used them in sequence as the operating conditions demanded. A satisfactory general procedure for correlating data from such complex combustors over very wide ranges of operating conditions was not produced during the present study.

A phenomenological model for quick assessment of stability was formulated by a characteristic time method, whereby a mixing time scale is compared to a chemical reaction time scale for a critical value determining flame extinction. Pertinent empirical data were incorporated into these times, and constants were established by means of a limit analysis. The ratio of these times was also related to a critical Karlovitz Number (flame stretch criterion) for flame extinction in the case of weak turbulence.

The drawback of this phenomenological stability parameter was that it involved local turbulence characteristics and flame speed, and therefore needed to be applied on a point–by–point basis throughout a calculated flowfield. It is hence best suited to incorporation into a CFD code. This removes it from the category of a "quick assessment" procedure! Beyond a brief but successful look at the PW100 combustor, (where it was applied during postprocessing of a cold–flow CFD calculation), exploration of the general utility of this stability parameter was not made as part of this program.

The mathematical modeling approach selected for investigation was the Eddy Dissipation Concept combustion model of Magnussen. The EDC combustion model concentrates on the physics of the

fine–scale turbulence where most of the dissipation of turbulence kinetic energy into heat takes place and where molecular mixing is accomplished. It makes the assumption that reactants are homogenously mixed within the fine–scale eddy structures, and therefore treats them as being well–stirred reactors. Since the scale of the fine eddy structures are normally well–below what could be resolved by any reasonable CFD computational grid, the EDC model is a subgrid scale combustion model.

The EDC model involves two parts, 1.) establishing from fluid dynamics the subgrid scale reactors and the surrounding fluid feed–stream conditions, and, 2.) establishing the chemical reaction rates within the subgrid scale reactors. The fluid dynamic portion can be reduced to the form of a series of residence time scales which may be compared with chemical kinetic time scales (from the second part) to establish flame extinction criteria. The turbulence model incorporated in the CFD code supplies the necessary information from which the fluid dynamic time scales may be calculated.

Incorporation of a chemical reaction kinetics mechanism into a CFD code involves a number of difficulties that should be addressed. A major one is that a transport equation must be solved for each individual chemical species involved in the mechanism. The additional computational burden so–arising may be manageable for very simple reacting flowfields, but it rapidly becomes unacceptable as flowfield complexity increases. Therefore, there is always a desire to find the simplest possible reaction mechanism that is appropriate. Another difficulty is that the rate constants in a reaction mechanism are not usually evaluated at conditions representative of LBO in an aircraft gas turbine. The simpler the reaction mechanism is, the more important it becomes that the rate constants be correct. Therefore, finding a reduced reaction rate mechanism for propane/air systems that reproduces appropriate (well–stirred reactor) LBO characteristics was a task of some importance. Success in this effort was not satisfactorily achieved, and it was necessary to fall back on an empirically–calibrated, single–step reaction mechanism due to Kretschmer & Odgers.

The EDC model was therefore implemented in the limit of fast chemistry. In this limit of fast chemistry, an extinction criterion was established, and this was applied as an extinction residence time for a reactor. In this form there was a great deal of similarity and consistency with the phenomenological stability parameter established as part of this program, although the EDC model accounted for intermittency which the stability parameter did not.

The fast chemistry version of the EDC model implemented in the Pratt & Whitney 2D–PREACH CFD code was able to successfully calculate flame lift for both classical jet diffusion flames from the literature and in the PW100 combustor. However, it was not able to calculate the attached flame condition in the PW100 combustor. Two possible reasons for this failure were identified: 1.) The lack of reaction kinetics allowed substantially all of the fuel to be consumed in the jet shear layers so that insufficient survived to be recirculated back to the combustor step to there generate the attached flame. 2.) The possibility in the actual experiment, that sufficient unreacted fuel to produce the attached flame was directly introduced into the step recirculation from the central fuel jet, by (unaccounted for in the calculation) nonstationary behavior in the mean flow. Had sufficient fuel survived the jet shear layers in the calculation to be returned to the step region of the combustor, the calculated extinction criterion in the step region would still have excluded the attached flame. It appears that some further adjustment of Magnussen's so–called "adjustment factors" might therefore be necessary. It was clear that temperature–broadening of the "flammability limits" on the rich–side was also a necessary improvement that should be made.

The CFD calculations made of the PW200 combustor yielded a stationary–state solution, that when used in conjunction with the OH and flame imaging, and, the CARS and LDV measurements, of the LS fuel injector in the PW150 combustor, together with the direct flame observations and the CARS measurements in the PW200 combustor, formed part of a most useful diagnostic package for understanding the combustion behavior in the PW200 combustor. Each diagnostic technique separately conveyed a certain amount of information about the complex reaction processes in the simplified generic combustor or its

component parts; used together they permitted a comprehensive picture of the behavior to be built up that helped to explain the LBO behavior and measurements.

When the calculated flowfields in the PW200 combustor were postprocessed in terms of Swithenbank's dissipation gradient approach, the complicated flow structures could be reduced to a simplified network of individual reactors of various kinds and sizes, together with their connectivities. In philosophy this is very similar to Magnussen's EDC approach, except that now, the scale is on the macro–plus level, i.e., it forms a supra–grid scale combustion model. With this network then, the combustor behavior could be studied in yet another way, in this case, in processing terms.

The smaller number of reactors involved, together with the uncoupling from the fluid dynamics, permits detailed chemical reaction mechanisms to be used in such processing solutions, without excessive computational cost. In the present instance, the chemical reaction mechanism of Kollrack for Jet–A/JP 8/air systems, used with propane properties, was utilized since this had been shown to give reasonable representation of the LBO curve for well–stirred reactors.

With this hybrid modeling approach the time–consuming and computationally–expensive CFD calculation is only performed once, at appropriate conditions representative of LBO. It is presumed that the calculated flowfield then does not change much with fairly wide variation in combustor operating conditions and minor changes in combustor airflow distribution. These presumptions follow as a "useful half–truth" from Spalding's partial modeling methods [34.], i.e., essentially, that to first order and for the approximately–correct Reynolds Number, the flowfield is established by the combustor geometry and the pressure drop across it only. Solution of the reaction ordinary differential equations for the network chemistry is computationally not inherently expensive, and can be performed relatively quickly. The hybrid approach therefore allows many blowout calculations over a range of combustor loadings to be performed rather rapidly, so that a stability curve for the combustor can be established. The stability curve is directly useful to the combustor designer who can use it to assess the blowout of the design at suitable engine operating conditions, for example.

The hybrid modeling approach proved to be rather successful in defining the stability behavior of the PW200 combustor. It correctly calculated the effects on overall equivalence ratio at lean blowout of primary zone airflow, combustor pressure, and, variations in dome flow split, to the level of accuracy with which LBO tests can be performed and correlated. The probable reason for this success is that LBO is chemistry–dominated, and a good job was done of that aspect in the hybrid modeling, while the fluid dynamics only needs to be approximately correct. Similarly, while the nonstationary flow aspects of LBO were not explicitly addressed in the hybrid modeling, the protocol for a blowout, in terms of a critical temperature, which can be set to a high enough value, probably covers nonstationary effects implicitly.

LBO is dominated by chemistry, and these effects must be accounted for in some suitable fashion in any modeling of the LBO process. In summary, the program investigating LBO in gas turbine engine combustors achieved its objective of creating a viable modeling procedure, in the form of the hybrid modeling, that is suitable for calculating the stability characteristics of a given design. The modeling procedure accounts for both flowfield and chemical kinetics in uncoupled fashion, but is still relatively time–consuming in that it requires three distinct steps. However, it is a viable procedure in the context of a time–scale associated with an engine development program. The total elapsed time to go through the procedure would benefit greatly from a speed–up in any of the three sequential steps – CFD analysis to establish the flowfield, postprocessing the calculated flowfield via dissipation gradient analysis to establish the reactor network, and, reactor network blowout calculations. The rate–controlling step is the CFD analysis, and the LBO calculation would be significantly shortened if the CFD analysis procedure could be accelerated. It is anticipated that development of unstructured–grid CFD will be of tremendous value here. The CFD calculation may be one performed with a simple combustion model, or a combustion model that is more complete if so–desired; it may even be a nonreacting flow case provided that the fuel is identified as a separate fluid to the air.

The approach is primarily a **design analysis** procedure as opposed to a **design synthesis** procedure. The effects of some combustor variables can be easily determined, provided that these variables do not substantially change the combustor flowfield. If the combustor changes are extensive enough to result in significant flowfield changes, then the LBO calculation procedure must be recommenced from the beginning. The effects of changing combustor operating conditions are easily determined without additional modification.

As implemented under the program the hybrid procedure only addresses gaseous fuels, although any gaseous fuel can be accommodated through use of alternative chemical reaction mechanisms and fuel properties. Extension of the method to liquid fuels is desirable.

THIS PAGE INTENTIONALLY LEFT BLANK

SECTION 9.0
CONCLUSIONS

As a result of the studies conducted under this program of research, the following conclusions could be reached:

1. LBO of enclosed diffusion flames, for both plain–jet and swirling–jet flows, involves a degree of flame–lift, and as a consequence, some amount of premixing or partial–premixing of reactants prior to combustion. The flame–lift takes place for both fuel–rich and fuel–lean conditions, although this may or may not be immediately obvious for rich flames. The partial premixing should be accounted for in any analysis of LBO.

2. Nonstationary behavior of the mean flowfield exists in enclosed diffusion burning when the bulk equivalence ratio is both above and below unity. This is so for both simple (plain–jet) and relatively complex (swirling–jet) combustion systems. In simple systems it manifests itself as axial movements of the flame front when the flame is lifted; for complex systems it manifests itself as a "puffing" behavior of the flame, and may involve a spiral mode. For simple systems at least, the nonstationary behavior can substantially affect the "turbulent" mass transport for overall fuel–rich conditions. As LBO is approached and the flame has lifted, the low–frequency nonstationary behavior increases in amplitude, and appears to play a direct role in the blowout.

3. The experimental roles of the nonstationary mean flow behavior observed in enclosed diffusion flames suggests that any stationary–state CFD solution of these flows will only have limited utility in providing detailed simulations of flame behavior; true time–dependent calculations are required for the research–study of enclosed diffusion flames, with time–step and grid sizes adequate to resolve the important phenomena.

4. Because of the partial–premixing phenomena, classical stirred–reactor concepts can play a useful role in modeling LBO of enclosed diffusion flames. Experimental LBO data from simple combustion systems are well–correlated by a combustor loading parameter developed from the stirred reactor concept. For complex combustion systems that can have more than a single potential flame–holding region, such a simple loading parameter fails to correlate LBO data, due to breakdown of the description of apparent reaction order, that governs pressure dependency.

5. For certain combustion situations, such as blowout, the kinetics of the chemistry has a dominant role. Any modeling using equilibrium, or infinitely–fast, chemistry is most unlikely to be appropriate. There are implied difficulties in this conclusion, for the computational costs associated with attempted solutions based on CFD methods, due to the need to solve transport equations for each species involved.

6. Adequate hydrocarbon/air chemical reaction mechanisms for representation of the LBO of propane, either full or reduced mechanisms, do not currently exist. The reason is most probably associated with the rate constants used.

7. For complex (swirl–stabilized) gas turbine engine generic combustion systems the combustor dome (fuel–rich usually) flows are closely–coupled with the downstream transverse air jet array supplying additional combustion air. Procedures aimed at calculating the LBO characteristics for such systems must account in some substantive way for these fluid dynamic interactions.

8. A successful hybrid modeling procedure that includes both fluid dynamic and chemical kinetic aspects of the LBO process, has been produced. This procedure accounts for the effects of flame–lift and partial premixing, and dome/jet flow interactions, but does not account for any nonstationary flow characteristics; it also includes relevant chemistry. It is successful because of the way blowout is defined through a critical temperature, whose observed value implicitly includes any effects not explicitly accounted for.

9. Increasing the amount of the total (gas turbine generic) combustor airflow that is introduced through the combustor dome reduces the stability of the combustor, as does increasing the overall airflow or reducing the operating pressure.

THIS PAGE INTENTIONALLY LEFT BLANK

SECTION 10.0
RECOMMENDATIONS

The present work by intent only investigated part of the overall LBO problem, so that many important aspects were not explored. In addition, certain gaps and unanswered questions were uncovered during the execution of this effort. Together, these issues remain to be addressed. As a result, some recommendations for future work are as follows:

1. Nonstationary behavior of the mean flowfield has been observed to be important in enclosed diffusion flames. The roles of nonstationary mean flow behavior in determining mass transport, combustion efficiency, and details of flame extinction, in such combusting flows is deserving of a thorough investigation.

2. The role of liquid fuels in modifying the nonstationary mean flow behavior of enclosed diffusion flames should be explored. In addition, potential coupling of the mean gas flow oscillations with the liquid fuel flow from high flow number (low liquid pressure drop) airblast–atomizing injectors (low fuel momentum), and the subsequent effects on time–dependent liquid atomization, local heat release rate, and pollutant formation, and on LBO, are extremely important. These aspects are worthy of study. Such a study could then be usefully extended to include the strong coupling that has been shown to exist between the dome flow and the transverse combustion air jet array in a generic gas turbine combustor.

3. Derivation is needed of suitable complete reaction kinetics mechanisms and rate constant sets for hydrocarbon/air systems, that are suitable for LBO conditions. Reduction of such sets, when obtained, to a number of species suitable for incorporation into CFD codes without unacceptable computational penalties, would then be a worthwhile effort. It is recognized that such reduced sets would likely only be of limited applicability, e.g., one set for LBO calculations, and perhaps another set needed for emissions calculations.

4. The next useful development of the hybrid modeling procedure for LBO would be to extend it to cover liquid fuels. It could also serve as a useful and pragmatic engineering tool for other combustion situations where reaction chemistry is important, e.g., in the emissions area. Development into this area is definitely worthwhile.

5. The EDC combustion model of Magnussen has great potential, despite its relative lack of success in the PW100 combustor test cases. The obvious short–comings with the extinction–time implementation should be addressed, and this is relatively easily accomplished. If a reduced chemical reaction mechanism should be forthcoming, as under Recommendation No. 3, the kinetics version of the EDC model should be developed and re–explored for LBO, and extended to emissions calculations.

6. The Stability Parameter phenomenological model should be tested against flames from the literature, and the links to a critical Karlovitz Number for LBO, investigated. It could be applied as a postprocessing function to a standard CFD calculation, or, implemented as an alternative in the EDC model.

7. The need for a revised correlating parameter for LBO data from complex combustors having more than a single potential burning zone has been demonstrated. Such a parameter would find great utility in the practical design world.

THIS PAGE INTENTIONALLY LEFT BLANK

SECTION 11.0
REFERENCES

1. Bahr, D.W., "Technology for the Design of High Temperature Rise Combustors," Paper No. AIAA–85–1292, AIAA/SAE/ASME/ASEE 21st. Joint Propulsion Conference, Monterey, California, July 8–10, 1985.

2. Lefebvre, A.H., *Gas Turbine Combustion,* Hemisphere Publishing Co., McGraw–Hill Book Co., 1983.

3. Jeffs, R.A., "The Flame Stability and Heat Release Rates of Some Can–Type Combustion Chambers," *Eighth Symposium (International) on Combustion,* Williams & Wilkins, Baltimore, 1962, pp. 1014–1027.

4. Stewart, D.G., *Selected Combustion Problems II,* AGARD/NATO, Butterworths Press, London, 1956, pp. 384–413.

5. Sturgess, G.J., McKinney, R.G. and Morford, S.A., "Modification of Combustor Stoichiometry Distribution for Reduced NOx Emissions from Aircraft Engines," (92–GT–108), Trans. ASME, *J. Engrg. Gas Turbines and Power,* Vol. 115, No.3, July 1993, pp. 570–580.

6. Sturgess, G.J., Sloan, D.G., Lesmerises, A.L., Heneghan, S.P. and Ballal, D.R., "Design and Development of a Research Combustor for Lean Blow–Out Studies," Trans. ASME, *J. Engrg. Gas Turbines and Power,* Vol. 114, No.1, January 1992, pp. 13–19.

7. Heneghan, S.P., Vangsness, M.D., Ballal, D.R., Lesmerises, A.L., and Sturgess, G.J., "Acoustic Characteristics of a Research Step Combustor," Paper No. AIAA–90–1851, presented at AIAA/SAE/ASME/ASEE 26th. Joint Propulsion Conference, Orlando, Florida, July 16–18, 1990.

8. Sturgess, G.J., Heneghan, S.P., Vangsness, M.D., Ballal, D.R. and Lesmerises, A.L., "Isothermal Flow Fields in a Research Combustor for Lean Blowout Studies," Trans. ASME, *J. Engrg. Gas Turbine and Power,* Vol. 114, No.2, April 1992, pp. 435–444.

9. Sturgess, G.J., Heneghan, S.P., Vangsness, M.D., Ballal, D.R., Lesmerises, A.L., and Shouse, D., "Effects of Back–Pressure in a Lean Blowout Research Combustor," Trans. ASME, *J. Engrg. Gas Turbines and Power,* Vol. 115, No.3, July 1993, pp.486–498.

10. Sturgess, G.J., Heneghan, S.P., Vangsness, M.D., Ballal, D.R. and Lesmerises, A.L., "Lean Blowout in a Research Combustor at Simulated Low Pressures," ASME Paper No. 91–GT–359, presented at the International Gas Turbine and Aeroengine Congress and Exposition, Orlando, Florida, June 306, 1991.

11. Roquemore, W.M., Reddy, V.K., Hedman, P.O., Post, M.E., Chen, T.H., Goss, L.P.,Trump, D., Vilinpoc, V., and Sturgess, G.J., "Experimental and Theoretical Studies in a Gas–Fueled Research Combustor," Paper No. AIAA–91–0639, presented at 29th. Aerospace Sciences Meeting, Reno, Nevada, January 7–10, 1991.

12. Sturgess, G.J., Hedman, P.O., Sloan, D.G., and Shouse, D., "Aspects of Flame Stability in a Research Dump Combustor," Paper No. ASME 94–GT–496, presented at International Gas Turbine and Aeroengine Congress and Exposition, The Hague, The Netherlands, June 13–16, 1994.

13. Johnson, B.V. and Bennett, J.C., "Mass and Momentum Turbulent Transport Experiments with Confined Coaxial Jets," (UTRC Rept. R81–915540–9) NASA Contractor Report NASA CR–165574, November 1981.

14. Morrison, G.L., Tatterson, G.B. and Long, M.W., "A 3–D Laser Velocimeter Investigation of Turbulent, Incompressible Flow in an Axisymmetric Sudden Expansion," AIAA Paper No. AIAA–87–0119, AIAA 25th. Aerospace Sciences Meeting, Reno, Nevada, 1987.

15. Pitz, R.W. and Dailey, J.W., "Combustion in a Turbulent Mixing Layer Formed at a Rearward Facing Step," *AIAA Journal,* Vol. 21, No. 11, 1983, pp. 1565–1569.

16. Stevenson, W.H., Thompson, H.D., Gold, R.D. and Craig, R.R., "Laser Velocimeter Measurements in Separated Flow Combustion," Paper, 11.5, presented at the Intl. Symp. of Laser–Doppler Anemometry in Fluid Mechanics, Lisbon, Portugal, 1982.

17. Chen, T.H., Air Force Wright Laboratory, private communication of unpublished work, 1991

18. Bragg, S.L., "Application of Reaction Rate Theory to Combustion Chamber Analysis," Aeronautical Research Council Pub. ARC 16170, Ministry of Defense, London, England, 1953.

19. Kretschmer, D. and Odgers, J., "Modeling of Gas Turbine Combustors – A Convenient Reaction Rate Expression," Trans. ASME, *J. Energy and Power,* 1972, pp. 173–180.

20. Longwell, J.P., Frost, E.E. and Weiss, M.A., "Flame Stability in Bluff–Body Recirculation Zones," *Ind. Engrg. Chem.,* Vol. 45, No.8, 1953, pp. 1629–1633.

21. Swithenbank, J., "Flame Stabilization in High Velocity Flow," *Combustion Technology* – Some Modern Developments, Edit. H.B. Palmer and J.M. Beer, Academic Press, 1974, pp. 91–125.

22. Lewis, B. and von Elbe, G., *Combustion, Flames and Explosion of Gases,* 3rd. Edition, Academic Press, 1961.

23. Ballal, D.R., Vangsness, M.D., Heneghan, S.P. and Sturgess, G.J., "Studies of Lean Blowout in a Research Combustor," presented at an AGARD meeting on *Fuels and Combustion Technology for Advanced Aircraft Engines*, AGARD Conf. Proc. 536, Fiuggi, Italy, 10–14 May, 1993.

24. Pratt, D.T. and Wormeck, J.J., "CREK – A Computer Program for Calculation of Combustion Reaction Equilibrium and Kinetics in Laminar or Turbulent Flow," Rept. No. WSU–ME–TEL–76, Dept. Mech. Engrg., Washington State University, 1976.

25. Roberts, R., Aceto, L.D., Kollrack, R., Teixeira, D.P. and Bonnell, J.M., "An Analytical Model for Nitric Oxide Formation in a Gas Turbine Combustor," *AIAA Journal,* Vol. 10, No. 6, June 1972, pp. 820–826.

26. Hedman, P.O., et al., "Investigation of the Combustion Characteristics of Confined Co–Annular Jets with a Sudden Expansion," Final Rept., Summer Research Extension Program, Aero Propulsion & Power Lab., Wright–Patterson Air Force Base, Ohio, Brigham–Young University, 1993.

27. Pyper, D.K., "The Study of Flame Stability Near Lean Blow Out in Non–Premixed, Non–Swirl and Swirl Burners, and the Design of a Research Combustor Facility." M.S. Thesis, Dept. Mech. Engrg., Brigham Young University, April 1994.

28. Warren, D.L., "Combustion Studies of a Swirled, Non–Premixed Flame Using Advanced Diagnostics," M.S. Thesis, Dept. Mech. Engrg., Brigham Young University, April 1994.

29. Hedman, P.O., Sturgess, G.J., Warren, D.L., Goss, L.P. and Shouse, D., "Observations of Flame Behavior from a Practical Fuel Injector Using a Gaseous Fuel in a Technology Combustor," ASME Paper No. 94–GT–389, presented at the ASME International Gas Turbine and Aeroengine Congress and Exposition, The Hague, The Netherlands, June 13–16, 1994, (to appear in Trans. ASME).

30. Sturgess, G.J. and Shouse, D., "Lean Blowout Research in a Generic Gas Turbine Combustor with High Optical Access," ASME Paper No. 93–GT–332, presented at the ASME International Gas Turbine and Aeroengine Congress and Exposition, Cincinnati, Ohio, May 24–27, 1993 (to appear in Trans. ASME).

31. Switzer, G.L. and Goss, L.P., "A Hardened CARS System for Temperature and Species Concentration Measurements in a Practical Combustion Environment," *Temperature: Its Measurement and Control in Science and Industry,* Edit. J.F. Schooley, American Institute of Physics, New York, 1982, pp.583–587.

32. Switzer, G., Sturgess, G.J., Sloan, D. G. and Shouse, D., "Relation of CARS Temperature Fields to Lean Blowout Performance in an Aircraft Gas Turbine Generic Combustor," Paper No. AIAA–94–3271, presented at 30th. AIAA/ASME/SAE/ASEE Joint Propulsion Conference, Indianapolis, Indiana, June 27–29, 1994.

33. Zelina, J. and Ballal, D.R., "Combustion Studies in a Well–Stirred Reactor," submitted to AIAA *Journal of Propulsion and Power,* 1994.

34. Spalding, D.B., "Performance Criteria of Gas–Turbine Combustion Chambers," *Aircraft Engineering Monograph,* August 1956.

35. Williams, F.A., *Combustion Theory,* 2nd. Edition, The Benjamin/Cummings Publishing Company Inc., California, pp. 408–410.

36. Janicka, J. and Peters, N., "Production of Turbulent Jet Diffusion Flame Lift–Off Using a PDF Transport Equation," *19th. Symposium (International) on Combustion,* The Combustion Institute, Pittsburgh, Pennsylvania, 1982, pp. 367–374.

37. Lockwood, F.C. and Megahed, I.A.E., "Extinction in Turbulent Reacting Flows," *Combustion Science and Technology,* Vol. 19, 1978, pp.77–80.

38. Chakravarty, A., Lockwood, F.C. and Sinicropi, G., "The Prediction of Burner Stability Limits," *Combustion Science and Technology,* Vol. 42, 1984, pp.67–86.

39. Kalghatgi, G.T., "Lift–Off Heights and Visible Lengths of Vertical Turbulent Jet Diffusion Flames in Still Air," *Combustion Science and Technology,* Vol. 41, 1984, pp. 17–29.

40. Eickhoff, H., Lenze, B. and Leuckel, W., "Experimental Investigation on the Stabilization Mechanism of Jet Diffusion Flames," *20th. Symposium (International) on Combustion*, The Combustion Institute, Pittsburgh, Pennsylvania, 1985, pp. 311–318.

41. Byggstoyl, S. and Magnussen, B.F., "A Model for Flame Extinction in Turbulent Flow," *Turbulent Shear Flows 4,* Edit. L.J.S. Bradberry, F. Durst, B.E. Launder, F.W. Schmidt and J.H. Whitelaw, Springer–Verlag, Berlin, 1985, pp. 381–395.

42. Semenov, N.N., "Thermal Theory of Combustion and Explosion; III – Theory of Normal Flame Propagation," *Progress of Physical Science (USSR),* Vol. 24, No. 4, 1940, (available as NACA Tech. Memo No. 1026, Sept. 1942).

43. Chomiak, J., *Combustion: A Study in Theory, Fact and Application,* Abacus Press/Gordon & Breach, New York, 1990.

44. Barnett, H.C. and Hibbard, R.R., (Editors) "Basic Considerations in the Combustion of Hydrocarbon Fuels with Air," NACA Report No. 1300, 1959.

45. Weinberg, F.J., "Geometric–Optical Techniques in Combustion Research," Progress in *Combustion Science and Technology,* Edit. J. Ducarme, M. Gerstein and A.H. Lefebvre, Pergamon Press, Vol. 1, 1960, pp. 111–144.

46. Spalding, D.B., *Convective Mass Transfer – An Introduction,* Edward Arnold (Publishers) Ltd., London, 1963.

47. Jones, W.P. and Lindstedt, R.P., "Global Reaction Schemes for Hydrocarbon Combustion," *Combustion and Flame,* Vol. 73, 1988, pp. 233–249.

48. Colket, M.B., private communication, United Technologies Research Center, 1989.

49. Paczko, G., Lefdel, P.M. and Peters, N., "Reduced Reaction Schemes for Methane, Methanol and Propane Flames," proc. *21st. Symposium (International) on Combustion,* The Combustion Institute, Pittsburgh, Pennsylvania, 1988, pp. 739–748.

50. Edelman, R. and Harsha, P.T., "Some Observations on Turbulent Mixing with Chemical Reactions," *Turbulent Combustion,* Progress in Astronautics and Aeronautics, Vol. 58, Edit. L.A. Kennedy, 1978, pp. 55–102.

51. Roberts, R., Aceto, L.D., Kollrack, R., Teixeira, D.P. and Bonnell, J.M., "An Analytical Model for Nitric Oxide Formation in a Gas Turbine Combustor," *AIAA Journal,* Vol. 19, No. 6, 1972, pp. 820–826.

52. Kollrack, R., "Model Calculations of the Combustion Product Distributions in the Primary Zone of a Gas Turbine Combustor," ASME Paper No. 76–WA/GT, presented at ASME Winter Annual Meeting, New York City, 1976.

53. Kretschmer, D. and Odgers, J., "Modeling of Gas Turbine Combustors – A Convenient Reaction Rate Equation," Trans. ASME, *Journal of Engineering for Power,* Vol. 94,1972, pp.173–180.

54. 54. Glarborg, P., Kee, R.J., Grcar, J.F. and Miller, J.A., "PSR: A Fortran Program for Modeling Well–Stirred Reactors," Sandia National Laboratories Report SAND 86–8209, VC–4, (reprint), October 1988.

55. Seydel, R., From Equilibrium to Chaos, Elsevier Science Publishing Company, New York City, New York, 1988.

56. Keller, H.B., "Numerical Solution of Bifurcation on Non–Linear Eigenvalue Problems, Applications of Bifurcation Theory, Edit. P. Rabinowitz, Academic Press, New York City, New York, 1977, pp. 359–384.

57. Keller, H.B., Lectures on Numerical Methods in Bifurcation Problems, Springer–Verlag, New York City, New York, 1987.

58. Kee, R.J., Miller, J.A. and Evans, G.H., "A Computational Model of the Structure and Extinction of Strained, Opposed Flow, Premixed Methane–Air Flames," proc. 22nd. Symposium (International) on Combustion, The Combustion Institute, Pittsburgh, Pennsylvania, 1988, pp. 1479–1494.

59. Giovangigli, V. and Smooke, M.D., "Calculation of Extinction Limits for Premixed Laminar Flames in a Stagnation Point Flow," Journal of Compuational Physics, Vol. 68, 1987, pp. 327–345.

60. Hottel, H.C., Williams, G.C., and Baker, M.L., "Combustion Studies in a Stirred Reactor," proc. 6th. Symposium (International) on Combustion, Reinhold Publishing Corporation, New York City, New York, 1957, pp. 398–411.

61. Clarke, A.E., Harrison, A.J. and Odgers, J., "Combustion Instability in a Spherical Combustor," proc. 7th. Symposium (International) on Combustion, Butterworths Scientific Publications, London, 1958, pp. 664–673.

62. Zelina, J. and Ballal, D.R., "Combustion Studies in a Well–Stirred Reactor, AIAA Paper No. 94–0114, 1994.

63. Magnussen, B.F. and Hjertager, B.H., "On Mathematical Modeling of Turbulent Combustion with Special Emphasis on Soot Formation and Combustion," proc. *16th.* Symposium (International) on Combustion, The Combustion Institute, Pittsburgh, Pennsylvania, 1977, pp. 719–729.

64. Magnussen, B.F., "Effects of Turbulent Structure and Local Concentrations on Soot Formation and Combustion in C_2H_2 Diffusion Flames," proc. *17th. Symposium* (International) on Combustion, The Combustion Institute, Pittsburgh, Pennsylvania,1979, pp.1383–1393.

65. Magnussen, B.F., "On the Structure of Turbulence and a Generalized Eddy Dissipation Concept for Chemical Reaction in Turbulent Flow," AIAA Paper No. AIAA–81–0042, Aerospace Science Meeting, St. Louis, Missouri, January 12–15, 1981.

66. Magnussen, B.F., "Modeling of Reaction Processes in Turbulent Flames with Special Emphasis on Soot Formation and Combustion," *Particulate Carbon Formation During* Combustion, Edit. D.C. Siegle and G.W. Smith, Plenum Press, New York, 1981, pp. 321–341.

67. Magnussen, B.F., "Heat Transfer in Gas Turbine Combustors – A Discussion of Mathematical Modeling of Combustion, Heat and Mass Transfer with Emphasis on Heat Transfer in Gas Turbine Combustors," AGARD Conference Preprint No. 390, *Heat Transfer and Cooling in Gas Turbines*, Paper No. 23, 1985.

68. Magnussen, B.F., "Modeling of Pollutant Formation in Gas Turbine Combustors Based on the Eddy Dissipation Concept," presented at the CIMAC Conference in Tainjin, China, 4–8 June, 1989.

69. Tennekes, H., "Simple Model for the Small–Scale Structure of Turbulence," *The Physics of Fluids*, Vol. 11, No. 3, March 1968, pp. 669–671.

70. Chomiak, J., "Dissipation Fluctuations and the Structure and Propagation of Turbulent Flames in Premixed Gases at High Reynolds," proc. *16th. Symposium (International) on Combustion*, The Combustion Institute, Pittsburgh, Pennsylvania, 1977, pp. 1665–1673.

71. Sturgess, G.J., series of private Pratt & Whitney internal memos, 1988.

72. Lilleheie, N.I., Byggstoyl, S. and Magnussen, B.F., "Developments in the Numerical Modeling of Turbulent Diffusion Flames with Finite Rate Chemistry, Based on the EDC," private communication, June 22, 1989.

73. Lilleheie, N.I., Byggstoyl, S. and Magnussen, B.F., "Numerical Calculations of a Methane/Air Turbulent Diffusion Flame Using Detailed Chemical Kinetics in the Eddy Dissipation Concept," private communication, December 16, 1989.

74. Sturgess, G.J., *Aerothermal Modeling Phase I, Final Report,* NASA Report No. CR–168202, May 1983.

75. Dahm, W.J.A. and Dibble, R.W., "Combustion Stability Limits of Coflowing Turbulent Jet Diffusion Flames," Paper No. AIAA–88–0538, AIAA Aerospace Sciences Meeting, Reno, Nevada, January 11–14, 1988.

76. Longwell, J.P. and Weiss, M.A., "High Temperature Reaction Rates in Hydrocarbon Combustion," *Industrial and Engineering Chemistry,* Vol. 47, No. 8, 1955, p. 1634.

77. Barat, R.B., "Behavior of Jet–Stirred Combustors Near Blow–Out," *Chemical and Physical Processes in Combustion*, Fall Technical Meeting of the Eastern Section of the Combustion Institute, Ithaca, New York, October 14–16, 1991.

78. Correa, S.M. and Overton, K.S., "A Model for Optimizing Emissions and Stability of a Gas Turbine Combustor," Paper No. AIAA–88–2858, presented at AIAA/ASME/SAE/ASEE 24th. Joint Propulsion Conference, Boston, Massachusetts, July 11–13, 1988.

79. Globus, A., Levit, C. and Lasinski, T., "A Tool for Visualizing the Topology of Three–Dimensional Vector Fields," Rept. No. RNR–91–017, NASA Ames Research Center, Moffett Field, California, April 1991.

80. Rhie, C.M. and Stowers, S.T., "Numerical Analysis of Reacting Flows Using Finite Rate Chemistry Models," AIAA Paper No. AIAA–89–0459, 1989.

81. Gerrard, A.J., "Methods of Flow Visualization By Means of Water," *Experimental Methods in Combustion Research*, Edit. J. Surugue, AGARD, Pergamon Press, 1961, Section 1–10, pp. 22–43.

82. Appleton, J.P. and Heywood, J.B., "The Effects of Imperfect Fuel–Air Mixing in a Burner on NO Formation from Nitrogen in the Air and the Fuel," proc. *14th. Symposium (International) on Combustion*, The Combustion Institute, 1973, pp. 777–786.

83. Pratt, D.T. and Pratt, B., MARK2X Computer Code, private communication, 1990.

84. Syed, S.A. and Sturgess, G.J., "Validation Studies and Combustion Models for Aircraft Gas Turbine Combustors," proc. ASME Symp. *Momentum and Heat Transfer Processes* in Recirculating Flows, Edit. B.E. Launder and J.A.C. Humphrey, HTD–Vol. 13, Winter Annual Meeting, Chicago, Illinois, November 16–21, 1980, pp. 71–89.

THIS PAGE INTENTIONALLY LEFT BLANK

APPENDIX A

DESIGN AND DEVELOPMENT OF A RESEARCH COMBUSTOR FOR LEAN BLOW-OUT STUDIES

By

G.J. Sturgess and D.G. Sloan
Pratt & Whitney, East Hartford, Connecticut

A.L. Lesmerises
WL/POSF, Wright-Patterson Air Force Base, Ohio

S.P. Heneghan and D.R. Ballal
University of Dayton, Dayton, Ohio

Published in Trans. ASME, *Journal of Engineering for Gas Turbines and Power,* Vol. 114, No. 1, January 1992, pp. 13-19

G. J. Sturgess

D. G. Sloan

Pratt & Whitney,
East Hartford, CT 06108

A. L. Lesmerises
WRDC/POSF,
Wright-Patterson AFB, OH 45433

S. P. Heneghan

D. R. Ballal

University of Dayton,
Dayton, OH 45429

Design and Development of a Research Combustor for Lean Blow-Out Studies

In a modern aircraft gas turbine combustor, the phenomenon of lean blow-out (LBO) is of major concern. To understand the physical processes involved in LBO, a research combustor was designed and developed specifically to reproduce recirculation patterns and LBO processes that occur in a real gas turbine combustor. A total of eight leading design criteria were established for the research combustor. This paper discusses the combustor design constraints, aerothermochemical design, choice of combustor configurations, combustor sizing, mechanical design, combustor light-off, and combustor acoustic considerations that went into the final design and fabrication. Tests on this combustor reveal a complex sequence of events such as flame lift-off, intermittency, and onset of axial flame instability leading to lean blowout. The combustor operates satisfactorily and is yielding benchmark quality data for validating and refining computer models for predicting LBO in real engine combustors.

Introduction

The provision of adequate stability in aircraft gas turbine combustors is a long-term problem that is exacerbated by several current design trends. Of particular concern is the phenomenon of lean blow-out (LBO). The solution to this problem is made difficult by deficiencies in present calculation methods and by conflicting design criteria. A joint U.S. Air Force, industry, and university research program is being carried out to improve the understanding of the physical processes involved in LBO and also the calculation procedures used. Recently, Sturgess et al. (1989) have provided a broad description of this overall program.

In a modern annular gas turbine combustor, flame is stabilized by producing a recirculation zone in the flow field. This zone is generated by a combination of *three* mechanisms, namely: an axial swirling air jet associated with each fuel introduction, sudden expansion of the axial swirling jets as they enter the primary zone, and back-pressure provided by an array of radial air jets at the end of the primary zone. The recirculation zone itself serves a *triple* purpose of: (*i*) producing a region of low velocity, (*ii*) providing high residence time for the flame to propagate into the incoming fresh mixture, and (*iii*) serving as a source of continuous ignition for the combustible fuel-air mixture.

To obtain low exhaust emissions, Pratt & Whitney currently tailors the combustor flow control mechanisms to produce an "inside-out" recirculation pattern, illustrated in Fig. 1. Therefore, the research combustor was required to reproduce this type of recirculation pattern. At the same time, it had to provide stable combustion over a wide variation in its loading, be geometrically simple for ease of experimentation and computation, and provide adequate optical access for measurements.

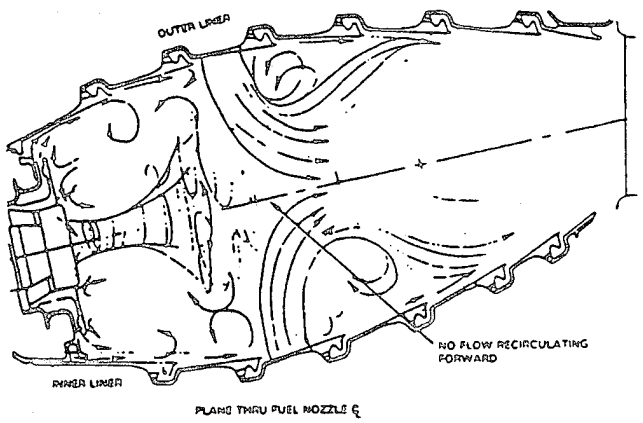

Fig. 1 Flow patterns in a modern annular combustor showing swirl and recirculation dominating the "inside-out" primary zone

Design Criteria

The following were established as the leading criteria to satisfy the above design requirements:

1 Introduce fuel and air separately to produce a turbulent diffusion flame.

2 Have geometric simplicity so that accuracy of CFD modeling is not affected by the combustor shape representation.

Contributed by the International Gas Turbine Institute and presented at the 35th International Gas Turbine and Aeroengine Congress and Exposition, Brussels, Belgium, June 11-14, 1990. Manuscript received by the International Gas Turbine Institute January 16, 1990. Paper No. 90-GT-143.

3 Be two-dimensional to minimize the cost of CFD modeling, and to simplify measurements and their interpretation.

4 Have well-defined boundary conditions so these may be correctly represented in CFD modeling.

5 Contain the flame fully near blow-out conditions for all loadings that should be achieved without recourse to exotic operating conditions.

6 Avoid flow field interference and nonstationary behavior due to acoustic resonance.

7 Provide good optical access for flow visualization and laser diagnostics.

8 Be inexpensive to manufacture and operate, but have structural robustness and durability.

These criteria contain several potential conflicts and indeed, simultaneous satisfaction of all criteria without some compromises proved not to be possible.

Design Constraints

The research combustor was to be operated in the Fundamental Combustion Laboratory of the U.S. Air Force, Wright Research and Development Center, Aero Propulsion and Power Laboratory, W-PAFB, Ohio. A layout and a detailed description of this laboratory are given by Ballal et al. (1987).

The research combustor was mounted vertically on the laboratory burner, which is bolted to a traverse platform capable of a vertical movement of 61 cm and a horizontal movement of 23 cm in each of the other two directions. An exhaust hood is located directly above the combustor exit section. A three-component LDA system for velocity measurements and a CARS system for flame temperature measurements are arranged on two separate 1.22 m × 2.44 m optics tables on either side of the combustor. By moving the combustor relative to the fixed optical diagnostics, the complexity of the optical arrangement is minimized. Of course, this imposes constraints on the combustor design. For example, the combustor dimensions must be chosen such that the scale of events of interest taking place inside the combustor is within the traverse distance of the platform. Similarly, the requirement to have the base of the combustor in line with the height of the laser beams above the optics table and the location of the exhaust hood above the optics table places a restriction on the maximum length of the combustor. Finally, the combustor has to pass through a 40 cm × 40 cm square cut-out in the breadboard optical bench that carries the LDA-CARS optics and also binds the other two optics tables.

Air was supplied to the combustor in the 510 kg/h to 4900 kg/h range at atmospheric pressure. The combustion laboratory provides gaseous propane and methane fuels. For propane, flow rates beyond 20 kg/h are difficult to obtain due to limitations of the facility. This fuel flow rate limit imposes additional constraints on the combustor design.

Aerothermochemical Design

At the outset, use of swirl generators was ruled out for establishing a recirculating flow field because Sturgess et al. (1986) found that they produce complex inlet boundary conditions for CFD codes and current turbulence modeling calculates swirling flows inaccurately (Sturgess and Syed, 1985). Also, Gupta et al. (1984) observe that a strongly swirling central jet induces exit flow into a combustor and produces precessing vortex cores. Therefore, jet expansion was used to generate the inside-out recirculation.

The jet expansion arrangement consists of a central gaseous fuel jet surrounded by a coflowing annular air jet. Both jets suddenly expand into a confinement that is symmetric about the jet axes. This configuration, which can be either planar or axisymmetric, represents a single sector of a practical annular combustor rather well. The back-pressure effects produced by the transverse air jets in a real combustor had to be considered for the research combustor as well. Individual air jets are three dimensional and do not provide the required uniformity. Therefore, the back-pressure effect was simulated by restricting the outlet from the research combustor by means of an orifice plate. This restriction was sufficiently far downstream from the sudden expansion that the step-recirculation zones were not affected.

In this research combustor, gaseous hydrocarbon fuel was burned because its chemistry resembles that of vaporized JP fuels. The choice between propane and methane was made based upon their peak flame temperatures, transition Reynolds numbers, flame lengths, lift-off heights, and blow-out characteristics.

Peak flame temperatures were important because the annealing temperature limit for fused quartz window is approximately 1450 K. Since, heat release would be confined to the central portion of the combustor, it seemed feasible to operate the combustor at 1700 K corresponding to $\phi = 0.6$ for propane–air mixture. This value of ϕ represents LBO conditions similar to well-stirred reactor performance (see Clarke et al., 1958).

Since the research combustor must operate in the fully developed turbulent region, the critical transitional Reynolds numbers for propane and methane fuel jets were obtained from Hottell and Hawthorne (1949) as 10,000 and 3000, respectively. Flame length is important because the combustor must confine the flame. For enclosed flames, Beer and Chigier (1972) and Lenze (1982) have shown that the flame length depends on the Thring–Newby criterion θ, and the excess air ratio, λ. Figure 2 shows a plot of flame length ratio L/L_f versus $1/\theta$.

Now, for $\phi = 0.6$, and $\lambda = 1.7$, the maximum flame length $L/L_f = 1.3$ occurs for zero recirculation (i.e., when $\theta < 1$). This condition determines maximum combustor length = 200 and 296 fuel jet passage heights for propane and methane respectively.

When conditions for critical Reynolds numbers, maximum propane flow rate, and maximum flame length are combined, the required combustor length for both fuels exceeds the available space in the facility. Therefore, recirculation ($1/\theta > 1.0$) becomes a prerequisite. At $\phi = 0.6$, less recirculation is re-

Nomenclature

B = blockage ratio
D = flameholder diameter
d = diameter
h = height
L = length
$\dot{m}$ = mass flow
p = pressure
r = radius
T = temperature
Tu = mainstream turbulence intensity
U = mean velocity
x, y, z = directions
θ = Thring–Newby parameter
λ = excess air ratio
ρ = density
ϕ = equivalence ratio

Subscripts

a = air, annulus
c = combustor
f = flame, fuel tube
FAR = fuel air ratio
i = equivalent fuel–air supply passage
LBO = lean blow-out
s = step, air passage radius

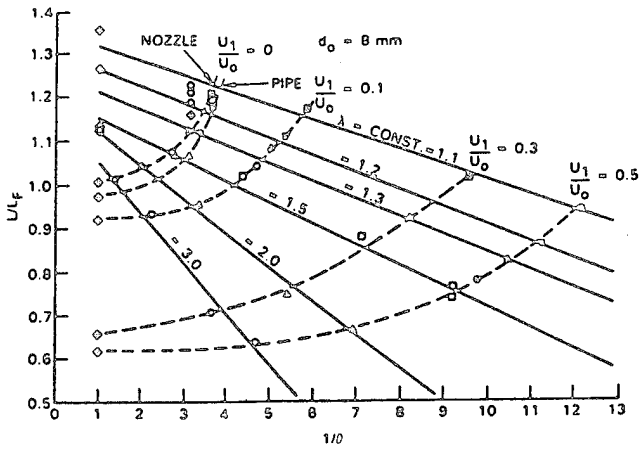

Fig. 2 Flame length ratio as a function of reciprocal Thring-Newby criterion for various values of excess air ratio for an enclosed, natural gas flame (Lenze, 1982)

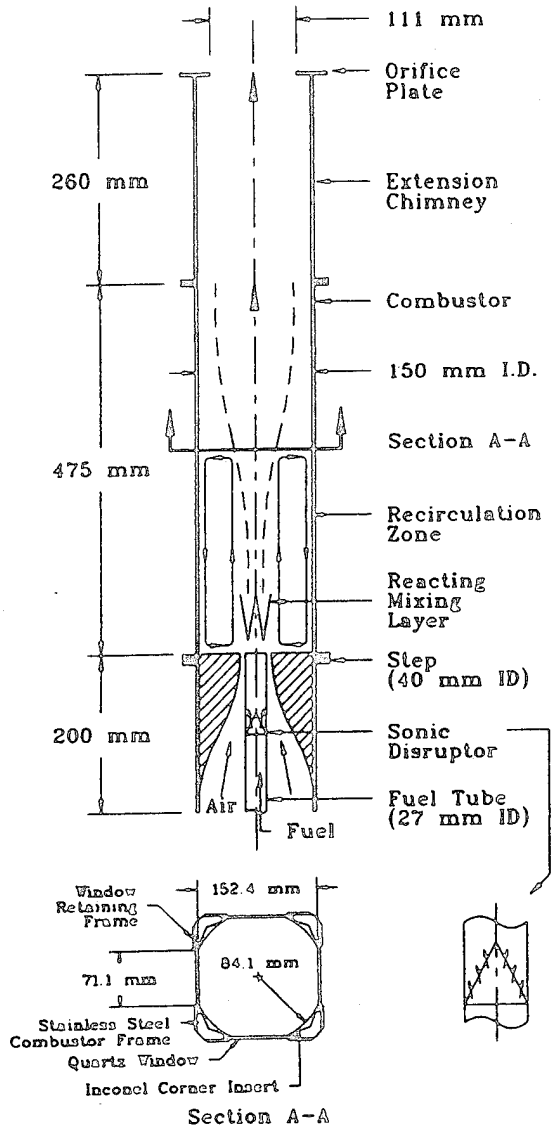

Fig. 3 Schematic diagram of the final configuration of the research combustor mounted on the burner (inset shows "sonic disruptor")

quired for a propane flame of the requisite length than is required for methane.

As the LBO condition is approached, the attached diffusion flame lifts from the fuel tube and is stabilized slightly downstream. This is the region of most interest and relevance to the present study. Thus, the combustor has to be long enough to contain the lifted flame region; and this region has to fall within the traverse window. Both Kalghatgi (1987) and Dahm and Dibble (1988) have shown that propane has less lift-off height than methane. Considering both flame length and lift-off heights, the choice of gaseous propane yields smaller combustor length.

Choice of Configuration

For easy optical access, the most ideal configuration for the research combustor was a planar cross section. However, experimentally it is extremely difficult to establish planar flows that are truly symmetric about the jet axes. In addition, the aspect ratio considerations for a planar rig resulted in propane flow rates that exceeded the capacity of the facility. Therefore, an axisymmetric jet arrangement was preferred.

A jet discharging into a quartz cylindrical working section provides an ideal axisymmetric configuration, but poses severe problems for optical measurements through curved glass surfaces. Corrective lens techniques have been developed by Durrett et al. (1985). However, these are too complex and immature for the advanced laser diagnostics (three-dimensional LDA and CARS) used in this program. A box-section combustor with corner fillets to reduce vorticity concentration and eliminate its effect on the bulk flow field in the combustor was an attractive alternative. CFD calculations made using Pratt & Whitney's 3D-TEACH computer code indicated, in agreement with Brundett and Baines (1964), that a single, linear corner fillet in a square-section duct reduces the peak vorticity by half. Therefore, corner fillets were provided for the research combustor.

Figure 3 shows a schematic of the final agreement for the research combustor. It consists of a central fuel tube surrounded by a co-annular air jet. This jet system supplies unmixed reactants at the exit to a dump-step inside the combustor. The burner contains the jet system and also supports the combustor vertically. The combustor is comprised of *two* separate sections. The first section holds windows (quartz or instrumented metal panels) on all four sides, and the second one is a short extension Inconel chimney. On the top of this chimney, orifice plates of specific blockage ratios can be fitted.

Combustor Sizing

To decide step height, the stability expression of Ballal and Lefebvre (1979) was used:

$$\phi_{LBO} = \left[\frac{2.25(1+0.4U_m[1+0.1Tu])}{p^{0.25}T_0\exp(T_0/150)D_b(1-B)}\right]^{0.16} \quad (1)$$

In the present context, $B = (D_b/D_c)^2$, where D_b is an effective diameter representing an orifice plate closed area.

Preliminary estimates made by assuming d_f = 13.2 mm, ϕ = 0.6, and $U_a/U_f > 1$, had yielded a value of 40 mm for an equivalent premixed passage diameter at the combustor inlet. Equation (1) was then used to generate the parametric curve of blow-out velocity versus step height for this value of passage diameter. Figure 4 shows plots of these calculations. From these data a step height of 55 mm was found appropriate for ϕ = 0.6. This value of step height with a 40 mm inlet gives a combustor diameter of 150 mm. This step will generate a symmetric recirculation zone with a reattachment point plane that depends on the step height, inlet Reynolds number, and equivalence ratio as is evident, for example, in the work of Morrison et al. (1987). Figure 5 shows reattachment lengths for reacting and nonreacting laminar and turbulent flows. For ϕ = 0.6 and Re = 10^4, the reattachment plane is about five step-heights downstream of the step. To accommodate this recirculation zone, and the one formed due to flow stagnation

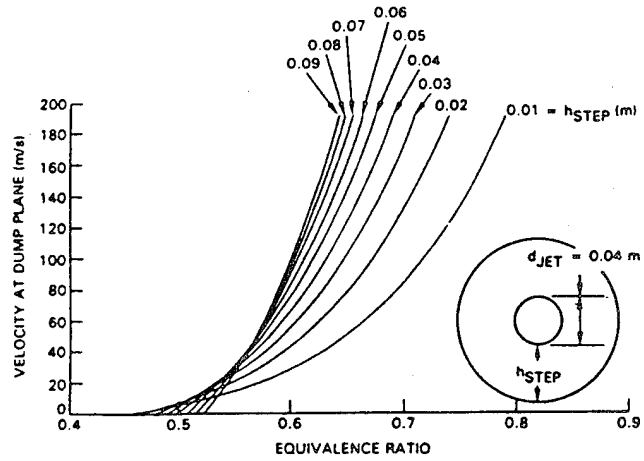

Fig. 4 Blowout velocity versus equivalence ratio for various values of step height as calculated by Ballal and Lefebvre (1979) correlation

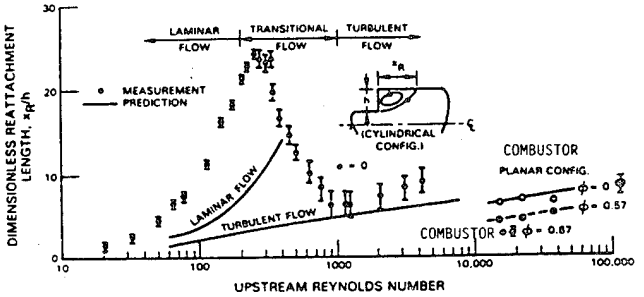

Fig. 5 Recirculation zone length for nonreacting and reacting cylindrical and planar flows

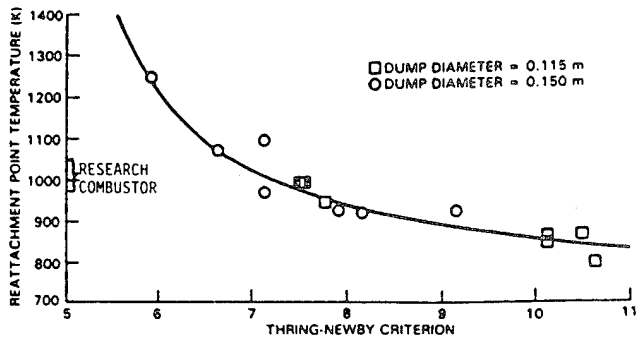

Fig. 6 Correlation of 2D-PREACH results for the stagnation temperature in terms of the Thring-Newby criterion

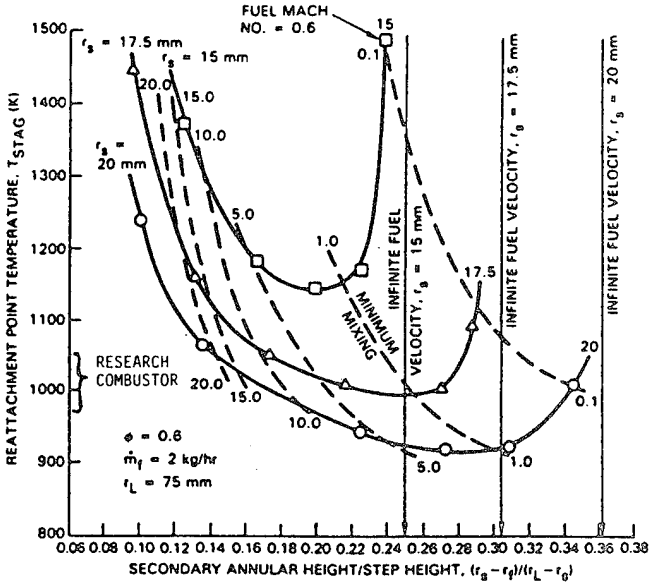

Fig. 7 Plots of reattachment point temperature versus annular/step height ratio for a 150 mm i.d. combustor

on the orifice plate at exit, a combustor length 2–3 times the reattachment length is required to avoid interference between the two zones, i.e., combustor length = 825 mm approximately.

Since the reactants are not premixed the velocity ratio should be high, e.g., $U_a/U_f > 10$, to provide good mixing. Also, the temperature of the combustion products in the step recirculation zone should be high enough to guarantee continuous ignition of fresh reactants when the flame is in lifted condition. For propane-air mixtures, Sturgess (1979) has shown, and CFD analysis for $\phi = 0.6$ suggests, that auto-ignition times become short and temperatures of 400–800 K exist in the shear layer when the gas temperature at reattachment was around 1000 K. Therefore, recirculation zone rettachment plane gas temperature at the combustor wall should not be less than 1000 K for continuous ignition of a lifted flame.

A CFD code was used to obtain the relationship between reattachment plane temperature and the Thring-Newby parameter, θ, for a duct with sudden expansion, namely:

$$\theta = \left(1 + \frac{1}{\text{FAR}}\right)(\rho_f/\rho_a)^{0.5}(r_i'/r_c) \tag{2}$$

where

$$r_i' = \frac{(\dot{m}_f + \dot{m}_a)}{\sqrt{\pi\bar{\rho}}\,(\dot{m}_f U_f + \dot{m}_a U_a)^{0.5}} \tag{3}$$

$$\bar{\rho} = (\dot{m}_a\rho_a + \dot{m}_f\rho_f)/(\dot{m}_a + \dot{m}_f) \tag{4}$$

Results of these calculations are plotted in Fig. 6. In this figure each data point represents a separate calculation and the line drawn through them serves as a design curve.

Based on manipulation of Fig. 6 and Eqs. (2)–(4), Fig. 7 plots the reattachment plane gas temperature in the 150 mm i.d. combustor versus the ratio of annular height to step height for the various secondary passage radii, r_s. The reattachment temperature has two asymptotes; one corresponding to choking in the air passage, and the other due to choking of the fuel passage. For each r_s, the reattachment temperature exhibits a minimum corresponding to $U_a/U_f = 1$. The left-hand side of the plot represents the strongly recirculated step flames of interest for this combustor. The position of minimum temperature occurs at lower values of the abscissa as r_s is decreased. This may be explained in two ways: First, as r_s gets smaller, the step height gets bigger in a fixed combustor and the reattachment plane moves downstream into the regions of increasing gas temperature. Second, as r_s gets smaller so does the air passage annular height for a fixed fuel passage. Therefore, the fuel source is relatively closer to the shear layer associated with the recirculation bubble at the step. Thus, for a given rate of jet expansion, higher temperature gases are delivered at the reattachment plane. For a given r_s, the annular/step height ratio is also changed by changing the fuel passage size. Then, the temperature changes because the jet velocity ratio and hence the rates of mixing jet expansion, are also changed. Plots similar to Fig. 7 can be produced at every equivalence ratio. For a given r_s, increasing the equivalence ratio increases the reattachment temperature at all velocity ratios.

From Fig. 7, geometric relationships may be found for specified mixing conditions or specified temperature conditions. This relationship is shown in Fig. 8 for $\phi = 0.6$, minimum

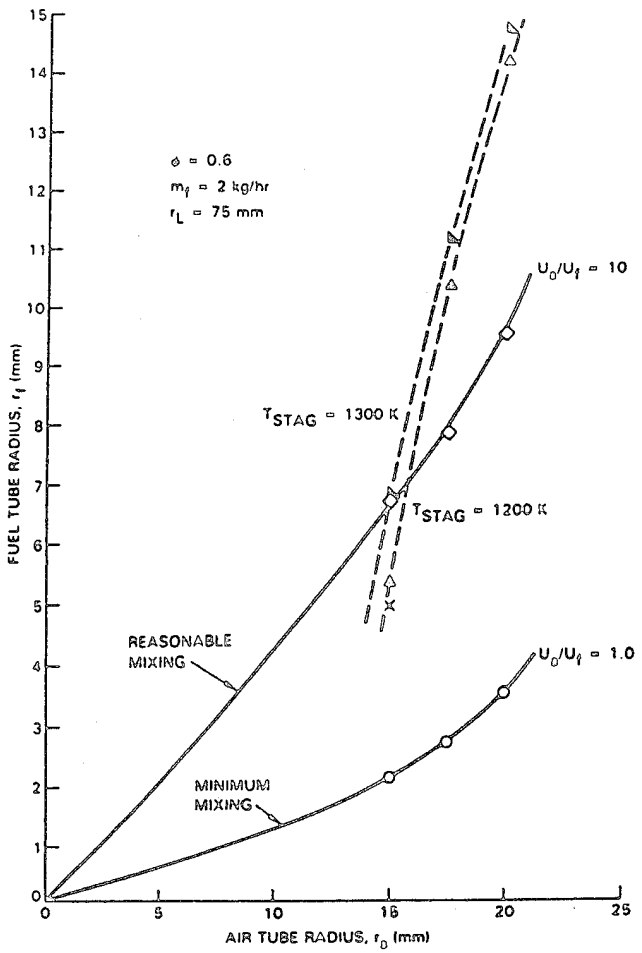

Fig. 8 Relationship between reactant supply tube dimensions, mixing, and stagnation point temperature in a 150-mm i.d. combustor

and moderately strong mixing (U_a/U_f = 1.0 and 10.0, respectively), and reattachment temperatures of 1200 K and 1300 K. Figure 8 indicates that for r_s = 20 mm, the fuel tube needs to be at least 12.5 mm radius to provide the desirable minimum reattachment plane temperature of 1000 K. Allowing for heat losses from the combustor, the fuel tube radius was increased to 13.5 mm. For this radius, Fig. 8 indicates that the reattachment plane temperature would be somewhat over 1100 K. In this way, combustor sizing is completed. The final combustor dimensions are given in Fig. 3.

Mechanical Design

The combustor frame establishes reference planes for the quartz windows. These reference planes ensure that windows on opposite sides of the combustor remain flat and parallel as the combustor is moved. Thus, the combustor frame had to be dimensionally stable, despite frequent and extreme thermal cycling. A thorough heat treatment, for stress relief, was performed on the combustor frame prior to final machining. This proved to be effective since follow-up inspection revealed that deviations from design dimensions were less than 0.25 mm.

The windows are spring-loaded against the window retaining frames by means of Inconel corner inserts. These inserts also form the corner fillets needed to minimize vortex formation. Inconel was used because of its high melting temperature, resistance to oxidation, and its better spring constant at high temperature. The corner insert concept has several advantages. The step discontinuity, where the insert meets the glass, is quite small since the inserts are only 0.81 mm thick. Thus, the combustor frame required less intricate machining. Also, the window can float between the lightly spring-loaded inserts and the frame, thus permitting its independent expansion and contraction.

The windows for this combustor had to meet several design requirements, such as a need to overlap LDA and CARS beams, a desire for cylindrical symmetry, the ability to withstand vibration and high temperature, optical clarity even under laser power approaching 1 GW/cm^2, the preclusion of beam steering as the combustor is moved, and the cost of high-quality quartz glass.

Quartz windows, while expensive, have proven to be quite durable, exhibiting lifetimes on the order of hundreds of hours. The quartz windows used in this combustor are only 3.2 mm thick and this keeps thermal stresses between inner and outer window surfaces to a minimum. Further, thermal shock to the windows was minimized by devising a proper light-off procedure for the combustor. Finally, the windows were designed such that they could easily be replaced, for example, with stainless steel plates equipped with thermocouples and pressure taps.

Window durability with the high-power CARS laser operation has been good except for where soot accumulates. A new short focal length lens is being incorporated in the CARS system to reduce laser power density incident on the window surface by a factor of 4. Insertion of plane windows in the path of the laser beams still causes the probe volume of both the CARS and LDS systems to move. Therefore, the overlap volume must be determined after the windows are in place. The window width was established to allow adequate probe distance perpendicular to the laser propagation direction, and still maintain sufficient cylindrical symmetry.

As illustrated in Fig. 3, the shape of the annular air passage is dictated by the inner contour of the combustor step. Early step designs exhibited poor flow characteristics because of too sudden a contraction. Also, the fuel tube was not concentric with the step. Eventually, a new step was designed, which produced uniform and symmetric annular air velocity profiles.

An Inconel extension is fitted to the downstream end of the research combustor. Prior to the combustor fabrication, it was recognized that the metal walls of the extension piece would get rather hot. This Inconel extension provides a passage with the same cross-sectional profile as the lower portion of the combustor and conveys the combustion products to the exhaust hood directly above the combustor. It may be equipped with either a top-hat restriction (available in various sizes), no restriction at all, or what is preferred, a simple orifice plate.

Combustor Light-Off

Several techniques for igniting the combustor were tested. These include:

Lighting at the exit plane
Lighting through a 6.3 mm hole in the step
Lighting in recirculating zone, 25 mm above the step, through a hole in the side plane.

Only the last of these gave smooth, successful, and reproducible ignition. Ignition in the recirculation zone has been satisfactorily accomplished with a small propane torch igniter attached to the side plate fitting. Normal light-off is accomplished by first establishing an airflow of 300 SLPM, then lighting the torch igniter, and finally admitting about 10 SLPM of fuel in the combustor. Upon successful ignition, air and fuel flows are increased, taking care to maintain constant fuel/air ratio, until the air flow reaches about 900 SLPM. At this flow rate, the flame is very stable, exhibiting lean blow-out at ϕ = 0.5. The only major problem is that at these ignition conditions there is a tendency for significant sooting on the

upper portion of the windows. Attempts to initiate combustion at lower equivalence ratios or higher initial flow rates were not successful. After a light-off is successful, the torch ignitor is removed and the fitting is capped.

Combustion Characteristics

Before performing combustion tests, acoustic characteristics of this research combustor were investigated because it was feared that eddy-shedding off the step might result in satisfying the Rayleigh criterion, and this may set up resonance in the combustor and fuel supply tube. A breadboard version of the combustor was tested and it revealed noisy combustion and flame flicker. Also, mechanical vibrations shortened the window life. Therefore, and after some development work, a "sonic disruptor" (see Fig. 3, inset), which can pass LDA seed particles but is acoustically closed, was introduced into the fuel tube. This device and the redesign of the annular air passage reduced pressure fluctuations in the combustor significantly. These developments are fully described by Heneghan et al. (1989).

Combustion tests revealed that the combustor operates as designed, with the reactants being ignited in the shear layer formed between the fuel and air jets. The shear layer flame appears removed from the confluence of the jets. In agreement with results shown in Figs. 6 and 7, reattachment point temperatures around 1000 K were obtained from the measurements of combustor wall temperatures. Also, in Fig. 5, we show measurements of flame recirculation zone length for Re = 20,000, ϕ = 0.87, and isothermal recirculation zone length for Re = 110,000 obtained by using an LDA instrument. These values are consistent with other isothermal and combusting flow data from the literature.

Figure 9 illustrates the sequence of events leading to lean blow-out in our research combustor for a variety of Reynolds numbers (based on fuel and air flows) and air loading parameters. As the overall equivalence ratio is reduced below unity, the luminosity of the recirculation zone vanishes and the shear-layer *attached* flame moves farther downstream into the combustor in a characteristic *lifted flame* position and form. Continuing reduction in the equivalence ratio produces an onset of flow instability in the lifted flame, increase in the amplitude of the instability, onset of intermittency, severe intermittency, and finally, an onset of strong axial flame instability. At this point, a slight increase in equivalence ratio results in an *attached* flame, while a slight decrease produces a *lean blow-out*. Provided the air jet is always turbulent and the velocity ratio u_a/u_f is sufficiently large, the above sequence of events was the same whether equivalence ratio is decreased by reducing fuel flow rate or by increasing air flow rate. This sequence of events leading to flame-out clearly highlights the complexity of the lean blow-out mechanism in a modern annular gas turbine combustor.

Figure 10 shows the LBO performance of our research combustor. It appears that the combustion characteristics of our research combustion are more similar to those of well-stirred reactors than those of the practical combustor designs of the past. Since high-performance annular combustors of the future will approach the combustion characteristics of the well-stirred reactors, it is reasonable to conclude that our research combustor correctly reproduces the LBO processes of a real gas turbine combustor.

Conclusions

A research combustor that simulates the "inside-out" recirculation pattern and LBO processes of a modern annular aircraft gas turbine combustor was designed and fabricated. This was accomplished using CFD-generated design curves and data available in the literature.

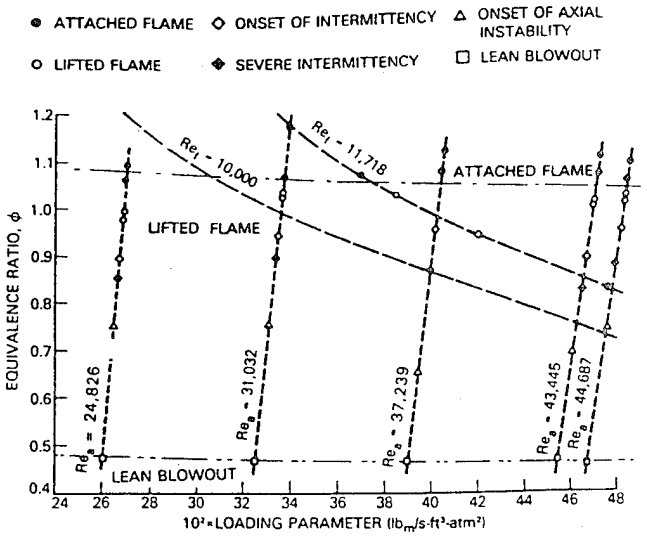

Fig. 9 Flame characteristics in the research combustor

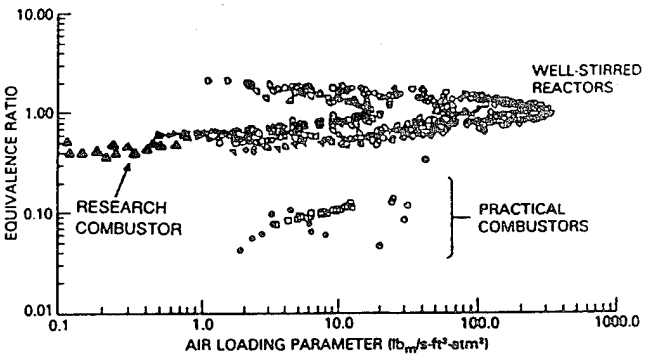

Fig. 10 Lean Blow-out (LBO) performance of the research combustor

It was found that the existing test facility, optics capabilities, and limit on fuel flow rate due to safety considerations imposed dimensional constraints on combustor length and shape. The requirement of simple inlet boundary conditions and two-dimensional flow field for CFD codes made it undesirable to use swirl for improved mixing and reduced flame length. Peak flame temperatures of 1700 K inside the combustor were dictated by the temperature limit of fused quartz.

An axisymmetric arrangement of fuel and air jets, 27 mm and 40 mm diameter, respectively, dumping unmixed reactants at a 55 mm wide step, emerged as the final preferred configuration of this combustor. The combustor is 735 mm long, has 150 mm square cross section with rounded corner fillets of 84 mm radius, and is fitted with an Inconel extension chimney with an orifice plate as its exit.

It was found that the combustor operates in a stable and predictable manner over a range of loadings. Measurements revealed a complex sequence of events such as flame lift-off, intermittency, and onset of axial flame instability eventually leading to lean blow-out. Also, the LBO performance of the research combustor was similar to that of well-stirred reactor. These tests confirmed the soundness of the combustor design for the intended purpose. This combustor is now making possible acquisition of more benchmark quality data on LBO.

Acknowledgments

This research was sponsored by the U.S. Air Force, Wright Research and Development Center, Aero Propulsion and Power

Laboratory, under Contract No. F33615-87-C-2822 to Pratt and Whitney, East Hartford, CT (Contract Monitor: 1Lt. A. L. Lesmerises) and Contract No. F33615-87-C-2767 to University of Dayton, Dayton, OH (Contract Monitor: Dr. W. M. Roquemore).

References

Ballal, D. R., Lightman, A. J., and Yaney, P. P., 1987, "Development of Test Facility and Optical Instrumentation for Turbulent Combustion Research," *AIAA Journal of Propulsion and Power*, Vol. 3, pp. 97–104.

Ballal, D. R., and Lefebvre, A. H., 1979, "Weak Extinction Limits of Turbulent Flowing Mixtures," ASME JOURNAL OF ENGINEERING FOR GAS TURBINES AND POWER, Vol. 101, pp. 343–348.

Beer, J. M., and Chigier, N. A., 1972, *Combustion Aerodynamics*, Wiley, New York.

Brundrett, E., and Baines, W. M., 1964, "The Production and Diffusion of Vorticity in Duct Flow," *Journal of Fluid Mechanics*, Vol. 19, pp. 375–394.

Clarke, A. E., Harrison, A. J., and Odgers, J., 1958, "Combustion Instability in a Spherical Combustor," *Seventh Symposium (International) on Combustion*, Butterworths Scientific Publications, London, pp. 664–673.

Dahm, W. J. A., and Dibble, R. W., 1988, "Combustion Stability Limits of Coflowing Turbulent Jet Diffusion Flames," AIAA Paper No. 88-0538.

Durrett, R. P., Gould, R. D., Stevenson, W. H., and Thompson, H. D., 1985, "A Correction Lens for Laser Doppler Velocimeter Measurements in a Cylindrical Tube," *AIAA Journal*, Vol. 23, pp. 1387–1391.

Gupta, A. K., Lilley, D. G., and Syred, N., 1984, *Swirl Flows*, Abacus Press, London, United Kingdom.

Heneghan, S. P., Vangsness, M. L., Ballal, D. R., Lesmerises, A. L., and Sturgess, G. J., 1989, "Acoustic Characteristics of a Model Step Combustor," in preparation.

Hottel, H. C., and Hawthorne, W. R., 1949, "Diffusion in Laminar Flame Jets," *Third Symposium (International) on Combustion, Flame, and Explosion Phenomena*, The Williams and Wilkins Co., Baltimore, MD, pp. 254–266.

Kalghatgi, G. T., 1987, "Lift-Off Heights and Visible Lengths of Vertical Turbulent Jet Diffusion Flames in Still Air," *Combustion Science and Technology*, Vol. 41, pp. 17–29.

Lenze, B., 1982, "The Influence of Recirculation and Excess Air on Enclosed Turbulent Diffusion Flames," *Nineteenth Symposium (International) on Combustion*, The Combustion Institute, Pittsburgh, PA, pp. 565–572.

Morrison, G. L., Tatterson, G. B., and Long, M. W., 1987, "A 3-D Laser Velocimeter Investigation of Turbulent, Incompressible Flow in an Axisymmetric Sudden Expansion," AIAA Paper No. 87-0119.

Sturgess, G. J., 1979, "Premixed Prevaporized Combustor Technology Forum," NASA Report CP-2078.

Sturgess, G. J., and Syed, S. A., 1985, "Calculation of Confined Swirling Flows," AIAA Paper No. 85-0060.

Sturgess, G. J., Syed, S. A., and McManus, K. R., 1986, "Importance of Inlet Boundary Conditions for Numerical Simulation of Combustor Flows," *International Journal of Turbo & Jet Engines*, Vol. 3, pp. 43–55.

Sturgess, G. J., Roquemore, W. M., and Lesmerises, A. L., 1989, "Enhancement of Computer Simulation as a Combustor Design Tool Through a Lean Blow Out Research Program," in preparation.

APPENDIX B

ACOUSTIC CHARACTERISTICS

OF A RESEARCH STEP COMBUSTOR

By

S.P Heneghan, M.D. Vangsness and D.R. Ballal
University of Dayton, Dayton, Ohio

A.L. Lesmerises
WL/POSF, Wright-Patterson Air Force Base, Ohio

G.J. Sturgess
Pratt & Whitney, East Hartford, Connecticut

Published as AIAA Paper No. AIAA-90-1851, July 1990. To appear in AIAA *Journal of Propulsion and Power.*

ACOUSTIC CHARACTERISTICS OF A RESEARCH STEP COMBUSTOR

S. P. Heneghan[1], M. D. Vangsness[1], D. R. Ballal[1], A. L. Lesmerises[2], and G. J. Sturgess[3]
[1]University of Dayton, Dayton, OH.; [2]WRDC, Wright-Patterson Air Force Base, OH.;
[3]Pratt and Whitney, East Hartford, CT.

Abstract

For a gas turbine combustor, combustion stability and freedom from acoustic coupling are the two essential design requirements. Here, acoustic characteristics of a research step combustor are investigated by measuring acoustic fluctuations, lean blowout, and visual observations of flame behavior. This combustor was designed to serve as a test bed for evaluating lean blowout and refining combustor design modeling codes.

It was found that inlet conditions, combustor geometry and size, and outlet blockage affected the acoustic characteristics. An acoustic isolator in the fuel tube and a step design that eliminated vortex generation at the inlet significantly decreased acoustic coupling. For a long combustor (L/D = 7.3), loud acoustic resonances resembling classic "rumble" were produced. In this combustor dominant frequencies around 55 Hz and 170 Hz were observed corresponding to eddy shedding from the step and the quarter-wave longitudinal mode respectively. The short combustor (L/D =3), simply did not exert enough back pressure to confine a steady burning flame. In general, top-hat outlet restrictors produced noisier combustion than orifice plates. Finally, a research step combustor with L/D = 4.9 and fitted with an orifice plate of blockage ratio = 0.45 provided the best combination of LBO and freedom from acoustic coupling. This combustor operated satisfactorily under all the conditions of interest and its LBO performance resembled that of a well-stirred reactor.

Nomenclature

A	=	cross sectional area (o-outlet, c-combustor)
ALP	=	air loading parameter ($\dot{m}/VP^n$)
B	=	outlet area blockage ratio (A_o/A_c)
D, d	=	equivalent diameter, obstacle dimension
f	=	frequency (o-fundamental, h-harmonic)
I	=	intensity, amplitude
L	=	combustor length
LBO	=	lean blowout
LPM	=	litres per minute
$\dot{m}$	=	mass flow through the combustor
n	=	reaction order, number
P	=	pressure
Re	=	Reynolds number
St	=	Strouhal number
U	=	mean velocity (a-air, f-fuel, j-jet)
V	=	combustor volume
$\dot{v}$	=	volume flow rate (a-air, f-fuel)
x	=	axial distance
ϕ	=	equivalence ratio
λ	=	wavelength, velocity ratio (U_a/U_f)
ν	=	kinematic viscosity

Copyright © 1990 American Institute of Aeronautics and Astronautics, Inc. All rights reserved.

1. Introduction

An essential requirement in the design of new stoichiometric combustors and high thrust output afterburners is that steady combustion can be initiated and sustained over a wide range of flight conditions. Combustion-induced oscillations commonly known as *rumble* and *screech* severely limit the flame stability range of practical combustors. They can also compromise hot-section durability, induce mechanical vibrations in the engine-airframe components, and couple with the aerodynamics of other engine modules. Therefore, knowledge of acoustic characteristics of combustors is important from a design viewpoint.

The provision of adequate combustion stability, and freedom from acoustic coupling in aircraft gas turbine combustors is a long-term problem that is exacerbated by several current design trends. Further, the solution to this problem is made difficult by deficiencies in present calculation methods and by conflicting design criteria. Therefore, a joint U. S. Air Force, Industry, and University research program is being carried out to (i) study acoustic coupling and its effects upon the combustor performance, (ii) improve understanding of the physical processes involved in lean blowout (LBO), and (iii) evaluate and refine the combustor design modeling codes on the basis of experimental measurements.

In a modern annular gas turbine combustor, flame is stabilized by producing a recirculation zone in the flowfield. As shown in Fig. 1, this zone is formed by a combination of *three* mechanisms, namely an axial swirling air jet associated with each fuel introduction, sudden expansion of the axial swirling jets as they enter the primary zone, and back-pressure provided by an array of radial air jets at the end of the primary zone. To achieve low unburned hydrocarbon emissions, Pratt & Whitney currently tailors these combustor flow control mechanisms to produce an "inside-out" recirculation pattern, as illustrated in Fig. 1. Recently, Sturgess et al. [1] designed and developed a research step combustor that reproduces the recirculation pattern of the practical combustor, and closely simulates those essential features of its flowfield that control flame stability and lean blowout. This combustor is geometrically simple for ease of experimentation and computation, and provides adequate optical access for nonintrusive measurements. Its configuration and dimensions represent a series of compromises between different design criteria.

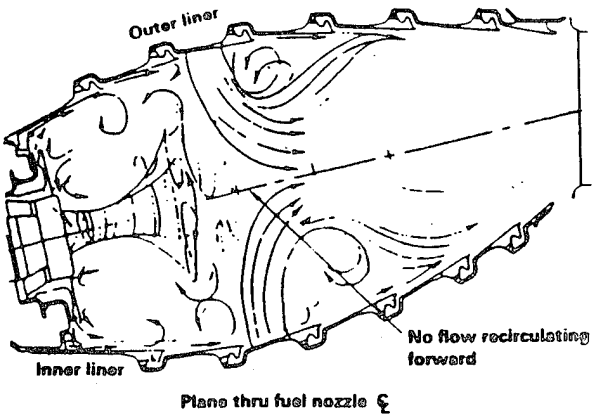

Fig. 1: Flow patterns in a modern annular combustor showing swirl and recirculation dominating the "inside-out" primary zone.

This paper describes *three* design stages in the development of the research step combustor. Acoustic analyses of the combustor prior to its manufacture were made using the lumped impedance-admittance techniques of Putnam [2] and also by the MSC/NASTRAN finite element code. These analyses suggested potentially strong acoustic coupling between the combustor, fuel tube, and the step. Acoustic characteristics of each design configuration were measured and improved upon (decoupled) in the subsequent design stage until a *final* design of the research combustor emerged that was relatively free of acoustic coupling effects. Experimental measurements of acoustic pressure fluctuations, lean blowout, and visual observations of the flame behavior are reported.

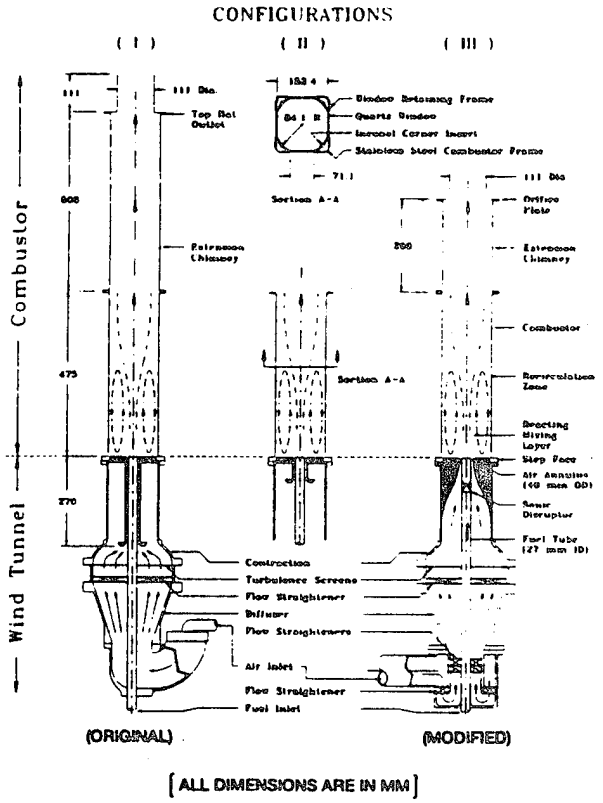

Fig. 2: Various configurations of the combustor, step, and vertical wind tunnel: (a) combustor configuration I-long combustor, (b) combustor configuration II-short combustor, (c) combustor configuration III-final (optimized) combustor.

2. Research Step Combustor

Configurations: Figures 2a-c show *three* configurations of the research combustor, three step designs, and a schematic diagram of the vertical wind tunnel which supplies reactants to the combustor. Common to all the combustor configurations is an arrangement of coannular air (40 mm O. D.) and fuel (27 mm I. D.) jets that feed air and gaseous propane to a 55-mm-wide sudden expansion step. The step establishes a recirculation zone which increases residence time, recycles hot combustion products, and thus provides a source of continuous ignition for the incoming cold reactants. In this manner, a flame is stabilized in the research combustor. The combustor is 475 mm long, 150 mm square cross section with rounded corner fillets of 84 mm radius, and has glass windows on all four sides for optical access. On the top of this combustor sits an inconel chimney extension, of either 508 mm or 260 mm length. The chimney may be fitted, at its exit, either with a top hat (Fig. 2a) or with an orifice plate (Fig. 2c) of different blockage ratios. This outlet restriction exerts a specific amount of back pressure for stabilizing the confined flame.

As illustrated in Fig. 2a, the research combustor is bolted to a 150 mm I. D., 200 mm long tube with a bellmouth annular inlet that supports the step. This tube is mounted on top of a vertical wind tunnel that supplies reactants to the research combustor. Figure 2b shows the research combustor with its plan view and a short inlet step. In Fig. 2c, the combustor is fitted with a short extension, an orifice plate, and a step having a smooth convergent inlet.

Figures 3a-b illustrate the influence of outlet configuration on the static pressure distribution along the combustor wall. Both these figures show plots of $\Delta P = (P_{atm} - P)$ vs. downstream distance. It is evident from Fig. 3b that outlet blockage causes atmospheric pressure to be attained well inside the combustor due to the *vena contracta* formed in the outlet restrictor. This terminates the combustion process and also defines the exit boundary condition for CFD calculations.

In general, combustion in any of the above combustor configurations can exhibit sensitivity to various physical processes such as:

(1) Transition from laminar to turbulent flow due to variation in throughput rate of reactants;

(2) Flame shifts due to pressure gradients created by step size, combustor length, outlet configuration, and stoichiometry;

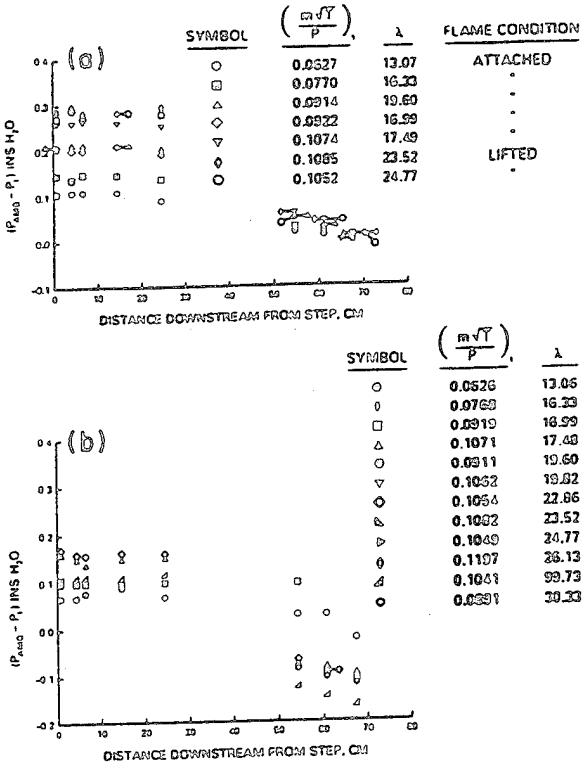

Fig. 3: Axial distribution of wall static pressure for reacting flow: (a) Pressure distribution with free outlet, (b) Pressure distribution with orifice plate (B = 0.45).

(3) Acoustic coupling that depends upon disturbances in the inlet streams, combustor length, inlet/outlet configuration, operating conditions, and flame type and location;

(4) Opposing effects of combustor back-pressure and acoustic resonance in the combustor;

(5) Opposing effects of chemical reaction-rate control and mixing-rate limit for a non-premixed flame.

Past Work: A good deal of research has been performed on the acoustic waves created by combustion in long pipes, multiple-port burners, residential heating units, and oil fired furnaces. This work is summarized by Putnam [2] and others [3-6]. Some of these instabilities can be predicted reasonably well by the Rayleigh criteria [2]. In contrast, practical combustors, some research combustors such as the one under investigation, and afterburners have complex flowfields with recirculation zones and swirl, elaborate fueling arrangements, and cross sections of varying shapes. The acoustics of these devices is unique and depends upon flow pattern, equivalence ratio, and hardware configuration. Research in this area is of relatively recent origin [7-10] and leads to a conclusion that significant differences in acoustic characteristics are realized with even *minor* changes in combustor configuration. Therefore, a combination of careful experimentation and phenomenological analyses was used to investigate the acoustic characteristics and then eliminate acoustic coupling in our research step combustor.

3. Acoustic Characteristics

Experimental Setup: Tests were made of the various research combustor configurations shown in Fig. 2. Gaseous propane and methane were used as fuels. Ignition was accomplished by means of a removable propane torch which protruded through a hole drilled in one wall of the combustor. A steady continuous blue flame filling the combustor indicated good combustion stability and relative freedom from acoustic coupling. The fuel burned in the reacting mixing layer (see Fig. 2c) to which the step recirculation zone fed hot products of combustion. For methane, flame could not be stabilized, even with complete tunnel length and a large outlet blockage. Acoustic frequency spectra were measured using a microphone and Kistler pressure transducers (Model 211 B5 series). These pressure signals were fed into a dual-channel FFT Spectrum Analyzer (Nicolet Model 660) the output of which was connected to a chart recorder (Hewlett-Packard Model HP 7035B). Acoustic spectra were recorded for several combinations of combustor inlet conditions, step and fuel tube designs, combustor lengths (475-983 mm), outlet restrictions (top-hats or orifice plates with B = 0-62%), and fuel and air flow rates given by $Re_a = 2.5\text{-}10.5 \times 10^4$ and $Re_j = 0.37\text{-}1.46 \times 10^4$ respectively.

Vertical Wind Tunnel

Acoustic Characteristics: As seen in Fig. 2, the research combustor-wind tunnel combination has a very complex geometry. Moreover, at an early stage, it was recognized that any air and fuel flow fluctuations produced within the wind tunnel itself would be amplified by the combustion process confined by the combustor. Initially, the wind tunnel shown in Fig. 2a was being supplied with a 25-mm-dia. line dumping air into a 100-mm-dia. U-shaped inlet. Two pressure transducers, one mounted in the wind tunnel air inlet, and the other at its exit, revealed the acoustic spectra shown in Fig. 4. The frequency peaks of 260, 390, 660, and 837 Hz were present in the wind tunnel (Fig. 4a). The amplitude of these peaks increased with an increase in airflow rate. When the research combustor configuration I was mounted on the top of this wind tunnel, additional frequency peak at 55 Hz appeared in the acoustic spectra (Fig. 4b). As will be explained later, this frequency is associated with the eddy-shedding frequency inside the combustor.

Acoustic Sources and Modifications: The acoustic fluctuations in the wind tunnel were traced to three sources, namely (i) sudden expansion of the airflow from the 25-mm-dia. flexible hose to the 100-mm-dia. U-shaped inlet produced extensive and periodic flow vortices, (ii) vortex shedding at the bell-mouthed entrance of the step, (iii) a short aggressive diffuser (area ratio = 2.172, included angle = 15°) which is not uniformly filled with the airflow at its entrance.

To significantly reduce, if not to totally eliminate, these acoustic fluctuations, the following design modifications to the

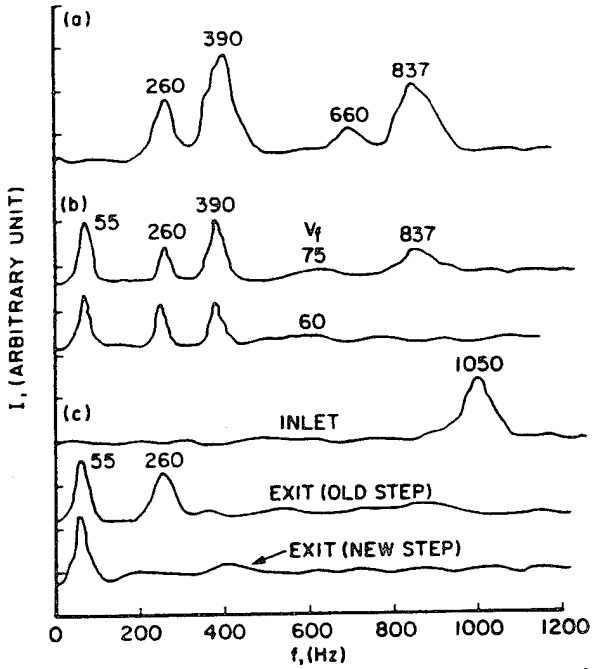

Fig. 4: Acoustic characteristics of the vertical wind tunnel: (a) Wind tunnel only (v_a = 1100 LPM), (b) Wind tunnel + Combustor configuration I + Outlet top-hat (B = 0.45) at v_a = 3200 LPM, (c) Modified wind tunnel (v_a = 3200 LPM)

wind tunnel were made. First, the 25-mm-dia. flexible air supply hose was replaced by a 7-m-long, 100-mm-dia. pipe. This pipe was connected to a newly designed 90 ° air inlet section sketched in Fig. 2c. This modification eliminated any sudden flow expansion and periodic vortex shedding. Second, the step intake length was shortened as shown in Fig. 2b to trap the toroidal shed vortex into a dead space just upstream of the combustor. Finally, an additional set of honeycombs and a flow straightening screen were added, just at the entrance to the short diffuser to improve the inlet airflow distribution. Figure 4c shows the acoustic characteristics of this modified wind tunnel. It can be seen that all frequencies, except the lowest one (260 Hz), have been eliminated.

As for the acoustic peak at 260 Hz, the following explanation is offered: vortex shedding off an obstacle (of the type presented by the bell-mouthed step entrance) usually has a Strouhal number, St = f d/U in the range 0.2 to 0.4. For an annulus air velocity of 35 m/s and the bell-mouth step width of 25.4 mm, vortex shedding frequencies fall in the range 177-354 Hz, or a mean value of 265 Hz represents the vortex shedding frequency of eddies shed off the entrance obstacle. It was recognized that this frequency was sufficiently low to interfere with the acoustic characteristics of our combustor. Therefore, and as shown in Fig. 2c, a new step was designed to eliminate the trapped vortex. Acoustic characteristics measured with the new step in place are plotted in Fig. 4c. These show an absence of any peak at 260 Hz. Finally, this new and modified wind tunnel was employed in the acoustic characterization of the following three combustor configurations.

Combustor

Acoustic Characteristics-Combustor Configuration I: Tests were performed on the research step combustor-configuration I shown in Fig. 2a. Acoustic frequency spectra were recorded for many combustor design and operating variables, such as different fuel and air velocities, fuel tube diameters, extension chimney lengths, and outlet blockage. When the flame was stabilized in the shear layer close to the fuel tube exit, combustion-generated noise increased dramatically. An oscillatory mode of burning was also observed in the vicinity of lean blowout (LBO). This oscillatory cycle comprised flame extinction in the shear layer, downstream re-ignition, flashback, shear layer burning, shear layer extinction, and so on. In the results plotted in Fig. 5, dominant frequencies around 55 Hz, 170 Hz, 390 Hz, and 850 Hz were observed.

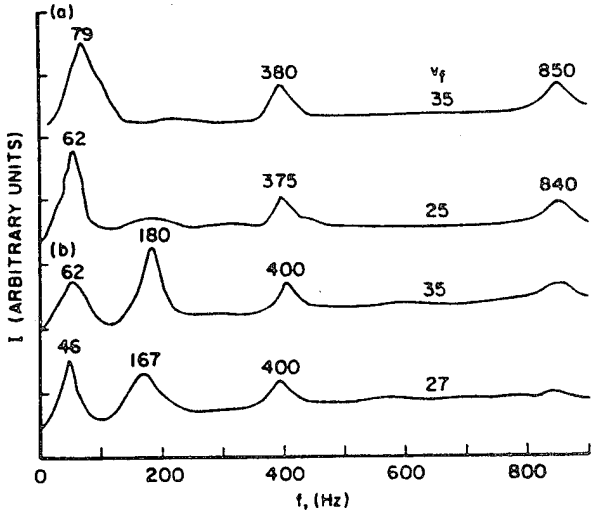

Fig. 5: Acoustic characteristics of the research step combustor configuration I at v_a = 1000 LPM: (a) Top-hat outlet (B = 0.45), (b) Orifice plate outlet (B = 0.45).

Acoustic Sources and Modifications: As described below, the frequency peaks noted in Fig. 5 correspond to eddy-shedding off the step, fundamental quarter-wave longitudinal acoustic mode for the combustor, and the two frequencies originating in the vertical wind tunnel. These latter frequencies coincide with the *calculated* organ-pipe harmonics of the 55 Hz frequency. Thus, the combustor-wind tunnel system was closely coupled and the Rayleigh criterion was being satisfied so that the oscillations were driven [2]. This meant that even the frequencies of 390 Hz and 837 Hz, well suppressed by the wind tunnel design modifications, were slightly augmented by the combustion process. To decrease the magnitude of all the observed acoustic fluctuations, various alternatives were considered, such as switching air and fuel flow lines and designing a tri-jet system. However, it was concluded that the acoustic isolation of the fuel tube from the combustor was the single best modification that would drastically attenuate noise and decrease acoustic coupling. Some experimental evidence that such a modification would work was available in the work of Whitelaw and coworkers [7-9]. These workers found

that by locating an orifice close to the pressure node, in the upstream duct, about one quarter of the wavelength from the dump plane, radiated sound intensity decreased by around 10 dB. Thus, it became clear that our modification should (i) eliminate line-of-sight access between fuel tube inlet and combustor inlet to prevent propagation of acoustic waves, (ii) decrease inlet length and thereby shift acoustic oscillations to higher frequencies, corresponding to the frequency of the quarter-wave mode for the new effective inlet length, (iii) add pressure drop to the fuel system to damp the acoustic over-pressure propagating from the combustor.

Various acoustic isolation schemes such as plugging the fuel tube with steel wool and/or ball (BB) shot were tried. Although these damped the acoustic fluctuations satisfactorily, they would not pass LDA seed particles through the tube. Finally, a perforated conical cap was designed as shown in Fig. 6, and fitted inside the fuel tube about 125 mm upstream of its exit. This device was very successful at acoustically decoupling the fuel tube from the vortex shedding frequency of 55 Hz in the main combustor. It significantly reduced the combustor noise and vibration. However, there was a trade-off in that the 125 mm (12% tube length) section of the fuel tube is still acoustically coupled. This length of the fuel tube is required for the fuel flow to develop a uniform velocity profile prior to issuing out into the combustor.

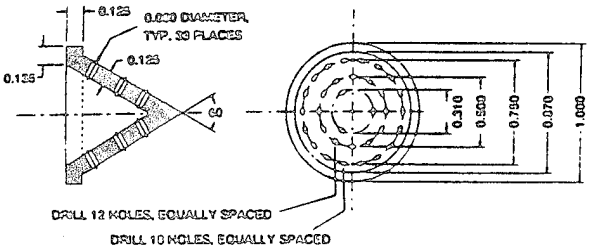

Fig. 6: Sketch of a perforated conical cap used for the acoustic isolation of the fuel tube from the main combustor.

Further tests, with the above modifications in place, still produced disappointingly loud acoustic resonance resembling the classic gas turbine combustor *rumble*. Also, the noise level increased with an increase in the reactant mass flow through the combustor, and as LBO was approached. Moreover, it visibly affected the flame lift and stability. Cylindrical combustors with long aspect ratios (L/D > 3) are generally known to be strongly susceptible to classic organ-pipe resonances [10] and lead to interesting side effects such a flame flashback [11].

In their work on axisymmetric dump combustors and gas turbine augmentors, Sivasegaram and Whitelaw [7] and Sivasegaram, et al. [8] have observed rough combustion and low-frequency oscillations around 55 Hz. For combustors with L/D > 6, these authors have suggested that the dominant frequency may be associated either with vortex shedding or with acoustic quarter-waves in their combustor.

The effects of large-scale eddy shedding and the acoustic-vortex interactions produced in Ramjet-type dump combustors are further elucidated by Kailasanath et al. [12, 13] and Schadow et al.[14]. In their earlier work, Kailasanath et al.[12] find a strong coupling between the first longitudinal acoustic mode frequency of 446 Hz and the unforced natural vortex shedding at 405 Hz. In their later work [13], the acoustics of both the inlet and the combustor are coupled. A low-frequency oscillation of 150 Hz, corresponding to the quarter-wave mode in the inlet, is observed and changing the inlet length changes this frequency. The merging patterns of the large-scale shed vortices are modified significantly [13, 14] when either the combustor acoustic mode or the inlet mode is changed.

For the combustor configuration I under study here, small air annulus passage and acoustic isolation of the fuel tube suggest that effectively the combustor dome region is acoustically closed. Depending upon the exit blockage, the combustor exit would be either acoustically open or closed. Assuming a uniform temperature in the combustor configuration I, a quarter-wave longitudinal acoustic frequency of 170 Hz was calculated. This suggests that the lowest frequency of 55 Hz detected by the pressure transducer is *not* the quarter-wave longitudinal frequency.

There is an additional non-stationary process present in the combustor, and that is the eddy-shedding off the step. For a Strouhal number in the range, St = 0.2-0.4, and assuming that the characteristic velocity is equal to the velocity of je shear layer (or annulus air velocity) we obtain the calculate range of eddy shedding frequency as 40-90 Hz. In general and as shown in Fig. 5, increasing the fuel flow (or combusto heat release) pushed the shedding frequency higher (up to 7 Hz) and also increased its amplitude. At high airflow rate (above 2000 LPM) and with large outlet blockage (> 45% shedding frequency was as high as 90 Hz. Without or with to hats (B = 45%), the observed shedding frequency was in th range 45-63 Hz, i. e., the mean observed value was close to 5 Hz. In contrast to the observations of Kailasnath et al. [12 coupling between shedding frequency and the quarter-wav frequency did not occur in our combustor.

Acoustic Characteristics-Combustor Configuration II: T eliminate these resonances, we performed tests with a sho (L/D < 3) configuration II combustor as sketched in Figure 2 These tests were with ϕ = 0.76, Re_a = 24,827, Re_j = 6,027 an U_a/U_j = 26.2. It was observed that peaks in the frequenc spectra for both combustor configurations I and II were th same despite the length reduction which should have produce higher frequencies. Finally, even with a large outlet blockag of 0.62, the combustor behaved as though it had a acoustically open outlet.

When the magnitude of the acoustic phenomena considered, the amplitude of lowest frequency of 55 Hz w almost 5-10 times lower for a short combustor than for a lor

combustor. For both the combustors I and II, amplitude of low frequency peaks sharply at the 45% outlet blockage condition. Now, since any resonance is destabilizing, it was expected that the shorter combustor (configuration II) would exhibit better stability than the longer combustor (configuration I) and LBO's would be clear and consistent. In practice, while the latter observation is found to be valid, the results of Fig. 7 show stability trends opposite to what was expected. A main reason is that the configuration II combustor was too short to contain the flame for equivalence ratios greater than lean blowout, and considerable back pressure was required to sustain burning in the combustor. Both Sivasegaram and Whitelaw [7] and Sivasegaram et al. [8] make similar observations with regard to flame holding in a short combustor (L/D < 2). For this reason, combustor configuration III of Fig. 2c was finally examined.

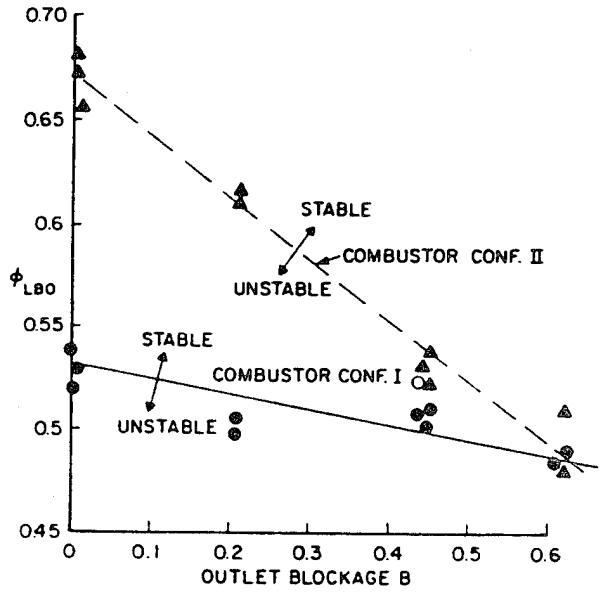

Fig. 7: Combustion stability (as measured by ϕ_{LBO} vs. B) of combustor configurations I and II in the near-turbulent flow regime (Re_a < 23,000). Note that m/VP^2 (U_a -U_f/U) = 0.8 configuration I and = 1.6 for configuration II.

Acoustic Characteristics-Combustor Configuration III: In all the tests, we observed that this combustor configuration operated at significantly reduced noise levels and exhibited much steadier combustion. As seen in Fig. 8a, acoustic spectra showed that the quarter-wave longitudinal mode frequency increases from 190 Hz to 222 Hz as the fuel flow is increased above its value for the LBO. These observations essentially remained valid even when the airflow was increased and when the shorter extension chimney was fitted with different outlet blockage (see Fig. 9). Figure 8b shows a comparison between the acoustic characteristics of combustor configurations I and III. It is observed that for combustor configuration III, peaks in the acoustic spectra exist at significantly higher frequencies, well above the eddy shedding frequency. This acoustic decoupling greatly attenuates the low-frequency *rumble* in this combustor configuration III. Moreover, for airflow rates all the way up to 7,000 LPM, combustor configuration III maintained a marked reduction in acoustic output at the step shedding frequency. Therefore, this configuration was adopted for further studies on the choice of a suitable combustor outlet configuration.

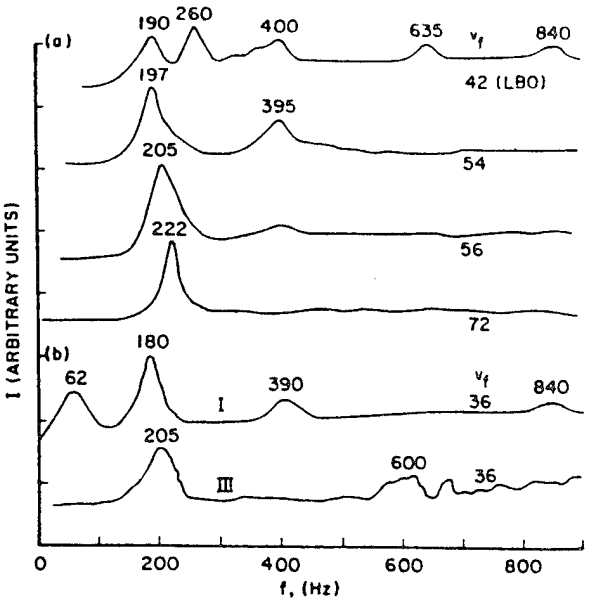

Fig. 8: Acoustic characteristics of the research step combustor configuration III with an orifice plate outlet (B = 0.45): (a) Effect of increasing the fuel flow rate at v_a = 2000 LPM, (b) Comparison of combustor configurations I and III at v_a = 1500 LPM.

Outlet Configuration: In deciding the optimum combustor outlet configuration, whether fully open, orifice plate, or short top-hat, the following *four* positive and *three* negative considerations come into play:

(1) back pressure stabilizing the flow in the step recirculation zone,

(2) outlet restriction accelerates the flow and terminates the chemical reactions for fuel-lean mixtures,

(3) top-hat configuration imposes the zero streamline gradient exit boundary condition for CFD calculation,

(4) the top-hat behaves as a high impedance to low-frequency pressure changes,

(5) outlet restriction necessitates additional combustor length to prevent the exit streamline curvature from influencing the step recirculation zone,

(6) outlet restriction produces acoustically closed exit boundary,

(7) outlet restriction provides a hot, potential source of reignition at LBO.

The combustor was run with three outlet configurations: free (B = 0), orifice plates (B = 0.45, 0.62), and top hats (B = 0.45 with L/D = 1 and 2.1). The following observations were made.

In general, the top hats resulted in noisier combustion than did the orifice plates. In Fig. 9, it is seen that for equal outlet blockage (i) orifice plate produced a broader acoustic frequency spectrum than the top-hat outlet, (ii) for an orifice plate, peaks in the acoustic spectra (205 Hz and 600 Hz) were found at a higher frequency than for a top-hat (140 Hz and 515 Hz). For an outlet blockage of 62%, both, top-hat and orifice plate were so loud that the combustor could not be operated comfortably over a long period.

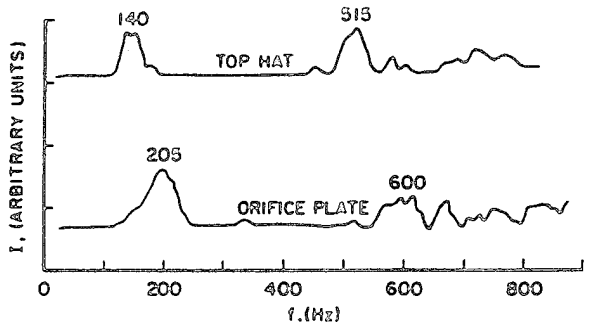

Fig. 9: Acoustic characteristics of top-hat and orifice plate outlet restrictions of same blockage ratio (B = 0.45) for combustor configuration III (v_a = 1500 LPM, v_f = 36 LPM).

Given the propensity of the top-hat restrictors to produce large acoustic fluctuations with strong peaks, and the requirement of the combustor to provide flame stability over a broad range of air and fuel flows, a choice of orifice plate with B = 0.45 was made. This choice was dictated by the conflicting requirements of low noise (B < 0.62), good flame stabilization (B > 0.21), and for achieving fully turbulent burning conditions without producing axial instability of the flame or LBO. In this way, the final configuration of the combustor for stable operation and relative freedom from acoustic coupling was arrived at.

4. Combustor Performance

Lean Blowout: The research combustor was designed to study LBO and other combustion processes such as attached flame, lifted flame, and large-scale axial instability eventually leading to LBO. Accordingly, visual observations of the flame, and a series of measurements of LBO, wall static pressure distribution, and wall temperature distribution were made. A wide range of fuel and air flows from semi-laminar to fully turbulent regime (Re_a = 2.5-10.5 x 10^4, and Re_j = 0.37-1.46 x 10^4) were investigated.

Figure 10 illustrates the LBO vs. air loading parameter (ALP) characteristics of this combustor. These values of LBO are in general agreement with experimental data from other well-stirred reactors [1]. Also, they are lower than the LBO values for combustor configurations I and II. This is because the acoustic fluctuations present in combustor configurations I and II augment flame instabilities in the combustor and cause premature LBO.

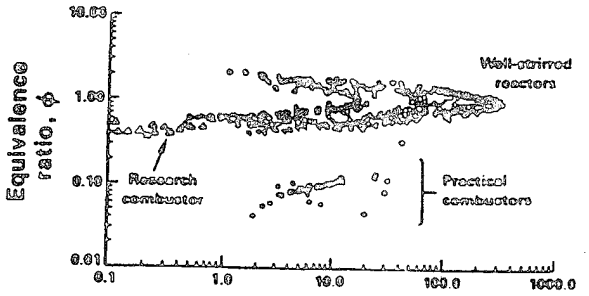

Fig. 10: Lean Blowout performance of the research step combustor as compared with the well-stirred reactor and practical gas turbine combustors.

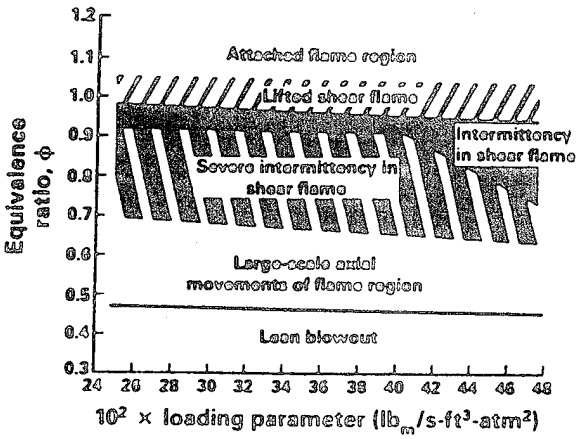

Fig. 11: Research step combustor performance illustrating the different flame regimes that eventually lead to LBO.

Flame Regimes: The flame features that appear in the combustor prior to LBO are sketched in Fig. 11. At a given airflow or ALP, a corresponding fuel flow can be found at which a distinct flame attaches itself around the inner edge of the step. This so called "attached flame" region is realized in our combustor for or above stoichiometric overall equivalence ratios. Also, the flame attachment is found to be very sensitive to acoustic fluctuations. An intense blue annular flame, in contact with the attached flame and anchored by it, appears in the jet shear layer region. The resultant flame structure has the appearance of an inverted "classic coke bottle" shape and is remarkably stable a little downstream of the confluence of the fuel and air jets. As the overall equivalence ratio falls below 0.9, the lifted shear flame develops severe intermittency, becomes ragged in appearance, and resembles a typical "turbulent flame brush." Below ϕ = 0.65, large-scale, oscillatory axial movement of the flame begins and this

eventually leads to LBO. Finally, as the ALP is increased, it is seen that the limits of each region are narrowed, each region intrudes sharply into the adjacent region, and eventually LBO occurs almost instantaneously.

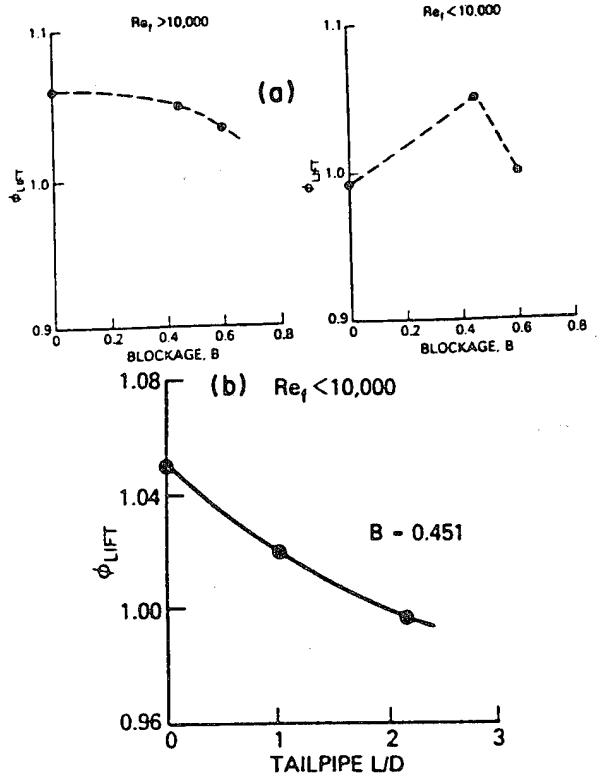

Fig. 12: Effect of outlet blockage, B on equivalence ratio for flame lift: (a) Orifice plate blockage, (b) Influence of top-hat aspect ratio.

The flame characteristics shown in Fig. 11 are influenced by the outlet blockage and the type of this blockage. For example, Fig. 12 compares equivalence ratios at flame lift for orifice blockage and for top-hat L/D at fixed blockage. These results show that the 45% blockage top-hat with a L/D = 2.11 and a 60% blockage orifice plate have the same ϕ_{lift}. Figure 13 shows the effect of orifice blockage on the equivalence ratio for the onset of large-scale axial movements of the flame that are an immediate precursor to blowout. A comparison between the data plotted in Figs. 12 and 13 shows the stabilizing effect of back pressure on combustion (low ϕ_{lift}) and the destabilizing effect of increased acoustic activity (high ϕ_{axial}).

5. Concluding Remarks

In this paper, we explored *three* combustor configurations and found influences of combustor upstream conditions, combustor geometry, combustor outlet blockage, and, to a minor extent, fuel/air flow conditions, on the acoustic characteristics of a research combustor. Broad similarities to the observations of other researchers [7, 10, 13, 14] were noted, and at the same time acoustic characteristics unique to our research step combustor were highlighted. Since this

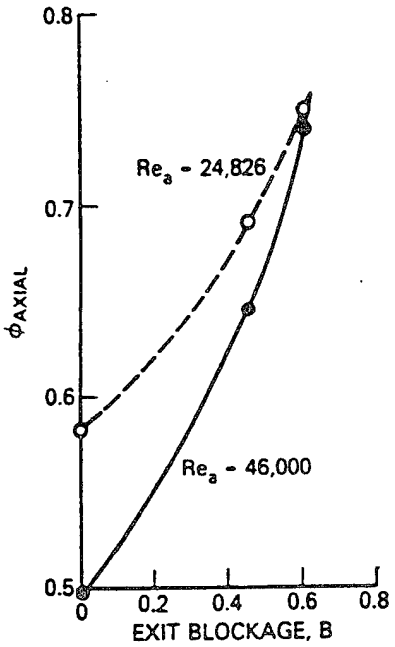

Fig. 13: Influence of orifice plate outlet blockage, B on the equivalence ratio for the onset of axial instability in the lifted flame.

research combustor simulates certain features of a practical gas turbine combustor, similar effects are likely to be present in practical combustors to a varying degree. This is especially disconcerting because the provision of steady combustion and freedom from acoustic coupling are the two main requirements of a good combustor design, be it a swirl combustor [7], a bluff body combustor [8], or a ramjet combustor [10].

We noted that both the fuel supply and the air supply had to be acoustically isolated from the main combustion process to significantly decrease acoustic coupling. In a modern annular gas turbine combustor, air swirl vanes and fuel metering inside the fuel injector provide the necessary acoustic isolation. However, and unless the air supply is sonically isolated from the combustion zone, combustor *rumble* or *screech* may be produced. Generally, the pressure drop across the combustor liner is low enough that the air boundaries for inflow are acoustically soft so that resonances can occur. Next, the aspect ratio (L/D) of the practical combustor should be well below 5 to prevent the generation of acoustic standing waves and quarter-wave longitudinal type resonances. While, the modern annular gas turbine combustor falls well within a safe range of aspect ratio, some types of the newer dual-stage combustors for low exhaust emissions may be approaching the upper limit of the safety criteria. Finally, most practical combustors provide sufficient back pressure to main a stable flame in the combustor. This is achieved by blocking the outlet via a smooth exit contraction or a turbine nozzle stator guide vane. All these design features contribute to producing favorable acoustic characteristics for the practical combustors.

The understanding of the acoustic characteristics of the research combustor and the subsequent development to eliminate spurious interactions have resulted in a vehicle that is well suited for its intended purpose of investigating flame stability with reference to aircraft gas turbine engines.

Acknowledgment

This work was supported by the U. S. Air Force, Wright Research and Development Center, Aero Propulsion and Power Laboratories, under Contract No. F33615-87-C-2767 to University of Dayton, Dayton, Ohio, (Monitor: Dr. W. M. Roquemore) and Contract No. F33615-87-C-2822 to Pratt and Whitney Aircraft, East Hartford, CT., (Monitor: 1Lt. A. L. Lesmerises).

References

1. Sturgess, G. J., Sloan, D. G., Lesmerises, A. L., Heneghan, S. P., and Ballal, D. R., "Design and Development of a Research Combustor for Lean Blowout Studies," ASME Paper No. 90-GT-143, To appear in *Transactions of ASME, Journal of Engineering for Gas Turbines and Power*, 1990.

2. Putnam, A. A., *Combustion Driven Oscillations in Industry*, Elsevier, New York, 1971.

3. Blackshear, P. L., Royle, W. D., and Tower, L. K., " Study of Screeching combustion in a 6-Inch Simulated Afterburner," *NACA TN 3567*, 1955.

4. Kilham, J. K., Jackson, E. G., and Smith, T. J. B., "An Investigation of Tunnel Burner Noise," *Institution of Gas Engineers Journal*, Vol. 1, pp. 251-266, 1961.

5. Marble, F. E., and Candel, S. M., "An Analytical Study of the Nonsteady Behavior of Large Combustors," *Seventeenth Symposium (International) on Combustion*, The Combustion Institute, Pittsburgh, PA, 1978, pp. 761-770.

6. El Banhawy, Y., Melling, A., and Whitelaw, J. H., "Combustion Driven Oscillations in a Small Tube," *Combustion and Flame*, Vol. 33, pp. 281-290, 1978.

7. Sivasegaram, S., and Whitelaw, J. H., "Oscillations in Axisymmetric Dump Combustors," *Combustion Science and Technology*, Vol. 52, pp. 413-419, 1987.

8. Sivasegaram, S., Thompson, B. E., and Whitelaw, J. H., "Acoustic Characterization Relevant to Gas Turbine Augmentors," *AIAA Journal of Propulsion and Power*, Vol. 5, pp. 109-115, 1989.

9. Heitor, M. V., Taylor, A. M. K. P., and Whitelaw, J. H., "Influence of Confinement on Combustion Instabilities of Premixed Flames Stabilized on Axisymmetric Baffles," *Combustion and Flame*, Vol. 57, pp. 109-121, 1984.

10. Crump, J. E., Schadow, K. C., Yang, V., and Culick, F. E. C., "Longitudinal Combustion Instabilities in Ramjet Engines: Identification of Acoustic Modes, " *AIAA Journal of Propulsion and Power*, Vol. 2, pp. 105-109, 1986.

11. Vaneveld, L., Hom, K., and Oppenheim, A. K., "Secondary Effects in Combustion Instabilities Leading to Flashback," *AIAA Journal*, Vol. 22, pp. 81-88, 1984.

12. Kailasanath, K., Gardner, J. H., Boris, J. P., and Oran, E. S., "Numerical Simulation of Acoustic-Vortex Interactions in a Central-Dump Ramjet Combustor *AIAA Journal of Propulsion and Power*, Vol. 3, pp. 525-533, 1987.

13. Kailasanath, K., Gardner, J. H., Boris, J. P., and Oran, E. S., "Acoustic-Vortex Interactions and Low-Frequency Oscillations in Axisymmetric Combustors," *AIAA Journal of Propulsion and Power*, Vol. 5, pp. 165-171, 1989.

14. Schadow, K. C., Crump, J. E., Mahan, V. A., Nabity, J. A., Wilson, K. J., and Gutmark, E., "Large Scale Coherent Structures as Drivers of Ramjet Combustion Instabilities," *1985 JANNAF Propulsion Meeting*, 1985.

APPENDIX C

ISOTHERMAL FLOW FIELDS IN A RESEARCH COMBUSTOR FOR LEAN BLOWOUT STUDIES

By

G. J. Sturgess
Pratt & Whitney, East Hartford, Connecticut

S.P. Heneghan, M.D. Vangsness and D.R. Ballal
University of Dayton, Dayton, Ohio

A.L. Lesmerises
WL/POSF, Wright-Patterson Air Force Base, Ohio

Published in Trans. ASME, *Journal of Engineering for Gas Turbines and Power,* Vol. 114, No. 2, April 1992, pp. 435-444.

G. J. Sturgess
Pratt & Whitney,
East Hartford, CT 06106

S. P. Heneghan

M. D. Vangsness

D. R. Ballal

University of Dayton,
Dayton, OH 45469

A. L. Lesmerises
Wright-Patterson Air Force Base, OH 45433

Isothermal Flow Fields in a Research Combustor for Lean Blowout Studies

A propane-fueled research combustor has been designed and developed to investigate lean blowouts in a simulated primary zone of the combustors for aircraft gas turbine engines. To understand the flow development better and to ensure that the special provisions in the combustor for optical access did not introduce undue influence, measurements of the velocity fields inside the combustor were made using laser-Döppler anemometry. These measurements were made in isothermal, constant density flow to relate the combustor flow field development to known jet behavior and to backward-facing step experimental data in the literature. The major features of the flow field appear to be consistent with the expected behavior, and there is no evidence that the provision of optical access adversely affected the flows measured.

Introduction

A propane-fueled research combustor (Fig. 1) has been designed (Sturgess et al., 1992) and developed (Sturgess et al., 1992; Heneghan et al., 1990) to investigate lean blowouts in a simulated primary zone of combustors for aircraft gas turbine engines. The fundamental flow and heat release features of a gas turbine combustor primary zone, within which the flame is held, are generated by the geometrically simple design of the research combustor.

The research combustor consists of co-axial jets with a 29-mm-i.d. central fuel jet, surrounded by a 40-mm-dia annular air jet. The fuel is gaseous propane. Inserted inside the fuel tube 5 diameters from the discharge is a perforated conical baffle that serves to isolate the fuel supply acoustically from the combustor (Heneghan et al., 1990). The confluence of the jets is centrally located in a 150-mm nominal diameter duct. The duct is closed at its forward end to give a backward-facing step of 55 mm height. The sudden expansion of the jets caused by the step provides a recirculation region that can stabilize the flame. The duct is usually restricted at its discharge by a 45 percent blockage orifice plate, and has an overall length from step to discharge of 735 mm.

The duct forming the combustor is uncooled and is made in two sections, consisting of a window section of 475 mm overall length and an extension chimney of 260 mm length. Provision for optical access is made in the window section of the duct. The construction of the window section consists of thin, flat quartz windows mounted in a stainless steel frame. The frame establishes reference planes to ensure that the pairs of windows on opposite sides of the combustor remain flat and parallel to each other. The windows themselves are spring-

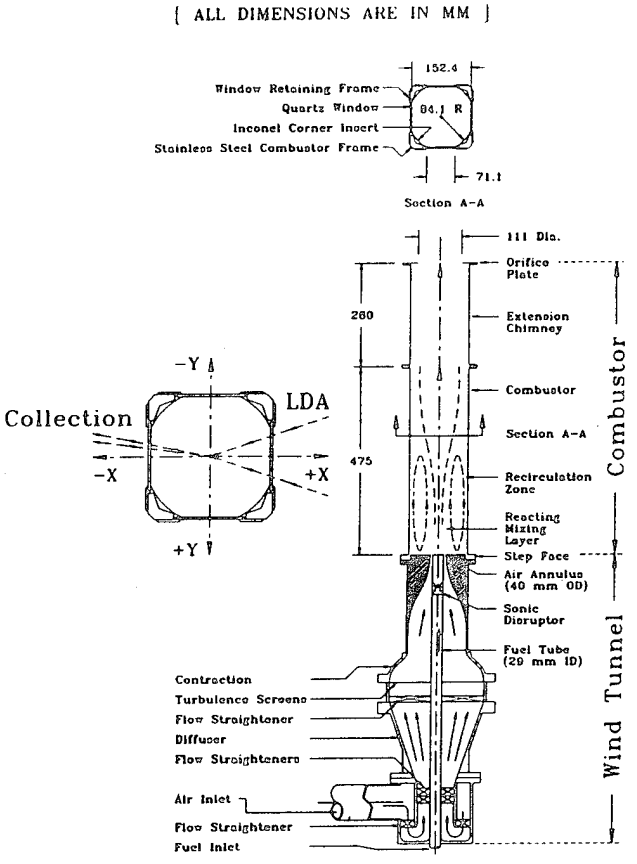

Fig. 1 Research combustor and axis convention

Contributed by the International Gas Turbine Institute and presented at the 36th International Gas Turbine and Aeroengine Congress and Exposition, Orlando, Florida, June 3-6, 1991. Manuscript received at ASME Headquarters February 6, 1991. Paper No. 91-GT-37. Associate Editor: L. A. Riekert.

loaded against the frames by means of 0.81-mm-thick Inconel corner inserts. The windows can float between the spring-loaded corner inserts and the rigid frames, thereby allowing differential thermal growth without stressing the windows.

The construction of the window section results in a duct cross section as shown in Fig. 1. The quartz windows are on a square of 152 mm inside dimension, within which the Inconel corner inserts form a circle of 84 mm. This results in a window width of 71 mm, and the length of the windows is 457 mm. The cross section of the window section is duplicated in the extension chimney, fabricated of Inconel.

The hybrid cross section of the combustor described above represents a hard-won compromise between the demands for geometric simplicity and flow two dimensionality, and the need for straightforward optical access to allow use of laser diagnostics. The flat windows avoid laser beam distortion, while the corner fillets distribute vorticity generation and reduce secondary flow developments due to interaction of the wall boundary layers on the flat windows. If unaddressed, corner-derived secondary flow vortices could influence combustion stability by providing spurious flame holding.

While the cross section of the combustor was designed to ameliorate the magnitude of secondary flow developments, it is not possible entirely to eliminate the local concentrations of vorticity where the circular-arc corner fillets run into the flat windows. However, the vorticity should be reduced in strength and distributed to a degree that secondary flow development does not substantially influence the bulk flow development in the combustor. While computational fluid dynamics (CFD) analyses showed that the introduction of the corner fillets resulted in the anticipated favorable modification of flow behavior, it was still necessary to demonstrate experimentally that such is the case. To this end, velocity field measurements were made in the combustor under isothermal, constant-density conditions. These measurements also serve to contribute to the understanding of the flow development in the combustor; in addition, they provide initial condition information and baseline data for testing subsequent CFD analyses employing blowout models being developed as part of this research.

LDA Arrangement

A custom-designed laser-Döppler anemometer (LDA) system was used for all the velocity measurements. The LDA uses the green (514.5 nm) and blue (488 nm) lines of a 15-W argon-ion laser as a source; two measurement channels of this system were separated by polarization, while the third uses the blue beam. The third channel optics were set up normal to the two-channel optics, and the scattered signal was collected in a forward direction at 10 deg off-axis. The effective probe volume was $50 \times 300 \times 750\ \mu m$. The instrument incorporates Bragg cells with a 5 MHz frequency shift for unambiguous measurements in recirculatory flows. A unique three-channel coincidence circuit with a 10 μs window for rapid validation of acquired data was also incorporated. This assists the integration of the LDA with CARS, Raman, or Rayleigh spectroscopic techniques to be used later with reacting flows.

A proprietary fluidized-bed seeder was used to inject submicron-sized Al_2O_3 or SiO_2 seed particles into the flowing streams. The primary source of error in the measurements is the statistical bias of the final measured velocity toward higher mass fluxes when number-weighted averages are used to calculate stationary statistics. Chen and Lightman (1985) and Glass and Bilger (1978) have discussed bias correction schemes. Seeding of the fuel and air stream separately and together was investigated. No differences of any significance were seen in the measured velocity profiles.

Scattered signals were detected by TSI Counter Processors, and were processed by custom-designed software to yield intensity, shear stresses, skewness and kurtosis, and pdf's. Typical sampling rates were up to 1 kHz. At each spatial location in the combustor, a total of 4096 realizations were acquired. A portion of these data (up to 2 percent), whose departure from the mean exceeded three standard deviations, was filtered to eliminate spurious signals due to seed agglomeration. Finally, a subroutine was used to correct for any particle and density biasing effect (nonreacting and reacting flows).

Error Analysis. Both the fuel stream and air stream flows were monitored and controlled by separate electronic flow control units to within 2 percent. Also, mass conservation balances in the exit plane of the fuel tube provided an additional cross-check against flow meter readings. After allowing for seeding bias, for single-stream seeding with the relatively high sampling rates used, the uncertainty in the measurement of mean velocity was 1 percent, for rms velocity 5 percent, and for skewness and flatness 7 percent. The long-term repeatability was found to be within 5 percent for the turbulence quantities.

Traverse Axes. The combustor is mounted vertically in the facility (Sturgess et al., 1992) and its centerline constitutes the z axis. Zero z is taken as the plane of the step. The x and y axes are diametral to the combustor cross section, with the x axis aligned with the LDA axis. The axis convention is shown

Nomenclature

a = upstream distance from step, defining effective origin of merged jets
D_L = combustor diameter
h = step height
i, j = Cartesian tensor coordinate directions
l_m = mixing length
L/D = length-to-diameter ratio
M_O/M_I = momentum ratio of outer jet to inner jet
n = exponent in definition of boundary layer velocity profile
R = radius
R_f = fuel tube interior radius
$R_{1/2}$ = radius at which $\bar{u}$ has fallen to $1/2\ \bar{u}_c$
$R_{u=0}$ = radius at which $\bar{u} = 0$
U, U_{AVE} = mass-averaged axial velocity
U_L = mass-averaged axial velocity in combustor
U_I = initial mass-averaged axial velocity of center jet
$\bar{u}$ = time-mean axial velocity
u_{max} = maximum axial velocity in X, Y scan
$\bar{u}_c$ = time-mean axial velocity on combustor centerline
$\bar{u}_{c,min}$ = time-mean minimum centerline axial velocity
u_1, u_2 = maximum and minimum velocity in shear layer
u_f = fuel jet axial velocity
u' = fluctuating axial velocity
$\overline{u_i' u_j'}$ = Reynolds stresses
$\bar{v}$ = time-averaged radial velocity
v' = fluctuating radial velocity
X, Y = diametral coordinate directions
y = distance normal to wall
Z = downstream coordinate direction from combustor step plane
z_p = conditional potential core length
δ = shear layer width
η = dimensionless distance across shear layer
ξ_2 = dimensionless radius

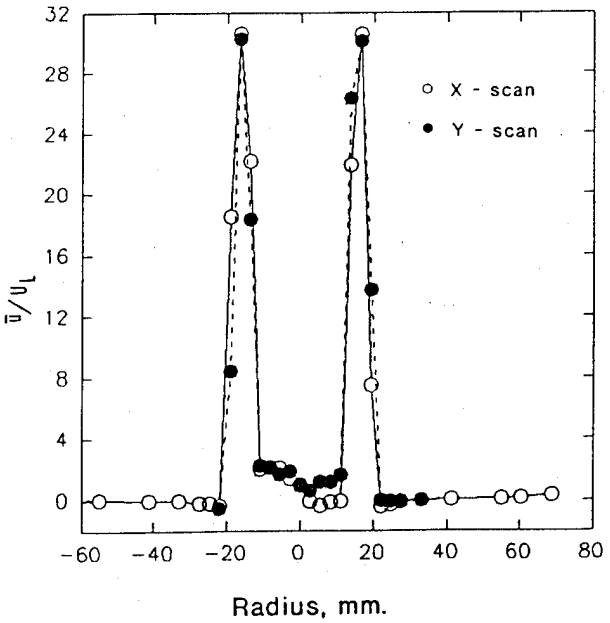

Fig. 2 *X* and *Y* scans of mean axial velocity at $z = 5$ mm with both jets flowing, showing induced asymmetry in central jet

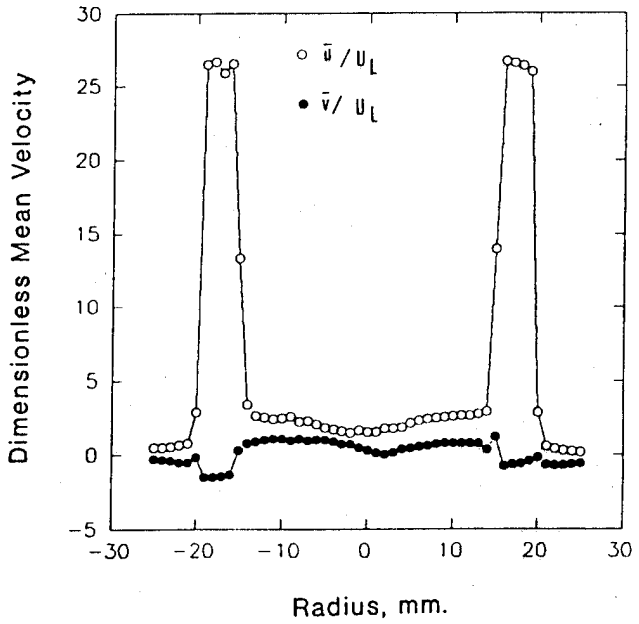

Fig. 3 Increased resolution *Y* scan of mean velocity profiles at $z = 5$ mm; combustor inlet condition

in Fig. 1. Velocities parallel to and increasing in the direction of the z axis, and velocities normal to and directed away from this axis, are also considered positive.

Windows. The geometric window sizes in the combustor, the LDA traverse mechanism (Sturgess et al., 1992), and the LDA beam focusing together define the effective windows within which data may be taken. This access window is given by $-68.7 \le x \le +68.7$ mm, and $-22 \le y \le +33$ mm; in the downstream direction it is $+2 \le z \le +358$ mm.

Test Conditions

Separate diametral traverses of the fuel jet and annular air jet were made by the LDA at the step with the combustor body removed, for a variety of inlet mass flow rates covering fuel jet Reynolds numbers from 1733 to 17,333, and air jet Reynolds numbers from 7233 to 72,322. Air was used for the fuel stream. This information was used to assess the uniformity of the inlet flows.

Detailed diametral traverses (both x and y scans) were made at a number of axial positions, together with a centerline axial traverse, with both jets flowing and the exit orifice plate removed. This information was to be used for comparison with round jet data from the literature. The jet inlet conditions resulted in an air jet Reynolds number of 56,413 and a fuel jet Reynolds number of 11,320 for this test. Some further centerline axial traverses were made at different inlet conditions as part of a study of the near-field jet development.

For reasons of safety and economy, the fuel stream was chosen to be air rather than gaseous propane. On a Reynolds number basis, the conditions at which the majority of the results to be presented were obtained correspond in this simulation to an actual lean blowout point for which the fuel jet is turbulent at inlet (Reynolds number > 9000) with an air jet Reynolds number appropriate to an equivalence ratio of about 0.5. The mass-averaged axial velocities for the fuel jet, air jet, and combustor at this condition are, respectively, 1.98, 20.6, and 3.06 m/s.

Results

Inlet Conditions. With the combustor removed, diametral LDA traverses (y scans) of the fuel jet alone at z of 2 mm from the step were made for several Reynolds numbers. The resulting diametral profiles of time-mean axial velocity were compared with Nikuradse's (Schlichting, 1960) turbulent profile for smooth pipes and Reynolds number around 100,000,

$$u/u_{\max} = (y/R_f)^{1/n} \quad (1)$$

where y is the distance from the fuel tube wall and n was taken as 7. The fluctuating axial and radial velocity profiles were compared with Laufer's (Hinze, 1975) data for smooth round pipes at a Reynolds number of 500,000.

The measured diametral profile of time-mean axial velocity was flatter than that for the familiar seventh power law. The flatness of the measured profile was increased for a Reynolds number of 8665, and reduced for one of 17,333. These changes are in accord with expected behavior (Schlichting, 1960) since the exponent $1/n$ is not constant, and n is a known function of Reynolds number. However, the excessive flatness results because the profile was generated by the acoustic isolator, and the jet does not represent true fully developed pipe flow. A slight asymmetry was observed in the measured data, and this was present over the range of Reynolds numbers.

The turbulence was reasonably isotropic, with higher values occurring toward the edges (wall) of the jet; levels were considerably above those measured by Laufer. For the lower Reynolds number of 8665, the turbulence was clearly anisotropic, but it was isotropic for the higher Reynolds number of 17,333. At the 17,333 Reynolds number, the trend of the fluctuating radial component of velocity with y appeared to be the reverse of Laufer's measurements, i.e., increasing values toward the jet center. Once again, the characteristics were strongly influenced by the presence of the acoustic isolator, which behaved similarly to a turbulence grid.

Velocity profile development in the annular air jet depends on the passage L/D, radius ratio, and weakly on Reynolds number. Although the convergent inlet to the annular jet is so short that the flow could not be fully developed (requiring an L/D of around 70), it was instructive to consider the measured radial profiles of mean axial velocity against the anticipated turbulent profiles.

The appropriate turbulent velocity profile for an annular jet was based on the experimental data of Rehme (1974), corrected to the radius ratio of 0.675 appropriate for the research combustor, and Nikuradse profiles with n appropriate to 60,000

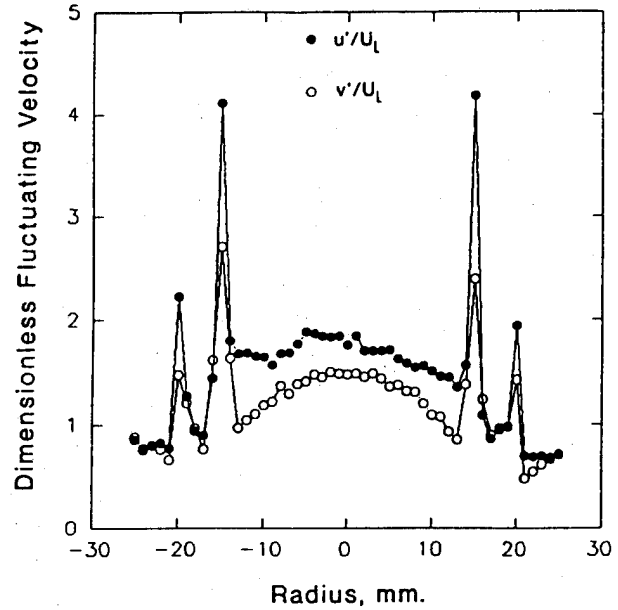

Fig. 4 High-resolution *Y* scan of fluctuating velocity profiles at $z=5$ mm; combustor inlet condition

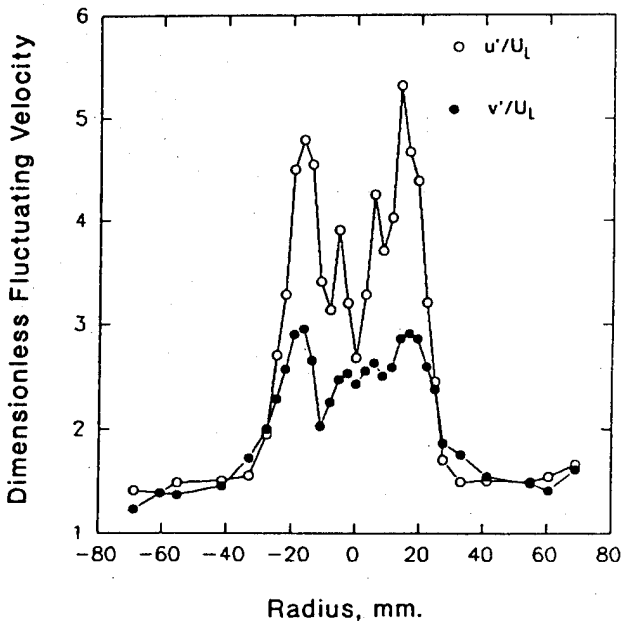

Fig. 6 *X*-scan diametral profiles of fluctuating velocities at $z=55$ mm

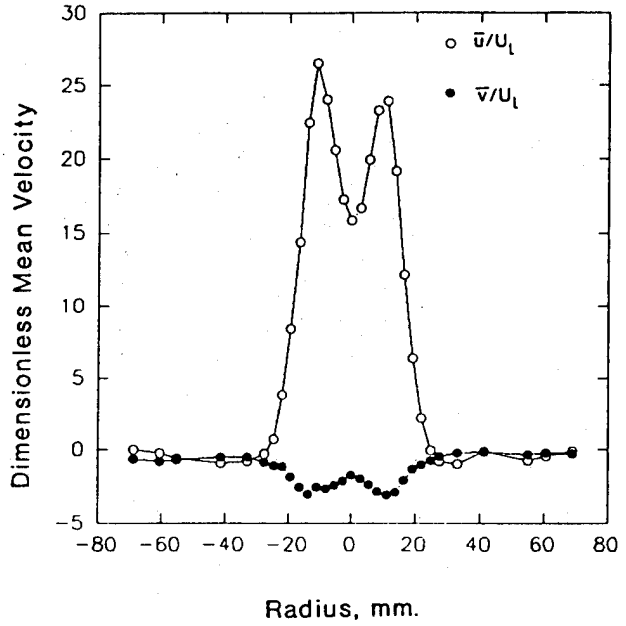

Fig. 5 *X*-scan diametral profiles of mean velocities at $z=55$ mm

Reynolds number. This procedure resulted in a radius at which the profile exhibited its maximum of 16.537 mm, or 46.7 percent of the annular height from the jet inner radius.

The radial profile (y scan) of measured time-mean axial velocities, in the form of $\bar{u}/\bar{u}_{max}$, for a Reynolds number of 83,330, was much flatter than for fully developed flow, and the peak velocity occurred at about 15 mm radius, i.e., inward-peaked compared to anticipation. There was considerable asymmetry across the traverse, with the ratio of maximum time-mean axial velocity to mass-averaged axial velocity, $\bar{u}/U_{ave}$, being 1.214 for negative R and 1.186 for positive R. For an x-scan radial profile, the position of the maximum velocity was at a radius ± 14.6 mm, i.e., slightly more inward-peaked than the y-scan profile, while the values of $\bar{u}_{max}/U_{ave}$ were about 1.23, i.e., slightly more peaked.

The radial profile of local axial turbulence intensity $u'/\bar{u}$ from a y scan at 83,330 Reynolds number, was fairly flat at about 6 percent across the center section of the annular jet. Increases at the edges of the jet were due not only to the mean axial velocities decreasing, but also to an increase in the local fluctuating velocities due to the increased shear generated at the tube walls.

Despite the careful design of the inlet, it is apparent that the annular air jet is not being fed uniformly around its circumference, and that a radial velocity component is being developed that results in an inward flow toward the outer wall of the fuel tube.

With the combustor body mounted on the step, the closest axial station to the step at which LDA data can be taken is 5 mm. At this position with the combustor mounted and both jets flowing, the annular air jet takes control of the fuel jet. This can be seen in Fig. 2 for x- and y-scan diametral traverses, where the time-mean axial velocity divided by the mass-averaged axial velocity in the combustor, $\bar{u}/U_L$, is shown. This traverse is for a fuel jet Reynolds number of 11,320 and an air jet Reynolds number of 56,413. Comparison of the x- and y-scan data in the central region of the traverses reveals that fuel jet profiles have been distorted by the influence of the nonuniform air jet to produce a flow reduction in the $+X$, $+Y$ quadrant (see Fig. 1) that results in a small reverse flow region the x scan. Thus, the relatively minor nonuniformities in the isolated fuel and air jet flows have been magnified when both jets are flowing to result in significant distortion of the lower momentum fuel jet.

Figure 3 is a repeat of the y scan of Fig. 2 at an increased density of measurement; the $\bar{v}/U_L$ profile is also included. The improved resolution of the annular air jet can be seen. These profiles would represent adequate initial condition information for computational fluid dynamics calculations. The appropriate turbulence information is shown in Fig. 4.

General Flow Development. Selected diametral (x-scan) profiles of nondimensional time-average and fluctuating velocities at various axial positions in the combustor, Figs. 5–10, together with Figs. 3 and 4, present the general flow development in the combustor at the selected operating conditions.

The distinct high-velocity co-annular jet and the low velocity central jet (Figs. 3 and 4) quickly merge as the annular jet fills in the velocity defect represented by the central jet (Figs. 5

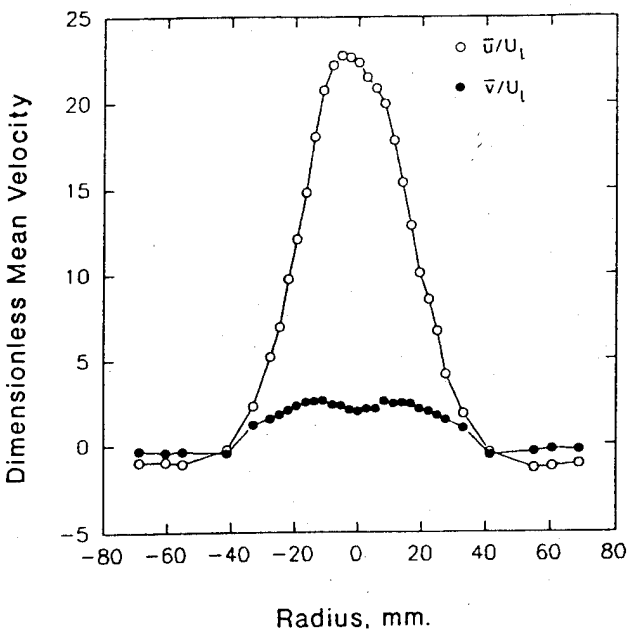

Fig. 7 X-scan diametral profiles of mean velocities at $z = 138$ mm

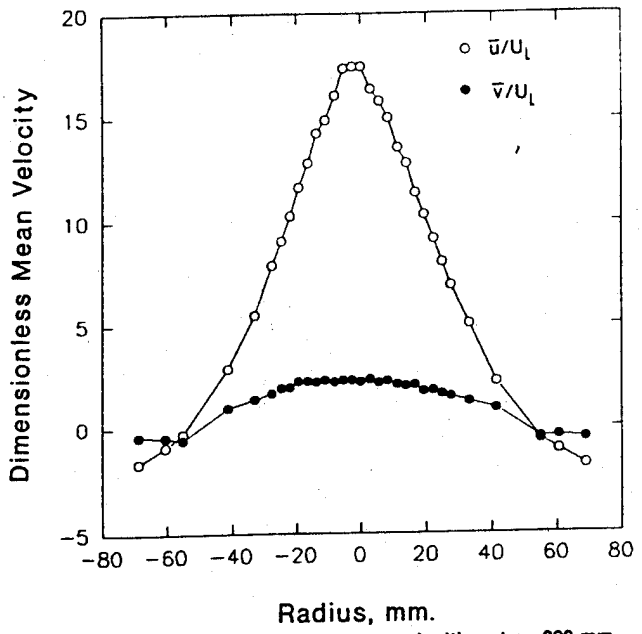

Fig. 9 X-scan diametral profiles of mean velocities at $z = 220$ mm

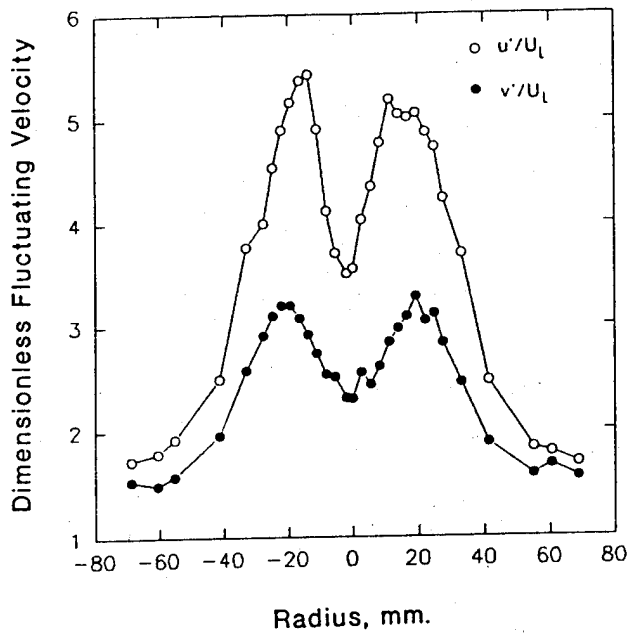

Fig. 8 X-scan diametral profiles of fluctuating velocities at $z = 138$ mm

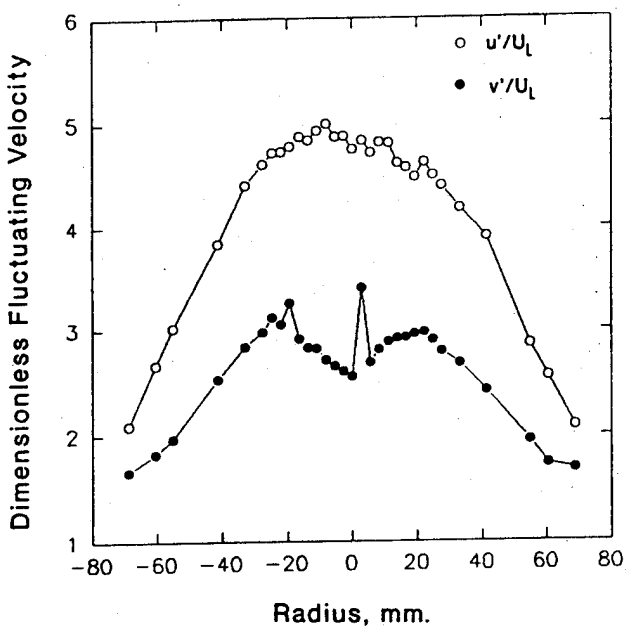

Fig. 10 X-scan diametral profiles of fluctuating velocities at $z = 220$ mm

and 6), and soon have the appearance of a single, central jet (Figs. 7–10). Note that the time-mean axial velocity profile reaches the single jet form (Fig. 7) before the fluctuating velocities do (Fig. 8). At all of the stations shown, the $\bar{u}$ profiles reveal the existence of the recirculation zone associated with the step; the window aperture does not permit full coverage of this region.

Figure 11 represents nondimensional time-averaged axial and radial velocity profiles from a y scan at an axial station of 138 mm. These plots should be compared with those in Fig. 7 (x scan) to obtain an assessment of the downstream asymmetry introduced into the flow by the upstream distortions due to the individual jet irregularities, Fig. 2.

The general characteristics are completed by Fig. 12, which gives centerline traverses of nondimensional time-averaged axial velocity. This shows that the initial momentum difference between the jets is so large that entrainment of the central jet by the annular jet results in the formation of a central recirculation bubble. Centerline axial velocity recovers and then overshoots as the annular jet expands to fill the central velocity deficit. Finally, the centerline axial velocity decays. High fluctuating axial velocities are associated with the fore and aft stagnation points of the central recirculation bubble.

Analysis of Results

Near-Field. The salient features of the near-field velocity development in the research combustor are displayed in Fig. 13, which is constructed from radial profile information.

Shown in Fig. 13 are data points and lines that represent the contours where the time-mean axial velocities are zero. These define the existence of the two recirculation zones noted above; one is associated with the step as expected, and the other on the centerline of the combustor is generated by jet

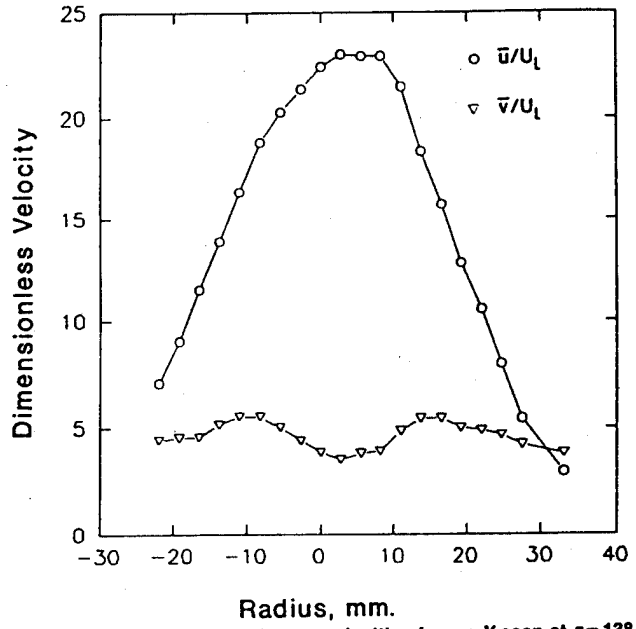

Fig. 11 Diametral profiles of mean velocities from a Y scan at $z = 138$ mm; for an assessment of flow distortion

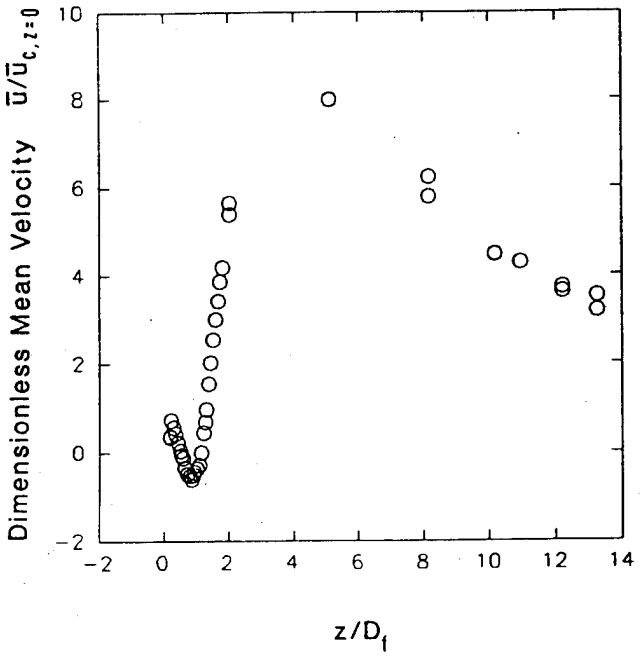

Fig. 12 Variation of axial mean velocity along combustor centerline, showing central recirculation zone

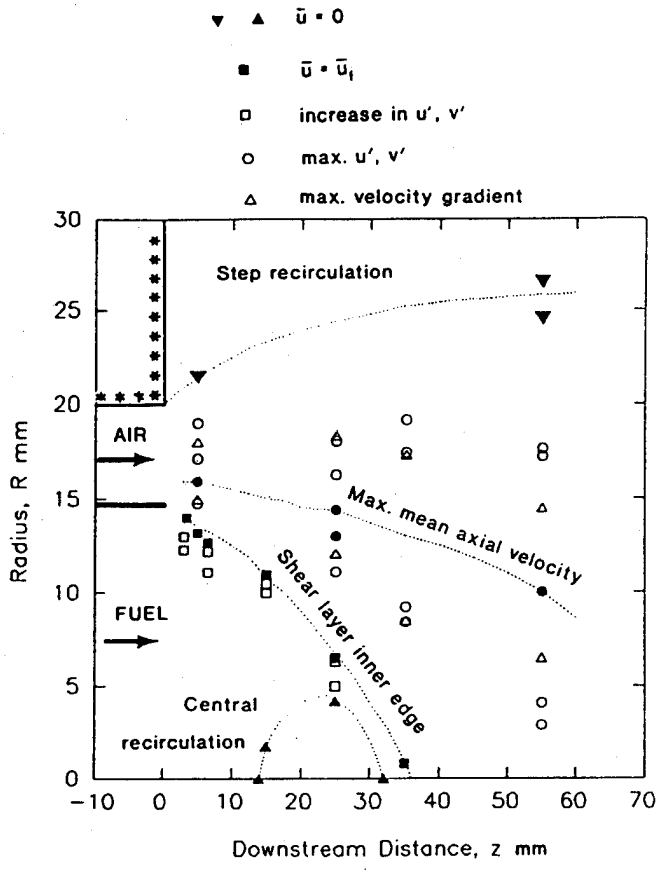

Fig. 13 Salient features of near-field development

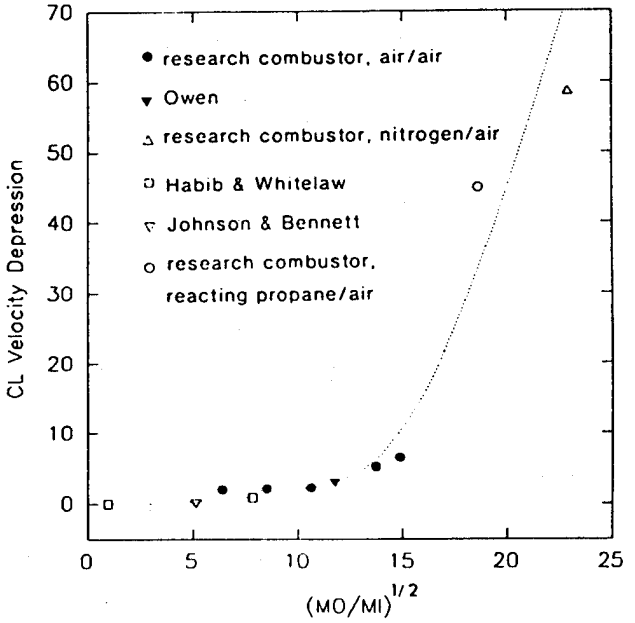

Fig. 14 Dependency of strength of centerline recirculation on jet momentum ratio, and comparison with data from the literature

interaction. These zero mean axial velocity lines delineate the beginnings and ends of the two separated flow regions, but not their radial extents. The central recirculation bubble is positioned on the combustor centerline at 14 mm downstream from the step, and extends downstream for another 18 mm.

Shear layers originate at the confluence of the central fuel jet and the concentric air jet. Shown are lines representing the locus of points where the local mean axial velocity is equal to the fuel mean axial velocity at the step, and also where it is equal to the maximum in the jet shear layer. The position of the inner edge of the jet shear layer can be checked by also plotting the locus of the radii where the fluctuating axial and radial velocity components exhibit a distinct increase from the fuel jet inlet values. This definition of the shear layer inner edge is at consistently reduced radii compared to the former definition.

The downstream distance where the inner edge of the jet shear layer intersects the combustor axis defines a conditional potential core length for the fuel jet. The fact that the fluctuating velocity definition of the shear layer inner edge is at smaller radii than the time-mean axial velocity definition is

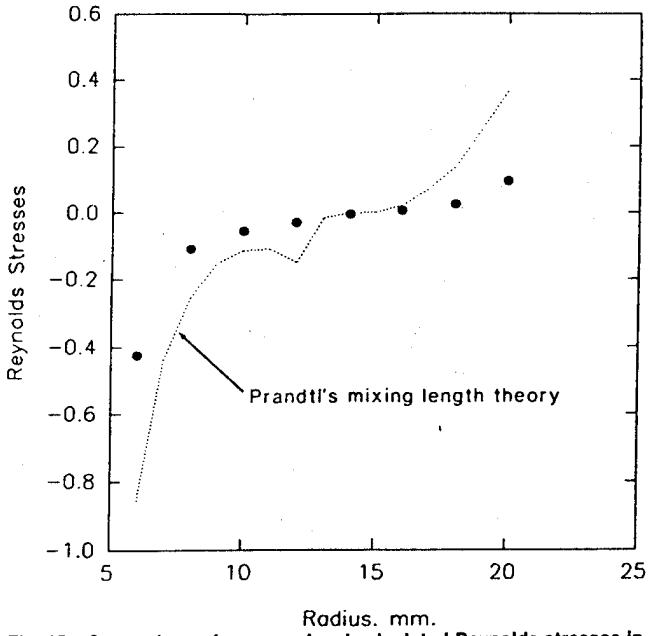

Fig. 15 Comparison of measured and calculated Reynolds stresses in jet shear layers at $z = 25$ mm

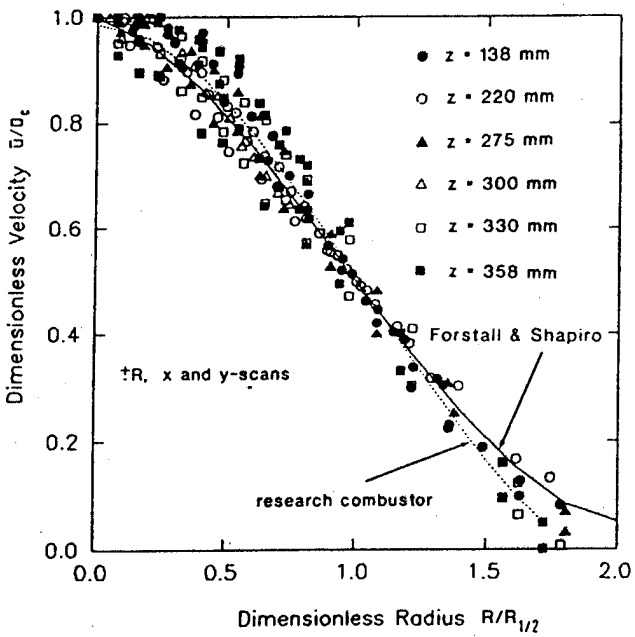

Fig. 17 Self-similarity of mean axial velocity profiles in far-field, and comparison with Shapiro's submerged round jet profile

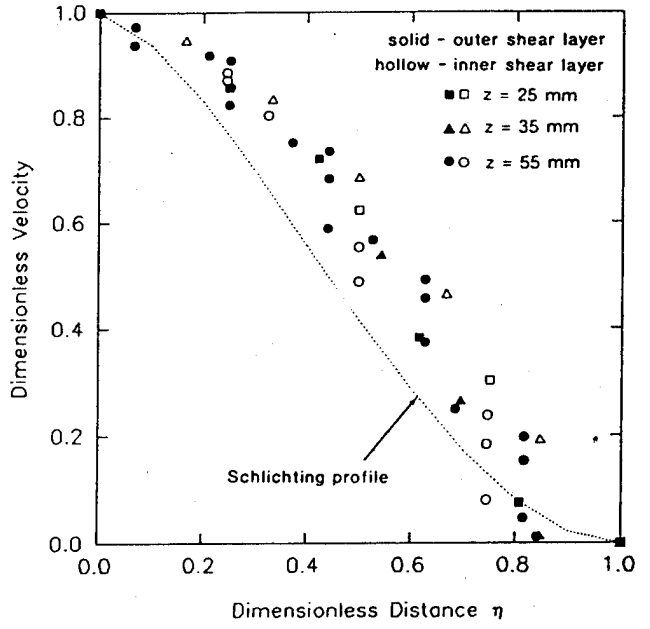

Fig. 16 Self-similarity of mean axial velocity profiles in jet shear layers, and comparison with Schlichting's profile

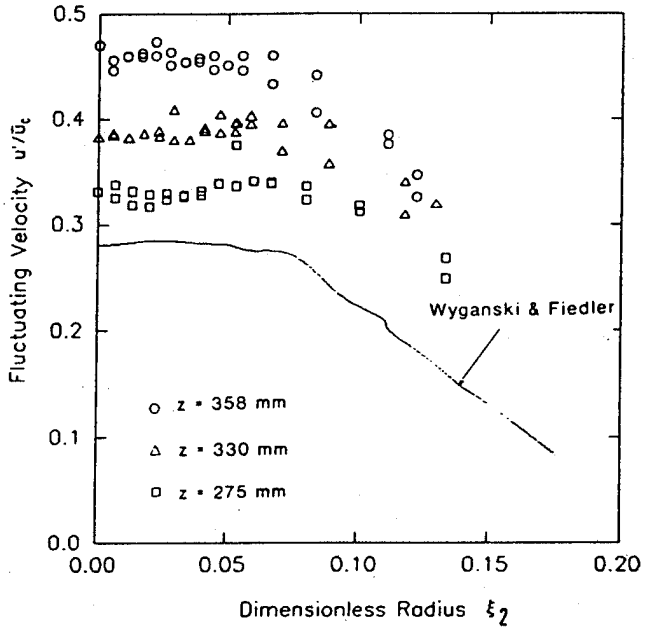

Fig. 18 Self-similarity of fluctuating velocity profiles in far-field, and comparison with Wyganski and Fiedler's free round jet profile

due to the existence of initial turbulence associated with boundary layer buildup on the interior surface of the fuel tube, upstream. Normal shear layer growth is linear, rather than the concave-downward curve seen in Fig. 13. This curvature is induced by the presence of the central recirculation bubble.

The dimensionless potential core length, z_p/R_f, is equal to 2.4. This value is in very good agreement with the theoretical calculations of Abramovich (1963) for coflowing jets with boundary layers.

The momentum difference that exists between the two jets initially results in entrainment of the low-momentum fuel jet by the high-momentum annular air jet surrounding it. The momentum difference is large enough to cause the centerline recirculation zone to form in the fuel jet. The strength of this effect can be characterized by the depression of the initial mean axial velocity on the combustor centerline, $(\bar{u}_{c,z=0} - \bar{u}_{c,\max})$. This velocity difference can be nondimensionalized by the maximum overall change, on a mass-average basis, that the center jet can undergo, i.e., $(U_I - U_L)$. Entrainment considerations would relate this ratio to the square root of the jet momentum ratio M_O/M_I.

Figure 14 is a plot of this relationship for the research combustor at a variety of operating conditions with air/air, air/nitrogen, and air/propane (reacting) flows, and for some similar geometries from the literature, e.g., Habib and Whitelaw (1979), Johnson and Bennett (1981), and Owen (1975). All of the present data points represent actual reverse flow conditions, while Habib and Whitelaw (1979) and Johnson and Bennett (1981) have points in which depression of the initial centerline velocity takes place, but no actual reverse flow occurs. This figure shows good agreement between the present data and those of other researchers.

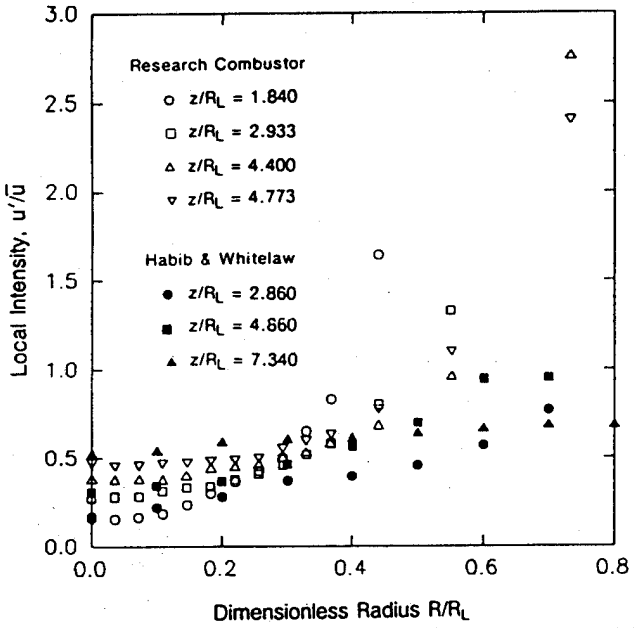

Fig. 19 Comparison of local turbulence intensities for Habib and Whitelaw with research combustor

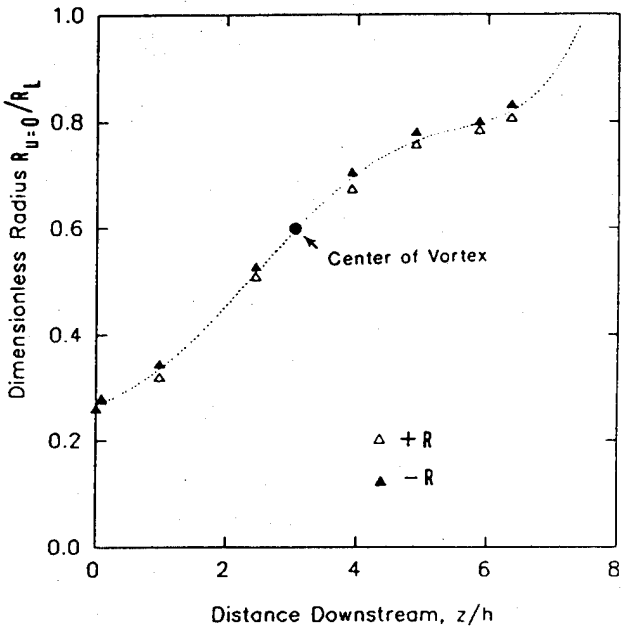

Fig. 20 Definition of step recirculation zone length

When considering Fig. 13, it was found that the locus of the radial positions in the jet shear layer where the fluctuating velocity components u' and v' reached a minimum coincided with the locus of the maximum mean axial velocity, and the maximum values of these components coincided with the loci of maximum velocity gradients in the mean velocity radial profiles. This is the case for a value of z equal to 35 mm, but only reasonably so at a station of z equal to 55 mm. For example, compare Figs. 5 and 6.

The implication of this behavior is that the local turbulence is generated by the local shear, through the local mean velocity profiles. This being so, the Reynolds stresses in the jet shear layer could be described by Prandtl's (1925) mixing length model (Abramovich, 1963),

$$\overline{u_i' u_j'} = l_m^2 \left|\frac{d\bar{u}_i}{dx_j}\right| \frac{d\bar{u}_i}{dx_j} \tag{2}$$

where for round jets the mixing length l_m is given by

$$l_m/\delta = 0.079 \tag{3}$$

and δ is the shear layer width.

Figure 15 compares a Reynolds stress radial profile calculated from Eqs. (2) and (3), and nondimensionalized by the square of measured local mean axial velocity, with the measured profile at z equal to 25 mm. The velocity gradients used in Eq. (2) were obtained from the measured mean velocity profiles.

By a z of 55 mm, the agreement between measured and calculated Reynolds stress profiles is only fair. This must be due to the upstream presence of the centerline recirculation zone, and the fuel jet high initial turbulence due to the presence of the acoustic isolator. By this axial station, the transport of turbulence is apparently becoming important in comparison with local shear generation.

The behavior of the shear layers with respect to Reynolds stresses suggests that the time-mean axial velocity profiles at different axial positions in these layers might be self-similar, that is, of the same shape but differing by a scale factor. To test this, several velocity profiles in both inner and outer layers were plotted in the dimensionless form,

$$\frac{u_1 - u}{u_1 - u_2} = F\left(\frac{y - y_2}{\delta}\right) \tag{4}$$

where u is the time-mean axial velocity in the shear layer at position y; u_1 and u_2, respectively, are the maximum and minimum velocities bounding the shear layer, and δ is its width. Inner and outer shear layer data were obtained from radial profiles at positive and negative radii for x scans and y scans at downstream positions of 25, 35, and 55 mm; the inner shear layer width at any axial position was defined from the positions of maximum jet velocity to that of the fuel jet (see Fig. 13), and the outer shear layer width from the position of maximum jet velocity to the zero velocity line in the step recirculation zone. The shear layer profiles are shown in Fig. 16.

Figure 16 demonstrates that the axial velocity profiles at the three positions downstream collapse onto a common relationship. There is no difference between the inner and outer layers. The flow asymmetries present in the flow should be recalled. The profiles, therefore, may be considered as being similar. Shown also on the figure is Schlichting's classical plane shear layer velocity profile (Schlichting, 1960)

$$\frac{u_1 - u}{u_1 - u_2} = (1 - \eta^{3/2})^2 \tag{5}$$

where

$$\eta = (y - y_2)/\delta \tag{6}$$

The correlated data have the same general form as Eq. (5), but differ from it in fullness. This difference is undoubted y associated with the streamwise curvature of the jet shear laye in the research combustor.

Far-Field. In this region the individual jets interact vigorously with each other and have merged by 138 mm from their confluence (Figs. 7 and 8). Having lost their individuality, subsequent development takes place as though the two jets were a single round jet.

One of the major characteristics of the round jet is the development of self-similar profiles. The condition of similarity in the radial profiles of time-mean axial velocity is examined in Fig. 17 for axial stations of 138, 220, 275, 300, 330, and 358 mm by plotting the dimensionless radial profile of mean axial velocity $\bar{u}/\bar{u}_c$ against $R/R_{1/2}$ where R is radius and $R_{1/2}$ is the radius where the velocity $\bar{u}$ has fallen to one half of its centerline value $\bar{u}_c$. The data for $\pm R$ and x and y scans are included.

Figure 17 contains a line (with correlation coefficient 0.9998) representing Forstall and Shapiro's (Abramovich, 1963) data for submerged round jets with a variety of blowing ratios. A curve fit to the present data agrees excellently with the curve for Forstall and Shapiro's data out to a dimensionless radius of about 1.5, after which the two curves approach their own boundary conditions (i.e., submerging jet or step recirculation).

The effective origin (point source) of the apparent single jet can be found by extrapolating the locus of the radii $R_{1/2}$ for various axial stations backward until it intercepts the combustor axis. This yields an effective origin that is about 140 mm upstream of the step.

With the effective origin of the combined jet so determined, the turbulence profiles in the far-field region can be compared with the self-similar form of the turbulence profiles from Wyganski and Fiedler's round, free jet (Hinze, 1975). The similarity form used is the dimensionless radius ξ_2, where,

$$\xi_2 = R/(z+a) \tag{7}$$

and a is the distance upstream from the physical origin of the individual jets to the effective origin of the merged jets.

Figure 18 compares the dimensionless fluctuating velocity $u'/\overline{u}_c$ against ξ_2 for z of 275, 330, and 358 mm for $\pm R$ from an x scan. The line represents Wyganski and Fiedler's self-similar data to a correlation coefficient greater than 0.999. It can be seen that the turbulence profiles do not collapse onto a similar curve, but increase in intensity with increasing axial position. The behavior for the $v'/\overline{u}_c$ profiles is the same.

The behavior of the present turbulence profiles is in sharp contrast to that of Wyganski and Fiedler's round jet, and is in direct conflict with Fig. 17 where the time-mean axial velocity profiles are shown to be self-similar. The inevitable conclusion from this conflict is that the fluctuating velocity profiles in the far-field are not directly associated with, or derived from, the mean velocity profiles at the same axial station. Thus, for the turbulence field, flow history effects, i.e., convection of turbulence, dominates.

If the turbulence profiles are plotted in the form of a local turbulence intensity $u'/\overline{u}$ and $v'/\overline{u}$ against ξ_2, and compared with Corrsin's isothermal, free, round jet (Hinze, 1975) a similar finding is obtained. The present $u'/\overline{u}$ on the jet centerline is about twice that of Corrsin's jet, while $v'/\overline{u}$ is in better agreement; in both cases the present turbulence intensities increase much more rapidly with increasing dimensionless radius due to the presence of the combustor wall condition.

Despite the turbulence intensities being about twice the free round jet values, they are in accord with what is to be expected for the research combustor geometry. Radial profiles of local turbulence intensity $u'/\overline{u}$ at several axial stations are compared in Fig. 19 with those measured in a similar geometry by Habib and Whitelaw (1979). The increases in intensity at larger dimensionless radii represent falling values of $\overline{u}$ as the inner edges of the step recirculation zone are approached.

Step Recirculation. The downstream extent of the step recirculation zone may be found by tracing the locus of zero axial mean velocity ($R(u=0)$) from the individual radial profile measurements, such as Figs. 5, 7, and 9. This has been done for the x-scan profiles ($\pm R$), which cover a greater radial extent than the y-scan profiles; see Fig. 1. The results are plotted in Fig. 20 in the form of $R(u=0)/R_L$ versus z/h, where R_L is the combustor equivalent radius and h is the step height. The line representing the data is a fifth-order polynomial with a correlation coefficient of 0.9987. A portion of this curve appears in Fig. 13.

Although there are some small differences, the data show that the step recirculation zone development is fairly symmetric about the combustor centerline. The boundary marking the division between upstream and downstream flow exhibits at least one point of inflection. Along this line, the zero velocity point defines the center of the vortex, and this is shown on the figure at about three step heights downstream from the step. The approximate length of the recirculation zone is found by extrapolating the fitted curve to a dimensionless radius of unity. Such extrapolation results in a value of about 7.7 step heights, i.e., a z/D_L of about 3. When this value is compared with the collected step recirculation zone length experience (Morrison et al., 1987) for the test Reynolds number, the agreement is good.

Discussion

Optical access to the research combustor is acceptable and permits the behavior of the flow field to be mapped with reasonable coverage of the important features.

Efforts to condition the inlet flows result in individual jet flows that are reasonably uniform. The provision of a necessary acoustic isolator (Heneghan et al., 1990) in the fuel jet supply tube elevates the central jet fluctuating velocities over what would normally be associated with straight pipe flow and also affect the mean profiles. When the jets coflow and are enclosed, they interact extremely strongly, and the individual jet anomalies are amplified so that the symmetry downstream in the combustor is not especially good. This jet interaction effect is felt in the fuel jet upstream of the step, i.e., before the geometric confluence of the two jets, and it changes the inlet profiles of the central jet from the free-flow ones.

The step generates a large wall recirculation that extends a considerable distance down the combustor. It appears to be fairly symmetric. Jet momentum effects result in the creation of a small, central recirculation just downstream of the fuel jet discharge.

Outside the confines of the step recirculation and downstream of the central recirculation, the jet development takes place apparently largely unaffected by the presence of the recirculation zones. This time-mean development, in both near-field and far-field regions, is self-consistent, and is in good agreement with classical jet and shear layer behavior described through measurements in the literature. The initial turbulence generation in the jet shear layers is in accord with Prandtl's mixing length theory, but downstream of the central recirculation bubble and after the end of the fuel jet conditional potential core, the high initial level of turbulence and the transport of turbulence, i.e., flow history effects, start to dominate. Downstream, the individual jets merge into a single, central jet that has many of the time-mean characteristics of the classic free round jet and the submerged round jet. In this region the turbulence profiles are totally unassociated with the local velocity profiles.

There is no evidence that the special, nonaxisymmetric cross section of the research combustor influences the isothermal flow development to any serious degree. The influence of mass transfer, chemical reaction, and heat release on this flow field development will make an interesting future study.

Conclusions

1 The optical access in the research combustor is adequate to establish the major flow features.

2 Reliable LDA measurements of time-mean and fluctuating axial and radial velocity components have been made for the isothermal flow condition.

3 Three regions of flow development were observed: a near-field region, a far-field region, and a step recirculation region. In the near-field shear layer development leads to a potential core, within which is a recirculation bubble generated by the jet momentum ratio. In the far-field the individual jets have lost their identity and exhibit self-similarity. The step

recirculation bounds the near-field and part of the far-field regions.

4 The component flows that make up the overall flow development within the research combustor are in remarkable agreement with the descriptions provided by classical fluid dynamics.

5 There is no evidence that the presence of the flat optical windows and their interfacing with the corner fillets in the combustor cross section introduce any adverse effects on the flows measured. The cross section used provides a reasonable compromise between flow two dimensionality and optical access.

6 The major time-mean flow features of the research combustor could be calculated by the classical integral techniques of fluid dynamics. This is somewhat surprising. However, the fluctuating velocity fields, except for a very limited initial region, are uncoupled from the time-mean features. Realistic calculation of the complete flow characteristics therefore requires the solution of transport equations.

7 Initial conditions have been established that can be used as the basis for computational fluid dynamic calculations in this combustor.

Acknowledgments

This work was supported by the U. S. Air Force Wright Research and Development Center, Aero Propulsion and Power Laboratory, under Contract No. F33615-87-C-2822 to Pratt & Whitney, East Hartford, CT (Contract Monitor: Lt. A. L. Lesmerises) and Contract No. F33615-87-C-2767 to University of Dayton, Dayton, OH (Contract Monitor: Dr. W. M. Roquemore). The authors wish to thank Dr. Paul Hedman, Brigham Young University, and also staff members of Systems Research Laboratories, Inc., for access to some of their unpublished experimental data obtained in the research combustor, and used in Figs. 3, 4, and 14.

References

Abramovich, G. N., 1963, *The Theory of Turbulent Jets*, M. I. T. Press, Cambridge, MA.

Chen, T. H., and Lightman, A. J., 1985, "The Effects of Particle Arrival Statistics on Laser Anemometer Measurements," ASME FED-Vol. 33, pp. 172-176.

Glass, M., and Bilger, R. W., 1978, "The Turbulent Jet Diffusion Flame in Coflowing Stream—Some Velocity Measurements," *Combustion Science and Technology*, Vol. 18, pp. 165-177.

Habib, M. A., and Whitelaw, J. H., 1979, "Velocity Characteristics of a Confined Coaxial Jet," ASME Paper No. 79-WA/FE-9.

Heneghan, S. P., Vangsness, M. D., Ballal, D. R., Lesmerises, A. L., and Sturgess, G. J., 1990, "Acoustic Characteristics of a Research Step Combustor," AIAA Paper No. AIAA-90-1851, presented at AIAA/SAE/ASME/ASEE 26th Joint Propulsion Conference, Orlando, FL, July 16-18.

Hinze, J. O., 1975, Turbulence, 9th ed., McGraw-Hill, New York.

Johnson, B. V., and Bennett, J. C., 1981, "Mass and Momentum Turbulent Transport Experiment With Confined Coaxial Jets," NASA CR-165574.

Morrison, G. L., Tatterson, G. B., and Long, M. W., 1987, "A 3-D Laser Velocimeter Investigation of Turbulent, Incompressible Flow in an Axisymmetric Sudden Expansion," AIAA Paper No. AIAA-87-0119, AIAA 25th Aerospace Sciences Meeting, Reno, NV, Jan. 12-15.

Owen, F. K., 1975, "Laser Velocity Measurements on Confined Co-axial Jet With Recirculation," AIAA Paper No. 75-d120, 13th Aerospace Sciences Meeting, Pasadena, CA, Jan.

Rehme, K., 1974, "Turbulent Flow in Smooth Concentric Annuli With Small Radius Ratios," *J. Fluid Mech.*, Vol. 64, Pt. 2, pp. 263-287.

Schlichting, H., 1960, *Boundary Layer Theory*, 4th ed., McGraw-Hill, New York.

Sturgess, G. J., Sloan, D. J., Lesmerises, A. L., Heneghan, S. P., and Ballal, D. R., 1992, "Design and Development of a Research Combustor for Lean Blowout Studies," ASME JOURNAL OF ENGINEERING FOR GAS TURBINES AND POWER, Vol. 114, pp. 13-19.

THIS PAGE INTENTIONALLY LEFT BLANK

APPENDIX D

EFFECTS OF BACK-PRESSURE IN A LEAN BLOWOUT RESEARCH COMBUSTOR

By

G.J. Sturgess
Pratt & Whitney, East Hartford, Connecticut

S.P. Heneghan, M.D. Vangsness and D.R. Ballal
University of Dayton, Dayton, Ohio

A.L. Lesmerises and D.T. Shouse
WL/POSF, Wright-Patterson Air Force Base, Ohio

Published in Trans. ASME, *Journal of Engineering for Gas Turbines and Power,* Vol 115, No. 3, July 1993, pp. 486-498

G. J. Sturgess
Pratt & Whitney,
East Hartford, CT 06108

S. P. Heneghan

M. D. Vangsness

D. R. Ballal

University of Dayton,
Dayton, OH 45469

A. L. Lesmerises

D. Shouse

Wright Laboratories,
Wright-Patterson Air Force Base,
Dayton, OH 45433

Effects of Back-Pressure in a Lean Blowout Research Combustor

Experimental information is presented on the effects of back-pressure on flame-holding in a gaseous fuel research combustor. Data for wall temperatures and static pressures are used to infer behavior of the major recirculation zones, as a supplement to some velocity and temperature profile measurements using LDV and CARS systems. Observations of flame behavior are also included. Lean blowout is improved by exit blockage, with strongest sensitivity at high combustor loadings. It is concluded that exit blockage exerts its influence through effects on the jet and recirculation zone shear layers.

Introduction

Combustion stability is extremely important in gas turbine engines for aircraft use. It is becoming more difficult to ensure that adequate stability margins can be maintained because of current design trends toward airblast atomization of liquid fuel, high temperature rise, and low emissions combustors.

As part of a comprehensive research program to investigate, understand, and model lean blowouts in the combustors of aircraft gas turbine engines (Sturgess et al., 1991a), three combustors are utilized. These vehicles consist of a research combustor, a technology combustor, and a generic gas turbine combustor, which reflect the three-phase approach to the problem. The purpose of the research combustor is to yield fundamental information on the lean blowout process to assist in understanding the events taking place during blowout, and so guide in modeling them.

In gas turbine combustor design, it is generally recognized that the end of the flame-holding primary zone is determined by the transverse combustion air jets entering through the combustor liners (Lefebvre, 1983). For combustors using either pure airblast or hybrid pressure-atomizing primary/airblast secondary fuel injectors, it has been observed that dynamic interactions can occur between the axially directed jets of atomized fuel/air mixture from the injectors, and these transverse combustion air jets. Recirculation zones of the "external" (Gupta et al., 1984) or "inside-out" type (Sturgess et al., 1990) seem to be especially prone to this behavior. The interaction can be exacerbated if the airflow through the combustor dome (including the injectors) is a significant proportion of the combustor total flow, and if the transverse air jets are close to the dome.

It was therefore felt that the important back-pressure effect exerted on the flame through the presence of the combustion air jets should be included in any simulation of a gas turbine combustor primary zone.

In the research combustor, which was intended for the study of the breakdown of flame stabilization in the primary zone, the essential features of a typical primary zone of modern combustors were reproduced in simplified form (Sturgess et al., 1992a). Combustion air jets were not included directly due to the complication involved; however, the back-pressure of these jets was represented by means of exit blockage from the combustor.

Research Combustor

The research combustor consists of a central fuel jet of gaseous propane surrounded by an unheated co-axial air jet, with the confluence of the jets centrally located in a nominally circular cross-sectional duct (Sturgess et al., 1992b). The duct is closed at its forward end to give a backward-facing step. The combustor exit is open to the atmosphere; low pressure effects on lean blowout are simulated by means of dilution through injection of excess nitrogen into the air supply (Sturgess et al., 1991b). The combustor is mounted vertically on an

Contributed by the International Gas Turbine Institute and presented at the 37th International Gas Turbine and Aeroengine Congress and Exposition, Cologne, Germany, June 1-4, 1992. Manuscript received by the International Gas Turbine Institute February 6, 1992. Paper No. 92-GT-81. Associate Technical Editor: L. S. Langston.

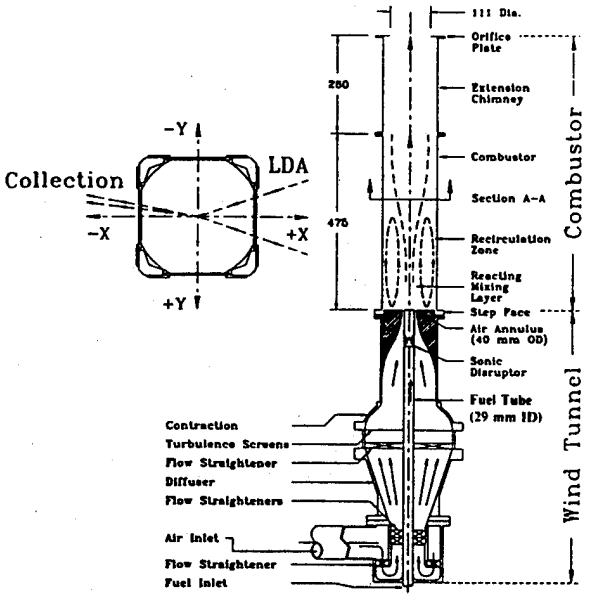

Fig. 1 Research combustor, showing axes convention

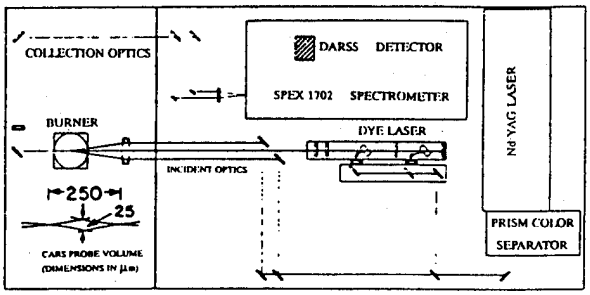

Fig. 2 Arrangement of the CARS system optics

airflow-conditioning unit, which traverses through a cutout in a fixed optical bench, Fig. 1.

The combustion tunnel was designed and constructed in two sections: a fixed upstream window section providing optical access as needed, and a replaceable downstream chimney. The chimney is available in two lengths, and the combustor can be run with either of these, or with no chimney at all. The combustor has a hydraulic diameter of 150 mm, giving length to diameter (L/D) ratios of 3.167, 4.9, and 6.513, respectively, depending on the chimney arrangement. The inner diameter of the fuel tube is 29.97 mm with a 2-deg half-angle taper over 120 mm of its length, and the outer diameter of the air passage at discharge is 40 mm.

Provision is made for combustor exit blockage. The geometric values of exit blockage are 21.0, 45.1, and 62.0 percent of the combustion cross section. These blockages are achieved by means of thin orifice plates. For the 45.1 percent geometric blockage, "top-hat" exits with tailpipe length to diameter (L/D) values of 1.0 and 2.1, respectively, are also available.

The optical windows can be replaced by metal plates containing arrays of thermocouples for wall temperature measurements, and tappings for static pressure measurements. The combustor may be run with any combination of windows and plates.

LDA Arrangement

Mean and fluctuating velocity component measurements are obtained by means of a laser-Döppler anemometer (LDA) system (Sturgess et al., 1992b), using 10-deg off-axis forward scattering. The effective probe volume is 50 × 300 × 750 μm.

The combustor is mounted vertically in the facility (Sturgess et al., 1992a), and its centerline constitutes the z axis, with zero taken as the plane of the step. The x and y axes are diametral to the combustor cross section, with the x axis aligned with the LDA axis. Velocities parallel to and increasing in the direction of the z axis, and velocities normal to and directed away from the axis, are considered positive.

The effective optical window within which data may be taken is defined by: $-68.7 < x < +68.7$ mm, and $-22 < y < 33$ mm; in the downstream direction it is $+2 < z < 358$ mm. This window permits reasonable access to the major flow field features (Sturgess et al., 1992b).

For error assessments, see Sturgess et al. (1992b).

CARS Arrangement

The laser source for the coherent anti-Stokes Raman Spectroscopy (CARS) optics is a Nd:YAG pulse laser with 10 ns time resolution. The frequency-doubled source green beam (532 nm) is equally divided into four parts: two of these serve as pump beams, while the remaining two pump a dye laser oscillator and amplifier. The dye laser is tuned to provide a red broad-band Stokes beam (110 FWHM) centered at 607 nm. The red Stokes beam and the two green pump beams are then focused together by a 25 cm focal length lens in a BOXCARS configuration. A 25 × 250 μm measuring spot size is achieved. The CARS signal is collected by a Spex 1702 spectrometer, 1024-element DARSS camera, and Tracor-Northern multichannel analyzer (Fig. 2). The raw data are processed by a MODCOMP minicomputer.

From the raw data the temperatures are determined by comparing the actual nitrogen spectra to the calculated spectra, using a least-squares fit. The calculation of a nitrogen CARS spectrum requires knowledge of the instrument slit function. Error problems associated with the assumption of a constant slit function when the optical path contains density and/or temperature gradients are avoided by use of a simple method of determining slit functions from the collected data at actual temperature and turbulence levels, by applying local thermodynamic equilibrium principles (Heneghan et al., 1991). This method has been shown to yield improvements in the precision of the CARS measurement (Heneghan and Vangsness, 1991).

Both fuel and air flows were monitored by separate electronic flow control units to within ±0.5 percent and ±1.5 percent, respectively. The combined error produced an uncertainty of ±1.5 percent in equivalence ratio, or ±30 K in temperature. Usually, 500 samples were taken for each CARS measurement to ensure that the error in rms temperature was less than 10 K. The rms temperature is susceptible to CARS instrument noise (Heneghan and Vangsness, 1990). However, in combusting flow the temperature fluctuations are much greater than the instrument noise, and thus the measurement precision (reproducibility) is good. It is estimated overall that the CARS mean temperature measurement accuracy is within 50 K, while the precision is well within 20 K. Unlike the LDA, CARS temperature measurements are time-averaged without density-biasing effects.

Isothermal Flow Field

Development of the isothermal flow field in the research combustor with a free outlet is fully discussed by Sturgess et al. (1992b). Briefly, at a simulated blowout condition, the

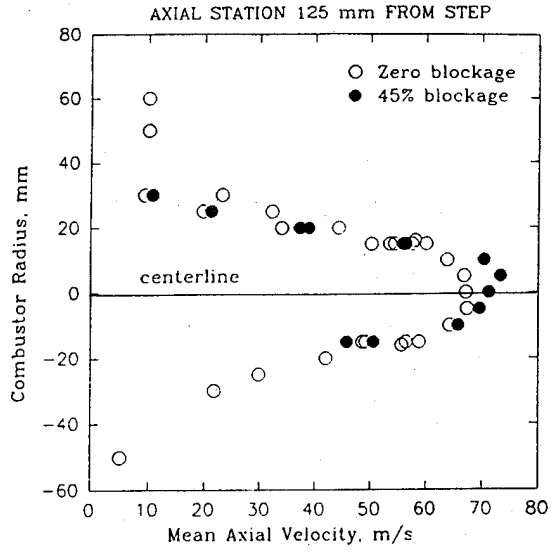

Fig. 3 Radial profiles of mean axial velocity in isothermal flow 125 mm downstream from the step-plane, showing central flow net acceleration with exit blockage

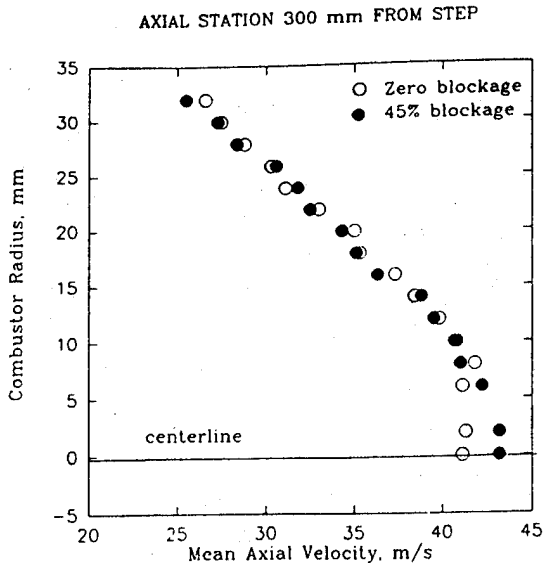

Fig. 4 Radial profiles of mean axial velocity in isothermal flow 300 mm downstream from the step-plane, showing central flow net acceleration with exit blockage

annular air jet immediately entrains the central fuel jet, generating a small central recirculation bubble of length 17 mm with a beginning about 15 mm downstream of the jet confluence. The individual jets thus quickly merge as they expand into the combustor, and soon lose their identities. This merging is complete by 138 mm from the step. The step generates a large recirculation zone of axial length 7.7 step heights, and with vortex centers about 3.1 step heights downstream.

The addition of exit blockage by orifice plate exerts an obvious effect on the radial profiles of mean axial velocity as the flow accelerates along the combustor centerline to form a vena contracta in the exit plane, with a toroidal recirculation zone forming on the forward face of the orifice plate. For the 4.9 L/D combustor the near-field is unaffected, but the centerline flow acceleration is evident as close as 125 mm downstream from the step-plane. Figures 3 and 4 demonstrate this at the 125 and 300 mm stations, respectively, for 45.1 percent blockage. Note that the acceleration effect is ameliorated to some extent by the expansion of the combined jets into the combustor.

There were no changes apparent in the fluctuating velocities with the addition of exit blockage.

The flow field with reaction present is the process of being measured. The features described under isothermal conditions are unchanged in character by the heat release.

Effects of Blockage on Flame Behavior

The research combustor operates with three basic flame conditions, depending on the equivalence ratio. For $\phi > 1.05$ approximately, a thin, sheathlike pilot flame is anchored close to the step near the outer diameter of the air passage (Sturgess et al., 1991b). The fuel source for this pilot flame is the step recirculation zone. The major heat release is then precipitated downstream in more or less distributed fashion, by the action of this pilot. Downstream flame-holding takes place in the shear layers associated with the central and step recirculation zones (Sturgess et al., 1992b). For $\phi < 1.05$ approximately, the pilot flame is highly intermittent (Roquemore et al., 1991), and the main flame is lifted (Sturgess et al., 1991b), allowing considerable premixing of reactants to take place prior to combustion. The lifted flame is positioned between 160 to 300 mm from the step-plane. When ϕ reaches 1.5 to 2.0 and before a rich blowout, a separated flame condition is again established where the pilot flame is no longer apparent to the eye, but the main flame does not lift in this case. It is located about 30 to 40 mm downstream from the step.

Lean blowout data were correlated on the basis of a combustor loading parameter (Sturgess et al., 1991b), derived from reaction rate theory as

$$LP = \dot{m}_{\mathrm{Tot}}/(VP^nF)$$

where for gaseous fuels and with simulation of low pressures by excess nitrogen injection,

$\dot{m}_{\mathrm{Tot}} = \dot{m}_{\mathrm{fuel}} + \dot{m}_{\mathrm{air}} + \dot{m}_{\mathrm{nitrogen}}$

V = reactor volume

P = effective pressure

n = apparent global reaction order

$= 2\phi/(1 + \dot{m}_{\mathrm{nitrogen}}/\dot{m}_{\mathrm{air}})$

ϕ = equivalence ratio

F = temperature correction factor (to 400 K)

$= 10^{0.00143T_{in}}/3.72$

T = inlet temperature of reactants in K.

Use of LP for blowout correlations follows from the adoption of a stirred reactor modeling approach (Sturgess et al., 1992a). It also forms a useful way of characterizing the degree of "flame straining" present in the combustor.

Figure 5 provides a map of flame behavior as a lean blowout is approached, obtained by visual observation. The combustor L/D was 4.9, and the exit was a 45.1 percent blockage orifice plate. Inlet temperatures for the reactants were constant at 293 K, and no excess nitrogen was injected. The Reynolds number of the annular air jet was in the range of 24,800 to 46,000. The attached and lifted flame conditions are illustrated in Fig. 2 of Sturgess et al. (1991b).

The range of the loading parameter in Fig. 5 is such that lean blowouts were obtained close to the flammability limits for propane/air mixtures at ambient conditions (Lewis and

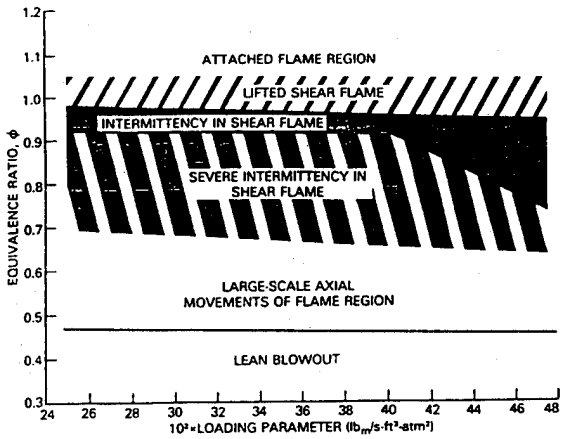

Fig. 5 Flame behavior as lean blowout is approached at low combustor loadings with 45 percent exit blockage

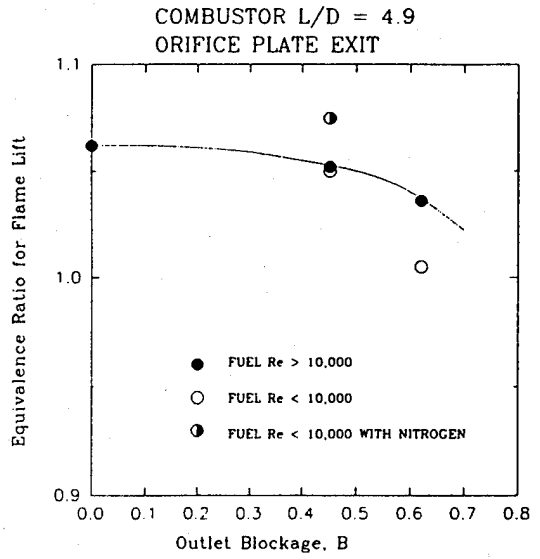

Fig. 6 Dependence of equivalence ratio for flame lift on exit blockage for low and intermediate combustor loadings

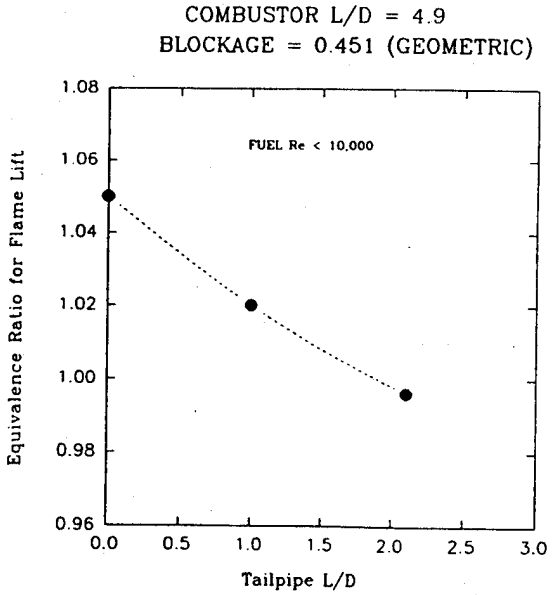

Fig. 7 Dependence of equivalence ratio for flame lift on tailpipe length for 45 percent geometric exit blockage

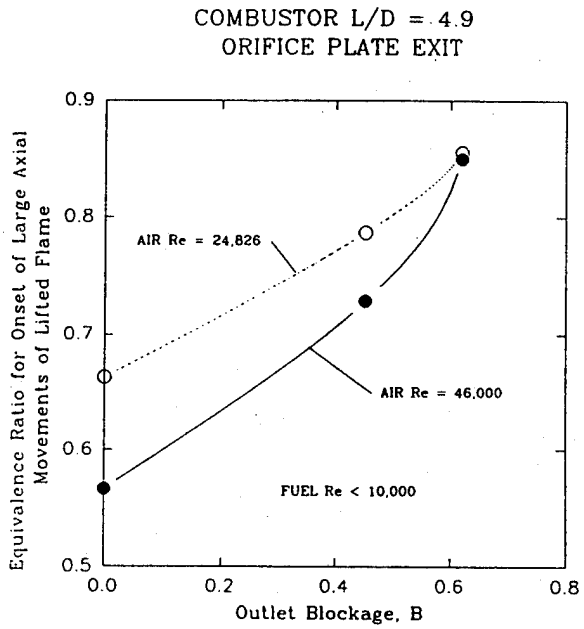

Fig. 8 Influence of exit blockage and combustor loading on equivalence ratio for onset of axial movements of the lifted flame

von Elbe, 1961). The flame behavior seen is both reversible and repeatable. Flame lift can be seen at about 1.05 equivalence ratio, and is insensitive to loading parameter over the limited range covered. Subsequent tests (Sturgess et al., 1991b) with injection of excess gaseous nitrogen into the air stream showed no effects on equivalence ratio for flame-lift. When the fuel flow was progressively reduced at constant airflow, or the airflow was progressively increased at constant fuel flow, the same sequence of flame events leading to a blowout took place. These events are shown in Fig. 5. Eventually, an oscillatory flow situation develops, with large-scale axial movements of the entire lifted flame about a mean position. This motion leads, in due course, to lean blowout.

The existence of the sequence of flame behaviors did not change qualitatively with differences in exit blockage. However, the equivalence ratio for flame lift was observed to decrease slightly with increase in blockage due to orifice plates (Fig. 6). Similar behavior was observed with increase in tailpipe L/D for the 45.1 percent blockage top-hat section (Fig. 7).

The significance of the 10,000 Reynolds number for the fuel jet in Figs. 6 and 7 is that this value represents a critical threshold for transition to turbulent flow for propane (Lewis and von Elbe, 1961).

A fairly strong influence on the equivalence ratio for the onset of the large-scale axial oscillation of the lifted flame was observed, as shown in Fig. 8. Increased blockage raises this equivalence ratio and is therefore destabilizing, opposite to the effect on flame lift. Note the significance of air jet Reynolds numbers.

It is apparent that the loss of the important pilot flame marks the beginning of a lean blowout sequence. A similar importance of the pilot flame is observed as a rich blowout is approached. Figure 9 shows the dependence of rich equivalence ratio for loss of the pilot flame (to result in a separated main flame), on exit blockage in the 4.9 L/D combustor. Note that on the rich side, decreasing equivalence ratio denotes a maximum loss

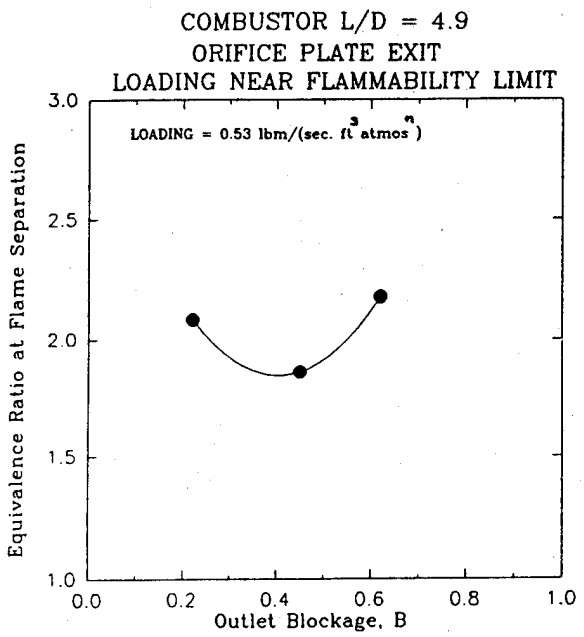

Fig. 9 Dependence of equivalence ratio for flame separation on exit blockage for low combustor loading

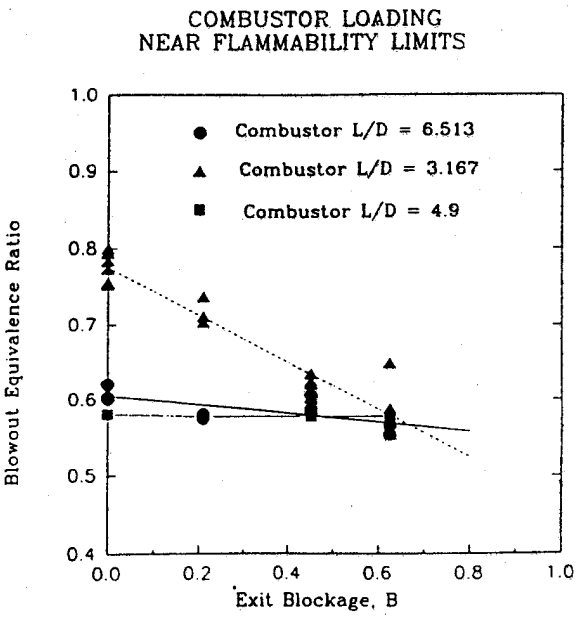

Fig. 11 Influence of exit blockage on lean blowout at low combustor loading in three combustor lengths

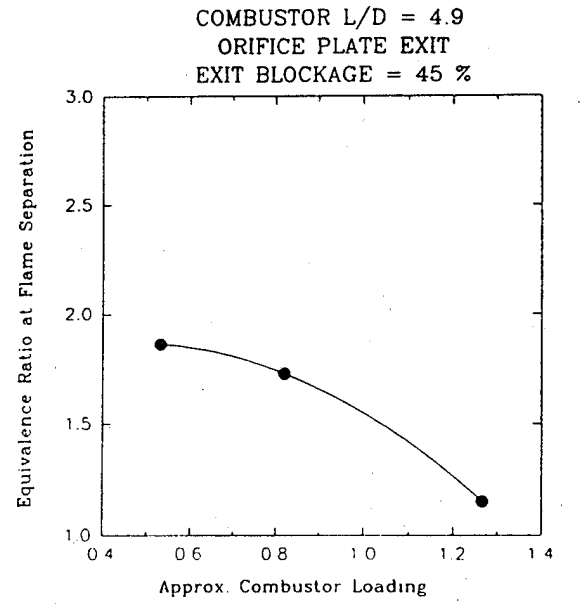

Fig. 10 Influence of combustor loading on equivalence ratio for flame separation at 45 percent exit blockage

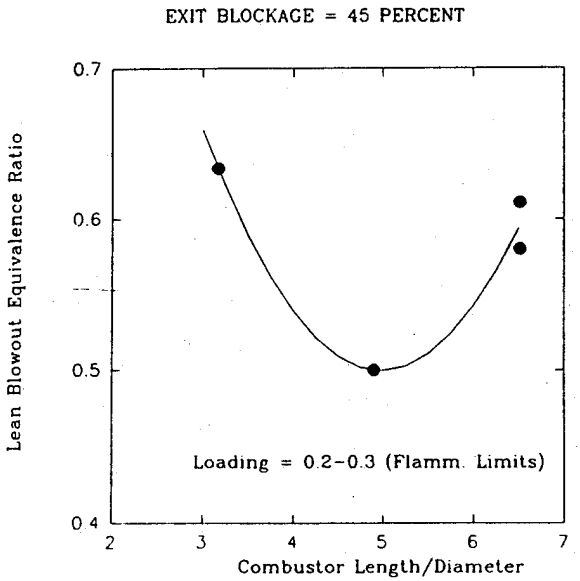

Fig. 12 Dependence of lean blowout at low loadings on combustor length with 45 percent exit blockage

of stability at 45.1 percent blockage. At given blockage this rich equivalence ratio for pilot flame loss decreases as the combustor loading is increased; Fig. 10 demonstrates this for the 4.9 L/D combustor at 45.1 percent exit blockage by orifice plate.

Direct Effects on Lean Blowout

It was observed for low values (about 0.18 $lb_m/(sec.ft.^3 atmos.^n)$ close to the flammability limits for propane/air mixtures at these conditions) of the loading parameter that the blowout equivalence ratio decreased linearly as the exit blockage by orifice plate was increased. This is shown in Fig. 11, and is somewhat surprising since the lifted flame is positioned (Roquemore et al., 1991) in the regions where the mean flow is beginning to be accelerated due to the blockage (Figs. 3 and 4), at least in isothermal flow. Heat release should increase the flow acceleration. The improvement in stability depended on the combustor L/D ratio; for a given blockage, the shorter the combustor the less stable it was and the greater its sensitivity to the exit blockage. For the 4.9 L/D combustor at this loading, the lean blowouts were virtually independent of exit blockage.

For a fixed exit orifice plate blockage of 45.1 percent at slightly higher loading parameter, the dependency on L/D is given in Fig. 12, where it can be seen that an optimum L/D

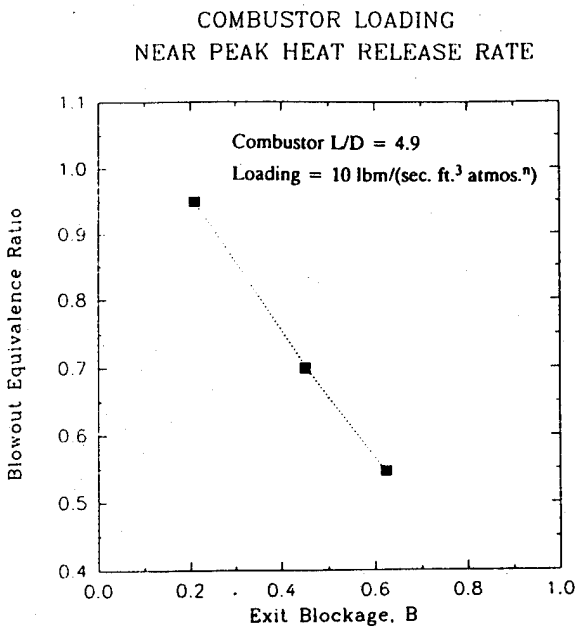

Fig. 13 Influence on lean blowout of exit blockage at high combustor loading

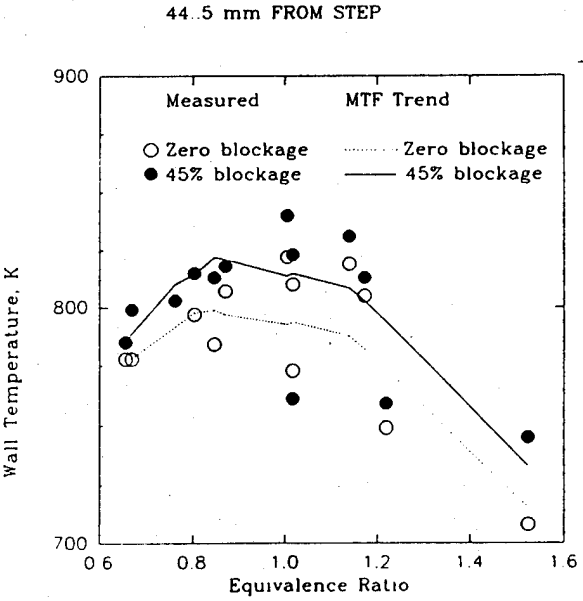

Fig. 14 Comparison of actual wall temperatures with smoothed values over a range of equivalence ratios, showing influence of exit blockage

exists. Close to the flammability limits there is also a fairly strong sensitivity of blowout equivalence ratio to combustor loading parameter. The existence of the optimum combustor length for maximum stability close to the flammability limits (Lewis and von Elbe, 1961) can be attributed to the occurrence of acoustic coupling (organ-pipe resonance driving eddy shedding off the step at 55 Hz) at large L/D (Heneghan et al., 1990), and outlet interference with flame holding at small L/D.

At 45.1 percent exit blockage the peak amplitude of the 55 Hz frequency signal measured inside the combustor by Kistler pressure transducers was increased by a factor of 5.5 when the combustor L/D was increased from 3.167 to 6.513. For the 4.9 L/D combustor with 45.1 percent exit blockage (and the acoustic treatment described by Heneghan et al., 1990), the peak-to-peak amplitudes for low-frequency oscillations (1–600 Hz) were less than 0.69 N/m^2, for high-frequency oscillations (1–5 kHz) the amplitudes were less than 6.9 N/m^2.

Figure 13 displays the sensitivity to exit blockage in the 4.9 L/D combustor operating at loadings (10 lb$_m$/(sec.ft.^{3}atmos.^{n})) near the peak heat release rate condition (obtained with a combination of high airflow rates and injection of excess nitrogen as a diluent). Again, the blowout equivalence ratio decreases linearly with increasing blockage. However, when contrasted with the sensitivity to blockage for this combustor near the flammability limits (Fig. 11), it is seen that blockage exerts a much more powerful influence on stability at this higher loading.

The general conclusion can be drawn that exit blockage improves the lean stability of the research combustor. The effectiveness of blockage in improving the stability in a combustor of given length depends on the loading at which the combustor is operated. Of the three combustor lengths evaluated (and for operation at low loadings at least), the 4.9 L/D combustor has the best stability at any blockage level between 0 and 62 percent. Exit blockage reduces the rich stability of the research combustor, and the extent of this also depends on the combustor loading.

Wall Temperature Behavior

The wall temperatures for the combustor are needed to provide boundary condition information for subsequent computational fluid dynamic calculations to be made in attempts to model the lean blowout process. They can also provide, by inference, additional information concerning development of major flow features in the combustor.

Wall temperatures are most conveniently expressed in nondimensional form, sometimes known as Metal Temperature Factor (MTF), and defined by

$$\text{MTF} = \frac{T_s - T_{in}}{T_{ad,fl} - T_{in}}$$

where

T_S = wall temperature
$T_{ad,fl}$ = adiabatic flame temperature.

For premixed flames, MTF represents a normalized wall temperature, and is particularly useful in the present case therefore, because of the partial premixing that takes place when the flame is lifted.

Figure 14 compares, at 44.5 mm downstream from the step and inside the step recirculation zone, actual thermocouple temperatures over a range of equivalence ratios against temperatures derived from the MTF trend with downstream distance. Data are provided for zero and 45.1 percent exit blockage in the 4.9 L/D combustor. The tests were made for a variety of jet velocity ratios and combustor flow functions. No effect of velocity ratio was apparent, and substantial increase in flow function resulted in only a negligible increase in MTF.

The figure shows that wall temperatures in the recirculation zone increase with combustor exit blockage by about 20 to 25 K for 45.1 blockage. Peak temperatures occur at equivalence ratios in the range of 0.9 to 1.1. For the attached flame condition ($\phi \geq 1.05$), temperature levels are about 820 K, and fall to about 780 K as lean blowout is approached.

The form of MTF variation with equivalence ratio is shown in Fig. 15 for a station 146 mm downstream from the step (still inside the recirculation zone). The behavior in the figure is typical of all axial stations along the combustor. MTF decreases with increasing equivalence ratio up to an equivalence ratio of about 0.95, and then becomes independent out to a

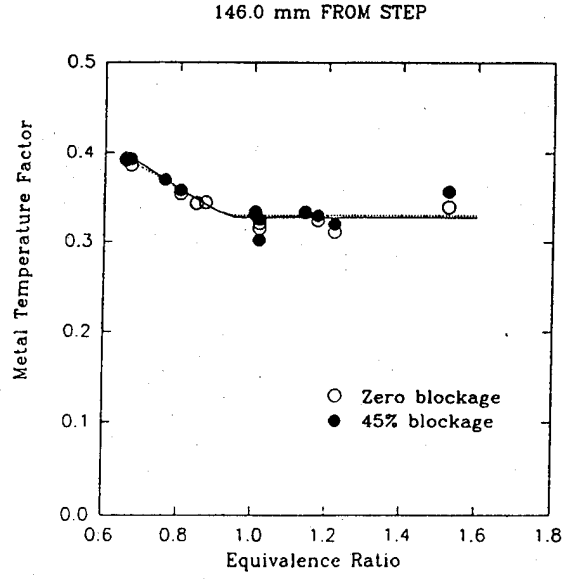

Fig. 15 Normalized wall temperatures at 126 mm from step-plane for zero and 45 percent exit blockage, showing influence of equivalence ratio

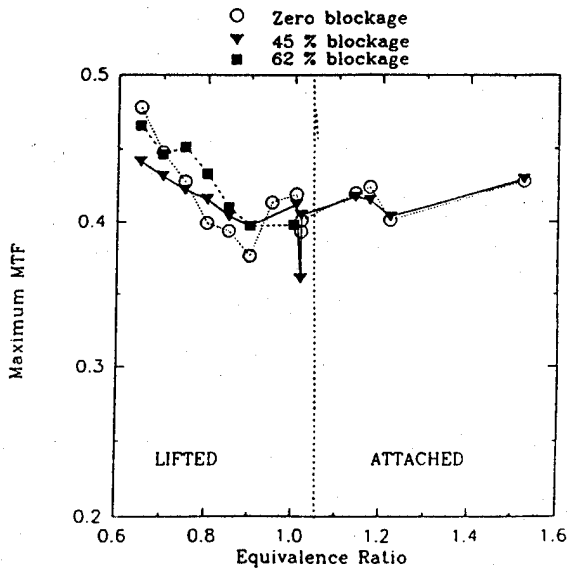

Fig. 17 Variations of maximum normalized wall temperatures for lifted and attached flames at several values of exit blockage

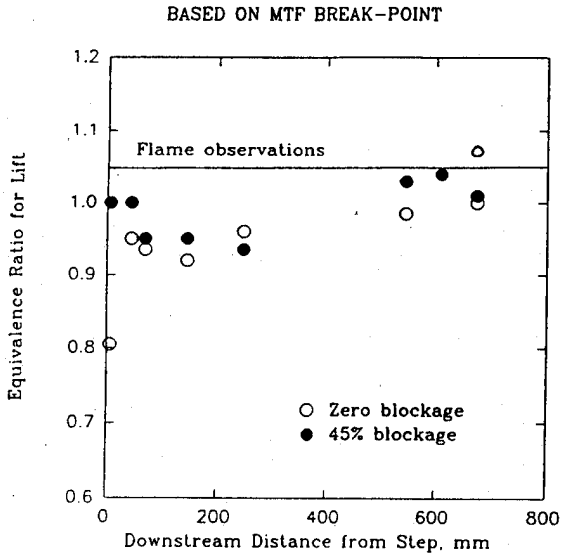

Fig. 16 Indicated equivalence ratios for flame-lift from wall temperatures, compared with direct observations

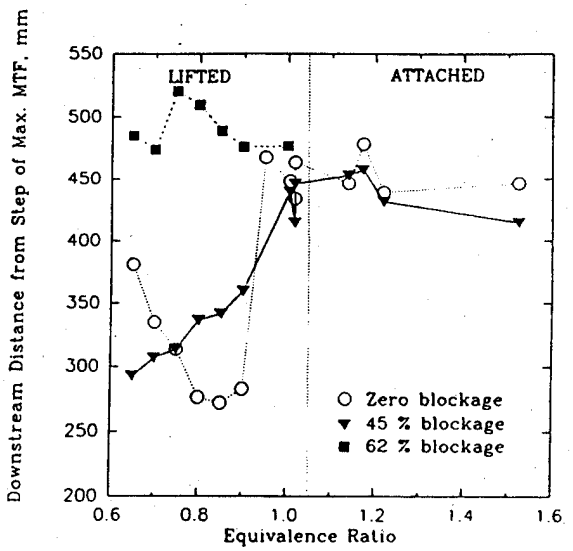

Fig. 18 Dependency of position of maximum normalized wall temperature on exit blockage for lifted and attached flames

value of 1.6. There is negligible effect of blockage on MTF at this station.

The "break" in the curve of Fig. 15 may be interpreted as representing the flame-lift condition. The inferred equivalence ratios for flame-lift based on this break for different axial locations are shown in Fig. 16 compared with the equivalence ratios for flame-lift based on direct observation (Fig. 6). As might be anticipated, inferences based on data from downstream are in better agreement with direct observations. No effect of blockage is apparent on the inferred flame-lift, which does not conflict with direct observation in Fig. 6.

The variations of the maximum value of MTF with equivalence ratio for 0, 45.1, and 62 percent geometric blockages are given in Fig. 17; the flame condition—lifted or attached—is delineated based on Fig. 6. The values of maximum MTF, and the positions at which they occur, were derived at each equivalence ratio from differentiation of curve fits to MTF versus axial distance information obtained from the curves in plots such as given in Fig. 15.

Figure 17 indicates that maximum MTF reaches its minimum value at about the equivalence ratio for flame-lift. Exit blockage does not affect the value of maximum MTF, but maximum MTF does increase as lean blowout is approached.

When the position at which maximum MTF is reached is plotted in similar fashion in Fig. 18, a strong effect of blockage is apparent for lifted flames; equivalence ratios for attached flames do not influence this position significantly. For the three blockages shown, the position of maximum MTF is roughly constant around 450 mm from the step for attached flames.

When equivalence ratio is reduced so that a lifted flame is established, an unrestricted combustor exit results in the position of maximum MTF initially moving back toward the step. However, for an equivalence ratio of 0.9, the closest position

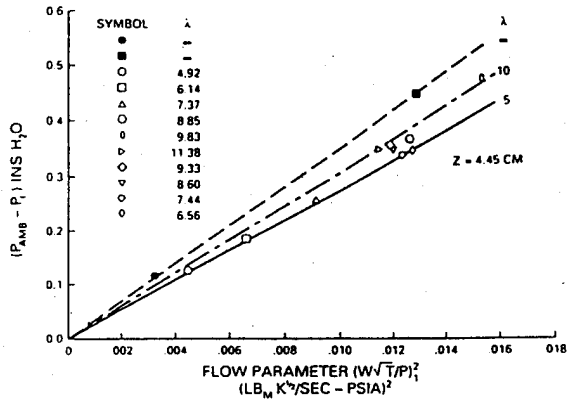

Fig. 19 Dependency of wall static pressures in the step recirculation zone on inlet flow parameter and jet velocity ratio in isothermal flow with a free exit

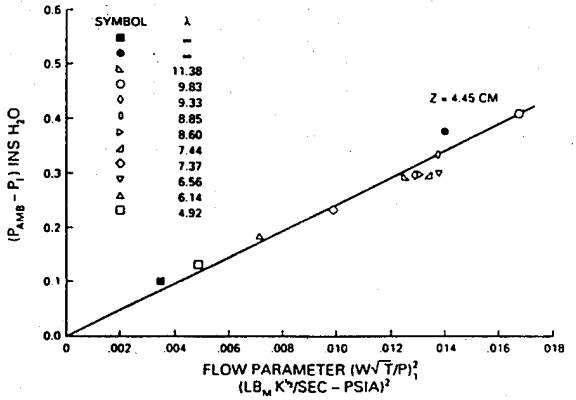

Fig. 20 Suppression of dependency of wall static pressure on jet velocity ratio by exit blockage (45 percent) in isothermal flow

to the step is reached at about 270 mm; thereafter, as equivalence ratio is further lowered toward a lean blowout, the position again moves downstream as the flame-lift increases.

The addition of exit blockage introduces an additional recirculation zone (on the orifice plate upstream face) into the combustor, and the existence of this recirculation is how blockage exerts an influence on the position of maximum MTF. The position of maximum MTF is associated with the reattachment plane of the step recirculation zone since this is where the jet shear layers reach the combustor wall (Sturgess et al., 1992b). These jet shear layers are where the majority of the heat release takes place during combustion, whether or not the pilot flame is attached (Sturgess et al., 1991a). Movements of the position of maximum MTF therefore reflect, albeit in crude fashion, movements of the reattachment plane for the step recirculation zone. The lack of blockage-effect on the value of maximum MTF (Fig. 17) indicates that heat release in the jet shear layers is not substantially changed by combustor exit blockage; however, the trajectory of these shear layers is (Fig. 18), possibly due to flow acceleration as a result of the heat release. The behavior evident in Fig. 18 for 45.1 and 62 percent blockage is the result of interactions between the step and orifice plate recirculation zones, due to heat release rate as equivalence ratio is varied, and modified by the two flame conditions.

With this flow model, the lifted-flame (partially premixed) behavior for maximum MTF in Fig. 18 at zero exit blockage is consistent with the findings of Morrison et al. (1987), Pitz and Daily (1983), and Stevenson et al. (1982) for premixed flames that a step recirculation zone at fixed (turbulent) Reynolds number decreases in size with increasing equivalence ratio. The minimum distance occurring at an equivalence ratio of 0.9 suggests that pilot flame attachment becomes evident before the directly observed equivalence ratio of 1.05 (Fig. 6). Examination of the intermittency of the pilot flame (Roquemore et al., 1991; Chen, 1991) tends to confirm this suggestion.

Wall Static Pressures

For an atmospheric pressure discharge combustor with exit blockage, wall static pressures provide means for a convenient assessment of the extent of the additional recirculation zone set up on the orifice plate upstream face. With a free exit, the difference between ambient pressure and wall static pressure in the combustor reaches zero in the exit plane. However, when the exit is restricted, this difference reaches zero at some position inside the combustor (Heneghan et al., 1990). The position where this occurs marks the stagnation plane for the aft recirculation zone on the orifice plate.

In isothermal flow the wall static pressure at a given station

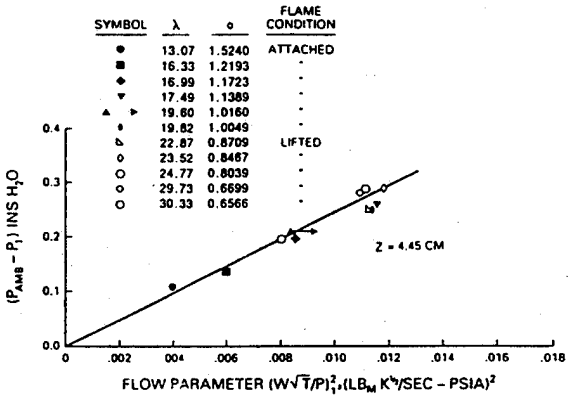

Fig. 21 Suppression of dependency of wall static pressure on jet velocity ratio by combustion with a free exit

is a function of the jet velocity ratio λ, and the inlet flow parameter, as can be seen for a station 44.5 mm downstream, in Fig. 19. As Fig. 20 demonstrates, when exit blockage is introduced, the dependency of wall static pressure on velocity ratio is suppressed. Combustion also suppresses the dependency on jet velocity ratio, even for a free exit. This is illustrated in Fig. 21, where it is also shown that the flame condition does not exert an influence.

Again using curve fits and differentiation, the axial positions along the combustor at which atmospheric pressure was attained were found. Typical wall static pressure axial distributions are given in Fig. 3 of Heneghan et al. (1990). Figure 22 shows that in isothermal flow this condition was reached at a constant 580 mm approximately, with 45.1 percent exit blockage, and was so regardless of inlet flow parameter or jet velocity ratio. With combustion and the same blockage, the position for atmospheric pressure was a strong function of equivalence ratio, as Fig. 23 shows, where the leading-edge of the aft recirculation zone moves progressively forward in the combustor as equivalence ratio is reduced, independent of flame condition.

At 62 percent blockage the position at which atmospheric pressure was attained was always greater than 600 mm from the step, and thus could not be accurately determined from the static tap positions available.

Relationship Between Recirculation Zones

The information on the end of the step recirculation zone inferred from MTF data (Fig. 18) can be combined with the

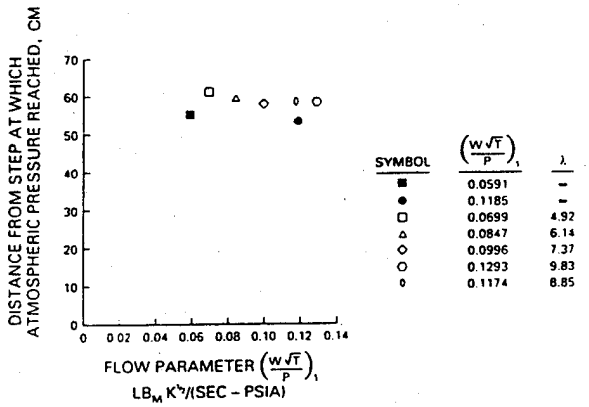

Fig. 22 Independence from inlet flow parameter and jet velocity ratio of position where atmospheric pressure is reached on the combustor wall, in isothermal flow with 45 percent exit blockage

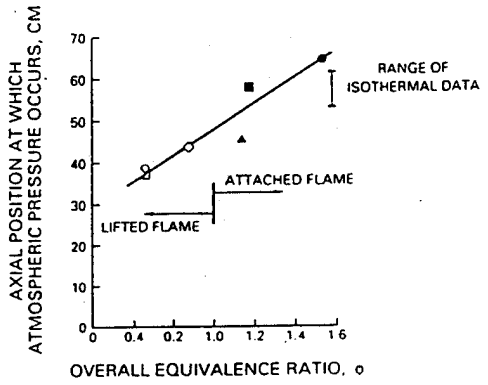

Fig. 23 Variation of downstream position where wall static pressure reaches atmospheric with equivalence ratio at 45 percent exit blockage

information on the beginning of the orifice plate recirculation zone from the static pressure data (Fig. 23) in order to examine the relationship between these two important flow features in the restricted-exit combustor.

Figure 24 shows a combination of Figs. 18 and 23 for 45.1 percent exit blockage with combusting flow. It can be deduced that there is always positive separation between the end of the step recirculation zone and the beginning of the orifice plate recirculation zone for this blockage. Furthermore, for lifted flames, this separation is maintained at a constant distance of about 80 mm, so that direct interference never happens. For attached flames, the separation distance increases, as Fig. 25 shows.

For 62 percent blockage, it appears as though direct interference between zones does not occur either, despite the fact that the inferred position of the end of the step recirculation zone is farther downstream at around 500 mm for all equivalence ratios (Fig. 18).

Gas Temperature Profiles

Limited gas temperature measurements were made using the CARS system. Profiles along the combustor centerline and, radially, close to the step, were taken at 0, 45.1, and 62 percent exit blockage by orifice plates in order to assess what blockage did to the all-important step recirculation zone. This was a quick preliminary look made prior to more extensive field-mapping of temperature to be reported separately.

The axial profiles of mean temperature along the combustor centerline at 45.1 percent exit blockage for lifted and attached

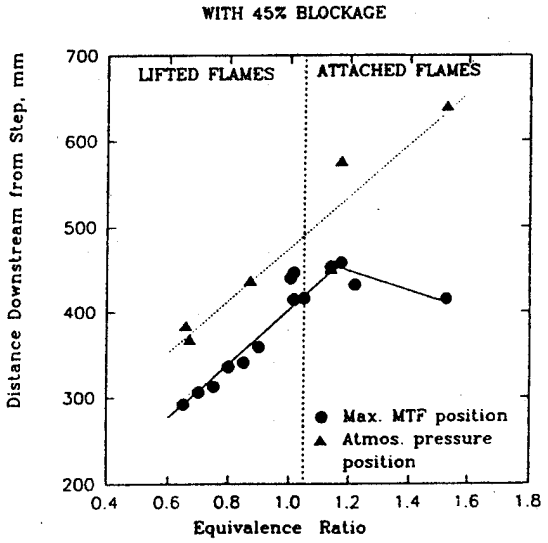

Fig. 24 Downstream positions where atmospheric pressure and maximum normalized wall temperature are attained as equivalence ratio is varied for fixed exit blockage

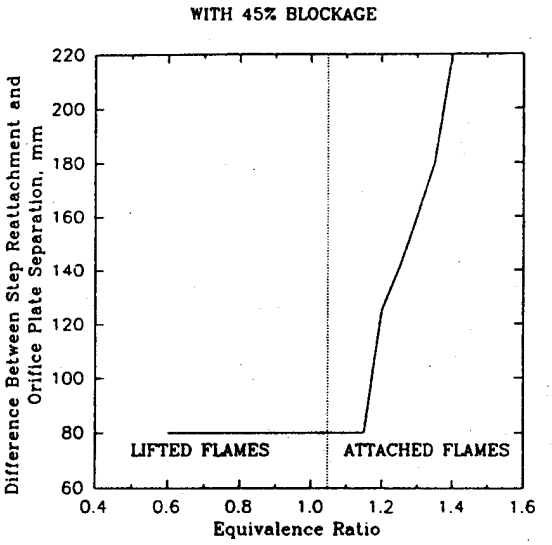

Fig. 25 Distance between recirculation zones for lifted and attached flames at fixed exit blockage

flames are given in Fig. 26, where the temperatures are presented as the ratio of actual temperature to the adiabatic flame temperature. The combustor loadings in both cases are in the range of 0.7 to 0.76 $lb_m/(sec.ft.^3atmos.")$, i.e., fairly near the lean flammability limit. For both flames the temperature initially falls, and then increases again for distances greater than 100 mm from the step-plane. By consideration of Sturgess et al. (1992b), the increases in centerline mean temperature can be associated with the inner edge of the reacting jets shear layer reaching the centerline and thereby introducing sufficient oxidant for extensive chemical reaction to take place on the centerline. The initial distance in this profile can therefore be viewed as a conditional thermochemical potential core region. Note that the position of mean temperature increase is in the region where in isothermal flow the centerline mean axial velocity begins to accelerate with the 45.1 percent exit blockage (Fig. 3). Also, for the attached flame, the dimensionless mean temperature level is generally increased over that for the lifted flame.

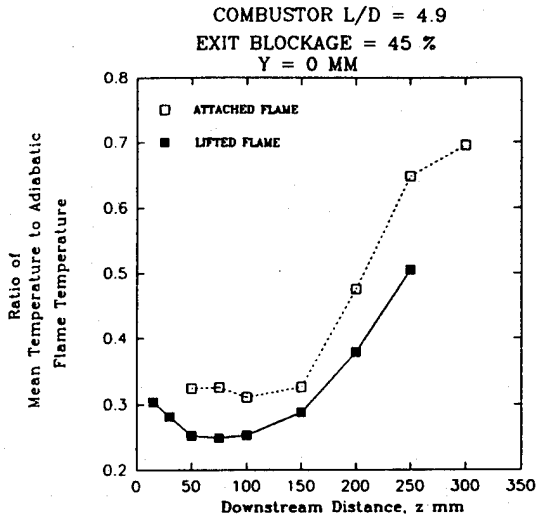

Fig. 26 Centerline profiles of dimensionless mean gas temperature for attached and lifted flames at fixed exit blockage

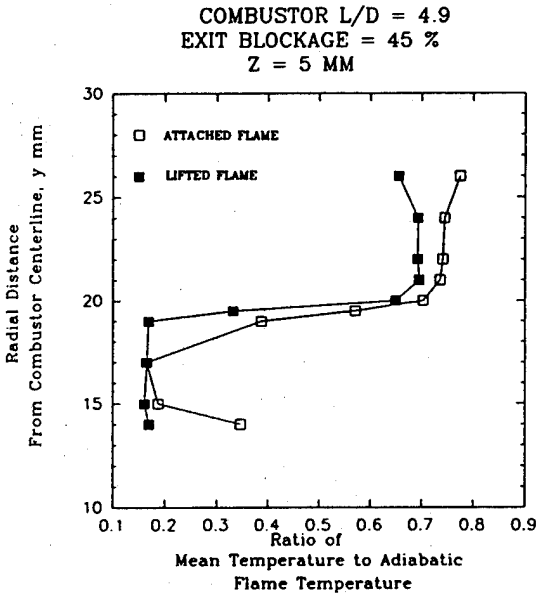

Fig. 27 Radial profiles of dimensionless mean gas temperature in the step region for attached and lifted flames at fixed exit blockage

Radial profiles of dimensionless mean temperature for the condition above are given in Fig. 27 for a downstream station 5 mm from the step. Comparison of these profiles reveals the effect of the attached flame on mean temperature, and shows the pilot flame to be located at a radius of 17 to 20 mm. The probability distribution functions (p.d.f.) confirm this definition. This is somewhat consistent with the mean position of 24 mm radius for the attached flame determined at 10 mm downstream with thin filament pyrometry (TFP) (Roquemore et al., 1991). Again, the levels of dimensionless temperature are higher at all radial positions for the attached flame condition. The p.d.f.'s for the lifted flame condition agree with the measurements of the spontaneous OH emission given by Roquemore et al. (1991), that there is a finite probability of the pilot flame being present part of the time, even though the main flame is fully lifted and an anchored pilot flame is not directly observed. For both lifted and attached flames, the step

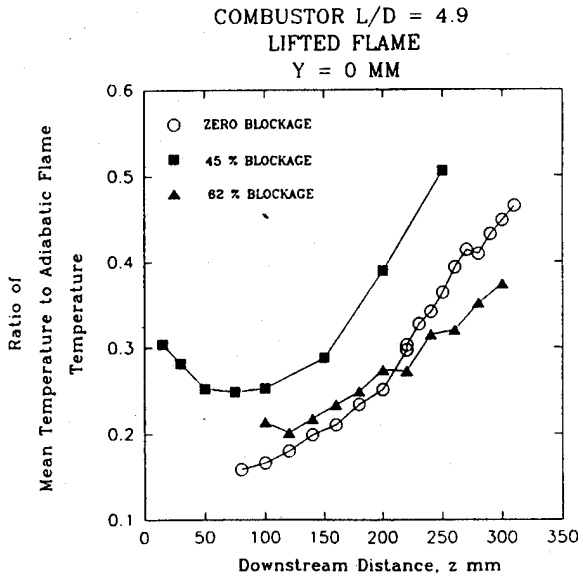

Fig. 28 Comparison of centerline profiles of dimensionless mean gas temperatures for lifted flames at various exit blockages

recirculation zone provides a significant high-temperature reservoir for the combustion processes developing in the shear layers.

Note that both Figs. 26 and 27 indicate an elevation of gas temperatures over the inlet conditions close to the confluence of the jets and around the region encompassing the small, central recirculation bubble (Sturgess et al., 1992b). Although not yet supported by strong direct evidence, it has been hypothesized (Sturgess et al., 1992a) that nonstationary flow interactions of the fuel and air jets with the central recirculation bubble result in additional radial mass transport of reactants. Such mass transport could account for early chemical reaction and hence, the observed elevated temperatures close to the orifice. The p.d.f. at a radius of 14 mm for an equivalence ratio of 1.36 at a combustor loading of 0.428 $lb_m/(sec.ft.^3 atmos.^n)$ shows that there is an equal probability of the flame being present and of fluid at inlet temperatures. This radius marks the position of the outer edge of the fuel tube. For this temperature condition to be so, either direct flame or a hot gas ignition source from the step recirculation zone must be transported completely across the annular air-jet path (see Fig. 1).

The addition of blockage increases the centerline mean temperatures for lifted flames at loadings fairly near the lean flammability limit. The effect is particularly strong for distances closer to the confluence of the jets than 100 mm as Fig. 28 shows. The radial profiles of dimensionless mean temperature indicate that blockage slightly increases the temperature in the step recirculation zone.

The centerline profiles of the ratio of the rms value of fluctuating temperature to mean temperature for 0, 45.1, and 62 percent exit blockage in the 4.9 *L/D* combustor are given in Fig. 29. The equivalence ratios are such that the flames were all lifted, and the combustor loadings were 0.7 to 0.76 $lb_m/(sec.ft.^3 atmos.^n)$. The fluctuating temperatures superimposed on the mean temperatures are not significantly affected by exit blockage. What is noteworthy, however, is the dramatic increase in the fluctuating component for distances closer than 50 mm to the jet origins. This is associated in particular with the forward stagnation point of the small, central recirculation zone, which for isothermal flow is situated at about 14 mm from the origin.

Figure 30 presents radial profiles of the ratio of rms tem-

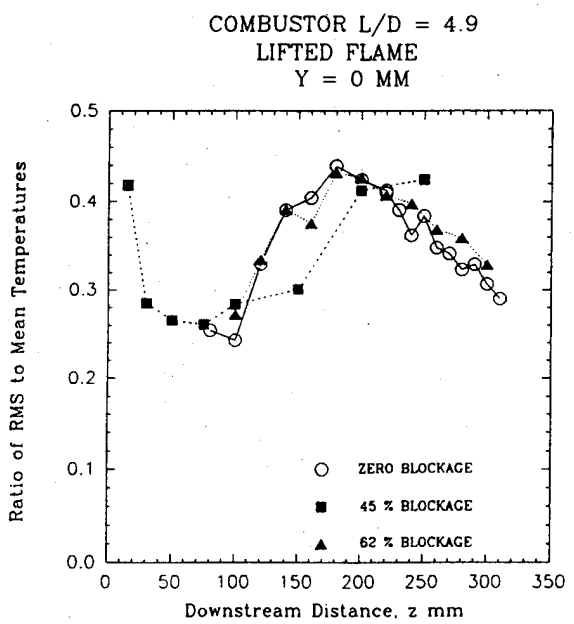

Fig. 29 Comparison of centerline profiles of dimensionless fluctuating gas temperatures for lifted flames at various exit blockages

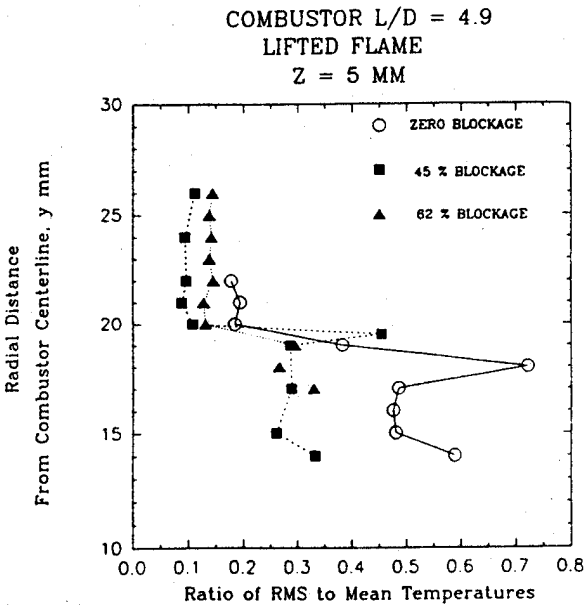

Fig. 30 Radial profiles of dimensionless fluctuating gas temperatures in the step region for lifted flames at various exit blockages

perature to mean temperature at 5 mm downstream from the step-plane for a range of exit blockage at the same operating conditions as for the previous figure, i.e., lifted flame at light loadings. Temperature fluctuations in the step recirculation zone are not much affected by the exit blockage. In sharp contrast, the existence of any blockage at all exerts a powerful suppressing effect on fluctuations in the jet shear layers.

Whether the flame is lifted or attached, there are no changes in temperature fluctuations in the step recirculation zone at 5 mm downstream with 45.1 percent exit blockage. There appear to be some differences for the two flame conditions in the shear layers (possibly the pilot flame), but the present data are not sufficient to be sure.

Discussion

The long-term intent for the research program, of which this effort is but a part, is to derive calculation procedures for lean blowout in gas turbine engine combustors. One of the calculation procedures being developed for this purpose is computational fluid dynamics (CFD). For viability, CFD should be able to provide a reasonable simulation of the real physical behavior involved in the lean blowout process. It is therefore required that significant flame events in the blowout process be experimentally identified and characterized. The attached, separated, and lifted flames, and the influence of combustor geometry on the operational conditions under which these are encountered, hence form a significant part of the data base. The ability to calculate these characteristics will form a critical test of the efficacy of any CFD modeling of lean blowout.

The research combustor exhibits a distinct and repeatable flame pattern change as it blows out on the lean side (Fig. 5). There are similarities in the flame changes for both rich and lean blowouts. A key element in these sequences of flame change is the loss of the thin, sheathlike pilot flame anchored at the outer diameter of the air jet. This pilot flame serves as a continuous ignition source for the main flame that then originates in the shear layers associated with the fuel and air jets, and the recirculation zones. For rich blowouts, loss of the pilot flame does not result in obvious changes in the main flame, either in position or character. It tends to remain concentrated in the shear layers. However, for lean blowouts, loss of the pilot flame causes the main flame to lift to a downstream position. This clearly allows significant premixing of reactants to occur, with the result that the main flame in its lifted position is more distributed across the width of the combustor. Blowout in the separated rich flame takes place suddenly; in the lifted lean flame, blowout is preceded by the onset of large-scale axial oscillations of the main flame about its mean position (Fig. 5).

The flame events described are controlled by the operating equivalence ratio of the combustor (Figs. 5 and 10). The equivalence ratios at which flame events occur are modified by the existence of back-pressure applied at the exit from the combustor (Figs. 6–9). The sensitivity of the event-equivalence ratios to the exit back-pressure depends on the combustor loading, and this sensitivity generally increases with the loading (Figs. 8 and 10).

The application of exit back-pressure to the research combustor exerts a favorable influence on the lean blowout (Fig. 11). At fixed combustor loading, the effect depends on the combustor length-to-diameter ratio. When acoustic effects and direct loss of the step recirculation zone (Fig. 12) are eliminated through use of an appropriate combustor length, the changes in blowout due to exit blockage are sensitive to combustor loading (Figs. 11 and 13). Predictably, they are strongest at high loadings approaching the peak heat release rate condition. At low combustor loadings, the improvement in stability due to blockage is consistent with a more persistent anchored flame (Figs. 6 and 7), but conflicts with an earlier onset of large-scale axial movements of the lifted flame (Fig. 8).

The presence of the outlet blockage changes the isothermal flow field in the combustor by causing acceleration of the mean axial velocities about the centerline (Figs. 3 and 4), and by introducing an additional recirculation zone on the upstream face of the orifice plate placed at the combustor exit. Acceleration of the central flow is evident as close as 125 mm downstream from the step plane (Fig. 3), or, at an L/D of 0.83 in the 4.9 L/D combustor at 45.1 percent blockage. This is upstream of the reattachment plane for the step recirculation, which is at about 2.82 L/D (Sturgess et al., 1992a). With a

free exit in isothermal flow, the central flow decelerates as the fuel and air jets merge and expand into the combustor around the step recirculation zone. The net acceleration that results with exit blockage represents a modification of the shear layers, and thus, flame holding in these shear layers can be expected to be changed.

The wall static pressure measurements in the step recirculation zone show that combustion suppresses a sensitivity to jet velocity ratio that is apparent in isothermal flow (Figs. 19 and 21); the addition of exit blockage in isothermal flow exercises a similar effect (Fig. 20).

With combustion, it can be inferred from wall thermocouple measurements that the position of the step recirculation zone reattachment shifts according to the equivalence ratio (Fig. 18). For lifted flames, the dependency on equivalence ratio is modified by the degree of outlet blockage (Fig. 18). From wall static pressure tap measurements, it is inferred that the size of the orifice plate recirculation is also influenced by combustion (Fig. 23). For a lifted flame at a given blockage, the movement of these two stagnation planes with equivalence ratio is such that a constant separation between them exists (Figs. 24 and 25), i.e., there is no direct interference. When the attached pilot flame condition is established, movement of the step recirculation zone attachment essentially ceases (Fig. 24). However, the orifice recirculation zone continues to decrease in size (Fig. 24), with the result that the separation between stagnation planes is increased (Fig. 25). Therefore, it is unlikely that the lean blowout improvement with exit blockage is associated with direct modification of the step recirculation zone.

The "quick-look" at mean gas temperature profiles shows the existence of the pilot flame for equivalence ratios when it is present (attached flame), and indicates slightly increased temperatures in the step recirculation zone and on the combustor centerline in the near-field. For lifted flames, exit blockage exerts its greatest effect in the near-field on the combustor centerline, particularly associated with the small, central recirculation bubble; there is little effect in the step recirculation zone. The CARS p.d.f.'s confirm earlier findings by OH emission and TFP measurements that the pilot flame is intermittently present even when direct observations indicate that it is lost and the main flame is lifted.

Fluctuating gas temperatures along the combustor centerline are insensitive to exit blockage (Fig. 29); however, they once again confirm the strong dynamic nature of the flow associated with the central recirculation bubble that is generated by entrainment of the central fuel jet by the much stronger surrounding annular air jet (Sturgess et al., 1992b). In the near-field (at 5 mm) the radial profiles of fluctuating temperature suggest that exit blockage is a dampening effect, only slightly in the step recirculation, but much more strongly in the jet shear layers (Fig. 30).

Back-pressuring the flame (by exit blockage in this case) exerts a powerful stabilizing effect on lean blowout, especially at the high combustor loadings that can represent critical operating conditions for military aircraft. Direct action of back-pressure on the step recirculation zone does not seem to take place. The back-pressure acts most strongly on the initial processes occurring in the jet shear layers by modifying their trajectories and turbulence characteristics. These initial processes emerge as being critical to the overall flame stabilization, whether the main flame is attached or lifted. Evidence is building (here and in earlier work) that dynamic behavior of the flow in the near-field can control the combustion process, perhaps through radical changes in radial mass transport.

The present results confirm that future attention should be directed at the pilot flame, the circumstances of its existence, and its contribution to the main flame. The dynamic interactions of the central recirculation bubble with the jet shear layers and of the jet shear layers with the step recirculation zone must be explored in detail, and characterized if possible. It would be desirable if such future studies could include a mass transport experiment, and time-resolved flow visualization of the combustion in the shear layers.

Conclusions

1 Back-pressure by means of exit blockage does exert an effect on the lean blowout characteristics of a combustor. The effect is weakest at low combustor loadings near the flammability limits, and strongest at high combustor loadings near the peak heat release rate. Modification of the effect occurs with changes in combustor length-to-diameter ratio.

2 Direct interference effects of exit blockage on the step recirculation zone do not occur.

3 The major effects of exit blockage on lean blowout are due to changes in the fuel and air jet shear layers, and in the interaction of this shear layer with the step recirculation zone and with the central recirculation bubble. Dynamic processes appear to play a significant part in these interactions.

4 Future experimental work should concentrate on the near-field region, the dynamic interactions taking place there, and the circumstances governing the existence and role of the anchored flame.

5 The combustor exhibits consistent and well-characterized flame behavior that depends on equivalence ratio and exit blockage. The ability to represent this behavior will provide a stringent test of the realism of any numerical modeling (CFD) of this combustor.

Acknowledgments

The authors wish to acknowledge the contributions to this work from their colleagues at Wright-Patterson Air Force Base and Pratt & Whitney, and also from Dr. P. Hedman, Brigham Young University, Provo, Utah. The University of Dayton work was supported by the U.S. Air Force Wright Laboratories, under Contract No. F33615-87-C-2767 (Contract Monitor Dr. W. M. Roquemore), and Pratt & Whitney was supported under Contract No. F33615-87-C-2822 (Contract Monitors 1st Lt. A. L. Lesmerises and Mr. D. Shouse). The authors thank the Air Force and Pratt & Whitney for permission to publish the results of this research.

References

Chen, T. H., 1991, private communication.

Gupta, A. K., Lilley, D. G., and Syred, N., 1984, *Swirl Flows*, Abacus Press.

Heneghan, S. P., and Vangsness, M. D., 1990, "Instrument Noise and Weighting Factors in Data Analysis," *Experiments in Fluids*, Vol. 9, pp. 290–294.

Heneghan, S. P., Vangsness, M. D., Ballal, D. R., Lesmerises, A. L., and Sturgess, G. J., 1990, "Acoustic Characteristics of a Research Step Combustor," AIAA Paper No. AIAA-90-1851 (to appear in *Journal of Propulsion and Power*).

Heneghan, S. P., and Vangsness, M. D., 1991, "Analysis of Slit Function Errors in Single-Shot Coherent Anti-Stokes Raman Spectroscopy (CARS) in Practical Combustors," *Reviews of Scientific Instruments*, Vol. 62, pp. 2093–2099.

Heneghan, S. P., Vangsness, M. D., and Pan, J. C., 1991, "Simple Determination of the Slit Function in Single Shot CARS Thermometry," *Journal of Applied Physics*, Vol. 69, pp. 2692–2695.

Lefebvre, A. H., 1983, *Gas Turbine Combustion*, Hemisphere Publishing Corp., McGraw-Hill, New York.

Lewis, B., and von Elbe, G., 1961, *Combustion, Flames and Explosion of Gases*, 2nd ed., Academic Press, New York.

Morrison, G. L., Tatterson, G. B., and Long, M. W., 1987, "A 3-D Laser Velocimeter Investigation of Turbulent, Incompressible Flow in an Axisymmetric Sudden Expansion," AIAA Paper No. AIAA-87-0119.

Pitz, R. W., and Daily, J. W., 1983, "Combustion in a Turbulent Mixing Layer Formed at a Rearward Facing Step," *AIAA Journal*, Vol. 21, No. 11, pp. 1565–1569.

Roquemore, W. M., Reddy, V. K., Hedman, P. O., Post, M. E., Chen, T. H., Goss, L. P., Trump, D., Vilimpoc, V., and Sturgess, G. J., 1991, "Experimental and Theoretical Studies in a Gas-Fueled Research Combustor," AIAA Paper No. AIAA-91-0639.

Stevenson, W. H., Thompson, H. D., Gold, R. D., and Craig, R. R., 1982, "Laser Velocimeter Measurements in Separated Flow With Combustion," presented at the International Symposium of Laser-Doppler Anemometry in Fluid Mechanics, Lisbon, Portugal, Paper No. 11.5.

Sturgess, G. J., Sloan, D. G., Roquemore, W. M., Reddy, V. K., Shouse, D., Lesmerises, A. L., Ballal, D. R., Heneghan, S. P., Vangsness, M. D., and Hedman, P. O., 1991a, "Flame Stability and Lean Blowout—A Research Program Progress Report," *Proc. 10th ISABE*, Nottingham, United Kingdom, pp. 372-384.

Sturgess, G. J., Heneghan, S. P., Vangsness, M. D., Ballal, D. R., and Lesmerises, A. L., 1991b, "Lean Blowout in a Research Combustor at Simulated Low Pressures," ASME Paper No. 91-GT-359.

Sturgess, G. J., Sloan, D. G., Lesmerises, A. L., Heneghan, S. P., and Ballal, D. R., 1992a, "Design and Development of a Research Combustor for Lean Blowout Studies," ASME JOURNAL OF ENGINEERING FOR GAS TURBINES AND POWER, Vol. 114, pp. 13-19.

Sturgess, G. J., Heneghan, S. P., Vangsness, M. D., Ballal, D. R., and Lesmerises, A. L., 1992b, "Isothermal Flow Fields in a Research Combustor for Lean Blowout Studies," ASME JOURNAL OF ENGINEERING FOR GAS TURBINES AND POWER, Vol. 114, pp. 435-444.

APPENDIX E

LEAN BLOWOUT IN A RESEARCH COMBUSTOR AT SIMULATED LOW PRESSURES

By

G.J. Sturgess
Pratt & Whitney, East Hartford, Connecticut

S.P. Heneghan, M.D. Vangsness and D.R. Ballal
University of Dayton, Dayton, Ohio

A.L. Lesmerises
WL/POSF, Wright-Patterson Air Force Base, Ohio

Published as ASME Paper No. 91-GT-359, June 1991. To appear in ASME *Journal of Engineering for Gas Turbines and Power.*

THE AMERICAN SOCIETY OF MECHANICAL ENGINEERS
345 E. 47 St., New York, N.Y. 10017

The Society shall not be responsible for statements or opinions advanced in papers or in discussion at meetings of the Society or of its Divisions or Sections, or printed in its publications. Discussion is printed only if the paper is published in an ASME Journal. Papers are available from ASME for fifteen months after the meeting.
Printed in USA.

91-GT-359

G.J. Sturgess

Lean Blowout in a Research Combustor at Simulated Low Pressures

G. J. STURGESS, Pratt & Whitney, East Hartford, Connecticut
S. P. HENEGHAN, M. D. VANGSNESS and D. R. BALLAL
University of Dayton, Dayton, Ohio
A. L. LESMERISES, WRDC, Wright-Patterson Air Force Base, Ohio

ABSTRACT

A propane-fueled research combustor has been designed to represent the essential features of primary zones of combustors for aircraft gas turbine engines in an investigation of lean blowouts. The atmospheric pressure test facility being used for the investigation made it difficult to directly approach the maximum heat release condition of the research combustor. High combustor loadings were achieved through simulating the effects on chemical reaction rates of sub-atmospheric pressures by means of a nitrogen diluent technique. A calibration procedure is described, and correlated experimental lean blowout results are compared with well-stirred reactor calculations for the research combustor to confirm the efficacy of the calibration.

NOMENCLATURE

A	Pre-exponential rate constant (may also include convenient unit conversion factors)
B	Combustion efficiency
C	E/ℜ
E	Activation energy
F	Temperature correction factor
K	Mass ratio of excess nitrogen to fuel
m	Volumetric fractional concentration
$\dot{m}$	Mass flow rate
$\dot{m}'''$	Volumetric rate of oxidant mass consumption
n	Effective order of global chemical reaction
P	Pressure
R	Global reaction rate expression
ℜ	Universal gas constant
T	Reaction temperature
V	Volume associated with combustion
α	Molar fraction of CO in products of reaction
β	Molar fraction of CO_2 in products of reaction
γ	Defined by Eq. (4)
ϕ	Fuel/air equivalence ratio

Subscripts

air	Air
f	Carbon monoxide in products of reaction, fuel
LBO	Lean blowout
N_2	Excess nitrogen as diluent
o	Oxygen in products of reaction
Tot	Inlet sum of air, propane and excess nitrogen

INTRODUCTION

A propane-fueled research combustor, Fig. 1, has been designed (Sturgess et al., 1990) and developed (Heneghan et al., 1990) to investigate lean blowouts in simulated primary zones of the combustors for aircraft gas turbine engines. The fundamental flow features of a gas turbine combustor primary zone, within which the flame is held, are generated by the geometrically-simple design of the research combustor.

The research combustor consists of co-axial jets with a 29.7 mm inside diameter central fuel jet surrounded by a 40 mm diameter annular air jet. The fuel is gaseous propane. The jets are located centrally in a 150 mm nominal diameter duct. A backward-facing step at the jet discharge plane completes the sudden expansion, giving a step height of 55 mm. The step provides a recirculation region that can stabilize the flame. The combustor test section incorporates flat quartz windows to provide optical access. Curved metal fillets, located in the corners of the test section, reduce and distribute the vorticity generation due to wall secondary flows, and so eliminate their impact on the bulk flowfield in the combustor. An orifice plate with a 45 percent blockage ratio forms the exit from the combustor.

When operated in a fuel-rich mode, the flame in the combustor is very stable and is anchored in the jet shear layers by a pilot flame attached to the step near the outer edge of the air supply tube. Fuel for this flame is recirculated from downstream by the step recirculation zone; ignition is by hot

Presented at the International Gas Turbine and Aeroengine Congress and Exposition
Orlando, FL June 3-6, 1991

gases also recirculated. As the bulk equivalence ratio is reduced the flame becomes less stable, and eventually reaches a point where the pilot flame becomes detached from the base region (lifts), and the entire flame structure becomes stabilized downstream, Fig. 2. Thus, there are two distinct operating modes for the combustor: a fully anchored flame, and a lifted flame.

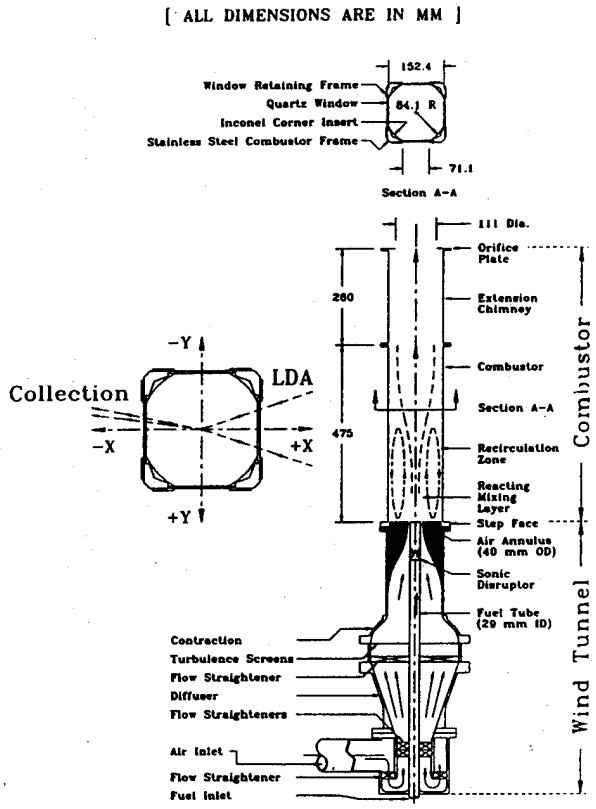

Fig. 1 Cross-Section of Research Combustor

As a consequence of the flame-lift, a significant degree of partial premixing of the reactants takes place upstream of the lifted flame position. When the equivalence ratio is further reduced, the flame becomes progressively less stable (Heneghan et al., 1990) in its lifted condition, and eventually flows out. This lean blowout limit at atmospheric pressure has been found to correspond to a fuel equivalence ratio (around 0.5) that is very close to the lean flammability limit of propane in air (Lewis and von Elbe, 1987). Due to the partial premixing, the combustor lean blowout performance characteristic has been observed to be consistent with that of well-stirred reactor data (Sturgess et al., 1990).

Lean blowout is strongly affected by chemical reaction rates. Application of chemical reaction rate theory to well-stirred reactors has resulted in the formulation of the gas loading parameter $\dot{m}/(VP^nF)$, where n is the effective order of the reaction, F is a temperature correction factor, V is the reactor volume, $\dot{m}$ is the oxidant mass flow rate, and P the operating pressure, against which the equivalence ratio at blowout is frequently plotted. The concept of the well-stirred reactor can provide a simplified description of practical combustors. Bragg (1953) originated the view that any reasonably efficient practical combustor should consist of an initially well-stirred reactor section for ignition and flame holding, followed by a plug-flow reactor section for burnout. Since the research combustor was designed specifically to reproduce the major features of an aircraft gas turbine combustor primary zone (Sturgess et al., 1990), it might be expected to conform to well-stirred reactor behavior. The lean blowout behavior supports this expectation. Therefore, the loading parameter can be used to define lean blowout performance.

The research combustor is being tested in a facility that operates at atmospheric pressure and which was limited to maximum propane flow rates of about 20 kg/hr. Under these circumstances, sufficient loading to approach the maximum heat release condition of the research combustor cannot be achieved. However, to investigate the lean blowout phenomenon thoroughly, it is desirable to probe the flowfields for flames that are anchored and lifted at both lightly-strained and heavily-strained flame conditions. Heavily-strained flames occur at high loadings, and in practice, result from combustor operation at a given airflow with low air inlet temperatures and low (sub-atmospheric) pressures. Reducing air inlet temperatures alone to achieve high loadings without choking the combustor requires very low temperatures, and this demands drying of the air to avoid severe icing problems. Given these difficulties, alternative methods of achieving heavily-strained flames were needed.

The quantities involved in the loading parameter are those which influence the speed at which chemical activity converts reactants to products. When the combustor inlet conditions cannot be manipulated to achieve a desired loading, the chemical reaction can be influenced by some other means to yield a similar rate of reactants conversion. If pressure is made the variable of influence, then a suitably altered chemical reaction would reflect the "simulated pressure".

Low pressures can be simulated by the introduction of an inert diluent that slows down the chemical reaction in approximately the same way that low pressures do. The addition of the diluent has two effects - first, it lowers the concentration of reactants, and second, it lowers the reaction temperature by virtue of its heat capacity. Thus, tests may be made at atmospheric pressure and high loading still achieved.

Such a simulation technique for achieving high loadings while operating at room temperature and atmospheric pressure was developed for the research combustor.

SIMULATION TECHNIQUE

A number of techniques for simulating low combustion pressures are available, e.g. Lefebvre and Halls (1959), Lefebvre (1961) and Greenhough and Lefebvre (1956), using water as the diluent. However, water is inconvenient for the present purposes. It requires pre-heating of the inlet air to ensure complete vaporization of the droplets. Gaseous nitrogen has also been used with success (Norster, 1968), and does not require pre-heating. Although a direct calibration for nitrogen was not available, nitrogen as a diluent is extremely convenient for the present purposes, and was therefore selected.

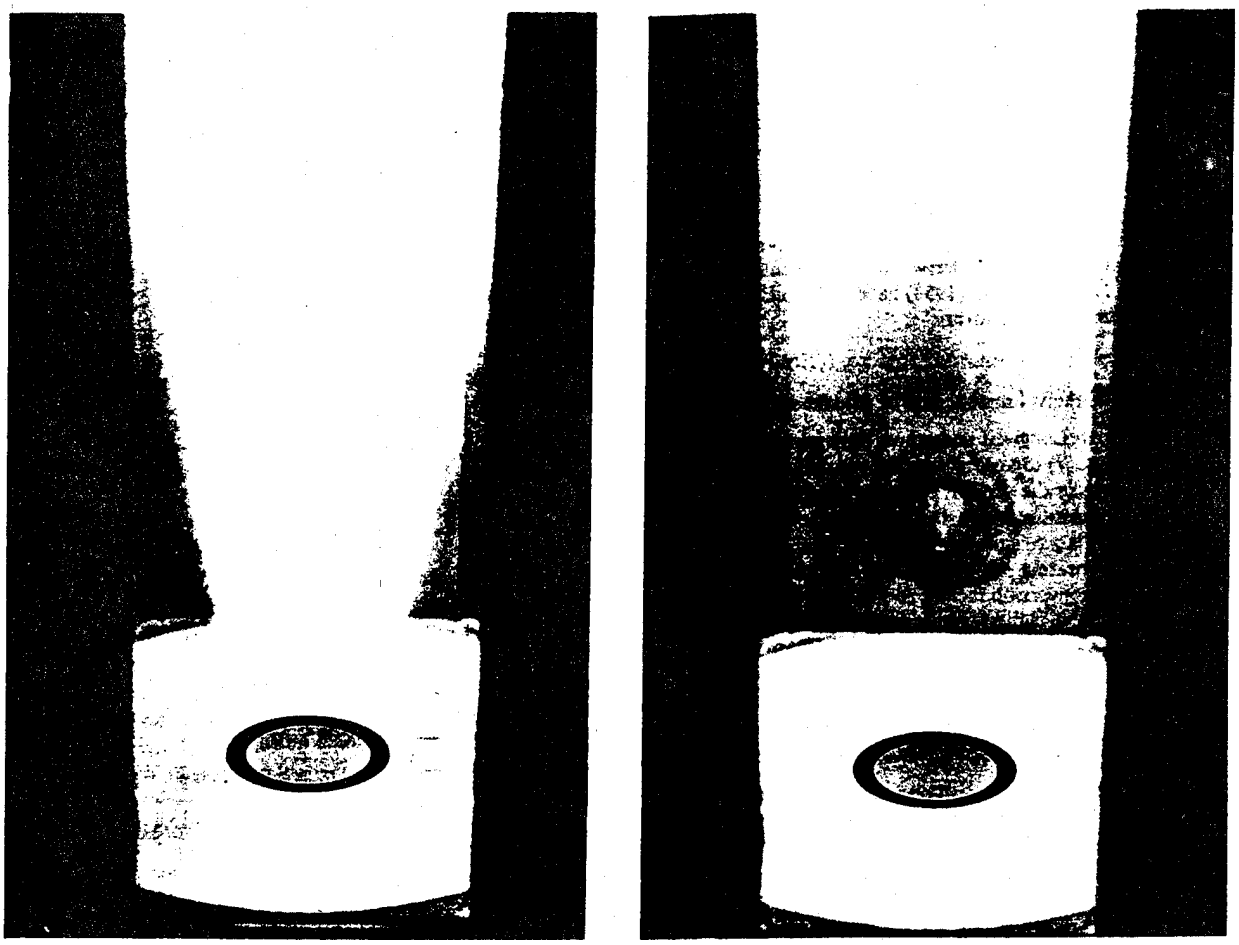

Fig. 2 Photographs of Anchored and Lifted Flame Operation

THEORETICAL BACKGROUND

Consider the combustion of the general hydrocarbon C_xH_y in air, and let the equivalence ratio ϕ be such that there is an excess of air, i.e., $\phi < 1.0$. Also, let the combustion efficiency be such that B is the fraction of fuel that is actually burned. The unburned fuel will not pass through the combustor unchanged, but will, in general, appear in the exhaust as carbon monoxide, hydrogen and lower hydrocarbons. In modern combustors the lower hydrocarbons are always small in quantity under normal circumstances; further, the fast reaction rate of hydrogen suggests that it too, will not be a significant product. Therefore, a simple bimolecular global reaction can be proposed,

$$\phi C_xH_y + (x + y/4)O_2 + 79/21(x + y/4)N_2 = \alpha CO + \beta CO_2 + y/2\phi H_2O + 79/21(x + y/4)N_2 + (1 - \phi B)(x + y/4)O_2 \quad (1)$$

where all of the hydrogen in the fuel is burned to water vapor, and the inefficiency is reflected solely in the CO/CO_2 balance. This is reasonable because of the relatively slow conversion of CO to CO_2. Nitrogen is assumed inert. The molar fractions α and β are found from C/O balances.

For propane this reaction becomes,

$$\phi C_3H_8 + 5O_2 + 18.8095N_2 = 10\phi(1-B)CO + \phi(10B - 7)CO_2 + 4\phi H_2O + 18.8095N_2 + 5(1 - \phi B)O_2 \quad (2)$$

Note that with this simple reaction mechanism CO_2 disappears from the products for a fractional conversion less than or equal to 0.7.

Let K be the mass ratio of diluent nitrogen to fuel. The reaction expression becomes,

$$\phi C_3H_8 + 5O_2 + 18.8095\gamma N_2 = 10\phi(1 - B)CO + \phi(10B - 7)CO_2 + 4\phi H_2O + 18.8095\gamma N_2 + 5(1 - \phi B)O_2 \quad (3)$$

so that the additional mass of N_2 is 18.8095 x 28 (γ - 1).

Hence,

$$\gamma = (\phi K/11.9697 + 1) \quad (4)$$

Eqs. (3) and (4) together provide the volumetric fractional concentrations of oxidant and fuel present in the exhaust, i.e.,

$$m_f = \frac{10\phi(1-B)}{G} \quad (5)$$

where,

$$G = 10\phi(1 - B) + \phi(10B - 7) + 4\phi + 18.8095\gamma + 5(1 - \phi B)$$

and,

$$m_o = \frac{5(1-\phi B)}{G} \qquad (6)$$

From the kinetic theory of gases a reaction rate expression in Arrhenius form can be derived for bimolecular, single-step reactions. Longwell et al. (1953) have proposed that for lean mixtures this takes the form,

$$\phi B\dot{m}''' = Am_o m_f P^2 T^{-3/2} \exp(-E/\Re T) \qquad (7)$$

where $\dot{m}'''$ is the volumetric rate of oxidant mass consumption.

Although Longwell and others have proposed fractional indices in Eq. (7) to accord with the results of various experiments, for the present purposes a pure second order reaction in pressure and first order in concentrations is taken. In Eq. (7), E is a reaction rate constant (activation energy), and A can incorporate a pre-exponential rate constant as well as various unit conversion factors and other constant terms as may be convenient. T is the reaction temperature, and $\Re$ the universal gas constant.

Rearranging Eq. (7) into a form incorporating the loading parameter yields,

$$\frac{\dot{m}_{air}}{VP^2} = \frac{Am_o m_f}{\phi B} \frac{1}{T^{3/2}\exp(E/\Re T)} \qquad (8)$$

Combining Eqs. (5), (6) and (8) gives,

$$\frac{\dot{m}_{air}}{VP^2} = \frac{A(1-B)}{B} \frac{2(1-\phi B)}{(\phi(1.4-B)+79/21\gamma+1)^2} \frac{1}{T^{3/2}\exp(E/\Re T)} \qquad (9)$$

Eq. (9) represents the appropriate global kinetic expression for the reaction rate of propane in air with additional nitrogen. With K equal to zero, it also represents a similar expression for propane in pure air.

A reaction rate simulation can be obtained if,

$$\left(\frac{\dot{m}_{air}}{VP^2R}\right)_{simulation} = \left(\frac{\dot{m}_{air}}{VP^2R}\right)_{desired} \qquad (10)$$

where R is the appropriate reaction rate expression from the right-hand side of Eq. (9), i.e., with $K > 0$ and $P = 1$ atmos. for simulation and $K = 0$ and $P < 1.0$ atmos. for desired reaction rate. If it is taken that the presence of the diluent has no effect on the rate constants, the identity represented by Eq. (10) can be written,

$$\left(\frac{P^2R}{A}\right)_{simulation} = \left(\frac{P^2R}{A}\right)_{desired} \qquad (11)$$

Thus, A does not have to be described explicitly. A typical value for E is 26,613 gm.cal./gm.mole, for near-stoichiometric mixtures (Clarke et al., 1960).

Figs. 3 and 4 may be used to compare the left- and right-hand sides of the identity for an equivalence ratio of 0.9 and inlet temperature of 300K. Fig. 3 shows the effect of pressure on propane/air combustion, while Fig. 4 shows the effect of nitrogen addition on the combustion at one atmosphere pressure. The similarities of the two curves are obvious.

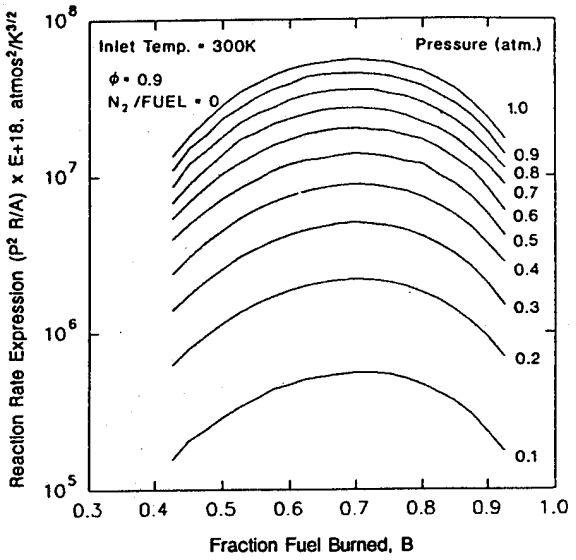

Fig. 3 Variation of Reaction Rate Expression (Eq. 11) with Pressure

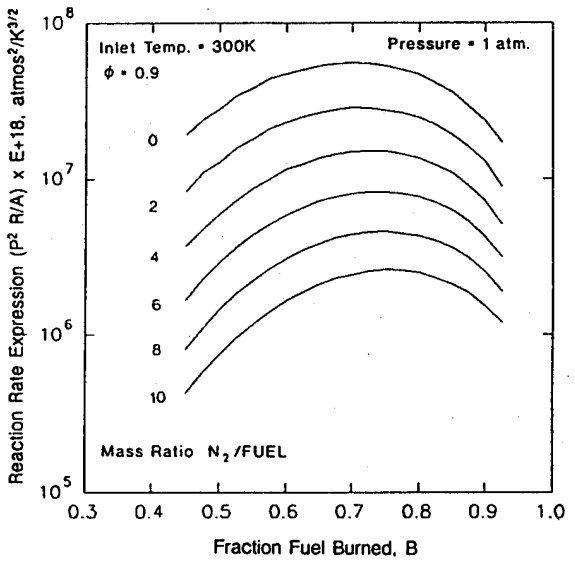

Fig. 4 Variation of Reaction Rate Expression (Eq. 11) with Diluent Addition

NEED FOR CALIBRATION

The simplified reaction mechanism and rate expression used to derive the simulation are only a convenient representation of reality. A given rate expression cannot be expected to adequately represent all the actual reactions taking place so that the expression is appropriate over wide ranges of operating conditions. Therefore, if the simulation technique is to be used for other than merely comparative purposes, some form of calibration is required.

Various global Arrhenius rate expressions have been published in the literature to represent propane/air combustion at different conditions, e.g., Greenhough and Lefebvre (1956), Clarke et al. (1960) and Herbert (1960). One that is more appropriate for low equivalence ratios (around 0.5) is given by,

$$\dot{m}''' = A m_o^{0.5} m_f^{0.5} P T^{-0.5} \exp(-56{,}600/\Re T) \qquad (12)$$

This has the form of Eq. (7), but different fractional indices and rate constants. When the simulation is based on Eq. (12) rather than Eq. (7), considerable differences result.

As is to be described, comparison of curves like Figs. 3 and 4 can be used to obtain the relationships between nitrogen to fuel mass ratio and the equivalent reaction pressure. This has been done in Figs. 5 and 6 for an equivalence ratio of 0.9 and a mixture initial temperature of 300K, using simulations based on Eqs. (7) and (12) respectively. For given combustion efficiency and nitrogen/fuel mass ratio, the differences in equivalent pressure from the two curves are marked. This illustrates vividly the need for calibration of the technique.

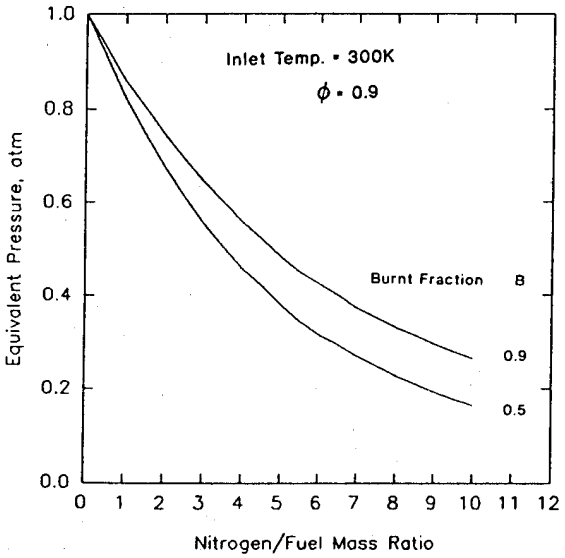

Fig. 5 Dependency of Simulated Pressure on Diluent Addition for a Global Reaction Rate Based on Indices for ϕ = 1.0 (Eq. 7)

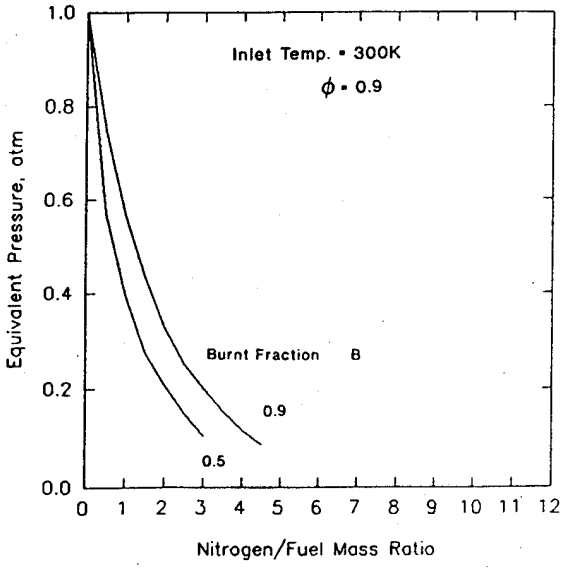

Fig. 6 Dependency of Simulated Pressure on Diluent Addition for a Global Reaction Rate Based on Indices for ϕ = 0.5 (Eq. 12)

CALIBRATION

An ideal calibration would be based on a comparison of the simulated pressure technique against true low pressure tests in the same reactor. Unfortunately, such a direct approach was not immediately available for the research combustor. Therefore, an indirect approach is used. This maintains the bimolecular reaction mechanism Eq. (3), unchanged, but calibrates the Arrhenius reaction rate expression that goes with it.

Fortunately, a calibration of the Arrhenius rate expression for propane/air/excess nitrogen systems has already been carried out by Kretschmer and Odgers (1972), and their work has been utilized here.

Kretschmer and Odgers used for their calibration experimental results from spherical stirred reactors and gas turbine combustors, burning fuels from propane to aviation kerosene over a wide range of operating conditions including pressures from 0.1 to 5.4 atmospheres and inlet temperatures from 200K to 900K; equivalence ratios equal to and less than unity were included. Analysis of these data resulted in a rate expression giving the calibrated form for Eq. (8) as,

$$\frac{\dot{m}_{air}}{VP^2\phi} = \frac{A(m_o m_f)^{\phi}}{\phi B} \frac{1}{T^{2\phi-0.5}\exp(C/T)} \qquad (13)$$

where C is E/$\Re$. For an equivalence ratio of unity, Eq. (13) is identical to Eq. (8); while for an equivalence ratio of one-half, it is identical with the form of Eq. (12). Now, however, the exponential rate constant contained in C is a complex function of equivalence ratio and reactant inlet temperature. This variation arises because of the empirical character given to the rate equation.

Fig. 7 gives the dependency on ϕ of B at blowout for 300K inlet temperature as produced by Kretschmer and Odgers. This dependency is compared with earlier recommendations also given in Kretschmer and Odgers (1972).

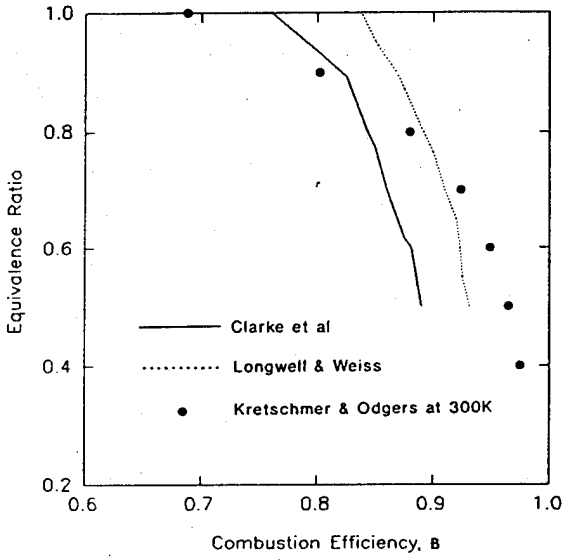

Fig. 7 Variation of Combustion Efficiency at Blowout with Equivalence Ratio, from Several Sources

Unfortunately, Kretschmer and Odgers assumed a reaction mechanism that was different from that given in Eq. (2). Hence, their expression for m_f was different from that given in Eq. (5). Therefore, it was necessary to derive a variation of C, containing the exponential rate constant, with ϕ that was appropriate to the present reaction mechanism.

The derivation of an appropriate C was done through Eq. (13) so that,

$$C = T\,[\ln (m_{f,new}/m_{f,Kretschmer})\, \exp(C/T)_{Kretschmer}] \quad (14)$$

A comparison between the variations of two C's with equivalence ratio for an inlet temperature of 300K is shown in Fig. 8. Although the differences are small, it should be remembered that C is eventually to be used in an exponential relationship. The variation of C for the present reaction mechanism is conveniently represented by the polynomial,

$$C = 14{,}926.5 + 73{,}774.7\phi - 109{,}826\phi^2 + 35{,}933.3\phi^3 \quad (15)$$

which has a correlation coefficient of 0.99998 and a maximum error of -54.3K in the range $0.4 < \phi <= 1.0$.

Eqs. (13) and (15) establish the form of the global reaction rate, and relate it to the selected reaction mechanism.

The calibration of simulated pressure may now be constructed for a range of equivalence ratios. The appropriate reaction rate expressions, one with variation in pressure and the other with variation in diluent mass flow rate, can be compared as functions of pressure and nitrogen/fuel mass ratio respectively. The intersection of these expressions represents a common value of reaction rate expression indicating equivalency of pressure and nitrogen/fuel mass ratio. This enables the relationship between diluent mass flow rate and simulated pressure to be established. Fig. 9 gives an example of this technique for a ϕ of 0.8; Fig. 10 shows the resulting calibration curves for an inlet temperature of 300K.

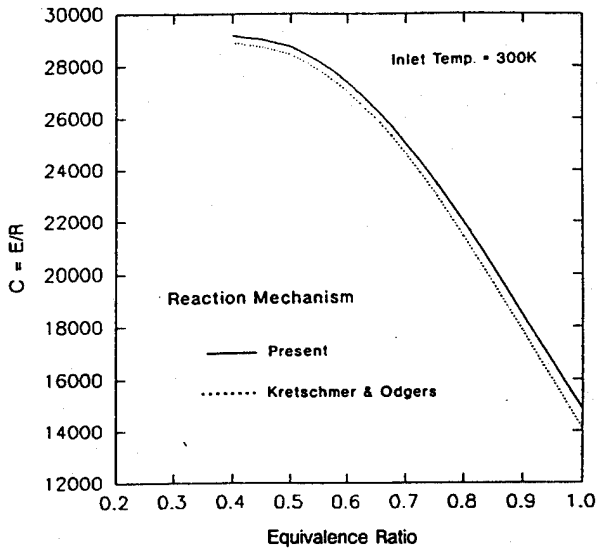

Fig. 8 Comparison of Dependencies of Activation Energy on Equivalence Ratio for Kretschmer and Odgers Reaction Mechanism and Present Reaction Mechanism

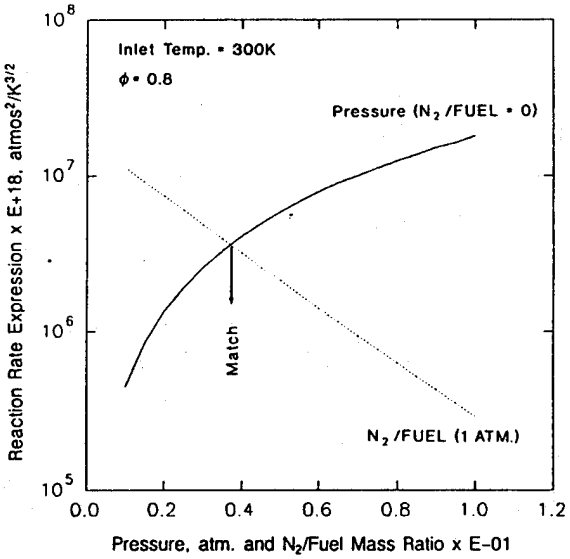

Fig. 9 Relationship Between Low Pressure and Simulated Reation Rates for ϕ = 0.8

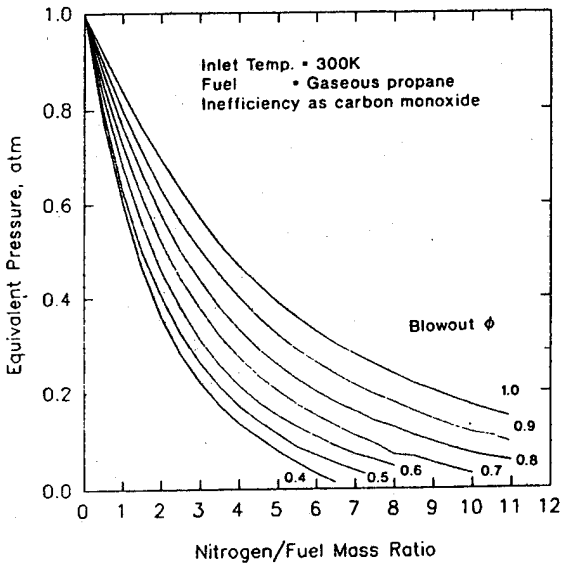

Fig. 10 Nitrogen–Simulation Calibration Curve at 300K

Fig. 10 can be considered valid for well-stirred and partially-stirred reactors. Although the empirical adjustment of the global Arrhenius reaction rate expression may be considered as being valid for a wide variety of hydrocarbons burning in air, the simulation calibration is for propane only. Further, it is limited to fuel-lean mixtures, as the figure indicates. The calibration shown is for 300K inlet temperatures; Swithenbank (1974) contains sufficient information to construct curves for inlet temperatures from 200K to 900K.

EXPERIMENTAL RESULTS

After the ignition sequence was completed and the desired airflow established with the anchored flame condition (Sturgess et al., 1990), gaseous nitrogen was introduced into the air supply line to the research combustor. This was done far upstream so that the excess nitrogen was uniformly mixed with the air entering via the annular air jet surrounding the fuel jet. The nitrogen flow rate was set at a desired level, and a blowout sequence obtained by reducing the fuel flow rate until the flame was extinguished. Ignition was reestablished, the airflow reset at the previous value in conjunction with the fuel flow, a new nitrogen flow rate was selected, and blowout was again obtained.

This procedure was repeated until a maximum nitrogen flow condition was reached. The combustor has been operated with nitrogen mass flow rates up to 55 percent of the air mass flow rate. No difficulties were encountered at this extreme condition. Repeatability and hysteresis were checked through obtaining blowouts by turning down the nitrogen flow rate range, and also by holding nitrogen and fuel flow rates constant while the airflow rate was increased. In addition, test points were repeated on different days with a different observer.

Examples of the basic results are displayed in Fig. 11, and show at a given airflow that increasing the nitrogen flow rate linearly increases the fuel flow rate at which a blowout takes place. In the figure, the multiple tests points shown at a given nitrogen flow rate for the 0.653 lbm/sec (0.075 kg/sec) airflow represent the day-to-day repeatability of the blowout.

Increasing the combustor airflow increases the fuel flow at which blowout occurs, but does not change its dependency on the nitrogen flow rate.

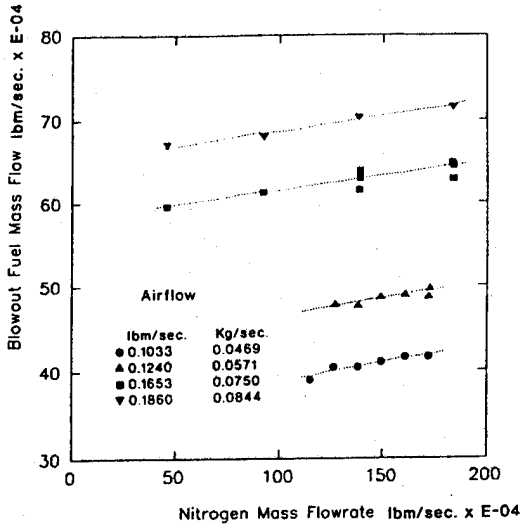

Fig. 11 Relationship Between Fuel Flow at Blowout and Nitrogen Flow at Several Airflows in the Research Combustor

Fig. 12 gives an indication of the range of equivalent pressures represented by the nitrogen simulation, for various airflows. It ranges from just less than one atmosphere down to one-tenth of an atmosphere for these tests. The equivalent pressures were obtained from Fig. 10 for the blowout conditions given in Fig. 11. When the equivalent pressures are displayed against the mass ratio of nitrogen to fuel at blowout in this form, the data for the different airflows collapse onto a single curve representing the blowout characteristic for the research combustor. Note that for nitrogen to fuel mass ratios greater than about 5, there is a loss of effectiveness of the technique.

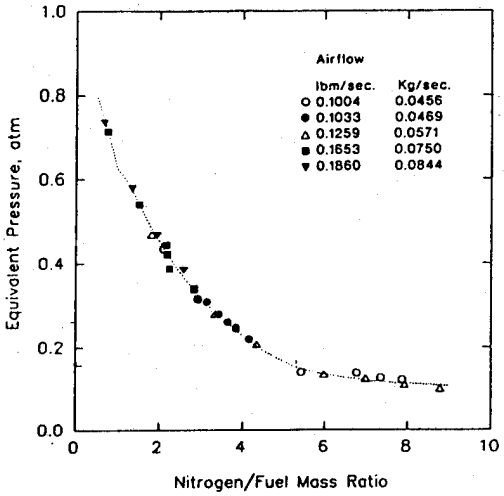

Fig. 12 Relationship Between Equivalent Pressure and Nitrogen to Fuel Mass Ratio at Blowout in the Research Combustor

When excess nitrogen is introduced into the air supply, the visual appearance of the flame and its behavior does not change from that observed for zero excess nitrogen, (Sturgess et al., 1990), (Heneghan et al., 1990). Fig. 13 gives a description of the flame behavior at constant airflow as the nitrogen flow rate is increased. Visually, there is no change in the equivalence ratio at which flame lift takes place. The equivalence ratio for lean blowout does increase, in accord with the behavior of Fig. 11. Blowout with excess nitrogen follows the same sequence of events as was observed for zero excess nitrogen (Sturgess et al., 1990), (Heneghan et al., 1990).

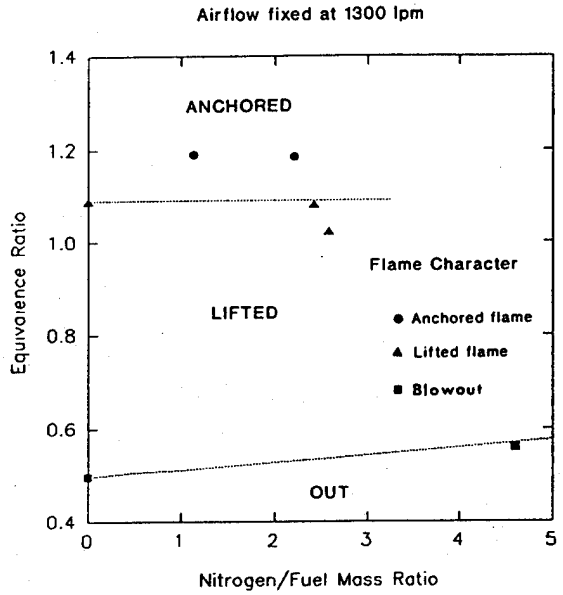

Fig. 13 Flame Behavior in the Research Combustor at Fixed Airflow as Nitrogen to Fuel Mass Ratio Is Varied

CORRELATION OF EXPERIMENTAL DATA

As described above, the equivalence ratio at blowout, ϕ_{LBO}, of a well-stirred reactor can be related to the gas loading parameter, $\dot{m}/VP^nF$, for the combustor. Here, the mass flow rate is interpreted as $\dot{m}_{Tot}$, which is the sum of the air, excess nitrogen and fuel mass flow rates. The fuel is included in this sum since its volume is not insignificant; the nitrogen flow rate is generally several times that of the fuel. Thus, the residence time in the reactor is materially affected by these flows.

For the present experiments the temperatures of the reactants were not varied, and the values for air, excess nitrogen and propane were sensibly equal. Therefore, the temperature correction factor F, is taken as unity as a matter of convenience.

The pressure is interpreted as the effective pressure, and depends on the quantity of excess nitrogen flowing, as given by Fig. 12.

The (constant) volume is taken as the total combustor volume minus the volume of the combustor associated with flame lift.

The apparent order of the reaction, n, is taken as equal to 2 ϕ for lean mixtures. However, this is for propane/air systems. When a diluent is present, the order is reduced. The expression,

$$n = \frac{2\phi_{LBO}}{(1+\dot{m}_{N2}/\dot{m}_{air})} \qquad (16)$$

is used to account for this. When no excess nitrogen is present, Eq. (16) reverts to the pure air form.

In Fig. 14 the data in terms of ϕ_{LBO} and $\dot{m}_{Tot}/VP^n$ are plotted in logarithmic form. The measured data define most of the lean portion of the stability loop for the research combustor. The data cover points at atmospheric pressure with zero excess nitrogen, as well as those at atmospheric pressure with excess nitrogen; a variety of airflows were used.

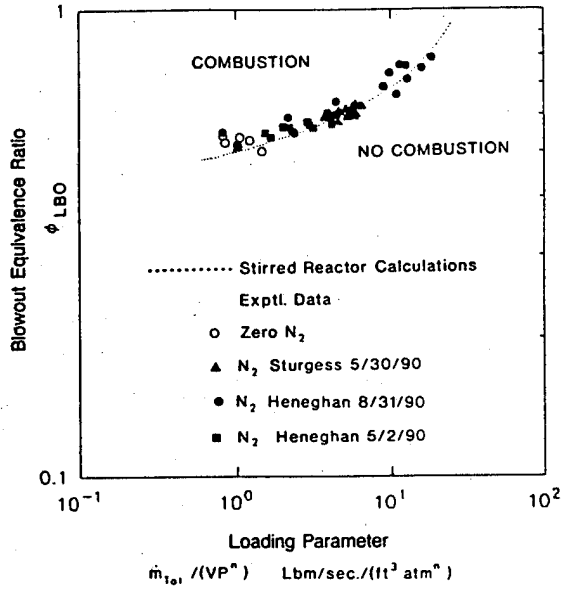

Fig. 14 Correlated Blowout Data for the Research Combustor, and Comparison with the Calculated Well-Stirred Reactor Blowout Characteristic for the Research Combustor

The figure shows that the loading parameter correlates the blowout equivalence ratios very well. This can be appreciated when considering the repeatability shown in Fig. 11. The blowout data extend over three orders of magnitude of loading parameter, and range from a blowout equivalence ratio of around 0.5 to around 0.8.

VERIFICATION OF CALIBRATION

Use of the simulation calibration curves for effective pressure (Fig. 12), resulted in a very satisfactory correlation of experimental lean blowout data obtained at constant true pressure for wide ranges of air and excess nitrogen flows. Fortunately, since the research combustor with zero excess nitrogen appeared to behave like a well-stirred reactor (Sturgess et al., 1990), (Heneghan et al., 1990), an independent check of the calibration can be made through the use of well-stirred reactor theory.

Swithenbank (1974) presented a dissipation gradient approach for defining perfectly-stirred regions of combustors. This approach was applied to the research combustor, using a

computational fluid dynamics (CFD) calculation to provide the turbulence characteristics.

Based on the dissipation gradient analysis, the rapid-stirring region of the research combustor was identified as the volume enclosing the highly turbulent portion of the flow. It was found that the surface contour enclosing 96 percent of the turbulence kinetic energy and 99 percent of its rate of dissipation corresponded to a surface over which the total dissipation gradient had a value of 10.0, which is 100 times the value recommended by Swithenbank. This well-stirred region extended over most of the length of the combustor, with exceptions of portions of the step recirculation zone and the stagnation region on the upstream face of the orifice plate placed at the combustor exit.

While the turbulence characteristics of a flow can be used to define a region of rapid mixing, this alone is not a sufficient condition for a well-stirred reactor. For stable reaction to take place within the rapid mixing region, the fuel and air mixture must locally fall inside the flammability limits, a source of continuous ignition (mixture at exit temperature) must be present, and local flow velocities must not exceed the local turbulent burning velocity.

CFD analysis was again used to provide necessary information to determine places within the defined rapid mixing region where stable combustion could take place for conditions close to blowout. On the basis of these calculations and the observations of the lifted flame position, which was found to remain roughly constant as equivalence ratio was reduced, a suitable well-stirred reactor volume was defined. This was 44 percent of the total combustor volume, and corresponded to a lifted flame mean position of about 40 cm (16 inches) from the central portion of the step, assuming that the flame completely filled the cross-section. Visual observations of the flame indicated that on the centerline of the combustor the closest position to the step-plane of the lifted flame was about 16 cm (6 inches) downstream. Of course, the real flame never completely filled the cross-section.

With a well-stirred reactor defined, the stirred reactor network code MARK2I by David Pratt and Brian Pratt was used to make calculations for the research combustor. The MARK2I code uses the CREK chemical kinetics code (Pratt and Wormeck, 1976) and a hydrocarbon reaction mechanism by Roberts et al. (1972). The research combustor near blowout was modeled in MARK2I as a single, perfectly-stirred reactor with separate air and fuel inlets, and a single discharge of products; there was no recirculation of products. It was operated with gaseous propane as fuel and air as oxidant, with equal inlet temperatures of 293K. The volume was that defined above, although two other volumes were used for spot-checks to see the sensitivity to volume. This was done because of the uncertainty associated with the flame position. (The results for the range of volumes were subsequently correlated successfully by the loading parameter, via the volume term incorporated in it.) The model was operated at a number of air mass flow rates, with several pressure levels of atmospheric and less, for each airflow. No cases with excess nitrogen were run.

Shown on the stability plot of Fig. 14 is a line representing the blowout characteristic calculated by the well-stirred reactor code. The line runs through the correlated experimental blowout data very nicely, thereby confirming that the research combustor is behaving as a well-stirred reactor. Furthermore, since the loading variation in the well-stirred reactor calculations was achieved through variations in mass flow rate and true operating pressure while the experimental data were correlated on the basis of mass flow rate and equivalent pressure, the agreement verifies the calibration (Fig. 12) of the nitrogen dilution technique.

DISCUSSION

A technique has been presented whereby the lean reaction of gaseous propane in air at sub-atmospheric pressures can be simulated by approximating the sub-atmospheric pressure reaction rate with a reaction rate at atmospheric pressure in the presence of excess gaseous nitrogen as a diluent.

The technique has been calibrated through the assumption of a one-step global reaction mechanism for propane/air/excess nitrogen systems in which nitrogen remains inert, and where combustion inefficiency is accounted for solely through the CO/CO_2 balance in the products. A global reaction rate expression in Arrhenius form for a bimolecular, single-step reaction was calibrated using experimental data from the literature. Finally, the relationship between excess nitrogen and the equivalent pressure was established by comparing appropriate reaction rate expressions with separate variation in pressure and diluent mass flow rate. This relationship forms a calibration for the simulation technique at blowout conditions. The calibration is valid for well-stirred and partially-stirred reactors using propane as a fuel in a lean mixture with air. The specific calibration curve presented is for 300K inlet temperature of reactants, although similar curves for other temperatures are readily constructed.

Lean blowout data in a research combustor, obtained using the simulation technique, were successfully correlated using the conventional loading parameter in which the pressure term was taken as the equivalent pressure obtained from the calibration. The range of equivalence ratios covered by the variation in loading parameter was from near the flammability limit to near the maximum heat release rate; the range of loading parameter obtained extended over three orders of magnitude. These were achieved at atmospheric pressure and with a limited range of mass flow rates. The lean stability of the research combustor was completely defined by these data.

The combustor was operated without difficulty with an excess nitrogen mass flow rate up to 60 percent of the air mass flow rate. At this condition the equivalent pressure corresponded to 0.1 atmosphere. However, it is not recommended that the maximum excess nitrogen flow rate be greater than about 45 percent of the air mass flow rate. This is because of inaccuracies in the calibration curve (lower right-hand corner of Fig. 10), at operating conditions with very high levels of excess nitrogen.

The effective order of the reaction when excess nitrogen is used becomes a function of the mass ratio of excess nitrogen to air, as well as equivalence ratio at blowout. There was no visual evidence that the excess nitrogen changed the flame characteristics in any way from that observed without excess nitrogen.

A final check on the accuracy of the calibration was made by comparing the correlated experimental results using the simulation against well-stirred reactor calculations based on propane/air systems for true sub-atmospheric pressures. This comparison was justified since it was known from the initial test

results (Sturgess et al., 1990), (Heneghan et al., 1990) that the research combustor had well-stirred reactor lean blowout performance when operated at atmospheric pressure without any excess nitrogen. The subsequent agreement in the stirred reactor calculation comparison confirmed the accuracy of the calibration.

The demonstration of the successful calibration for the nitrogen dilution simulation of low operating pressures opens an important possibility for small-scale facility combustion experiments. Their operating range may be extended for certain low pressure effects in an easy, inexpensive and safe fashion while the convenience of operating at atmospheric pressure is maintained.

Experimental lean blowout data have been obtained in the research combustor over a wide range of equivalence ratios. These data will provide a good data base for lean blowout modeling. The fact that the research combustor has been definitively shown to behave as a well-stirred reactor when operated in the lifted flame condition is an important help in understanding, and hence modeling, the lean blowout process.

CONCLUSIONS

1. The nitrogen dilution technique for simulating the effects on chemical reaction rates of low pressures has been successfully calibrated. The calibration removes the simulation from being a qualitative technique, to being a quantitative one. It permits certain low pressure combustion effects to be examined while maintaining the convenience of operating at atmospheric pressure.
2. The lean blowout data obtained in a research combustor via the low pressure simulation technique were correlated by the familiar loading parameter when the effective pressure was used for actual pressure and the reaction order was made a function of the excess nitrogen.
3. Nitrogen dilution enables the loading parameter for the research combustor to be extended over three orders of magnitude, and the blowout equivalence ratio to be increased from near the flammability limit to close to the maximum heat release condition. This enables the lean stability of the combustor to be adequately defined.
4. The research combustor at blowout conditions behaves like a classical well-stirred reactor.

ACKNOWLEDGEMENTS

This work was supported by the U.S. Air Force Wright Research and Development Center, Aero Propulsion and Power Laboratory, under Contract No. F33615-87-C-2822 to Pratt & Whitney, East Hartford, CT, (Contract Monitor: Lt. A. L. Lesmerises) and Contract No. F33615-87-C- 2767 to University of Dayton, Dayton, OH, (Contract Monitor: Dr. W. M. Roquemore).

REFERENCES

Bragg, S. L., Aeronautical Research Council, Paper No. 16170, CF 272, U.K., September 1953.

Clarke, A. E., Odgers, J., and Ryan, P., "Further Studies of Combustion Phenomena in a Spherical Reactor," *Proc. 8th. Symposium (International) on Combustion*, The Combustion Institute, 1960, pp. 983-994.

Greenhough, V. W., and Lefebvre, A. H., "Some Applications of Combustion Theory to Gas Turbine Development," *Proc. Sixth Symposium (International) on Combustion*, Reinhold Publishing Co., 1956, pp. 858-869.

Heneghan, S. P., Vangsness, M. D., Ballal, D. R., Lesmerises, A. L., and Sturgess, G. J., "Acoustic Characteristics of a Research Step Combustor," AIAA Paper No. AIAA-90-1851, presented at AIAA/SAE/ASME/ASEE 26th. Joint Propulsion Conference, Orlando, Florida, July 16-18, 1990.

Herbert, M. V., "A Theoretical Analysis of Reaction Rate Controlled Systems; Part II," *Proc. 8th. Symposium (International) on Combustion*, The Combustion Institute, 1960, pp. 970-982.

Kretschmer, D., and Odgers, J., "Modeling of Gas Turbine Combustors - A Convenient Reaction Rate Equation," Trans. ASME, *Journal of Energy Power*, July 1972, pp. 173-180.

Lefebvre, A. H., and Halls, G. A., "Simulation of Low Combustion Pressures by Water Injection," *Proc. Seventh Symposium (International) on Combustion*, Butterworths Scientific Publications, London, 1959, pp. 654-658.

Lefebvre, A. H., "Some Simple Techniques for the Performance Evaluation of Gas Turbine Combustion Systems," Experimental Methods in Combustion Research, Edit. J. Surugue, AGARD, Pergamon Press, 1961.

Lewis, B., and von Elbe, G., Combustion, Flames and Explosion of Gases, 3rd. Edition, Academic Press, 1987.

Longwell, J. P., Frost, E. E., and Weiss, M. A., "Flame Stability in Bluff-Body Recirculation Zones," *Ind. Eng. Chem.*, Vol. 45, No. 8, 1953, pp. 1629-1633.

Norster, E. R., "Subsonic Flow Flameholder Studies Using a Low Pressure Simulation Technique," *Proc. Intl. Prop. Symp. Combustion in Advanced Gas Turbine Systems*, Edit. I. E. Smith, Cranfield Intl. Symp. Series, Vol. 10, Pergamon Press, 1968, pp. 79-94.

Pratt, D. T., and Wormeck, J. J., "CREK - A Computer Program for Calculation of Combustion Reaction Equilibrium and Kinetics in Laminar or Turbulent Flow," Rpt. No. WSU-ME-TEL-76, Dept. Mech. Engrg., Washington State University, 1976.

Roberts, R., Aceto, L. D., Kollrack, R., Teixeira, D. P., and Bonnell, J. M., "An Analytical Model for Nitric Oxide Formation in a Gas Turbine Combustor," *AIAA J.*, Vol. 10, No. 6, June 1972, pp. 820-826.

Sturgess, G. J., Sloan, D. J., Lesmerises, A. L., Heneghan, S. P., and Ballal, D. R., "Design and Development of a Research Combustor for Lean Blowout Studies," ASME Paper No. 90-GT-143, presented at the Gas Turbine and Aeroengine Congress and Exposition, Brussels, Belgium, June 11-14, 1990.

Swithenbank, J., "Flame Stabilization in High Velocity Flow," Combustion Technology - Some Modern Developments, Edit. H. B. Palmer and J. M. Beer, Academic Press, 1974, pp. 91-125.

THIS PAGE INTENTIONALLY LEFT BLANK

APPENDIX F

EXPERIMENTAL AND THEORETICAL STUDIES IN A GAS-FUELED RESEARCH COMBUSTOR

By

W.M Roquemore and V.K. Reddy
WL/POSF Wright-Patterson Air Force Base, Ohio

P.O. Hedman
Brigham Young University, Provo, Utah

M.E. Post, T.H. Chen, L.P. Goss, D.Trump, and V. Vilimpoc
Systems Research Laboratories, Inc., Dayton, Ohio

G.J. Sturgess
Pratt & Whitney, East Hartford, Connecticut

Published as AIAA Paper No. AIAA-91-0639, January 1991.

AIAA 91-0639

Experimental and Theoretical Studies in a Gas-Fueled Research Combustor

W. M. Roquemore and V. K. Reddy
WL, Wright-Patterson Air Force Base, OH
P. O. Hedman
Brigham Young University
M. E. Post, T. H. Chen, L. P. Goss, D. Trump, V. Vilimpoc
Systems Research Laboratories, Inc.
G. J. Sturgess
Pratt and Whitney, East Hartford, CT.

29th Aerospace Sciences Meeting
January 7-10, 1991/Reno, Nevada

For permission to copy or republish, contact the American Institute of Aeronautics and Astronautics
370 L'Enfant Promenade, S.W., Washington, D.C. 20024

Experimental and Theoretical Studies in a Gas-Fueled Research Combustor

W. M. Roquemore and V. K. Reddy
Wright Laboratory
Aero Propulsion and Power Directorate
Wright Patterson AFB, OH 45433-6563

P. O. Hedman
Chemical Engineering Department
Brigham Young University
Provo, UT 84602

M. E. Post, T. H. Chen, V. Vilimpoc, L. P. Goss, B. Sarka, D. Trump
Systems Research Laboratories, Inc.
A Division of Arvin/Calspan
Dayton, OH 45440-3696

G. J. Sturgess
Pratt and Whitney
East Hartford, CT 06108

ABSTRACT

This paper reports the results of an investigation to determine the flow and flame characteristics of a burner which has been carefully designed to "specifically reproduce recirculation patterns and lean-blow-out (LBO) processes that occur in a real gas turbine combustor" [1]. When operated in a fuel rich mode, the flame is very stable and is anchored in the jet shear layer by a pilot flame attached to the step, near the outer edge of the air supply tube. As the equivalence ratio is reduced, the flame becomes less stable, and eventually reaches a point where the pilot flame becomes detached (lifts) from the base region, and the entire flame structure becomes stabilized downstream. Thus, there are two distinct operating modes for the combustor: a fully attached flame and a lifted flame. As the fuel equivalence ratio is further reduced, the flame becomes progressively less stable in its lifted condition, and eventually blows out. Photographs of the flame clearly illustrate the attached and lifted flame operational regimes of the combustor. However, visual observation and conventional photographic techniques are unable to quantify the precise details of the flame transition from an attached to a lifted condition. A Computational Fluid Dynamics (CFD) model with one step chemistry was used to investigate the time-averaged features of the reacting and non-reacting flow fields. The difficulties of predicting the characteristics of the attached flame with a time averaged CFD type model are discussed. Measurements, using OH emissions and graybody radiation from 14 μm diameter filaments located near the base of the flame, clearly indicate the dynamic or intermittent nature of both the attached and lifted flames. It is theorized that unburned hydrocarbon combustion products are transported into the recirculation zone by the intermittent process; and it is these products that provide the fuel needed for the flame to attach to the outer edge of the step.

INTRODUCTION

Advancements in gas turbine engine technology are reducing design tolerances and increasing the need to have precise design methods. Of all the design requirements for combustion chambers, several may be categorized as being critical to safety and reliability. One of these is combustion stability, an aspect of which is lean-blow-out (LBO). LBO is of special concern since recent design trends appear to result in an erosion of stability margins. This concern is exacerbated by the weakness in current methods of calculating LBO limits, and by the limited design criteria for obtaining good stability. A research program that results in improved calculation procedures for LBO enhances design capability and will provide a most valuable contribution.

There are several difficulties that make modeling LBO a serious challenge. LBO is usually encountered during engine transients and it may, therefore, be difficult to separate overall system behavior from the combustor characteristics. The phenomenon itself is a transient process, and it may involve non-stationary flow behavior. Hence, LBO is rather difficult to study in detail. The physics involved can be extremely complex since it concerns interactions between several processes. This means that the mechanisms of blow-out in one combustor

design might be different from that of another design so that the impact of changing operational parameters, such as pressure or air flow, could have opposite effects. Also, the blow-out process may be very sensitive to small design changes even to the point that manufacturing and assembly tolerances in a system component, such as the fuel nozzle, may be a significant factor. An equal challenge is presented by the state-of-the-art in computational fluid dynamic (CFD) based codes for engineering use. In general, these provide stationary-state solutions, and the near-term prospects for realistic time-dependent calculations for engineering applications are not good.

This paper presents the results of an investigation to determine the flow and flame characteristics of a burner designed for the study of the fundamental LBO process. The burner has confined, coannular jets that discharge into a sudden expansion. This simple geometry provides a recirculation zone that is similar to those in modern gas turbine combustors. The present work is part of a larger study to investigate the flow and flame structure within the combustor over a wide range of fuel equivalence ratios and loading conditions. The results presented in this paper are considered preliminary in that the Reynolds numbers associated with flow conditions are lower than those found in gas turbine combustors. The transitional Reynolds number limitation was required to prevent overheating of the facility exhaust hood. The facility is currently being modified to accommodate the higher heat loads associated with fully turbulent flows. Future studies performed in this facility will be conducted at engine representative Reynolds number flow conditions. The general descriptions of the flame attachment and lifting processes reported in this paper were also observed in the facility at fully turbulent Reynolds number conditions. However, these conditions were only maintained for only short periods of time. Earlier studies conducted with this combustor were performed in a high Reynolds number flow facility that did not have the heat load problem [1,5,6].

The objectives of this paper are to: 1) characterize the flame structure for a wide range of equivalence ratios; 2) identify phenomena that contribute to the transition from an attached to a lifted flame since this clearly represents the beginning of lean blowout; and 3) gain insight into the characteristics that a model must have to correctly predict the LBO process.

The experimental approach used in this study involves: 1) visual observations, 2) 2-D flow visualization of the combustion flows using Reactive Mie Scattering, 3) spontaneous OH emission measurements in the ultraviolet (uv) to characterize the fuel equivalence ratio where the flame transitions from an attached flame to a lifted flame, 4) uv laser sheet lighting to stimulate OH laser induced fluorescence (LIF) emission, and 5) thin filament graybody radiation studies of the flame frequency oscillations. A CFD model is also used to investigate the time averaged flow field characteristics of the burner. Experimental and model results are discussed in the following sections.

EXPERIMENTAL DESCRIPTION

Combustor. The combustor is shown schematically in Figure 1. The combustor has been carefully designed to "specifically reproduce recirculation patterns and LBO processes that occur in a real gas turbine combustor"[1]. The research combustor consists of coaxial jets with a 29.7 mm inside diameter central fuel jet surrounded by a 40 mm diameter annular air jet. The fuel is gaseous propane. The jets are located centrally in a 150 mm diameter duct. A backward facing step at the jet discharge plane completes the sudden expansion, giving a step height of 55 mm. The step provides a recirculation region that can stabilize the flame. The combustor test section incorporates flat quartz windows to accommodate laser and other optical access to the flame. Curved metal fillets, located in the corners of the test section, reduce and distribute the vorticity, generated by secondary wall flows, and thereby minimizes its impact on the bulk flow field in the combustor. This hybrid cross-section of the combustor allows reasonable optical access for laser diagnostics, while providing a good two-dimensional, axisymmetric flow approximation.

Test Conditions. Tests reported herein were all conducted at an air flow rate of 1000 lpm (referenced to 1 atm and 21°C) with a mean velocity of 31.6 m/s. Nominal propane flow rates were 30, 41, 52, and 63 lpm propane (referenced to 1 atm, and 0°C) with velocities of 0.8, 1.01, 1.35, and 1.64 m/s, respectively. These flow rates correspond to fuel equivalence ratios of 0.78, 1.05, 1.31, and 1.56, respectively. The Reynolds number for the annular air jet based on the width of the air jet is 18,360. Fuel jet Reynolds numbers are 5,223, 7,138, 9,053, and 10,968, respectively. Thus both the air and fuel jets are in the transitional flow region.

Reactive Mie Scattering (RMS). Mie scattering of a laser sheet from TiO_2 particles was used to obtain instantaneous (10 ns) images of the flame and flow patterns. The TiO_2 seed was obtained from the near instantaneous reaction of $TiCl_4$ vapor and moisture to form the TiO_2 particles. Either dry air or dry propane were seeded with $TiCl_4$ vapor. Moisture was added to the opposite flowing stream to provide ample H_2O for the chemical reaction. Moisture generated in the combustion process also participated in the chemical reaction. A sheet of light from a frequency doubled Nd-Yag laser was used to illuminate a cross section of the flow through the centerline of the burner. Images were collected with a 1024x1024 array unintensified CCD camera that was located normal to the laser sheet.

OH Emissions. An instrument was set up to observe the spontaneous emission from the OH radical through a very narrow region of the flame near the flame attachment point. A simple lens and aperture were used to focus a narrow, cylindrical region of the combustor into a spectrometer. The waist of the focal volume was located about 15 mm above the base of the burner and in the region where the characteristic blue flame sheet was observed when the flame was attached. The focal volume integrated the OH emission along the entire path across the burner, but the most intense region, at least from visual observations was in the circular ring just outside of the air jet, where the flame appeared to attach.

The spectrometer was tuned to an OH emission line near 308 nm that gave a strong signal. The signal was captured with a photomultiplier tube, amplified, converted to a digital signal, and recorded on a mini computer. The 20,000 separate digital points collected over a 20 second time period were used to obtain a mean and standard deviation of the measured signal. Even though the spectrometer and photomultiplier tube were shielded from the radiation of the combustor, there was sufficient thermal loading to cause considerable background instrument noise that changed during a test. Consequently, an average background was obtained for each set of OH emission measurements. An average background was obtained from 20,000 data points collected after each test with the entrance to the spectrometer blocked. The average background signal was subtracted from each of the uv signal data points to obtain as representative a set of uv emission data as possible.

Laser-Induced Fluorescence (LIF). A thin sheet of laser light was also used to capture instantaneous (10 ns) two dimensional images of the flame and flow structure from the laser induced fluorescence (LIF) emission of OH. A frequency doubled Nd-Yag laser was used to generate a uv laser beam at about 283 nm. This frequency was used to pump a fluorescence transition of OH which resulted in a LIF signal at about 308 nm. As in the $TiCl_4$ seeded experiments, the plane of the laser light bisected the centerline of the test section. A 384x576 element intensified CCD camera, located normal to the laser sheet, was used to capture the rather faint images from the laser induced OH fluorescence. The intensified CCD camera was able to capture the full width of the optical window, but was limited in vertical height to about a 77 mm section of the combustor. To get a more complete record of the OH images, data were collected at four axial locations: 0 mm, 75 mm, 150 mm, and 225 mm.

Thin-Filament Pyrometer (TFP). A thin-filament pyrometer was used to study the time variations in temperature of the flame near the inlet of the combustor. The 14 μm SiC_4 filament is capable of measuring temperatures at high sampling rates and is described in detail in [7]. The filament was not calibrated for these studies and was used only to indicate relative temperatures. The emissivity of the SiC_4 filament is independent of temperature which means that the intensity of the radiation from the filament is exponentially proportional to the temperature as determined by Planck's blackbody radiation law. The response time of the filament is of the order of 700 Hz, which causes the intensity signal from the filament to rise and fall as the temperature varies inside the combustor. The lower detectable temperature limit of the filament was about 1300 K, based on past experiences [7]. The radiation from a chosen filament was imaged onto a single InGaAs photodiode detector through the use of a cylindrical lens and a rotating mirror. The filament was located about 1 cm above the exit of the fuel-air jet. The filament radiation scanned and imaged with 256 pixels, digitized, and stored during each gated scan. For a fixed optical layout, the physical length scanned can be adjusted by changing the mirror scan rate and the digitization rate. This scanned length divided by 256 yields the pixel resolution. In this study the pixel resolution was ~ 75 μm.

To achieve the high sampling rates used in this experiment, a transient recorder was used. The output signal from the InGaAs detector was amplified and fed into the memory unit of the transient recorder. During the gated time period, 256 bytes of data were digitized at a selected rate in the range 1 - 4 Mbyte/s. The digitized data, which can be used to derive the line temperature profile, were then fed into a micro computer for data processing and storage. For this study, the line TFP signal was scanned at 250 and 500 lines per second. It was found that inside the recirculation zone near the step surface, the flame oscillation occurs at very low frequencies, i.e., less than 20 Hz. Therefore, only the results of scans at 250 lines per second are shown.

From the stored line signal taken at known scan rate, spectral information related to the flame oscillation can be obtained by spectral analysis using fast Fourier transform (FFT). For example, once a spatial location was chosen for the spectral analysis, the intensity data corresponding to that location was graphed as a function of time. Then, that array of data was fed into an FFT routine to yield spectral density. The FFT results are used to identify significant frequency patterns in the temperature signal produced by the filament.

CFD MODEL DESCRIPTION

Both the nonreacting and the reacting flows in the research combustor are numerically simulated using a not-yet-published CFD code that is capable of predicting nonequilibrium and weakly compressible flows. It uses a non-staggered grid system and solves time-dependent

governing equations that are written in cylindrical polar coordinate system. An isotropic k-ε turbulence model has been used. When N_S number of species are considered in the given problem then, this two-dimensional code solves (N_S+5) governing equations namely; two momentum, continuity, turbulent energy, turbulent energy dissipation, enthalpy and (N_S-1) species conservation equations. Density is obtained from the state equation while pressure is directly obtained by solving the Poission pressure equation instead of the continuity equation. One species mass fraction is always determined from the global species continuity equation. The specific enthalpy of each species is calculated from a polynomial curve-fit. In the present version of the code, all the species transport properties such as viscosity, thermal conductivity and diffusivity are assumed to be constant and identical to those of nitrogen.

The finite-difference form of the nondimensional governing equations are obtained by using a hybrid numerical scheme [8]. In general, it uses central differencing for the convective terms everywhere in the flow domain except at the locations where the local Peclet number falls below 2. In these regions the scheme automatically switches over to an upwind or backwind differencing to improve the convergence. Even though all the governing equations are solved in an uncoupled manner, the turbulence equations and the species conservation equations are coupled through the source terms in the solution process. Solution for the system of algebraic equations deduced from each governing equation at all grid points is obtained by adopting an Alternate Direct Implicit (ADI) technique. When the grid aspect ratio (Dx/Dr) is large, this ADI technique fails to converge. To circumvent this problem, the u-momentum equation is solved using a point-relaxation scheme. Finally, the usual no slip, adiabatic and chemically inert wall boundary conditions are made. Also the wall functions approach [9] is employed to avoid grid clustering near the walls.

In the present analysis for the combusting flows, a simple global reaction scheme involving propane, oxygen, water, carbon dioxide and inert nitrogen species is used and is expressed as follows:

$$C_3H_8 + 5O_2 + N_2 \Longrightarrow 4H_2O + 3CO_2 + N_2 \quad (R1)$$

The specific reaction rate is written in Arrhenius form and the pre-exponential is adjusted to match the peak temperatures for the experimentally measured propane diffusion flames.

Parabolic velocity profiles have been specified at the inlets of the fuel and air tubes. During cold flow simulations, the air jet is replaced with a pure oxygen jet and the thermophysical properties of both propane and oxygen are set equal. This enables identification of fuel mixing patterns when there is no flame. All the cold flow simulations are made on a 89 x 46 uniformly spaced grid system, whereas the reacting flow solutions are obtained on a relatively coarse mesh having 40 x 40 nodes. Due to the small recirculation bubble in the fuel jet, calculations are made with a Courant-Friedrichs-Lewy (CFL) number close to 0.9 and the converged solution is obtained after several thousand time steps.

RESULTS

Visual Observations. When operated in a very fuel rich mode with gaseous propane fuel, the flame is very stable and is attached to the bluff body near the outer edge of the air tube. Figure 2a shows a photograph of such an attached flame at a fuel equivalence ratio (ϕ) of 1.56. As ϕ is reduced, the flame becomes less stable, and eventually reaches a point where it detaches (lifts) from the base region, and is stabilized about 150 mm downstream on the outer recirculation zone as shown in Fig. 2b. The end of the outer recirculation zone is located at a height very near the base of the very bright flame zone shown in Fig. 2b. As the fuel equivalence ratio is further reduced, the flame becomes very unstable, and eventually blows out. The lean blowout limit was found [1] to closely correspond to a fuel equivalence ratio (ϕ = 0.5) very close to the lean flammability limit (ϕ = 0.51) of the propane fuel and air [2]. Other studies suggest the combustor may behave like a well stirred reactor [3, 4] when the flame is in the lifted condition [1,5,6] . The instability that results just before blowout appears visually to correspond to a longitudinal oscillation of the lifted flame in the interfacial shear layers of the jets. The flame lifting process is required before lean blow out can occur. It is believed that an understanding of how the flame attaches and detaches from the combustor at rich and lean equivalence ratios will provide insight into the blowout process.

OH Emissions. The time-average view of the flame, as obtained from visual observations and photographs of the flame, clearly illustrates the qualitative effect of fuel equivalence ratio on the attached and lifted flame regimes of the burner. However, visual observation and conventional photographic techniques were unable to quantify the precise fuel equivalence ratio where the flame transitioned from an attached flame to a lifted flame. This was made difficult by the stochastic nature of the flame, and the integrating nature of observations by the human eye. At a given fuel equivalence ratio, the flame would appear to alternately attach then lift similar to what happens near lean blowout but not as vigorously. The visual appearance was such that the flame appeared to be attached most of the time, when the burner was operated very fuel rich; and lifted most of the time, when the burner was operated near or below a stoichiometric fuel equivalence ratio. Consequently, a measurement technique was sought that would give a more quantitative

measurement of the fuel equivalence ratio where the flame transitioned from an attached flame to a fully lifted flame.

It was reasoned that the signal obtained from the uv emission detection device described in the Experimental Section would be sensitive to the spontaneous OH uv emission, and would show a strong signal when the flame was attached, and a rather weak signal when the flame was lifted. The device could also give some insight into the periodicity of the flame attachment phenomena. Visual observations suggested that the flame would be attached for some period of time, and be lifted for some period of time. The fraction of time for attachment and fraction of time for lifted flames appear to be a function of fuel equivalence ratio. It was also thought that the intensity of the flame (i.e., the concentration of OH in the flame) would be somewhat proportional to the fuel equivalence ratio - a higher fuel equivalence ratio should lead to higher OH concentration, and consequently, a higher signal as measured by the device.

Measurements of OH emission from the flame in the region of the attachment point are presented in Fig. 3. Both the mean signal intensity and the standard deviation of the signal intensity show the same trends. Reproduced data points show that the data were very repeatable. In the fuel rich region, a general decrease in signal intensity with decreasing fuel equivalence ratio (decreased fuel flow at an air flow fixed at 1000 lpm) was readily apparent down to a fuel equivalence ratio of about 1.05. It was at about this fuel equivalence ratio that visual observations had suggested that the flame was fully lifted. Further reductions in fuel equivalence ratio cause little further change in the signal until the fuel equivalence ratio falls below about 0.8. After this point, the signal intensity continued to drop as the flame became more unstable, and as the fuel equivalence ratio approached the lean blow out limit of about 0.5.

These measurements identify the two operational regions of the flame, and have quantified a point of demarcation between the regimes of attached and lifted flames at a fuel equivalence ratio of about 1.05. Measurements at higher air flow rates showed different levels of signal intensity, but the curve had the same characteristic shape shown in Fig. 3, and the point of demarcation was always at a fuel equivalence ratio of about 1.05 even at the highest air flow rate tested, which was 3000 lpm. Consequently, further measurements were performed for two lifted conditions (the point of demarcation, $\phi = 1.05$ and a fuel lean case $\phi = 0.78$), and at two fuel rich cases where the flame was expected to be well attached ($\phi = 1.31$, and $\phi = 1.56$ respectively).

RMS Results. Figure 4a shows an example of results obtained by seeding the air stream with $TiCl_4$ vapor and adding moisture to the fuel tube. The flow conditions were 30 lpm of propane and 1000 lpm of air, which gave a lifted flame. The flame is stabilized near the end of the recirculation zone and is not visible in Fig. 4a. The flow structure associated with the flow through the fuel tube, the eddies in the shear layer between the fuel jet and the annular air jet, and the turbulent structure downstream are clearly evident. It appears that the turbulent eddies that exist between the fuel and air jets are of about the same scale as the gap between the edge of the fuel tube and the outer diameter of the annular air jet.

A recirculation zone, where there is a high concentration of TiO2 particles, is also observed near the fuel tube exit in Fig. 4a. The recirculation zone is similar to that formed behind bluff bodies and originates in much the same way. The high velocity annular air jet expands and entrains surrounding fluid as it enters the combustion chamber. The entrainment requirements of the air jet cannot be satisfied by the relatively small mass of fuel exiting the fuel jet and the air fuel mixture turns back on itself and is entrained back into the air jet much like the flow behind a bluff body. The recirculation zone appears to be somewhat egg-shaped and is very unstable. At relatively low fuel flow rates, it would momentarily attach at one location on the edge of the fuel tube and then move to another location. It seemed to dance back and forth around the fuel tube, always being attached to one edge or another; however, there appeared to be one location where it preferentially attached. This egg-shaped recirculation can be seen in Fig. 4a, and appears to be attached to the right side of the fuel tube. This appears to be a low Reynolds number effect since an increase in fuel flow caused the recirculation zone to lift out of the fuel tube, reduce in size, and became more or less stable in a location on the centerline of the burner above the jet exit.

CFD Model Results. The steady state CFD streamline calculation in Fig. 4b also shows the recirculation zone at the base of the fuel jet. The calculation is for a nonreacting flow of air in both the annular and central jets but for the same volumetric flow conditions as the reacting flow shown in Fig. 4a. The nonreacting flow calculation seems appropriate, since in the combusting flow case, the lifted flame sits near the end of the outer recirculation zone and no reaction is taking place in the near field shown in Fig. 4b. The spatial scales for Figs. 4a and 4b are about the same so only the flow observed in the width of the combustion chamber window is shown. The calculated recirculation zone has about the same size and shape as that determined experimentally and shown in Fig. 4a. Also, the streamlines converge towards the centerline just above the recirculation zone much like the experimentally observed shear layer. However, the calculated streamlines do not diverge further downstream as is observed experimentally.

The outer or step recirculation zone plays a major role in characterizing the performance of the research combustor. The recirculation zone is critical to the

understanding of the attached flame because it is responsible for the transport of unburned fuel and hot products that maintain this flame. In the case of a lifted flame as shown in Fig. 4a, it is particularly important to understand how much fuel and air are transported into the recirculation zone. This may determine whether a flammable fuel to air mixture might exist in the recirculation zone. If so, the flame, stabilized at the end of the recirculation zone, could ignite and flash back towards the face of the combustor. Such a process can be envisioned as being responsible for the low frequency oscillation of the lifted flame that will be reported later. It seems appropriate to use the model in a nonreacting flow simulation to examine the characteristics of the recirculation zone for the lifted flame.

The calculated steady-state or time-averaged streamlines and fuel mixture fraction contours for a nonreacting flow in the combustor are shown in Fig. 5a. The calculation is for the same nonreacting flow condition as shown in Fig. 4b. The zero axial velocity surface and the vortex center are important to the understanding of the fuel and air transport around the recirculation zone and are also shown in Fig. 5a. As noted by the radial component of the fuel mass flux vector on the zero axial velocity surface, the fuel is being transported out of the recirculation zone at axial locations up-stream of the vortex center and is transported into the recirculation zone at axial locations downstream of the vortex center. The magnitude of the radial component of the fuel flux vectors suggests that the largest transport of fuel into the outer recirculation zone occurs near the attachment point and the largest transport out of the recirculation zone occurs near the face of the combustor. The fraction of fuel at different axial locations can be obtained by integrating the mass flux between the outer wall and the zero axial velocity surface. A plot of the integrated mass fraction, shown in Fig. 5b, peaks at an axial location very near that of the vortex center. Although not shown, the integrated air mass fraction in the recirculation also peaks at an axial location corresponding to the vortex center. The integrated fuel to air ratio in the recirculation zone as a function of axial location is also shown in Fig. 5b. The fuel to air ratio is larger near the end of the recirculation zone and decreases as the flow is transported back towards the combustor base. The fuel to air ratio is essentially constant once the reverse flow passes the vortex center. This constant fuel to air ratio in the near field of the recirculation zone is about the same as the inlet fuel to air ratio. The stoichiometric fuel to air ratio by mass is 0.0638 and the largest fuel to air ratio in the recirculation zone is 0.023 which is below the flammability limit of 0.0319. Thus, a flammable mixture does not exist for this condition in the recirculation zone, according to the calculation.

Additional nonreacting flow calculations show that the trends noted in Fig. 5 also apply for other fuel and air flow rate conditions. The fuel to air ratio in the recirculation zone is of prime importance because it determines whether a flammable mixture exists that might flash back into the recirculation zone if ignited. Plots for the fuel to air ratio at the end of the recirculation zone and at the face of the combustor are shown in Fig. 6. Inlet air flow rates of 1000 and 3000 lpm were used in these calculations. The fuel to air normalization appears to be good choice and there was no impact of air flow rate on the plotted results. The model predicts that there will be a linear relationship between the fuel to air ratio in the recirculation zone and inlet fuel to air ratio. Indeed, the calculations suggest that the recirculation zone behaves something like a well stirred reactor with the fuel to air ratio in the near region of the recirculation zone being approximately the same as the inlet fuel to air ratio even though the sources of fuel and air into the combustor are different.

The isotherms and streamlines calculations for an attached flame are shown in Fig. 7. Comparisons of Figs. 5a and 7 illustrate that the recirculation zone for the combusting flow is much smaller than for the nonreacting case. The attachment point of the zero axial velocity surface at the face of the combustor is located much closer to the wall than that for the nonreacting case. This is not understood but may be associated with the large volumetric expansion of the heated gases. The shape of the experimental flame surface, as taken from photographs like that shown in Fig. 2, and the computed flame surface are also shown in Fig. 7. The calculated and measured flame surfaces nearly coincide for axial locations above 50 mm. However, the calculated and measured locations of the attachment point at the combustor face are different. Experimentally, the flame attaches at the outer edge of the step; whereas, in the calculation, the flame attaches near the edge of the fuel jet. The calculations are obviously reflecting the incomplete physics and chemistry that have been put into the model. Indeed, the calculation does not require any high temperature sources or flammable fuel and air mixture ratios in order to burn. Also, there is no provision for incomplete combustion in a computational cell except when fuel remains unburned because the local equivalence ratio is larger than one. However, attempts have been made to put these features, as well as wall quenching effects, into a CFD model. The result is that the flame always appears to attach near the edge of the fuel tube. Even when the rate of chemical reaction is slowed down, it was not possible to get the flame to attach in a way similar to that observed experimentally. Indeed, it is difficult to understand the physics and chemistry that lead to an attached flame on the step side of the air jet . This difficulty will be considered in the Discussion Section. However, for present purposes it is suggested that the source of the difficulty may be associated with an intermittent property of the flame. This line of thinking led to using diagnostic techniques that provide the

temporally and spatially resolved measurements reported below.

LIF Results. A series of images were obtained at four axial locations (0, 75, 150, and 225 mm) and at four propane flow rates (30, 41, 52, and 63 lpm). These fuel flow rates corresponded to equivalence ratios of $\phi = 0.78$, 1.05, 1.31, and 1.56, respectively. Two of the flow rates corresponded to a lifted flame ($\phi = 0.78$ and 1.05), and the other two corresponded to an attached flame ($\phi = 1.31$, and 1.56) These images have been used to examine the location and shape of the flame zones in the burner. An example of an image for the attached flame when $\phi = 1.56$ is shown in Fig. 8. The image shows regions of high OH concentration, and consequently illustrates the actual flame structure that existed during the 10 ns exposure. Note that the OH appears to be concentrated in vortex structures that are apparently shed from the rearward facing step. There is evidence that the vortices merge and the burning becomes more intense as they move downstream. This is suggested by the vortex train on the left side of the step. The flame surface, as marked by the OH fluorescence, is not continuous but has holes that appear to be located in the braid region of the vortex train. The flame is not symmetric in an instantaneous view. Rayleigh scattering from the fuel is also apparent and some scattered light from the edge of the windows can also be observed. Nevertheless, the instantaneous image of the flame at axial locations between 0 and 70 mm clearly indicates the complex structure of the flame and the importance of thinking about the combustion processes in a dynamic way instead of on a time-averaged basis.

A sequence of images at different equivalence ratios and at different axial locations is presented in Fig. 9. The four images at the extreme left of Fig. 9 correspond to a fuel flow rate of 30 lpm. They show no OH image in the two regions from 0 to 152 mm. Significant OH emission (flame) is apparent in the region from 150 mm to 227 mm and evidence of a rather thick flame zone exists in the shear layers shown in the region from 225 mm to 302 mm. It is clear from this set of images that the flame is lifted, and is being stabilized by the outer recirculation zone. Examination of the images at the four different axial positions that correspond to a fuel flow rate of 41 lpm show a similar trend, i.e., no OH flame structure in the region from 0 to 152 mm, but significant flame stabilized by the outer recirculation zone in the regions above 150 mm. There is a faint image in the primary fuel jet that shows some evidence of the jet mixing structure between the fuel and air jets. Flame has never been seen visually in this region. Consequently, this image has been caused by a mechanism other than LIF. This image is thought to have been caused by Rayleigh scattering of the dye laser beam by the propane in the fuel tube.

The two sets of images on the right-hand side of Fig. 9 correspond to conditions for an attached flame ($\phi =$ 1.31 and 1.56). Not only has the intensity of the OH emission in the two downstream zones increased, but there is OH emission evident for both ϕ's in the regions between 0 and 152 mm. In the bottom region (0 to 77 mm), the OH emission shown in the moderately attached case ($\phi = 1.31$) is not continuous, but shows some evidence of being fragmented and only partially attached. This is consistent with visual observations where the flame seemed to be attached part of the time, and lifted part of the time. The OH emission shown in the $\phi =$ 1.56 case between 0 and 77 mm clearly shows the sheet like nature of the flame zone, and also shows that the flame is wrapped up into one of the vortices associated with the eddy mixing between the fuel and air jets.

The thin flame structure near the entrance to the combustor in the well attached flame, $\phi = 1.56$, is clearly evident in Fig. 9 (also see Fig. 8). However, the flame zone appears to thicken in the downstream locations. The discontinuous and unsymmetrical nature of the flame is also apparent in all of the images. The packets of flame appear to be increasing in size as the flame progresses downstream. One might speculate that these flame packets represent vortices that have merged.

These observations suggest that the flame will be attached or lifted depending on the fuel equivalence ratio and attachment between the lifted point of demarcation and the well attached flame is periodic with the degree of attachment increasing as the fuel equivalence ratio is increased above $\phi = 1.05$. These results also suggest that the major heat release in the reactor occurs in the region above about 150 mm whether the flame is attached or lifted.

Thin-Filament Pyrometer Results. A time sequence of nearly instantaneous radial profiles of relative temperature 1 cm above the face of the combustor is shown in Fig. 10 at an equivalence ratio of 1.56 and an air flow of 1000 lpm. Each profile was obtained in 266 μs and are separated by 8 ms. Approximately one period of the time evolving profile is shown. The graybody radiation intensity profiles along a SiC_4 filament were obtained using a rotating mirror arrangement, as described in the Experimental Section. The intensities are proportional to the instantaneous temperatures along the filament with a resolution in the radial direction of better than 75 μm. Visual observations of the glow of the filament indicated that a temperature region of 1300 K or more extended from near the edge of the step to about 20 mm from the wall of the combustor. However, the combustion chamber window limited the radial observation of the filament, when the rotating mirror was used. The zero radial position in Fig. 10 is the approximate location of the edge of the step that is 20

mm from the combustor centerline. The sharp drop in intensity at 15.5 mm denotes the edge of the window.

Figure 10 shows that the flow behind the step is hot (e.g., higher than the cut-off-temperature of 1300 K) all the time, and that the temperature peaks at different radial location in time. The temperature peak is about 5 mm wide and is believed to be associated with the visible flame shown in Fig. 2a and the LIF image in Figs 8 and 9. Indeed, the radial motion of the temperature peak may be the result of vortices, like those shown in Figs. 8 and 9, convecting pass the measurement station. If this is the case, the radial displacement of the temperature peak can be taken as the width of the vortices at about 10 mm above the combustor face. This scale is about 4 mm and is comparable to the size of the vortices shown in Figs 8 and 9. The average radial location of the mean temperature peak is approximately 4 mm from the edge of the step.

The intermittent nature of the flame was investigated by observing the graybody radiation at one location on the filament. Time traces and frequency data are shown for both attached and lifted flames in Fig. 11a and 11b, respectively. In both flames, there appears to be an intermittent process that brings hot products down near the face of the combustor at a low frequency rate of less than 10 Hz, which is similar to the period for the time traces shown in Fig. 10. There was a continuum of frequencies above 25 Hz that continued for several hundred Hz but, no distinguishing high frequency peaks were observed in the TFP spectra.

DISCUSSIONS

Results of this study show that the operation of the combustor is very complex. The combustor operates in two distinct modes. In one mode, the flame is attached to the face of the combustor near the edge of the step, Figs. 2a. and 7. In the second mode, the flame is stabilized downstream near the end of the recirculation zone established by the step, Fig. 2b. The sheet lit LIF visualizations of OH in Figs. 8 and 9 and the TFP measurements in Figs 10 and 11 show that even when the flame is fully "attached", there is a degree of lifting, i.e., the flame fluctuates between an attached mode and the lifted mode with some degree of periodicity. The spontaneous OH emissions measurement in Fig. 3 suggests that when the inlet flow equivalence ratio is greater than 1.05, the flame is attached most of the time, whereas it is lifted most of the time when the equivalence ratio is less than this. As the equivalence ratio nears 0.5, the flame becomes very unsteady to the eye and goes out. This lean blow out limit is about the same as the lower flammability limit of propane and air mixtures.

The modeling results shown in Figs. 5-7, provide some insights into the time averaged flow field, but considerable difficulties have been encountered in correctly predicting the attached flame condition. The problem is that the model does not predict sufficient entrainment of fuel into the step recirculation zone to stabilize a flame on the face of the combustor, near the edge of the step. Attached flames are observed at fuel rich conditions and the model predicts that almost all of the excess fuel exits the combustor unburned. The challenge is to understand the physics and chemistry responsible for the entrainment, mixing, transport, and combustion of fuel and hot products into the step recirculation zone so that a physically sound model can be developed. Unfortunately, the presented results are not sufficient to establish a confident explanation of the observed characteristics of this research combustor. However, there is sufficient information to allow some speculation about the possible causes of the observed effects.

Figure 12 illustrates the authors' postulate of the key characteristics of the reacting flow field of the research combustor. Several zones of distinct thermal/fluid action are identified. In the reported experiments, the air flow rate (1000 lpm) is much higher than the fuel flow rates (23, 30, 45, and 63 lpm). As a result, a fuel jet recirculation zone is formed at the fuel jet exit. This is also indicated in the CFD model results. The Rayleigh images in Figs. 8 and 9 show that only a small percentage of air is entrained into the fuel recirculation zone so it is probably above the rich flammability limit and unable to support combustion. Also, the computed isotherms in Fig. 7 show that the temperature in the fuel recirculation zone is about 400 K, which is not sufficient to ignite and sustain a flame even if a flammable mixture were present.

In the case of an attached flame, intense combustion and mixing is taking place in the region where the shear layers of the step and fuel jet intersect. This interaction occurs about two air jet diameters downstream and involves the merging of vortices shed from the step (air jet) and the fuel jet. The vortex merging is believed to be responsible for the thickening of the flame observed in Fig. 2a. This is illustrated between stations 2 and 3 in Fig. 12. The intersection of the shear layers and the merging of flame vortices from the step are clearly shown in Fig. 8 at a distance of 35 to 40 mm downstream. This is illustrated by location 2 in Fig. 12. It was observed that this also occurs at an axial location where the time averaged attached flame shown in Fig. 2a, extends radially toward the centerline before being pulled toward the wall by the outer, or step, recirculation zone. The time averaged result of the merging of the vortices may give the appearance that the flame moves toward the centerline. Since this maximum inward motion of the flame occurs near the end of the fuel recirculation zone established behind the fuel jet the two events may be related.

The flame established in the merged shear layer between locations 2 and 3 in Fig. 12 is being fed directly

by fuel coming from the fuel jet, as noted in Fig. 7. However, this region of intense combustion is actually piloted by the weaker flame that is attached to the face of the combustor near the edge of the step as illustrated by location 1 in Fig. 12. The fuel and the high temperature combustion products that sustain the attached flame appear to come from the step recirculation zone. A major concern is how the unburned fuel crosses the intense flame zone in the shear layer of the step and enters the step recirculation zone without being consumed.

Entrainment of a rich fuel and product mixture into the step recirculation zone for the attached flame is believe to involve an intermittent process. The entrainment into the step recirculation zone occurs in the merged shear layer between locations 2 and 3. This is a region of intense combustion. However, the combustion process is discontinuous in that it involves regions of intense burning and regions where there appears to be holes in the flame as shown by the OH images in Figs 8 and 9. The holes appear to be formed in the braid regions of the vortex train. Stretching and fast mixing normally occur in the braid regions which might lead to quenching of the flame (i.e. formation of holes) by finite rate chemistry. It is proposed that entrainment into the step recirculation zone is by an intermittent process involving discrete packets of fuel and products. Rich fuel packets may be transported through the holes into the recirculation zone essentially unburned. The probability of hole formation increases the probability that unburned fuel is transported into the recirculation zone. This probability is extremely high in the shear region between stations 2 and 3. TFP data shown in Figs. 10 and 11 indicate that the gases in the recirculation zone are sufficiently hot to ignite the fuel if oxygen is present. Thus, it is believed that most of the oxygen is consumed in the shear layer and only a small quantity enters into the recirculation zone. The predominance of fuel over oxygen in the recirculation zone is favored for fuel rich inlet conditions. This is believed to be the reason why the attached flame only occurs at equivalence ratios greater than one. The unburned fuel is mixed with the hot products and transported by the recirculation zone to location 1 in Fig. 12. The hot fuel mixes with the air in the step shear layer and burns as a relatively thin flame between the face and location 2 shown in Fig. 12. This flame may be fuel starved at discrete times due to the intermittent way it was initially entrained into the step recirculation zone. Thus, the flame might attach and lift periodically, which is consistent with observation.

As the inlet fuel equivalence ratio is reduced, a condition will develop in which the amount of fuel entrained into the step recirculation zone cannot sustain the flame stabilized at location 1 in Fig. 12. Since this pilots the flame at location 2, the flame will lift and reestablish near location 3. This is most likely to occur at fuel lean conditions, since very little fuel will be entrained into the recirculation zone. Once lifting has occurred, the intense mixing of fuel, air, and hot combustion products from the step recirculation zone sustains the flame which becomes more like a premixed flame than a diffusion flame. The model calculation in Fig. 5 indicates that the fuel and air mixture in the recirculation zone under noncombusting conditions will be about the same as that entering the combustor. It seems possible that intermittent entrainment of hot products could ignite the fuel and air mixture in the step recirculation zone. This would result in a premixed flame propagating to the face of the combustor. This would account for the measured low frequency oscillations (3 to 10 Hz) noted in the TFP data in Fig. 11.

At increasing lean inlet conditions, the probability of having insufficient fuel inside the step recirculation zone increases. In this case, the flame will be lifted most of the time. Decreasing the fuel flow rate further results in a fuel-air mixture in the recirculation zone that is too lean to support combustion. Although intense mixing of the fuel, air, and combustion products is taking place in the primary fuel-air mixing zone, combustion does not take place because there is not sufficient heat and unburned combustion products coming from the recirculation zone to sustain a flame. Lean blow out results.

CONCLUDING REMARKS

The operational characteristics of a step stabilized research combustor designed to study lean blow out processes have been established at low Reynolds number conditions. A variety of measurement techniques and CFD modeling are used to examine both the time averaged and dynamic nature of the flame for a wide range of equivalence ratios. The flame appears to be attached near the combustor face at the edge of the step most of the time for equivalence ratios greater than 1.05. It is stabilized at the end of the recirculation zone for lower equivalence ratios. The presented measurements are not sufficient to establish the fundamental processes responsible for this behavior. However, they do show that the flame established near the mixing layers is not continuous in space and time. This suggests that unburned fuel is transported into the recirculation zone in discrete packets in an intermittent process that involves holes in the flame. Packets of hot fuel and products in the recirculation zone are mixed and transported to the face of the combustor where they are mixed with the air in the shear layer of the step. The fuel and air is sufficiently hot that an attached flame results. This process is most likely to occur at fuel rich conditions. At lean conditions, insufficient fuel is entrained into the recirculation zone to sustain the flame; lifting then occurs.

The potential importance of the intermittent nature of the burning process in this combustor offers significant challenges to conventional combustion

models. The biggest difficulty is to correctly model the processes responsible for entraining and transporting fuel, products, and heat into and out of the recirculation zone. The models must account for mixing of fuel, air, and hot products by relatively large vortices in the shear layers of the fuel jet and air jets. Also, they must account for burning in the vortex structures, holes in the flame, and intermittent transport and mixing of fuel and hot products into the recirculation zone. These requirements are believed to be beyond the capabilities of the current models.

ACKNOWLEDGEMENTS

This research was supported by the Air Force Office of Scientific Research (AFOSR) through a Summer Faculty Research Program (SFRP) and direct funding to the Aero Propulsion and Power Laboratory. Special appreciation is given to Mr. Royce Bradley, Dr. Tom Jackson, Dr. Tim Edwards, and Dr. David Sloan for their helpful comments and suggestions during this study and to Ms Gayle Byrd and Ms Carol Lucas for editorial corrections and aid in printing.

REFERENCES

1. Sturgess, G.J., D.G. Sloan, A.L. Lesmerises, S.P. Henneghan and D.R. Ballal. "Design and Development of a Research Combustor for Lean Blowout Studies", 35th International Gas Turbine and Aeroengine Congress and Exposition. Brussels, Belgium (June 1990).

2. Lewis, B., and G. von Elbe, Combustion, Flames and Explosions of Gases, 3rd Edition, Academic Press, Inc. (1987).

3. Longwell, J.P., E.E. Frost, and M.A. Weiss, "Flame Stability in Bluff Body Recirculation Zones", Industrial and Engineering Chemistry, 45 (8), pp 1629-1633 (August 1953).

4. Longwell, J.P., and M.A. Weiss, "High Temperature Reaction Rates in Hydrocarbon Combustion", Industrial and Engineering Chemistry, 47 (8), pp 1634-1643 (August 1955).

5. Sturgess, G. J., et al., "Lean Blowouts in a Research Combustor at Simulated Low Pressures." To Be Presented at the 36th ASME International Gas Turbine and Aeroengine Congress and Exposition, Orlando, FL, June 1991.

6. Henneghan, S.P., et al. "Acoustic Characteristics of a Research Step Combustor." AIAA Paper 90-1851, AIAA/SAE/ASME/ASEE 26th Joint Propulsion Conference, Orlando, FL, July 1990.

7. L. P. Goss, V. Vilimpoc, B. Sarka, and W. F. Lynn, "Thin-Filament Pyrometry: A Novel Thermometric Technique for Combusting Flows," J. Engrg. Gas Turbines & Power, Transactions ASME, vol. 111, pp. 46-52, January 1989.

8. Spalding, D. B., A Novel Finite Difference Formulation for Difference Expressions involving both First and Second Derivatives, International Journal for Numerical Methods in Engineering, Vol. 4, 1972, pp. 551-559.

9. Launder, B. E. and Spalding D. B., The Numerical Computation of Turbulent Flows, Computer Methods in Applied Mechanics and Engineering, Vol. 3, 1974, pp. 269-289.

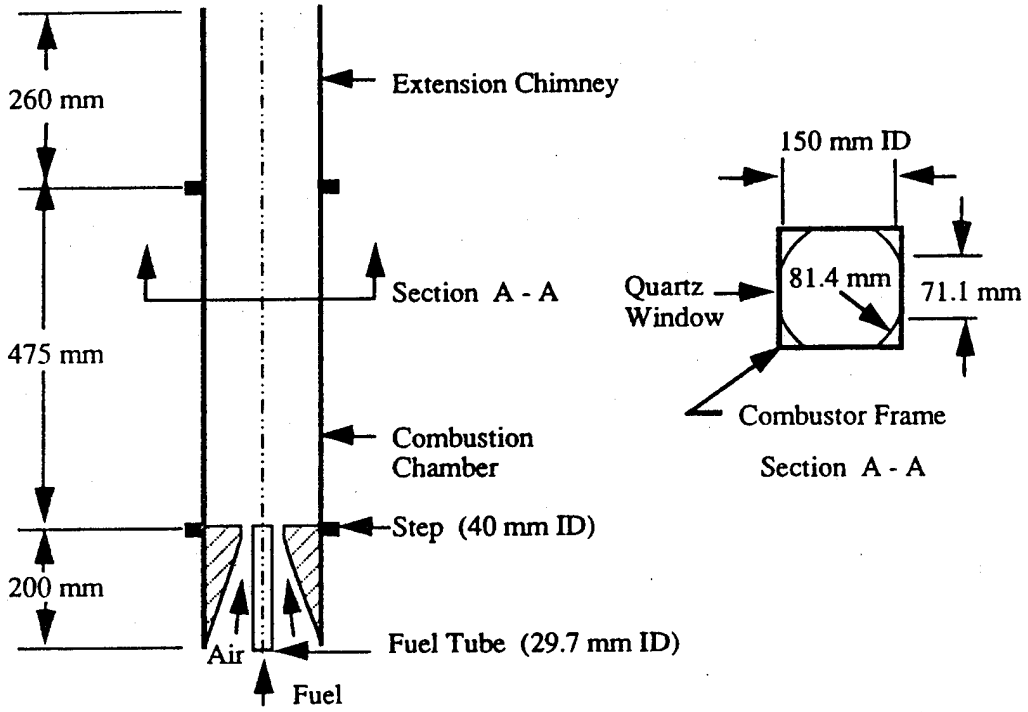

Figure 1. Schematic of the Confined Coaxial Jet Combustor with a Sudden Expansion [1].

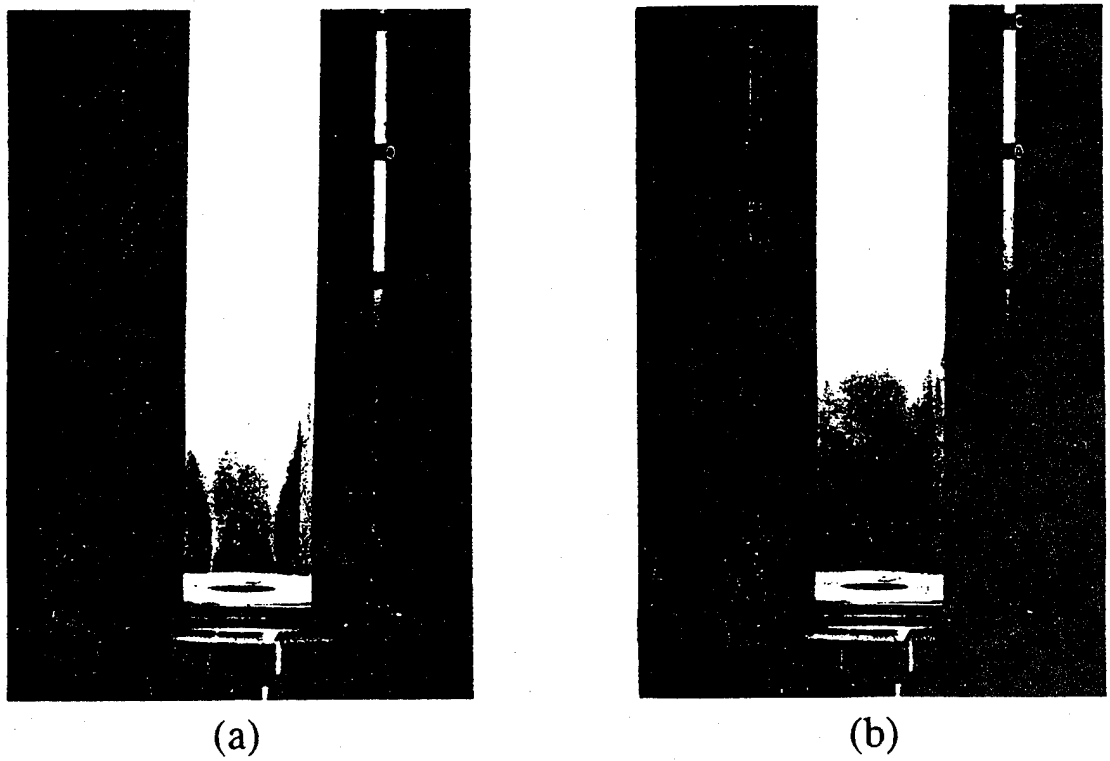

Figure 2. Photographs of Combustor with (a) Attached Flame 63 lpm Propane, $\phi = 1.56$, and (b) Lifted Flame 30 lpm Propane, $\phi = 0.78$, Air = 1000 lpm.

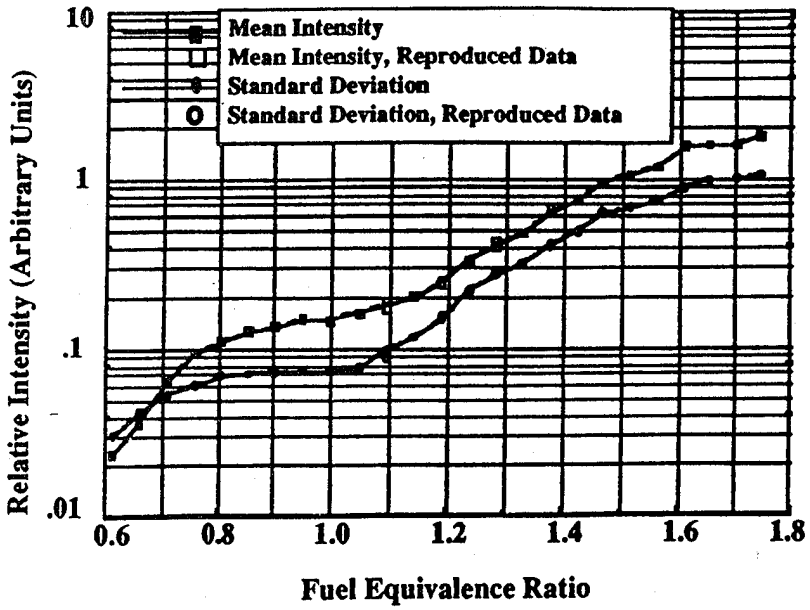

Figure 3. Relative Intensities of OH Emission for Different Equivalence Ratios with Air Flow Rate of 1000 lpm.

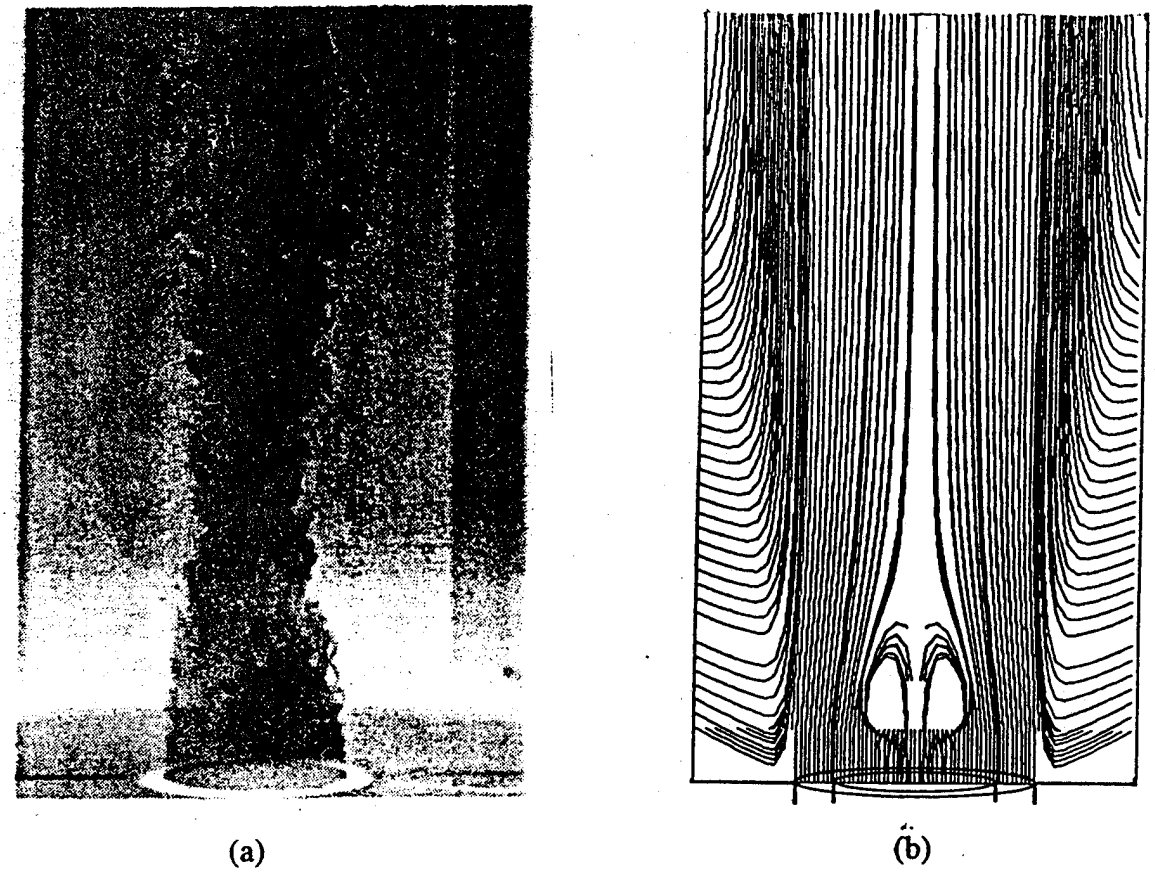

Figure 4. a) Laser Sheet Lighted Image of TiCl4 Seeded Flame 1000 lpm Air, 30 lpm Propane, TiCl4 Seed in Air, H20 in Fuel, $\phi = 0.78$. b) CFD Model Streamline Calculations for Nonreacting Flow Conditions 1000 lpm Air and 30 lpm Air in the Fuel Jet.

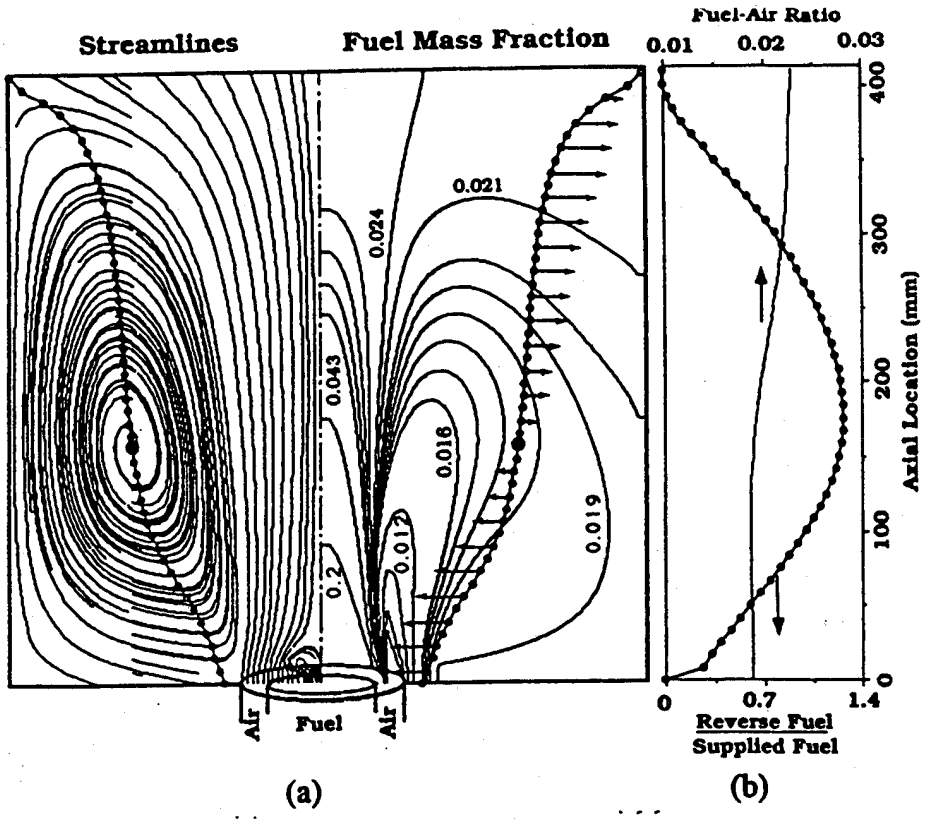

Figure 5. a) CFD Calculations of Streamlines, Fuel Mass Fraction and Zero Axial Velocity Surface and b) Integrated Fuel Mass Fraction and Fuel to Air Ratio in the Recirculation Zone for Air in Both Fuel and Annular Jets with $\phi = 0.78$.

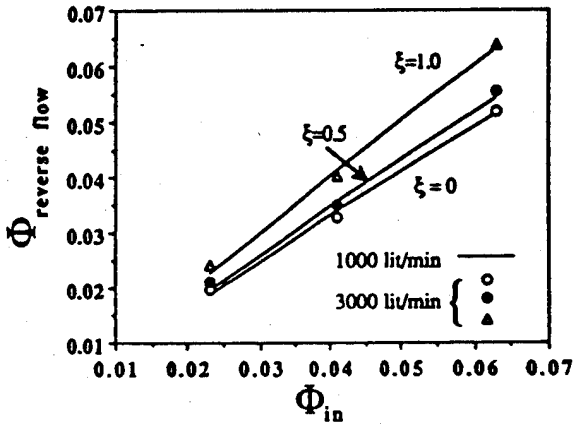

Figure 6. Calculated Fuel to Air Ratio in the Recirculation Zone for Nonreacting Flow with $\phi = 0.78$ and at Axial Locations Measured by the Fraction of the Recirculation Zone Length ξ.

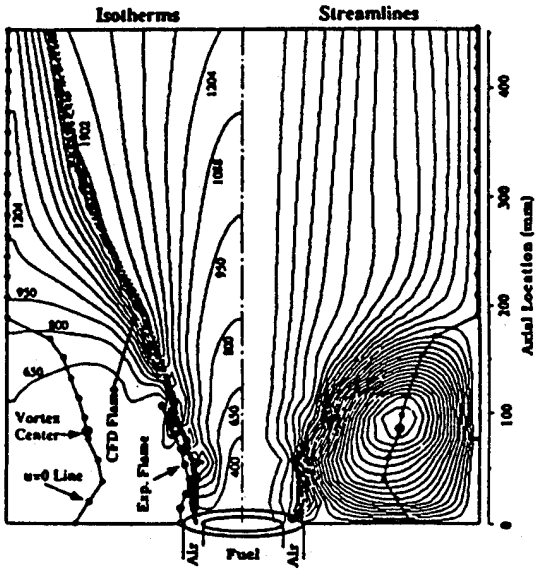

Figure 7. Calculated Isotherms, Streamlines and Flame Surface for Propane Flame with $\phi = 1.56$.

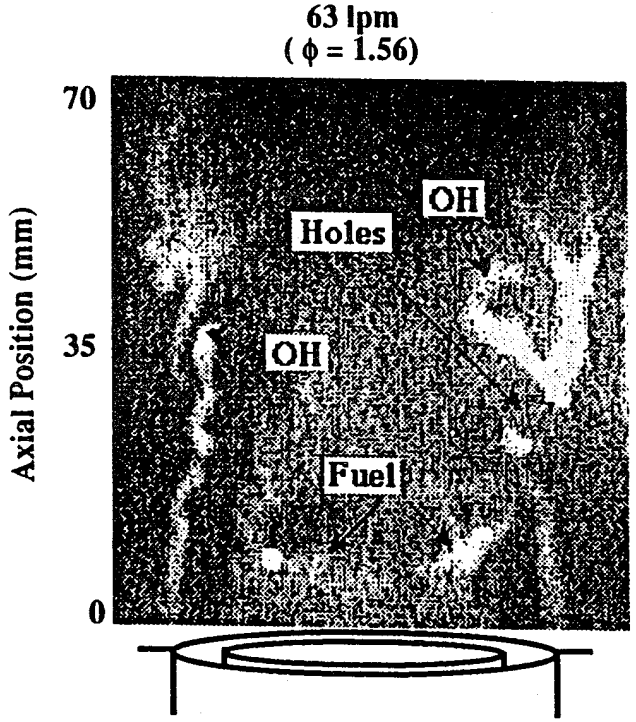

Figure 8. Image of Laser Induced OH Fluoresence for the Attached Flame with 63 lpm Propane, 1000 lpm Air, ϕ = 1.56.

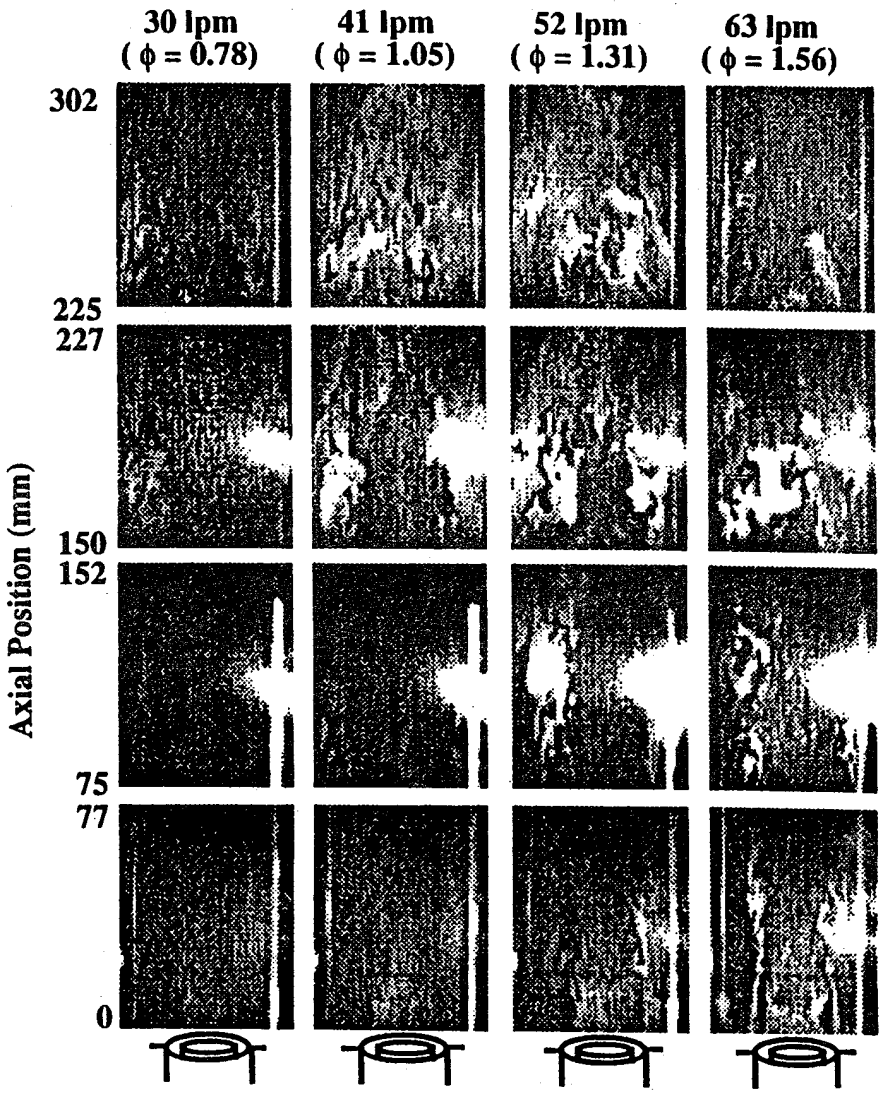

Figure 9. Images of Laser Induced OH Fluoresence at Various Axial Positions, and at Various Fuel Equivalence Ratios (1000 lpm Air)

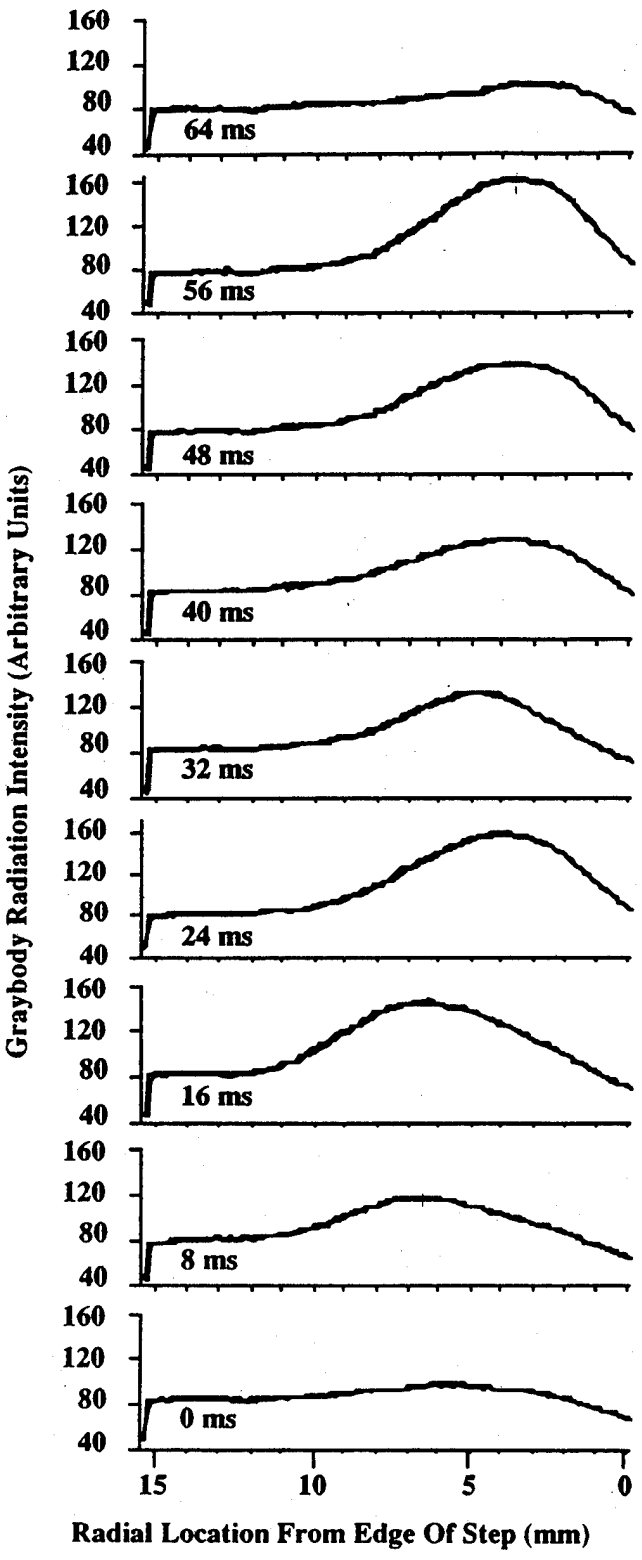

Figure 10. TFP Radial Traces at Indicated Times for Filament 10 mm Above Face of Combustor with $\phi = 1.56$.

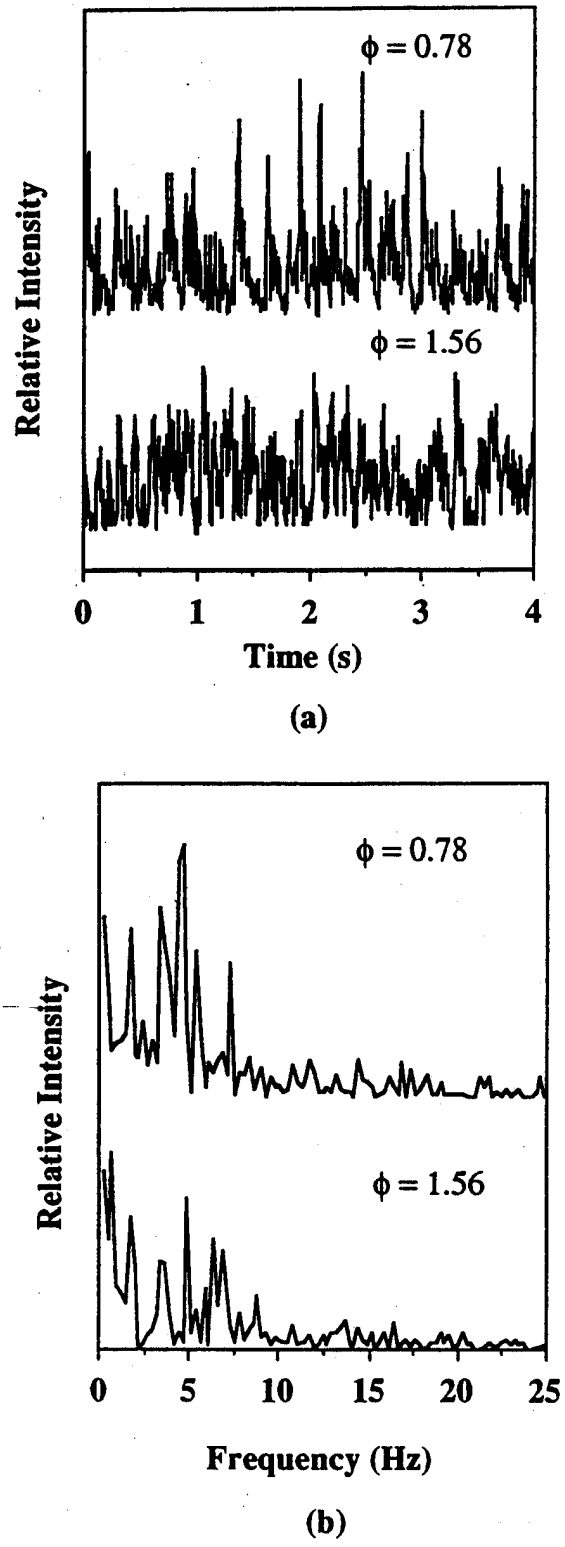

Figure 11. Time Trace and Spectrum of Filament, 10 mm Above Combustor Face, r ~ 4 mm from Step, $\phi = 1.56$.

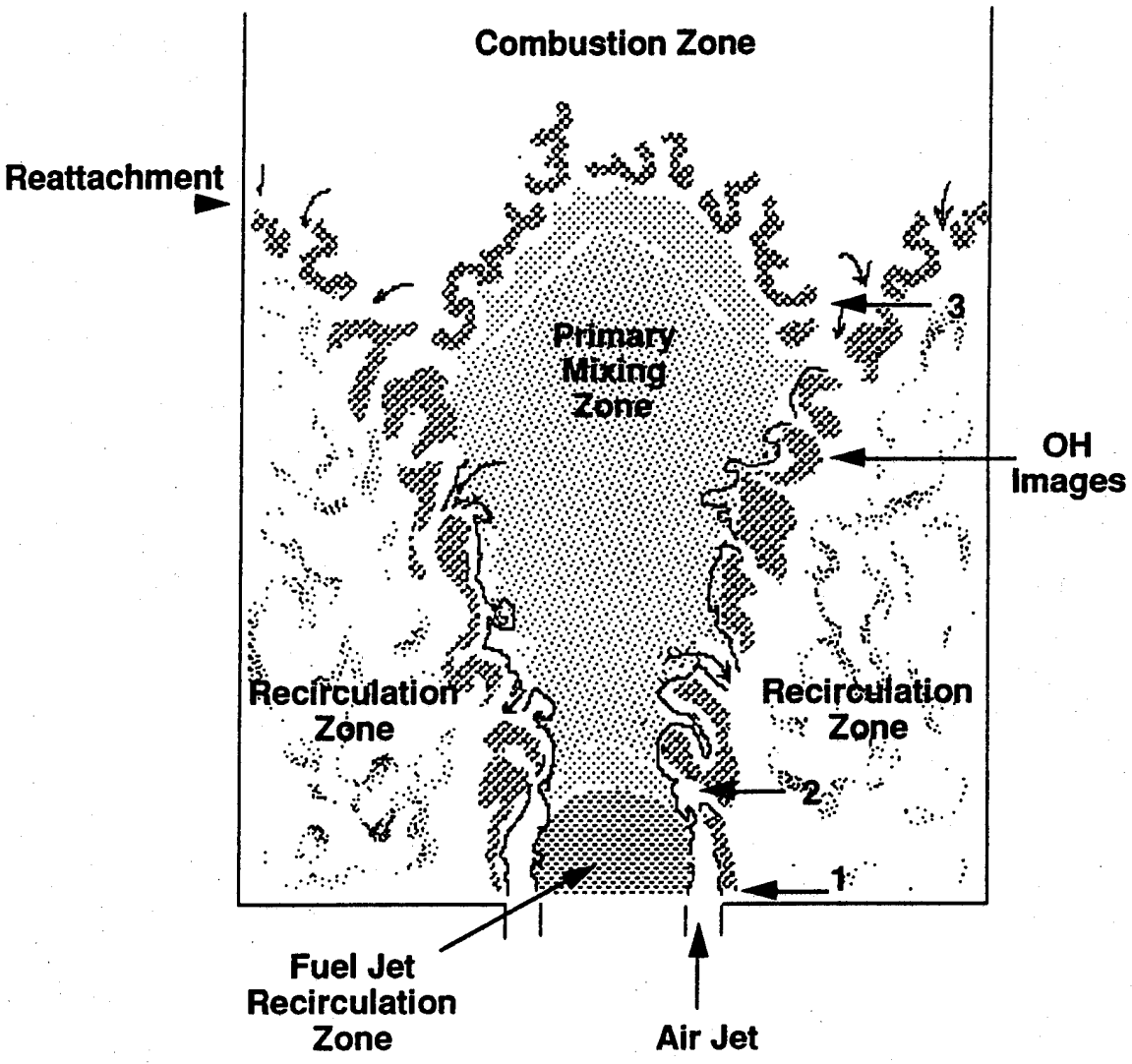

Figure 12. General flame/flow characteristics of near-fieldof research combustor.

APPENDIX G

ASPECTS OF FLAME STABILITY IN A RESEARCH DUMP COMBUSTOR

By

G.J. Sturgess and D. G. Sloan
Pratt & Whitney, East Hartford, Connecticut

P.O. Hedman
Brigham Young University, Provo, Utah

D.T. Shouse,
WL/POSF Wright-Patterson Air Force Base, Ohio

Published as ASME Paper No. 94-GT-496, June 1994.

THE AMERICAN SOCIETY OF MECHANICAL ENGINEERS
345 E. 47th St., New York, N.Y. 10017

The Society shall not be responsible for statements or opinions advanced in papers or discussion at meetings of the Society or of its Divisions or Sections, or printed in its publications. Discussion is printed only if the paper is published in an ASME Journal. Papers are available from ASME for 15 months after the meeting.

Printed in U.S.A.

94-GT-496

ASPECTS OF FLAME STABILITY IN A RESEARCH DUMP COMBUSTOR

G. J. Sturgess
Pratt & Whitney
East Hartford, Connecticut

P. O. Hedman
Brigham Young University
Provo, Utah

D. G. Sloan
Pratt & Whitney
East Hartford, Connecticut

D. Shouse
Wright Laboratory
Wright-Patterson AFB, Ohio

ABSTRACT

The lean blowout process is studied in a simplified, nominally diffusion flame, research combustor that incorporates the essential features of the combustor primary zone for an aircraft gas turbine engine. The research combustor is provided with extensive optical access. To investigate the blowout, a variety of diagnostic techniques are employed, including direct flame observation, laser-Doppler anemometry, spontaneous OH-imaging, thin-filament pyrometry, laser-induced fluorescence OH-imaging, coherent anti-Stokes Raman spectroscopy, and computational fluid dynamics. Lean blowouts in the research combustor are related to well-stirred reactor blowout. A blowout sequence is found to initiated by the loss of a key flame structure in the form of an attached pilot flame. The behavior of this attached flame is investigated. It is concluded that a major contribution to the existence of the attached flame is near-field, non-stationary radial transport of reactants directly into the recirculation zone, rather than by mean flow recirculation of hot products. "Lift" of the attached flame is the reason that lean blowout in the research combustor is related to well-stirred reactor blowout since it allows at least partial premixing of reactants to take place .

NOMENCLATURE

D	total dissipation rate of turbulence kinetic energy
F	Longwell temperature correction factor
KE_{mean}	loss in kinetic energy associated with distortion of mean velocity profile
LP	combustor loading parameter
P	combustion pressure
T	reactant temperature at inlet to reactor
V	effective reactor volume
$\dot{m}_a$	air mass flow rate
$\dot{m}_f$	fuel mass flow rate
$\dot{m}_{N2}$	excess nitrogen mass flow rate
n	apparent global reaction order
q_1	reactor inlet dynamic head
$\overline{u}_1$	time-averaged axial velocity component at reactor section where mean velocity profile is uniform
x	combustor co-ordinate direction, along LDA beam axis, from combustor center
y	combustor co-ordinate direction, normal to LDA beam axis, from combustor center
y^+	dimensionless 'law of the wall' co-ordinate
y_{max}	maximum value of cross-stream co-ordinate over which mean velocity profile varies
z	combustor co-ordinate direction, along combustor centerline from plane of step
ΔP	loss in total pressure across reactor
ϕ	equivalence ratio
λ	constant about 0.03, associated with eddy size

INTRODUCTION

Combustion stability is extremely important in gas turbine engines for aircraft use. However, it is increasingly more difficult to ensure that adequate stability margins can be maintained in the future because of current design trends towards improved atomization of liquid fuel, high temperature rise, and low emissions combustors, and their associated technologies. The potential difficulties are exacerbated by the lack of a satisfactory and reliable *a priori* prediction procedure for lean blowout.

To address the developing need, the U.S. Air Force Wright Laboratory, Aero Propulsion and Power Directorate (WL/PO), Wright-Patterson Air Force Base, Ohio, is conducting a comprehensive joint Government, Industry and University research program aimed at improving the design and analysis capabilities for flame stability and lean blowout (LBO) in the combustors of aircraft gas turbine engines (*Sturgess et al., 1991a*).

The approach adopted in this program is a step-by-step one that moves from giving an understanding of the basic flow behavior at blowout in a simplified environment, through progressively more realistic situations, to a simplified version of a real gas turbine combustor. The experimental portion of the program utilizes three combustors as test vehicles to achieve this progression. These combustors consist of a research combustor, a technology-development combustor, and a generic gas turbine combustor. The three combustors together reflect the step-by-step approach that is unique to this program.

Presented at the International Gas Turbine and Aeroengine Congress and Exposition
The Hague, Netherlands — June 13–16, 1994

The majority of the published work on flame stability is for bluff-body flameholders of various types, or, for well-stirred reactors, as reviewed by *Lefebvre, 1983*. The amount of experimental data published in the open literature for practical gas turbine combustors is much less extensive, and systematic investigations are largely lacking, although some limited investigations for can-type combustors are reported by *Jeffs, 1962* and *Stewart, 1956*. Almost all the information on the annular-type combustors currently used for aircraft applications is confined to relatively inaccessible private company reports.

RESEARCH COMBUSTOR CONCEPT

The intent of the research combustor was to study the fundamentals of flame stability, and specifically, the breakdown of flame stabilization as a lean blowout is approached. To facilitate such a study it was essential that the research combustor be provided with high optical access. To ensure relevancy, the essential features responsible for flame stabilization in an annular-configuration gas turbine combustor were to be incorporated in the design of the research combustor, while preserving geometric simplicity for subsequent computational fluid dynamic (CFD) modeling, together with high optical access for direct observation and interrogation by laser diagnostic techniques.

In a gas turbine combustor flame is stabilized by means of a recirculating flow of hot gases and chemically-active species to ensure continuous ignition of entering fresh reactants. The recirculation is generated by a combination of three mechanisms: an axial swirling air jet associated with each fuel introduction, sudden expansion of the axial swirling jets as they enter the combustor at its front end with critical swirl number, and, back-pressure provided by the blockage of an array of radial air jets at some downstream distance from the plane of the fuel sources. The region of the combustor containing the recirculating flow is known as the **primary zone**. The arrangement of these flows in combustors of modern Pratt & Whitney design produces an "inside-out" recirculation pattern (Figure 1). A small central recirculation zone close to the fuel injector can also exist. It is not visible in this sketch of flow patterns observed in a water tunnel.

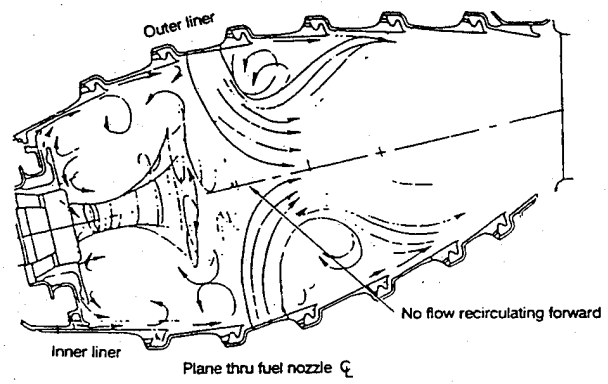

Fig. 1 Flow Patterns in a Typical Modern Pratt & Whitney Combustor, Showing the "Inside-Out" Recirculation Zone

The term "inside-out" follows from its difference to "conventional" gas turbine combustor recirculation zones as described by *Lefebvre,1983*. The reason for the inside-out feature of the recirculation is associated with the low emissions character of these modern combustors (*Sturgess et al., 1993a*).

In the design of the research combustor it was necessary to reproduce this "inside-out" recirculation. However, it was decided not to be necessary to reproduce swirl; a backward-facing step in the combustor wall would suffice to generate the required recirculation. In addition, the complications that would have resulted from the inclusion of the radial air jets were avoided by simulating their back-pressure by means of an exit-plane orifice plate fitted to the research combustor.

As an overall program decision it was decided to approach the lean blowout problem in two distinct stages - initially, with gaseous fuels (propane and methane). and then, with liquid fuels (ethanol and JP8). By this means the effects of liquid fuel atomization and spray evaporation could be separated from the aerothermochemical effects. The research combustor was therefore restricted to operation on gaseous fuels.

RESEARCH COMBUSTOR DESCRIPTION

The research combustor consists of a central jet of gaseous fuel surrounded by an unheated co-axial air jet, with the confluence of the jets centrally located in a nominally circular cross-section duct (*Sturgess et al., 1992a*). The duct has a hydraulic diameter of 150 mm. The duct is closed at its forward end to give a backwards-facing step of 55 mm height. The discharges from the supply tubes are flush with each other and with the step. The fuel tube has an inner diameter at exit of 29.97 mm with a 2-degree half-angle taper over 120 mm of its interior length to give a thin lip at its exit. The outer wall of the air passage converges sharply to its discharge, where the exit diameter is 40 mm.

The combustor is designed and constructed in two sections - a fixed upstream window section of 475 mm length providing optical access as needed, and a replaceable downstream chimney. The chimney is available in two lengths, and the combustor can run with either one of these, or both, or, with no chimney at all, to give length to diameter ratios of 4.9, 6.513 and 3.167 respectively. (The combustor has never been run with both chimeys mounted simultaneously.) Provision is made for exit blockage, with geometric values of 21.0, 45.1 and 62.0 percent tunnel blockage. These blockages are achieved by thin orifice plates. For the 45.1 percent geometric blockage, "top-hat" exits with tailpipe length to diameter values of 1.0 and 2.1 respectively, are also available.

The combustor has been subject to considerable development work to ensure that spurious acoustic effects were minimized (*Heneghan et al., 1990*). To this end a baffle is installed in the fuel tube to acoustically isolate the fuel supply system from the combustor. The desired configuration for extensive test evaluation was the 4.9 L/D combustor with 45.1 percent exit blockage by orifice plate.

The combustion tunnel cross-section (Figure 2) represents a compromise between the need for a simple axisymmetrical configuration, the demands of distortion-free and convenient optical access, and the requirement to minimize corner effects. The optical windows are flat fused-quartz, and are retained in the corner-frames by thin, curved metal corner fillets that reduce and distribute the vorticity generation due to wall secondary flows at the change in section contour (*Sturgess et al., 1992a*). The resulting effective optical window within which data may be taken is defined by $-68.7<x<+68.7$ mm and $-22<y<+33$ mm, where x and y are defined in Figure 2. In the downstream direction the window is $+2<z<+358$ mm, where the z-origin is the plane of the step.

The optical windows can be replaced by metal plates containing either arrays of thermocouples for wall temperature measurements, or, tappings for static pressure measurements. The combustor may be run with any combination of windows and plates.

Ignition in the combustor is accomplished by means of a

removeable propane torch ignitor that is inserted via an access boss mounted flush on the single permanently installed metal side-plate. The combustor is uncooled.

The combustor assembly is mounted vertically on the air-conditioning unit, Figure 2, that delivers a smooth flow of reactants to the combustor. The combustor and air-conditioning unit together translate vertically and horizontally through a cut-out in a fixed optical bench so that traversing with laser diagnostics may be made. A cooled exhaust extractor is positioned vertically above the combustor exit.

Both the fuel and air flows are continuously monitored and controlled by separate electronic flow control units to within 2 percent. It was therefore relatively easy to set and hold a given operating condition, within these constraints. A lean blowout of course, is not a precise event and is determined by local fluctuations about the mean flows. However, blowouts were found to be reasonably consistent, with a typical repeatability on equivalence ratio at fixed operating conditions being within 0.06.

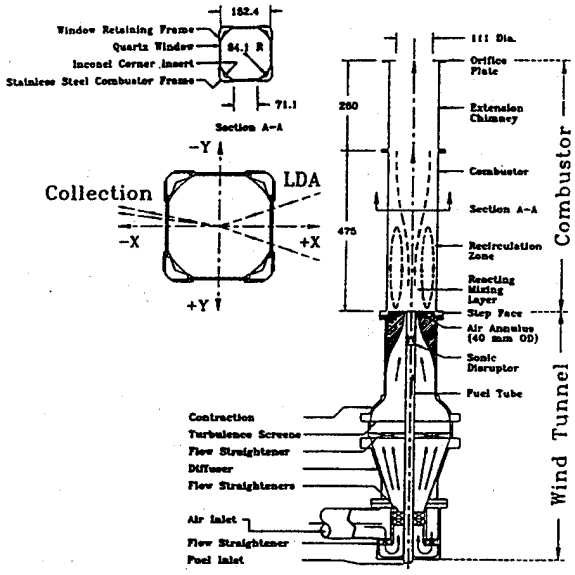

[ALL DIMENSIONS ARE IN MM]

Fig. 2 Cross-Sectional Drawings of the Research Combustor, Showing Axes Convention

ISOTHERMAL FLOW FIELD

A laser-Doppler anemometer (LDA) was used to measure axial and radial mean and fluctuating velocity components in the combustor for non-reacting flows (*Sturgess et al., 1992b*). Air was used for both entering streams, and the jet momentum ratios were set to values representing a typical blowout point. The air jet Reynolds Number was 56,413 and the simulated fuel jet Reynolds Number was 11,320, for which the mass-averaged velocity in the combustor was 3.06 m/s. Note that air jet momentum is always greater than that of the fuel jet, regardless of whether the flow is reacting or not, and, whether or not the operating conditions are near blowout.

From the LDA measurements the flow field in the combustor was constructed. Figure 3 shows the near-field features. The small central recirculation bubble is generated by entrainment of the fuel jet by the air jet. It has a length of 17 mm with a diameter of 9 mm, and begins 15 mm downstream from the plane of jet confluence. The inner edge of the jet shear layers reaches the combustor centerline about 36 mm downstream from the jet confluence. The step generates a large recirculation zone of 7.7 step heights, with vortex centers about 3.1 step heights downstream from the step. The individual jets are fully merged and have lost their identities by 138 mm from the step-plane. Not shown in Figure 3 is a relatively small recirculation zone existing on the forward face of the exit orifice plate. It has been shown (*Sturgess et al., 1993b*) that this zone does not interfere directly with the step recirculation zone.

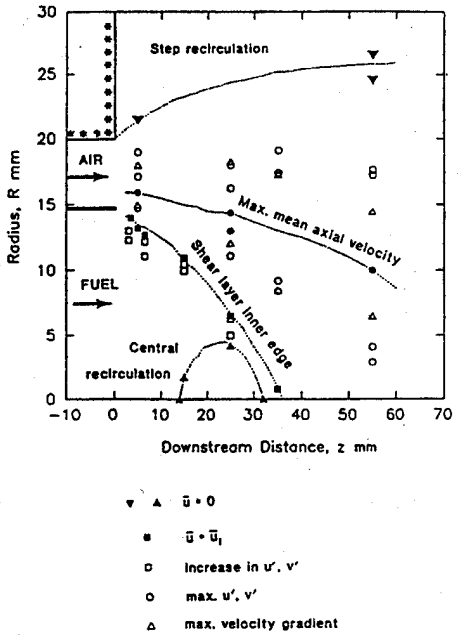

Fig. 3 Combustor Flow Features in the Near-Field

The general flow field characteristics of the research combustor do reproduce the basic features of a typical modern Pratt & Whitney primary zone, as was the intent.

TURBULENCE CHARACTERISTICS

A CFD-based study was made of the fluctuating velocity components generated in the combustor by the mean flow field to assess its relation to those of stirred reactors.

Following *Swithenbank,1974,* it can be shown that the **minimum condition** for a **perfectly stirred reactor** is represented by,

$$\frac{\Delta P}{q_I} \geq 3.0 \qquad (1.)$$

An energy balance shows that the **pressure loss factor** is made up of the sum of losses associated with distortion of the mean velocity profile, the generation of turbulence, and the total dissipation of turbulence energy, i.e.

$$\frac{\Delta P}{q_1} = \frac{K.E._{max}}{q_1} + 3\left(\frac{u'}{\bar{u}_1}\right)^2 + \frac{D}{q_1} \qquad (2.)$$

It can then be shown that the total dissipation of turbulence energy is given by,

$$\frac{D}{q_1} = \frac{2}{\lambda y_{max}} \int_0^x \left(\frac{u'}{\bar{u}_1}\right)^3 dx \qquad (3.)$$

where $u' = u'(x,y)$

Since mixing is proportional to dissipation, Equation 3 is an appropriate basis for determining well-stirred portions of a flow. However, the maximum value of D/q_1 is approached asymptotically, so, differentiating Equation 3 yields,

$$\frac{d(D/q_1)}{dx} = \frac{y^2}{\lambda_{max}} \left(\frac{u'}{\bar{u}_1}\right)^3 \qquad (4.)$$

which depends only on the value of $(u'/\bar{u}_1)$ over y at each x-station. This quantity will be zero initially, rise to a maximum due to shear effects, and then decline to zero downstream at the asymptotic condition. Equation 4 therefore allows a rather precise determination of the extent of well-stirred regions of a flow.

It is not necessary for $d(D/q_1)/dx$ to be zero; based on grid-turbulence *Swithenbank, 1974* recommended a value ≤ 0.1 for negligible further mixing. Typical turbulence intensities in a combustor will normally be far in excess of grid turbulence. Examination of CFD calculations in isothermal flow for the research combustor made with the Pratt & Whitney 2D-PREACH code (*Sturgess, 1983*), show that fields of both the specific kinetic energy of turbulence and its rate of dissipation fall to very low levels long before the combustor exit is reached. K.E. is down to 4.0 percent of its maximum and D is down to 1.0 percent of its maximum **inside** the gradient contour with value **10.0**. Therefore, the limiting condition for $d(D/q_1)/dx$ was taken as 10.0 for the research combustor.

Figures 4 and 5 display the distribution of total dissipation gradient through the research combustor, where the x-gridlines are parallel to the combustor z-axis (Figure 2) and the y-gridlines are normal to the z-axis. In Figure 6 are shown spatial contours, constructed from Figures 4 and 5, in the research combustor of total dissipation gradient for values of 10.0 and 1.0.

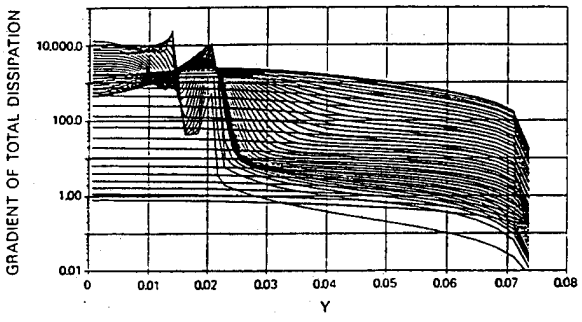

Fig. 4 Dissipation Through the Research Combustor Total Dissipation Gradient (x-gridlines)

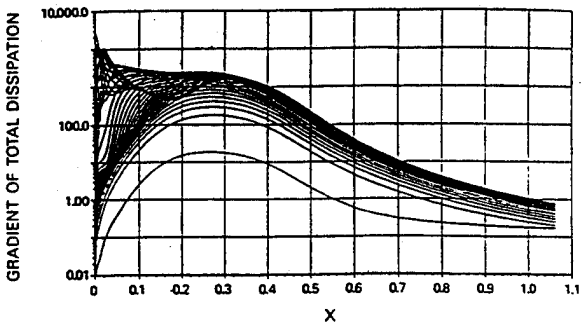

Fig. 5 Dissipation Through the Research Combustor of Total Dissipation Gradient (y-gridlines)

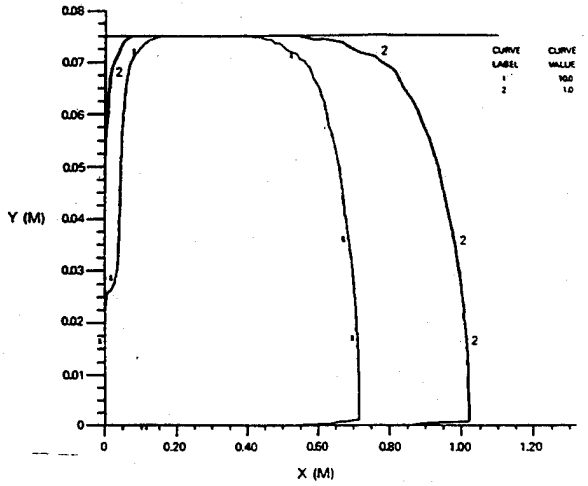

Fig. 6 Iso-Contours of Total Dissipation Gradient at Swithenbank and Present Cut-Off Levels in the Research Combustor

Based on the 10.0 contour from Figure 6, it can be seen that most of the research combustor can be classified as well-stirred. Included in this classification are the jet shear layers, the central recirculation bubble, the step recirculation zone, and the region immediately downstream of the step recirculation zone.

LEAN BLOWOUTS

Using the calibrated nitrogen diluent technique to simulate low pressures (*Sturgess et al., 1991b*) together with variation of throughput, to achieve high combustor loadings, the LBO portion of the stability loop of the research combustor was obtained experimentally (*Sturgess et al., 1991*), (*Sturgess et al., 1993b*), with gaseous propane as the fuel. This is shown in Figure 7.

The experimental LBO equivalence ratio data were correlated on the basis of well-stirred reactor theory, using the combustor loading parameter,

$$LP = \frac{\dot{m}_{Total}}{V P^n F} \qquad (5.)$$

where,

$\dot{m}_{Total}$	$= \dot{m}_f + \dot{m}_a + \dot{m}_{N2}$	*lbm / sec.*
V	*= effective reactor volume*	ft^3
P	*= combustion pressure*	*atmos.*
n	$= 2\phi_{LBO} / (1 + \dot{m}_{N2} / \dot{m}_a)$	
	apparent global reaction order	
F	$= \frac{10^{0.00143T}}{3.72}$	*to correct to* $400K$
T	*= fuel / air inlet temperature*	K
ϕ_{LBO}	*= equivalence ratio at LBO*	

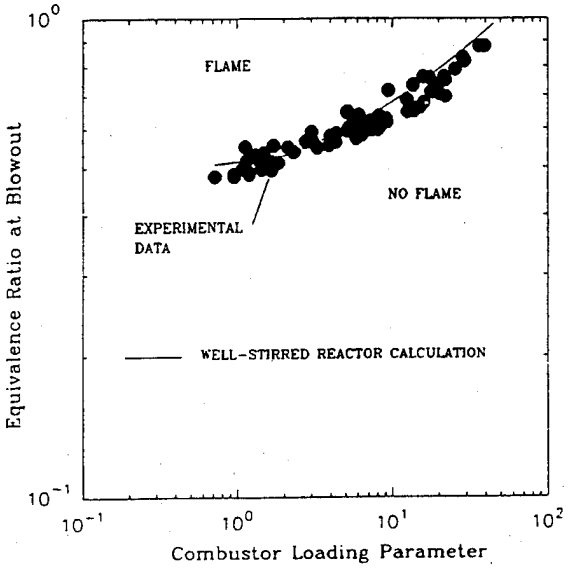

Fig. 7 Measured Lean Portion of Stability Loop Compared with Well-Stirred Reactor Calculation

This application of well-stirred reactor theory follows *Bragg, (1953)*, who proposed that a gas turbine combustor could be modeled as a well-stirred reactor followed by a plug-flow reactor. The general form of the loading parameter follows *Kretschmer & Odgers,1972,* and has been in common use for many years; presently, it has been modified to account for the use of excess nitrogen as a diluent (*Sturgess at al., 1991b*). Correction of the data to a constant 400K inlet temperature represents tribute to the pioneering well-stirred reactor work of *Longwell et al., 1953,* where an actual inlet temperature of 400K was used. Determination of the effective volume for the research combustor was based on Figure 6 with account of flame lift, and is described in detail in *Sturgess et al., 1991b* .

Shown on Figure 7 is a line representing a well-stirred reactor calculation (*Sturgess et al., 1991b*). It passes through the data. When the experimental LBO data from the research combustor are compared to experimental LBO data from actual well-stirred reactors in the literature (*Sturgess et al., 1992a*), (*Ballal et al., 1993*) the agreement is excellent. At low combustor loadings the blowout equivalence ratios attained approach the flammability limit for propane/air mixtures (*Lewis & von Elbe, 1961*).It therefore appears as though the research combustor at lean blowout behaves as a well-stirred reactor. The calculated turbulence characteristics of the research combustor, a necessary but not sufficient condition for a well-stirred reactor, would certainly permit this to be so.

FLAME CHARACTERISTICS

Visual

It is observed for overall fuel-rich operation over wide ranges of jet Reynolds Numbers, that a steady sheath-flame originates on the combustor step at the outer-edge of the air jet. This attached flame appears quite thin at its origin, and maintains a roughly constant overall diameter and thickness for about 20 mm downstream. Beyond this 20 mm station the thickness of the flame increases by growing significantly towards the combustor centerline, and also radially outwards; strong radial expansion of the reacting jet shear layers begins thereafter. It appears that the attached flame exists in the outer shear layer (see Figure 3), and that the initial thickening at 20 mm is due to the ignition of the inner shear layer, where the thickened flame has a "turbulent flame-brush" appearance i.e. "fuzzy blue."

As fuel flow is reduced at constant airflow the attached flame remains steady but becomes visibly intermittent in both circumferential and axial extent, and at an equivalence ratio of 1.05 (for propane/air mixtures) and less, is no longer evident to the eye. The intermittency of the inner shear layer burning is much more severe than that in the outer shear layer. Eventually, the shear layer burning is no longer apparent, and the flame lifts to move far downstream (160-300 mm) and exists in distributed fashion across most of the combustor diameter. The behavior has some of the appearance of conventional "lift" in jet diffusion flames (*Takahashi et al., 1988*). Figure 8 compares the attached and lifted flame conditions. Still further reductions in fuel flow result in periodic large-scale axial movements of the lifted flame, and LBO occurs as these movements increase in extent (*Sturgess et al., 1992a*), (*Ballal et al., 1993*).

When the bulk equivalence ratio reaches 1.5 to 2.0, depending on combustor loading (*Sturgess et al., 1993b*), and before a rich blowout, a separated flame condition is again established, where the attached flame originating from the outer-edge of the air jet is not visible to the eye. For low combustor loadings this takes place at an equivalence ratio of 1.8. However, for this loss of the attached flame the main flame does not lift; it is located about 30-40 mm downstream from the step plane. A rich blowout occurs suddenly at this condition, and does not involve flame-lift. A high value of combustor loading can be reached when the attached flame is not present at **any** equivalence ratio, either rich or lean (*Sturgess et al., 1993b*).

The attached/lifted flame behavior was also observed in the technology combustor, which is identical to the research combustor except that the jet system is replaced with a conventional fuel injector from the generic combustor. A similar occurence was noted in the generic combustor (*Sturgess & Shouse, 1993c*). It therefore appears that the research combustor is a satisfactory representation of a gas turbine combustor primary zone, and that the attached flame, and its loss, are fundamental features of the LBO process.

It seems as though the attached flame serves as a pilot for the inner shear layer. When the attached flame is no longer evident the subsequent increase in ignition delay for the inner shear layer that probably takes place appears to cause the flame to lift. The lifted flame then allows significant premixing of the reactants to take place. Since the lifted flame is within the region of the combustor that is classified as being well-stirred by the total dissipation gradient method, it is therefore not unexpected that the LBO behavior is consistent with well-stirred reactor blowout calculations and experimental data from the literature.

Spontaneous OH-Imaging

The hydroxl radical is produced in large quantities in reaction regions of hydrocarbon combustion where large amounts of heat release take place. It can thus be an important flame marker, although care has to be taken to allow for convection effects.Therefore, measurements of the spontaneous uv-emission from the OH radical provide a means for further study of the important attached flame and its lift.

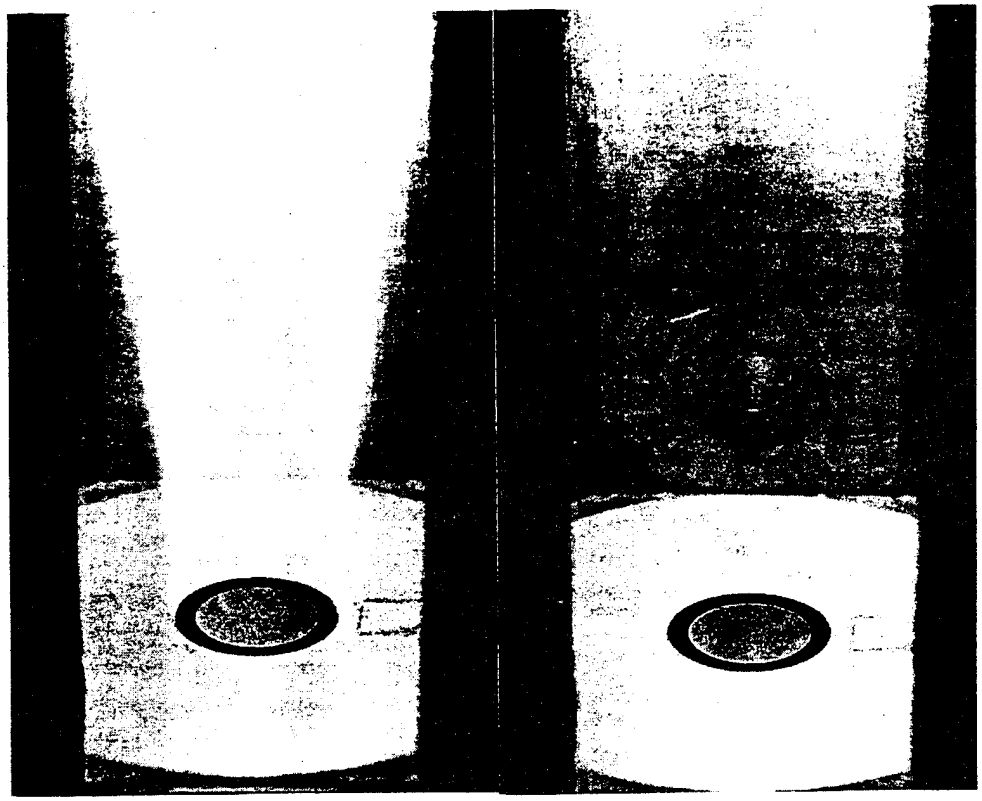

Fig. 8 Available Light, Time-Mean Photographs of Attached and Lifted Flame Appearances

A narrow view-angle, line-of-sight optical system, consisting of a simple lens and aperture, was set up and used to image a narrow cylindrical focal volume of a region of the reactor, located about 15 mm above the step, into a spectrometer that was tuned to an OH-emission line near 308 nm to give a strong signal. The signal was captured with a photomultiplier tube, then amplified, digitized, and recorded on a computer, Figure 9. Over a 20-second time period 20,000 separate digital points were collected, and a mean and standard deviation of the measured signal were obtained. To reduce noise from the hot combustor hardware, an average background was obtained from 20,00 data points collected with the spectrometer inlet blocked, and the average background signal was then subtracted from each of the 20,00 true data points to obtain representative uv-emission data.

Although the optical system integrated the observed emission signal completely across the combustor, the positioning of the view-volume was such that when the flame was attached a strong spontaneous OH uv-emission signal resulted, and when the flame was lifted the signal was rather weak. Fast Fourier Transform (FFT) analysis of the data could then provide an indication of the intermittency of the attached flame.

Figure 10 shows the variation of mean intensity and its standard deviation with bulk equivalence ratio; the repeatability is seen to be good, and both measurements show the same trends. It can be seen that there is a clear demarcation in the emission intensity occurring at an equivalence ratio of about 1.05. This is in excellent agreement with the flame-lift equivalence ratio obtained visually. For lower equivalence ratios the emission intensity remains roughly constant until the equivalence ratio falls below 0.8, which is approaching LBO, at which the intensity falls sharply.

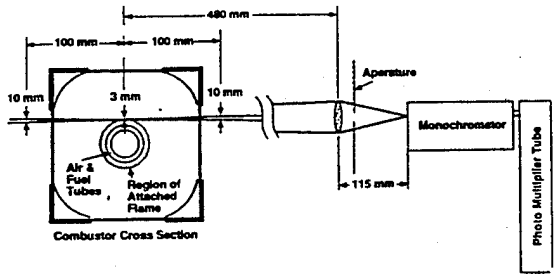

Fig. 9 System for Spontaneous OH-Imaging

Figure 10, together with the variations of emission intensity with time at given equivalence ratio, indicate that the attached flame is a periodic phenomenon. For $\phi \geq 1.05$ the flame is present more often than it is not; for $\phi \leq 1.05$ the flame is still present (although not visible), but is absent more than it is present.

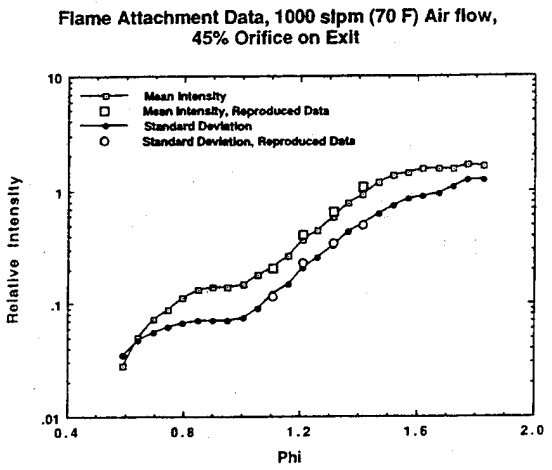

Fig. 10 Mean and Standard Deviation of Spontaneous OH-Image Intensity Variation With Equivalence Ratio for the Attached Flame

Thin-Filament Pyrometry (TFP)

For further study of the critical attached flame condition a 14 micron diameter silicon carbide filament was stretched across the combustor diameter at a height of 10 mm above the step plane. The emissivity of the filament is independent of its temperature, so that the radiation from it when heated is exponentially proportional to its temperature as determined by Planck's blackbody radiation law. The filament can thus serve as a pyrometer (*Goss et al., 1988*). The response time of the filament is of the order of 700 Hz and the lower limit of detectable temperature is about 1300K, so that such a TFP can yield the near-instantaneous time-variation of flame temperature radially at fixed axial position in the combustor.

The radiation from the filament was imaged by a cylindrical lens and rotating mirror into a single InGaAs photodiode detector. The filament was scanned and imaged with 256 pixels, with the signal being digitized at a rate of 1-4 Mbyte/sec. and stored on a transient recorder during each gated scan. For a fixed optical system the physical length of filament scanned can be adjusted by changing the mirror speed and the digitization rate. The pixel resolution is the scanned length divided by the pixel number; for this study the pixel resolution was approximately 75 microns. The digitized signal was scanned at 250 and 500 lines/sec. Spectral information was obtained from the stored line signal by using FFT analysis. In this instance the filament was not calibrated, and was only used to indicate relative temperatures.

The scanned region of the filament radially encompassed the attached flame region of the combustor. Each instantaneous radial relative temperature profile was obtained in 266 μs, and profiles were separated in time by 8 ms. The test conditions repeated those for the spontaneous OH-imaging.

The attached flame was found to be about 5 mm in thickness, i.e. thin, confirming the visual observations, and at the 10 mm downstream station the temperature peak was found to oscillate radially about a mean radius of 24 mm with a displacement of about 4 mm; the oscillation frequencies were less than 10 Hz. Reference to Figure 3 places the mean radius about which the flame oscillates in the outer shear layer region, again confirming the visual observations.

Figure 11 shows the time history of the attached flame (*Chen, 1991*) at equivalence ratios of 1.56 (visibly-attached flame) and 0.78 (visibly-lifted flame); also shown are the relative intensity frequency spectra at a radius of 24 mm for these two equivalence ratios. The figure demonstrates that the radial oscillation of the flame is independent of equivalence ratio, and depends on a flow phenomenon. It also illustrates the intermittent character of the attached flame that the spontaneous OH-imaging revealed. It confirms the flame is present some of the time when the attached flame is visibly-lifted, and that the intermittency increases at the lower equivalence ratio, when significant "holes" appear in the flame. This behvior is very similar to that observed in open jet diffusion flames, (*Chen et al., 1989*), (*Chen & Goss, 1989*).

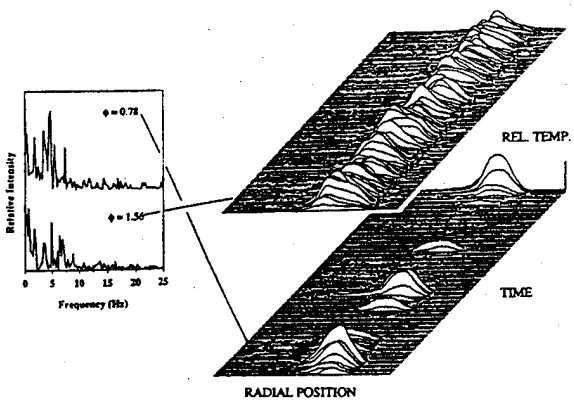

Fig. 11 Time History and Frequency Spectra of Relative Temperature From a Thin Filament Pyrometer in the Attached Flame at Fuel-Rich and Fuel-Lean Equivalence Ratios

Laser-Induced Fluorescence (LIF) OH-Imaging

Laser-induced fluorescence of OH was used to capture instantaneous (10 ns) two-dimensional images of the reaction regions in the research combustor (*Roquemore et al., 1991*).

A frequency-doubled Nd-Yag laser was used to generate a uv laser beam at about 283 nm. This frequency was used to pump a fluorescence transition of OH, which resulted in a LIF signal at about 308 nm. The plane of the laser light was passed through the research combustor as shown in Figure 12, at two angles of 0-degrees and 25-degrees relative to a bisector passing through the vertical centerline. A 384 x 576 element intensified CCD camera located normal to the plane of the laser beam was used to capture the induced images. The camera was able to view the full width of the optical window in the combustor in the 0-degree position, and almost to the combustor wall in the 25-degree position, but was limited to a vertical extent of 76 mm. To obtain a complete record, the camera was successively located for each operating condition at four different axial positions of z equal to 0, 75, 155, and 225 mm.

The data are presented as single images, and as spatial and time ensemble-averages of multiple images at each location and condition. The equivalence ratios covered both attached and lifted flames, and two values of combustor loading - low and moderate (see Figure 7); the loadings differed by a factor of 2.9.

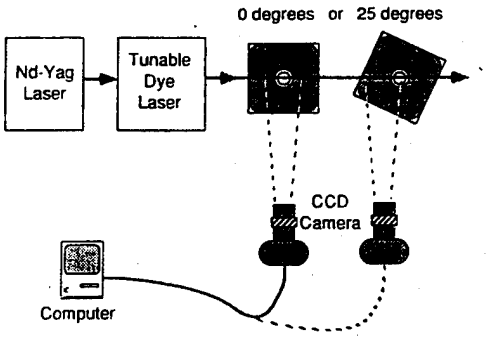

Fig. 12 System for Laser-Induced Fluorescence OH-Imaging

Figure 13 is a spatial composite of ensemble-averaged LIF images of OH at 0-degrees image plane angle for low combustor loading at an equivalence ratio of 1.56, and Figure 14 is for the 25-degree image plane angle that allows a more extensive view of a slightly different cross-section. Images at the higher combustor loading are very similar.

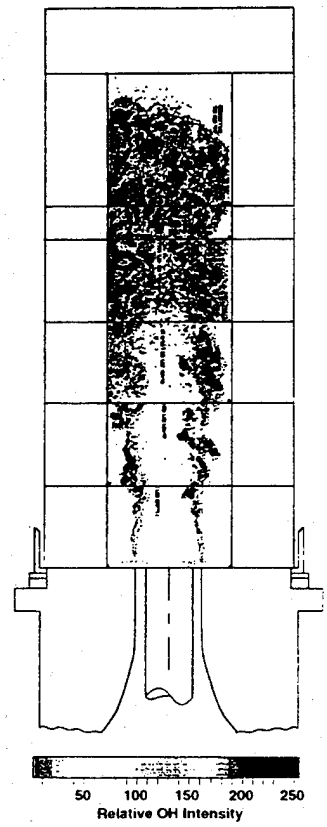

Fig. 13 Spatial Composite of LIF OH-Images at an Equivalence Ratio of 1.56 with Lower Combustor Loading (0-degree orientation)

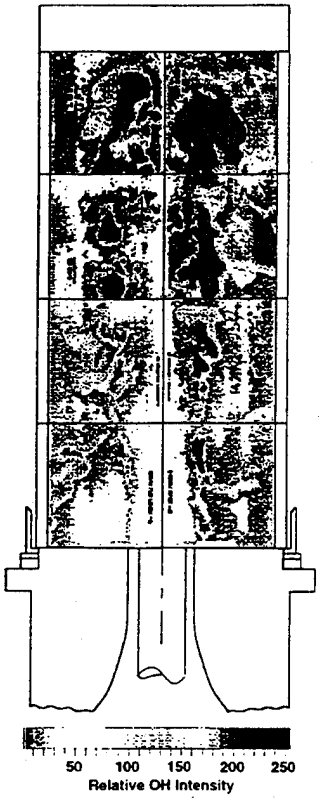

Fig. 14 Spatial Composite of LIF OH-Images at an Equivalence Ratio of 1.56 with Lower Combustor Loading (25-degree orientation)

Once generated, the hydroxl radical is persistent, and therefore, it can be convected to sites other than where it was generated. Care, therefore, must be taken in reading two-dimensional OH images.Interpretation of Figure 13 is relatively easy since, due to the limited field of view, there is little convection effect to cause confusion.

The spatial composite of ensemble-averaged images presents a picture that is similar to that obtained by direct visual observations, except that time-resolution is improved. For the higher equivalence ratio the thin attached flame existing in the outer shear layers can be seen, together with the thickening that takes place at about 40 mm downstream. The flame in the thickened region has a clear vortical structure, as expected in reacting shear layers. Downstream development of flame takes place in the vortical structures present in the developing shear layers, and chemical heat release does not take place on the combustor centerline until greater than 200 mm downstream from the step. The greater field of view provided in Figure 14 shows a likely convection of OH (low intensity and distributed) from the shear layers into the step recirculation zone, via the reattachment plane. However, there are snake-like tendrils of high OH intensity are present locally (in the near-field regions) in the step recirculation zone. These almost certainly represent the presence of local chemical heat release. The images are extremely suggestive that these tendrils of chemical reaction within the step recirculation zone are the result of radial ejections of fuel from the center of the combustor across the jet shear layer, by non-stationary behavior of the mean flowfield. Figure 15 shows clearly shows an instance of this at the higher combustor loading, as do the individual instantaneous images that contribute to the ensemble.

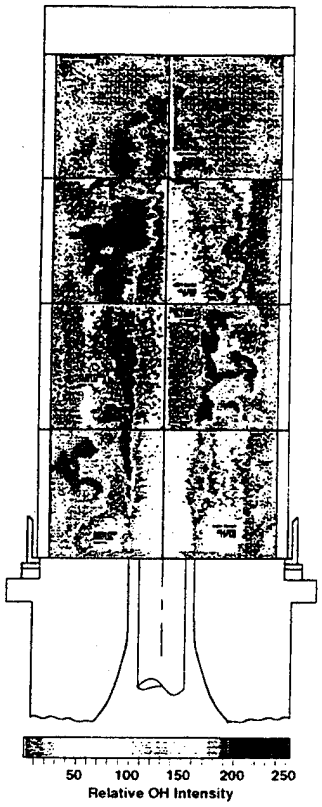

Fig. 15 Spatial Composite of LIF OH-Images at an Equivalence Ratio of 1.56 with Higher Combustor Loading (25-degree-orientation)

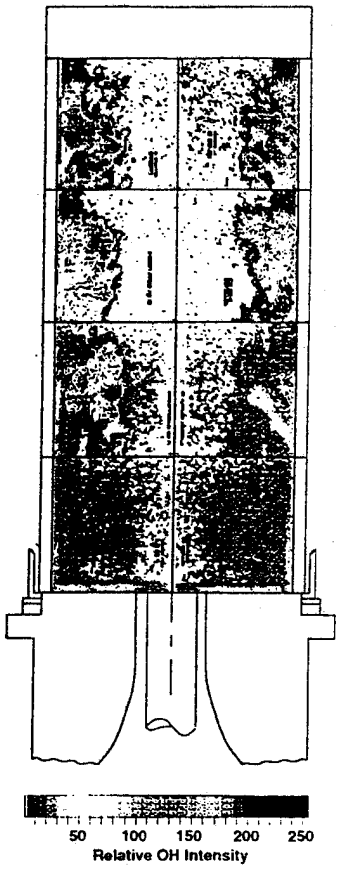

Fig. 16 Spatial Composite of LIF OH-Images at an Equivalence Ratio of 0.78 with Lower Combustor Loading (25 degree orientation)

Figure 16 shows an ensemble-average at 25-degrees image plane angle for low combustor loading at an equivalence ratio of 0.78. The attached flame is not in evidence. Reaction is absent from the center of the combustor, and reaction in the shear layers is reduced and is more diffuse. The step recirculation zone in the near-field is dominated by convection effects, and there is no evidence of local reaction due to radial ejection of fuel through the shear layers. Any fuel that enters the step recirculation from the shear layers at the reattachment plane is reacted long before it is returned to the step region.

Near-Field CARS Temperatures

Mean and fluctuating temperature measurements were made in the near-field using a Coherent Anti-Stokes Raman Spectroscopy (CARS) system in BOXCARS configuration (*Sturgess et al., 1993b*).

Figure 17 shows partial radial profiles of normalized mean temperature at 5 mm downstream from the step-plane of the combustor. The CARS measurements at this section show for visually-lifted flames that in the region 14 to 19 mm radii the flow is relatively cool, i.e. mostly air. This is in agreement with the isothermal, non-reacting LDA measurements that, at 5 mm downstream, define the air jet as existing from radii of 14 to 20 mm, and the fuel jet for radii less than 14 mm. For visually-attached flames, the cold air jet exists for $14 \le r \le 17$ mm, but for $r \ge 17$ mm there is a rapid increase in mean temperature as the inner edge of the attached flame is encountered. The main region of the attached flame is

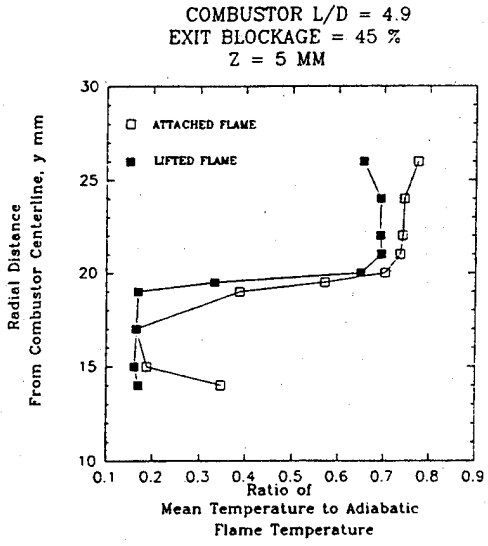

Fig. 17 Partial Radial Profiles of Normalized Mean Temperatures Measured By CARS at 5 mm Downstream From Step for Lifted and Attached Flames

encountered by a radius of 21 mm, and exists for at least 5 mm more. This is in good agreement with the values obtained from the TFP. The radial dimensionless temperature profile for the visually-lifted flame is very similar in this region, and, although the sudden temperature increase is not encountered until 19 mm radius, the elevated temperature region is again at least 5 mm in extent. Absolute temperatures for the attached flame are, of course, much higher than those for the lifted flame.

Examination of the CARS probability distribution functions (p.d.f's) at a z of 5 mm for low Reynolds Number, visually-attached flames, reveals that they are strongly bimodal for radii between 14 and 19 mm, as the example in Figure 18 shows. These radii encompass the nominally cold air jet ($15 \leq r \leq 17$ mm) and the inner part of the attached flame region. The bimodal p.d.f's reveal that there is a strong probability of encountering either hot or cold gas in this range of radii. Further into the attached flame itself, $r \geq 19.5$ mm, the p.d.f's are **not** bimodal. Thus, the jet shear layer (inner) part of the attached flame has a large-scale non-stationary behavior that may be associated with the vortical structure revealed somewhat further downstream in the LIF OH images.

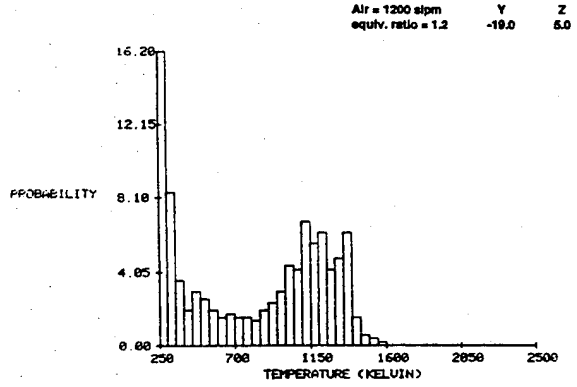

Fig. 18 CARS Temperature P.D.F. at 5 mm Downstream in the Air Jet, Showing Bimodal Form

CFD Calculations

CFD calculations were used to study the thermal boundary layer on the combustor wall upstream of the reattachment plane for the step recirculation zone, and on the step itself. Two combustion models were used in these calculations: the "mixed-is-burned" eddy break-up (EBU) model of *Magnussen & Hjertager (1973)* and, *Mason & Spalding (1973)*, and the eddy dissipation concept (EDC) model of *Magnussen (1985), Sloan & Sturgess (1994)*. The EBU model is familiar. The EDC model used fast chemistry, and bases chemical reaction on the sub-grid level to the ratio of two characteristic times, such that if the residence time in an individual grid volume is greater than a blowout time, then reaction in the volume is allowed. A further constraint is applied that the fuel/air mixture within the volume must be inside independent flammability limits for combustion. Finally, the action of turbulence eddies on limiting combustion through flame speed was included.

The dimensionless length of the step recirculation zone is a function of flow Reynolds Number and equivalence ratio (*Sturgess et al., 1992a*). The calculations were made for a Reynolds Number lower than desirable, but are to be compared to CARS data obtained at similar values. For the conditions of the calculations, the EBU model calculated the reattachment plane of the step recirculation zone at just less than 300 mm for 0.6 equivalence ratio (lifted flame), with maximum temperatures in the interior of the recirculation of the order of 800K, i.e. indication that all the fuel was consumed in the shear layers, and that there was no chemical reaction taking place within the recirculation itself. The EDC model at these conditions calculated a length of 350 mm, with interior temperatures of the order 1300-1400K. i.e. indication that not all of the fuel was consumed in the shear layers. Experimental estimate of the reattachment plane position at this equivalence ratio was 285 mm from the step; flame was not visible within the recirculation zone. At an attached flame condition with 1.05 equivalence ratio the EDC model gave a reattachment length of 300 mm, compared to an experimental estimate of 400 mm; recirculation zone interior temperatures were around 1500K. At an equivalence ratio of 1.62 (attached flame) the EDC model gave the reattachment length as 300 mm versus 400 mm from the measurements; the calculated interior temperatures were 1700-1800K. For an attached flame condition at 1.56 equivalence ratio, the TFP indicated interior recirculation zone temperatures (at z=10 mm) greater than 1300K (the cut-off value for the uncalibrated filament) to within about 20 mm from the combustor wall. For higher equivalence ratios, the EDC model showed that the interior temperatures of the step recirculation zone fall.

While these calculations are not defintive, they strongly suggest that the EBU combustion model is not capable of reproducing the attached flame. The EDC model appears at this point to be more promising.

In the experiments, with heat losses through the wall, wall quenching effects, and recirculation zone interior temperatures that increase with bulk equivalence ratio (up to about 1.6 equivalence ratio), an extensive thermal boundary layer is formed on the combustor surfaces within the step recirculation zone. Fuel entering this thermal boundary layer upstream (at the reattachment plane) is unlikely to be reacted. Quantities of such unreacted fuel would increase with bulk equivalence ratio, particularly suddenly as the jet shear layers become fuel-rich. It would be returned to the step by the recirculation, where it would then be entrained in the jet flows. There, it could be reacted and so form the attached flame.

A downstream plane of 5 mm from the step will be just outside this thermal layer, but will be influenced by it. As indicated above, the attached flame is encountered for radii around 20-25 mm. Therefore, Figure 19 compares the CFD calculations made with the EDC model, of temperature at (5,25) mm with CARS mean temperatures at 24 and 26 mm radii. The calculations show gas temperatures only increasing slightly from 1300K at 0.5 equivalence ratio (lifted flame) to 1350K at 1.6 bulk equivalence ratio (attached flame condition). The quantity of unburned fuel on the combustor wall is such that mixtures returned to the jet system are always outside the imposed flammability limits. The CARS measurments are in fairly good agreement with the calculations for 0.7 equivalence ratio (lifted flame) and even for 1.43 bulk equivalence ratio (attached flame). However, at 1.51 bulk equivalence ratio the measurements indicate a sudden and dramatic increase in gas temperature to around 1500K that is not reflected in the calculations.

To address the thermal boundary layer problem more realistically, measured wall temperatures were used as a thermal boundary condition. Typically, for lifted flames measured wall temperatures at z of 44.5 mm were around 810K, and for attached flames they were less than 815K, falling to less than 750K for an equivalence ratio of 1.5 (*Sturgess et al., 1993a*). Heat losses to the wall and step, and removal of active radicals by these impervious surfaces, inhibit flame propagation along the surfaces, resulting in an intervening dark region between them and the flame. This is known as the **deadspace.** The existance of the deadspace was accounted for by incorporating a wall-quenching model that precluded chemical reactions on the combustor wall and step. This model operated to quench reactions out from each surface to a value of y^+ equal to 100.

In order to elevate the mass of unreacted fuel returned to the air jet origin via the combustor wall and step in the step recirculation

zone, the bulk equivalence ratio was increased to just over 2.0 and the revised boundary conditions applied to the calculation. The calculated stoichiometric contour crossed the step recirculation zone and reached the combustor wall about half-way to the calculated reattachment plane. The amount of unreacted fuel returned to the origin of the air jet was increased through the existance in the calculation of the thermal boundary layer. However, the mixtures returned still remained outside the imposed flammability limits. The calculated temperature at the (5, 25) mm co-ordinate position is shown on Figure 19, and is therefore consistent with the other calculations.

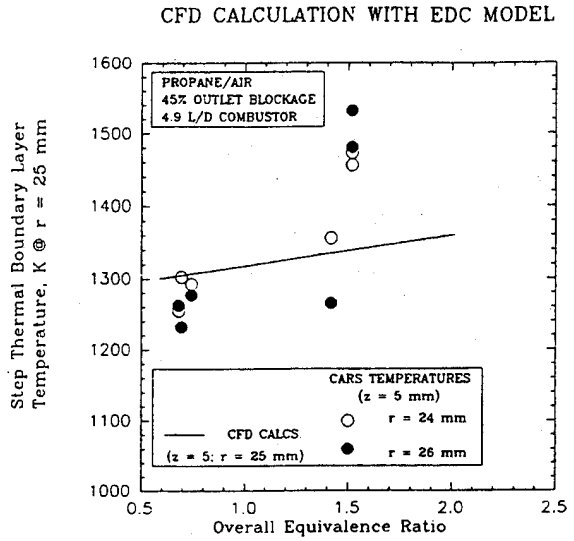

Fig. 19 Comparison of the Variation with Equivalence Ratio of CARS Mean Temperatures and CFD Calculations at a Co-ordinate Position in the Attached Flame, (5, 25) mm

The calculations show that the EDC model cannot correctly calculate the attached flame over the complete range of equivalence ratios. The CARS measurements indicate that something additional to recirculation of unburned fuel from the reattachment plane occurs for over-rich mixtures on a bulk basis.

DISCUSSION

It is apparent that the existance of the attached 'pilot' flame (Figure 8) is the key to where the majority of the fuel is reacted, and its "loss" denotes the beginning of a lean blowout sequence in the research combustor. When the attached flame is lost and the main flame lifts, considerable mixing of the separately-introduced reactants takes place prior to reaction. This accounts for the lean blowout data being so well correlated by a combustor loading parameter derived from well-stirred reactor theory (Figure 7), and for the resulting lean blowout curve agreeing with well-stirred reactor experimental lean blowout data from the literature, and with a well-stirred reactor calculation for the research combustor.

The blowout behavior of the research combustor provides good support for the argument that blowout of a lifted turbulent diffusion flame is controlled by **premixing**, where merging of neighboring vortices of hot burnt, and cold unburnt but mixed reactants, controls local extinction (*Williams, 1985*), (*Lockwood & Megahed, 1978*), etc. However, this is only part of the problem, since "lift" must also be explained. In the case of the research combustor there are in fact, two things that must be explained: First, loss of the attached flame leading to lift, and second, the existance of the attached flame in the first place!

Contrary to visual observations, the thin attached flame is revealed by the spontaneous OH-imaging and the TFP results as being a continuously-occurring phenomenon over fairly wide ranges of equivalence ratio, including equivalence ratios at which the main flame is lifted. At these latter equivalence ratios it is not a continuous flame (Figure 10) but has "holes" and is highly intermittent (Figure 11). Under such conditions it just does not supply enough energy and active radicals to serve as an adequate pilot for the jet shear layers.

The visually-lifted flame has been observed to vary in position with bulk equivalence ratio and combustor Reynolds Number (slightly), but is typically in the range of 160-300 mm downstream from the step. With normal airflow rates and air jet expansion rates in the combustor (based on isothermal LDA flow measurements) these distances represent mean ignition delay times in the range of 0.0033 to 0.0061 seconds. For hot-gas ignition of stoichiometric propane/air mixtures, (*Barrett & Hibbard, 1959*), these delay times correspond to ignition temperatures of 1340-1400K, which are in good agreement with the CARS temperatures measured in the outer shear layer just off the step (Figure 19) for lifted-flame equivalence ratios.

The holes and intermittency in the attached flame and its loss of visual luminosity, at equivalence ratios for which the main flame lifts ($\phi \leq 1.05$), could arise from two possible causes: First, a reduction in unburned fuel being delivered to the air jet outer shear layer by the recirculation zone. Figure 19, and the ignition delay estimates, support this as a plausible mechanism. The fuel returned by the step recirculation would be reduced as almost all of the supplied fuel would be consumed in the shear layers prior to reaching the reattachment plane. Second, local flame-stretch and/or quenching of the attached flame as cold vortices formed in the air jet move radially to impinge on and cross the front of the attached flame. Such vortices, if of comparable dimension to the flame thickness, could result in local extinctions by either process, or both. This dual-process is the hypothesis for flame lift advanced by Dahm (*Broadwell et al., 1985*), (*Dahm & Dimotakis, 1987*), (*Dahm & Dibble, 1988*). The amplitude of the attached flame oscillations detected in the research combustor by the TFP investigation are of the same order as the measured flame thickness. The frequencies of the oscillation, less than 10 Hz, are somewhat consistent with vortical motions in shear layers. The scale of the distortions revealed in the attached flame by the LIF OH-imaging are also of the same order as the flame thickness, Figures 14 and 15. These pieces of evidence do strongly suggest that there is a strong interaction of the attached flame with shear layer vortices. It is most likely that all three of the processes described are taking place simultaneously.

A major difficulty comes in convincingly explaining the existance of the attached flame in the research combustor.

A conventional view of flame stability in the research combustor would be as follows: A shear layer is formed between the inner fuel jet and the co-annular air jet. The sudden expansion at the step forms a step recirculation zone, around which the jet shear layers expand. Fuel/air mixtures inside the flammability limits are formed in the shear layers, and, where the expanding shear layers local velocities fall to the level of the local turbulent burning velocity, chemical reaction takes place. The majority of the heat release occurs in these shear layers. The step recirculation zone returns hot products of combustion upstream from the reattachment plane to the outer edges of the air jet entering the combustor. Mixing raises the temperature of the air jet, so that the fuel/air mixture formed in the inner shear layer is raised to ignition temperature and combustion is initiated. The position of the ignition in the shear layers would vary with bulk equivalence ratio, but there should **always** be an ignition delay that results in **some degree of flame lift.** Figures 8 and 19, and the ignition delay calculations given above, indicate that the process described is essentially the mechanism for low equivalence ratios.

A companion paper (*Sloan & Sturgess, 1994*) shows that CFD calculations also yield this result for **all** equivalence ratios. For bulk equivalence ratios that are fuel-rich (visually attached flame) there is not enough air introduced to burn all of the fuel. However, the temperature in the reacting jet shear layers is very high, and almost all of the fuel that can be reacted is reacted there, together with most of the oxygen. Very little oxygen enters the recirculation zone. Of the fuel that is unburned, most exits the combustor; very little extra enters the recirculation zone. Fuel that does enter the recirculation zone is returned to the jet shear layers in oxygen-deficient mixtures via a thermal boundary layer existing on the combustor interior surfaces. When reacted with air from the air jet there is too little fuel delivered in this way to result in sufficient temperature rise to evidence the attached flame.

It is apparent that **additional** unburned fuel somehow enters the recirculation zone **directly**, (i.e. **not** via the reattachment plane), and in sufficient quantities at bulk equivalence ratios over 1.05, to raise the temperature of the step thermal boundary layer to ignition levels or greater, and to result in local equivalence ratios in the air jet outer layer that are inside the flammability limits and also give high heat release. The LIF OH-imagining, Figures 14 and 15, shows instances of such a mechanism whereby there are sudden and local violent radial ejections of reacting mixture from the reacting shear layers into and radially across, the step recirculation zone long before the reattachment plane is reached. The recirculating flow carries these tendrils of high temperature reacting mixture upstream to the step, and thence, to the outer air jet. These tendrils could well be the cause of the sudden rise in temperature recorded by the CARS apparatus at the co-ordinates (5, 25) mm shown in Figure 19. Of course, the OH-imaging cannot detect unreacted propane that is similarly ejected, but since there are holes (Figure 14) in the shear layer, unreacted fuel could likewise be ejected radially into the recirculating flow directly.

The method for radial transport directly into the step recirculation zone has been demonstrated. The mechanism that produces the behavior must now be explained.

The TFP results show that at 10 mm downstream, the 'attached' flame, at a 24 mm mean radius, oscillates with a 4 mm displacement at frequencies below 10Hz for equivalence ratios from 0.78 to 1.56. At 5 mm downstream, the CARS p.d.f.'s were found to be strongly bimodal for radii between 14 and 19 mm when the flame was visibly attached ($\phi \geq 1.05$). At this axial position these radii encompass the region of the air jet, which has an initial thickness of 3 mm. From these pieces of evidence it therefore appears that the non-stationary behavior of the attached flame is driven from the **inside** of the jet system.

Figure 3 shows the near-field stationary flow characteristics of the research combustor for isothermal flow. Contained on the centerline of the combustor in the fuel jet, is the small central recirculation bubble, whose mean leading-edge position is at a z of 15 mm, with an axial extent of 17 mm and a maximum radius of 4.5 mm. This bubble is in extremely close proximity to the inner edge of the jet shear layers, which reach the combustor centerline at 36 mm from the step-plane, just immediately downstream of the bubble. The bubble and jet shear layers are thus closely-coupled.

The bubble is generated because the air jet rapidly entrains the fuel jet. This is because the momentum of the co-annular air jet is many times that of the central fuel jet, typically 15-20 for combusting flow (*Sturgess et al., 1992b*). At typical equivalence ratios, the centerline mean axial velocity of the fuel entering the combustor is very low, being of the order of the mass-averaged combustor velocity. The axial and radial fluctuating velocities as measured by the LDA, however, are high on the centerline, and are about 1.5 times the mass-averaged combustor velocity. The centerline reverse-flow mean axial velocity in the bubble is about equal to the fuel centerline inlet velocity. The central bubble is therefore highly unstable.

Free-stream recirculation bubbles are known to be unstable. The presence of standing waves in a flow also provides a feedback mechanism to allow any small initial disturbance that might be introduced in the entering flow to be sustained. The shear layer formed around the recirculation bubble is inherently unstable, and can act as a fluid amplifier for these initial disturbances. Thus, if there is a correct phase relationship between the feedback and the natural frequency of the bubble shear layer, a self-excited oscillation can be set up. This self-excitation can cause the dimensions of the major and minor axes of the bubble to vary in time, and for the position of the bubble to move along its major axis. Periodic oscillations have been observed experimently for both non-reacting and reacting flows (*Gouldin et al., 1983*), (*Vu, 1983*), (*Halthorne & Gouldin, 1984*).

Visualization of the near-field, center region of the combustor has been made using reactive Mie scattering (RMS), (*Roquemore et al., 1991*). Titanium tetrachloride was added to dry propane, and moisture was added to the air stream to supplement the water generated by chemical reaction. TiO_2 seed particles generated by the near-instantaneous reaction of $TiCl_4$ with H_2O, were illuminated with a sheet of frequency-doubled Nd-Yag laser-light, and the images produced were collected by a CCD camera that was normal to the laser sheet.

The RMS images reveal that the vortices generated by the jet shear layer are about 3 mm in diameter, i.e. the same size as the air jet passage, and the same as the amplitude of the attached flame oscillation. The images also confirm that the central recirculation bubble is very unstable. It precesses around the circumference of the fuel tube and moves axially to actually enter the fuel tube opening at times. Although recirculation bubble formation is essentially an inviscid process, the movements of the bubble appear to be Reynolds number dependent. An increase in fuel flow rate moved the bubble out of the fuel tube, and tended to reduce the precessing. This behavior is consistent with strengthening the reverse flow velocity in the bubble.

Given the close-coupling between the jet shear layers and the central recirculation bubble, it is reasonable to believe that the movements of the attached flame derive from those of the bubble. Since the vortices in the jet shear layers are comparable in size to the attached flame thickness and the radial movements are also comparable in size, it is also entirely possible to accept that random movements of the bubble could project shear layer eddies of reacting mixture, pure air, pure fuel, and of non-reacting mixture, through into the step recirculation zone.

CONCLUSIONS

Following are the conclusions of this research concerning lean stability in a research combustor:

1. The research combustor satisfactorily reproduces the major features of a gas turbine combustor primary zone, as was the intent.

2. The research combustor behaves like a well-stirred reactor during lean blowout. This is because flame-lift at a bulk equivalence ratio of 1.05 causes partial-premixing of the reactants prior to reaction. The onset of a lean blowout sequence is the loss of the piloting action of an attached flame for the fuel/air jet shear layers, thereby resulting in the flame-lift.

3. The attached flame is continuously present over a wide range of both fuel-rich and fuel-lean equivalence ratios; however, at equivalence ratios less than 1.05 it does not supply sufficient energy to pilot the jet shear layers.

4. The attached flame is both non-stationary and intermittent, with intermittency increasing rapidly below 1.05 equivalence ratio. This behavior is a result of eddies from the jet shear layers impinging on, stretching, and penetrating, the flame front.

5. The step recirculation zone does not of itself, return sufficient unburned fuel to sustain the attached flame. The attached flame is fueled by periodic ejections of appropriate eddies from the jet shear layers, directly into the upstream regions of the step recirculation zone.

6. The mechanism for the non-stationary behavior of the attached flame and for the ejection of eddies from the jet shear layers into the step recirculation zone, is the close-coupling of the upstream portion of the jet shear layers with a non-stationary and dimensionally-unstable, central recirculation bubble. The central recirculation bubble is generated by entrainment of the low momentum central fuel jet by the high momentum, co-annular air jet.

7. Domination of the critical mass transport by non-stationary behavior of the mean flow has potentially-serious implications of the efficacy of stationary-state CFD codes in the calculation of combusting flows.

8. With respect to implications for lean stability in practical combustors, the research suggests that recirculation zone-stabilized combustion may not operate the way it is thought to do.

ACKNOWLEDGEMENTS

The authors wish to acknowledge the contributions to this work from their colleagues at Wright-Patterson Air Force Base, Pratt & Whitney and Brigham Young University. The enthusiasm, encouragement, support and contributions of Dr. W. M. (Mel.) Roquemore of Wright Laboratory have been particularly appreciated. The work was supported by the U.S. Air Force Wright Laboratory under Contract No. F33615-87-C-2822 to Pratt & Whitney, East Hartford, Connecticut, and the U.S. Air Force Office of Scientific Research (AFOSR) through a Summer Faculty Research Program grant, Contract No. F49620-88-C-0053. Special thanks are due to Dr. Julian Tishkoff of AFOSR. The authors wish to thank Pratt & Whitney for permission to publish these results.

REFERENCES

Ballal, D.R., M.D. Vangsness, S.P. Heneghan, and G.J. Sturgess, 1993, "Studies of Lean Blowout in a Research Combustor," presented at AGARD 81st. Symposium of the Propulsion and Energetics Panel *Fuels and Combustion Technology for Advanced Aircraft Engines,* Colleferro, Italy, 10-14 May.

Barnett, H.C. and R.R. Hibbard, (Edit.), 1959, *Basic Considerations in the Combustion of Hydrocarbon Fuels with Air,* NACA Report 1300.

Bragg, S.L., 1953, "Application of Reaction Rate Theory to Combustion Chamber Analysis," Aeronautical Research Council Pub. ARC 16170, London.

Broadwell, J.E., W.J.A. Dahm, and M.G. Mungal, 1985, "Blowout of Turbulent Diffusion Flames," proc. *20th. Symposium (International) on Combustion,* The Combustion Institute, Pittsburgh, Pennsylvania, pp. 303-310.

Chen, T.H., 1991, private communication.

Chen, T.H. and L.P. Goss, 1989, "Flame Lifting and Flame/Flow Interactions of Jet Diffusion Flames," Paper No. AIAA-89-0156, AIAA 27th. Aerospace Sciences Meeting, Reno, Nevada, January 9-12.

Chen, T.H., L.P. Goss, D.Talley and D. Mikolaitis, 1989, "Stabilization Zone Structure in Jet Diffusion Flames from Liftoff to Blowout," Paper No. AIAA-89-0153, AIAA 27th. Aerospace Sciences Meeting, Reno, Nevada, January 9-12.

Dahm, W.J.A. and R.W. Dibble, 1988, "Combustion Stability Limits of Coflowing Turbulent Jet Diffusion Flames," Paper No. AIAA-88-0538, AIAA 26th. Aerospace Sciences Meeting, Reno, Nevada, January 11-14.

Dahm, W. J. A. and P.E. Dimotakis, 1987, "Measurements of Entrainment and Mixing in Turbulent Jets," *AIAA Journal,* Vol. 25, No. 9, pp.1216-1223.

Goss, L.P., V. Vilimpoc, B. Sarka and W.F. Lynn, 1988, "Thin-Filament Pyrometry: A Novel Thermometric Technique for Combusting Flows," Paper No. 88-GT-28, ASME Gas Turbine and Aeroengine Congress and Exposition, Amsterdam, The Netherlands, June 5-9.

Gouldin, F.C., J.S. Depsky and S.L. Lee, 1983, "Velocity Field Characteristics of a Swirling Flow Combustor," Paper No. AIAA-83-0314, AIAA 21st. Aerospace Sciences Meeting, Reno, Nevada, January 10-13.

Halthore, R.N. and F.C. Gouldin, 1984, "Laser Scattering Measurements for Density in a Swirling Flow Combustor," Paper No. AIAA-84-0199, AIAA 22nd. Aerospace Sciences Meeting, Reno, Nevada, January 9-12.

Heneghan, S.P., M.D. Vangsness, D.R. Ballal, A.L. Lesmerises, and G.J. Sturgess, 1990, "Acoustic Characteristics of a Research Step Combustor," Paper No. AIAA-90-1851, AIAA/SAE/ASME/ASEE 26th. Joint Propulsion Conference, Orlando, Florida, July 16-18.

Jeffs, R.A., 1962, "The Flame Stability and Heat Release Rates of Some Can-Type Combustion Chambers," proc. *8th. Symposium (International) on Combustion,* Williams and Wilkins, Baltimore, pp. 1014-1027.

Kretschmer, D. and J. Odgers, 1972, "Modeling of Gas Turbine Combustors - A Convenient Reaction Rate Expression," Trans. ASME, *J. Energy and Power,* pp.173-180.

Lefebvre, A.H., 1983, *Gas Turbine Combustion,* Hemisphere Publishing Co., McGraw-Hill.

Lewis, B. and G. von Elbe, 1961, *Combustion, Flames and Explosion of Gases,* 3rd. Edition, Academic Press.

Lockwood, F.C. and I.A.E. Megahed, 1978, "Extinction in Turbulent Reacting Flows," *Combustion Science and Technology,* Vol. 19, pp. 77-80.

Longwell, J.P., E.E. Frost and M.A. Weiss, 1953, "Flame Stability in Bluff-Body Recirculation Zones," *Ind. Eng. Chem.,* Vol. 45, No. 8, pp.1629-1633.

Magnussen, B.F. and B.H. Hjertager, 1973, "On Mathematical Modelling of Turbulent Combustion with Special Emphasis on Soot Formation," proc. *16th. Symposium (International) on Combustion,* Academic Press, pp. 601-606.

Magnussen, B.F., 1985, "Heat Transfer in Gas Turbine Combustors - A Discussion of Mathematical Modelling of Combustion, Heat and Mass Transfer with Emphasis on Heat Transfer in Gas Turbine Combustors," AGARD Conference Preprint No. 390, *Heat Transfer and Cooling in Gas Turbines,* Paper No. 23.

Mason, H.B. and D.B. Spalding, 1973, "Prediction of Reaction Rates in Turbulent Premixed Boundary Layer Flows," proc. *First Symposium (European) on Combustion,* Academic Press, pp. 601-606.

Roquemore, W. M., V.K. Reddy, P.O. Hedman, M.E. Post, T.H. Chen, L.P. Goss, D. Trump, V. Vilimpoc and G.J. Sturgess, 1991, "Experimental and Theoretical Studies in a Gas-Fueled Research

Combustor," Paper No. AIAA-91-0639, 29th. Aerospace Sciences Meeting, Reno, Nevada, January 7-10.

Sloan, D.G. and G.J. Sturgess, 1994, "Modeling of Local Extinction in Turbulent Flames," submitted to ASME Turbo-Expo '94.

Stewart, D.G., 1956, *Selected Combustion Problems II,* AGARD/NATO, Butterworths, London, pp. 384-413.

Sturgess, G.J., 1983, *Aerothermal Modeling - Phase I, Final Report,* NASA Report CR-168202, May.

Sturgess, G.J., D.G. Sloan, W.M. Roquemore, V.K. Reddy, D. Shouse, A. L. Lesmerises, D.R. Ballal, S.P. Heneghan, M.D. Vangsness, and P.O. Hedman, 1991a, "Flame Stability and Lean Blowout - A Research Program Progress Report," proc. *10th. International Symposium on Air Breathing Engines,* Nottingham, England, pp. 372-384.

Sturgess, G.J., S.P. Heneghan, M.D. Vangsness, D.R. Ballal, and A.L. Lesmerises, 1991b, "Lean Blowout in a Research Combustor at Simulated Low Pressures," Paper No. 91-GT-359, presented at the ASME Gas Turbine and Aeroengine Congress and Exposition, Orlando, Florida.

Sturgess, G. J., D.G. Sloan, A.L. Lesmerises, S.P. Heneghan, and D.R. Ballal, 1992a, "Design and Development of a Research Combustor for Lean Blowout Studies," Trans. ASME, *J. Engineering for Gas Turbines and Power,* Vol. 114, pp.13-19.

Sturgess, G.J., S.P. Heneghan, M.D. Vangsness, D.R. Ballal, and A.L. Lesmerises, 1992b, "Isothermal Flow Fields in a Research Combustor for Lean Blowout Studies," Trans. ASME, *J. Engineering for Gas Turbines and Power,* Vol. 114, pp. 435-444.

Sturgess, G.J., R. McKinney and S. Morford, 1993a, "Modification of Combustor Stoichiometry Distribution for Reduced NOx Emission from Aircraft Engines," Trans. ASME, *J. Enginneering for Gas Turbines and Power,* Vol.115, No.3, pp. 570-580.

Sturgess, G.J., S.P. Heneghan, M.D. Vangsness, D.R. Ballal, A.L. Lesmerises, and D. Shouse, 1993b, "Effects of Back-Pressure in a Lean Blowout Research Combustor," Trans. ASME, *J. Engineering for Gas Turbines and Power,* Vol. 115, No. 3, pp. 486-498.

Sturgess, G.J. and D. Shouse, 1993c, "Lean Blowout Research in a Generic Gas Turbine Combustor with High Optical Access," Paper No. 93-GT-332, ASME International Gas Turbine and Aeroengine Congress and Exposition, Cincinnati, Ohio, May 24-27.

Swithenbank, J., 1974, "Flame Stabilization in High Velocity Flow," *Combustion Technology - Some Modern Developments,* Edit. H.B. Palmer and J.M. Beer, Academic Press, pp. 91-125.

Takahashi, F., M. Mizomoto, and S. Ikai, 1988, "Structure of the Stabilizing Region of a Laminar Jet Diffusion Flame," Trans. ASME, *J. Heat Transfer,* Vol. 110, pp.182-189.

Vu, B.T., 1983, *Experimental Study of Turbulent Swirling Flows,* Ph.D. Thesis, Sibley School of Mechanical and Aerospace Engineering, Cornell University, Ithaca, New York.

Williams, F.A., 1985, *Combustion Theory,* 2nd. Edition, The Benjamin/Cummings Publishing Co., Inc., Menlo Park, California, pp. 408-410.

THIS PAGE INTENTIONALLY LEFT BLANK

APPENDIX H

STUDIES OF LEAN BLOWOUT IN A RESEARCH COMBUSTOR

By

D.R. Ballal, M.D. Vangsness and S.P. Heneghan
University of Dayton, Dayton, Ohio

G.J. Sturgess
Pratt & Whitney, East Hartford, Connecticut

Published in AGARD Conference Proceedings 536, *Fuels and Combustion Technology for Advanced Aircraft Engines,* May 1993, pp. 23-1 - 23-9.

STUDIES OF LEAN BLOWOUT IN A RESEARCH COMBUSTOR

by

D.R. Ballal, M.D. Vangsness and S.P. Heneghan
University of Dayton
300 College Park
Dayton, Ohio 45469
United States

G.J. Sturgess
Pratt and Whitney Engineering
East Hartford, CT 06108
United States

1. SUMMARY

A prime requirement in the design of a modern gas turbine combustor is good lean blowout (LBO) stability to ensure an adequate stability margin. Therefore, a geometrically simple, optically accessible, and acoustically decoupled research combustor was designed to reproduce the gross features of the flow field in a modern annular gas turbine combustor. Its LBO was measured using methane and propane fuels. We successfully observed and documented a systematic and detailed sequence of events comprising an attached flame, a lifted shear flame, an intermittent shear flame, the large-scale instability of the flame front, and LBO. Also, for the sake of comparison, a generic gas turbine combustor was tested and its LBO limits were measured.

We found that LBO in the research combustor behaved like a perfectly stirred reactor (PSR) for values of combustor-loading spanning three orders of magnitude. Also, LBO was successfully correlated using a simple PSR theory. Finally, Swithenbank's dissipation gradient approach and an eddy dissipation model with a built-in characteristic extinction time criterion, when coupled with CFD, offer the possibility of an *a priori* calculation of LBO. The lean stability of a generic gas turbine combustor at peak heat release rates was less than that in a research combustor. Also, in the generic combustor, the flame changes from a lifted to an attached position depending upon how combustor loading is achieved. Due to such complications, modeling of the LBO process that works reasonably well with the research combustor will be seriously challenged by the blowout behavior evidenced in the generic gas turbine combustor.

LIST OF SYMBOLS

C_μ	constant
D	laminar diffusion coefficient
E	activation energy
K	turbulent kinetic energy
LBO	lean blowout
LP	loading parameter
L/D	length/diameter ratio
m	mass flow rate
n	reaction order
P	pressure
PSR	perfectly stirred reactor
R	gas constant
Re	Reynolds number
S	species source term
T	temperature
V	combustion volume
x,y,z	radial, transverse, and axial distance resp.
ε	turbulent dissipation rate
ϕ	equivalence ratio
ν	kinematic viscosity
ρ	density
σ	Schmidt number
τ	residence time

Subscripts

a	air
ext	extinction
f	fuel
o	oxygen
nit,N_2	nitrogen
tot	total

2. INTRODUCTION

A prime requirement in the design of a modern gas turbine combustor is good combustion stability, especially near lean blowout (LBO), to ensure an adequate stability margin. For the aircraft engine, combustor blow-off limits are encountered during low engine speeds at high altitudes over a range of combustor air loading parameters. This is illustrated in Fig. 1 as a loss in the operating envelope. It is the task of the combustion engineer to design a combustor such that all its steady-state operating points lie inside the envelope. This envelope should be extensive enough to encompass the under- and over-shoots associated with the different response rates to the throttle movements of the fuel system and the rotating machinery. Further, the current and likely future design trends towards airblast atomization, high temperature rise, and low emissions are eroding the safety margins. For these reasons, the U.S. Air Force Wright Laboratory, Aero Propulsion and Power Directorate (WL/PO), Wright-Patterson Air Force Base, Ohio initiated a joint Government, Industry, and University research program to understand and model LBO in aircraft combustors. This paper describes the major results and discusses various factors that influence LBO in research and practical combustors.

In a modern annular gas turbine combustor (Fig. 2), flame is stabilized by producing a recirculation zone in the flow field. This zone is generated by a combination of three mechanisms: an axial swirling air jet associated with each

Presented at an AGARD Meeting on 'Fuels and Combustion Technology for Advanced Aircraft Engines', May 1993.

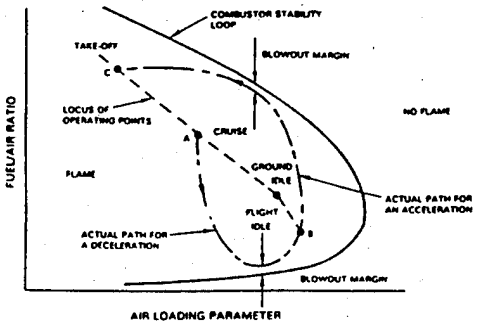

Fig. 1: Engine operating envelope superimposed on the combustor stability loop, illustrating the stability margins at blowout.

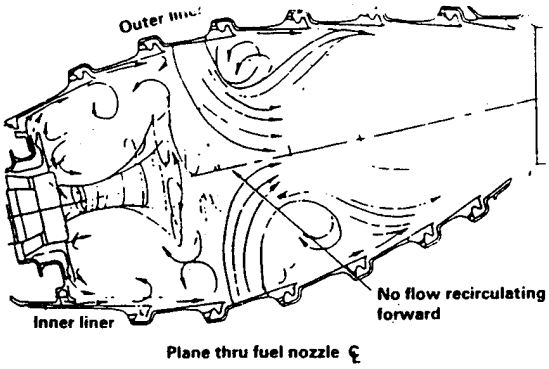

Fig. 2: Flow pattern in a modern annular combustor.

fuel introduction, sudden expansion of the axial swirling jets as they enter the primary zone, and back pressure provided by an array of radial air jets at the end of the primary zone. To obtain low exhaust emissions, Pratt & Whitney currently tailors the combustor flow control mechanisms to produce an "inside-out" recirculation pattern (Fig. 2). Therefore, the research combustor was required to reproduce this type of recirculation pattern. At the same time, it had to provide stable combustion over a reasonably wide variation in its loading, be geometrically simple for ease of experimentation and computation, and provide adequate optical access for measurements.

This paper discusses fundamental processes in the near-field region of the combustor that elucidate how LBO occurs in practical combustors, factors relating to combustor geometry (e.g., back pressure) and operating conditions (e.g., equivalence ratio, fuel and air velocity) that influence LBO, a map of flame behavior vs. combustor loading, and the application of reaction rate theory to the correlation of LBO results.

3. EXPERIMENTAL WORK

Research Combustor: We designed a research combustor to simulate three main features of the flow field in a modern annular gas turbine combustor; (i) a reactive shear layer formed between fuel and air jets, (ii) the inside-out type of recirculation zone, and (iii) the interaction between and back-pressure exerted by transverse combustion air jets and axially directed jets of fuel-air mixture. A complete description of the combustor design and development is provided by Sturgess et al. [1].

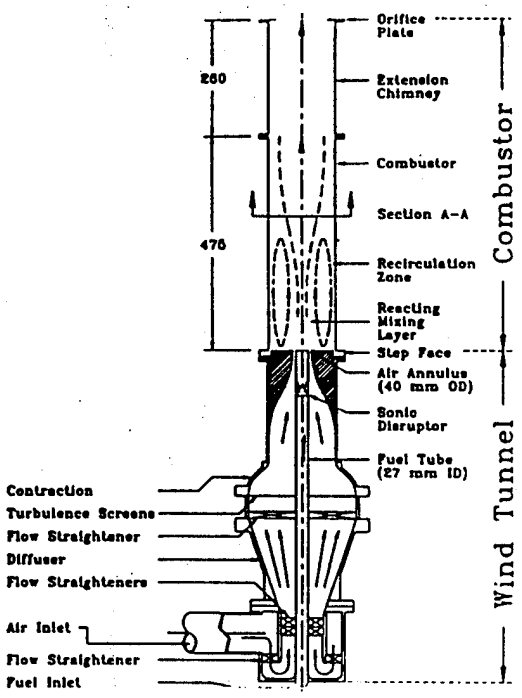

Fig. 3: Schematic diagram of a research combustor for LBO studies.

Fig. 3 shows a schematic diagram of the research combustor. It consists of a 27-mm (i.d.) central fuel tube of low-speed gaseous propane or methane surrounded by a 40-mm (i.d.) high-speed coaxial air jet exhausting into a dump combustor. This arrangement produces an intense reactive shear layer between fuel and airstreams. The duct is closed at its forward end to yield a 55-mm-high, backward-facing step. This step provides an inside-out recirculation zone which feeds high-temperature combustion products into the shear layer and thus provides a source of continuous ignition to

stabilize the flame. A perforated conical baffle inserted five diameters upstream of the fuel tube serves to acoustically isolate the fuel supply from the combustion process. As shown in Fig. 3, the step combustor is mounted vertically on a small wind tunnel. The combustor duct is comprised of two separate sections. The first section holds optical quartz windows (or metal panels with thermocouples and static pressure tappings for wall temperature and pressure measurements, respectively) on all four sides; the second one is a 250-mm extension inconel chimney. The chimney exit is blocked with an orifice plate which simulates the back-pressure effect of a practical combustor. The combustor has a hydraulic mean diameter of 150 mm, is 475 mm long, and has an exit orifice blockage of 21%, 45%, or 62%. The combination of combustor and its extension chimney yields (L/D) ratios of 3.17, 4.9, and 6.5, respectively.

Test Conditions: The combustion laboratory provides gaseous propane anane fuels up to 20 Kg/hr. Both fuelstream (Re = 1,733 to 17,333) and airstream (Re = 7,233 to 72,322) were monitored to within 1.5%. Ignition of the combustor was satisfactorily accomplished using a retractable torch igniter. As the LBO condition was approached, the attached diffusion flame lifted from the fuel tube and was stabilized slightly downstream. This was the region of most interest and relevance to the present study.

Instrumentation: A three-component LDA system for velocity measurements and a CARS system for flame-temperature measurements were used. The optical window size permitted data acquisition in the range x = -70 to + 70 mm, y = -33 to +33 mm, and z = 2 to 360 mm.

The LDA uses the green (514.5 nm) and blue (488 nm) lines of a 15 W Argon-ion laser as a source; two measurement channels were separated by polarization while a third uses the blue beam. The scattered signals were collected in a forward direction at 10 degrees off axis. The effective probe volume was 50 x 300 x 750 μm, the Bragg cell frequency shift was 5 MHz, and Al_2O_3 seed particles were used. After allowing for seed biasing, the measurement uncertainty in mean velocity was 1%, in rms velocity it was 5%, and in skewness and kurtosis it was 7%.

The CARS system employed a BOXCARS configuration. Here, the frequency-doubled source green beam (532 nm) was split into four beams. A 25-x-250-μm measuring spot size was achieved. The CARS temperatures were determined, see Heneghan et al., [2], by applying the principle of local thermodynamic equilibrium. Usually, 500 samples were taken for each CARS measurement. It was estimated that the overall CARS mean temperature measurement accuracy is within 50K, while the precision is well within 20K. Unlike the LDA, the CARS measurements are time-averaged without density-biasing effects.

4. RESULTS

Acoustic Decoupling: Combustion-induced acoustic oscillations can severely limit the operating range of some practical combustors--especially parallel-wall duct combustors. The acoustic characteristics of this research combustor were investigated because it was feared that eddy-shedding off the step might satisfy the Rayleigh criterion, which, in turn, could set up resonance in the combustor and fuel supply tube. Heneghan et al. [3] have described the results of this investigation in detail. It was found that an acoustic isolator in the fuel tube and an air inlet convergence that eliminated vortex generation at the inlet significantly decrease acoustic coupling. Finally, a research step combustor with an L/D = 4.9 and fitted with an orifice plate with a blockage ratio = 0.45 provided the best combination of LBO and freedom from acoustic coupling.

Isothermal Flow Field: Next, we measured the isothermal flow field in the combustor corresponding to the fuel and air-jet velocity ratios at the combustor blowout conditions. This investigation is described by Sturgess et al. [4]. Fig. 4 shows a typical result. The LDA measurements revealed the presence of the primary zone flow features (i.e., a near-field region comprising the jet shear layer and a small, central recirculation zone generated by the large momentum ratio between the fuel and the air jets; an outer recirculation zone stabilized on the step; and the far-field region, in which the individual jets lose their identity and exhibit self-similarity).

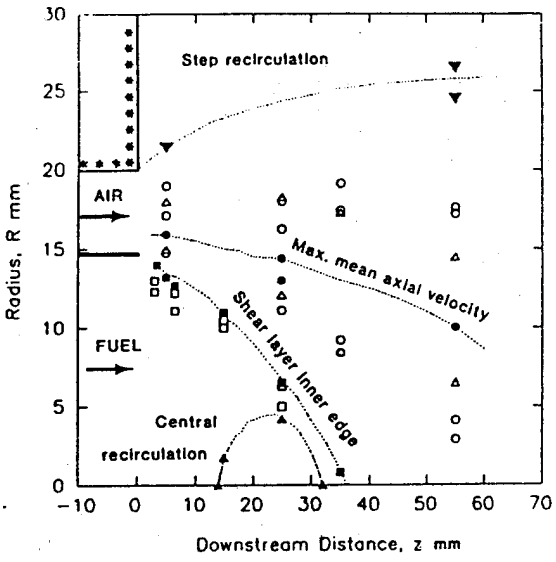

Fig. 4: Isothermal flow field results illustrating the near-field region, recirculation zones, and the far-field region; (■, ▲, ▼-mean axial velocity, □, ○-turbulence intensities, and Δ-max. velocity gradient).

Flame Visualization: Fig. 5 illustrates the sequence of events leading to LBO. As the overall equivalence ratio was reduced below unity, the attached flame moved further downstream into the combustor in a characteristic lifted flame position and form. Continuing reduction ir

equivalence ratio produces an onset of flow instability in the lifted flame, an increase in the amplitude of the instability, the onset of intermittency, severe intermittency, and, finally, the onset of strong axial flame instability. This sequence clearly highlights the complexity of the LBO mechanism in a modern annular gas turbine combustor.

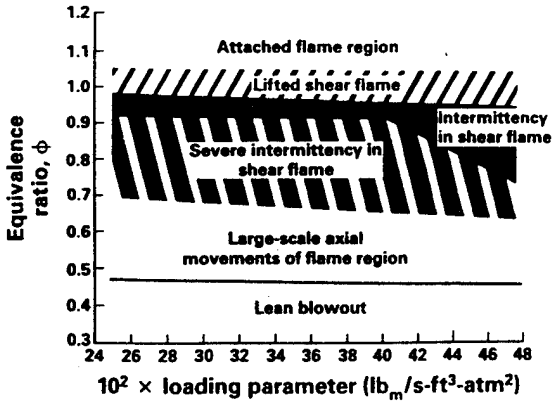

Fig. 5: Sequence of events leading to LBO as observed by flame visualization.

In our research combustor, the piloting action of the flame in the jet shear layers by the attached flame at the step appears to be crucial to combustor stability. Thus, successful modeling of the combustor stability requires the prediction of the attached flame and its lift. The OH images of the attached flame, see Sturgess et al., [5], show that its structure at any given time is associated with local vortices shed from the inner edge of the combustor step. Also, the instantaneous OH images reveal that combustion takes place in a more distributed form via relatively large "packets" of reaction.

Lean Blowout: We measured LBO as a function of air loading parameter (LP) over a range of propane fuel flows. However, this did not yield a complete combustor stability loop. To achieve a wide variation in LP with the simple atmospheric pressure research combustor, a subatmospheric pressure simulation was used. As explained in Ref. [6], excess gaseous nitrogen was introduced into the air supply upstream of the combustor as a diluent to lower the concentration of reactants and/or reaction temperature by virtue of its heat capacity. Fig. 6 illustrates a calibrated relationship between equivalent pressure and (nitrogen/fuel) mass ratio at blowout in the research combustor. This technique permitted (i) the simulation of subatmospheric pressure as low as 0.1 atm, (ii) the completion of the combustor stability loop (ranging from ϕ = 0.5 to 0.9), and (iii) increased LP by two orders of magnitude.

Fig. 7 shows the LBO performance of our research combustor and stability loops for several well-stirred reactors from the

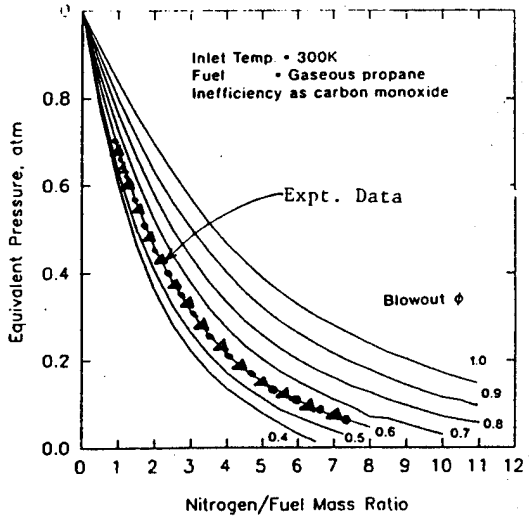

Fig. 6: Calibration curves for simulating subatmospheric pressure by using nitrogen dilution.

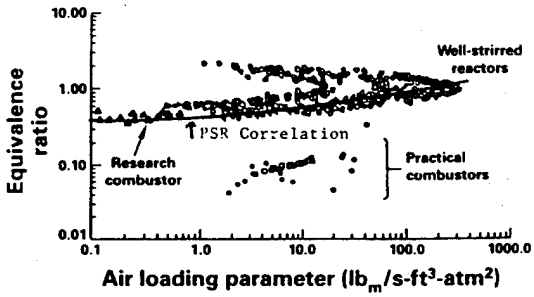

Fig. 7: LBO vs. LP data for the research combustor showing a comparison between the measured and the predicted results.

literature, as well as two partial loops for practical gas turbine combustors. For these results, the standard LP was derived from the global reaction rate theory, but modified to include the effects of inert excess nitrogen;

$$LP = m_{tot}/(VP^n), \quad (1)$$

$$m_{tot} = m_f + m_a + m_{nit}, \quad (2)$$

and $$n = 2\,\phi_{LBO}/(1 + m_{nit}/m_a). \quad (3)$$

The trend of LBO vs. air loading shown in Fig. 7 is very similar to that found for a perfectly stirred reactor (PSR); the latter approaching the characteristics of a future generation of

ideal premixed, prevaporized, near-stoichiometric combustors. Thus, it is reasonable to conclude that our research combustor correctly reproduced the LBO processes of a real gas turbine combustor. Also plotted in this figure are results for a gas turbine combustor fitted with a vaporizer tube and another one fitted with a strongly swirling prefilming airblast atomizer. In addition to their different fuel injection patterns, these two combustors had completely different flow fields (as compared to the combustor of Fig. 1) due to their different shapes, method of fuel introduction, and liner hole patterns. These results clearly suggest that a simple and general correlation for LBO is not possible. However, as will be shown later, direct calculation for each combustor offers the only possibility of making reliable *a priori* estimates of stability in gas turbine combustors.

To simulate the presence of dilution air jets, we investigated the effects of back pressure on the LBO in our research combustor. These results are discussed in detail in Ref. [7]; a typical result is presented in Fig. 8. As seen in the figure, LBO was improved by increasing the exit blockage. However, we found that (see Ref. 7) above a blockage of 45%, (i) significant interference occurs between the outlet and the combustor flame holding, and (ii) LBO does not improve much. Thus, we concluded that an exit blockage of 45 percent provides the best combustion stability and optimal configuration (i.e., for a combustor of exit blockage = 45 percent and L/D = 4.9, the LBOs were virtually independent of blockage and acoustic coupling). For a lightly loaded combustor (near the flammability limits), exit blockage exerts a weak influence on LBO, primarily through its effect on the jet and the recirculation zone shear layers. For high combustor loadings (near the peak heat release rate), exit blockage had a strong effect on the LBO via the dynamic behavior of the flow in the near-field (especially the interaction of the central recirculation bubble with the jet shear layers) and of the jet shear layers with the step recirculation zone.

5. ANALYSIS

Complete calculation of stability by using the CFD techniques to define the combustor flow field locally is not a viable approach. LBO is dominated by the kinetics of chemical reaction; therefore, CFD calculations of a large number of chemical reactions would be required to yield the correct heat release. For example, for hydrocarbon fuels, a general transport equation of the form,

$$\partial/\partial x_j \langle \rho u_j m_i - \Gamma_{eff} (\partial m_i/\partial x_j) \rangle = S_m \qquad (4)$$

where i denotes chemical species, m_i is the mass fraction of i, and S_m is a species source term, would have to be solved for each species. The computational burden of doing so is presently unacceptable in the context of the complicated flow field and confining boundaries of the real gas turbine combustor. Therefore, the chemistry was uncoupled from the fluid dynamics and analysis of LBO was addressed at three levels of increasing difficulty:

1. characteristic time modeling based on a phenomenological approach, with CFD providing local flow properties,
2. stirred reactor network modeling established on the basis of CFD analysis of the flow field, and
3. subgrid-level stirred reactor modeling using reactor extinction criteria based on the characteristic time model (1) above.

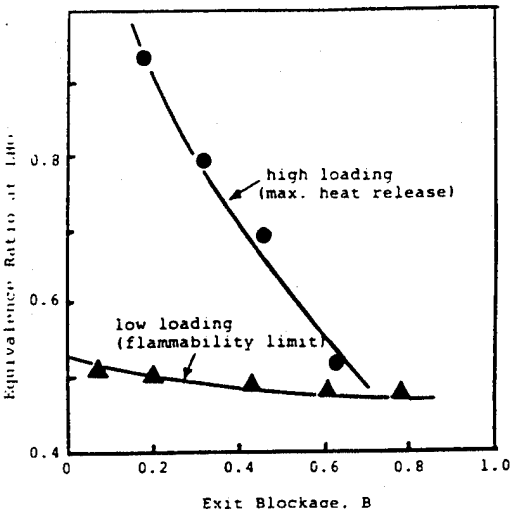

Fig. 8: Influence of exit blockage on LBO at low and high combustor-loadings.

Characteristic Time Approach: This approach is based on the reaction-quench model which assumes that, at LBO, flame propagation will cease when the rate of mixing between small turbulent eddies of cold reactants and hot products is greater than the local chemical reaction rate. This quenching criteria finds its origin in the work of Lockwood and Megahed [8] and yields:

$$1.5\{D + C\mu K^2/\sigma_t \varepsilon)/\nu\{1 + S_L/(\varepsilon\nu)^{0.25}\} > 1.0 \qquad (5)$$

where D is the laminar diffusion coefficient, K is the kinetic energy of turbulence, ε is the dissipation rate, C_μ is a constant, σ_t is the turbulent Schmidt number, and S_L is the laminar flame speed.

Since the quenching criterion requires turbulence parameters for evaluation, isothermal flow CFD calculations were performed to provide this information at each grid node. Quenching was examined on a point-by-point basis to ascertain if any part of the flow field could support combustion. Further, two additional conditions were imposed; (i) local fuel/air ratio must be within the flammability limits, and (ii) local mean velocities should be

less than or equal to turbulent burning velocity. In a somewhat limited evaluation, Eq. (5) showed promise in the step combustor in delineating between operating conditions where combustion was possible and where it was not. Eventually, this approach provided the reactor extinction criteria for the subgrid-level stirred reactor modeling.

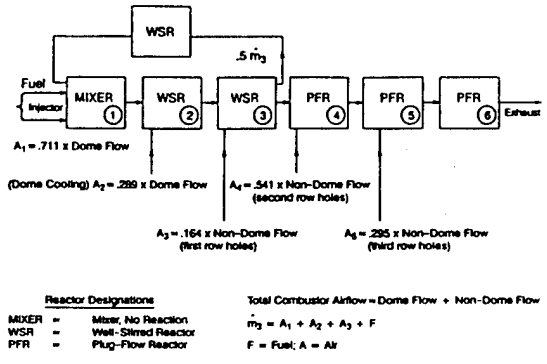

Fig. 9: A typical simulation of a combustor primary zone using the PSR network.

Local Stirred Reactor Modeling: In this approach, the combustor volume is represented by an equivalent global stirred reactor network. This enables the calculation of stability from thermo-chemistry considerations. We applied Swithenbank's [9] dissipation gradient approach for defining PSR regions in the combustor. Fig. 9 shows a typical reactor network that simulates the generic combustor primary zone. To establish such a global reactor network, considerable and careful post-processing of a CFD solution for the generic combustor was performed. Flow structures were identified by visualization, connectivity and local mass flow rates were assigned, and flow topology mapping techniques, e.g., Ref. [10], were used. Based on the Swithenbank approach [9], a rapid mixing region of the combustor was established from CFD calculations. This region was defined as the volume contained within a surface contour containing 96% of the turbulence kinetic energy and 99% of its dissipation rate, and over which the total dissipation gradient was not less than ten times the minimum value recommended by Swithenbank. From within this rapid-mixing region, a PSR volume was defined by super-imposing an additional space encompassing fuel/air mixtures falling inside the flammability limits for propane and air. For the research combustor, the resulting reactor was 44% of the combustor volume and corresponded reasonably well to the lifted flame observed in the real combustor. As shown in Ref. [6], good agreement was found between predictions and experiments for the research combustor.

Thus, networks of stirred reactors, particularly when established from CFD calculations, appear to offer possibilities for calculating limiting LBO performance. However, care may be needed in interpreting the results of such calculations since only the thermochemical limits to combustion can be determined.

Subgrid Scale Reactor Modeling: The eddy dissipation concept (EDC) of Byggstoyl and Magnussen [11] represents a general model for chemical reaction in turbulent flow. In the EDC model, the reactants are homogeneously mixed within the fine structure (Kolmogoroff eddies) of turbulence; therefore, these fine structures can be treated as PSRs. If the volume and the mass exchange rate between the reactors and the surrounding fluid are known, chemical reactions occurring within the PSRs can be calculated using a system of equations. Since the Kolmogoroff scale is always less than the CFD grid size, the modeling represents a subgrid scale approach. In contrast to the characteristic time analysis and local stirred reactor modeling, this approach tests the individual reactor stability within the CFD calculations.

Use of full or even reduced chemical kinetics imposes a high cost on the calculations. Therefore, an alternative approach was to assume a one-step, irreversible reaction step and/or fast chemistry, then use a local quenching criterion. The validity of the calibrated, global, single-step reaction mechanism approach was tested by comparing it to the data of Kretschmer and Odgers [12] and Clarke et al. [13]. Also, an extinction residence time was defined as $\tau_{ext} = (\rho / \dot{m})_{ext,,}$ where $\dot{m}$ is the total inlet mass flow rate per unit volume of the reactor. Thus, when $\tau_{hydro} \leq \tau_{ext}$ reactions occur, the hydrodynamic residence time in the fine scales can be related to the bulk fluid through the mass fraction of fine structures present in the flow. This characteristic time approach to LBO within the EDC model was implemented with fast chemistry for propane-air combustion and tested for an attached flame at fuel-rich conditions.

The axisymmetric CFD calculations were made using the Pratt and Whitney two-dimensional PREACH code. Three constraints were applied on the chemical reaction; (i) the EDC model with characteristic time-based extinction criterion was implemented, (ii) the local mixture should be within flammability limits (lean ϕ = 0.2 or 0.5 depending upon reactant temperature and upper ϕ to 2.0), and (iii) turbulence effects on the flame burning velocity. Fig. 10 shows typical calculated isotherms for what should be the attached-flame condition. These results show that the stoichiometric contour crosses the step recirculation zone from the confluence of the jets and reaches the combustor wall about halfway between the step and the recirculation reattachment plane. We can infer from these temperature contours that the main flame exists in the jet shear layers and originates about 10 cm from the step-plane (i.e., it is lifted and not attached). It is thick and follows the stoichiometric contour across the recirculation zone. There is some agreement between the characteristics of the inferred flame and the actual flame observed in the time-mean photographs and in the near-instantaneous pictures of laser-induced OH fluorescence where concentrated islands of reaction in the jet shear layer thicken the flame region. However, it was found that this model calculated the lifted-flame condition but was

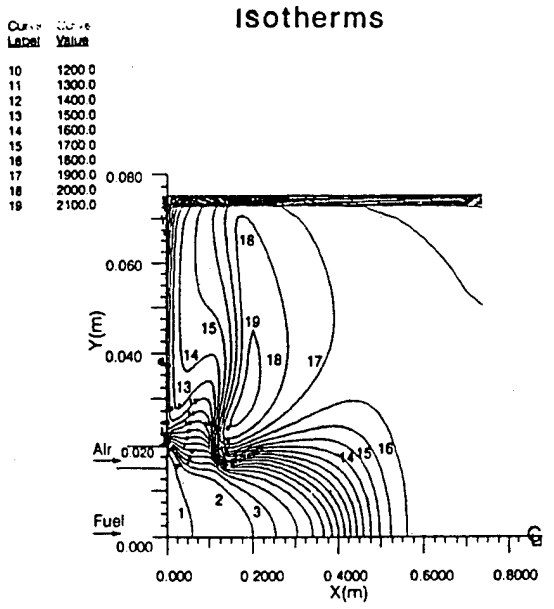

Fig. 10: Isotherms (curve values in degrees K) calculated using the EDC model for the attached-flame conditions in a research combustor

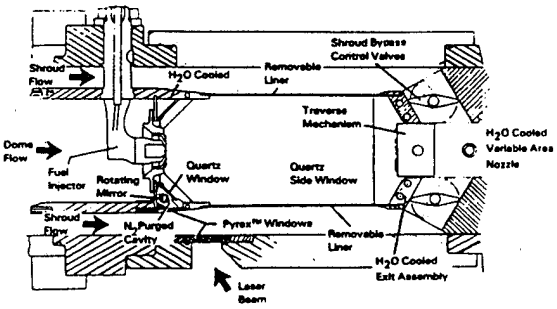

Fig. 11: Schematic diagram illustrating the design features of the generic gas turbine combustor.

unsuccessful in predicting the all-important attached-flame condition. Summarizing:

(a) A research step combustor was successfully developed. It produced three important features of the flow field that affect LBO in a practical combustor; (i) a reactive shear layer at the exit to the fuel nozzle, (ii) inside-out recirculation zones, and (iii) back pressure provided by dilution air jets.

(b) The step combustor acoustic characteristics were optimized; this permitted its operation in a stable and predictable manner. A detailed sequence of events leading to LBO and comprising the attached-flame region, lifted shear flame, intermittent shear flame, and the large-scale instability of the flame front was observed.

(c) The combustor flow-field measurements revealed three regions: near-field, step-recirculation, and far-field regions. In these regions, the turbulent fuel-air mixing and entrainment were governed by a potential core, a central recirculation bubble, and a self-similar jet development, respectively.

(d) The LBO process (ϕ = 0.4 to 1.2) in the step combustor behaved like a PSR for LP values in the range of 0.1 to 100 lb/s-ft^3-atm^2. Also, the LBO was successfully correlated with a standard LP derived from the PSR theory. Finally, Swithenbank's [9] dissipation gradient approach and an EDC model (Ref. 11) with a built-in characteristic extinction time criterion offer the possibility of an *a priori* calculation of LBO.

6. GENERIC GAS TURBINE COMBUSTOR

A final test of this research and modeling effort is to be able to predict LBO in an actual gas turbine combustor. To perform such a test, a generic gas turbine combustor was designed with three special requirements; (i) its LBO performance should be consistent with that of an actual gas turbine combustor, (ii) its geometric configuration and flow distribution should be variable so that the effects of residence time and mixture ratio on the LBO can be studied, and (iii) good optical access should be available for descerning the flow field and combustion zone.

Fig. 11 shows a schematic of a Pratt and Whitney designed generic combustor which is a four-injector, planar-section, simplified geometry version of a modern Pratt and Whitney annular combustor sector. This sector employs airblast-atomizing fuel injectors, an engine-type injector/dome interface, and the "inside-out" recirculation zones. The liners, upper and lower, are removable and may contain any desired pattern of air ports. The metal liners do not have any specific internal film cooling but are provided with a thermal-barrier coating and are convectively cooled by the shroud flows. Ignition is accomplished by means of a hydrogen torch ignitor. Individually metered air is supplied to the dome and upper and lower shrouds, provisions are made to supply gaseous nitrogen for subatmosheric pressure simulation, and, finally, fuel can be either propane or methane. This combustor is designed to operate at 65 psia with a variation in dome air from 10% to 40% of the total combustor air flow. The facility in which the combustor is installed is capable of supplying air up to 30 lbs/sec at ambient temperature and fuels up to 30 lbs/hr. Finally, side walls made of fused quartz and contained in water-cooled housings are provided for flow visualization. Sturgess and Shouse [14] have provided a detailed description of the construction, operation, and LBO tests on this combustor.

Fig. 12 illustrates the primary zone stability (LBO) of the generic combustor with lifted and attached flames against the LBO data obtained from the research combustor as well as

the predictions for the research combustor. The generic combustor data were obtained for the 10%, 15%, and 20% dome flow. Since the flames near blowout in the research combustor were all lifted, the partial premixing characteristic of the lifted flames in both combustors should be similar. The LBO stability of the generic combustor at peak heat release rates appears to be less than that of the research combustor. One likely reason may be the different fuel-air mixing rates in the generic combustor.

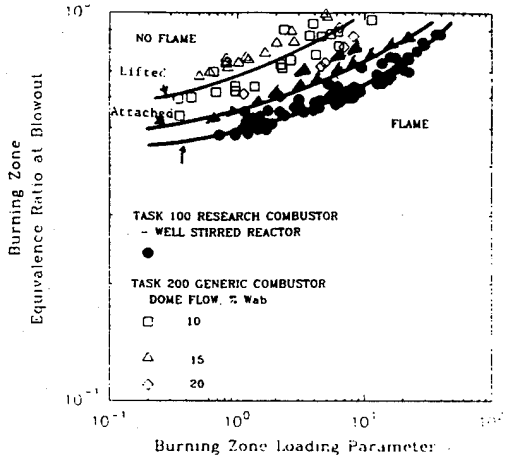

Fig. 12: LBO vs. LP data for the generic gas turbine combustor operating in the lifted- and attached-flame modes compared with data for the research combustor.

It appears that the gross features of the LBO can be successfully correlated by the combustor-loading parameter based on the PSR approach for a specific combustor. However, a simple phenomenological correlation is unlikely to explain the details of the LBO process. For example, the LBO process at simulated low pressures is rather complicated in a generic combustor. It contains quasi-staging of fuel as the loading increases with subsequent flame stabilization by the combustion air jets as well as the primary zone. When jet stabilization exists, LBO is insensitive to dome airflow and vice versa. Finally, the flame changes from a lifted to an attached position and, at a given loading, either flame can exist depending on how combustor-loading is achieved. Due to such complications, correlations of experimental data cannot be general enough to form a unique design curve which can determine the LBO stability margin of a practical gas turbine combustor. Thus, modeling of the LBO process, which works reasonably well with the research combustor, will be seriously challenged by the blowout behavior evidenced in the generic gas turbine combustor.

7. CONCLUSIONS

Following is the summary and conclusions of our research.

1. A geometrically simple, optically accessible, and acoustically decoupled research combustor to reproduce the gross features of the flow field in a modern annular gas turbine combustor was designed and its LBO was measured.

2. We successfully observed and documented a systematic and detailed sequence of events comprising an attached-flame, lifted shear flame, intermittent shear flame, large-scale instability of the flame front, and the LBO. These individual events clearly highlight the complexity of the LBO mechanism.

3. Simple phenomenological correlation based on PSR theory was successful. The LBO process (ϕ = 0.4 to 1.2) in the research combustor behaved like a PSR for LP values in the range of 0.1 to 100 lb/s-ft^3-atm^2. Also, the LBO was successfully correlated with a standard LP derived from the PSR theory. Finally, Swithenbank's [9] dissipation gradient approach and an EDC model (Ref. 11) with a built-in characteristic extinction time criterion offer the possibility of an *a priori* LBO calculation.

4. LBO stability at peak heat release rates in a generic gas turbine combustor was less than in the research combustor. Also, the flame changes from a lifted to an attached position and, at a given loading either flame can exist depending on how combustor-loading is achieved. Due to such complications, it was not possible to uniquely determine the LBO stability margin of a practical gas turbine combustor. Thus, modeling of the LBO process, which works reasonably well with the research combustor, will be seriously challenged by the blowout behavior evidenced in the generic gas turbine combustor.

8. ACKNOWLEDGEMENTS

This research was supported by the U.S. Air Force Wright Laboratory, Aero Propulsion and Power Directorate, Wright-Patterson Air Force Base, OH, under Contract No. F33615-92-C-2207. Mr. C. M. Frayne served as the Technical Monitor.

9. REFERENCES

1. Sturgess, G. J., Sloan, D. G., Lesmerises, A. L, Heneghan, S. P., and Ballal, D. R., "Design and Development of a Research Combustor for Lean Blowout Studies," ASME Journal of Engineering for Gas Turbines and Power, *114*, 1990, pp 13-19.

2. Heneghan, S. P., Vangsness, M. D., and Pan, J. C., "A Simple Determination of the Slit Function in Single Shot CARS Thermometry," Journal of Applied Physics, *69*, 1991, pp 2692-2695.

3. Heneghan, S. P., Vangsness, M. D., Ballal, D. R., Lesmerises, A. L., and Sturgess, G. J., "Acoustic Characteristics of a Research Step Combustor," AIAA Paper No. AIAA-90-1851, to appear in AIAA Journal of Propulsion.

4. Sturgess, G. J., Heneghan, S. P., Vangsness, M. D., Ballal, D. R., and Lesmerises, A. L., "Isothermal Flow Fields in a Research Combustor for Lean Blowout Studies," ASME Journal of Engineering for Gas Turbines and Power, *114*, 1992, pp 435-444.

5. Sturgess, G. J., Sloan, D. G., Roquemore, W. M., Shouse, D., Lesmerises, A. L., Ballal, D. R., Heneghan, S. P., Vangsness, M. D., and Hedman, P. O., "Flame Stability and Lean Blowout-A Research Program Progress Report," in Proceedings of Tenth ISABE, Nottingham, England, 1991, pp 372-384, Paper No. 91-7037.

6. Sturgess, G. J., Heneghan, S. P., Vangsness, M. D., Ballal, D. R., and Lesmerises, A. L., "Lean Blowout in a Research Combustor at Simulated Low Pressures," ASME Paper No. 91-GT-359, to appear in ASME, Journal of Engineering for Gas Turbines and Power, 1992.

7. Sturgess, G. J., Heneghan, S. P., Vangsness, M. D., Ballal, D. R., Lesmerises, A. L., and Shouse, D., "Effects of Back Pressure in a Lean Blowout Research Combustor," ASME Paper No. 92-GT-81, to appear in ASME, Journal of Engineering for Gas Turbines and Power, 1992.

8. Lockwood, F., and Megahead, I. E. A., "Extinction of Turbulent Reacting Flows," Combustion Science and Technology, *19*, 1978, pp 77-80.

9. Swithenbank, J., "Flame Stabilization in High Velocity Flows," Combustion Technology-Some Modern Developments, ed. H. B. Palmer and J. M. Beer, Academic Press, New York, NY, 1974, pp 91-125.

10. Perry, A. E., and Chong, M. S., "A Description of Eddying Motions and Flow Patterns Using Critical-Point Concepts," Annual Reviews of Fluid Mechanics, *19*, 1987, pp. 125-155.

11. Byggstoyl, S. and Magnussen, B. F., "A Model for Flame Extinction in Turbulent Flow," Turbulent Shear Flows-4, edts. L. J. S. Bradbury, F. Durst, B. E. Launder, F. W. Schmidt, and J. H. Whitelaw, Springer-Verlag, Berlin, 1985.

12. Kretschmer, D., and Odgers, J., "Modeling of Gas Turbine Combustors-A Convenient Reaction Rate Expression," ASME, Journal of Engineering for Power, *94*, 1972, pp 173-180.

13. Clarke, A. E., Harrison, A. J., and Odgers, J., "Combustion Stability in a Spherical Combustor," Seventh Symposium (Int.) on Combustion, The Combustion Institute, Pittsburgh, PA, 1958, pp 664-673.

14. Sturgess, G. J., and Shouse, D., "Lean Blowout Research in a Generic Gas Turbine Combustor with High Optical Access," A Paper Submitted to the 38th ASME Gas Turbine and Aeroengine Congress and Exposition, Cincinnati, OH, May 24-27, 1993.

Discussion

Question 1. D.K. Hennecke
In the experiments, you did not simulate the cooling films. Don't you think that they would influence the size and shape of the "inside out" vortex as the films flow against the vortex flow?

Author's Reply
The influence of the cooling film on the size and shape of the "inside out" recirculation zone is negligibly small. This is because in modern annular combustors the cooling air film is pretty much confined to the wall boundary layer. Also, the mass and momentum of the "inside out" recirculation zone is perhaps two orders of magnitude (or more) greater than that of the cooling film. Therefore, the cooling film, at best, causes only a minor perturbation of the "inside out" vortex flow. For this reason, it was not considered worthwhile to add complexity of simulating the cooling film in the research combustor hardware.

APPENDIX I

OBSERVATIONS OF FLAME BEHAVIOR FROM A PRACTICAL FUEL INJECTOR USING GASEOUS FUEL IN A TECHNOLOGY COMBUSTOR

By

P.O. Hedman and D.L. Warren
Brigham Young University, Provo, Utah

G.J. Sturgess
Pratt & Whitney, East Hartford, Connecticut

L.P. Goss
Systems Research Laboratories, Inc., Dayton, Ohio

D.T. Shouse
WL/POSF, Wright-Patterson Air Force Base, Ohio

Published as ASME Paper No. 94-GT-389, June 1994. To appear in ASME *Journal of Engineering for Gas Turbines and Power.*

THE AMERICAN SOCIETY OF MECHANICAL ENGINEERS
345 E. 47th St., New York, N.Y. 10017

The Society shall not be responsible for statements or opinions advanced in papers or discussion at meetings of the Society or of its Divisions or Sections, or printed in its publications. Discussion is printed only if the paper is published in an ASME Journal. Papers are available from ASME for 15 months after the meeting.

Printed in U.S.A.

94-GT-389

OBSERVATIONS OF FLAME BEHAVIOR FROM A PRACTICAL FUEL INJECTOR USING GASEOUS FUEL IN A TECHNOLOGY COMBUSTOR

Paul O. Hedman
Dept. of Chemical Engineering
Advanced Combustion
Eng. Research Center
Brigham Young Univ.
Provo, Utah

Geoffrey J. Sturgess
Pratt & Whitney Aircraft Co.
East Hartford, Connecticut

David L. Warren
Dept. of Mechanical Eng.
Advanced Combustion
Eng. Research Center
Brigham Young Univ.
Provo, Utah

Larry P. Goss
Systems Research Laboratories, Inc.
A Division of Arvin/Calspan
Dayton, Ohio

Dale T. Shouse
Wright Laboratory
Wright-Patterson AFB, Ohio

ABSTRACT

This paper presents results from an Air Force program being conducted by researchers at Brigham Young University (BYU) Wright-Patterson Air Force Base (WPAFB), and Pratt and Whitney Aircraft Co (P&W). This study is part of a comprehensive effort being supported by the Aero Propulsion and Power Laboratory at Wright- Patterson Air Force Base, and Pratt and Whitney Aircraft, Inc. in which simple and complex diffusion flames are being studied to better understand the fundamentals of gas turbine combustion near lean blowout. The program's long term goal is to improve the design methodology of gas turbine combustors.

This paper focuses on four areas of investigation: 1) digitized images from still film photographs to document the observed flame structures as fuel equivalence ratio was varied, 2) sets of LDA data to quantify the velocity flow fields existing in the burner, 3) CARS measurements of gas temperature to determine the temperature field in the combustion zone, and to evaluate the magnitude of peak temperature, and 4) two-dimensional images of OH radical concentrations using PLIF to document the instantaneous location of the flame reaction zones.

INTRODUCTION

As part of a comprehensive Air Force program, three different combustors have been utilized to investigate lean blowout in aircraft gas turbine engines. These vehicles consist of a simplified research combustor (Task 100), a technology combustor (Task 150), and a simplified, generic gas turbine combustor (Task 200). The technology combustor (Task 150) incorporates the practical fuel injectors used in the generic gas turbine combustor (Task 200) into the simpler research combustor (Task 100), to permit study of injector characteristics in isolation. The work presented concerns work with the Task 150 technology combustor. While many detailed studies exist in the literature concerning jet flames, both free and enclosed, almost nothing is available on the flame characteristics produced by practical ways of introducing the reactants into an engine combustor. This work goes some way towards remedying this situation.

The Task 150 technology combustor uses a practical liquid fuel injector with a classic gas turbine engine air blast atomizing configuration, involving co-swirling airsheets on either side of a co-swirling annular (normally liquid) fuel sheet, with the outer air passage and the fuel passage both converging on the central air passage. For this study, the burner was fueled by gaseous propane. Two injectors of this same configuration have been used, high-swirl (HS) and low-swirl (LS) injectors. Only data from the high-swirl configuration are reported in this paper. The technology combustor has been configured so that the geometry around the injector is nearly axi-symmetric with a diameter of about 150 mm. However, the combustor incorporates flat quartz windows about 60 mm in width on each of four sides so that laser based optical diagnostic instruments can be used. This unique configuration allows complex diagnostic measurements to be made in a simpler geometry than the Task 200 generic gas turbine combustor, but which embodies most of the features of an actual jet engine combustor in a near axi-symmetric configuration that is easier to mathematically model. Four methods of measurements have been used to characterize the flame. These include still film photographs, LDA measurements of velocity, CARS measurements of gas temperature, and images from PLIF measurements of the OH radical.

Experimental tests have been conducted on the research combustor at both BYU and WPAFB locations. These tests included operational characteristics, flow partitioning in various injector passages, visual flame structure, planner laser induced fluorescence (PLIF) imaging of OH radicals in the flame boundary, laser Doppler anemometry (LDA) velocity information, and coherent anti-Stokes Raman spectroscopy (CARS) temperature data. The effects of various parameters on the fuel equivalence ratio at lean blowout (LBO), an important operational characteristic, have also been investigated but are not reported in this paper.

Presented at the International Gas Turbine and Aeroengine Congress and Exposition
The Hague, Netherlands — June 13–16, 1994
This paper has been accepted for publication in the Transactions of the ASME
Discussion of it will be accepted at ASME Headquarters until September 30, 1994

Intriguing flame structures have been visually observed, and captured in video images, digitized still photographs, and PLIF images of the OH radical with the Task 150 configuration. The digitized images from still photographs have characterized the flame shapes observed visually. The instantaneous two-dimensional PLIF images have frozen flame structures missed with the visual observations. The partitioning of air flows through the dome and insert jets, and the primary and the secondary air swirlers was also determined. Preliminary analysis of PLIF images of the OH radical, combined with air flow split information, have helped describe the basic mixing patterns observed as the fuel equivalence ratio is changed. The flame attaches to the burner or lifts from the burner as the fuel equivalence ratio is changed.

LDA measurements have quantified the axial, radial, and tangential velocity components in the combustor for two operating conditions ($\phi = 0.72$ and $\phi = 1.49$) at an air flow rate of 500 slpm. This information has yielded local velocity and turbulence data and preliminary analysis of zero axial velocity contours has been used to identify the major recirculation zones. Data from both isothermal flows and combusting hot flows have been collected. Mean axial, tangential, and radial velocity LDA data for combusting hot flow data are presented in the paper. This data is also useful for model validation.

CARS gas temperature data have also been collected for the Task 150 technology combustor with the high swirl injector at an air flow rate of 500 slpm and at fuel equivalence ratios (ϕ) of 0.75, 1.00, 1.25, and 1.50. This unique set of data shows the corresponding geometrical changes in the structure of the mean gas temperature distribution as fuel equivalence ratio is changed, and quantifies the change in the magnitude of the peak temperature as the fuel equivalence ratio changes from lean, to stoichiometric, to fuel rich. Mean gas temperature data for $\phi = 0.75$, 1.00, and 1.50 are presented in the paper.

COMBUSTOR TEST FACILITY

Three burners are being utilized as part of a comprehensive Air Force program to investigate lean blowout in the combustors of aircraft gas turbine engines (Sturgess, et al., 1991b). These vehicles consist of the simplified Task 100 research combustor, the Task 150 technology combustor, and the Task 200 simplified, generic gas turbine combustor. This work provides a bridge between the combustion characteristics of confined, coannular fuel and air jets discharged into a sudden expansion (Task 100 research combustor) and the characteristics of a linear array of four swirling fuel injectors installed in a rectangular combustion chamber that simulates a segment of a real jet engine combustor (Task 200 simplified, generic gas turbine combustor). The Task 150 technology combustor incorporates one of the practical fuel injectors used in the Task 200 generic gas turbine combustor into the simpler Task 100 research combustor, to permit study of its characteristics in isolation. The use of the Task 150 technology combustor allows the combustion characteristics of a real injector to be investigated in a simple geometry where various diagnostic measurements (primarily laser-based optical measurements) can be more easily made.

In an actual engine combustor, additional combustion and cooling air is added to the combustor downstream of the actual fuel injector. This adds an additional complexity to the flow and combustion characteristics which is being investigated in a subsequent study. Only the characteristics in the zone near the injector are presented in this paper.

The work reported herein was accomplished in identical burners available in the Combustion Laboratories at BYU and WPAFB respectively. The burners were designed by researchers at P&W (Sturgess, et al., 1992a) and fabricated at WPAFB. The features of the dome and injector can be seen in Figure 1. The type injector used in this study is a classic gas turbine engine air blast atomizing configuration, involving co-swirling airsheets on either side of a co-swirling annular (normally liquid) fuel sheet, with the outer air passage and the fuel passage both converging on the central air passage.

Two injectors of this same configuration were used. The high-swirl (HS) injector has a nominal swirl number (based on vane angle) of 1.41, and the low-swirl (LS) injector has a nominal swirl number of 1.05. The total air passage effective areas were 0.176 in^2 for the HS injector and 0.266 in^2 for the LS injector, with outer to inner flow splits of 2.8 and 2.2 respectively. The outer swirler vane angle was 55 degrees for both injectors, while the inner swirler vane angle was 70 degrees for the HS injector and 45 degrees for the LS injector. The injectors were mounted in a plain bulkhead dome containing insert jets angled at 12.5 degrees into the flame, and radially outwards flowing film cooling jets. This arrangement closely simulates that of an engine combustor. The total effective air flow area of the dome, excluding the fuel injector, was 0.160 in^2.

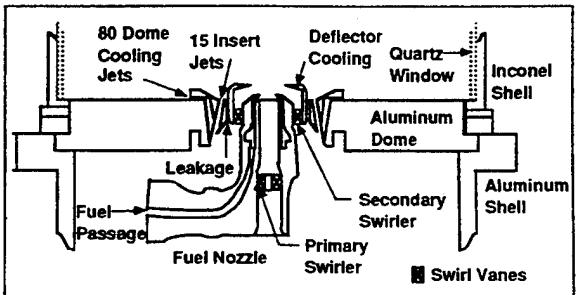

FIGURE 1. SCHEMATIC OF THE T150 HIGH SWIRL INJECTOR

The combustion chamber, shown in Figure 2, has been designed to be nearly axisymmetric and incorporate quartz windows to allow optical diagnostics (primarily laser-based optical measurements) to be made. The combustor cross-section is square with generously filleted corners to minimize secondary flow development. The hydraulic diameter is 150 mm. This box-section combustor with corner fillets allows reasonable optical access while providing a cross section that approximates a two-dimensional axisymmetric cross section. The bluff body provides a recirculation region which can stabilize the flame. Optical windows of fused quartz are provided on the four flat sides for a downstream length of 490 mm. The combustor overall length to hydraulic diameter ratio is 4.9, and the exit blockage is 45 percent by means of an orifice plate. The only air addition in this configuration is through the dome.

The combustor is mounted on a 240 mm length spool piece containing a mounting pad for the fuel injector flange. The combustor and spool piece are situated on an inlet air conditioning section, also shown in Figure 2. Reactants are supplied at ambient temperature and pressure. Ignition is by means of a removable torch-ignitor. This combustion chamber allows the combustion characteristics of a practical injector to be investigated in a simple geometry where various diagnostic measurements can be made.

In order to separate the effects of liquid fuel atomization and spray droplet evaporation from the effects associated with fuel/air mixing and aerodynamic flow pattern, these first evaluations involved the use of a gaseous propane fuel. Planned subsequent evaluations will use liquid ethanol. Liquid ethanol is expected to closely simulate the combustion characteristics of the liquid jet fuels, but without significant soot formation. Extensive sooting could cloud the quartz windows precluding easy optical access. The present paper deals exclusively with propane results with the HS injector.

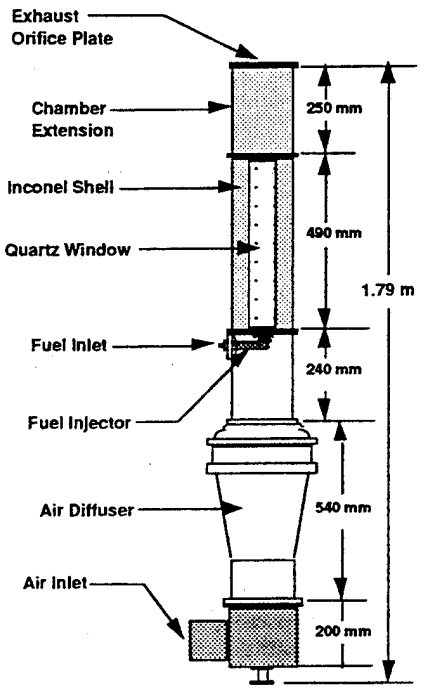

FIGURE 2. LABORATORY-SCALE GAS TURBINE COMBUSTOR

The results presented concern work with the Task 150 technology combustor using the high-swirl injector and gaseous propane fuel. While many detailed studies exist in the literature concerning jet flames, both free and enclosed, almost nothing is available on the flame characteristics produced by practical ways of introducing the reactants into an engine combustor. This work goes some way towards remedying this situation.

PHOTOGRAPHIC FLAME CHARACTERIZATION

A complex series of intricate flame structures have been observed in the Task 150 technology combustor according to the operating conditions and fuel injector used. Some of the flame behavior could be related to that seen in the Task 100 research combustor (Sturgess et al., 1991a; Sturgess et al., 1992b), and some of the structures to those seen in the Task 200 generic combustor (Sturgess and Shouse, 1993). These flame structures were studied directly with use of visual observations, video recordings, and still photography. The still film photographs have been digitized and filtered using computer techniques to produce isochromatic contour plots, Figure 3, for quantitative purposes.

One of the traits of the Task 150 technology combustor is the wide variety of flame structures that are observed. Each flame shape indicates a different mode of operation, which differ from one another in the location of the flame fronts, or by some structure such as thickness or intensity. The different structures observed arise from changes in the flow fields, mixing patterns, or fuel equivalence ratio as operating conditions are varied. The differences and similarities of the flame structures for the swirling injectors together with the results from the co-axial jet diffusion flame (Task 100 combustor) provide significant insights to the combustion processes. The shape of the flame, at the minimum, provides qualitative information on the mixing process and location of flame fronts. Such information can yield insights into the processes present. Flames fronts exist because fuel and oxidizer have been transported to a point where combustion can be supported. The location of these fronts relative to the outlet orifices of fuel and air are of obvious interest.

The fuel equivalence ratios where the transitions from one flame structure to another were determined as a function of fuel flow rate. The flames for both Task 150 injectors were attached to the outside of the insert air jets when the burner was operated very fuel rich. The flame would then lift, reattach, and lift again as the fuel equivalence ratio was progressively reduced depending on the injector (high swirl versus low swirl) and the air flow rate. During the reattachment phase, the flame would take on many of the characteristics of a strong vortex, and shared many features associated with a tornado. Consequently, the terminology of funnel cloud, tornado, and debris cloud were adopted to differentiate some of the observed flame structure from the general description of a vortex flow.

The characterization of the flame structure was carried out by visual observations. Still film photographs were taken of the different structures. These images were digitized and manipulated using various computer programs into the isochromatic contour plots found in Figure 3 for the high swirl injector. The major factor affecting in flame structure was the overall fuel equivalence ratio in the burner determined from total air and fuel flow rates, and to a much lesser extent the air flow rate. At a given air flow rate, the fuel would be reduced until a transition in flame structure was judged to have been reached. These observations were not easily made. With the high swirl nozzle, the flame structures flowed smoothly from one mode to another. These smooth transitions left no sharp break point in flame behavior. Consequently, the images presented in Figure 3 are only representative of the types of flame structures observed.

At very fuel rich conditions (ϕ = 2.38 and ϕ = 1.72), the flame was attached to the insert jets, in a manner similar to

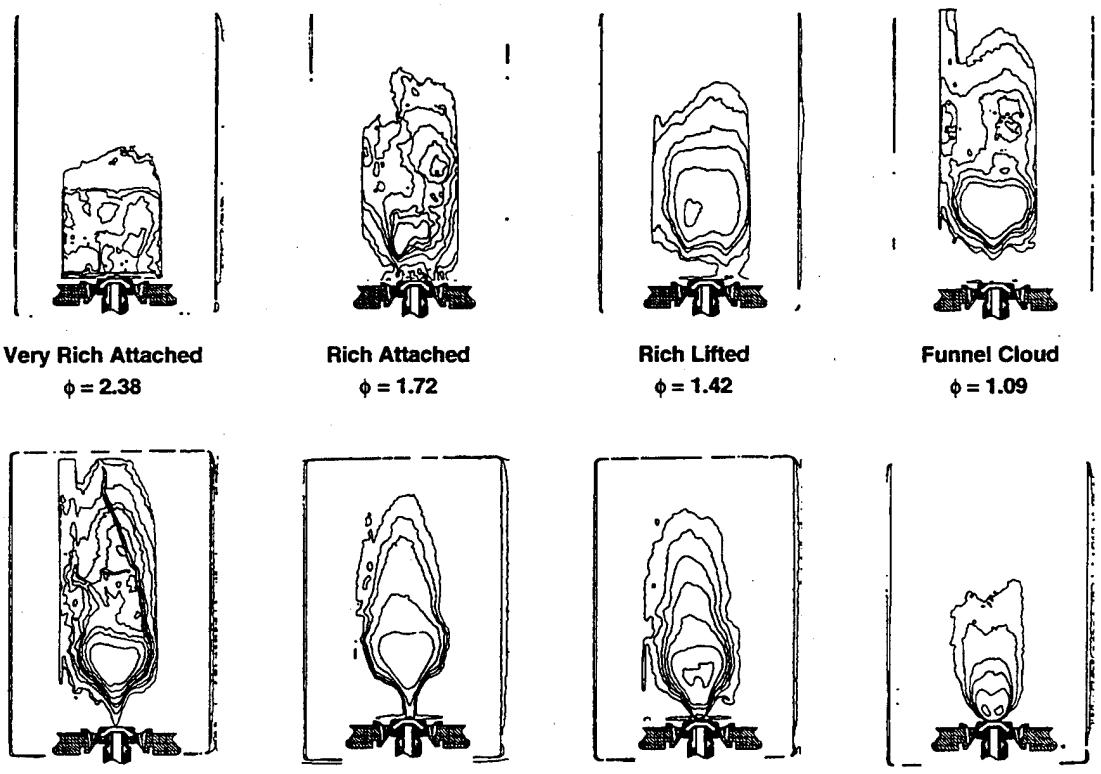

FIGURE 3. CHARACTERISTIC FLAME SHAPES FROM DIGITIZED STILL PHOTOGRAPHS (T150-HS NOZZLE, 310 SLPM AIR)

that observed with the Task 100 technology combustor at rich conditions. Unlike the Task 100, however, these flames were very short, presumably because of the much faster mixing due to the swirling motion of the gases. As the amount of fuel was further reduced (decreasing fuel equivalence ratio at a constant air flow rate), the still rich flame lifted and stabilized on a downstream recirculation zone that appeared to be associated with the injector (ϕ = 1.42). The primary combustion zone continued to lengthen as relatively less fuel entered the combustion chamber (ϕ = 1.42 to ϕ = 1.09).

After the rich lifted condition, further reductions in fuel equivalence ratio caused the flame to stabilize in the rapidly swirling vortex at the center of the combustor, with flame structures that resembled the development of a tornado. As seen in Figure 3, a structure that resembled a funnel cloud formed within the rich lifted flame (ϕ = 1.09) and gradually descended as the fuel flow was continually decreased (ϕ = 1.09 to ϕ = 0.93) forming a tornado like flame structure. Further reductions in ϕ caused the tornado like flame to enter the primary swirler passage in the injector (ϕ = 0.93). Continued reduction in fuel equivalence ratio caused a flame in the shape of a bowl, which looked much like the debris cloud of a tornado, to attach to the nozzle on the outside of the tornado like structure (ϕ = 0.85). The minute detail of the debris cloud was lost in the process of converting from the still photograph to the image presented in Figure 3. Continued reduction of the fuel flow resulted in the growth in size and intensity of the debris cloud like flame structure while the funnel cloud like structure was simultaneously decreasing. The total disappearance of the funnel cloud structure marked a transition to a fully developed flame that was strongly attached to the center of the injector (ϕ = 0.78). At lower air flow rates (less than ca 500 slpm), this strongly attached flame would weaken until the lean blowout limit (ϕ = 0.46) was reached (blowout occurred from an attached flame). At high air flow rates (greater that ca 500 slpm), the flame would once again lift, attach to a down stream recirculation zone, and eventually

blowout from the separated flame structure ($\phi = 0.42$), much like that observed in the Task 100 research combustor.

GAS VELOCITY MEASUREMENTS

A laser Doppler anemometer (LDA) was used to make extensive measurements of gas velocity in the burner at five separate experimental conditions. The experimental conditions used are summarized in Table 1.

TABLE 1
SUMMARY OF EXPERIMENTAL CONDITIONS FOR LDA MEASUREMENTS

Injector	Flow	Air slpm (70 F)	C_3H_8 slpm (0 C)	N_2 slpm (0 C)	ϕ
T150HS	Cold	500		14	0.72
T150HS	Hot	500	14		0.72
T150HS	Cold	500		29	1.49
T150HS	Hot	500	29		1.49
T100	Cold	1000		23	0.59

The LDA measurements reported in this paper are for the Task 150 burner with the high swirl injector installed. Measurements were made for lean conditions ($\phi = 0.72$) where the flame was well attached to the central part of the injector, and also at fuel rich conditions ($\phi = 1.49$) where the flame was attached to the dome and insert jets. LDA measurements were also obtained in isothermal, non-reactive flows where nitrogen was substituted for the propane fuel. This has allowed the effect of the flame temperature on the flow field and gas velocities to be determined for at least two of the test conditions used. However, only the data from the combusting flow experiments are reported in this paper.

A schematic of the LDA experimental set-up is presented in Figure 4. The beam from the argon-ion laser was split into two beams, frequency shifted (40 and 34 MHz), polarized, and focused into a diagnostic volume in the test section. The forward-scattered LDA signals for the radial (or tangential) and axial velocity components were focused into fiber optic cables and passed to a photo multiplier tube to be amplified and converted to electrical signals. These electrical signals were collected with TSI, Inc. counters and analyzed with a Macintosh IIfx computer. A Le Croy 9314L Quad 300 MHz oscilloscope was used to monitor the Doppler bursts to help in the alignment of the LDA system and to insure quality data was being collected. Even with careful alignment, there was still some noise which was filtered using a data analysis program.

A brief investigation was made to evaluate the effect of the number of points taken at a given test location on the accuracy of the gas velocity measurement. Three different sets of data were collected, a set with 5000 points, a set with 2000 points,and a set with 1000 points. In general, there was little difference observed in the mean axial and tangential velocities determined from the different number of points in the data sets. However, the fluctuating velocity components (i.e. rms velocities) were better described by the data sets containing the largest number of points. Nevertheless, for this study, 1000 data points were collected at each test location. This allowed a greater number of experimental conditions and geometries to be evaluated, albeit at slightly reduced data accuracy.

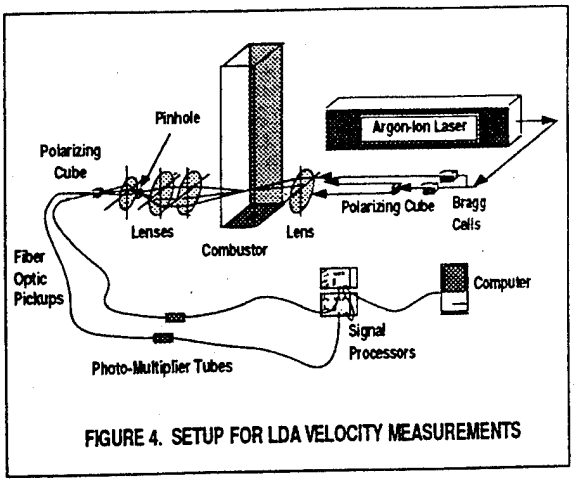

FIGURE 4. SETUP FOR LDA VELOCITY MEASUREMENTS

The two component velocity data (either axial and radial, or axial and tangential) were obtained for each of the test conditions described above (Table 1). The burner was translated with respect to the laser diagnostic volume in an X, Y, and Z coordinate system. Translation in the Z coordinate direction allowed different axial locations to be sampled. Translation in the X or Y axis allowed different radial locations to be sampled. For these tests, the X or Y translations were done along a coordinate centerline. Translation in the X coordinate direction along the Y coordinate centerline allowed axial and radial velocity data to be obtained. The edge of the windows limited translation in this coordinate direction to about ± 30 mm. Translation in the Y coordinate direction along the X coordinate centerline allowed axial and tangential velocity data to be obtained. As the diagnostic volume was brought near the quartz windows, significant optical noise was added to the Doppler signals. The quartz windows were approximately ± 75 mm from the center of the reactor. The optical noise from the windows generally limited data collection to ± 65 mm, although with especially clean windows, it was sometimes possible to get good data at ± 70 mm.

Typically, data was collected at 0.5 or 1.0 mm radial increments where the velocity gradients were large. Data was collected at up to 10 mm increments where velocity profiles were relatively flat. A typical set of data was taken at axial locations of 10, 15, 20, 25, 50, 75, 100, 125, 150, 200, and 240 mm above the dome of the reactor. Occasionally, other intermediate locations were examined where large velocity gradients or other interesting behavior were found.

The basic flow field in the combustor was derived by interpolation of the velocity data obtained. The field is dominated by multiple regions of flow recirculation. The axial velocity from both the X and Y coordinate traverses has been combined for one of the Task 150-HS cold flow cases (14 slpm N_2, 500 slpm air), interpolated, and the zero axial velocity contours plotted in Figure 5. Each zero axial velocity contour bisects a recirculation zone. While the data have not been

analyzed in the detail needed to totally quantify the recirculation patterns, estimates of the recirculation zones are indicated. Eventually, flow streamlines will be plotted to better identify the various flow fields. However, for this paper, only axial, tangential, or radial data have been used.

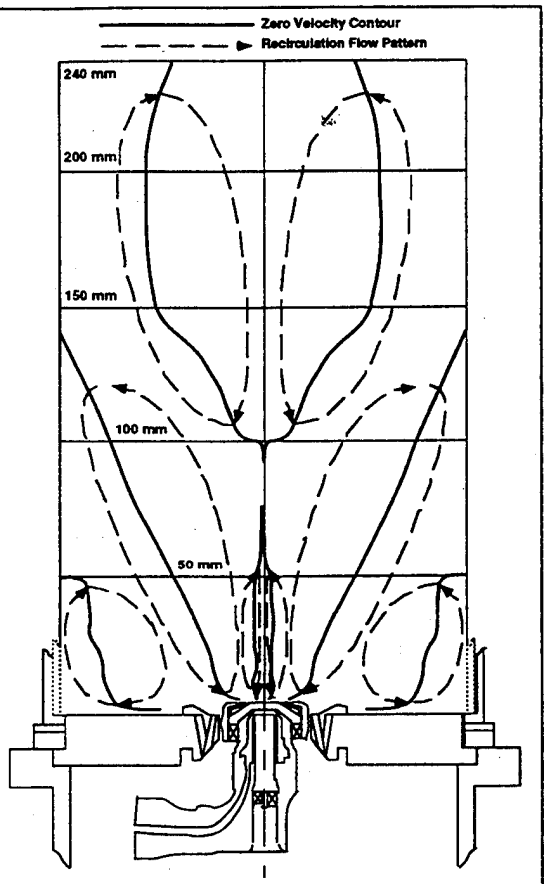

FIGURE 5. RECIRCULATION PATTERNS WITH THE HIGH-SWIRL FUEL INJECTOR

Figure 5 identifies several important recirculation zones. Although the near-field is similar to that in a real gas turbine combustor, the downstream region in not due to the absence of air addition by means of transverse jets, as is usual practice. Since current interest is concentrated on the near-field, this deviation is not of great significance. It is interesting to note that there is a zone of flow reversal on the centerline of the burner very near the discharge of the injector. This flow reversal is undoubtedly caused by the highly swirling flow, and is consistent with the strong vortex structures observed earlier (Figure 3). A recirculation zone is also apparent in the lower corners of the combustion chamber. This zone appears to be driven by the dome cooling jets, and is consistent with the observed horizontal flow in the radial direction that emanates from these cooling jets.

Another major recirculation zone is centered on the zero axial contour that angles from the face of the injector outward till it reaches the wall of the combustor at a down stream location at about 140 mm. This large recirculation zone seems to have a major impact in stabilizing the flame under certain operating conditions. The last observed recirculation zone surrounds the zero iso-velocity contours that exist between the 100 mm and 240 mm axial locations. This recirculation pattern was very weak as judged by the magnitude of the velocities measured, and was only observed in the isothermal case. It was not seen in the combusting cases. The influence of the combustion was sufficient to eliminate this pattern from the flow field. Combustion also altered the shape and location of the other recirculation zones, but each of the other zones remained in the combustion cases.

Figure 6A, 6B, and 6C present the iso-contour plots for the mean axial, mean tangential, and mean radial velocity measurements respectively for the fuel lean case ($\phi = 0.72$). In each figure, the velocity contour plot from the centerline to the maximum measurement radius was created using commercial computer software, duplicated, and reversed. The reversed image was combined with the original image and superimposed on a schematic of the burner to provide an indication of the flow characteristics with respect to the burner. The data presented in Figure 6A and 6B were collected along the Y coordinate direction out to about 60 mm. The data in Figure 6C are limited to a radial location of about 30 mm because of the width constraints of the windows. The flow fields and recirculation patterns presented here are generally consistent with those observed in Figure 5.

The flame at this operating condition was well attached to the center of the injector, and was considered to be fully developed as was shown earlier in the discussion of Figure 3. Mass balance calculations based on isothermal axial velocity measurements have been used to determine the overall accuracy of the LDA measurements. It was found that the mass flow rate was strongly influenced by the gradient assumed near the wall, but reasonable velocity interpolations gave reasonable mass balance closure.

The sharp peak in axial velocity component shown in Figure 6A near the injector is clearly evident. The rapid decay of the high velocity region near the injector as one moves down stream is also apparent. The recirculation zone directly over the injector is dramatic, and clearly shows a significant region of flow reversal. The tangential velocity in this zone is very high as seen in Figure 6B. The other major recirculation pattern in the combustor is of a somewhat different shape and in a somewhat different location than observed in the isothermal case (Figure 5). The recirculation patterns caused by the dome jets are notably absent. Visual observations confirmed that the corner recirculation still existed in the combustion flow cases, but it was not possible to collect LDA data close to the window near the bottom of the reactor because of excess optical noise.

The radial velocity data are presented in Figure 6C. These data are limited to a radial location of about 30 mm. The radial flow velocities are all very low in magnitude, but do showsomeinteresting structures. The low magnitudes of these velocities are close to the resolution of the LDA instrument A similar set of gas velocity data for the Task 150-HS combustor operating at a fuel equivalence ratio of 1.49 is presented in Figures 7A, 7B, and 7C for the mean axial, mean

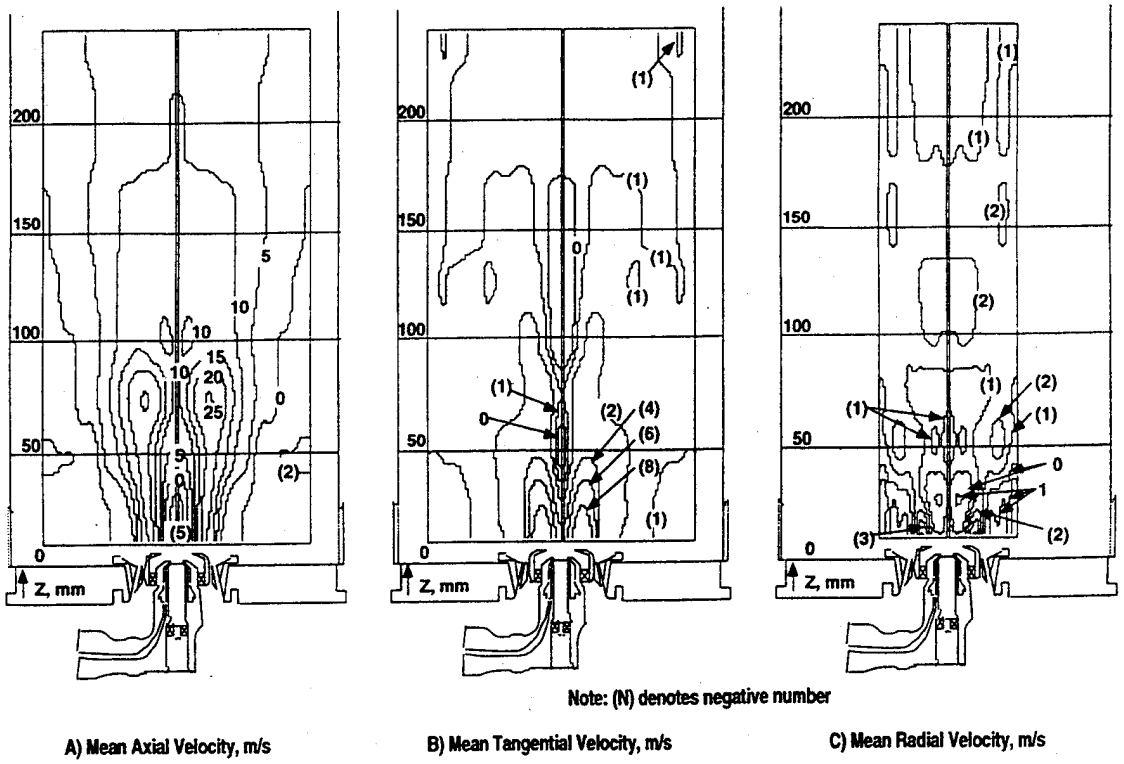

FIGURE 6. ISO-VELOCITY CONTOURS FOR THE T150-HS BURNER AT ϕ = 0.72 AND 500 SLPM AIR FLOW RATE

tangential, and mean radial velocity measurements, respectively. The flame at this operating condition was attached to the insert and dome jets as was shown earlier in the discussion of Figure 3. As above, the radial data in Figure 7C are limited to a radial location of about 30 mm, but the axial and tangential data in Figures 7A and 7B were collected out to about 60 mm. The flow fields and recirculation patterns presented here are also generally consistent with those observed in Figures 5 and 6.

As for the $\phi = 0.72$ case, the sharp peaks in mean axial velocity component associated with the injector are still clearly evident, but seem to decay more rapidly than in the $\phi = 0.72$ case. The recirculation zone directly over the injector is still dramatic, and shows little difference in the magnitude of the reversed velocity or in the size and shape of the recirculation pattern when compared to the $\phi = 0.72$ case. The other major recirculation pattern in the combustor is of a similar shape to that observed with the $\phi = 0.72$ case, but seems to be much stronger (i.e. has much larger reversed flow velocity components). The recirculation patterns caused by the dome jets are still absent. As in the $\phi = 0.72$ case, visual observations confirmed that the corner recirculation still existed in this combustion flow case, but it was not possible to collect LDA close to the window near the bottom of the reactor because of optical noise near the quartz windows.

The radial velocity data are presented in Figure 7C. Again, the radial flow velocities are all very low in magnitude, but do show some interesting structures, that are quite different than seen with the lean flame. The low magnitudes of these velocities are also close to the resolution of the LDA instrument.

The differences in velocities between the lean flame and the rich flame show that there is a strong influence of the location of the flame zone on the flow fields as characterized by the measured velocity fields.

GAS TEMPERATURE MEASUREMENTS

Coherent anti-Stokes Raman spectroscopy (CARS) was used to obtain a set of gas temperature measurements in the Task 150-HS combustor at fuel equivalence ratios of 0.75, 1.00, 1.25, and 1.50; and at an air flow rate of 500 slpm. The details of the CARS facility has been well documented in previous publications (Boyack and Hedman, 1990; Hancock et al., 1991, 1992). The CARS setup used for this study, as shown inFigure 8, is very similar to the folded box-CARS phase matching scheme employed by Boyack (Boyack and Hedman, 1990). Boyack located his combustor directly on the CARS optical table, and was able to easily focus the laser beams

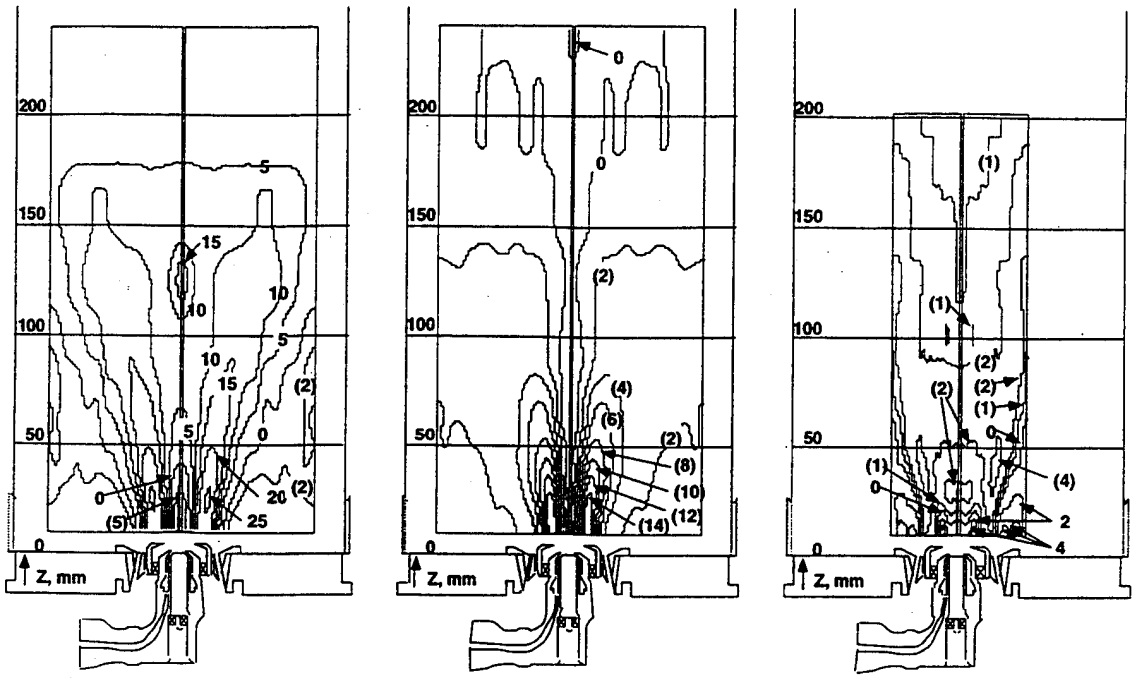

FIGURE 7. ISO-VELOCITY CONTOURS FOR THE T150-HS BURNER AT ϕ = 1.49 AND 500 SLPM AIR FLOW RATE

directly into his combustor. In this experimental setup, the combustor was remotely located. Consequently, the laser beams were directed off the optics table over a distance of about 10 m onto a set of optical bread boards located on either side of the Task 150-HS combustor. The optical components needed to create the box-CARS phase matching were located on these remote optical breadboards. As with Boyack's work, the CARS signal was focused into the end of the fiber optic used to transfer the signal back to the spectrometer. The CARS lasers and spectrometer were keep in an optics room distant from the combustion facilities in an effort to keep the optical components relatively clean.

Like the gas velocity measurements, the CARS temperature measurements were taken at closely spaced radial increments where large gradients in temperature were found and in a courser grid where the temperature gradients were found to be relatively shallow. Temperature data was take at similar axial locations as well. The temperature data were taken along the X coordinate, and consequently are available only out to a radius of about 30 mm, but were taken to an axial location of about 300 mm. Attempts at obtaining data along the Y axis to radial locations near the quartz window resulted in laser damage to the quartz window. Nevertheless, the CARS temperature data obtained have provided adequate temperature measurements to well quantify the temperatures in the region of most interest near the injector.

Figure 9 presents an iso-contour plots of temperature data for the Task 150-HS combustor operating with an air flow rate of 500 slpm and at fuel equivalence ratios of 0.75, 1.00, and 1.50. The data at ϕ =1.25 have been excluded from the paper because of space considerations. Two hundred discrete temperature data points were taken at each of 92 separate diagnostic locations from the centerline to a 30 mm radial location, and from 10 mm to 300 mm axial location. These sets of data were used to determine the mean temperatures used to create the iso-thermal contour plots shown. In order to show the symmetry of the flame, the contour plot was duplicated, and computer software was used to flip the image and add it to the opposite side of the combustor. The flow fields are very symmetric about the centerline in this highly swirled flame. The doubled image gives a better representation of the temperature field in the vicinity of the injector.

The relatively cold region (600 K to 1000 K) directly above the injector in all three cases generally corresponds the central recirculation zone seen in the gas velocity plots (Figures 6 and 7). Surrounding the cold central zone is an intermediate temperature region that seems to be associated with thepenetration of the very high axial velocity into thecombustor. Higher temperatures exist on either side of this penetration zone. It is unfortunate that temperature data could not be obtained in the lower corners of the combustor where

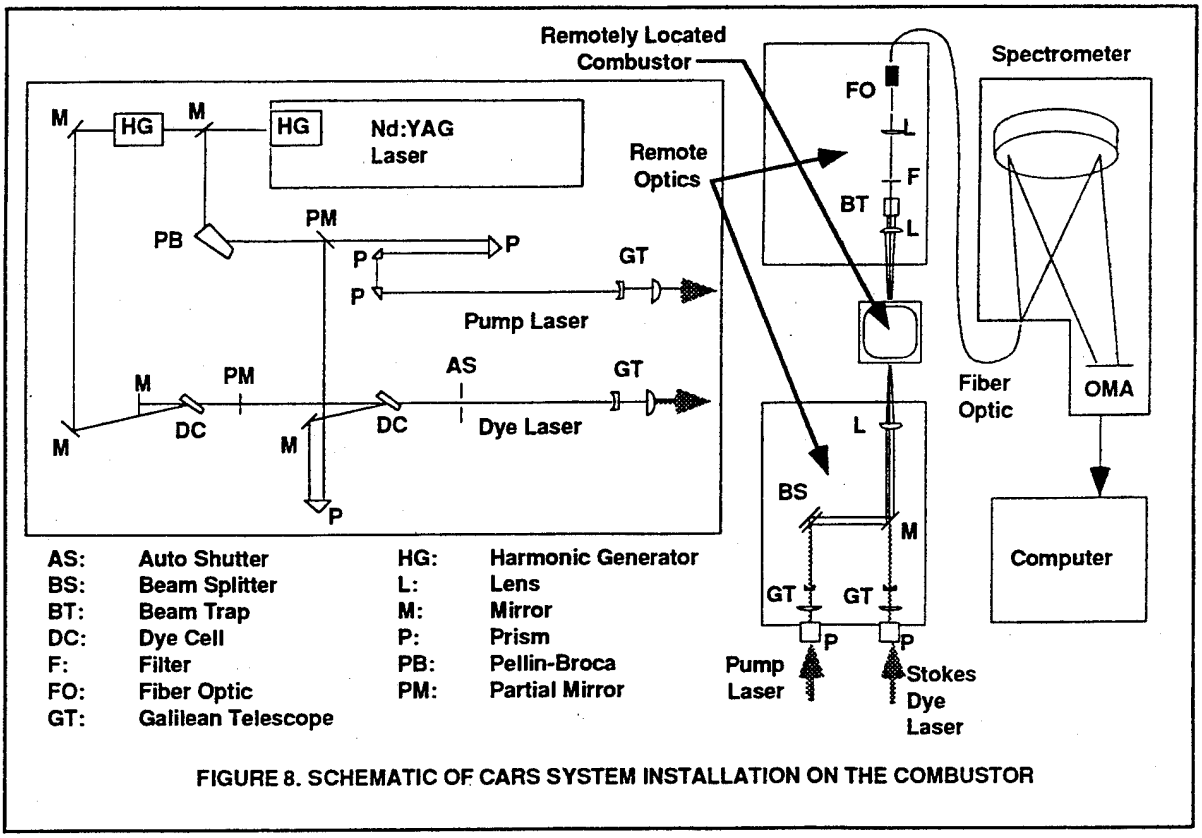

FIGURE 8. SCHEMATIC OF CARS SYSTEM INSTALLATION ON THE COMBUSTOR

the recirculation zones near the dome are located. The data do suggest that this region is relatively cool for the $\phi = 0.75$ case, but seem to indicate a relatively hot region in this corner recirculation zone for the $\phi = 1.5$ case. This observation seems to be consistent with the observed relocation of the flame zone from the central core of the vortex when operating fuel lean to the outer recirculation zone when operating fuel rich, as noted in the digitized film images and in the PLIF images of OH radical discussed in the last section of this paper.

Temperatures in excess of the $\phi = 0.75$ adiabatic flame temperature (1963 K) are seen in a zone near the centerline at an axial location of about 100 mm for the fuel lean case. Since this is a non-premixed flame, this suggests that this diffusion zone may be operating with near stoichiometric ($\phi = 1.00$) mixtures of fuel and air. The peak temperature that was measured was 2085 K which is about 178 K below the theoretical stoichiometric adiabatic flame temperature of 2263 K.

In the stoichiometric case ($\phi = 1.00$), the peak measured temperature is 67 K below the theoretical stoichiometric adiabatic flame temperature of 2263 K. The zone of near peak temperature extends from an axial location of about 100 mm to about 170 mm and forms a toroidal shaped ring around the centerline. Beyond the high temperature region, the temperatures decrease, dropping to about 1800 K at the combustor exit (not shown).

Iso-contour plots of gas temperature measurements for the $\phi = 1.50$ case are shown in Figure 9C. It is interesting to note that the peak temperature (1875 K) in the fuel rich case, like the stoichiometric case, is just below the predicted ($\phi = 1.50$) adiabatic flame temperature of 1974 K It seems reasonable that the peak measured temperature in this case would be close to the adiabatic flame temperature, since all of the oxygen would be consumed early in the flame preventing a zone near stoichiometric to ever exist.

The variation in temperature field as the fuel equivalence ratio changes from fuel lean to fuel rich seems to be consistent with the observations made from the still photographs. At $\phi = 0.75$, the flame is well attached to the burner, with a narrow vortex penetrating into the injector and a fully developed flame structure attached to the injector. The temperature distributions at $\phi = 1.0$ and $\phi = 1.25$ (not shown) were very similar, and seemed to agree with the flame structures described in Figure 3 as a rich lifted flame and a funnel shaped flame. At $\phi = 1.50$ (Figure 9C), the center cold zone has been reduced in size, and there are higher temperatures at the outer edge of the measurement region that support the visual observation that the flame is attached to the insert jets.These results also suggest that a fairly high temperature exists in the corner recirculation zone when the combustor is operating in a fuel rich mode. In general, the temperature measurements are consistent with the visual flame conditions,

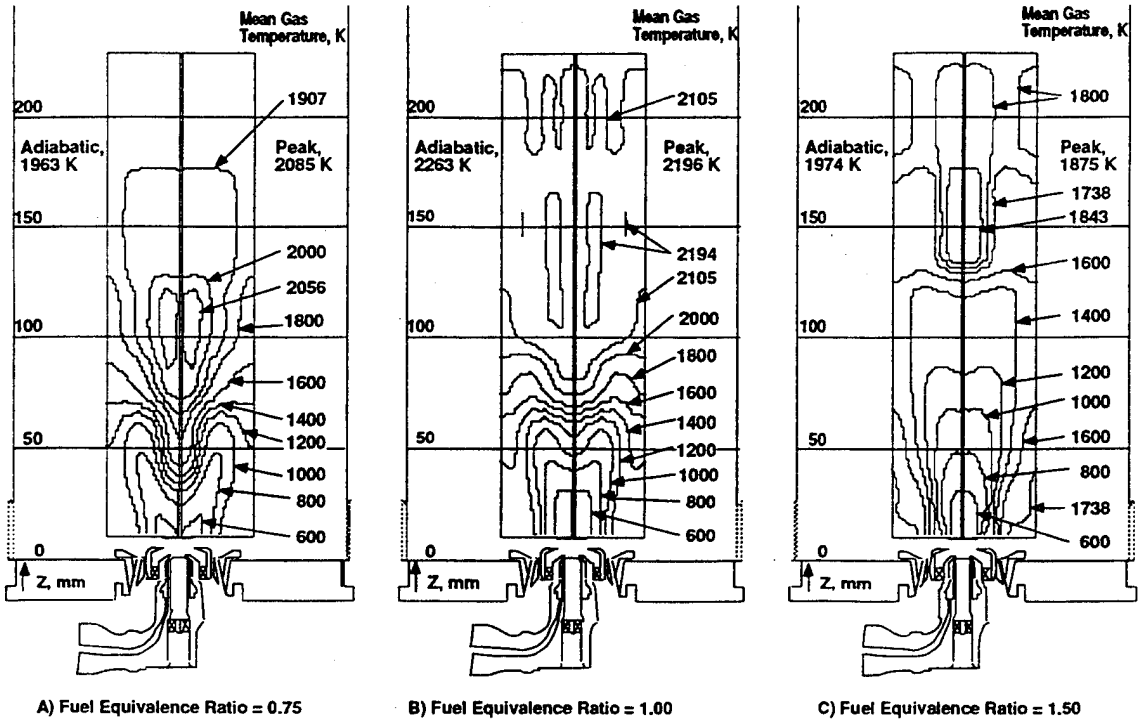

FIGURE 9. MEAN GAS TEMPERATURE ISO-CONTOURS FOR THE T150-HS BURNER AT 500 SLPM AIR FLOW RATE

the PLIF images of the OH radical, and the velocity measurements for this particular test condition.

PLIF IMAGING OF OH RADICAL

In PLIF (planner laser induced fluorescence) imaging, a dye laser is tuned to a resonant frequency which causes the particular combustion radical or molecule to fluoresce at a different resonant frequency. This fluorescence is then recorded and the two-dimensional image preserved with an electronic camera. In these experiments, OH radicals were excited with an ultra-violet (ca 283 nm) light sheet produced by a tunable dye laser pumped with a 10 ns pulse from a Nd:Yag laser. This sheet of laser light was passed through centerline of the reactor. An intensified CCD camera, located normal to the laser sheet, captured the 75 mm high two-dimensional uv (ca 308 nm) image (Figure 10). This nearly instantaneous map of OH radical concentration in the flame zone was then stored by a Macintosh computer. The images have been analyzed and enhanced using conventional computer software.

OH radicals are commonly chosen for PLIF because they are important markers in hydrocarbon flames. These radicals are produced in large quantities during the combustion process, and are a good indicator of flame fronts. However, in some circumstances, these radicals may persist for long distances downstream of the actual flame front, limiting their usefulness. Also, as in any laser diagnostic technique, there is a concentration level below which the OH radical will not be detected. With these limitations in mind, conclusions based solely on PLIF images of the OH radical must be carefully drawn.

Many PLIF images of the OH radicals were obtained in the Task 150-HS combustor at 500 slpm air flow and at fuel equivalence ratios that ranged from 0.62 to 1.75. Images were taken at values of fuel equivalence ratio that roughly correspond to the changes in flame structure that had been observed visually and documented with still photographs (Figure 3). Comparison of the two types of flame image, and the relation of these images to the time-mean flow field and bulk equivalence ratios, explains much about the flame structures. However, comparison of a sequence of instantaneous OH images at fixed operating conditions, e.g. Figure 11, also reveals the highly non-stationary character of the flame zone. This behavior is similar to that observed previously in the Task 100 research combustor (Roquemore, et al, 1991).

The experimental behavior of the Task 100 research combustor is quite different than the predictions by computational fluid dynamics (CFD) programs. These computer codes predict the flame to be anchored in the jet shear layer for all fuel equivalence ratios. However, the flame has been experimentally observed (Roquemore, et al. 1991) to attach to the backward facing step just outside the air tube at

fuel equivalence ratios (ϕ) in excess of 1.08. In these operating conditions, a small "coke bottle" shaped flame pilots a thicker flame sheet which is much lower in the combustor than the CFD programs predict. A waisting in the flow field is predicted by the CFD code, but the mixture is predicted to be too lean to burn. Roquemore postulates that a discrete and intermittent process is responsible for the entrainment of the fuel into the step recirculation zone. This type of transport would require passageways in the flame in order to deliver the unburned fuel from the fuel tube to the step recirculation zone. These passageways would appear as a region with little to no OH radical present.

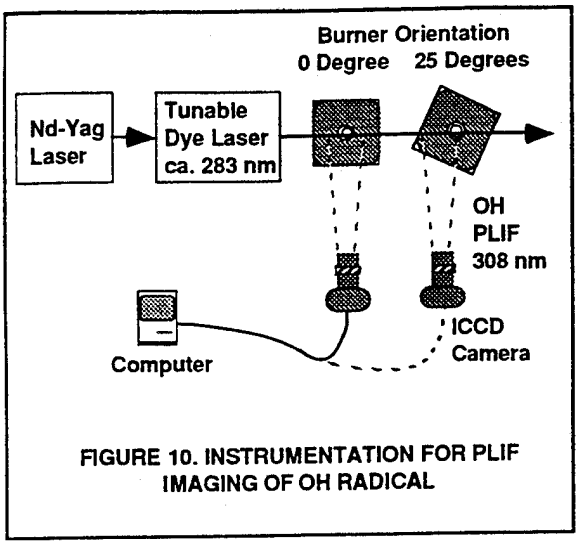

FIGURE 10. INSTRUMENTATION FOR PLIF IMAGING OF OH RADICAL

Much of what Roquemore postulated has been found in PLIF images of the OH radical collected in the Task 100 research combustor. In the well-attached flame (ϕ=1.56), the OH radicals appear in vortex structures being shed off the backwards step. These structures were very clear in the images collected. In the lean condition, OH radicals were not observed below 150 mm in the reactor, with relatively small amounts between 150-200 mm and very large amounts beyond. Similar observations have been made in the PLIF images of the OH radical for the Task 150 technology combustor (e.g. Figure 11 and Figures 12A, 12B, and 12C). Figure 11 shows four separate instantaneous images at two different axial locations at ϕ = 1.29. Figure 12 shows composites of several single PLIF images of OH radical grouped as a collage in the appropriate locations within the combustor at a fuel lean condition (ϕ = 0.62), near stoichiometric (ϕ = 1.08), and at a fuel rich condition (ϕ = 1.49). These images dramatically illustrate the characteristics of swirling flames and the highly variable nature of the instantaneous flame shape. Therefore, it seems likely that the conclusion reached for the co-axial jet system of the Task 100 research combustor (Roquemore et al., 1991; Sturgess et al., 1992; Sturgess et al., 1991b), that mass transport in axisymmetric, turbulent, recirculating flames is dominated by non-stationary flow phenomena, and not by gradient transport is confirmed, even in a practical injection system. The implication of this finding for accurate mathematical modeling of practical turbulent combustion systems is very important.

It is informative to correlate these OH images with the information known about the partitioning of the air flow rates through the various air passageways through the nozzle. The local fuel equivalence ratios shown in Table 2 were calculated from the air flow through each of the different passageways and the total fuel flow. Implicit in these calculations are two assumptions. First, the fuel is assumed to mix uniformly within each combination of partitions before mixing with remaining air. Second, any fuel blockage effects (which would change the partitioning as a function of fuel flow) are assumed to be negligible. At this air flow rate (500 slpm), LBO occurs at a fuel equivalence ratio of about 0.42.

TABLE 2
LOCAL ϕ FROM TOTAL FUEL FLOW AND AIR FOR EACH FLOW PASSAGE COMBINATION

Overall ϕ	ϕ with air from primary swirler	ϕ with air from primary + secondary swirlers	ϕ with air from primary + secondary swirlers + insert jets
0.62	4.17	1.11	0.80
1.08	7.26	1.94	1.39
1.49	10.02	2.67	1.92

With these assumptions in mind, and knowing the flammability limits (ϕ) of propane are roughly 0.5 to 2.5, some conclusions can be cautiously applied to these images. In every case, the air in the primary swirler alone does not provide sufficient oxidizer to permit combustion. Thus, the fuel must mix with at least the secondary swirled air before combustion is possible. As shown in Figure 12A, with a fuel equivalence ratio of 0.62, the funnel structure expected in a swirl stabilized flame is clearly evident. The local fuel equivalence ratio with the air from the two swirled jets is 1.11, indicating little air from the insert jets is needed to complete the combustion. Although Figure 12A shows high concentrations of OH radical extending above the funnel like structure, visual observations reveal the visible flame region is apparently only a thin sheet, much like a horn, or funnel, with a rounded cusp.

As the overall fuel equivalence ratio is increased to 1.08 (Figure 12B), the swirled air/fuel mixture was still within flammability limits. What changed was the extra fuel left to mix with the insert jets. This additional fuel, as shown in Figure 12B, apparently burned on the shoulders of the funnel like structure. Finally, as the overall fuel equivalence ratio is increased to 1.49 (Figure 12C), the very fuel-rich swirled air directly over the injector can no longer support combustion. The estimated fuel equivalence ratio in this central zone is estimated to be about 2.67 which exceeds the rich flammability limits for propane and air. The characteristic funnel of a swirl stabilized flame is no longer visible in Figure 12C. The combustion is only taking place where air from the insert and dome jets has reduced the local fuel equivalence ratio to within the flammability limits of propane and air. This can

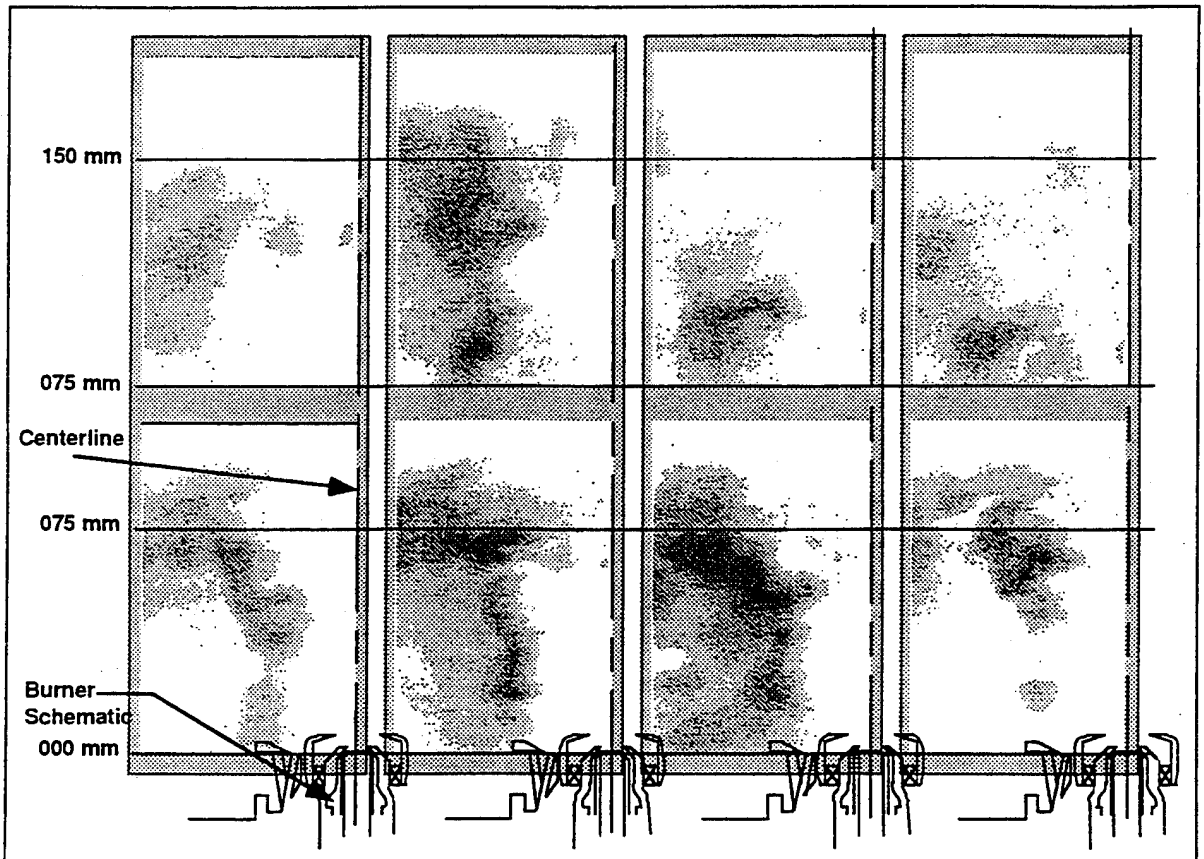

FIGURE 11. INSTANTANEOUS FLAME IMAGES BY PLIF OF THE OH RADICAL (T150-HS NOZZLE, 500 SLPM AIR, PHI 1.29)

be illustrated by comparing Figure 12A with Figure 12C. These two images appear to be negatives of each other--where one is black the other is white. This tends to support an assumption of the fuel mixing with each air passageway in turn from the inside-out.

OBSERVATIONS AND CONCLUSIONS

There have been considerable insights into the operational characteristics of a practical injector gained from this study. However, there is much to be done before a full understanding of the combustion characteristics of a practical gas turbine combustor is achieved.

A complex series of intricate flame shapes have been observed in the Task 150 technology combustor. Each flame shape indicates a different mode of operation, which differ from one another in the location of the flame fronts, or by some structure such as thickness or intensity. The different structures observed arise from changes in the flow fields, mixing patterns, or fuel equivalence ratio as operating conditions are varied. The fuel equivalence ratio where the flame transitions from one structure to another is the major operating variable affecting flame structure. The flames were attached to the insert air jets when the burner was operated very fuel rich. The flame would then lift, reattach, and lift again as the fuel equivalence ratio was progressively reduced. During the reattachment phase, the flame would take on many of the characteristics of a strong vortex and showed characteristics much like a tornado. Consequently, the terminology of funnel cloud, tornado, and debris cloud were adopted to describe some of the observed flame structure.

Gas velocity measurements were made where the flame is well attached to the injector ($\phi = 0.72$), at fuel rich conditions ($\phi = 1.49$) where the flame is attached to the dome and insert jets, and in isothermal, non-reactive flows where nitrogen was substituted for the propane fuel. These velocity data have allowed the effect of the flame temperature on the flow field and gas velocities to be determined.

Gas velocity data near the injector have shown sharp peaks in mean axial velocity near the outlet of the injector, and a corresponding strong tangential component in this same location. The insert jets had a marked influence on the axial and radial components, but seemed to have little effect on the tangential velocity components. The sharp gradients in axial velocity component were observed to decay quite rapidly with

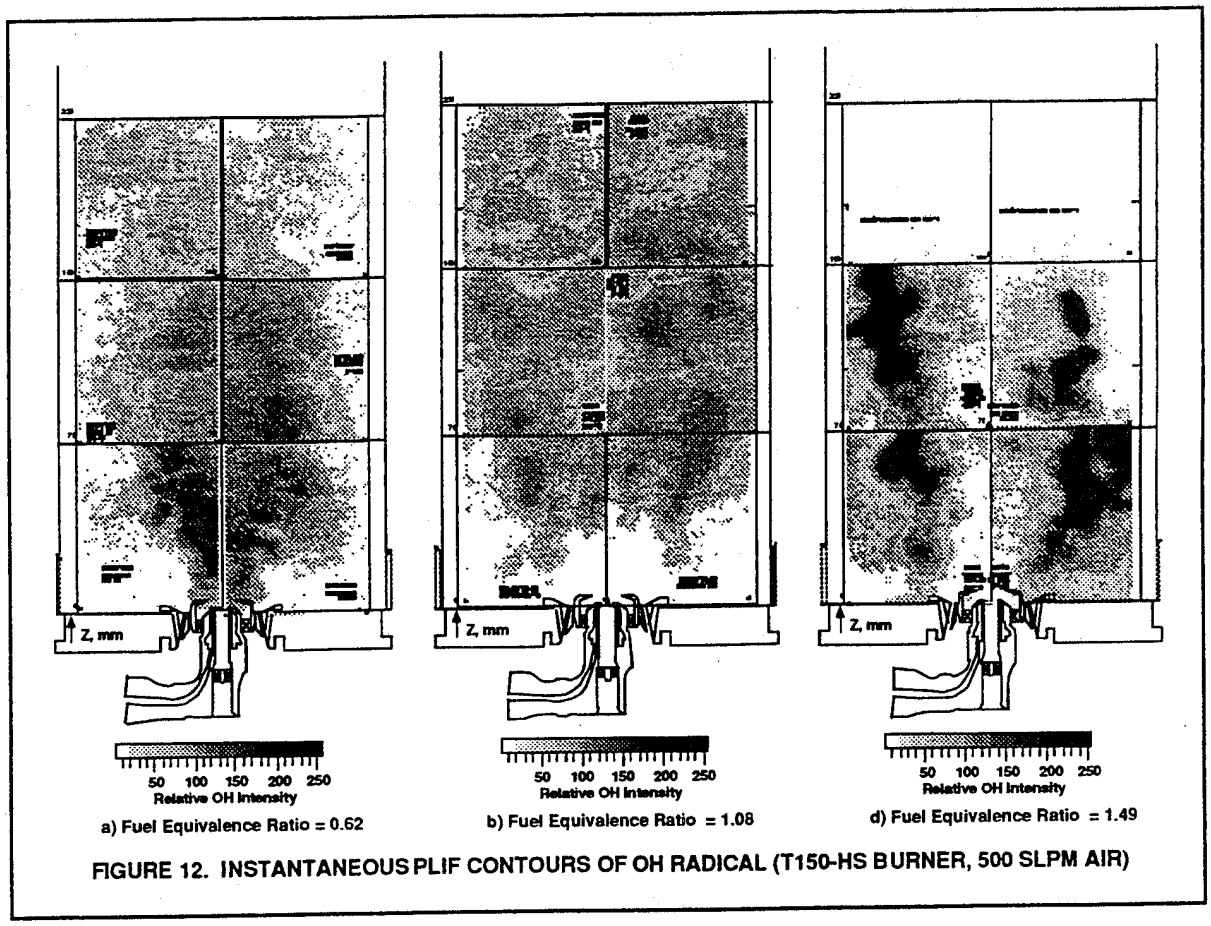

FIGURE 12. INSTANTANEOUS PLIF CONTOURS OF OH RADICAL (T150-HS BURNER, 500 SLPM AIR)

increasing downstream position. The strong tangential velocities associated with the injector rapidly decayed and diffused to the outer edges of the reactor becoming nearly uniform (ca -1 m/s) across the duct by the 150 mm axial location. Mass balance calculations based on isothermal axial velocity measurements have been used to determine the accuracy of the LDA measurements, and to assist in the extrapolation of the velocity to the wall. The mass flow rate is strongly influenced by the gradient assumed near the wall, but reasonable velocity interpolations gave reasonable mass balance closure.

Images from still photographs and angular velocity data deduced from the tangential velocity measurements have shown that the flow in the region behaves much like that observed in a strong vortex, with the rotational speed in rpm increasing towards infinity as the zero radius position is approached. The high rotational speeds are consistent with visual observations of the flames. The steep gradients in angular velocity suggest the shear stresses in the swirling eddies are very high.

An analysis of the zero axial velocity contours for one of the iso-thermal flow cases (14 slpm N_2, and 500 slpm air) has been used to show the complex flow structure that includes four recirculation zones: one at the bottom edge of the reactor driven by the dome jets., a second small but intense recirculation zone associated with the injector swirlers directly over the injector, a third major recirculation zone that begins at the edge of the injector and angles upward to the wall of the reactor, and a weak fourth recirculation zone high up in the combustor. The weak fourth zone was not seen in the combusting flows. The recirculation zones are consistent with the visual observations and video images taken of the reactor.

CARS gas temperature measurements have been successfully made in the Task 150 technology combustor. The measured peak temperatures were slightly below the predicted adiabatic flame temperature for the stoichiometric and fuel rich cases. The peak temperature was slightly higher than the adiabatic flame temperature for the lean case, which suggests a local diffusion zone within the flame that is close to a stoichiometric fuel equivalence ratio.

The variation in temperature field as the fuel equivalence ratio changes from fuel lean to fuel rich seemed to be consistent with the observations made from the still photographs. In general, the temperature measurements are consistent with the visual flame conditions, the PLIF images of the OH radical, and the velocity measurements for this particular test condition.

The PLIF images of the OH radical taken with the Task 150-HS technology burner dramatically illustrate the characteristics of swirling flames and the highly variable nature of the flame shape. The air from the insert jets significantly affects the flame structure, and the different modes of operation observed. Correlation of these OH images with the partitioning of the air flow rates through the various air passageways of the injector showed a consistent correlation between the local fuel equivalence ratio and the location of the flame structure. The images at low overall fuel equivalence ratio where the flame is well attached to the burner, and the images at high overall fuel equivalence ratio where the flame is attached to the insert jets are negatives of each other– where one is black the other is white. This supports the assumption of the fuel mixing with each passageway in turn from the inside-out.

ACKNOWLEDGMENTS

This paper presents results from an Air Force Office of Scientific Research (AFOSR) program being conducted at Brigham Young University (BYU), Provo, Utah and at Wright-Patterson Air Force Base (WPAFB). This study is part of an extensive research effort being carried out by the Fuels Combustion Group of the Aero Propulsion and Power Laboratory at Wright- Patterson Air Force Base (APPL, WPAFB), Dayton, Ohio, in which simple and complex diffusion flames are being studied to better understand the fundamentals of gas turbine combustion. The program's long term goal is to improve the design methodology of gas turbine combustors.

REFERENCES

Boyack, K.W., and Hedman, P.O., (1990), "Dual-Stokes CARS System for Simultaneous Measurement of Temperature and Multiple Species in Turbulent Flames," Twenty-third Symposium (International) on Combustion, The Combustion Institute, Pittsburgh, PA

Hancock, R.D., Hedman, P.O., and Kramer, S.K., (1991), "Coherent Anti-Stokes Raman Spectroscopy (CARS) Temperature and Species Concentration Measurements in Coal-Seeded Flames," Combustion and Flame, Vol. 71, pp 593-604

Hancock, R.D., Boyack, K.W., and Hedman, P.O., (1992), "Coherent Anti-Stokes Raman Spectroscopy (CARS) in Pulverized Coal Flames," Advances in Coal Spectroscopy, pg 373-407, ed by Henk L.C. Meuzelaar, Plenum Publishing Company

Roquemore, W.M., Reddy, V.K., Hedman, P.O., Post, M.E., Chen, T.H., Goss, L.P., Trump, D., Vilimpoc, V., and Sturgess, G.J., (January 7-10, 1991), "Experimental and Theoretical Studies in a Gas-Fueled Research Combustor," Paper No. AIAA 91-0639, 29th Aerospace Sciences Meeting, Reno, Nevada

Sturgess, G.J., Heneghan, S.P., Vangsness, M.D., Ballal, D.R., and Lesmerises, A.L., (June 3-6, 1991a), "Lean Blowout in a Research Combustor at Simulated Low Pressures," ASME Paper No. 91-GT-359, International Gas Turbine Congress and Exposition, Orlando, FL

Sturgess, G.J., Sloan, D.G., Roquemore, W.M., Reddy, V.K., A.L. Shouse, D., Lesmerises, A.L., Ballal, D.R., Heneghan, S.P., Vangsness, M.D., and Hedman, P.O., (1991b) "Flame Stability and Lean Blowout - A Research Program Progress Report," Proceedings of the 10th ISABE Conference, Nottingham, England, pp 372-384

Sturgess, G.J., Sloan, D.G., Lesmerises, A.L., Heneghan, S.P., and Ballal, D.R., (1992a), "Design and Development of a Research Combustor for Lean Blowout Studies," ASME Journal of Engineering for Gas Turbines and Power, Vol. 114, pp. 13-19

Sturgess, G.J., Heneghan, S.P., Vangsness, M.D., Ballal, D.R., Lesmerises, A.L., and Shouse, D., (June 1-4, 1992b), "Effects of Back-Pressure in a Lean Blowout Research Combustor," ASME Paper No. 92-GT-81, ASME International Gas Turbine Congress and Exposition, Cologne, Germany

Sturgess, G.J., and Shouse, D., (May 1993), "Lean Blowout Research in a Generic Gas Turbine Combustor with High Optical Access," ASME International Gas Turbine Congress and Exposition, Cincinnati, OH

THIS PAGE INTENTIONALLY LEFT BLANK

APPENDIX J

LEAN BLOWOUT RESEARCH IN A GENERIC GAS TURBINE COMBUSTOR WITH HIGH OPTICAL ACCESS

By

G.J. Sturgess
Pratt & Whitney, East Hartford, Connecticut

D.T. Shouse
WL/POSF, Wright-Patterson Air Force Base, Ohio

Published as ASME Paper No. 93-GT-332, May 1993. To appear in ASME *Journal of Engineering for Gas Turbines and Power.*

THE AMERICAN SOCIETY OF MECHANICAL ENGINEERS
345 E. 47th St., New York, N.Y. 10017

The Society shall not be responsible for statements or opinions advanced in papers or discussion at meetings of the Society or of its Divisions or Sections, or printed in its publications. Discussion is printed only if the paper is published in an ASME Journal. Papers are available from ASME for 15 months after the meeting.

Printed in U.S.A.

93-GT-332

LEAN BLOWOUT RESEARCH IN A GENERIC GAS TURBINE COMBUSTOR WITH HIGH OPTICAL ACCESS

G. J. Sturgess
Pratt & Whitney
East Hartford, Connecticut

D. Shouse
Wright Laboratories
Wright-Patterson Air Force Base
Dayton, Ohio

ABSTRACT

The U.S. Air Force is conducting a comprehensive research program aimed at improving the design and analysis capabilities for flame stability and lean blowout in the combustors of aircraft gas turbine engines. As part of this program, a simplified version of a generic gas turbine combustor is used. The intent is to provide an experimental data base against which lean blowout modeling might be evaluated and calibrated. The design features of the combustor and its instrumentation are highlighted, and the test facility is described. Lean blowout results for gaseous propane fuel are presented over a range of operating conditions at three different dome flow splits. Comparison of results with those of a simplified research combustor is also made. Lean blowout behavior is complex, so that simple phenomenological correlations of experimental data will not be general enough for use as design tools.

NOMENCLATURE

B.Z.	Burning zone
F	Temperature correction factor
LBO	Lean blowout
L.P.	Reactor loading parameter
P	Pressure in reactor
P.Z.	Primary zone
T	Reactants inlet temperature
V	Reactor volume
W_{ab}	Combustor total (cold) airflow
$W_{cooling}$	Dome cooling air, entering as film at dome/liner interface
W_{dome}	Total (cold) airflow entering combustor through dome, (including fuel injectors)
$W_{insertjets}$	Smoke-control airflow, as jets around fuel injectors
$W_{jets,1}$	Airflow for first row of transverse air jets (upper and lower liners)
$W_{P.Z.}$	Primary zone airflow
W.S.R.	Well stirred reactor
$l_{B.Z.}$	Burning zone length
$\dot{m}_a$	Air mass flowrate in reactor
$\dot{m}_f$	Fuel mass flowrate
$\dot{m}_{N2}$	Excess nitrogen mass flowrate in reactor
$\dot{m}_{Tot}$	Reactor total gaseous mass flowrate
n	Apparent global reaction order
ϕ	Fuel/air equivalence ratio by mass

INTRODUCTION

Combustion stability is extremely important in gas turbine engines for aircraft use. It is becoming increasingly more difficult to ensure that adequate stability margins can be maintained in the future because of current design trends toward improved atomization of liquid fuel, high temperature rise, and low emissions combustors, and their associated technologies.

In 1987 the U.S. Air Force established the Combustor Design Model Evaluation (CDME) program, with the goal of improving physical modeling to facilitate design work. Under the CDME effort, a joint industry/Government laboratory/university research program was initiated to address stability (Sturgess *et al.*, 1991a).

The intent of the stability research program is to investigate, understand and model lean blowouts in the context of combustors for aircraft gas turbines. The experimental portion of the program utilizes three combustors as test vehicles. These consist of a research combustor, a technology-development combustor, and a generic gas turbine combustor. The research combustor underwent extensive development (Sturgess *et al.*, 1990 and Heneghan

Presented at the International Gas Turbine and Aeroengine Congress and Exposition
Cincinnati, Ohio May 24–27, 1993
This paper has been accepted for publication in the Transactions of the ASME
Discussion of it will be accepted at ASME Headquarters until September 30,1993

et al., 1990) and is providing basic information on lean blowout (LBO) for a combustor that is simple in configuration but, nevertheless, contains the essential primary zone flow features of a practical gas turbine combustor (Roquemore *et al.*, 1991; Sturgess *et al.*, 1991b, 1991c and 1992a). A preliminary description of the generic gas turbine combustor is given in Sturgess *et al.* (1991a).

The majority of the published work on flame stability is for bluff-body flame-holders of various types, or, for well-stirred reactors, as reviewed by Lefebvre (1983). The amount of experimental data published in the open literature for practical gas turbine combustors is much less extensive. Given the large number of possible geometric variables that govern flow pattern, systematic investigations are largely lacking, although some basic studies are reported by Jeffs (1962) and Stewart (1956). However, the commonly-used form of practical combustor in these studies is the can-type; almost all information on the annular-type of combustor currently used in aircraft applications, is confined to relatively inaccessible company reports. The intent of this paper is to experimentally describe the lean stability behavior of an annular combustor, with an aim of eventually modeling this behavior.

DESIGN OF GENERIC COMBUSTOR

The purpose of the generic gas turbine combustor (known as the Task 200 combustor) is to provide an experimental data base against which lean blowout modeling of various types might be evaluated and calibrated. This purpose places three major requirements on the design of the Task 200 combustor: First, that it be as close to a real aircraft gas turbine combustor as possible in terms of LBO characteristics and flowfield. Second, that it be flexible enough to allow sufficient variation in relevant geometry and flow distribution to afford some investigation of the important primary zone design parameters, such as equivalence ratio and residence time. Third, that sufficient optical access be provided so that laser diagnostics might yield details of important flow features and their role in providing stability. Finally, it was decided to approach the LBO problem in two distinct stages – initially, with gaseous fuels (propane and methane), and lastly, with liquid fuels (ethanol). By this means the effects of liquid fuel atomization and spray evaporation can be separated from the aerothermochemical effects.

The aerothermodynamic design of the annular combustor was based on present Pratt & Whitney design practice, and it utilized airblast-atomizing fuel injectors and "inside-out" recirculation (Sturgess *et al.*, 1990 and 1991a). The configuration adopted for the Task 200 combustor is a four-injector, planar-section, simplified geometry version of this annular combustor design. The fundamental rig design to accommodate this combustor was carried out by United Technologies Research Center (UTRC), with subsequent modifications made by Wright Laboratories to improve handling, access and window durability. The distance between fuel injector centerlines is 7.62 cm (3.0 in), and the height between liners is 9.91 cm (3.9 in), while the length of the combustor is 20.83 cm (8.2 in) from the fuel injector face to the exit nozzle entrance.

The fuel injectors are actual engine hardware, with sets modified, calibrated and individually balanced with Lee-jets to flow gaseous or liquid fuels. Low and high swirl versions of the injector were provided. The fuel injector/combustor dome interfaces simulated engine practice. The major dimensions of combustor dome height, length and injector spacing are based on those of the engine from which the fuel injectors were taken. Cooling air is introduced as a surface film at the dome/liner interfaces. The liners, upper and lower, are removeable and may contain any desired pattern of air ports. Metal liners do not have any specific internal film cooling, but are provided with a thermal barrier coating and are convectively cooled by the shroud flows.

The diameters of the ports in the three rows of air addition are 0.635, 1.303 and 0.897 cm (0.250, 0.513 and 0.353 in) respectively, with a lateral spacing between ports in each row of 3.81 cm (1.5 in). Ports in a given row are staggered half a port pitch relative to adjacent rows, while the ports in each row in upper and lower liners are directly opposed. The ports in the first row are positioned with a port directly inline with a fuel injector. The spacings between rows of ports are as follows: first to second – 4.267 cm (1.68 in), and second to third – 3.962 cm (1.56 in); the centerline of the first row of ports is positioned 4.902 cm (1.93 in) downstream from the fuel injector faces.

The current pattern of circular air ports in the liners is one successfully developed at Pratt & Whitney for an in-service engine. Careful *in situ* measurements were made of the discharge coefficients for the dome, liner ports and fuel injectors.

Two domes are available; one a plain bulkhead (also provided with thermal barrier coating) and the other a vertically-symmetrical configuration having filleted upper and lower corners (Fig. 1). Dome cooling is provided by means of impingement jets, with spent dome cooling air being discharged at the dome/liner interfaces as a liner film. Ignition is by means of a hydrogen torch-ignitor mounted in the dome.

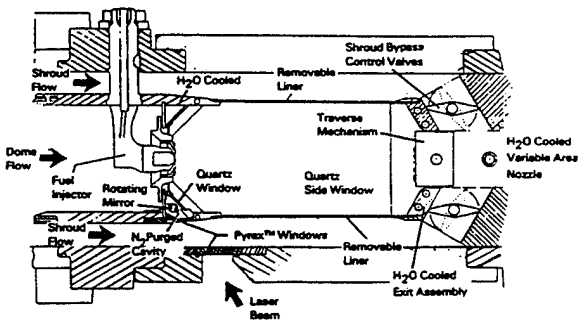

Fig. 1 Cross Section of the Task 200 Generic Combustor, Showing Optical Access and Flexibility Features of the Design

Air is supplied to the dome and upper and lower shrouds by individually-metered supplies that are always isolated from each other by means of an upstream array of sonic venturis. At the exits from the combustor and shrouds are independent water-cooled valves that control the bypass flows.

Fig. 2 shows the partially assembled rig; the combustor dome, the fuel injectors and one liner can be seen.

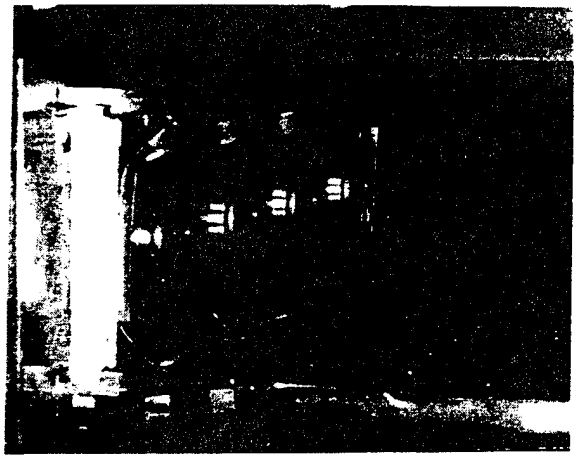

Fig. 2 Partially-Assembled Combustor, Showing Dome, Fuel Injector/Dome Interfaces, and One Liner

OPTICAL ACCESS

Direct optical access to the combustor for visualization and laser diagnostics is provided primarily by the side-walls enclosing the four-injector section. These side-walls are of fused quartz and are contained in water-cooled housings. Two thicknesses of sidewall are available – 1.905 cm (0.75 in) for operation at internal pressures up to 448.2 kN/m^2 (65 psia), and 0.318 cm (0.125 in) for operation at atmospheric pressure.

A further optical path is provided by windows in the base of the rig (Fig. 1), that allow laser beam access to a high-speed rotating mirror contained by the dome lower fillet-piece (this dome configuration only). Through selectively-opened slits up the height of the dome, the rotating mirror can scan the combustor with vertical, planar sheets of laser light for imaging purposes. For thermal protection, the mirror cavity is purged with a small, pressure-balanced flow of gaseous nitrogen.

A set of liners, containing the current air port hole pattern, is available in fused quartz for direct vertical access to the reacting flow.

RIG AND FACILITY

The rig is mounted horizontally in a test cell (Room 20) of Wright Laboratories, Wright-Patterson Air Force Base, Dayton, Ohio. It provides flow, metering and control of air, fuel, nitrogen and cooling water to the Task 200 combustor. A schematic flow path for the rig is given in Fig. 3.

Compressor air is supplied to the facility via a delivery system and isolating valve. The rig divides this air into three separate streams that respectively feed the upper shroud, dome and lower shroud. The passage flow splits are set by means of control valves, and each stream is pressure-isolated from its companions on the valve upstream side by means of appropriately-sized sonic venturis. Individual stream flows are then measured by calibrated orifice plates downstream of the control valves. For simulation of low pressures, gaseous nitrogen from a bottled supply is introduced into the main air line far upstream from the three-way split, so that it is thoroughly mixed with the incoming air prior to the sonic venturis.

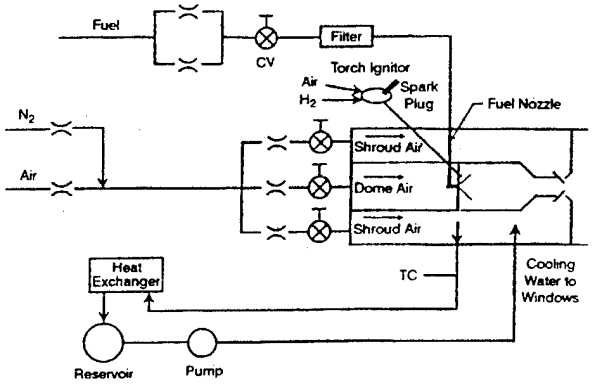

Fig. 3 Schematic of Facility, Showing Air, Fuel, Excess Nitrogen, and Cooling Water Circuits

Gaseous propane from a tank farm is metered by low-range and high-range turbine flow meters, and the filtered supply is delivered to a manifold feeding the four fuel injectors.

The torch ignitor is mounted on the rig and discharges directly into the dome. It is supplied separately with air and gaseous hydrogen; ignition is by spark plug. After a successful light of the main combustor, the torch ignitor is turned off.

Cooling water for the window frames is pumped from a reservoir to the frames where it flows upstream (counterflow heat exchanger). As the heated water leaves the rig, its temperature is monitored by a thermocouple. Before being returned to the reservoir, the heated water is first passed through a heat exchanger.

The discharge from the rig enters an atmosphere-pressure exhaust ejector and exits the facility to ambient conditions.

Fig. 4 shows the rig mounted in the facility. Flow is from left to right, and the rig exhausts from the facility via the circular duct on the right. Mounted under and on either side of the test section may be seen the hardened LDA and CARS system currently being used to map the combustor velocity and temperature fields.

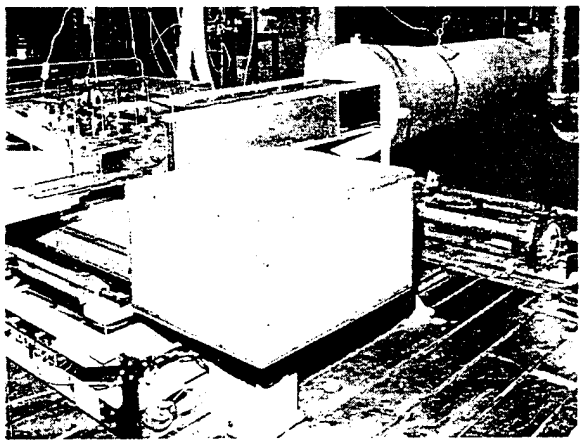

Fig. 4 Rig Mounted in the Facility, Showing Exhaust Arrangement and Hardened LDA/CARS Instruments

The facility in which the rig is installed is capable of supplying up to 13.61 kg/sec (30.0 lbm/sec) of air at ambient temperature, and up to 10.433 kg/sec (23 lbm/sec) at temperatures up to 922K (1200F) (nonvitiated); the air can be delivered at pressures up to 5171 kN/m^2 (750 psia). The fuel supplies in the facility are, for propane, up to 0.227 kg/min (0.5 lbm/min) at 689.5 kN/m^2 (100 psig); for methane, up to 0.181 kg/min (0.4 lbm/min) at 1034.2 kN/m^2 (150 psig); and for liquid fuels, up to 6.804 kg/hr (15 lbm/hr) at 1379 kN/m^2 (200 psig). The bottled nitrogen supply is capable of delivering up to 9.072 kg/min (20 lbm/min) at 3447.4 kN/m^2 (500 psig) for a limited period of time.

COMBUSTOR FLOW SPLITS

Fig. 5 shows diagrammatically the flow distribution in the combustor rig.

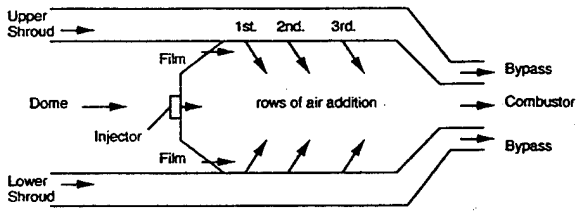

Fig. 5 Diagrammatic Representation of Combustor Flow Splits

The minimum levels of bypass flows were always set for convective cooling of the liners. The combustor total airflow was defined as the sum of the metered dome flow and the calculated jet flows based on measured pressure drops and pre-established hole effective areas, i.e.,

$$W_{ab} = W_{dome} + W_{jets} \quad (1)$$

The dome flow was made up of the injector, insert jets (around the individual injectors) and dome cooling airflows, i.e.,

$$W_{dome} = W_{injectors} + W_{insertjets} + W_{cooling} \quad (2)$$

The primary zone airflow consisted of the dome flow plus 27.9 percent of the first row jet air. This value of primary zone-active jet air has been established separately (Sturgess *et al.*, 1992b) for the particular primary zone aerodynamic flow pattern used. Thus,

$$W_{PZ} = W_{dome} + 0.279W_{1st.jets} \quad (3)$$

For a particular run, flow split information was established at the set point without combustion, prior to each blowout test point.

The measured effective areas for the liner air ports, top and bottom respectively, are as follows: first row – 1.516 and 1.632 cm^2 (0.235 and 0.253 in^2); second row – 4.968 and 5.394 cm^2 (0.77 and 0.836 in^2); and third row – 2.845 and 2.852 cm^2 (0.441 and 0.442 in^2). The total effective area of the dome is 8.652 cm^2 (1.341 in^2), and that of the fuel injector air passages is 5.929 cm^2 (0.919 in^2) (total of four injectors).

BLOWOUTS WITH PROPANE

Testing with gaseous propane has been completed for three values of dome flow, consisting of 10, 15 and 20 percent of the total airflow entering the combustor. For each flow split, lean blowouts were taken for a series of total airflows, and for a range of excess nitrogen flows at each airflow. Flame characteristics during the blowouts were recorded on videotape with viewing through the side-windows. The liner hole patterns remained fixed for all tests reported. The low-swirl fuel injectors were used for all the data presently reported.

Without combustion, the required airflow rate and dome/shroud bypass flow splits were established. The combustor was lit and the torch ignitor turned off. Once thermal stability was established, the flow rates and flow splits were again taken. Fuel flow was then reduced in a series of progressively smaller steps, with allowance for thermal stabilization at each fuel decrement. Blowout was detected visually through the side windows. Instrumentation was automatically scanned both before and immediately after the ultimate fuel decrement.

Shown in Fig. 6 is the atmospheric pressure LBO fuel mass flow rate (all four injectors) with increase in primary zone airflow for zero excess nitrogen flow at 15 percent dome flow. The effect of nitrogen addition is given in Fig. 7 over a series of primary zone airflows. Both flow relationships are linear for the ranges covered, with LBO fuel flow increasing with both airflow and nitrogen flow. For the range of air and excess nitrogen flows covered at 15 percent dome flow, the primary zone equivalence ratio remains less than unity, as Fig. 8 indicates for zero excess nitrogen.

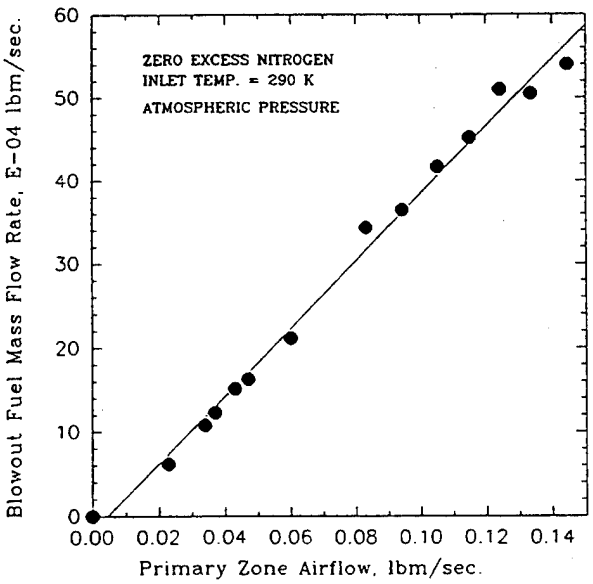

Fig. 6 Dependence of Blowout Fuel Mass Flowrate on Primary Zone Airflow for the 15 Percent Dome Flow Combustor at Atmospheric Pressure

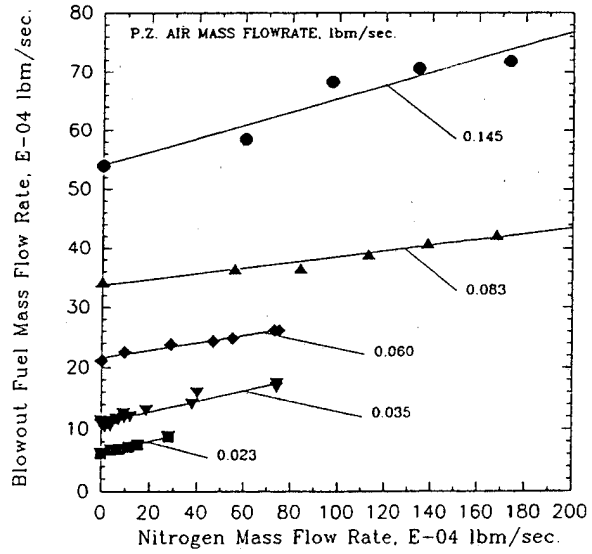

Fig. 7 Dependence of Blowout Fuel Mass Flowrate on Excess Nitrogen Mass Flowrate at Several Primary Zone Airflows in the 15 Percent Dome Flow Combustor

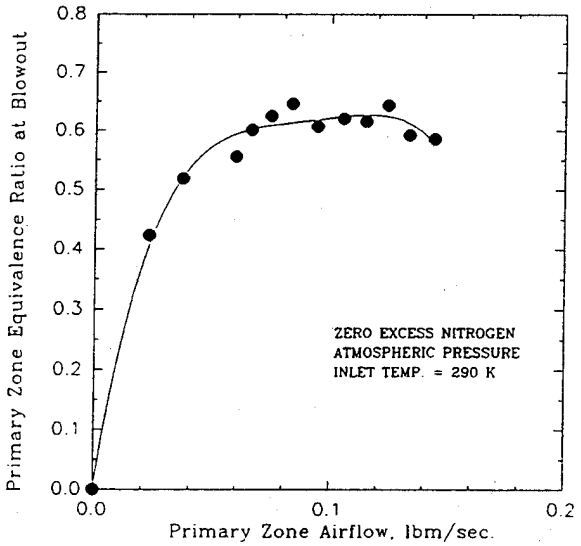

Fig. 8 Relation Between Primary Zone Equivalence Ratio at Blowout and Primary Zone Airflow at Atmospheric Pressure in the 15 Percent Dome Flow Combustor

For 10 percent dome flow, the primary zone equivalence ratio can exceed unity when the combustor airflow is low and/or the nitrogen flow rate is high. Under these circumstances, the burning zone is greater in length than the primary zone, and extends to encompass sufficient air to burn all the fuel. When this happens, the flame extends around the first row of transverse air jets. Eventually, the local equivalence ratio can again exceed a value of unity, and the second row of air jets becomes involved in the combustion process. The result of this behavior is that as combustor loading is increased, a quasi fuel staging process (Sturgess *et al.*, 1992b) develops. Quasi fuel staging for the Task 200 combustor at 10 percent dome flow is illustrated in Fig. 9, with the corresponding changes in burning zone length being shown in Fig. 10. When quasi fuel staging occurs, it is more realistic to refer to "burning zone" rather than primary zone. The burning zone length is determined by adding to the primary zone downstream air in bulk fashion until a local equivalence ratio of unity is reached or exceeded.

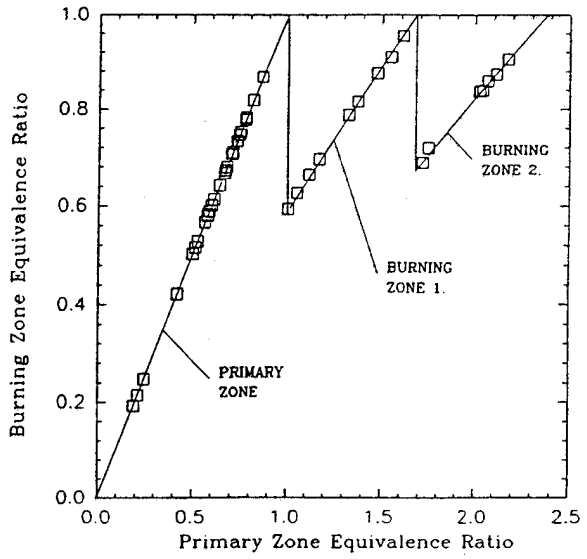

Fig. 9 Relationship Between Burning Zone and Primary Zone Equivalence Ratios in the 10 Percent Dome Flow Combustor to Illustrate Quasi-Staging of Fuel

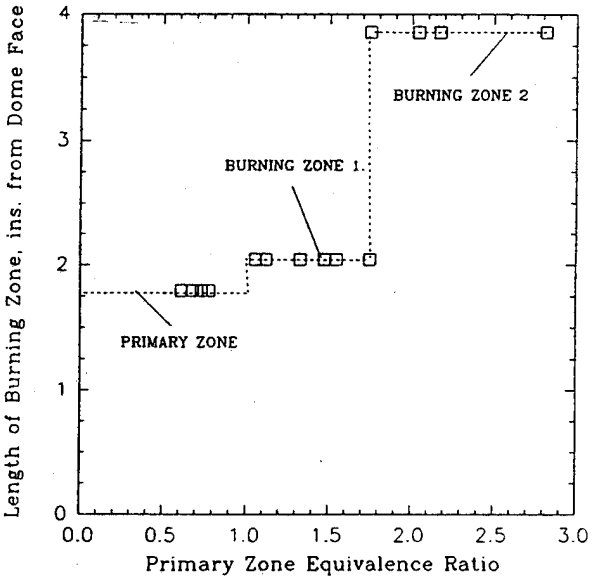

Fig. 10 Variation of Burning Zone Length with Primary Zone Equivalence Ratio in the 10 Percent Dome Flow Combustor as a Result of Quasi-Staging of Fuel

The inert gas, excess nitrogen dilution technique (Sturgess *et al.*, 1991c) simulates low pressures through slowing chemical reaction rates by lowering the concentration of reactants, and through reduction in reaction temperature by virtue of the nitrogen heat capacity. If the mass flow rate of nitrogen is high relative to that of the air, it will also result in a reduction of residence time in the reaction zone. The viability of the technique depends on the assumption that combustion is not residence time limited. Fortunately, for LBOs the flame does not fill the complete combustor, even with quasi fuel staging. The presence of the excess nitrogen must be accounted for if constant residence time/ reference velocity comparisons are to be made. It must be remembered that although the inert diluent can slow chemical reaction rates in a similar fashion to true low pressures, the actual pressure in the reactor is not reduced. Thus, reference velocity and residence time are conveniently independent of simulated pressure.

The calibration of excess nitrogen as an inert diluent for simulation of low pressures is presented graphically in Sturgess *et al.* (1991c). Using the calibration of the inert diluent, an equivalent pressure for the LBOs can be obtained. The relation between equivalent pressure and burning zone excess nitrogen to fuel mass ratio is shown in Fig. 11 for burning zone airflows of 0.018 to 0.045 kg/sec (0.040 to 0.100 lbm/sec) at 10 percent dome flow, and for 10, 15 and 20 percent dome flows at 0.045 kg/sec (0.100 lbm/sec) burning zone airflow. Extremely low values of equivalent pressure can be achieved, although the technique does reach saturation for excess nitrogen to fuel mass ratios greater than 8.0.

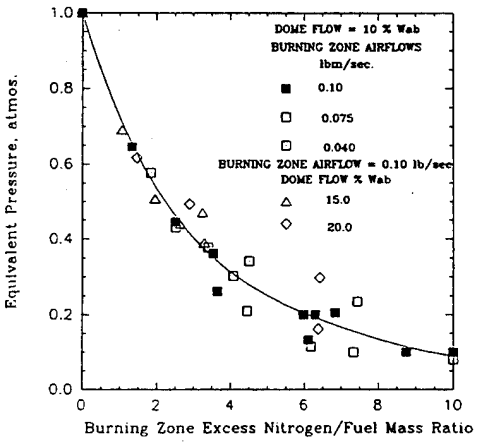

Fig. 11 Effect of Equivalent Pressure Due to Excess Nitrogen on Blowout Characteristic for Task 200 Combustor

The effect of equivalent pressure on blowout primary zone equivalence ratio with increasing primary zone airflow can be seen by comparing Fig. 12 (0.4 atmosphere) against Fig. 8 (1.0 atmosphere). Fig. 12 is corrected to the same residence times as for Fig. 8. The correction is to multiply the observed blowout equivalence ratio at fixed inlet airflow by the ratio of total mass flows entering the primary zone without and with excess nitrogen. The equivalence ratio-plateau observed at atmospheric pressure is reduced in presence at the lower pressure. This decrease appears to be due to the changing slope of the overall blowout curve (see Fig. 20 for example) at the higher combustor loadings associated with the lower pressure.

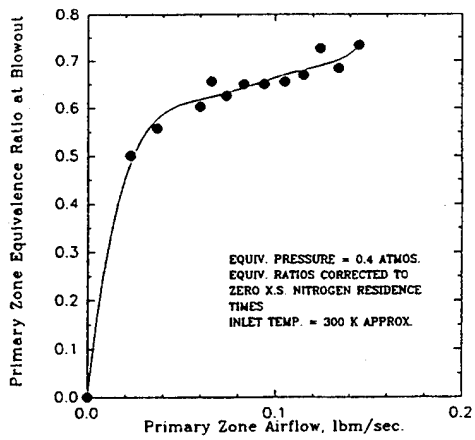

Fig. 12 Dependence of Primary Zone Blowout Equivalence Ratio on Primary Zone Airflow in the 15 Percent Dome Flow Combustor at 0.4 Atmospheres Equivalent Pressure

For 10 percent dome flow, the effect of equivalent pressure is complicated by the change in burning zone that takes place as combustor loading is increased. Fig. 13 shows the variation in LBO burning zone equivalence ratio with equivalent pressure for burning zone airflows of 0.018 to 0.045 kg/sec (0.040 to 0.100 lbm/sec), where the data have been linearly corrected to zero excess nitrogen residence times. The three burning zone airflows correspond to constant (cold) reference velocities of 1.372, 1.036 and 0.549 m/s (4.5, 3.4 and 1.8 ft/sec), respectively. The blowout data for the three reference velocities collapse within the scatter of an individual reference velocity.

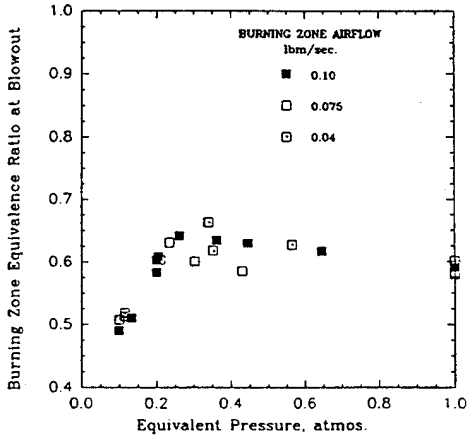

Fig. 13 Effect of Equivalent Pressure on Burning Zone Equivalence Ratio at Blowout in the 10 Percent Dome Flow Combustor for Several Constant Values of Burning Zone Airflow

It can be seen that as the equivalent pressure is reduced the burning zone equivalence ratio at blowout increases slightly from the value at atmospheric pressure (loss of stability) to a maximum value of about 0.65 at 0.3 atmosphere. Thereafter, it decreases

sharply with further decrease in effective pressure (gain of stability). The peak in blowout occurs at an equivalent pressure that corresponds to a condition at which the primary zone reaches unity (uncorrected) equivalence ratio. (The peak blowout equivalence ratio is at a value less than unity due to the residence time correction necessary because of the excess nitrogen.) Thus, for equivalent pressures greater than 0.3 atmosphere, the flame at blowout is stabilized in the primary zone; for equivalent pressures less than 0.3 atmosphere, the flame is stabilized in a burning zone that includes and extends beyond the primary zone. Flame holding in this condition is provided by the first row of air jets supplementing the regular primary zone.

The discrete character of the air addition to the combustor and the burning zone (B.Z.) definition together allow the possibility that the uncorrected equivalence ratio could be below unity at quasi-staging, and that as the burning zone extends itself, the corrected equivalence ratio would fall as the equivalent pressure falls. The residence time correction then applied to the equivalence ratio will also increase as the equivalent pressure falls, due to the growing quantities of excess nitrogen introduced.

Fig. 14 shows the variation of the uncorrected primary zone equivalence ratio at blowout with equivalent pressure for a constant B.Z. airflow of 0.045 kg/sec (0.100 lbm/sec) [constant cold reference velocity of 1.372 m/s (4.5 ft/sec)] in the 10 percent dome flow combustor. The behavior is similar to that shown in Fig. 13 for the B.Z.'s, and shows unity equivalence ratio is reached at an equivalent pressure of 0.3 atmosphere. This confirms the interpretation of the minimum stability point in Fig. 13.

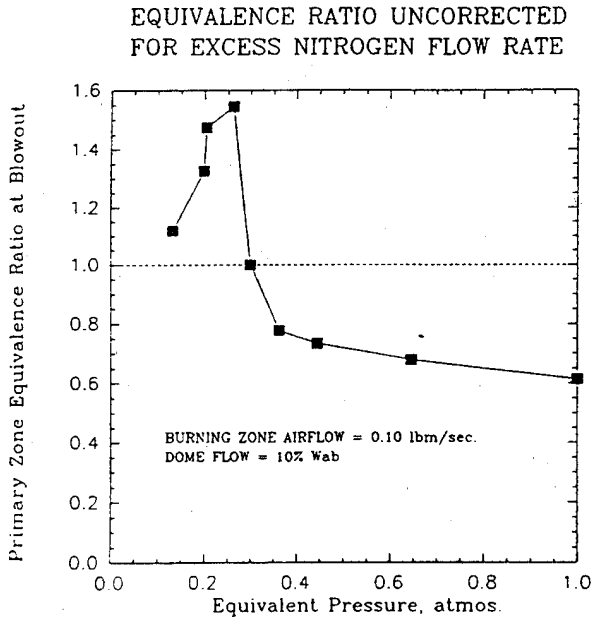

Fig. 14 Variation of Primary Zone Equivalence Ratio at Blowout with Decreasing Equivalent Pressure in the 10 Percent Dome Flow Combustor at a Fixed Burning Zone Airflow

Fig. 15 gives the combined B.Z. blowout behavior with different dome flows at constant B.Z. airflow, as the equivalent pressure is reduced. There is more scatter but the characteristics are again very similar to those of Fig. 13. The 20 percent dome flow combustor has a P.Z. that reaches an uncorrected unity equivalence ratio at 0.4 atmosphere (from a plot similar to Fig. 14). The peak corrected B.Z. equivalence ratios at blowout depend on the dome flow, and increase with increasing dome flow. The peak corrected B.Z. equivalence ratio at LBO occurs at higher equivalent pressures for higher dome flow splits. Although Fig. 15 is for a constant cold reference velocity of 1.372 m/s (4.5 ft/sec), the higher dome flow combustor has a shorter P.Z. residence time than does the lower dome flow combustor. Note that the B.Z. stability for both dome flow splits is independent of dome flow when the flame holding also depends on jet-stabilization as well as on the dome.

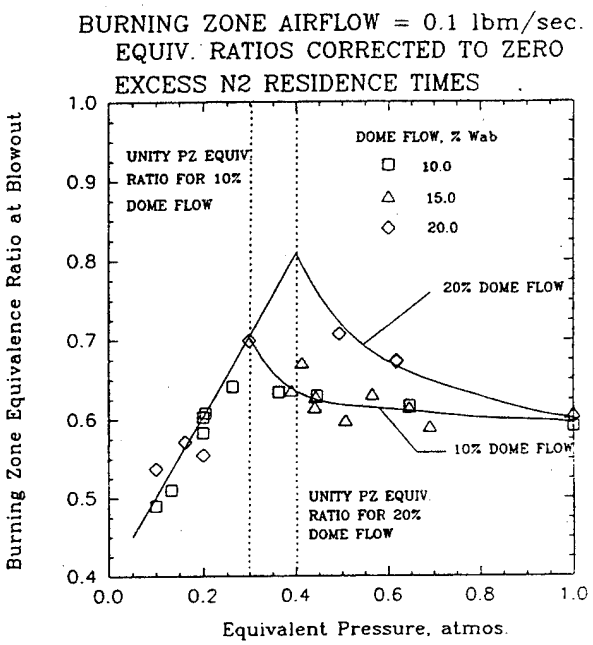

Fig. 15 Variation of Burning Zone Equivalence Ratio at Blowout with Equivalent Pressure at Fixed Burning Zone Airflow, Showing the Dependence on Dome Flow for Primary Zone Burning and the Independence of Dome Flow for Downstream Burning

The lines shown on the figure for 10 and 20 percent dome flows are curve fits to the data that are forced to intersect the combined (linear) line at the respective value of equivalent pressure for which the P.Z. equivalence ratio reaches unity.

FLAME PATTERN CHANGES

For the 15 percent dome flow split, it was observed for high values of primary zone airflow that a marked change in primary

zone flame shape took place, and this was also accompanied by a marked reduction in combustion noise. The two flame patterns have been denoted as a "lifted flame" (normal condition) and an "attached flame" (occurring at the higher flows). Fig. 16 displays photographs of the two flames. Fig. 17 is a repeat of Fig. 8 but with delineation of the flame type and some additional (no blowout) points to illustrate this effect. Comparison of Figs. 8 and 17 suggests that the attached flame condition might represent a more stable combustion situation. The reduction in combustion noise also suggests this.

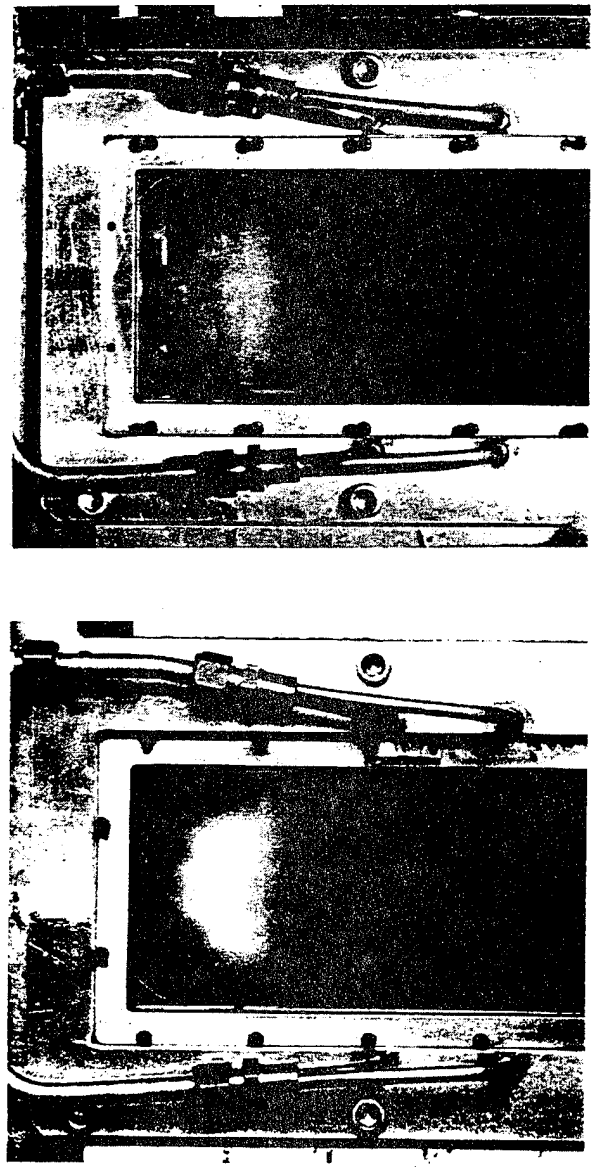

Fig. 16 Attached and Lifted Flames in the Task 200 Combustor

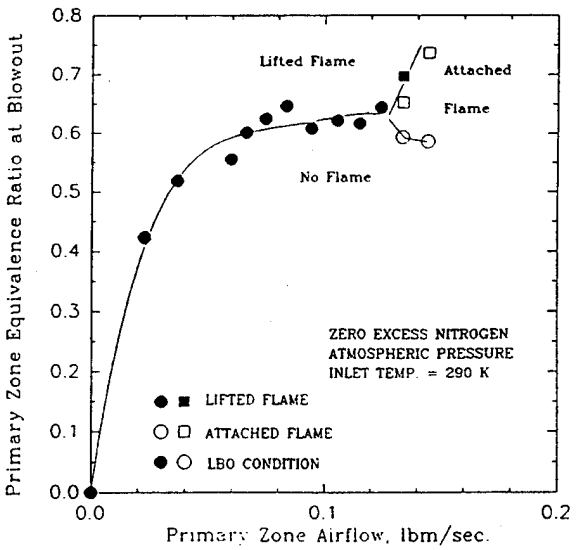

Fig. 17 Demonstration of Different Flame Conditions at Atmospheric Pressure in the 15 Percent Dome Flow Combustor with Primary Zone Burning

The blowout data presented up to Fig. 17 are all of a single flame type – the lifted flame. This is believed to be the more usual burning mode in combustors of the present type at these operating conditions. The attached flame was only encountered for extremely high values of airflow at the lower primary zone airflow splits. It was almost never encountered at the 20 percent dome flow. Since a significant proportion of the flow through the dome is air passing through the (airblast) fuel injectors, the injectors at these conditions are being operated "off-design." There is evidence from the technology combustor (to be reported) that the local flame characteristics immediately adjacent to the injector discharge are dictated by local stoichiometry distributions associated with the injector, i.e., a local flammability window is opened between the rich and lean limits that permits combustion close to the injector.

A definitive explanation of the circumstances of the attached flame/lifted flame phenomenon is not yet available, and it is being further explored in the (Task 150) technology-development combustor, which is a single Task 200 fuel injector element mounted in a version of the (Task 100) research combustor. The phenomenon has been reproduced in the Task 150 combustor and so, is clearly associated with the design of the fuel injectors. The behavior appears to be analogous to the attached/lifted flame behavior observed in the (Task 100) research combustor (Sturgess *et al.*, 1991c and 1992a).

CORRELATED DATA

Some of the blowout modeling being developed as part of this research effort is based on well-stirred reactor networks. Because of this, the collected blowout data have been correlated on the basis of well-stirred reactor theory. LBO data from the research combustor were successfully correlated (Sturgess *et al.*, 1991c) by the combustor loading parameter, defined as,

$$L.P. = \frac{\dot{m}_{Tot}}{VP^nF}$$

where,

$\dot{m}_{Tot}$	=	$\dot{m}_f + \dot{m}_a + \dot{m}_{N2}$	lbm/sec
V	=	reactor volume,	ft^3
P	=	pressure,	atmospheres
n	=	$2\phi_{LBO}/(1+\dot{m}_{N2}/\dot{m}_a)$	apparent global reaction order
F	=	$\frac{10^{0.00143T}}{3.72}$	(to correct to 400K)
T	=	inlet temperature,	K

Correction of the data to a constant inlet temperature of 400K represents tribute to the pioneering well-stirred reactor work of Longwell, since 400K was the inlet temperature used in his original experiments (Longwell *et al.*, 1953).

The general form of the W.S.R. loading parameter correlation group follows Kretschmer and Odgers (1972), and has been in common use for many years; here, it has been modified to account for the use of excess nitrogen as a diluent, as described in Sturgess *et al.* (1991c). The intended use of the group is as a correlating parameter for experimental data. In general, the equivalence ratio of a combustor primary zone will be established at a specific design point by considerations other than flame stability. It will, therefore, be known at off-design point operating conditions where stability becomes important. The design engineer then desires to check whether or not the combustor as designed remains alight at these off-design conditions. This is done by determining if the operating line for the combustor falls within the previously-determined appropriate stability loop for the type of combustor under consideration (see Sturgess *et al.*, 1991a, for an example).

Well-stirred reactor modeling is a convenient and inexpensive method to introduce a (reasonably) full chemical reaction mechanism into consideration for calculations of lean blowout. A difficulty is in defining a suitable network to represent a practical combustor. One of the procedures being developed under this research effort is network definition via computational fluid dynamics (CFD) modeling (Sturgess *et al.*, 1991a). For this reason, it is presently convenient to use the well-stirred reactor approach for the purposes of experimental data comparison.

Shown in Fig. 18 are the correlated blowout data for lifted flames only, in the 10 percent dome flow combustor. The blowout equivalence ratio is for the complete combustor, as is the reactor volume used in the loading parameter. The complete combustor airflow is the sum of (Fig. 5) dome and first, second, and third rows of transverse jet airflows, and this is used to calculate the overall equivalence ratio. The correlation achieved is quite satisfactory.

It can be seen that the behavior up to a loading of 10 lbm/sec(ft^3 $atmos^n$) follows the traditional lean-side stability loop characteristic form. The flame is stabilized only in the primary zone for these loadings. For loadings greater than 10, quasi-staging comes into effect as the flame grows first around the first row of transverse air jets in the combustor, and then, eventually extends to involve the second row of jets. The behavior can be easily related to Fig. 9. It is interesting to note that the staging behavior observed in the Task 200 generic combustor might also explain the LBO characteristic of another practical combustor presented in Sturgess *et al.* (1991a).

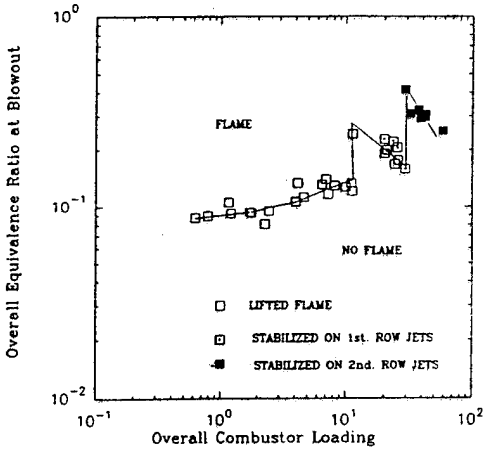

Fig. 18 Correlated LBO Data, Demonstrating Quasi-Staging in the 10 Percent Dome Flow Combustor for Lifted Primary Zone and Jet-Stabilized Flames

The correlated data for the 15 percent dome flow combustor do not exhibit quasi-staging up to a loading parameter of 15 lbm/sec(ft^3 $atmos^n$), and the 20 percent dome flow combustor does not evidence it up to loadings of 20 lbm/sec(ft^3 $atmos^n$). This is because of the higher primary zone airflows of these combustors.

In Fig. 19 the correlated LBO data for the attached and lifted flames up to the first quasi-staging point for the 10 percent dome flow combustor are compared. The loading parameters are based on the actual burning zones containing the flame. It can be seen that either flame can exist at a given loading parameter, and that the attached flame does indeed have improved stability over the lifted flame, as was suggested by Fig. 17. Again, there is, as yet, no definitive explanation for the circumstances that result in an attached or lifted flame condition.

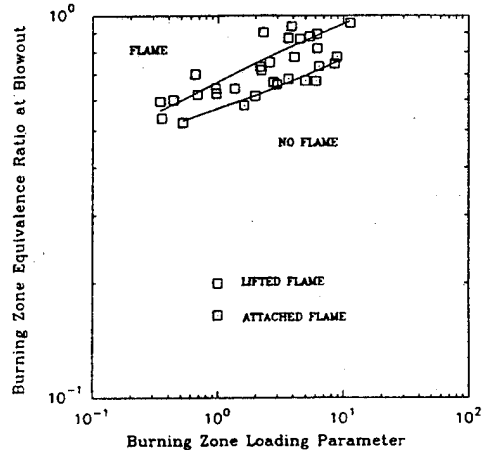

Fig. 19 Correlated LBO Data in the 10 Percent Dome Flow Combustor, Prior to Quasi-Staging (i.e., Primary Zone Burning) for Lifted and Attached Flames, Showing Improved Stability with Attached Flames

The effect of dome flow for primary zone burning only is shown in Fig. 20 by comparing the correlated data for the 10 and 20 percent dome flow combustors. For the 10 percent case, both attached and lifted flame data are shown, and the flame effect is almost as strong an influence on stability as is the percent dome flow. Only two data points for attached flames in the 20 percent dome were available at the time of writing, and these fall in with the lifted flame data for this dome. The lifted flame data for the 15 percent dome flow combustor fall between the data for the 10 and 20 percent domes. Note that the higher primary zone loading for the 20 percent dome results in an increased sensitivity of LBO equivalence ratio to loading when overall loading exceeds 10 lbm/sec(ft^{3}atmos^n). The effect of increased dome flow is to reduce the combustor stability.

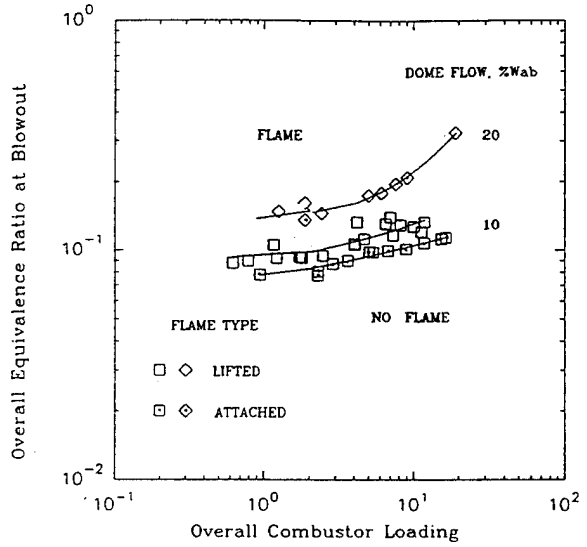

Fig. 20 Effect of Dome Flow for Primary Zone Burning in the Task 200 Combustor, for Lifted and Attached Flames

COMPARISON WITH WELL-STIRRED REACTOR

The stability performance of a combustor can be usefully compared with that of a well-stirred reactor (W.S.R.), which achieves its peak heat release rate (unity equivalence ratio) at very high values of loading parameter and whose lean blowout tends to the lean flammability limit of the reactants at very low values of loading parameter.

In order to make this comparison for practical gas turbine combustors, it is necessary to account for the (combustion) redundancy of the dilution zone of such combustors. This is because the dilution zone is generally not involved in the combustion process. In the case of the Task 200 generic combustor, the burning zone definition is used to describe the effective reactor portion of the total combustor.

In Sturgess *et al.* (1991c), it was established that the Task 100 research combustor, operating on propane at near-blowout, was behaving as a well-stirred reactor. Therefore, well-stirred reactor performance is represented by the lean blowout results obtained (also using the excess nitrogen dilution technique for low pressures) in the Task 100 combustor.

Fig. 21 compares the Task 100 research combustor stability characteristic with the collected burning zone equivalence ratios at lean blowout for the 10, 15 and 20 percent dome flow Task 200 generic combustors, on a basis of burning zone loading parameter.

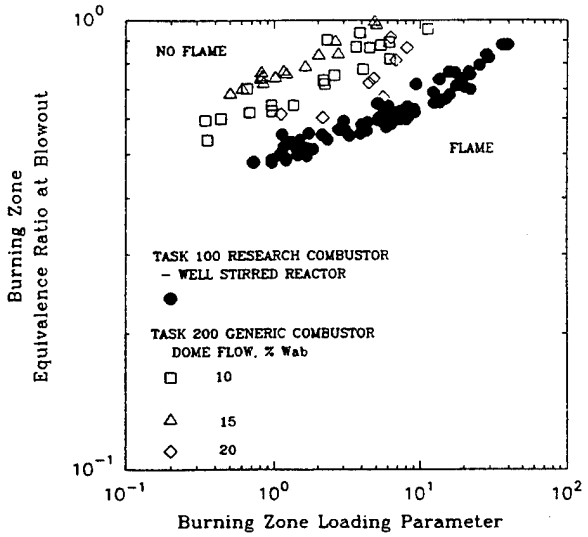

Fig. 21 Comparison of the Generic Combustor Primary Zone Stability with Lifted Flames Against Well-Stirred Reactor Stability

For the generic combustor data presented, the burning zone is confined to the conventional primary zone. Furthermore, only lifted-flame data are shown. Thus, quasi-staging data have been excluded so that consistent types of flame-holding behavior in the generic combustor are compared with the W.S.R. Since the flames near blowout in the research combustor were all lifted, the partial-premixing character of the lifted flames in both combustors should be similar.

The figure shows that the generic combustor data, although not well-correlated, show no systematic variation with dome flow, as they do for example in Fig. 20. For the range of loading parameters covered, the stability of the generic gas turbine combustor is less than that of the research combustor (W.S.R.). The W.S.R. reaches its peak heat release rate at a loading of about 50 lbm/sec(ft^{3}atmos^n) at 400K inlet temperature, while the primary zone of the generic combustor appears to reach its peak heat release rate at a loading of roughly 8 to 10 lbm/sec(ft^{3}atmos^n). The W.S.R. is asymptotically tending to a blowout equivalence ratio of about 0.5 at low values of loading, less than 1.0 lbm/sec(ft^{3}atmos^n). The lean flammability limit for propane in air is about 0.5 at atmospheric pressure and temperature (Lewis and von Elbe, 1987). Although the data do not extend to sufficiently low values of loading parameter for either combustor, it appears from the respective slopes that the two stability curves might cross at values of loading parameter less than 0.1 lbm/sec(ft^{3}atmos^n). Such a crossing would imply better stability on a bulk equivalence ratio basis for the generic combustor than the flammability limits for the reactants. This can only arise because of imperfect mixing of fuel and air in the generic combustor, so that local burning takes place at other than bulk equivalence ratios.

On the evidence of the above comparison, it would appear that the primary zone of the generic combustor is behaving relative to the W.S.R., exactly as might be expected from theory.

Fig. 22 is a repeat of Fig. 21, except that only attached flame data for the generic combustor are presented. Attached flame data for the 20 percent dome flow combustor case are not extensive enough to be worth including.

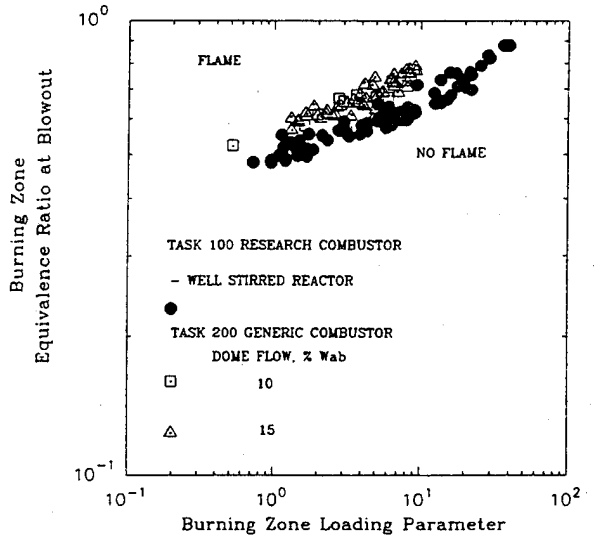

Fig. 22 Comparison of the Generic Combustor Primary Zone Stability with Attached Flames Against Well-Stirred Reactor Stability

The attached flame data are correlated extremely well and give a stability characteristic for the primary zone that is quite close to that for the W.S.R. over the range of loadings covered. The Task 200 attached flame data do not cover a sufficient range of loading parameter to permit observations concerning peak heat release rates, etc. It is not clear from consideration of Figs. 21 and 22 of the respective roles of mixing and combustion noise in the stability of lifted and attached flames.

DISCUSSION

The Task 200 generic combustor rig has achieved its major design objectives of geometric flexibility and good optical access. The separately-metered and controlled air supplies, interchangeable dome configurations, removeable combustor liners, and alternative fuel injectors, allow a large number of combinations of major design variables to be explored. Aerothermochemical and liquid fuel atomization/vaporization aspects can be addressed through use of different gaseous and liquid fuels. The optical access permits superb direct viewing of the flame. The complex lean blowout behavior observed could not have been untangled to the extent that it has without reference to flame-visuals. The "instant-replay" capability provided by the monitoring color videotapes formed valuable records and were particularly important in this. Three-dimensional temperature fields within the operating combustor are being mapped (not reported here) with CARS via the windows, and reasonably successful penetration deep across the combustor is being obtained. The planar imaging capability provided by the rig has not yet been used, however.

The simulation of low pressures by means of an inert diluent (nitrogen) and developed in the research combustor, has been successfully carried over to the generic combustor. Lean blowout data obtained in the generic combustor are consistent, repeatable and reliable.

The combustion behavior as lean blowout is approached at simulated low pressures is extremely complicated. It contains quasi-staging of the fuel as loading in the combustor is increased. When quasi-staging takes place, the flame becomes stabilized by the combustion air jets, as well as in the primary zone. When jet-stabilization exists, the lean blowouts are insensitive to dome airflow; without it, blowouts are sensitive to dome airflow. Flame changes from lifted to attached flames can occur, and at given loading either flame can exist, depending on how the loading is achieved.

Common flow features and behavior can be seen in the Task 100 research combustor, the Task 150 technology combustor, and the Task 200 generic combustor. However, there is much still to be understood in the generic combustor behavior. This complicated behavior will serve as a serious challenge when testing the efficacy of lean blowout modeling.

The blowout data can, in general, be successfully correlated by the combustor loading parameter based on the well-stirred reactor approach. However, as a result of the various flow aspects, a universal correlation did not result. This was not unexpected. Given the strong effects of the combustor geometric variables on burning zone flow patterns, a simple phenomenological correlation of experimental data is most unlikely ever to be general enough to form a unique design curve for lean blowout stability margin. The behavior of the correlated data in Fig. 18 confirms that for modeling purposes, the classical representation (Bragg, 1953) of a practical combustor as a single W.S.R. followed by a single plug-flow reactor, does not result in an adequate description of the combustion behavior during lean blowout. For this reason, it is essential to develop successful modeling techniques for lean blowout.

Lean blowout is a process that is dominated by chemical reaction effects. The use of well-stirred reactor modeling does allow a convenient introduction of full chemistry, whereas the cost of this is prohibitive with a CFD code. The efficacy of the W.S.R. approach depends on how well the chosen reactor network that must replace the classical description of a single W.S.R., represents the real combustor under consideration. The CFD calculation itself (with rudimentary chemistry at best) can be used to establish this network (Sturgess *et al.*, 1991a). The influences of turbulence on chemical reaction rates are still unaccounted for, even with this procedure. Although it is possible in principle to extend the method to allow for unmixedness, using stochastic methods, this has not yet been done.

CONCLUSIONS

1. Experimental LBO data have been provided for a generic gas turbine combustor over wide ranges of operating conditions and can serve to test modeling of the lean blowout process.

2. The lean blowout behavior of the generic gas turbine combustor is much more complicated than had been suspected and would not have been understood without direct visual access to the flame structure. According to operating conditions, quasi-staging and flame structure changes were exhibited.

3. A universal correlation of LBO data, using a well-stirred reactor loading group, was not obtained when the major variables were confined to total air mass flow rate, primary zone air flow split, and operating pressure. Simple phenomenological correlations of experimental blowout data are not likely to be good enough to serve as design tools for stability margin in a gas turbine combustor. Some form of blowout modeling will be necessary for this purpose.

4. The classic representation of a gas turbine combustor, as consisting of a single well-stirred reactor followed by a plug-flow reactor, is not sufficient to represent LBO behavior. If stirred reactor modeling of LBO is to be used, it must consist of a reactor network capable of adequately representing the flow field and fuel distributions, and their changes with operating conditions.

ACKNOWLEDGEMENTS

The authors wish to acknowledge the contributions to this work from their colleagues at Wright-Patterson Air Force Base and Pratt & Whitney. The enthusiasm, encouragement and support of Dr. W. M. Roquemore of Wright Laboratories has been particularly appreciated. Thanks also to Mr. Brian Knight of United Technologies Research Center who did the basic design work on the rig and who provided much help with operating procedures, and to Dr. David G. Sloan of Pratt & Whitney who conducted the fuel injector and combustor effective area measurements. Mr. Irwin Segalman of Pratt & Whitney kindly arranged for engine hardware for this program. The work was supported by the U.S. Air Force Wright Laboratories, under Contract No. F33615-87-C-2822 to Pratt & Whitney, East Hartford, Connecticut. The authors thank Pratt & Whitney Engineering for permission to publish these results.

REFERENCES

Bragg, S. L., 1953, "Application of Reaction Rate Theory to Combustion Chamber Analysis," Aeronautical Research Council Pub. ARC 16170, London.

Heneghan, S. P., Vangsness, M. D., Ballal, D. R., Lesmerises, A. L. and Sturgess, G. J., 1990, "Acoustic Characteristics of a Research Step Combustor," AIAA Paper No. AIAA-90-1851, presented at AIAA/SAE/ASME/ASEE 26th. Joint Propulsion Conference, Orlando, Florida (to appear in the *Journal of Propulsion*).

Jeffs, R. A., 1962, "The Flame Stability and Heat Release Rates of Some Can-Type Combustion Chambers," *Eighth Symposium (International) on Combustion*, Williams and Wilkins, Baltimore, pp. 1014-1027.

Kretschmer, D. and Odgers, J., 1972, "Modeling of Gas Turbine Combustors – A Convenient Reaction Rate Expression," Trans. ASME, *J. Energy Power*, pp. 173-180.

Lefebvre, A. H., 1983, Gas Turbine Combustion, Hemisphere Publishing Co., McGraw-Hill.

Lewis, B. and von Elbe, G., 1987, Combustion, Flames and Explosion of Gases, 3rd. Edition, Academic Press.

Longwell, J. P., Frost, E. E. and Weiss, M. A., 1953, "Flame Stability in Bluff-Body Recirculation Zones," Ind. Eng. Chem., Vol. 45, No. 8, pp. 1629-1633.

Roquemore, W. M., Reddy, V. K., Hedman, P. O., Post, M. E., Chen, T. H., Goss, L. P., Trump, D., Vilimpoc, V. and Sturgess, G. J., 1991, "Experimental and Theoretical Studies in a Gas-Fueled Research Combustor," AIAA Paper No. AIAA-91-0639, presented at the 29th. Aerospace Sciences Meeting, Reno, Nevada.

Stewart, D. G., 1956, *Selected Combustion Problems II*, AGARD/NATO, Butterworths, London, pp. 384-413.

Sturgess, G. J., Sloan, D. G., Lesmerises, A. L., Heneghan, S. P. and Ballal, D. R., 1990, "Design and Development of a Research Combustor for Lean Blowout Studies," ASME Paper No. 90-GT-143, presented at the Gas Turbine and Aeroengine Congress and Exposition, Brussels, Belgium. (Also, ASME *Journal of Engineering for Gas Turbines and Power*, Vol. 114, 1992, pp. 13-19.)

Sturgess, G. J., Sloan, D. G., Roquemore, W. M., Reddy, V. K., Shouse, D., Lesmerises, A. L., Ballal, D. R., Heneghan, S. P., Vangsness, M. D. and Hedman, P. O., 1991a, "Flame Stability and Lean Blowout – A Research Program Progress Report," Proc. 10th. ISABE, Nottingham, England, pp. 372-384.

Sturgess, G. J., Heneghan, S. P., Vangsness, M. D., Ballal, D. R. and Lesmerises, A. L., 1991b, "Isothermal Flow Fields in a Research Combustor for Lean Blowout Studies," ASME Paper No. 91-GT-37, presented at the Gas Turbine and Aeroengine Congress and Exposition, Orlando, Florida. (Also, ASME *Journal of Engineering for Gas Turbines and Power*, Vol. 114, 1992, pp. 435-444.)

Sturgess, G. J., Heneghan, S. P., Vangsness, M. D., Ballal, D. R. and Lesmerises, A. L., 1991c, "Lean Blowout in a Research Combustor at Simulated Low Pressures," ASME Paper No. 91-GT-359, presented at the Gas Turbine and Aeroengine Congress and Exposition, Orlando, Florida (to appear in Trans. ASME, *Journal of Engineering for Gas Turbines and Power*).

Sturgess, G. J., Heneghan, S. P., Vangsness, M. D., Ballal, D. R., Lesmerises, A. L. and Shouse, D., 1992a, "Effects of Back-Pressure in a Lean Blowout Research Combustor," ASME Paper No. 92-GT-81, presented at the Gas Turbine and Aeroengine Congress and Exposition, Cologne, Germany (to appear in Trans. ASME, *Journal of Engineering for Gas Turbines and Power*).

Sturgess, G. J., McKinney, R. and Morford, S., 1992b, "Modification of Combustor Stoichiometry Distribution for Reduced NOx Emission from Aircraft Engines," ASME Paper No. 92-GT-108, presented at the Gas Turbine and Aeroengine Congress and Exposition, Cologne, Germany (to appear in Trans. ASME, *Journal of Engineering for Gas Turbines and Power*).

THIS PAGE INTENTIONALLY LEFT BLANK

APPENDIX K

RELATION OF CARS TEMPERATURE FIELDS TO LEAN BLOWOUT PERFORMANCE IN AN AIRCRAFT GAS TURBINE GENERIC COMBUSTOR

By

G. Switzer
Systems Research Laboratories, Inc., Dayton ,Ohio

G.J. Sturgess and D.G. Sloan
Pratt & Whitney, East Hartford, Connecticut

D.T. Shouse
WL/POSF, Wright-Patterson Air Force Base, Ohio

Published as AIAA Paper No. AIAA-94-3271, June 1994.

AIAA 94-3271

Relation of CARS Temperature Fields to Lean Blowout Performance in an Aircraft Gas Turbine Generic Combustor

G. Switzer, Systems Research Labs., Inc., Dayton, OH
G. Sturgess, D. Sloan, Pratt & Whitney, East Hartford, CT
and D. Shouse, Wright Laboratory, Dayton, OH

30th AIAA/ASME/SAE/ASEE Joint Propulsion Conference
June 27-29, 1994 / Indianapolis, IN

For permission to copy or republish, contact the American Institute of Aeronautics and Astronautics
370 L'Enfant Promenade, S.W., Washington, D.C. 20024

RELATION OF CARS TEMPERATURE FIELDS TO LEAN BLOWOUT PERFORMANCE IN AN AIRCRAFT GAS TURBINE GENERIC COMBUSTOR

G.L. Switzer, Systems Research Laboratories, Inc., Dayton, Ohio,
G.J. Sturgess* Pratt & Whitney, East Hartford, Connecticut,
D.G. Sloan, Pratt & Whitney, East Hartford, Connecticut,+
D. Shouse, Wright Laboratory, Wright-Patterson Air Force Base, Ohio.

Abstract

A four-injector representation of a practical annular combustor has been made in planar configuration and tested. Although the desirable test matrix for full understanding and description of the lean blowout behavior of this combustor is large, sufficient has been accomplished to present a reasonably complete picture of this behavior. Phenomenological modeling has been used to order the data, and provided correlation of blowout equivalence ratios. Field information for the combustor has been provided through isothermal flow computational fluid dynamic calculations, and CARS temperature measurements in reacting flow. The pictures of the combustor behavior at blowout provided by these three approaches are complimentary, and are remarkably consistent.

Introduction

Combustion stability is extremely important in gas turbine engines for aircraft use. However, it is becoming increasingly more difficult to ensure that adequate stability margins are maintained in the future because of current design trends. These trends include enhanced fuel/air mixing, via better atomization of the liquid fuel in airblast-type injectors for improved temperature traverse quality, high temperature rise (increased fuel turndown ratio), and, low emissions combustors and their associated technologies. At the higher pressure, higher temperature operating conditions of current and projected engines, considerations of combustor durability demand minimum surface area designs, with consequent tendencies to reduce combustor volume. The potential stability difficulties due to these trends are exacerbated by the lack of a satisfactory and reliable *a priori* prediction procedure for lean blowouts.

The majority of the relevant published material on flame stability is for bluff-body flameholders of various types or, is for well-stirred reactors, as reviewed by Lefebvre[1]. The quantity of experimental data published in the open literature for practical gas turbine combustors is much less extensive, and systematic investigations are largely lacking, although some such work of limited scope for can-type combustors is reported by Jeffs[2] and Stewart[3]. Almost all of the information on the annular-type of combustor currently used for aircraft applications is confined to relatively inaccessible private company reports. The information that is available for practical combustors is expressed in global terms, and there are no detailed interior flowfield descriptions at near-blowout conditions. The large number of geometric and flow variables encountered makes rational comparison of data difficult.

In 1987 the U.S. Air Force Wright Laboratory, Aero Propulsion and Power Directorate (WL/PO), established the Combustor Design Model Evaluation (CDME) program, with the goal of improving physical modeling to facilitate design work. To address the developing stability concerns, the Air Force under the CDME effort, initiated a comprehensive joint Government, Industry and University research program aimed at improving the design and analysis capabilities for flame stability and lean blowout (LBO) in the combustors of aircraft gas turbine engines[4].

The intent of the stability research program is to investigate, understand, and model lean blowout in the context of combustors of aircraft gas turbine engines. The approach adopted in this program is a step-by-step one that moves from gaining an understanding of the basic flow behavior in, initially, a simplified environment, and then through progressively more realistic situations, leading to a simplified version

---

* Member, AIAA.
+ Current address: Asea Brown Boveri, Windsor, Connecticut.

of a real gas turbine combustor. In order to separate the effects of liquid fuel atomization and spray evaporation from the aerothermochemical effects, it was decided to approach the LBO problem in two distinct stages - initially, with gaseous fuels (propane and methane) and then, with liquid fuels (ethanol and JP8).

The experimental portion of the program utilizes three combustors as test vehicles to achieve the desired progression in flow complexity. These combustors consist of a research combustor[5], a technology-development combustor[6] and a generic gas turbine combustor[7].

The research combustor is simple in configuration, but nevertheless, contains the essential primary zone flow features of a practical gas turbine combustor. The technology combustor incorporates the practical fuel injectors of the generic combustor into the simplicity of the research combustor to permit study of their characteristics in isolation. The generic combustor is a geometrically-flexible, highly-controllable, yet simplified, four injector, planar version of an annular gas turbine combustor. Its purpose is to provide an experimental database against which lean blowout modeling of various types might be evaluated and calibrated.

All three combustors feature high optical access to permit direct flame observation and extensive use of laser diagnostic techniques. They operate at atmospheric pressure, and utilize an excess-nitrogen dilution technique[8] to simulate the effects of low combustion pressure on LBO, by slowing down chemical reaction rates.

Modeling of the LBO process follows several approaches[4]. Conventional phenomenological modeling was applied to the research combustor to derive a stability criterion, as was a computational fluid dynamics (CFD) approach using a finite rate chemistry model[9] and one[10] using the Eddy Dissipation Concept combustion model of Magnussen[11]. A hybrid method was applied to the generic combustor using conventional CFD with the Eddy Break-Up combustion model, to establish a well-stirred reactor network to represent the combustor flowfield, and upon which the detailed chemistry is solved[4]. In addition, CFD calculations of the generic combustor are being made using finite rate chemistry with a reduced mechanism for propane.

Some of the results from the research combustor are presented in References 8, 9, 10, 12, 13, 14, 15; limited results from the technology combustor are given in Reference 6, and limited results from the generic combustor are contained in Reference 7.

The more sophisticated the modeling that is used in a calculation procedure to describe a phenomenon, the more complex is the validation process necessary for that modeling. If the overall procedure utilizes a number of physical models, as does any CFD-based approach for example, it is not sufficient just to validate these models individually. The interactions of these models when working together must also be validated. Furthermore, given current computer and calculation grid limitations, it is essential that a comprehensive validation be made in a geometry similar to that of the intended application. Unfortunately, the number of suitable validation test cases for modern gas turbine combustor applications extant in the open literature is extremely limited; Reference 16 is a recent exception. Cases with operating parameters representative of lean blowout do not exist.

Contribution

The intended purpose of the generic gas turbine combustor is to provide an experimental database against which LBO modeling might be evaluated. In this context, a set of temperature measurements obtained in reacting flow with suitable operating conditions is presented, together with a description of the basic flow field in the combustor as obtained by CFD calculation. Together, these data are used to explain the measured LBO behavior of the generic combustor.

Generic Combustor Rig and Test Facility

The generic combustor rig design was selected to satisfy the following criteria: 1.) The combustor should represent current design practice. 2.) The combustor geometric boundary conditions should be simple so as to avoid introducing any grid restraints on calculation accuracy. 3.) The rig configuration should permit high optical access for flame visualization and application of laser diagnostics. 4.) The rig design should maximize geometric flexibility and operating condition controllability to permit extensive parametric studies of the major combustor design parameters.

The aerothermodynamic design of the base annular combustor was selected to follow present Pratt & Whitney design practice, and it utilized airblast-atomizing fuel injectors with integral air swirlers, together with "inside-out" recirculation[4, 5, 15]. The

basic design is embodied in an engine that is currently in regular airline service throughout the world. The configuration adopted for the rig was a four-injector, planar-section, simplified geometry version of this annular combustor design.

The fundamental rig design to accommodate the combustor configuration was carried out by United Technologies Research Center, with subsequent modifications made by Wright Laboratory at Wright-Patterson Air Force Base, Dayton, Ohio. These Air Force modifications were made to improve rig handling, optical access and window durability. The fuel injectors used were actual engine hardware, with sets modified, calibrated and individually balanced with Lee-Jets to flow gaseous or liquid fuels. Sets with two swirl strengths air swirlers were available. The replaceable sets of combustion liners contain patterns of flush, circular air ports to admit additional air into the combustor. The port patterns were based on engine experience. On the shroud-side of the liners were welded several longitudinal I-beams for structural stiffness at high metal temperatures.

The rig delivers separately-metered air supplies to the combustor dome and, the upper and lower shrouds that feed the liners. These supplies were isolated from each other by means of an upstream array of sonic venturis. The exits from the combustor and shrouds are throttled by independent water-cooled valves that control bypass flows. The shroud bypass flows are set to realistic values to result in correct air jet trajectories into the combustor; bypass flows also provide backside convective cooling of the liners. Excess nitrogen, when used for low pressure simulation, is introduced and mixed with the main air supply upstream of the sonic venturis.

Major optical access to the combustor volume is provided by sidewall windows of fused quartz. In additon, direct vertical access can be provided via a set of fused quartz liners containing the appropriate pattern of air ports.

Fig. 1 gives a cross-sectioned elevation of the rig, that shows the major features described. Complete details of the combustor and rig, including leading dimensions, are given in Ref. 7.

The rig was mounted horizontally in a test cell (Room 20) of Wright Laboratory. The cell provides metering and control of air, fuel (gaseous propane), excess (gaseous) nitrogen, and cooling water to the combustor rig; gaseous hydrogen and separate air for the combustor torch ignitor are also provided. The discharge from the rig enters an atmospheric pressure exhaust duct, and exits the facility to ambient conditions. Mounted under and on either side of the rig test section is a hardened CARS system. The facility is also described in more detail in Ref. 7.

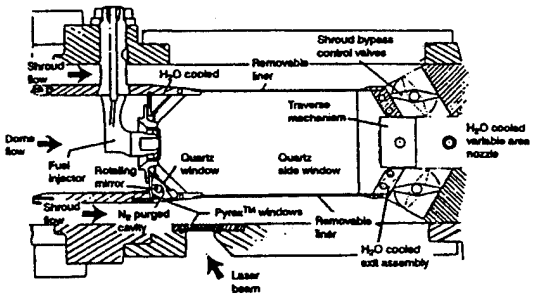

Fig. 1: Cross-section of the Generic Combustor

The planar configuration adopted for the combustor represents a compromise between realism and, optical access and simplicity. Jet flows into the rig combustor from the upper and lower shrouds via the liners will be into respective cross-sectional areas that are different from those of a real annular combustor due to the absence of wall circumferential curvatures. However, the rig upper and lower (planar) liners have identical hole sizes and patterns, just as they would have in the real outer and inner circular cross-section liners. Therefore, air jet penetration and jet lateral spreading will be slightly different in the rig from what they would be in the equivalent annular combustor. The resulting net blockage, and its radial distribution across the combustor height, for the gases exiting primary zones will also be different. This will exert some second order influence on flame stability, but, based on experience, this is not as serious for LBO as it is for some other aspects of combustor performance.

Lean Blowout Characteristics

The lean blowout characteristics of the generic combustor when operating on gaseous propane as fuel are described in Ref. 7. They are complex, and would have been difficult to understand with direct observations of flame behavior over the range of combustor loadings at which blowouts were obtained.

Combustor loading was set by air mass flow rate, (determining residence time) and the quantity of excess nitrogen that was introduced (determining the

simulated low pressure); air inlet temperature and combustor actual pressure were constant at ambient values. Blowouts were obtained by incrementally reducing fuel mass flow rate at fixed loading, with thermal stability being re-established after each successive fuel decrement. This was continued until flame extinction took place.

The equivalence ratios at LBO were correlated by a generalized form of the Kretschmer & Odgers[17] combustor loading parameter LP, defined in Ref. 7 as,

$$LP = \frac{\dot{m}_{Tot}}{VP^n F}$$

where,

$\dot{m}_{Tot} = \dot{m}_f + \dot{m}_a + \dot{m}_{N2}$ *lbm/sec.*

$\dot{m}_f$ = *fuel mass flow rate*

$\dot{m}_a$ = *air mass flow rat*

$\dot{m}_{N2}$ = *excess nitrogen mass flow rat*

V = *reactor volume*, ft^3

P = *combustion pressure, atmos.*

$n = 2\phi_{LBO} / (1 + \dot{m}_{N2} / \dot{m}_a)$
apparent global reaction order

$F = \frac{10^{0.001437}}{3.72}$ *(to correct to* $400K$*)*

T = *inlet temperature,* K

This definition of loading parameter derives from phenomenological modeling that considers the flame-holding region of the combustor as a well-stirred reactor[7]. It may be applied on a global basis to the whole combustor (including the redundancy of the dilution zone), or, to a local burning zone within the combustor.

Figure 2 illustrates the lean stability characteristic for a configuration where 10 percent of the total combustor airflow is introduced through the combustor dome. The dome airflow consists of the sum of fuel injector, insert swirler (a smoke-control device[18] surrounding each fuel injector and consisting of a ring of small circular ports each with a compound angle to the injector centerline), and dome cooling airflows[7]. The appropriate volume is here based on the total for the combustor, and the equivalence ratio at blowout is an overall one involving the total fuel flow and all of the combustor airflow. This is the usual definition for this quantity as used in combustor/engine development.

The LBO behavior shown in Fig. 2 exhibits an initial region of continuous but slow loss of stability at low and moderate values of combustor loading, followed at higher loadings (where values greater than 10 *lbm/sec.*($ft^3 atmos.^n$)are reached) by a region of discontinuous behavior, where there are sudden losses in stability followed by recoveries and subsequent losses. This saw-tooth pattern of behavior has a net loss of stability that becomes increasingly severe as loading increases. A condition of peak heat release rate is not reached in these results.

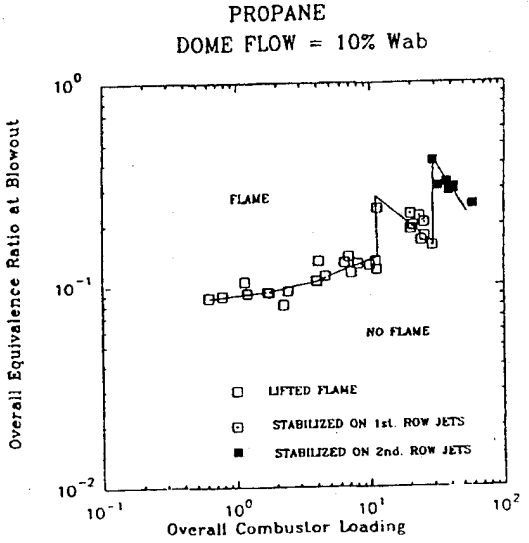

Fig. 2: Correlated LBO Data for 10% Dome Flow Combustor, Showing Different Flame Stabilization Modes

Flame observations confirmed conclusions based on estimates of local equivalence ratios, that up to a loading of 10 *lbm/sec.*($ft^3 atmos.^n$), flame was stabilized in the volume between the fuel injector discharges and the plane of the first row of combustion air jets, (commonly known as the "primary zone") and involved shear layer burning of fuel in the individual insert air jets surrounding each fuel injector. For the higher loadings (achieved by increasing excess nitrogen while essentially maintaining residence time through constant airflow), there can be insufficient oxygen to allow complete burning in this upstream position, so flame expands downstream to become anchored on the first tranverse row of combustion air jets. Eventually, at yet higher loadings achieved with additional excess nitrogen, the flame expands even further downstream to

become anchored on the second row of combustion air jets.

It is this progressive growth of the flame with increasing combustor loading, resulting in different methods and positions of flame holding, that gives the saw-tooth stability characteristic since the flame behavior as blowout is approached is different for each burning mode. LBO curves of this general character have been observed in other practical combustors, e.g. Ref. 4, where the reason for the behavior could only be speculated.

When the percentage of total combustor airflow introduced through the dome is increased, the saw-tooth stability behavior of overall LBO equivalence ratio is not encountered until much higher combustor loadings. This is because the local equivalence ratios in the primary zone do not approach unity until the higher loadings, by virtue of the additional dome air.

Figure 3 illustrates this behavior for 10 and 20 percent dome airflow combustor configurations. The term "burning zone" is now used to account for the expanding flame as equivalent pressure is reduced. Thus, "burning zone equivalence ratio" is based on the total fuel flow and the airflow associated with the axial extent of the visible flame in the combustor; the volume term in the loading parameter is determined similarly. The vertical dashed lines mark the appropriate equivalent pressures for each dome flow at which the primary zone reaches unity equivalence ratio. Values to the left of these lines represent equivalent pressures where the primary zone is over-rich, and the flame consequently extends beyond the primary zone.

The lines shown on the figure for 10 and 20 percent dome flows are curve fits to the data that are forced to intersect the combined (linear) data fit line at the respective values of equivalent pressure for which the primary zone equivalence ratio reaches unity. When the flame is anchored by the jets, the stability becomes independent of dome flow, as the correlated data show.

While the flame is stabilized in the primary zone, the effect of reducing pressure is to increase the burning zone blowout equivalence ratio. When the flame becomes stabilized on the transverse air jets, more air is involved even through fuel flow at blowout is increasing as pressure falls; therefore, the (extended) burning zone equivalence ratio at blowout falls.

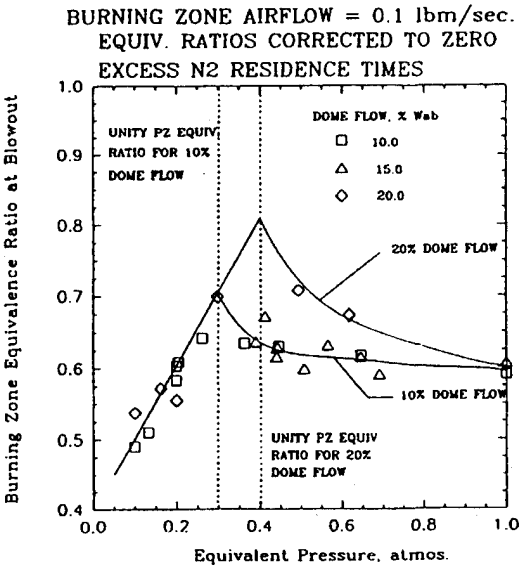

Fig. 3: Illustration of Change in Stability with Different Types of Flame Holding

The main flame structure in the primary zone for the 10 percent dome air configuration is characterized as being "lifted" for loadings less than $10\ lbm/\text{sec.}(ft^3 atmos.")$. A "lifted flame" was the normal operating mode, and was one where visual flame was distributed rather widely over the primary zone. It is associated with the flame being anchored in the shear layers associated with the individual insert swirler air jets surrounding each fuel injector.

At higher primary zone absolute airflows, and for lower primary zone equivalence ratios, the visual flame becomes distinctly attached in tight conical form to the fuel injectors. This is referred to as an "attached flame." Figure 4 illustrates the occurrence of this for the 15 percent dome flow combustor. In this condition there is sufficient air available for combustion to be associated with the shear layers formed between the swirling annulus of fuel introduced by the injector and the swirling air from the integral outer air swirler. As will be shown, the additional air comes from the first row of combustion air jets as well as the increased injector air. An attached flame condition is acoustically quieter than a lifted flame condition.

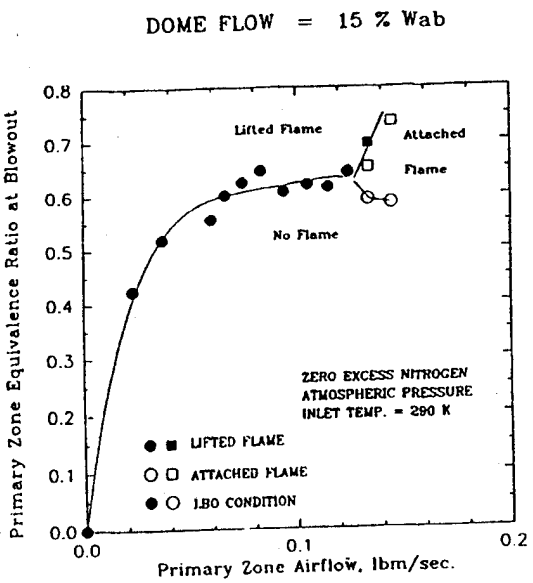

Fig. 4: Delineation of Lifted and Attached Flames at Atmospheric Pressure

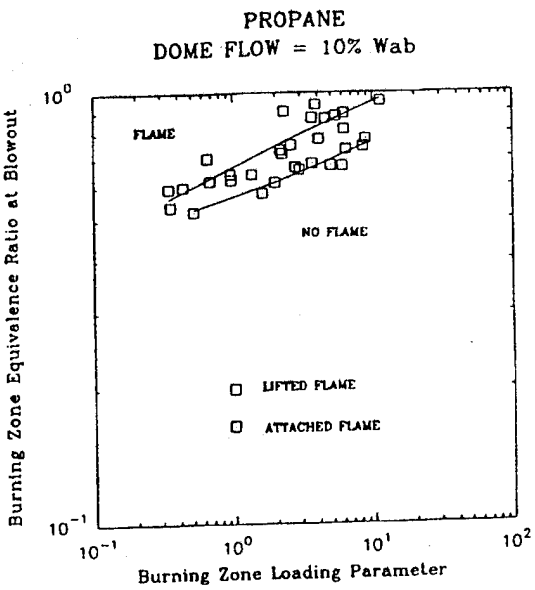

Fig. 5: Correlated LBO Data with Primary Zone Burning, Showing Improved Stability for Attached Flames

A given combustor loading in this rig can be obtained in two ways: 1.) low or zero excess nitrogen together with high airflow, or, 2.) low airflow together with high excess nitrogen. Therefore, at given combustor loading, the flame structure may be either lifted or attached, depending on how the loading is achieved. Therefore, since the flame holding can be different according to the flame structure, two stability curves at a given percentage dome flow are possible for primary zone-anchored flames. Fig. 5 demonstrates this for the 10 percent dome flow combustor, where it can be seen that the attached flame, in addition to being quieter, also has better stability than the lifted flame.

CFD Calculations of Flowfield

Direct observations of the flame structure and the LBO behavior described above and in Ref. 7, indicated that interactions of the swirling fuel/air jets issuing axially into the combustor from the fuel injectors with the transverse jets of combustion air introduced through the liners, are extremely important in this design of combustor. To better understand these interactions, computational fluid dynamics (CFD) calculations of the flow field were made.

The CFD calculations were made using the NASTAR[19] stationary-state solution computer code. The combustor configuration was represented as a (repeating) single fuel injector segment, to which periodic boundary conditions were applied on the lateral sides. The calculation domain was filled by a 109 x 53 x 49 (283,073 nodes) body-fitted grid; grid independent solutions are not claimed however, even with this nodal density. The operating conditions for the calculation were an air temperature of 304K and the combstor pressure was 14.31 psia. The combustor total airflow was 0.1716 lbm/sec., with flow splits of 15 percent dome flow, upper liner 42.41 percent and lower liner 42.56 percent. Liner flows were introduced as individual jets, according to the hole patterns and effective areas given in Ref. 7.

The calculation was made for isothermal flow to avoid questions concerning the suitability of various combustion models for these operating conditions. Air was the sole fluid used. This is considered as acceptable since the major flow features in the combustor will not be significantly modified by the heat release associated with combustion at near-blowout conditions.

Fig. 6 shows calculated iso-surfaces of mean axial velocity at fixed velocity of, for reference purposes, magnitude 1. This figure conveys a good three-dimensional impression of the flow field existing in the combustor. Immediately identifiable, from the front of the combustor, are the axial swirling jet from the

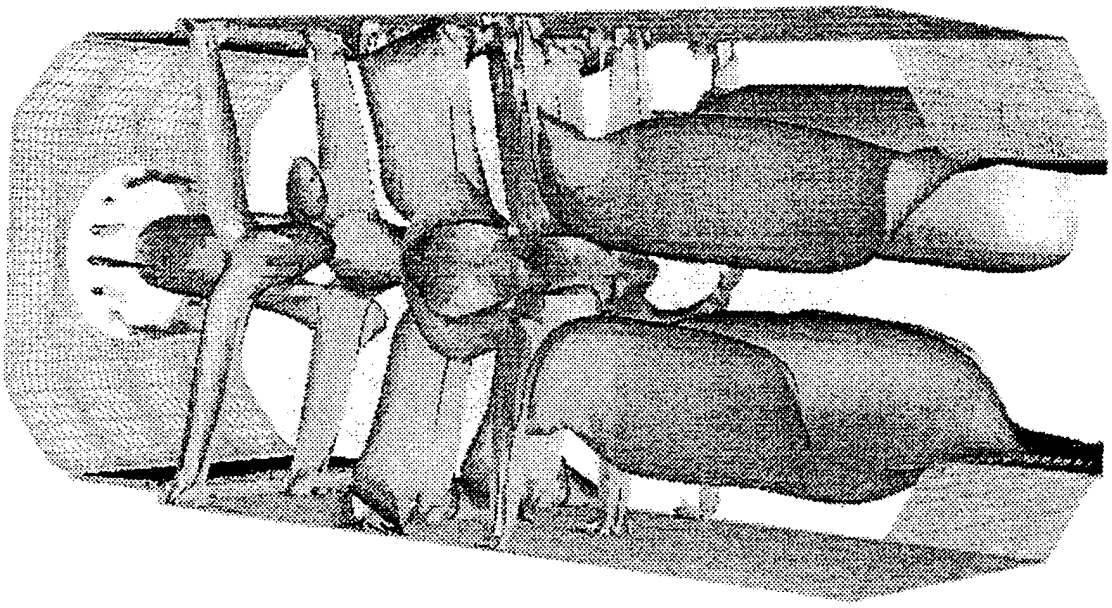

Fig. 6: Isothermal CFD Calculation with Iso-Surfaces of Mean Axial Velocity at Level 1 Magnitude, Showing Swirling Jet from Fuel Injector with Lobate Formation at First Row Combustion Air Jets

airblast fuel injector, the individual insert swirler jets (surrounding the fuel injector and with zero relative swirl in this instance, and zero angle relative to the injector discharge centerline), the first row of combustion air jets as opposed pairs on either side of, and inline with, the fuel injector jet, the second row of liner air jets as larger diameter, opposed pairs that are laterally disposed between the first row jets, and so on, along the combustor. Note that the effects of shroud bypass flows on liner jet initial angles are accounted for in the calculation (as a boundary condition, calculated separately from phenomenological modeling). The spent dome impingement cooling air is discharged axially as a liner cooling film at the upper and lower liner/dome interfaces.

The insert swirler jets act to prevent the weakly-swirling jet leaving the fuel injector from spreading much radially. It can be seen that the first row air jets penetrate to the combustor horizontal centerline before completing their turn to flow axially downstream.

The lateral spreading of the combustion air jets resulting from their high penetration and resulting collision can be seen in Fig. 7, where Level 2 velocity is less than Level 1 velocity in Fig. 6. The view in Fig. 7 is from the top of the combustor, with the upper liner removed for clarity. As in Fig. 6, the bounds of the calculation domain that are physical wall are shown by means of the calculation grid projected onto these surfaces.

The consequential blockage to primary zone flow represented by the colliding combustion air jets causes the coherent swirling jet from the airblast fuel injector to divide into two, diagonally-opposed lobes in order to escape from the combustor primary zone. The asymetric splitting of the fuel injector jet into two lobes is due to the swirl velocity component that this jet contains.

Figs. 8 and 9 respectively show contour plots of mean axial velocities on vertical planes inline with, and between, the fuel injectors; the plots reveal the regions of flow reversal (shown as hatched areas).

Note that the blockage of the pair of combustion air jets inline with the injector produces reverse flow in the center of the fuel injector jet as it begins to split into lobes, and that this causes diagonally-opposed lateral flows of combined combustion jet air and injector fluid into the regions between fuel injectors. Thus, the major recirculation zones are between injectors, with smaller recirculation zones in the injector plane that are placed

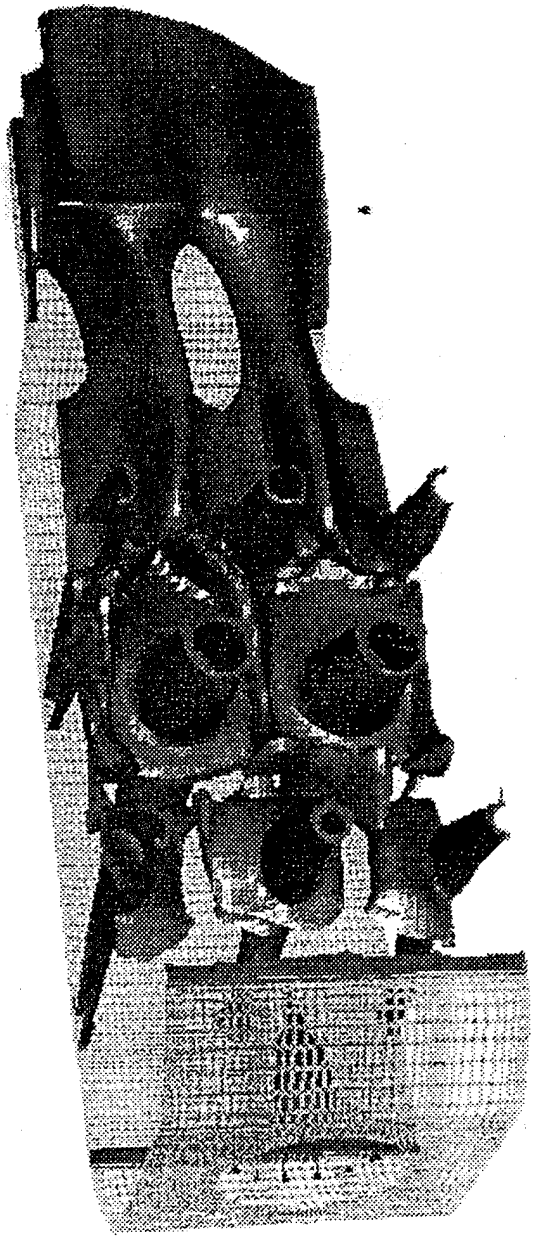

Fig. 7: Vertical View of Isothermal CFD Calculation with Iso-Surfaces of Mean Axial Velocity at Level 2 Magnitude, Showing Lateral Spreading of Colliding Transverse Combustion Air Jets

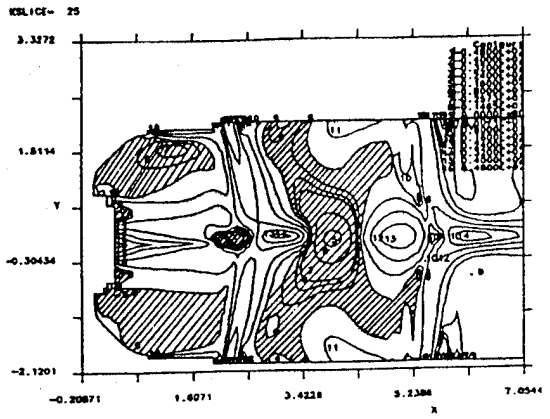

Fig. 8: Section Through Fuel Injector with Calculated Iso-Vels of Mean Axial Velocities Showing Reverse Flow Regions

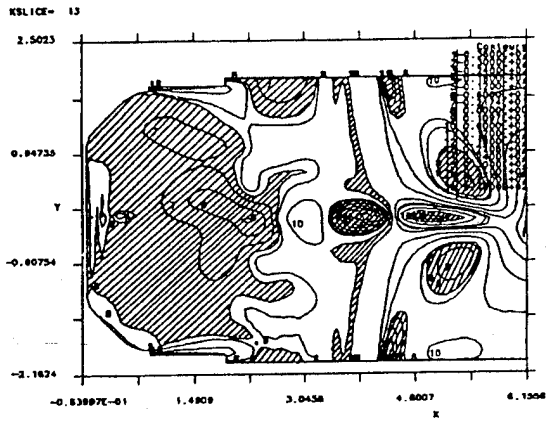

Fig. 9: Section Out of Fuel Injector Plane with Iso-Vels of Calculated Mean Axial Velocities, Showing Reverse Flow Regions

radially about the injector jets, outboard of the insert swirler jets. Further regions of reverse flow exist in the wake structures downstream of the first row combustion air jets and, upstream and downstream of the second row of combustion air jets.

The isothermal flow CFD calculations confirm that the swirling jet of fluid from the fuel injector is closely coupled with the first row of opposed combustion air jets. The swirling jets from the fuel injectors are sufficiently confined by their surrounding insert swirler air jets that fuel does not have much opportunity for spreading radially prior to reaching the combustion air jets. The combustion air jet system establishes ample

regions of reverse flow to provide jet flameholding if supplied with suitable fuel/air mixture.

Test Conditions for Temperature Measurements

As indicated above, the normal operating mode of the combustor was a lifted flame. However, the attached flame was interesting because of its quiet operation and improved stability (Fig. 5). It was therefore decided to make the temperature measurements to also include this condition.

The more typical engine combustor dome flow was the 15 percent case, so this was selected for the temperature measurements. Fig. 4 was used to determine the attached flame operating point. The total combustor airflow (all four injectors) was 0.7383 lbm/sec., with a primary zone airflow of 0.1422 lbm/sec. (see Ref. 7 for detailed calculation information); there was no excess nitrogen used, and the fuel was gaseous propane. The normal lifted flame became an attached flame at 0.69 primary zone equivalence ratio, and the combustor blew out for this airflow at just less than 0.60 equivalence ratio. Measurements were taken for a propane flow rate of 0.35 lbm/min. The combustor loading for these conditions was a low one so that the attached flame holding is confined to the primary zone.

CARS System

Temperature measurements in the combustor were performed using Coherent Anti-Stokes Raman Spectroscopy (CARS); the CARS system is described in detail by Switzer & Goss[20]. It is based on a frequency-doubled Nd:YAG laser that provides 8 nano-second pulses at 532 nano-meters wavelength with a repetition rate of 10 hertz, and, a broadband dye laser that is tuned to the Stokes vibrational frequency of the nitrogen molecule. The system is configured to employ a folded BOXCARS optical geometry[21] with a 50 cm focal length focussing lens. This combination yields a sampled spatial probe volume of about 1 mm^3, with the CARS information being generated within a path-length of 2 mm. The anti-Stokes signal produced within the probe volume is collected and directed into a spectrometer where its spectral content is dispersed; signal detection is then accomplished with a gate-diode array detector which allows single-shot temperature determination from the Q-branch spectrum of nitrogen.

The accuracy of the CARS temperature determination made in this manner is estimated to range between 10 percent at near-room temperatures and 5 percent at near-stoichiometric flame temperatures, with the largest contribution to uncertainty resulting from shot-to-shot variation in the Stokes-laser spectral distribution.

Four important combustion-diagnostic parameters are determined from the CARS data. Temperature means, fluctuations about the mean, probability distribution functions (pdf's), and the ratio of standard deviation of the distribution of temperature to the mean temperature, were obtained from instantaneous temperatures obtained in populations ranging from 1250 to 2000 at each measurement location.

Data repeatability is a difficult issue to resolve satisfactorily. It takes considerable elapsed time to acquire adequate data for extensive mapping. In this situation, repeatability is not determined by the CARS system, but by the constancy of the combustor air and fuel flows, and the precision with which a selected operating condition can be set and held. Both the fuel and air flows are continuously monitored and are electronically controlled to within 5 percent.

Measurement Considerations

The most desirable region to take detailed field measurements in this planar combustor is about the rig centerline, i.e. with two injectors on either side. This would result in minimum effect on the data due to the unwanted presence of the rig side-walls. However, use of this central region would necessitate that the laser beams traverse the maximum width of the combustor. Initial measurements made along this path, as feared, gave unreliable results because of insufficient CARS signal strength. The lack of signal was found to be the result of turbulent beam-steering as the laser beams passed through the flows associated with the near-pair of fuel injectors. The beam-steering was sufficient to prevent the essential overlap of the CARS pump and Stokes beams, (Fig. 10).

This problem was avoided in subsequent measurements by defining a measurement grid that extended through the first and second near-pair of injectors, and terminated at the line of local symmetry between the second and third injectors. This assumes that the flow field is identical on either side of this line of symmetry. It also supposes that data from the first injector, nearest to the side-wall, might have to be rejected due to side-wall effects. This indeed was found to be the case.

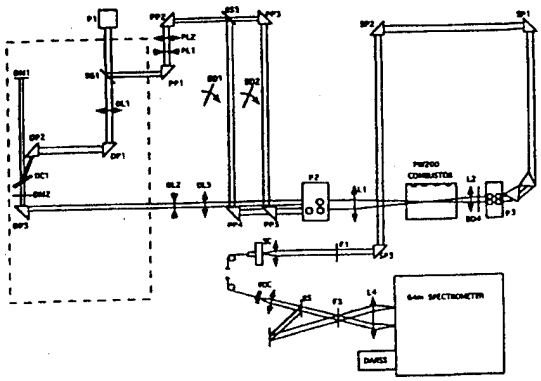

Fig. 10: Layout of CARS Optical Path in BOXCARS Configuration

A further consideration that influenced the determination of the measurement grid locations was the potential for damage to the optical windows by the laser beams. Initially, holes were burned in the combustor windows by the beams. To ensure that the high intensity laser beam focus would be a safe distance from the admitting windows, the sample region was restricted to a maximum distance of 11 cm from the combustor symmetry line, towards the sidewall.

With these two constraints to the possible measurement grid, a horizontal plane through the centerline of all four injectors (y = 0 cm) was selected. This plane extended transversely across the combustor from the axis of symmetry (x = 0 cm) to 11 cm towards the near-side combustor wall. It extended axially (z axis) from 1 - 15 cm downstream from the combustor dome. This area was covered with a 1 cm square measurement grid. An additional, smaller, transverse grid was applied normal to the horizontal grid at z = 5 cm, approximating the position of the first row of combustion air jets. The width of this vertical plane extended from x = 0 cm to x = 7 cm; thus, the second fuel injector centerline was located near its center. Again, a 1 cm square grid covered the region of this plane for 3 cm above and below the horizontal plane.

A caution is appropriate. As was unfortunately learned, the focussed laser beams contained sufficient energy to serve as an ignition source for flammable mixture in the combustor. Attention is necessary therefore, in sequencing purging system on shut-down, laser beam aligning, and start-up procedures, when attempting such measurements!

Temperature Fields

It was found that the major effect of the rig side-walls on the flow and temperature fields in the combustor was through their effects on the shroud flows. The combination of the structural-support I-beams on the shroud-sides of the liners, and the presence of the rig side-walls, reduced the local velocities in the shroud flows near the walls significantly from the mean values. This in turn increased the initial trajectory angles of all the combustion and dilution air jets nearest to the walls. For example, on the combustor horizontal center-plane, the center of the first row air jet is only displaced downstream by one port diameter, compared to three to four port diameters for the jets away from the side-walls.

In the primary zone, the steeper angles of the first row air jets near the side-walls resulted in the reverse flow region at the impact plane of these jets (Fig. 8) exerting more influence on the axial jets of fuel/air mixture from the fuel injectors (Nos. 1 and 4) nearest the side-walls. The lobe formation (Fig. 6) takes place earlier, and is more effective in recirculating combustion jet air forward into the fuel injector jet. Consequently, the combustion region of highest temperatures (1500K) is pushed upstream, well inside the swirling fuel/air jet. In turn, this increases the temperature of the hot gases recirculated back to the combustor dome between injectors number 1 and 2, and, 4 and 3. The temperatures at the dome are about 1250K versus 1150-1200K between injectors 2 and 3.

With the spurious, side-wall affected, data removed from consideration, only the field between the centers of injectors 2 and 3 can be considered as being reasonably representative of the real combustor. Discussion of the temperature field is therefore confined to this region of measurements only.

Fig. 11 shows the measured mean isotherms on the horizontal (on the left of the figure) and vertical (on the right of the figure) cross-sectional planes, placed with

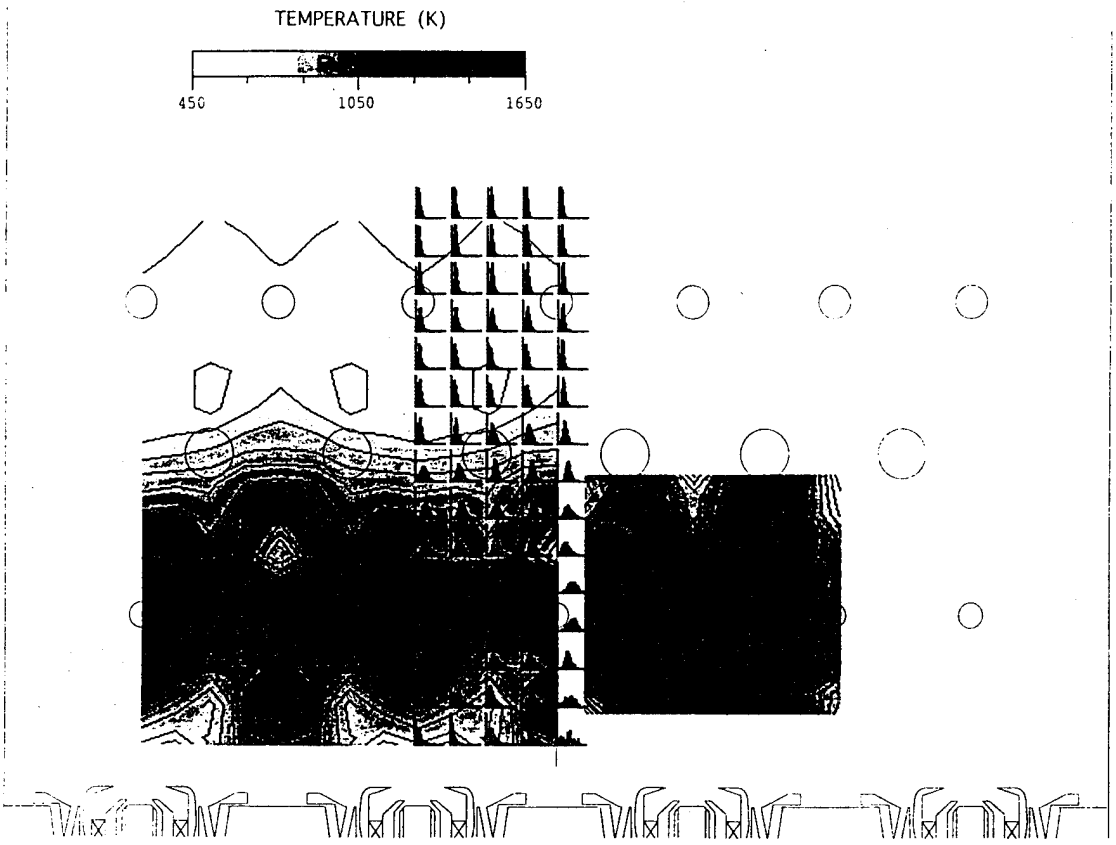

Fig. 11: Isotherms Representing Measured Mean Temperatures on Central Horizontal Plane and a Vertical Plane 5 cm Downstream, Together with PDF's for the Horizontal Plane Temperatures

the horizontal center of the vertical plane at its correct downstream position (just downstream of the first row of air jets) and the vertical center correctly aligned with an injector centerline. The vertical plane is viewed from the rear of the combustor. Super-imposed on the horizontal plane are the temperature pdf's at each measurement point in the plane. Note that the measured data in the horizontal plane for the right-hand side of injector No. 2 have been flipped to the left-hand side also. The symmetrical image so-formed makes it easier to understand the temperature field for a single, representative injector. While this is convenient, it should be remembered that the effects of swirl introduce some asymmetries in reality. For this particular set of fuel injectors the effective swirl strength is low, so that any asymmetries would not be especially large. The data in the vertical plane are not flipped.

On the horizontal plane the peak gas temperatures of around 1500K are reached inline with the fuel injectors at 5 - 6 cm downstream, and are clearly associated with the region of recirculating flow (Fig. 8) in the center of the combustor just upstream of the colliding opposed jets of the first row combustion air.

In the vertical plane one of the diagonally-opposed lobes (Fig. 6) formed by the splitting fuel injector jet can be identified as being a region of high temperature (about 1350 - 1400K). Regions of high temperature (about 1300K) move laterally at mid-

combustor height following the spreading due to jet impact (Fig. 7). It should be noted that, inline with the injectors, the penetration of the lower combustion air jet is not so evident as that for the upper air jet in this (z = 5 cm) plane. This indicates different jet penetrations, top to bottom of the combustor. It can also be observed that between injectors both combustion air jets can be seen at this plane, but again, the lower jet appears to have lesser penetration than the upper one.

Note the downstream displacement of temperature events on the central horizontal plane at the position of the first row of air ports due to the initial jet trajectory angles not being normal to the liner surfaces. The hot gases moved laterally from inline with the injectors enter the reverse flow region between injectors, (Figs. 11, 6 and 9), and, are mixed with jet air and recirculated back upstream to the combustor dome at temperatures about 1150 - 1200K.

Temperatures downstream of the first row of combustion air jets are fairly uniform on the central horizontal plane at 1000 - 1200K, until the second row of combustion air jets is encountered. Combustion is essentially over on the center plane when the second row of combustion air jets is added, with temperatures falling to less than 800K. This is the dilution zone of the combustor, and was referred to earlier in connection with the definition of loading parameter, as "redundant" at LBO conditions. The reason for this description is now apparent. At higher values of combustor loading, when the flame region expands beyond the primary zone, some of this redundancy is lost.

The flow from the injectors is initially cold at inlet temperatures. Temperature increases radially outwards from the injector centerlines as the insert swirler jets entrain the hot gases recirculated to the dome from downstream. By 2 cm downstream the local temperatures in these jets is about 750 - 800K. By 2 - 3 cm downstream, temperature rise is evident on the centerline of the jets issuing from the fuel injectors. This is clearly induced by the lobe-splitting of this jet due to the central reverse flow from the first row combustion air jets, and does not propagate from the peripheral shear layers associated with the insert swirler jets.

At the conditions for this test the equivalence ratio of the flow emerging from the fuel injector is 1.488, and with account of all the insert swirler air it would fall to 1.159. All of the insert air could not be involved in any case, so the additional air for combustion has to be provided by the reverse flow of combustion jet air. If this is so, then the reverse flow of combustion air penetrates forwards of the order of 2 - 3 cm on the centerline of the injector jet. It is most probably this penetration that gives the attached flame its conical shape, by introducing a radial velocity component into the injector jet. The CFD velocity vector results (not shown) confirm this.

The average of the mean temperature levels in the downstream regions of the measured horizontal field indicate that if they are typical of the complete exit plane from the combustor, then the upstream combustion efficiency is far from 100 percent. This is not too surprizing at these operating conditions.

Consideration of the temperature pdf's reveals behavior that is not unexpected. In the injector fuel/air jet region the probabilities are skewed towards the lower inlet temperature, with evidence of intermittency towards the jet edges. In the downstream region where the bulk of the heat release takes place, they are more symmetrical about the mean values. For the dome recirculation zones they show broadened peaks, indicating equal probabilities of a wide range of temperatures as poorly-mixed combustion products and unreacted combustion air and fuel are returned together towards the dome region by the reverse-flow velocities present. The isotherms confirm that chemical reaction does take place in this recirculating flow.

Note that the region where pdf's are shown represents the only side-to-side extent of this plane where the measured data are considered to be acceptable.

Fig. 12 shows the fluctuating temperatures, expressed as a local intensity. As might be expected, the highest temperature intensities, 40 - 50 percent, are encountered on the centerline of the fuel/air jet issuing from the injector, and in the flow recirculated back to the dome. Intensities in the insert jets are about 30 percent, rising to 36 - 38 percent in the lobes of the dividing fuel/air injector jet. In the reverse flow region immediately upstream of the first row of combustion air jets (where the highest mean temperatures are attained) the intensities are 30 percent or less. Downstream of the second row of combustion air jets the temperature fluctuations increase to give intensities of 32 - 36 percent, reflecting the mixing activity that might be anticipated from Figs. 8 and 9.

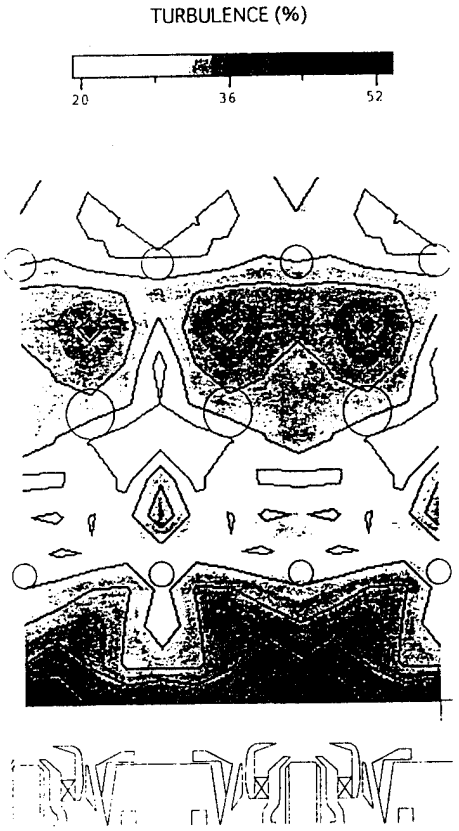

Fig. 12: Dimensionless Turbulent Fluctuations (RMS Values) of Temperature on the Central Horizontal Plane

Discussion

The conflicting difficulties of achieving a satisfactory benchmark test case in reacting flows for practical annular combustor geometries that have any pretence of reality, are well-demonstrated in the present work. A planar configuration is necessary to provide adequate optical access for the essential non-intrusive laser diagnostic probing. There are certain compromises that are inherent in making this configurational change to the combustor. In addition, the artificial side-walls so-introduced then perturb the flows near to them, and do so for significant distances normal to the walls, out into the reacting flowfield, causing non-typical behavior. To minimize this effect, a large number of fuel injectors pitches are necessary, four as a minimum with five being better. However, advantage of the increased combustor lateral dimension so obtained cannot be taken due to optical distrubances resulting from the extensive turbulent, reacting near-field through which the laser beams must then pass in order to reach the central, unperturbed flow region.

With due care, it is possible to obtain flow field measurements that are reasonably representative of real combustor flow (to the degree that a planar combustor can be considered to adequately represent an annular combustor). Such results can certainly be of value as a diagnostic in explaining aspects of combustor behavior. Their value as a database for evaluating combustion modeling in CFD codes remains to be established.

For the present combustor, three separate approaches have been used to describe one feature of its behavior: 1.) Phenomenological modeling to correlate LBO data, 2.) isothermal CFD analysis of an unperturbed segment of the flowfield at near-LBO conditions, and, 3.) CARS measurements of a narrow, but representative section of the temperatures in the reacting flow at near-LBO conditions. Each of the three approaches separately yields information that is remarkably consistent with that of the other two approaches. No single approach on its own provides an adequate picture of blowout. Taken together, the lean blowout behavior of the inside-out recirculation primary zone is extremely well described.

Many questions have been answered, but several more have been raised. For an example of the answers, the saw-tooth behavior (Fig. 2) of the lean stability loop as peak heat release rate is approached (seen in many combustors) is explained as a change in the flame holding mechanism as combustor loading increases above critical values. For just two examples of the new questions, how much air is recirculated back to the dome, and, what is the exact role of the insert swirler air jets in confining the fuel injector jet, and, in determining the coupling with the first row of combustion air jets?

It is apparent from the information presented for this combustor, that a simple, or even relative complex, phenomenological approach to modeling LBO in practical combustors is doomed to failure. The flow behavior even in the few geometric variations presented here and in Ref. 7, is far too complex to permit a useful generalized description to be obtained. Phenomenological modeling will only be useful with practical combustors for correlation of fairly wide-ranging experimental data sets for a particular combustor, or for a family of similar designs with only limited geometric variation. In this capacity

phenomenological modeling can make a useful contribution in combustor development of a particular design, and for small, incremental design or scale changes to an existing combustor configuration.

For an *a priori* design tool it is abundently clear that a CFD-based approach is necessary for LBO. Unfortunately, the combustion model required to make this realistic is a major stumbling block at this time; for example, see Ref. 10. Significant research is necessary in this area.

The aerodynamic and combustion close-coupling of the fuel/air jet from the fuel injectors with the first row of combustion air jets in this combustor illustrates why airblast-atomizing fuel injectors have to be designed in close co-operation with the engine companies, and developed in conjunction with the combustor. "Off-the-shelf" and "plug-in" fuel injectors of this type are now virtually items of the past.

The general primary zone characteristics revealed in this simplified gas turbine generic combustor can be related to the basic flow field established and studied in the research combustor7, and the fuel injector behavior studied separately in the technology combustor6, using more comprehensive diagnostics in both instances. The information gathered in the additional combustors greatly assisted in interpreting the present results.

The CARS temperature measurements confirm that the recirculated partially-mixed flow of hot combustion products and reactants back to the dome is important in providing flame stability. However, they reveal the major role played by the reverse flow of a small but important quantity of first row combustion jet air directly into the centers of the otherwise fuel-rich, swirling axial jets from the airblast fuel injectors. The blockage to the injector jets established by the colliding and laterally-spreading first row combustion air jets, then produces the necessary low velocity regions that allow flame-holding. It is the heat release associated with these flames that contributes enthalpy and chemically-active species to the between-injector dome recirculation, which results in further combustion in this dome region.

The action of the insert swirler individual jets in confining the mixture from the injector, increases the coupling of the injector flow to that of the first row combustion air jets.

Conclusions

1. Correlated experimental LBO data for a generic gas turbine combustor have been presented which show that the prime flame holding mechanism can change as the combustor loading increaes, to give a lean stability characteristic that becomes saw-tooth in shape as the condition of peak heat release rate is approached.

2. The primary zone flow behavior of the generic combustor, due to its basic design, is such that the discharges from the airblast fuel injectors are closely-coupled with the first row of combustion air jets, and this coupling dominates LBO for lower values of combustor loading.

3. The CFD results and CARS temperatures show that the close-coupling in the primary zone is due to excessive confinement of the discharge from the airblast fuel injectors by the surrounding insert-swirler air jets, and by the severe blockage produced by the penetration and lateral spreading of the first row of combustion air jets.

4. The difficulties of making laser-based measurements for benchmarking in a practical combustor configuration are severe, and limit the extent of the field for which reliable data can be obtained. The reliability itself is generally determined by the constancy of flows within the rig over the lengthy measurement times involved, rather than the behavior of the optical and electronic processing systems.

5. The best approach to generalized modeling or calculation of LBO lies in the CFD approach, although this will require combustion models that are beyond the current state-of-the-art.

Acknowledgements

The authors wish to acknowledge the contributions to this work from their collegues at Wright-Patterson Air Force Base and Pratt & Whitney. Special thanks are due to J.S. Stutrud and M. Russell at Wright Laboratory for support with the experimental work, and to A. Cheung at Pratt & Whitney for assistance in producing the manuscript. The enthusiasm, encouragement and support of Dr. W.M. Roquemore of Wright Laboratory has been particularly appreciated. The work was supported by the U.S. Air Force Wright Laboratory under Contract No. F33615-87-C-2822 to Pratt & Whitney, East Hartford, Connecticut, and Contract No. F33615-90-C-2033 to Systems Research Laboratories, Inc., (Division of Calspan), Dayton,

Ohio. The authors thank Pratt & Whitney for permission to publish these results.

References

1. Lefebvre, A.H., Gas Turbine Combustion, Hemisphere Publishing Co., McGraw-Hill Book Co., 1983.

2. Jeffs, R.A., "The Flame Stability and Heat Release Rates of Some Can-Type Combustion Chambers," Eighth Symposium (International) on Combustion, Williams and Wilkins, Baltimore, 1962, pp. 1014-1027.

3. Stewart, D.G., Selected Combustion Problems II, AGARD/NATO, Butterworths, London, 1956, pp. 384-413.

4. Sturgess, G.J., Sloan, D.G., Roquemore, W.M., Reddy, V.K., Shouse, D., Lesmerises, A.L., Ballal, D.R., Heneghan, S.P., Vangsness, M.D., and Hedman, P.O., "Flame Stability and Lean Blowout - A Research Program Progress Report," Proc. Tenth International Society on Air-Breathing Engines, Nottingham, England, 1991, pp. 372-384.

5. Sturgess, G.J., Sloan, D.G., Lesmerises, A.L., Heneghan, S.P., and Ballal, D.R., "Design and Development of a Research Combustor for Lean Blowout Studies," Trans. ASME, J. Engineering for Gas Turbines and Power, Vol. 114, 1992, pp. 13-19.

6. Hedman, P.O., Sturgess, G.J., Warren, D.L., Shouse, D., and Goss, L.P., "Observations of Flame Behavior from a Practical Fuel Injector Using Gaseous Fuel in a Technology Combustor," to be presented at ASME Intl. Turbo Expo '94, The Hague, The Netherlands, June, 1994.

7. Sturgess, G.J. and Shouse, D., "Lean Blowout Research in a Generic Gas Turbine Combustor with High Optical Access," ASME Paper No. 93-GT-332, presented at the ASME Intl. Turbo Expo '93, Cincinnati, Ohio, May 1993, (to appear in ASME Transactions).

8. Sturgess, G.J., Heneghan, S.P., Vangsness, M.D., Ballal, D.R. and Lesmerises, A.L., "Lean Blowout in a Research Combustor at Simulated Low Pressures," ASME Paper No. 91-GT-359, presented at the Gas Turbine and Aeroengine Congress and Exposition, Orlando, Florida, 1991.

9. Roquemore, W.M., Reddy, V.K., Hedman, P.O., Post, M.E., Chen, T.H., Goss, L.P., Trump, D., Vilimpoc, V. and Sturgess, G.J., "Experimental and Theoretical Studies in a Gas-Fueled Research Combustor," AIAA Paper No. AIAA-91-0639, 29th. Aerospace Sciences Meeting, Reno, Nevada, January 1991.

10. Sloan, D.G. and Sturgess, G.J., "Modeling of Local Extinction in Turbulent Flames," to be presented at ASME Intl. Turbo Expo '94, The Hague, The Netherlands, June 1994.

11. Magnussen, B.F., "Heat Transfer in Gas Turbine Combustors - A Discussion of Mathematical Modeling of Combustion, Heat and Mass Transfer with Emphasis on Heat Transfer in Gas Turbine Combustors," AGARD Conference Preprint No. 390, Heat Transfer and Cooling in Gas Turbines, Paper No. 23, 1985.

12. Heneghan, S.P., Vangsness, M.D., Ballal, D.R., Lesmerises, A.L. and Sturgess, G.J., "Acoustic Characteristics of a Research Step Combustor," AIAA Paper No. AIAA-90-1851, AIAA/SAE/ASME/ASEE 26th. Joint Propulsion Conference, Orlando, Florida, July 1990.

13. Sturgess, G.J., Heneghan, S.P., Vangsness, M.D., Ballal, D.R., and Lesmerises, A.L., "Isothermal Flow fields in a Research Combustor for Lean Blowout Studies," Trans. ASME, J. Engineering for Gas Turbines and Power, Vol. 114, 1992, pp. 435-444.

14. Sturgess, G.J., Heneghan, S.P., Vangsness, M.D., Ballal, D.R., Lesmerises, A.L. and Shouse, D., "Effects of Back-Pressure in a Lean Blowout Research Combustor," Trans. ASME, J. Engineering for Gas Turbines and Power, Vol. 115, No.3, 1993, pp. 486-498.

15. Ballal, D.R., Vangsness, M.D., Heneghan, S.P. and Sturgess, G.J., "Studies of Lean Blowout in a Research Combustor," AGARD Conference Proceedings No. 536, Fuels and Combustion Technology for Advanced Aircraft Engines,Section 23, September 1993.

16. Nikooj, M., Mongia, H.C., Sullivan, J.P. and Murthy, S.N.B., "Flow Interaction Experiment - Aerothermal Modeling II," Final Report, Vols. I and II, NASA Rept. CR-189192, November 1993.

17. Kretschmer, D. and J. Odgers, "Modeling of Gas Turbine Combustors - A Convenient Reaction Rate Expression," Trans. ASME, J. Energy Power, 1972, pp. 173-180.

18. Sturgess, G.J., McKinney, R. and Morford, S., "Modification of Combustor Stoichiometry Distribution for Reduced NOx Emissions from Aircraft Engines," Trans. ASME, J. Engineering for Gas Turbines and Power, Vol. 115, July 1993, pp. 570-580.

19. Rhie, C.M. and Stowers, S.T., "Numerical Analysis of Reacting Flows Using Finite Rate Chemistry Models," AIAA Paper No. AIAA-89-0459, 1989.

20. Switzer, G.L. and Goss, L.P., "A Hardened CARS System for Temperature and Species Concentration Measurements in a Practical Combustion Environment," Temperature: Its Measurement and Control in Science and Industry, Ed. J.F. Schooley, American Institute of Physics, New York, 1982, pp. 583-587.

21. Eckbreth, A.C., "BOXCARS: Crossed-Beam-Phase-Matched CARS Generation in Gases," Appli. Phys. Lett., Vol. 32, 1978, p. 421.

APPENDIX L

DEADSPACE MODELING

L–1.0: Introduction

In the PW100 combustor, application of the measured wall temperatures as a boundary condition to CFD calculations showed the existance of extremely severe radial temperature gradients at the wall and the step. These gradients suggested that wall–quenching of combustion reactions might be important in this combustor.

Close to an impervious surface the luminosity that is associated with visible flame does not extend completely to the surface. The intervening dark region is known as the deadspace. Deadspace is caused by quenching of chemical reactions due to heat losses to the wall and removal of active radicals, a sufficient quantity of which must be transferred ahead of the flame if propagation is to continue.

Several correlations for deadspace exist in the literature [L1.]; however, they are limited in scope and are inconvenient to use. Therefore, a suitable model was required for inclusion in the CFD modeling of the PW100 combustor. For this reason a simplified, more general correlation of wall deadspace for use in CFD analyses has been produced.

Since flame quenching affects flame propagation, quenching distances are frequently determined by the minimum tube size, or minimum distance between two parallel plates, at which a given fuel/air mixture will only just **not** flashback into the incoming mixture. The critical tube diameters and critical slit widths, the quenching distances, so determined are not the same, but are related by a fixed geometrical factor for given mixtures. Given the dependency on flame quenching, a reasonable definition of deadspace might seem to be one–half of the quenching distance as determined by the parallel plate method. Unfortunately, actual measurements show that deadspace is usually less than this distance. Although measurement of deadspace is complicated by uncertainties associated with defining the "edge" of the flame, it should not be unexpected that there are differences. This is because the measurement of quenching distances involves prevention of flame propagation, while the flame is still propagating for true deadspace determinations.

Unfortunately, there is not a large volume of experimental data available for true deadspace [L2.]; on the other hand, there is a large amount of information on quenching distance in the literature [L3.]. Therefore, for the present purposes, deadspace is taken as being one–half of the critical slit quenching distance. This is a conservative assumption. For the intended application this is not a serious supposition either, since in a CFD calculation it is grid distribution near the walls that will ultimately determine the achievable resolution of deadspace. This grid spacing at walls will frequently be greater than deadspace distances.

L–2.0: Data Analysis

Consider the temperature distribution in the gaseous fuel/air mixture layer near and flowing parallel to the combustor wall, as shown in Figure L–1. The temperature increases from T_w on the wall to T_b, the flame temperature, at distance L from the wall. The flame heat release rate is assumed to be so much greater than the heat transfer rate through the wall that the flame temperature may be taken as that of the adiabatic flame. The distance L consists of two elements: the reaction zone of thickness δ, and the deadspace d. The temperature increases through the deadspace as heat is conducted and diffused into it from the reaction zone, until the mixture temperature reaches a critical value. The critical temperature is a hypothetical ignition temperature T_i, for the mixture. After the ignition temperature is attained, the gas temperature increases rapidly in almost linear fashion to reach T_b.

A chemical ignition delay time τ, for the deadspace can be expressed in Arrhenius form, i.e.,

$$\tau = \frac{A \exp(\pm E / R T_i)}{P^n \quad \hat{A}} \qquad \text{L–1}$$

where: A = pre–exponential rate constant
E = activation energy
R = universal gas constant
n = apparent reaction order

If τ is written as d / S, where S is an appropriate propagation velocity,

$$dP^n = AS \exp(\pm E/R\ T_i)$$

or,

$$\ln(dP^n) = B + (\pm E / R T_i) \qquad \text{L–2}$$

In the deadspace, quenching reduces S to the local flow velocity V. In a boundary layer, $VR\ \ 0$ as the wall is approached, so

$$\ln(dP^n) R \pm E / R T_i \qquad \text{L–3}$$

For most hydrocarbons burning in air as lean mixtures, $T_i\ R\ T_b$ [L4]. Taking this condition results in the maximum reaction speed. Thus, for correlation of data for a given mixture,

$$dP^n = f(T_b) \qquad \text{L–4}$$

The reaction order n, would be expected to be around unity [L5.]. The temperature T_b is taken as the adiabatic flame temperature, and this was calculated from the equilibrium chemistry computer code EQLBRM [L6.].

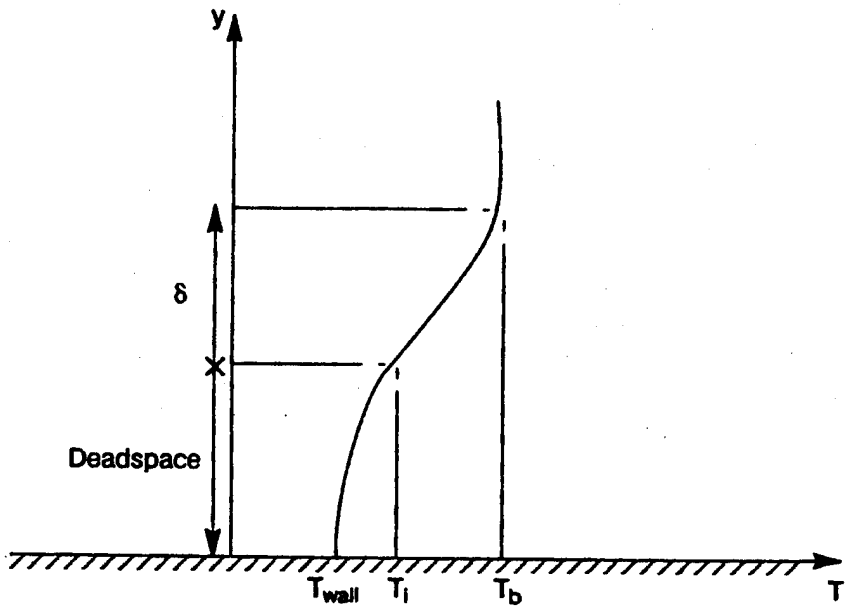

Figure L–1. Temperature Distribution for a Flame Near an Impermeable Wall

L–3.0: Experimental Data

In Reference L3 are contained narrow slit quenching data for propane/oxygen/nitrogen systems. The conditions covered are as follows:

(i) Propane/air at atmospheric pressure for inlet temperatures of 300–558K over equivalence ratios from 0.70–1.4.

(ii) Propane/air at 297K inlet temperature for pressures from 0.08–1.0 atm. over equivalence ratios from 0.7–1.4.

(iii) Stoichiometric mixtures of propane/oxygen/nitrogen with mole fractions of oxygen from 0.17 (excess nitrogen) to 0.70 (excess oxygen), at 300K inlet temperature, and pressures of 0.25 and 0.40 atm.

These data almost completely cover all the necessary conditions for the PW100 combustor.

In addition, there were quenching data at one atmosphere pressure and 373K inlet temperature for benzene, iso–octane and n–heptane/air mixtures over equivalence ratios from 0.7–1.7. These data were examined also to ascertain the generality of the propane data correlation.

For all cases, the deadspace was taken as equal to one–half of the measured quenching distance.

L–4.0: Results of Correlation Studies

For propane, the pressure dependency was determined from Data Set (ii) above. The apparent reaction order "n" was found to be 0.82, slightly less than the value of unity anticipated on the

basis of autoignition [L5]. Similar values are quoted in the literature [L3.]. Use of the adiabatic flame temperature for ignition temperature may account for some of the apparent reduction in reaction order. This is because there is a small pressure effect accounted for in the calculation of adiabatic flame temperature.

Figure L–2 shows the collected propane data correlated in the form indicated by Equation L–4. The higher values of flame temperature shown arise from Data Set (iii) for mixtures with excess oxygen. The exponential character of the correlation is obvious, with deadspace tending towards a constant value for very high flame temperatures. In Figure L–3, a blowup of Figure L–2 is shown for the PW200 combustor working region. The correlation for the collected data is seen to be most satisfactory. Note that Figures L–2 and L–3 both contain data for all the fuel–lean and fuel–rich propane mixtures measured.

The results at atmospheric pressure for the fuels other than propane are shown in Figure L–4. In this plot it can be seen that each fuel results in a distinct loop, i.e. the deadspaces at a given flame temperature depend on whether or not the mixture is fuel–rich or fuel–lean. This is unlike the propane behavior. For fuel–rich mixtures and for all three fuels, the deadspace is roughly constant at about 1.00 mm for flame temperatures from 2400 to 1800K, increasing slightly as temperature decreases. For the fuel–lean mixtures, deadspace decreases with increasing flame temperature at about the same rate as for propane, but is slightly different for each fuel.

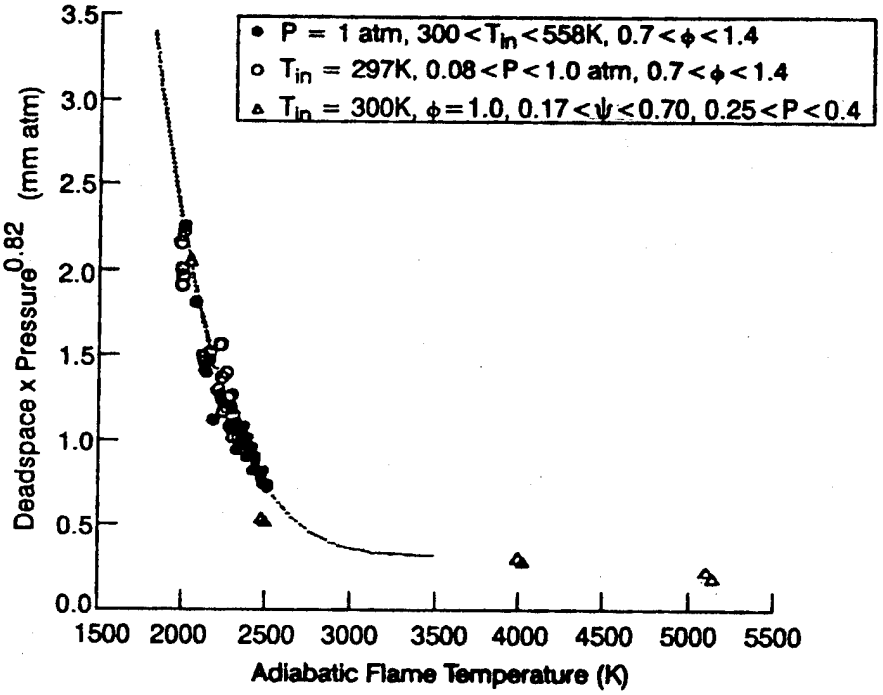

Figure L–2. Correlation of Deadspace Data for Propane Over a Wide Range of Operating Conditions for Propane/Oxygen/Nitrogen Systems

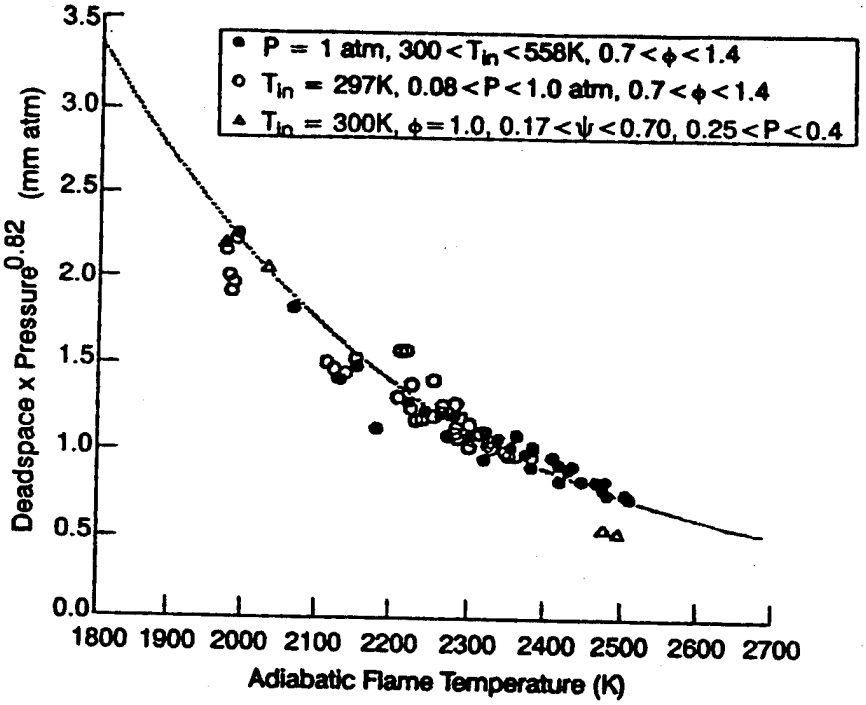

Figure L–3. **Enlargement of Figure L–2 for Variable Range of Interest in the PW1000 Combustor at Blowout**

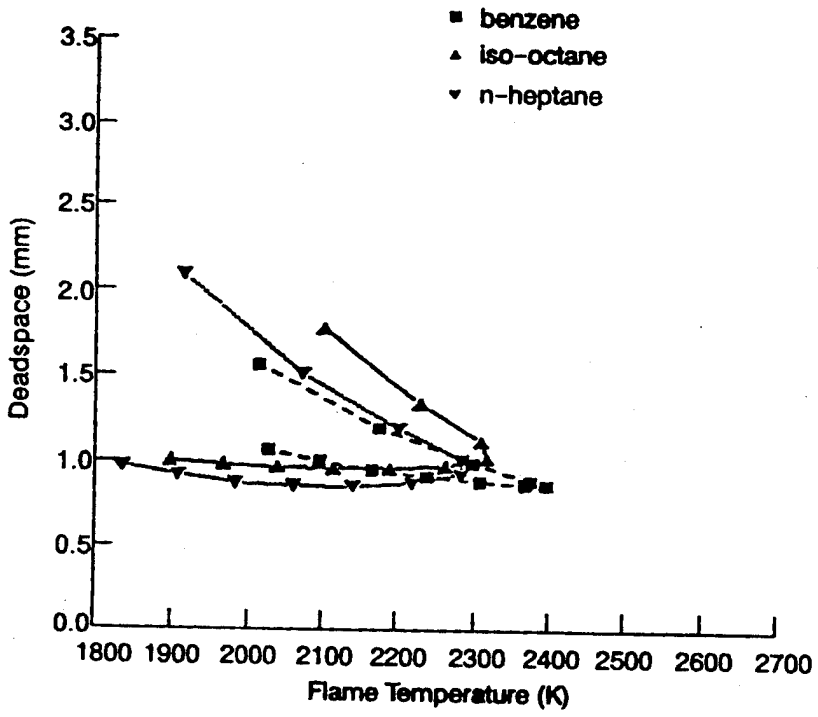

Figure L–4. **Reason for Failure of Simple Correlation for Several Fuels Other Than Propane, Burning in Air at Atmospheric Conditions**

L–5.0: Discussion of Results

The relationship used for correlating the experimental data, Equation L–4, is strictly for fuel–lean mixtures, and is specific for a given mixture. It should not be surprising therefore, that Figure L–4 is as it is. What is surprising is that Figures L–2 and L–3 show such good correlation of both fuel–rich and fuel–lean propane mixutres. The shapes of the adiabatic flame temparture curves are the same for each fuel (Figure L–5 at 300K initial temperature). The fuel–dependent difference lies in the shape of the curves for deadspace with equivalence ratio. For propane, this curve has the same symmetry with equivalence ratio as does flame temperature. For the other fuels, this symmetry does not exist. The implications of this observation follow from Equation L–3, i.e. the effective activation energies for deadspace are different for different hydrocarbon fuels, and the fuel–lean and fuel–rich mixtures of these fuels in air.

A more rigorous analysis of the experimental data is necessary to obtain a generalized plot for any hydrocarbon fuel. For each fuel, a plot of the logarithm of (dP^n) against the reciprocal of flame temperature (an Arrhenius plot) would enable the effective activation energy to be determined from the resulting straight line that could be drawn through the measured data. This would be required for rich and lean mixtures separately. Correlation of the collected data could then be attempted on the basis of Equation L–3.

Figure L–6 is an Arrhenius plot for the propane/air data at 300K inlet temperature and atmospheric pressure; both lean and rich points are shown. A very satisfactory straight line results, from which the effective activation energy was found to be 19.416 kcal/gmol. This can be compared with generally accepted values from the literature for the *combustion* of propane in air [L7.] of 27.8 kcal/gmol for lean mixtures and 26.592 kcal/gmol for rich mixtures. A similar plot for n–heptane is contained in Figure L–7, where it can be seen that separate straight lines do exist for the fuel–lean and fuel–rich region, just as was speculated. The appropriate effective activation energies were found to be 17.154 kcal/gmol and 4.671 kcal/gmol, respectively.

Lower activation energy values that are closer to the apparent 19.416 kcal/gmol found presently, have been reported for some of the chain reactions involved in proposed reaction mechanisms for the oxidation of propane, e.g. 15.0 kcal/gmol [L8.] for the reaction of CO with OH. Since the deadspace arises due to both thermal losses and active radical losses at the wall, the effective activation energy might well be related to that of the individual chain reaction steps that are broken by quenching. Stringer et. al. [L9.], in studies of autoignition of liquid fuel sprays in flowing systems at elevated pressures and temperatures, reported apparent activation energies for the ignition delay of lean mixtures of n–heptane of 14.189 kcal/gmol. This is close to the present value, but below that of 40 kcal/gmol given for stoichiometric mixtures of n–heptane in air in Reference L10.

When the individual rate constants for each fuel/air mixture are determined separately, through plots like Figures L–6 and L–7, the generalized plot shown in Figure L–8 can be drawn for lean mixtures in air at atmospheric pressure of n–heptane, iso–octane and benzene, and for rich and lean mixtures of propane in atmospheric pressure air. An excellent linear correlation results. The data are represented by the equation:

$$dP^{0.82} = 0.99872 \exp(E/R\,T_b + B) + 0.006173 \qquad \text{L–5}$$

with a correlation coefficient of 0.99925, and where d is the deadspace in ft., P is the pressure in lb_f / ft^2, T_b is the adiabatic flame temperature in K, and R is the universal gas constant, 1.986 $cal / gmol\ K$. The rate constants E and

B are related to hydrocarbon fuel type through the structure of the fuel molecule as represented by the number of carbon atoms it contains. Figure L–9 shows the dependency of the reduced rate constants ($E / E_{propane}$ and $B / B_{propane}$) on the fuel molecule. For propane, Figure L–6 yields,

$$E = 19.4166 \quad kcal / gmol$$

$$B = \pm 3.5641 \quad ft.lb_f / ft^2$$

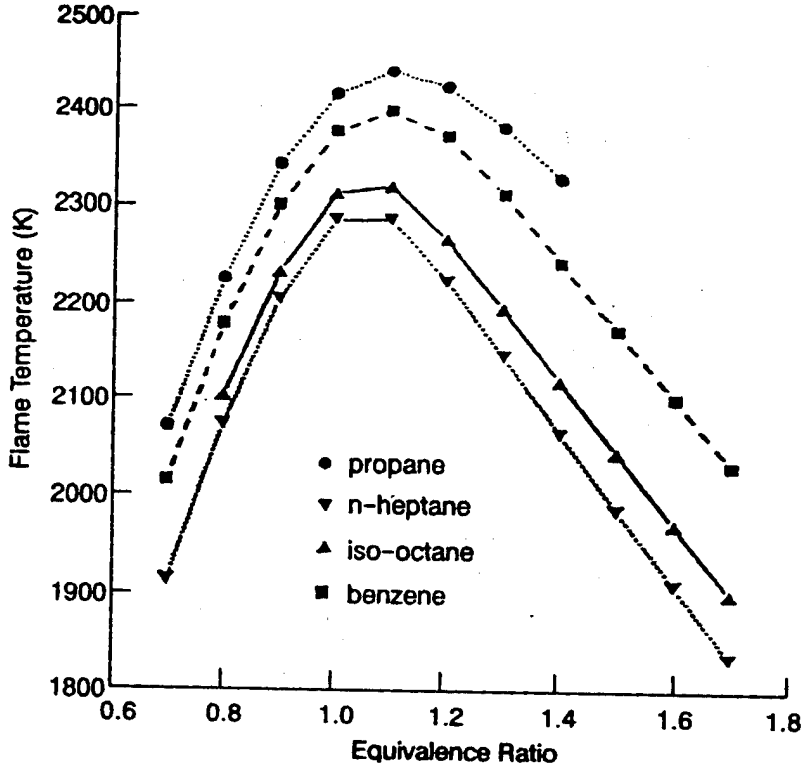

Figure L–5. Adiabatic Flame Temperatures at Atmospheric Pressure and 300K Inlet Temperature for Propane, n–Heptane, Iso–octane and Benzene In Air

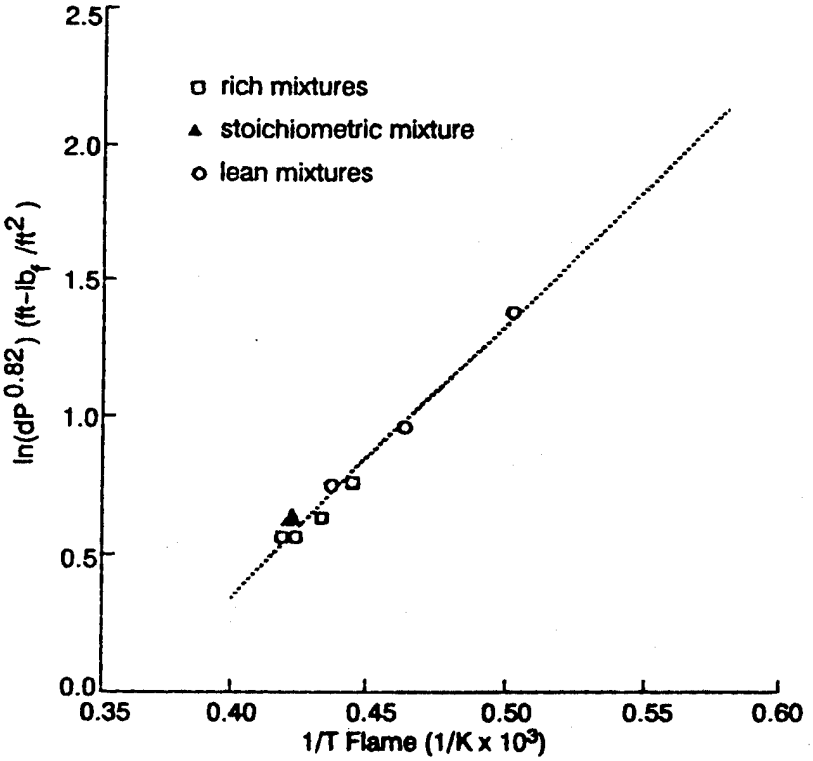

Figure L–6. Arrhenius Plot for Deadspace in Propane/Air Mixtures Burning at 300K Initial Temperature and Atmospheric Pressure (Rich and Lean Mixtures)

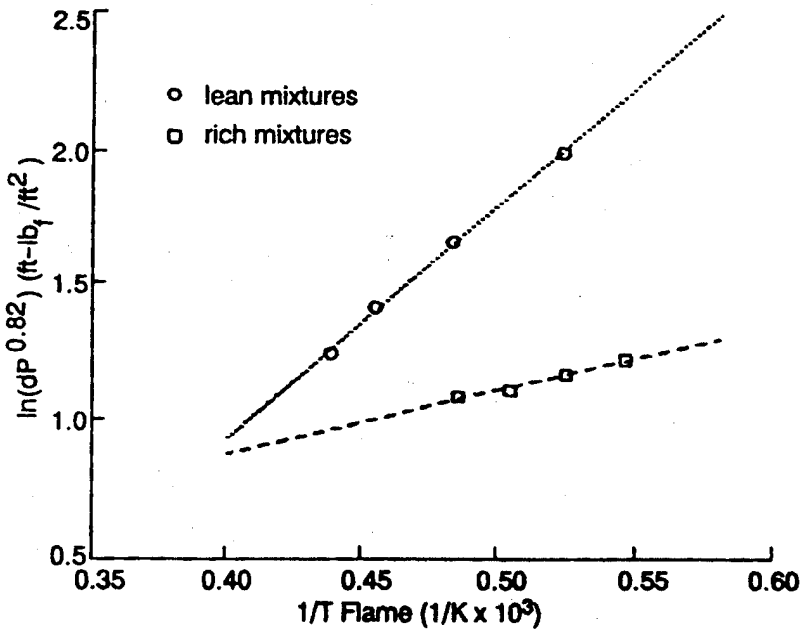

Figure L–7. Arrhenius Plot for Deadspace in n–Heptane/Air Mixtures Burning at 300K Initial Temperature and Atmospheric Pressure (Rich and Lean Mixtures)

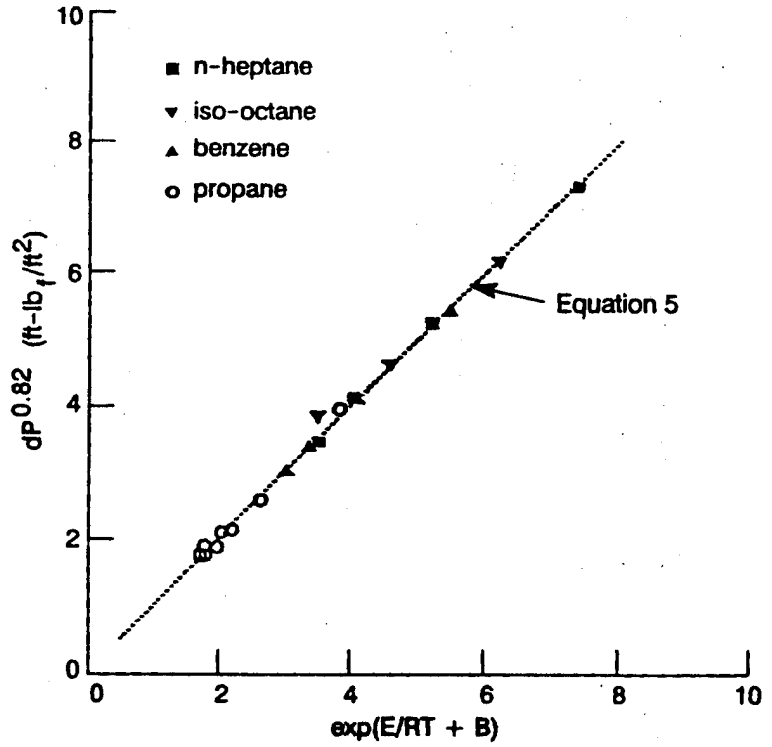

Figure L–8. Deadspace Correlation Plot for Combustion in Air of Propane, n–Heptane, Iso–octane and Benzene at 300K Initial Temperature and Atmospheric Pressure (Lean Mixtures Only, Except for Propane)

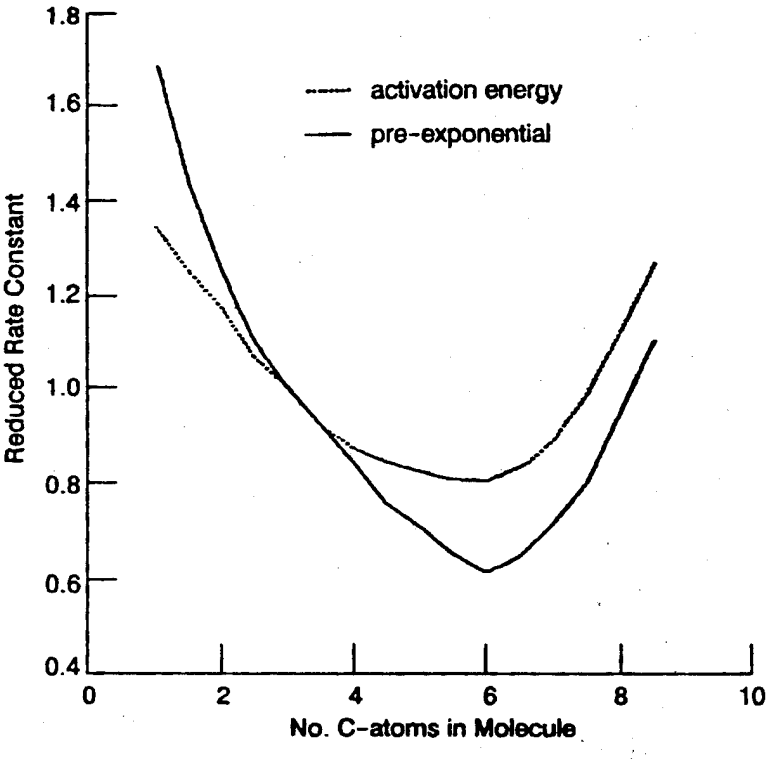

Figure L–9. Dependency of Reduced Rate Constants on Hydrocarbon Molecule

L–6.0: Test of Relationship

The validity of Equation L–5 was tested against some lean methane/air data at atmospheric pressure and 300K initial temperature [L11] and some lean butane/air data at 300K initial temperature and pressure of 1.0, 0.081 and 0.125 atm., [L12.]. The methane/air data are based on parallel plate quenching, and the butane/air data are based on burner rim quenching together with true deadspace quenching. In Reference L2, it was shown experimentally that wall deadspace is about one–half the rim deadspace for lean mixtures, and theoretically that wall deadspace is approximately one–quarter the parallel plate quenching distance. For consistency, all data were corrected to parallel plate quenching distances using these relationships.

Figure L–10 is a correlation plot for the calculated versus measured deadspaces for the methane/air and butane/air data. The accuracy achieved is satisfactory.

Figures L–8 and L–10 together establish the efficacy of the simplified (but convenient) correlation shown in Figures L–2 and L3 for propane/oxygen/nitrogen mixtures.

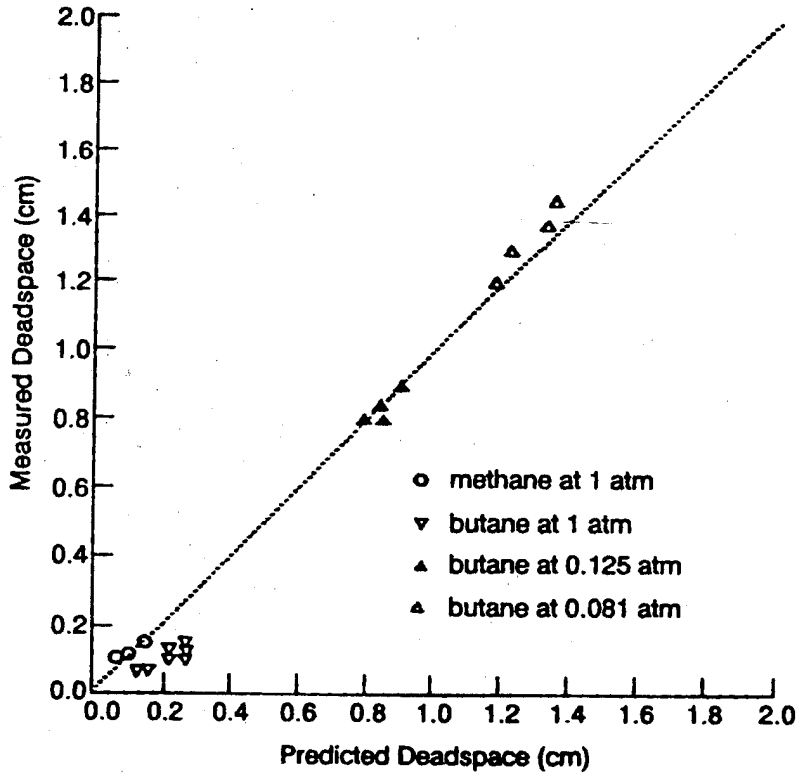

Figure L–10. Accuracy of Deadspace Prediction for Methane/Air at Atmospheric Pressure, and Butane/Air at Atmospheric and Sub–Atmospheric Pressures

L–7.0: References

L1. Lefebvre, A.H., *Gas Turbine Combustion,* McGraw–Hill Book Co., 1983.

L2.. Wohl, K., "Quenching, Flash–Back, Blow–Off–Theory and Experiment," proc. *4th. Symposium (International) on Combustion,* Williams & Wilkins Co., 1953, pp. 68–69.

L3. Barnett, H.C. and Hibbard, R.R., (editors), "Basic Considerations in the Combustion of Hydrocarbon Fuels in Air," NACA Report No. 1300, 1959, pp. 83–91.

L4. Semenov, N.N., "Thermal Theory of Combustion and Explosion, III– Theory of Normal Flame Propagation," *Progress of Physical Science (USSR),* Vol. 24, No. 4, 1940 (translation available as NACA TM No. 1026, September 1942).

L5. Sturgess, G.J., proc. *Symp. Premixed, Prevaporized Combustor Technology Forum,* NASA Rept. CP–2078, 1979.

L6. Pratt, B.S. and Pratt, D.T., "An Interactive Code for Calculation of Gas–Phase Chemical Equilibrium: EQLBRM," NASA Rept. CR–168337, April 1984.

L7. Clarke, A.E., Odgers, J., Stringer, F.W. and Harrison, A.J., "Combustion Process in a Spherical Combustor," proc. *10th Symposium (International) on Combustion,* The Combustion Institute, 1965, pp. 1151–1166.

L8. Kydd, P.H. and Foss, W.I., "Combustion of Fuel–Lean Mixtures in Adiabatic Well–Stirred Reactors," proc. *10th. Symposium (International) on Combustion,* The Combustion Institute, 1965, pp. 101–110.

L9. Stringer, F.W., Clarke, A.E. and Clarke, J.S., "The Spontaneous Ignition of Hydrocarbon Fuel in a Flowing System," proc. *Institute of Mechanical Engineers,* London, England, January 1970, pp. 198–211.

L10. Lewis, B. and von Elbe, G., *Combustion, Flames and Explosion of Gases,* 2nd. Edit., Academic Press, 1961, p.186.

L11. *ibid,* p. 338.

L12. Wohl, L., Kopp, N.M. and Gazely, C., proc. *3rd. Symposium (International) on Combustionm Flame and Explosion Phenomena,* Williams & Wilkins Co., 1949, p.3.